

Development of an Intervertebral Disc Implant,
BioModelling Methodology
and a
Femoral Endoprosthesis

A thesis
submitted in partial fulfilment
of the requirements for the Degree
of
Doctor of Philosophy in Mechanical Engineering
in the
University of Canterbury

by

Iain A. McMillan, B.E. (Honours)

University of Canterbury

2004

Abstract

The intervertebral discs of the lumbar spine can be damaged as a result of trauma, disease or deformity. If an intervertebral disc becomes too compromised the current surgical solution is to fuse the vertebra at the affected spinal level. Spinal fusion presents its own complications which can limit its short and long term success. One of the key limiting factors is the loss of mobility at the affected level, this causes additional loading and accelerated degradation of the adjacent intervertebral discs. Therefore, the aim of this project was to develop an intervertebral disc implant which allowed natural motion at the affected level.

The implant developed consists of a fluid filled welded bellows assembly. This arrangement is similar to a healthy intervertebral disc in which the fluid nucleus pulposus is contained by the annulus fibrosus. The proposed implant also incorporates overload and motion-restricting features to prevent the implant and spinal column being damaged.

Artificial disc implants have been developed by other researchers. The implant developed in this project is unique as it does not generate any wear debris. This is significant as wear debris can cause a macrophage response and osteolysis, thus ultimately limiting the long term viability of implants which do produce wear debris.

This thesis also details the development of BioModelling methodology for producing graphical reconstructions from medical scan data. These reconstructions can be used to produce plastic and metallic models for pre-operative planning purposes and implants for *in-vivo* use. While originally intended for the spinal implant work, it was ultimately used for other tasks. A case study illustrates its use in producing a maxilla implant.

The final component of this project was to design and produce a femoral endoprosthesis for a patient with Osteogenesis Imperfecta. The patient's existing implants had failed and as a result an implant was required which could fully support all the applied loads whilst still allowing the patient's healthy hip and knee joints to be retained.

To Julie

Thank you for your patience and support.

Acknowledgements

I would like to thank Dr Keith Alexander for supervising this project. His aid and direction during the course of this project have been invaluable. I would also like to acknowledge his ongoing efforts regardless of circumstances.

I would also like to thank my other supervisor, Mr James Burn, for his help with clinical matters, refinement of the problem statement and his enthusiasm for the project and all its possible applications.

I would also like to acknowledge the support I have received from the staff of Enztec Limited though out this project. However, in particular I would like to highlight the help, encouragement and support I have received from Paul Morrison.

I am very grateful to all the staff within the Department of Mechanical Engineering for helping with various aspects of this research. In particular I would like to thank Paul Southward, Scott Amies, Ken Brown, Paul Wells and Adam Latham.

Finally I would like to sincerely thank my family and friends for their support and encouragement. This contribution has been invaluable.

Contents

| | |
|------------------------|-------|
| Abstract | ii |
| Acknowledgements | iv |
| Contents | v |
| List of Figures | xi |
| List of Tables | xix |
| Glossary | xxi |
| Foreword | xxvii |

Part A - Development of an Intervertebral Disc Implant

| | |
|--|----|
| CHAPTER 1 - PROBLEM STATEMENT | 3 |
| 1.1 References | 4 |
| CHAPTER 2 - ANATOMY & PHYSIOLOGY OF THE LUMBAR SPINE | 5 |
| 2.1 Vertebral Column | 5 |
| 2.2 Basic Biomechanics – Rotations and Translations | 7 |
| 2.3 Lumbar Spine Overview | 10 |
| 2.4 Vertebrae | 12 |
| 2.5 Intervertebral Disc | 17 |
| 2.6 Zygapophysial Joints | 27 |
| 2.7 Lordosis Curve | 31 |
| 2.8 Nerves | 33 |
| 2.9 Effects of Age | 35 |
| 2.10 Lumbar Spine Pain | 37 |
| 2.11 Summary | 42 |
| 2.12 References | 43 |

| | |
|--|-----|
| CHAPTER 3 - TRADITIONAL SURGICAL SOLUTIONS..... | 43 |
| 3.1 Spinal Fusion Implants..... | 43 |
| 3.1.1 Interbody Spacers..... | 44 |
| 3.1.2 Posterior Instrumentation..... | 46 |
| 3.2 Surgical Approach for Spinal Fusion..... | 49 |
| 3.3 Disadvantages of Spinal Fusion..... | 57 |
| 3.4 References..... | 59 |
| | |
| CHAPTER 4 - SPECIFICATION & ANALYSIS OF EXISTING ARTIFICIAL DISCS | 63 |
| 4.1 Expansion of Problem Statement in Engineering Terms..... | 63 |
| 4.1.1 Load Carrying Requirements..... | 63 |
| 4.1.2 Kinematics..... | 65 |
| 4.1.3 Centre of Rotation..... | 67 |
| 4.1.4 Fatigue Requirements..... | 69 |
| 4.1.5 Materials..... | 75 |
| 4.1.6 Geometry..... | 77 |
| 4.1.7 Stiffness..... | 86 |
| 4.1.8 Fixation to Bone..... | 87 |
| 4.1.9 Failsafe..... | 88 |
| 4.1.10 Specification..... | 89 |
| 4.2 Artificial Discs..... | 90 |
| 4.2.1 Articulating Discs..... | 90 |
| 4.2.2 Hydraulic Discs..... | 101 |
| 4.2.3 Elastic Discs..... | 103 |
| 4.3 Summary..... | 105 |
| 4.4 References..... | 106 |

| | |
|---|---------|
| CHAPTER 5 - CONCEPTUAL DESIGN | 111 |
| 5.1 Conceptual Design Process | 111 |
| 5.2 Conceptual Design of the Intervertebral Disc Implant | 115 |
| 5.3 References | 118 |
| CHAPTER 6 – EMBODIMENT DESIGN | 119 |
| 6.1 Principles of the Bellows Intervertebral Disc Implant | 119 |
| 6.2 Components | 121 |
| 6.2.1 Metallic Bellows | 121 |
| 6.2.2 Internal Support | 138 |
| 6.2.3 Fill Medium Selection | 162 |
| 6.2.4 Endplates | 165 |
| 6.2.5 Motion Restriction | 175 |
| 6.2.6 Protective Outer Sheath | 179 |
| 6.2.7 Surface Treatment | 181 |
| 6.2.8 Surface Marking | 183 |
| 6.2.9 Insertion/Extraction Tooling | 185 |
| 6.3 Assembled Implant Renders and Drawings | 187 |
| 6.4 Advantages and Disadvantages of Bellows Intervertebral Disc Implant | 190 |
| 6.5 Patent | 192 |
| 6.6 References | 193 |
| CHAPTER 7 - TEST RIG DESIGN | 197 |
| 7.1 Introduction | 197 |
| 7.2 Background | 197 |
| 7.3 Common Features | 200 |
| 7.4 Single-Axis Testing | 203 |
| 7.5 Vertical Load Testing | 209 |
| 7.6 Multi-Axis Testing | 212 |
| 7.7 Conclusion | 218 |
| 7.8 References | 219 |
| CHAPTER 8 - CONCLUSION | 221 |

Part B - Development of BioModelling Methodology and a Femoral Endoprosthesis

| | |
|---|-----|
| CHAPTER 9 - BIOMODELLING | 227 |
| 9.1 Problem Statement | 227 |
| 9.2 Medical Imaging | 229 |
| 9.3 Medical Reconstruction | 233 |
| 9.3.1 Reconstruction Process | 235 |
| 9.3.2 Standard Voxel Manipulation Tools | 238 |
| 9.3.3 Software Solutions Tried | 241 |
| 9.3.4 Final Software Package Chosen | 246 |
| 9.3.5 Problem Highlighted With Use | 247 |
| 9.4 Rapid Prototyping | 249 |
| 9.5 BioModelling Ordering Process | 258 |
| 9.6 Machined BioModels | 261 |
| 9.7 Case Study | 271 |
| 9.8 Summary and Conclusion | 280 |
| 9.9 References | 281 |
| CHAPTER 10 - FEMORAL ENDOPROSTHESIS | 283 |
| 10.1 Problem Statement | 283 |
| 10.2 Case History | 283 |
| 10.3 Literature Review | 286 |
| 10.4 Proposed Solution | 290 |
| 10.5 Endoprosthesis Geometry | 292 |
| 10.6 Final Solution | 295 |
| 10.7 Analysis | 300 |
| 10.8 Instrumentation | 302 |
| 10.9 Surgical Outcome | 304 |
| 10.10 Potential Improvements | 305 |
| 10.11 Summary and Conclusion | 309 |
| 10.12 References | 310 |

Part C - Appendices

| | |
|---|-----|
| APPENDIX 1 - CONCEPTUAL DESIGNS | 313 |
| APPENDIX 2 - TITANIUM | 327 |
| A2.1 Background | 328 |
| A2.2 Available Alloys | 329 |
| A2.3 Ti-6Al-4V | 330 |
| A2.4 Commercially Pure Titanium | 345 |
| A2.5 Summary | 346 |
| A2.6 References | 347 |
| APPENDIX 3 - STAINLESS STEEL | 349 |
| A3.1 Background | 350 |
| A3.2 316L Stainless Steel | 350 |
| A3.3 Summary | 353 |
| A3.4 References | 354 |
| APPENDIX 4 – NITINOL | 355 |
| A4.1 History | 356 |
| A4.2 Characteristic Properties of Nitinol | 357 |
| A4.3 Properties of Nitinol | 366 |
| A4.4 Theory of the Austenite to Martensite Transformation | 368 |
| A4.5 Shape Memory Alloy Mechanisms | 373 |
| A4.6 Fatigue Characteristics | 383 |
| A4.7 Biocompatibility | 385 |
| A4.8 Conclusions | 386 |
| A4.9 References | 387 |

| | |
|--|-----|
| APPENDIX 5 – SAMPLE Z-SPRING CALCULATION..... | 389 |
| A5.1 Analysis of the Z-Spring Concept..... | 390 |
| A5.2 Arc Deflections (A-B)..... | 392 |
| A5.3 Cantilever Deflections (B-C)..... | 394 |
| A5.4 Arc Deflections (C-D)..... | 395 |
| A5.5 Total Deflections..... | 397 |
| A5.6 Peak Stress..... | 398 |
| A5.7 Effect of Varying Length and Radius..... | 399 |
| A5.8 Summary..... | 402 |
| | |
| APPENDIX 6 - EVALUATION SUBTASKS..... | 403 |
| | |
| APPENDIX 7 - INITIAL BELLOWS SPECIFICATION..... | 407 |
| | |
| APPENDIX 8 - TECHNICAL DATA SHEETS..... | 411 |
| A8.1 Silbione 40047..... | 413 |
| A8.2 NuSil Med-1511..... | 415 |
| A8.3 NuSil Med1-4213..... | 419 |
| A8.4 NuSil SP-120..... | 423 |
| A8.5 NuSil SP-124..... | 425 |
| | |
| APPENDIX 9 - NEW ZEALAND PATENT APPLICATION..... | 429 |
| | |
| APPENDIX 10 - FEMORAL ENDOPROSTHESIS CONCEPTUAL DESIGNS..... | 461 |
| | |
| APPENDIX 11 - FEMORAL ENDOPROSTHESIS DRAWINGS..... | 467 |

List of Figures

| | | |
|-------------|--|----|
| Figure 1.1 | Common intervertebral disc problems..... | 3 |
| Figure 2.1 | Vertebral column..... | 6 |
| Figure 2.2 | Planes and direction of motion: Anatomical system..... | 7 |
| Figure 2.3 | Axes and directions of motion: Biomechanical system..... | 8 |
| Figure 2.4 | Lumbar spine vertebrae, intervertebral discs and zygapophysial joints..... | 10 |
| Figure 2.5 | Sacrum and Coccyx..... | 11 |
| Figure 2.6 | Parts of the lumbar vertebrae..... | 12 |
| Figure 2.7 | Schematic internal structure of the vertebral body..... | 13 |
| Figure 2.8 | Vertebral spongiosa and veins..... | 14 |
| Figure 2.9 | Vertebral foramen and intervertebral foramina..... | 15 |
| Figure 2.10 | Posterior elements of the vertebral body..... | 16 |
| Figure 2.11 | Structure of the intervertebral disc..... | 17 |
| Figure 2.12 | Detailed structure of the annulus fibrosus..... | 17 |
| Figure 2.13 | Incomplete lamellae of the annulus fibrosus..... | 18 |
| Figure 2.14 | Structure of the vertebral endplates..... | 19 |
| Figure 2.15 | Annulus fibrosus and nucleus pulposus interaction under applied load..... | 21 |
| Figure 2.16 | Annulus fibrosus and nucleus pulposus weight bearing mechanisms..... | 22 |
| Figure 2.17 | Distraction and sliding of the intervertebral disc..... | 23 |
| Figure 2.18 | Bending of the intervertebral disc..... | 24 |
| Figure 2.19 | Twisting of the intervertebral disc..... | 25 |
| Figure 2.20 | Zygapophysial joints resist shear loads..... | 27 |
| Figure 2.21 | Posterior and superior views of the L3-4 zygapophysial joints..... | 28 |
| Figure 2.22 | Flat zygapophysial joints..... | 28 |
| Figure 2.23 | Curved zygapophysial joints..... | 29 |
| Figure 2.24 | Impaction of the zygapophysial joints..... | 30 |
| Figure 2.25 | Lumbosacral angle..... | 31 |
| Figure 2.26 | Spinal nerves..... | 33 |
| Figure 2.27 | Innervation of the lumbar spine..... | 34 |
| Figure 2.28 | Torsion injuries..... | 40 |
| Figure 2.29 | Intervertebral disc degradation..... | 41 |
| Figure 2.30 | Grades of radial fissure..... | 42 |

| | | |
|-------------|---|-----|
| Figure 3.1 | Titanium mesh gage packed with autogenous cancellous bone..... | 44 |
| Figure 3.2 | Cage placed at the fusion site..... | 44 |
| Figure 3.3 | BAK/L™ implant..... | 45 |
| Figure 3.4 | LT-CAGE™..... | 45 |
| Figure 3.5 | Ovation™ Polyaxial pedicle screw fixation system..... | 47 |
| Figure 3.6 | Claris pedicle screw fixation system..... | 47 |
| Figure 3.7 | Facet screw fixation..... | 48 |
| Figure 3.8 | Anterior interbody fusion utilizing a cage and buttress plate..... | 50 |
| Figure 3.9 | Retraction of the nerve roots to facilitate posterior interbody fusion..... | 52 |
| Figure 3.10 | Postoperative anterior-posterior x-rays of a TLIF..... | 55 |
| | | |
| Figure 4.1 | Instantaneous axis of rotation..... | 68 |
| Figure 4.2 | Intervertebral disc wedge angles..... | 77 |
| Figure 4.3 | Ejection of the implant from the disc space..... | 79 |
| Figure 4.4 | Vertebral body dimension parameters..... | 81 |
| Figure 4.5 | Allowance for using of the implant at contiguous levels..... | 84 |
| Figure 4.6 | Summary of implant geometry requirements..... | 85 |
| Figure 4.7 | Link SB Charité Disc..... | 92 |
| Figure 4.8 | Link SB Charité Disc mobile sliding core..... | 92 |
| Figure 4.9 | ProDisc implant..... | 94 |
| Figure 4.10 | Bryan Cervical Disc..... | 96 |
| Figure 4.11 | Kostuik Disc..... | 97 |
| Figure 4.12 | Bristol Cervical Disc..... | 99 |
| Figure 4.13 | Prosthetic Disc Nucleus (PDN)..... | 102 |
| Figure 4.14 | Acroflex Disc..... | 104 |

| | | |
|-------------|--|-----|
| Figure 6.1 | Stylised bellows intervertebral disc implant components..... | 119 |
| Figure 6.2 | Sectioned view of welded bellows showing common terminology..... | 122 |
| Figure 6.3 | Types of bellows..... | 122 |
| Figure 6.4 | Formed bellows manufacturing process..... | 123 |
| Figure 6.5 | Welded bellows manufacturing process..... | 125 |
| Figure 6.6 | Bellows solid height..... | 126 |
| Figure 6.7 | Welded bellows diaphragm contours..... | 127 |
| Figure 6.8 | Welded bellows multi-ply convolution..... | 128 |
| Figure 6.9 | Load carrying capabilities of annulus fibrosus following discectomy.. | 134 |
| Figure 6.10 | Support separation and contact..... | 138 |
| Figure 6.11 | Bellows natural centre of rotation..... | 140 |
| Figure 6.12 | Internal support causing sliding at interface..... | 140 |
| Figure 6.13 | Internal support causing rolling at interface..... | 141 |
| Figure 6.14 | Sphere in a spherical socket..... | 142 |
| Figure 6.15 | Thickness of sliding support socket..... | 143 |
| Figure 6.16 | Cylindrical-to-spherical tangency comparison for the internal support. | 143 |
| Figure 6.17 | Rolling support contact point radius during deflection..... | 144 |
| Figure 6.18 | Lift as a result of rolling support deflection..... | 145 |
| Figure 6.19 | Required roller radius (R2) for varying socket and contact point radii. | 146 |
| Figure 6.20 | Lift resulting from 8° angular deflection for varying socket and contact point radii..... | 147 |
| Figure 6.21 | Contact stress for varying socket and contact point radii..... | 148 |
| Figure 6.22 | FEA contact stress plot for chrome cobalt-chrome cobalt sliding support..... | 153 |
| Figure 6.23 | FEA contact stress plot for chrome cobalt-chrome cobalt rolling support..... | 155 |
| Figure 6.24 | FEA contact stress plot for Radel R5500-Radel R5500 rolling support..... | 156 |
| Figure 6.25 | Average surface roughness..... | 157 |
| Figure 6.26 | Wear resulting from rough surface..... | 158 |
| Figure 6.27 | Wear resulting from smooth surface..... | 158 |
| Figure 6.28 | Contact couple of differing hardness..... | 159 |

| | | |
|-------------|---|-----|
| Figure 6.29 | Example of a typical endplate weld preparation..... | 167 |
| Figure 6.30 | Rendered of implant endplates showing fixation features..... | 171 |
| Figure 6.31 | Exploded view showing the preferred endplate fill port arrangement..... | 173 |
| Figure 6.32 | Alternative endplate fill port..... | 173 |
| Figure 6.33 | Endplate socket..... | 174 |
| Figure 6.34 | Schematic diagrams of bump stops..... | 176 |
| Figure 6.35 | Schematic diagrams of externally tethered implant..... | 177 |
| Figure 6.36 | Schematic diagram of internally tethered implant..... | 177 |
| Figure 6.37 | Tether retaining components..... | 180 |
| Figure 6.38 | Example of laser engraving on the outer face of the top endplate..... | 184 |
| Figure 6.39 | Suggested intervertebral disc implant insertion tooling..... | 186 |
| Figure 6.40 | Rendered partial isometric of bellows intervertebral disc..... | 187 |
| Figure 6.41 | General assembly of bellows intervertebral disc implant..... | 188 |
| Figure 6.42 | Sectioned view of bellows intervertebral disc implant..... | 189 |
| | | |
| Figure 7.1 | Schematic diagram of the multi-axis test rig designed by Wilke et al. .. | 198 |
| Figure 7.2 | Flexion/extension and axial twisting module for a MTS machine..... | 199 |
| Figure 7.3 | CAD model of the single-axis test rig..... | 206 |
| Figure 7.4 | Single-axis test rig range of motion..... | 207 |
| Figure 7.5 | As built single-axis test rig..... | 208 |
| Figure 7.6 | Single-axis test rig constraint mechanisms, fluid vessels and heating coils..... | 208 |
| Figure 7.7 | CAD model of the vertical load test rig..... | 211 |
| Figure 7.8 | CAD model of the multi-axis test rig..... | 216 |
| Figure 7.9 | Multi-axis test rig axes..... | 217 |

| | | |
|-------------|---|-----|
| Figure 9.1 | Schematic of modern CT scanner..... | 229 |
| Figure 9.2 | Relationship of the x-ray tube, patient, detector, and image reconstruction computer..... | 230 |
| Figure 9.3 | Simulation of the x-ray beam path during spiral CT scanning..... | 231 |
| Figure 9.4 | Axial CT image of the lumbar spine..... | 232 |
| Figure 9.5 | CT planar images and three-dimensional reconstruction image..... | 233 |
| Figure 9.6 | BioModels of craniopagus twins..... | 234 |
| Figure 9.7 | Gantry tilt schematic..... | 235 |
| Figure 9.8 | Organise images dialogue box..... | 236 |
| Figure 9.9 | CT slices with increasing contrast..... | 238 |
| Figure 9.10 | CT slices with varying thresholding limits..... | 239 |
| Figure 9.11 | Draw and Erase tools..... | 240 |
| Figure 9.12 | 3D Doctor workspace and image mosaic..... | 242 |
| Figure 9.13 | Mimics workspace..... | 243 |
| Figure 9.14 | Velocity2 Pro workspace (Unix Version)..... | 245 |
| Figure 9.15 | Rapid prototyping part creation..... | 249 |
| Figure 9.16 | Addition of support material..... | 250 |
| Figure 9.17 | Stereo-lithography model of a maxilla and mandible..... | 251 |
| Figure 9.18 | Fusion deposition model of a maxilla and mandible..... | 253 |
| Figure 9.19 | Human skull model created using three dimensional printing..... | 254 |
| Figure 9.20 | CT Data Archive Request form..... | 259 |
| Figure 9.21 | Area of Interest Diagrams supplied to the surgeon..... | 260 |
| Figure 9.22 | Simple CAD generated model exported in STL format..... | 261 |
| Figure 9.23 | IGES contour file of a reconstructed femoral head..... | 263 |
| Figure 9.24 | Lofted model of a partial femoral head developed from IGES curves..... | 263 |
| Figure 9.25 | Anterior view of the right femur and pelvis..... | 264 |
| Figure 9.26 | Hip geometry produced in Rhinoceros® from an imported STL file..... | 265 |
| Figure 9.27 | Data input and pre-processing..... | 268 |
| Figure 9.28 | Surface generation and patch manipulation..... | 268 |
| Figure 9.29 | Final NURBS model..... | 269 |
| Figure 9.30 | Left zygomatic bone and maxilla in-situ..... | 271 |

| | | |
|--------------|---|-----|
| Figure 9.31 | Rendering of the reconstructed CT data..... | 271 |
| Figure 9.32 | Rendering of the implant parent data..... | 272 |
| Figure 9.33 | Rendering of the implant template data..... | 273 |
| Figure 9.34 | Skull implant prototypes..... | 274 |
| Figure 9.35 | Rendering of the raw implant template data..... | 276 |
| Figure 9.36 | Rendering of the modified implant template and contact patch..... | 277 |
| Figure 9.37 | Rendering of the bridge between the implant template and contact patch..... | 277 |
| Figure 9.38 | Rendering of the final implant and contact patch..... | 278 |
| | | |
| Figure 10.1 | Examples of existing fixation devices..... | 283 |
| Figure 10.2 | X-ray of the patient's left femur..... | 284 |
| Figure 10.3 | Marcove et al total femur and knee replacement..... | 287 |
| Figure 10.4 | Steinbrink et al total femoral prostheses..... | 288 |
| Figure 10.5 | Kotz distal femoral modular endoprosthesis..... | 289 |
| Figure 10.6 | Tee section positioned in femur..... | 290 |
| Figure 10.7 | Geometry extracted from x-ray..... | 292 |
| Figure 10.8 | Endoprosthesis geometry..... | 294 |
| Figure 10.9 | Assembled & exploded views of the femoral endoprosthesis..... | 295 |
| Figure 10.10 | Endoprosthesis body..... | 296 |
| Figure 10.11 | Hip and knee screws..... | 297 |
| Figure 10.12 | Locking plug..... | 298 |
| Figure 10.13 | Knee screw simplified for FEA purposes..... | 300 |
| Figure 10.14 | FEA deflection and stress plots..... | 301 |
| Figure 10.15 | Hip and knee screw introducer..... | 302 |
| Figure 10.16 | Femur endoprosthesis photos..... | 303 |
| Figure 10.17 | Hip screw length issue and in theatre solution..... | 304 |
| Figure 10.18 | Hip and knee screw castellation design..... | 306 |
| Figure 10.19 | Locking screw profiles..... | 307 |
| Figure 10.20 | Endoprosthesis body, supplied and preferable grain directions..... | 308 |

| | | |
|--------------|--|-----|
| Figure A2.1 | Ti-6Al-4V - Effect of shot peening and electropolishing on fatigue life..... | 332 |
| Figure A2.2 | Slip band formation mechanism..... | 336 |
| Figure A2.3 | Typical Ti-6Al-4V Widmanstätten microstructure..... | 337 |
| Figure A2.4 | Formation of lamellae microstructure..... | 338 |
| Figure A2.5 | Ti-6Al-4V - Lamellar microstructure..... | 339 |
| Figure A2.6 | Ti-6Al-4V - Equiaxed microstructure..... | 340 |
| Figure A2.7 | Processing path for recrystallization and duplex annealed microstructures..... | 341 |
| Figure A2.8 | Ti-6Al-4V - Duplex microstructure..... | 342 |
| Figure A2.9 | Ti-6Al-4V - Duplex microstructure and fatigue..... | 342 |
| Figure A2.10 | CP Grade 4 Titanium Alloy - Rotating beam fatigue strength..... | 346 |
| Figure A3.1 | S-N curve for 316 stainless steel in air..... | 352 |
| Figure A3.2 | Effect of pH on fatigue strength of stainless steel..... | 353 |
| Figure A4.1 | Homer Mammalok®, shown in retracted and deployed configurations..... | 357 |
| Figure A4.2 | Longitudinal and transverse views of a Simon vena cava filter in its deployed state..... | 358 |
| Figure A4.3 | Kink resistance 1 mm diameter grasper designed for use in urology..... | 359 |
| Figure A4.4 | Stress-Strain curve for Nitinol compared to Stainless Steel..... | 360 |
| Figure A4.5 | Nitinol orthodontic arch-wires apply constant stress to the teeth..... | 361 |
| Figure A4.6 | An intervertebral disc spacer in martensitic and deployed super-elastic states..... | 362 |
| Figure A4.7 | SMA stent in the process of being deployed from a catheter..... | 363 |
| Figure A4.8 | Biased stiffness illustrated in a stent..... | 365 |
| Figure A4.9 | Schematic showing super-elasticity descriptors..... | 367 |
| Figure A4.10 | 2d schematic of the austenite to martensite transformation..... | 368 |
| Figure A4.11 | Stress-induced martensitic shape and volume accommodation mechanisms..... | 369 |
| Figure A4.12 | Microstructure of martensite..... | 370 |

| | | |
|--------------|---|-----|
| Figure A4.13 | Microstructure of stress-induced martensitic..... | 370 |
| Figure A4.14 | Relationship between free energy of martensite (M) and austenite (β)..... | 371 |
| Figure A4.15 | Temperatures hysteresis..... | 372 |
| Figure A4.16 | Nickel Titanium alloy atomic arrangement upon cooling..... | 373 |
| Figure A4.17 | Deformation of lattice or de-twinning..... | 373 |
| Figure A4.18 | Transformation between high and low temperature structures..... | 374 |
| Figure A4.19 | Schematic diagram of the two-way memory effect..... | 375 |
| Figure A4.20 | All-round shape memory effect..... | 376 |
| Figure A4.21 | Two-way motion using a biasing (steel) spring..... | 376 |
| Figure A4.22 | Stress-Strain for a super-elastic material..... | 377 |
| Figure A4.23 | Effect of temperature on transformation stress..... | 378 |
| Figure A4.24 | Idealised temperature hysteresis..... | 380 |
| Figure A4.25 | Three dimensional stress-strain-temperature diagram for a Nitinol..... | 382 |
| Figure A4.26 | Strain controlled fatigue..... | 384 |
| Figure A4.27 | Stress controlled fatigue..... | 384 |
| | | |
| Figure A5.1 | Schematic showing the loads applied to the Z-Spring concept..... | 390 |
| Figure A5.2 | Simplified Z-Spring geometry..... | 391 |
| Figure A5.3 | Z-Spring peak stress location..... | 398 |
| Figure A5.4 | Z-Spring stiffness as a function of length and radius..... | 400 |
| Figure A5.5 | Z-Spring peak stress as a function of length and radius..... | 401 |
| | | |
| Figure A10.1 | Cross section sketches..... | 462 |
| Figure A10.2 | First endoprosthesis concept sketch..... | 463 |
| Figure A10.3 | Endoprosthesis designs for retaining a tri-fin nail..... | 464 |
| Figure A10.4 | Endoprosthesis designs for retain the hip screw..... | 465 |
| | | |
| Figure A11.1 | Femoral Endoprosthesis General Assembly..... | 468 |
| Figure A11.2 | Endoprosthesis Body..... | 469 |
| Figure A11.3 | Hip Screw..... | 470 |
| Figure A11.4 | Knee Screw..... | 471 |
| Figure A11.5 | Locking Plug..... | 472 |

List of Tables

| | | |
|------------|---|-----|
| Table 2.1 | Descriptive terms of motion..... | 9 |
| Table 4.1 | Mean values of range of motion of L4-5..... | 65 |
| Table 4.2 | Design range of motion..... | 66 |
| Table 4.3 | Mean (\pm SD) lumbar motion and percentage of normalised flexion for four daily activities..... | 70 |
| Table 4.4 | Lumbar spine angular deflections when walking..... | 71 |
| Table 4.5 | Mean movements coupled with flexion and extension of the lumbar spine..... | 72 |
| Table 4.6 | Estimated cycles per time period for typical daily activities..... | 72 |
| Table 4.7 | Estimates of daily activities, angular deflections and frequencies..... | 73 |
| Table 4.8 | Fatigue requirements of implant in flexion over 40-year life span..... | 74 |
| Table 4.9 | Intervertebral disc wedge angles..... | 78 |
| Table 4.10 | Average stiffness coefficients from representative functional spines..... | 86 |
| Table 4.11 | Specification..... | 89 |
| Table 5.1 | Sample evaluation table..... | 113 |
| Table 5.2 | Key mechanical properties of the materials investigated..... | 116 |
| Table 5.3 | Intervertebral disc evaluation table..... | 117 |
| Table 6.1 | Bellows fatigue requirements..... | 131 |
| Table 6.2 | Summary of socket and contact point radii effects..... | 149 |
| Table 6.3 | Summary of internal support material properties..... | 151 |
| Table 6.4 | Sliding support contact stresses..... | 152 |
| Table 6.5 | Rolling support contact stresses..... | 154 |
| Table 9.1 | Comparison of three rapid prototyping formats..... | 256 |

| | | |
|------------|---|-----|
| Table A2.1 | Ti-6Al-4V – Mechanical properties at room temperature..... | 330 |
| Table A2.2 | Surface effects on high cycle fatigue..... | 331 |
| Table A2.3 | CP Titanium grades and composition (% Weight)..... | 345 |
| Table A2.4 | CP Titanium - Mechanical properties at room temperature..... | 345 |
| Table A3.1 | 316 Stainless steel grades and composition (% Atomic)..... | 350 |
| Table A3.2 | Mechanical properties of 316LS annealed bar at room temperature.. | 351 |
| Table A3.3 | 316LS - Mechanical properties as a function of cold work..... | 351 |
| Table A4.1 | Stored energy of different materials..... | 379 |

Glossary

Aetiology – The cause or causes of a disease or abnormal condition.

Allograft Bone – Sterile bone derived from another human that is used for grafting procedures.

Anterior – Front of the body or situated nearer the front of the body.

Arthrodesis – The fusion of bones across a joint space, thereby limiting or eliminating movement. It may occur spontaneously or as a result of a surgical procedure, such as fusion of the spine.

Arthropathy – Any disease or disorder involving a joint.

Arthroplasty – The surgical remodelling of a diseased or damaged joint.

Autogenous Bone – Bone originating from the same individual; i.e., an individual's own bone.

Autogenous Weld – A weld formed by melting the parent material until it fuses without the addition of filler material.

Autograft Bone – Bone transplanted from one part to another part of the body in the same individual.

Axon – Usually a long, single nerve cell process that conducts impulses away from the cell body.

CAD – Computer Aided Design.

Caudal – A position more towards the cauda or tail than a specified point of reference, same as inferior.

Cephalad – In a direction towards the head.

Convolution – Two diaphragms welded together on their inner edge.

Cortical Bone – The layer of dense bone that forms the outer surface of bone.

Diaphragm – An annular ring of material which is used as the base unit for constructing welded bellows. Diaphragms often have a contoured surface and are produced in male and female configurations.

Discectomy – Surgical removal of part or all of an intervertebral disc in order to remove material which is impinging on the neural elements.

Endoprosthesis – An artificial device which is placed inside the body to replace a missing body part.

Exenteration – Surgical removal of the contents from a bodily cavity.

FDM – Fusion Deposition Modelling.

FEA – Finite Element Analysis.

Functional cadaver spinal segments – Two or more adjacent vertebrae harvested from a human cadaver with the intervertebral disc(s), zygapophysial joints and ligaments intact.

Hypertrophic – Excessive development of an organ, specifically an increase in bulk (as by thickening of muscle fibres) without multiplication of parts.

Iliac Crest – The large, prominent portion of the pelvic bones which can be felt at the belt line.

Inferior – Situated below or directed downward.

In-vitro – Describing biological phenomena that are made to occur outside the living body, traditionally in a test tube. In-vitro is Latin for in glass.

In-vivo – Within a living body. In-vivo is Latin for in life.

Ischial Weight Bearing Brace – A long leg brace with a thigh cuff which provides posterior ischial (hip bone) weight bearing support. Such a brace allows patients to stand upright and bear weight.

Ligamentous Laxity – A stretched or loose ligament which allows hyper deflection to occur.

Lordosis – Curvature of the spine with the convexity forward. Not a disease state, but the normal anterior concavity of the neck or lower back.

Macrophage Cells – Play an important role in killing bacteria and tumour cells. They release substances that stimulate other cells of the immune system and are involved in antigen delivery but they may also fuse to form foreign body giant cells.

Maxillectomy – Surgical removal of the maxilla.

Morphology – The configuration or the structure of a patient.

Myelopathy – Any disease or disorder of the spinal cord or bone marrow.

NC – Numerical Control.

Ossification – The process of forming bone in the body.

Osteogenesis Imperfecta – A genetic disease characterized by abnormal brittleness of the long bones.

Osteolysis – The abnormal loss of bone and tissue as a result of a pathological condition.

Osteophyte – A bony outgrowth or protuberance.

Oswestry Score – Indicates the level of disability in patients with lower back pain.

Paraesthesia – A sensation of pricking, tingling, or creeping on the skin having no objective cause and usually associated with injury or irritation of a sensory nerve or nerve root.

Periprosthetic – Around, about or near a prosthesis or implant.

Pitch – The height of one convolution, measured from the outer edge of one diaphragm to the next.

Posterior – The back of the body or situated nearer the back of the body.

Radicular Pain – Radicular pain arises as a result of irritation of a spinal nerve or its root.

Radiculopathy – Any pathological condition of the nerve roots.

Reflect – To fold back tissue to gain exposure or access. It is common surgical practice to cut a hinged flap into the anterior of the annulus during Anterior Lumbar Interbody Fusion. This process is often referred to as reflecting the annulus. At the completion of this procedure the reflected annulus is stitched back in place and will often re-grow into the vertebral bodies with time.

Resorption – The loss of substance through physiologic or pathologic means.

Sagittal – Longitudinal.

Sarcoma – A form of cancer that occurs in supportive tissues such as bone, cartilage, fat or muscle.

Sclerotic – Hard.

SLA – Stereo-Lithography.

Spondylolisthesis – A defect in the construct of bone between the superior and inferior facets with varying degrees of displacement. The vertebra with the defect and the spine above that vertebra are displaced forward in relationship to the vertebrae below. This is usually due to a developmental defect or as the result of a fracture.

Spongiosa – When filled with blood, the trabecular bone that fills the cavity of the vertebral body appears to be sponge like, and for this reason it is sometime referred to as the vertebral spongiosa.

Squamous Cell Carcinoma – A carcinoma that is made up of or arises from squamous cells, normally sited in areas of the body which have been exposed to strong sunlight for extended periods of time.

Stenosis – Reduction in the diameter of the spinal canal due to new bone formation that may result in pressure on the spinal cord or nerve roots.

STL – A stereolithography file format which is the standard input for most rapid prototyping machines. It consists of a list of triangular surfaces which describe a computer generated solid model.

Subsidence – Sinking or settling of an implant.

Superior – Situated above or directed upward toward the head of an individual.

Test Specimen – May be either the assembled bellows intervertebral disc implant or its constituent components.

Toolpath – Generation of code for NC machining components.

Varus Malalignment – Bowing of the femur(s) sometime referred to colloquially as ‘bandy legs’. This condition can be caused by the outer cortex of the femur(s) failing in tension thus allowing bending of the femur(s) to occur. Alternatively it can occur if one or more knee ligaments are damaged.

<Blank Page>

Foreword

This thesis consists of three components:

Part A - Development of an Intervertebral Disc Implant

The primary objective of this project was to develop an intervertebral disc implant for the lumbar spine. This implant was required to support the applied loads and to allow angular deflections to occur. Part A of this thesis details the structures and functions of the lumbar spine, development of an engineering specification and design of the implant. This section of the thesis also details the design of test rigs to aid in the development and testing the implant and its components.

Part B - Development of BioModelling Methodology and a Femoral Endoprosthesis

The original project brief also stipulated that BioModelling methodology should be investigated and developed to aid in the design of the intervertebral disc implant. As it turned out these tools were unnecessary for the development of an intervertebral disc implant. BioModelling tools can be used for visualisation and preoperative planning purposes. Therefore, given these other visualisation and planning applications, the decision was made to complete research into BioModelling techniques. The outcomes of this research are presented in Chapter 9.

Chapter 10 of this thesis details the development of a femoral endoprosthesis. This additional work was undertaken following a request to design a femoral implant, for a patient who had the brittle bone disease, Osteogenesis Imperfecta. This additional work was seen as a valuable experience that contributed to an understanding of surgical issues arising in the main project.

Part C - Appendices

The final section of this thesis contains appendices for the intervertebral disc implant and femoral endoprosthesis.

Part A

Development of an Intervertebral Disc Implant

<Blank Page>

Chapter 1 – Problem Statement

Debilitating lower back pain due to damage or failure of the intervertebral discs is a common complaint which affects a large percentage of the adult population⁴. Intervertebral disc disorders may arise from trauma, disease, or deformity. Some examples of common intervertebral disc disorders are shown in Figure 1.1. Once an intervertebral disc has degenerated to a point where it is completely compromised and discectomy is no longer an option, one viable surgical treatment presently available to surgeons is to fuse the affected vertebral level(s).

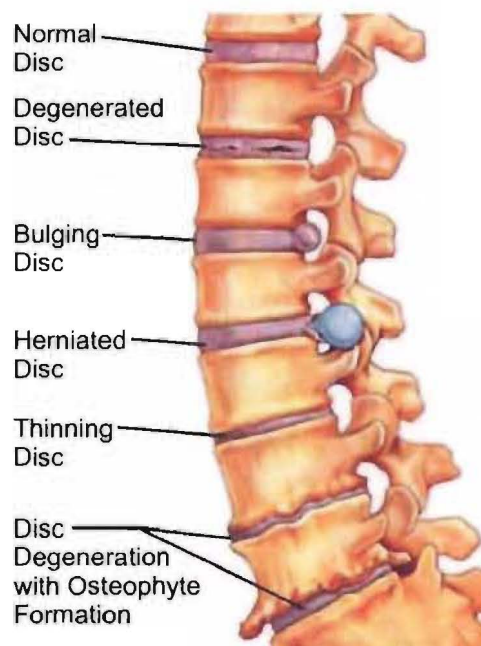


Figure 1.1 Common intervertebral disc problems.

[Source: <http://www.spineuniverse.com/displayarticle.php/article1523.html>]

The aim of spinal arthrodesis (fusing) is to remove the pain generating mechanism(s) at the affected vertebral level. This procedure typically involves removing degenerated bone and intervertebral disc tissue and in some cases fixation devices are also added to stabilise the adjacent vertebrae. Fusing the spine is most effective when treating conditions giving rise to instability in the spine or pain secondary to instability. Disadvantages of fusing the spine include reduced mobility, increased wear and stress on the adjacent vertebral levels, subsidence of the implants and in some cases failure of the vertebrae to fuse together. Any of these factors may, in turn, ultimately lead to the adjacent intervertebral discs needing to be fused as well.

In recent years several groups have developed implants for the lumbar spine which allow normal spinal motion to be preserved. However many of these implants have their own complications such as the generation of wear debris. Therefore for chronic back pain conditions the status is as it was for arthritic hips before hip replacements became available, immobility and a life of constant pain. In 1997 it was estimated that over 150,000 lumbar fusions were performed annually in the United States² and that in 2000 the US spinal market was worth an estimated \$US910 million¹.

Prior to Sir John Charnley revolutionizing modern orthopaedics with the development of the total hip replacement the long term prognosis for patients suffering from degenerative hip disease was also poor³. Today hip arthroplasty is the most successful surgical procedures in terms of patient satisfaction. Potentially, the development of a stable, fully functional, artificial disc could improve the treatment of degenerative intervertebral discs in a similar fashion.

Therefore the aim of this project was to develop an intervertebral disc implant that enables normal and uninhibited pain-free movement without the addition of complicating factors such as wear debris generation.

1.1 References

1. *Biomet 2000 Annual Report*. Biomet Inc, [cited Mar 2003]. Available from <http://www.biomet.com/investors/2000annual/mktreview.html>.
2. American Academy of Orthopaedic Surgeons. *Inpatient Hospital Back and Spine Procedures United States 1990 to 1997*. American Academy of Orthopaedic Surgeons, Updated: 26 May 2000 [cited Mar 2003]. Available from <http://www.aaos.org/wordhtml/press/bksppro.htm>.
3. Charnley J, *Total Hip Replacement*. Journal of the American Medical Association (JAMA), 1974. Vol 230 (7): pp 1025–1028.
4. Williams K D, Park A L, *Lower back pain and disorders of intervertebral discs*, in Canale S Terry (Eds). *Campbells Operative Orthopaedics*, 2002, Elsevier Science. pp 1955-2028.

Chapter 2 – Anatomy & Physiology of the Lumbar Spine

2.1 Vertebral Column

The vertebral column is formed by a series of bones called vertebrae. There are 33 vertebrae in total and they are grouped according to their position in the spinal column. There are 7 vertebrae in the cervical region, 12 in the thoracic, 5 in the lumbar, 5 in the sacral, and 4 in the coccygeal.

The cervical, thoracic and lumbar vertebrae remain distinct throughout life, and are known as true or movable vertebrae. The sacral and coccygeal vertebrae, are termed false or fixed vertebrae because in adults they are united with one another forming two bones, the sacrum and the coccyx.⁴

Between each of the true vertebrae there are three flexible joints which allow the spine to deflect and deform. The intervertebral disc is the largest and most significant of these joints as it provides flexibility and is responsible for transferring loads between the adjacent vertebrae. The intervertebral discs also have small shock absorbing qualities. The other joints between the vertebrae are the zygapophysial joints, these restrict the range of motion and help to stabilise the spine.

Figure 2.1 shows a typical adult spine with the cervical, thoracic and lumbar vertebrae groups identified.

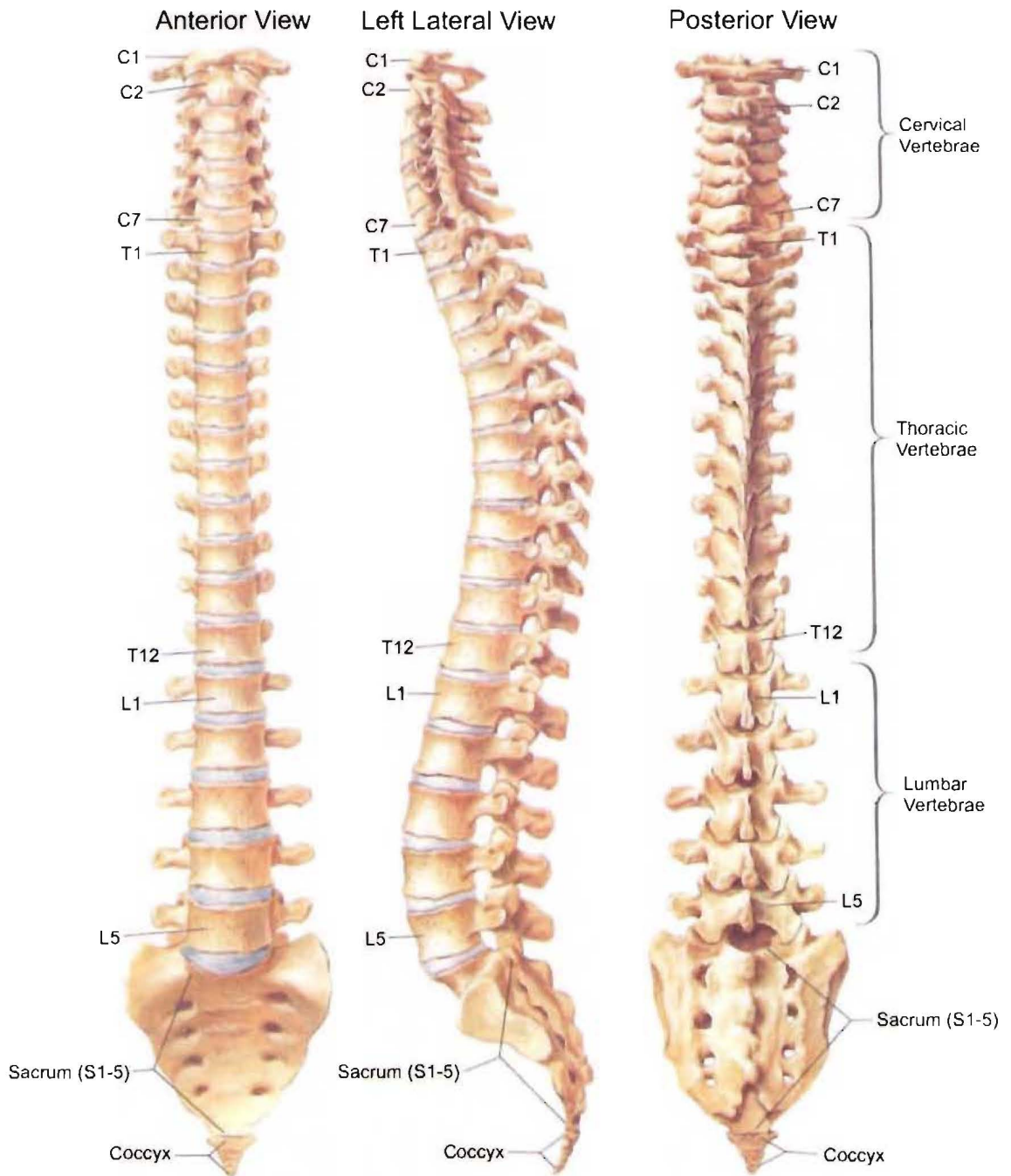


Figure 2.1 Vertebral column.
[Source: Plate 142 Netter¹⁰]

2.2 Basic Biomechanics – Rotations and Translations

There are two common methods of describing rotations and translations of the spine, these are the anatomical and biomechanical systems.

The anatomical system defines three orthogonal planes which are labelled as the sagittal, coronal and horizontal planes, as shown in Figure 2.2. Sometimes the horizontal plane is also referred to as the transverse plane. Backward and forward bending of the spine occurs in the sagittal plane, side or lateral bending is rotation in the coronal plane and axial twisting occurs in the horizontal plane.

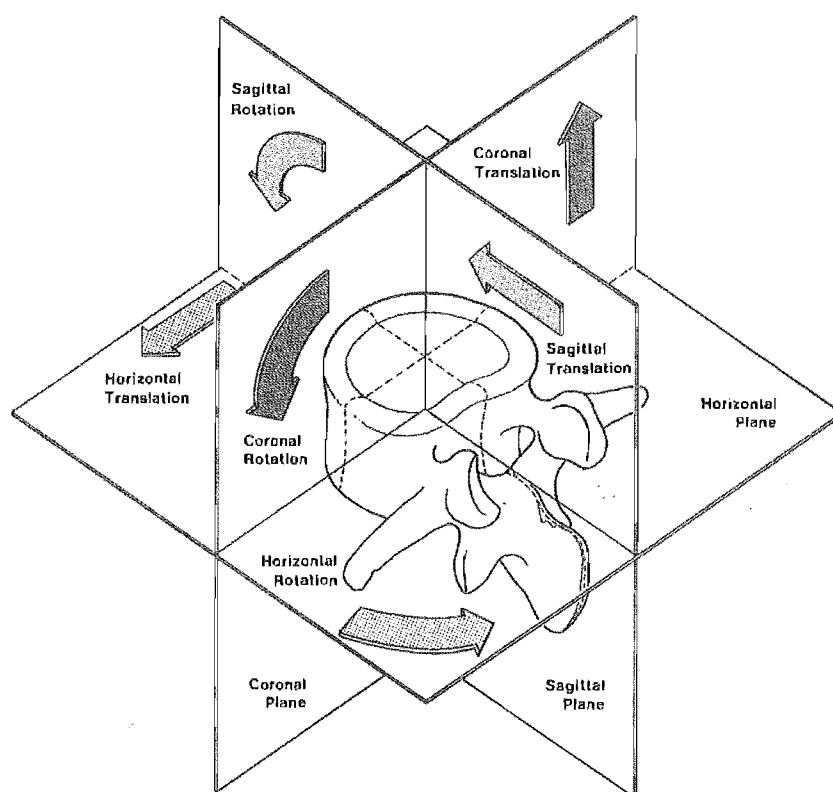


Figure 2.2 Planes and direction of motion: Anatomical system.

[Source: Bogduk et al¹]

The biomechanical system defines movements relative to three axes, as shown in Figure 2.3. The key to this system is the prepositions used, translation movements are *along* the axis and rotations are movements *around* the axis. For example forward bending can be described as positive rotation *around* the X axis, and left horizontal displacement is a positive translation *along* the X axis.

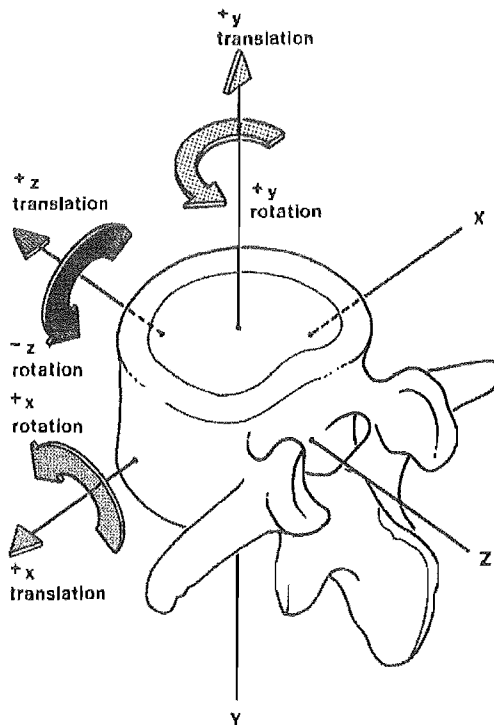


Figure 2.3 Axes and directions of motion: Biomechanical system.

[Source: Bogduk et al¹]

The advantage of the biomechanical system is that dimensions of movements can be accurately and unambiguously defined, however orientation of the axes can be unfamiliar if not used regularly. As the terms sagittal, coronal and horizontal are commonly used in other areas of anatomy they are therefore the more popular way to describe the motions of joints.

Table 2.1 shows the comparative terms for both the anatomical and biomechanical systems along with the colloquial description of each term.

| | Anatomical System | Biomechanical System | Colloquial Description |
|---------------------|--------------------|----------------------|-----------------------------------|
| Translations | Anterior sagittal | +Z translation | Forward Slide or Glide |
| | Posterior sagittal | -Z translation | Backward slide |
| | Cephalad coronal | +Y translation | Longitudinal or Axial Distraction |
| | Caudal coronal | -Y translation | Longitudinal or Axial Compression |
| | Left horizontal | +X translation | Left Lateral Slide |
| | Right horizontal | -X translation | Right Lateral Slide |
| Rotations | Anterior sagittal | +X rotation | Forward Bend "Flexion" |
| | Posterior sagittal | -X rotation | Backward Bend "Extension" |
| | Left coronal | -Z rotation | Left Lateral Bend |
| | Right coronal | +Z rotation | Right Lateral Bend |
| | Left horizontal | +Y rotation | Left Axial Rotation |
| | Right horizontal | -Y rotation | Right Axial Rotation |

Table 2.1 Descriptive terms of motion.

[Source: Bogduk et al¹]

The terms flexion and extension are commonly used to describe forward and backward bending of the spine respectively. However it should be noted that flexion and extension are not pure rotations of the lumbar spine. Instead flexion and extension of the lumbar spine involve a combination of sagittal rotation and sagittal translation.

As the term horizontal rotation can be confusing axial rotation is often used instead, as shown in Table 2.1. This also applies to the coronal translations which are regularly referred to as axial compression and distraction.

2.3 Lumbar Spine Overview

As previously described the lumbar spine consists of 5 vertebrae. The vertebrae are labelled according to their position in the spinal column with the upper most vertebrae labelled L1 and the lower most vertebrae labelled L5.

Between each adjacent pair of vertebrae there are three joints. The intervertebral disc is sited between the vertebral bodies. The zygapophysial joints are formed by the articulation of the inferior articular processes of one vertebra and the superior articular processes of the vertebrae below.

The joints are identified by referencing the adjacent vertebral. For example the intervertebral disc between L1 and L2 is referred to as L1-2. Individually the zygapophysial joints can also be specified this way, e.g. the 'left L1-2 zygapophysial joint'.

Figure 2.4 shows the lumbar vertebrae and associated joints with their nomenclature.

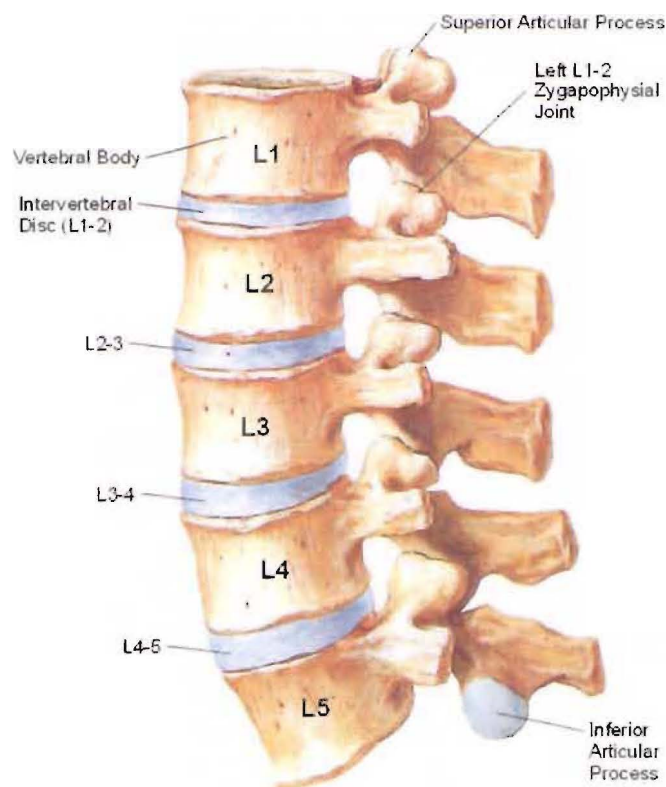


Figure 2.4 Lumbar spine vertebrae, intervertebral discs and zygapophysial joints.

[Source: Plate 144 Netter¹⁰]

The sacrum, shown in Figure 2.5, is positioned at the base of the lumbar spine and lies between the two iliac wings, forming the posterior wall of the pelvis. Although it is a continuous mass of bone the naming convention used for the rest of the spinal column is continued with aspects of the sacrum labelled S1 to S5. The intervertebral disc between the L5 and the lumbosacral articular surface of the sacrum is referred to as L5-S1. This intervertebral disc is normally considered to be part of the lumbar spine functional unit.

The primary purpose of the sacrum is to transfer load from the spine to the iliac wing where the loads are then transferred to the lower limbs. Conversely shock loading can also be transmitted from the lower limbs thru the pelvis, sacrum and lumbar spine. The sacrum is not fused to the rest of the pelvis rather there is a joint on each side of where it meets the iliac wing. Despite the size of this joint, the movements associated with it are small and there are no muscles groups capable of performing active movements of the joint. In essence the sacroiliac joint acts as a stress reliever.

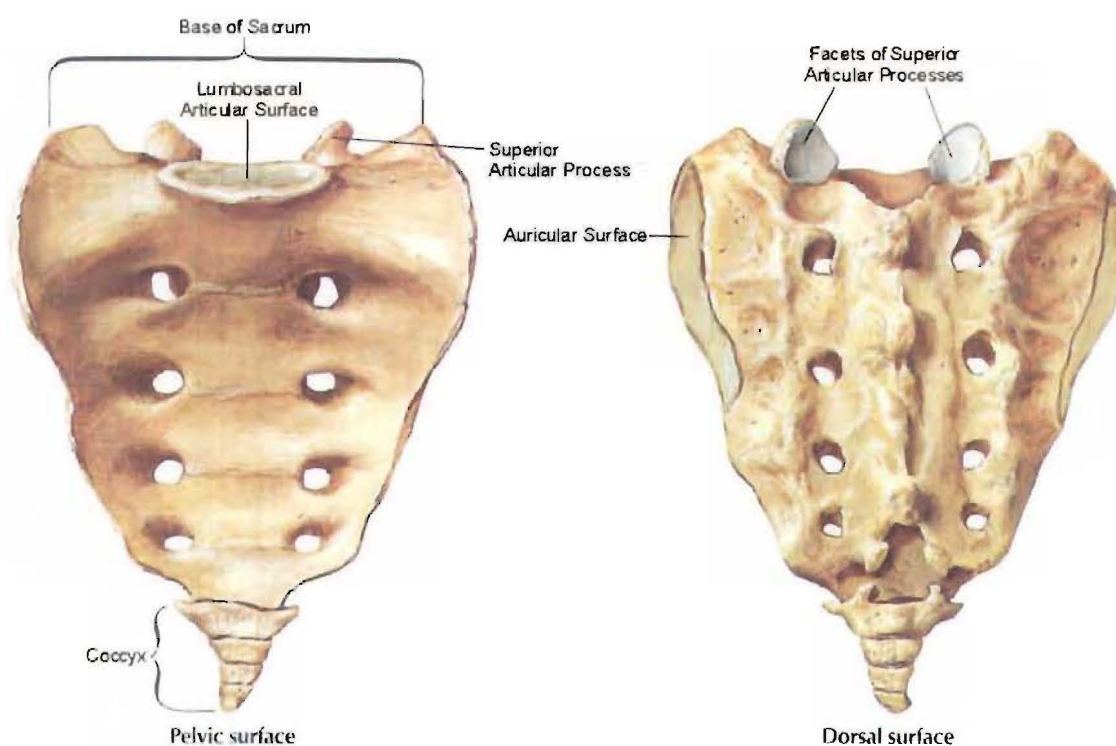


Figure 2.5 Sacrum and Coccyx.

[Source: Plate 145 Netter¹⁰]

The construction and functions of the vertebrae, intervertebral discs and zygapophysial joints are detailed in Sections 2.4 to 2.6 respectively.

2.4 Vertebrae

2.4.1 Components

The vertebrae can be broken down into three components based on function. These components are the vertebral body, pedicles and posterior elements as shown in Figure 2.6(a). The function of each of these sections is detailed over the page.

Figure 2.6 also shows the main features of the vertebral body and associated nomenclature.

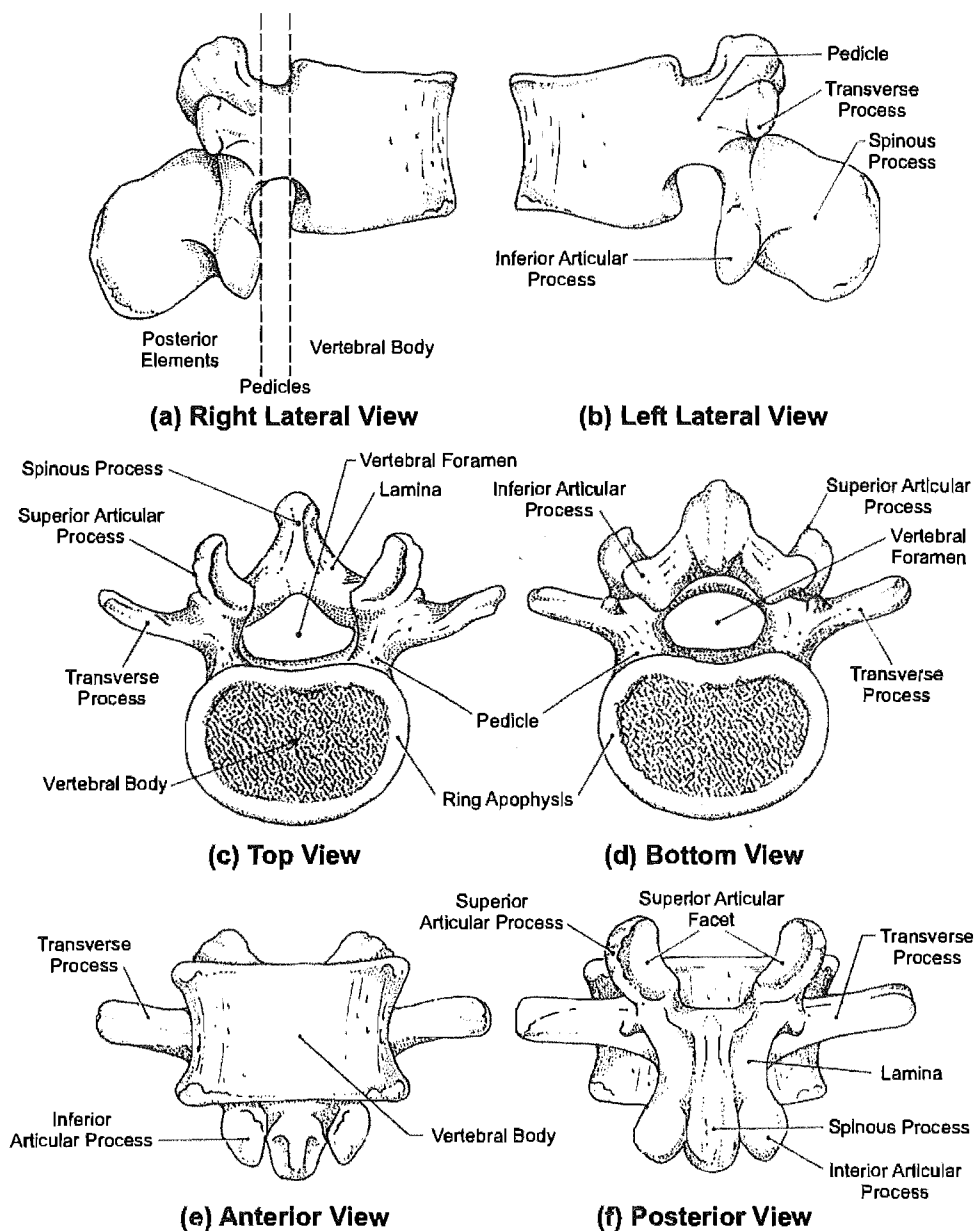


Figure 2.6 Parts of the lumbar vertebrae.

[Source: Bogduk et al¹]

2.4.1.1 Vertebral Body

The vertebral bodies carry the loads applied to the spine and are therefore required to be strong and resilient. If the vertebral bodies were constructed of solid bone, they would be very heavy and tend to fracture with the application of shock loads. Instead the vertebral bodies have a honeycomb structure.

The outer wall of the vertebral body is constructed from high strength cortical bone. However, if load was applied to this shell alone the wall would buckle and collapse as shown in Figure 2.7(b)

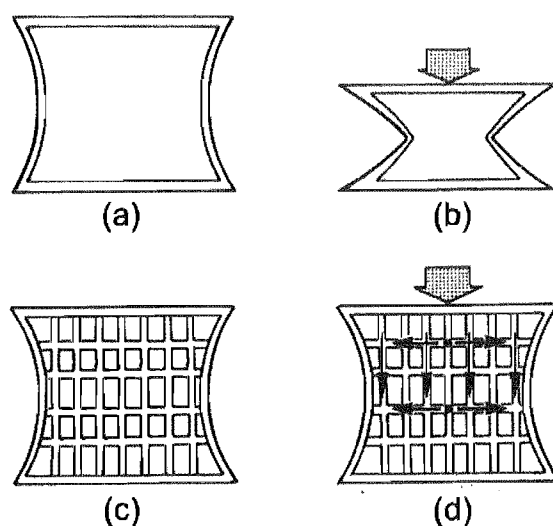


Figure 2.7 Schematic internal structure of the vertebral body.

The cortical bone shell alone (a) would not have sufficient rigidity to withstand the applied vertical loads and would buckle as a result (b). The vertebral body is instead filled with vertical and transverse trabeculae (c) which prevent buckling of the outer cortical shell (d).

[Source: Bogduk et al¹]

To prevent the cortical shell from buckling thin rods of bone, called vertical and transverse trabeculae, fill the cavity of the vertebral body. The trabeculae provide the cortical shell with the ability to bear weight while also providing resilience. When load is applied to the vertebral body the load is transferred to the vertical trabeculae. Should the vertical trabeculae start to buckle they are prevented from doing so by the transverse trabeculae, as shown in Figure 2.7(d).

The space between the trabeculae is also used to transfer blood to and from the vertebral bodies. When filled with blood the trabeculae can appear sponge-like and these structures are therefore often referred to as the vertebral spongiosa. Figure 2.8 shows the trabeculae and veins associated with the lumbar vertebrae.

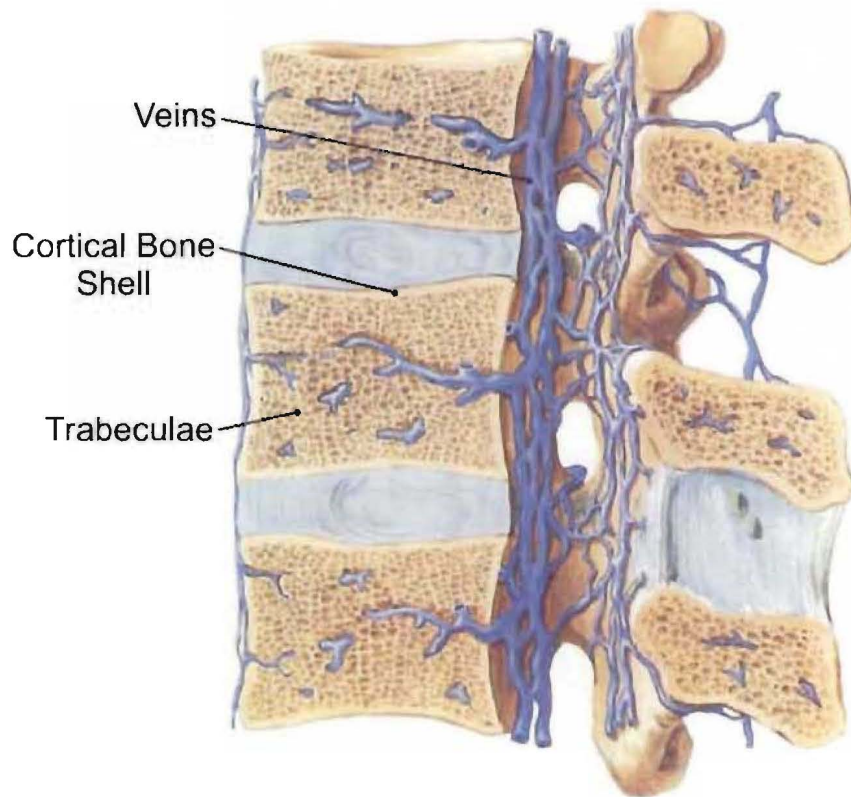


Figure 2.8 Vertebral spongiosa and veins.

[Source: Plate 159 Netter¹⁰]

2.4.1.2 Pedicles

The pedicles are oval in shape and consist of a thick cortical bone outer wall and inner trabecular structures which are a continuation of those found in the vertebral body. The primary function of the pedicles is to transfer tension loads and bending moments from the posterior elements to the vertebral bodies.

Tension loads arise when the vertebrae bodies try to slide forward and the motion is resisted by the zygapophysial joints, as detailed further in Section 2.6. Alternatively when the spine is bent, by applying muscle forces to the processes, the pedicles act as lever arms transmitting the bending moments to the vertebral bodies.

The pedicles also form two boundaries of the vertebral foramen and intervertebral foramen as shown in Figure 2.9.

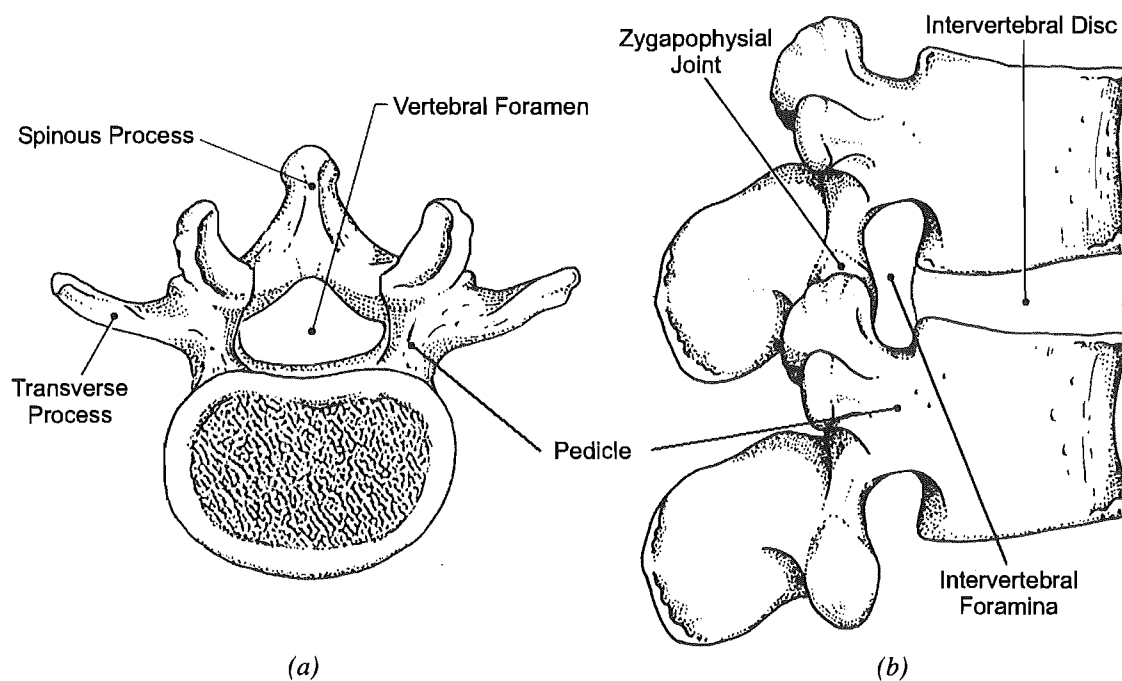


Figure 2.9 Vertebral foramen and intervertebral foramina.

(a) Top view.

(b) Right lateral view.

[Source: Bogduk et al¹]

2.4.1.3 Posterior Elements

The posterior elements consist of the articular surfaces, processes and laminae, as shown in Figure 2.10.

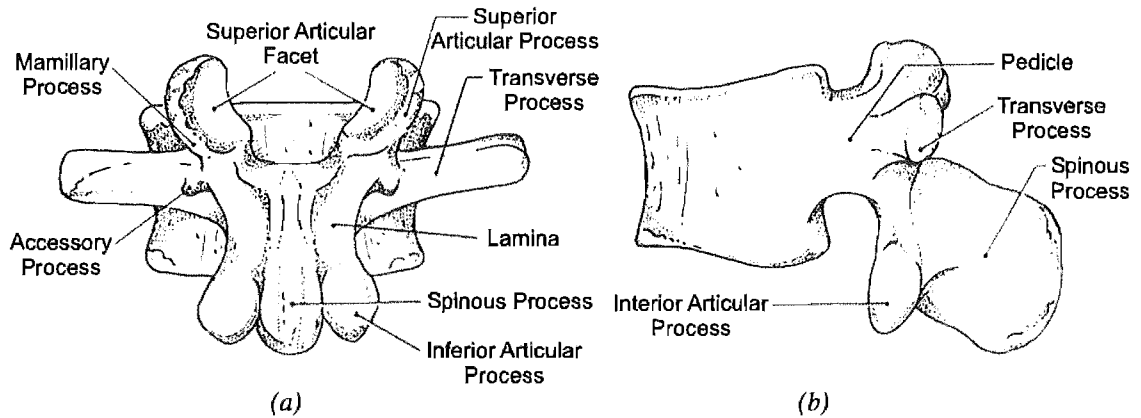


Figure 2.10 Posterior elements of the vertebral body.

(a) Posterior view.

(b) Left lateral view.

[Source: Bogduk et al¹]

The spinous, transverse, accessory and mamillary processes vary in length and provide areas for muscle attachment. The longer the processes are, the greater the lever arm and thus the greater amplitude of bending moment the back muscles are able to apply to the vertebrae. It should also be noted that all the functional muscles which act on the lumbar vertebral column are attached to the posterior elements.

The laminae are positioned centrally and transfer loads from the processes and articular facets to the pedicles. The laminae also provide protection for the spinal cord, however this role is not considered to be critical as patients who have had laminae surgically removed suffer no ill effects on their nervous systems¹.

As previously mentioned the superior and inferior articular processes form the zygapophysial joints. These joints are also sometimes referred to as the facet joints or apophysial joints. The construction and function of these joints is described in Section 2.6.

2.5 Intervertebral Disc

2.5.1 Components

The intervertebral discs consist of three parts the annulus fibrosus, nucleus pulposus and the vertebral endplates, as shown in Figure 2.11.

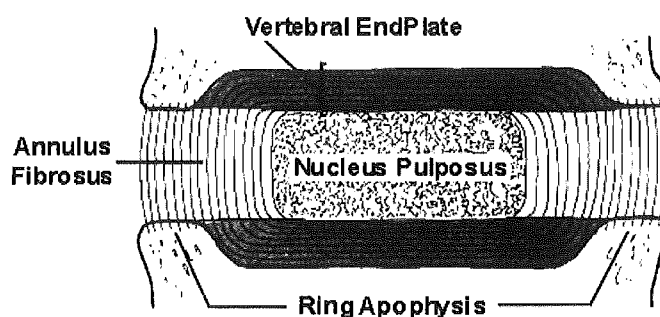


Figure 2.11 Structure of the intervertebral disc.

[Source: Bogduk et al¹]

2.5.1.1 Annulus Fibrosus

The annulus fibrosus is constructed from 15 to 25 layers of collagen fibres⁷. Each layer of fibres is called a lamella. In each lamella the collagen fibres are orientated parallel to each other and run from the vertebrae above to the vertebrae below. The orientation of the fibres in each lamella is therefore the same. However the angle of inclination alternates between each lamella, as shown in Figure 2.12. Viewed from the front the angle of the fibres (θ) is normally 65° to the left and those in the next layer are orientated 65° to the right^{7,18}.

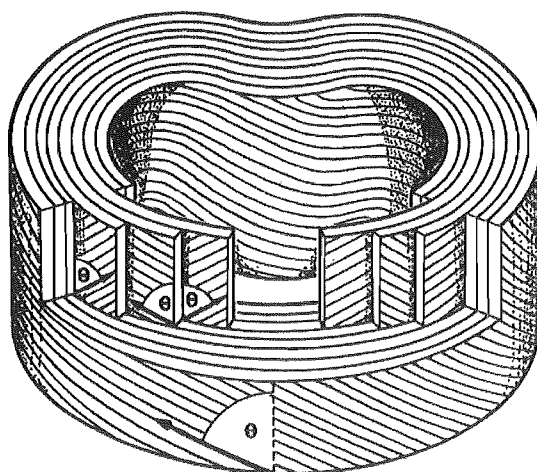


Figure 2.12 Detailed structure of the annulus fibrosus.

[Source: Bogduk et al¹]

However, the ideal structure of the annulus fibrosus, as shown in Figure 2.12, does not typically occur. Instead, in any given 90° segment of the annulus fibrosus, approximately 40% of the lamellae are incomplete⁷. As shown in Figure 2.13, these incomplete lamellae do not pass around the entire circumference of the intervertebral disc.

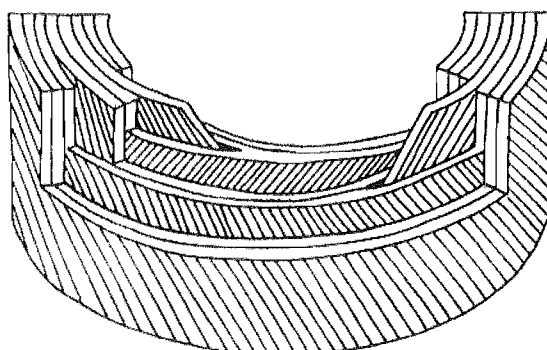


Figure 2.13 Incomplete lamellae of the annulus fibrosus.

[Source: Bogduk et al¹]

The lamellae increase in size towards the centre of the intervertebral disc⁷. The thickness of the lamellae also varies around the periphery of the intervertebral disc with thicker fibres in the anterior portion of the annulus fibrosus and finer and more closely packed fibres in the posterior portion⁷. As a result the cross sectional thickness of the annulus fibrosus varies across the intervertebral disc with the posterior portion being thinnest.

2.5.1.2 Nucleus Pulposus

In a healthy intervertebral disc the nucleus pulposus is a yellowish coloured, soft, pulpy, highly elastic substance which fills the cavity in the annulus fibrosus^{2,17}. The consistency of this fluid is similar to toothpaste or uncured silicone sealant.

The classical description of the annulus fibrosus being a ring of material surrounding the nucleus pulposus is not entirely accurate. Instead the nucleus pulposus is quite distinct at its centre and the annulus fibrosus is distinct at its periphery, however at the junction of the two there is no clear boundary. Rather the peripheral parts of the nucleus pulposus merge with the deeper parts of the annulus fibrosus^{2,8}.

2.5.1.3 Vertebral Endplates

There are two vertebral endplates associated with each intervertebral disc, as shown schematically in Figure 2.14. The vertebral endplates are 0.6 to 1 mm thick and cover the area of the vertebral body surrounded by the ring apophysis^{12,17}. The endplates therefore cover the entire nucleus pulposus but do not extend far enough to cover the entire annulus fibrosus.

There is some debate as to whether the vertebral endplates are components of the vertebral bodies or intervertebral disc^{2,13,15}. However, Inoue⁵ and Coventry² determined there were no anchoring structures between the endplate and underlying bone. Therefore, for the purposes of this project, the vertebral endplates are considered to be part of the intervertebral disc.

The endplates contain collagen fibres which are orientated parallel to the transverse plane. These fibres are a continuation of the inner third of the annulus fibrosus fibres^{5,15}. This seamless merging of the annulus fibrosus fibres and vertebral endplate fibres results in a strong bond between the two⁸, effectively encapsulating the nucleus pulposus in a sphere of fibres.

The outer fibres of the annulus fibrosus, which are not covered by the endplates, enter the vertebral bodies and are firmly anchored to the underlying bone⁵.

These structures are illustrated schematically in Figure 2.14.

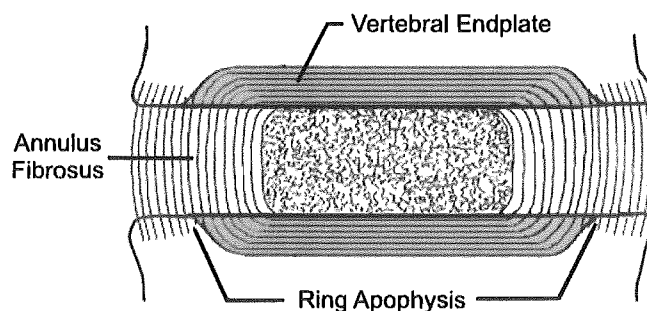


Figure 2.14 Structure of the vertebral endplates.

The inner annulus fibrosus fibres sweep around into the vertebral endplate. The peripheral fibres of the annulus fibrosus are anchored to the vertebral bodies.

[Adapted from: Bogduk et al¹]

2.5.2 Function

The intervertebral disc is responsible for transferring weight between the vertebral bodies and allowing relative motion between the adjacent vertebrae.

2.5.2.1 Weight Bearing

There are two mechanisms which allow the intervertebral discs to carry the applied loads.

The first load carrying mechanism involves the annulus fibrosus working in conjunction with the nucleus pulposus. The nucleus pulposus is a fluid which can be deformed under an applied load however it cannot be compressed. Therefore when a vertical load is applied to the nucleus pulposus it tends to reduce in height and expand outward radially. The radial expansion of the nucleus pulposus exerts pressure on the annulus fibrosus, tending to stretch the lamellae outwards. The lamellae fibres resist this stretching and oppose the outward pressure exerted on them. Equilibrium is reached when the pressure exerted on the nucleus pulposus is balanced by the tension in the annulus fibrosus fibres. In a healthy intervertebral disc the annulus fibrosus only bulges slightly under such applied loads.

The nucleus pulposus also exerts a pressure on the vertebral endplates however these are supported by the vertebral bodies and thus resist deformation too.

This creates a situation where the nucleus pulposus is unable to deform either radially or axially despite the application of a load, resulting in a pressure increase in the nucleus pulposus. This mechanism is illustrated in Figure 2.15.

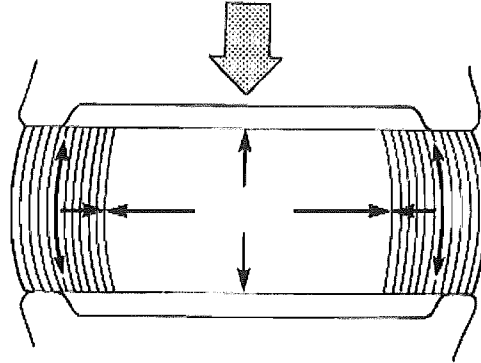


Figure 2.15 Annulus fibrosus and nucleus pulposus interaction under applied load.

Compression raises the pressure in the nucleus pulposus, which in turn exerts a radial pressure on the annulus fibrosus and an axial pressure on the endplates. The annulus fibrosus and endplates resist this pressure and prevent expansion of the nucleus pulposus.

[Source: Bogduk et al¹]

The second load carrying mechanism involves the annulus fibrosus alone. The closely packed lamellae fibres make the annulus fibrosus a relatively stiff structure. As long as the annulus fibrosus is healthy and the fibres remain closely bound together the annulus fibrosus will resist buckling. It has been shown that when a compressive load is applied to an intervertebral disc with nucleus pulposus removed, the annulus fibrosus alone is capable of supporting virtually the same load as an intact intervertebral disc^{1,8}. However if an isolated annulus fibrosus is loaded in compression for a sustained period of time, it will deform and buckle.

Markolf et al⁸ noted that the performance of an isolated annulus fibrosus does vary depending on the method used to extract the nucleus pulposus. When the nucleus pulposus was removed without cutting the annulus fibrosus there was no noticeable difference in performance to an intact intervertebral disc. However, when the nucleus pulposus was removed using typical discectomy techniques there was a small change in intervertebral disc height under applied loads. The annulus fibrosus also exhibited some bulging after the initially loading of the intervertebral disc. However, regardless of this deformation of the intervertebral disc the response to repetitive loading was very similar to that of intact specimens.

Therefore the pressure exerted by the nucleus pulposus achieves two things. First, the pressure exerted on the endplates transmits some of the load from one vertebral body to the next. Secondly, the radial pressure exerted on the annulus fibrosus also braces the annulus fibrosus lamellae and helps to prevent buckling thus allowing load to be transferred through the annulus fibrosus for extended periods of time. Figure 2.16 illustrates these two load carrying mechanisms.

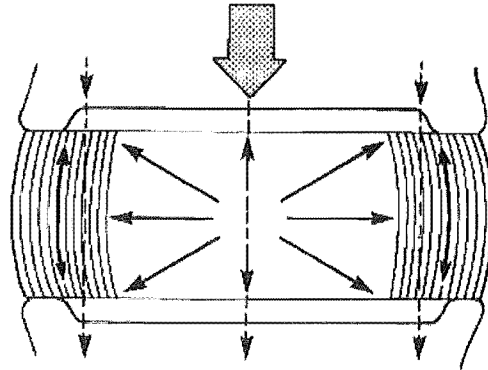


Figure 2.16 Annulus fibrosus and nucleus pulposus weight bearing mechanisms.

Weight is carried by both the annulus fibrosus and nucleus pulposus. The nucleus pulposus applies a radial pressure on the annulus fibrosus bracing it and the pressure on the endplates also transmits a portion the load from one vertebra to the next.

[Source: Bogduk et al¹]

These load carrying mechanisms also give the intervertebral discs an energy storage capability. As previously described when load is applied to an intervertebral disc the nucleus pulposus expands and some stretching of the lamellae fibres occurs. The collagen fibres are elastic and store the energy used to stretch them. When the applied load is removed from the intervertebral disc the collagen fibres contract exerting force on the nucleus pulposus which in turn restores any deformation that may have occurred. This process gives the intervertebral discs a degree of resilience.

This resilience also allows the intervertebral discs to act as shock absorbers. When a force is rapidly applied to a intervertebral disc, the load is briefly diverted into stretching the annulus fibrosus fibres. This stretching reduces the speed at which load is transferred to the adjacent vertebrae. It should be noted however that the average load remains the same, but by diverting the force through the annulus fibrosus, the peak load is reduced and the rate of load transfer is increased.

2.5.2.2 Movements

When considered on its own, i.e. without consideration of the zygapophysial joints, the intervertebral disc is capable of performing movements in all directions. The mechanics of compressing the intervertebral disc have been described in the previous section however, the intervertebral disc is equally capable of supporting the other forms of motion as well.

Distraction

When the spine is distracted, for example while hanging by the hands, the vertebral bodies separate. This separation results in all the fibres of the annulus fibrosus being stretched an equal amount, as shown in Figure 2.17(a). As the collagen fibres are densely packed and provide strong resistance to this movement hence only small levels of motion occur in this direction.

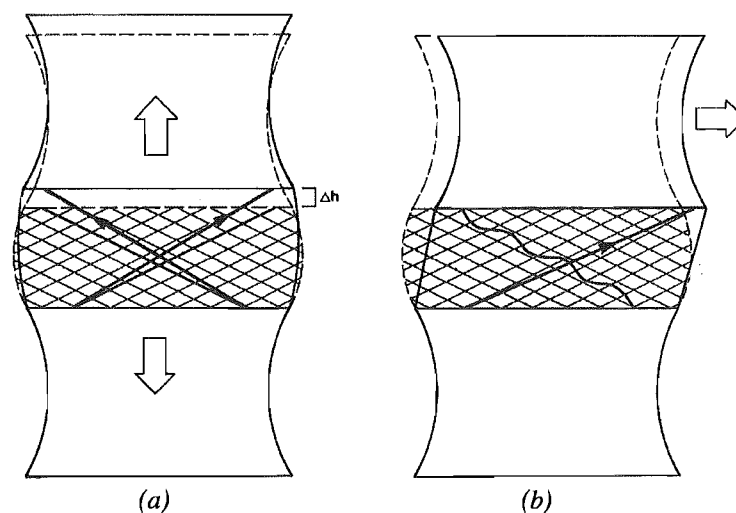


Figure 2.17 Distraction and sliding of the intervertebral disc.

- (a) Distraction of the intervertebral disc results in all the lamellae fibres stretching an equal amount.
 (b) During sliding of the intervertebral disc the fibres orientated in the direction of displacement are stretched, while the remaining fibres are relaxed.

[Source: Bogduk et al¹]

Sliding

The intervertebral discs also resist pure sliding. When the intervertebral disc is displaced sideways the endpoints of the annulus fibrosus all move an equal amount. However during sliding only some of the collagen fibres provide resistance depending on their orientation relative to the direction of movement.

For example during forward sliding the collagen fibres in the lateral portions of the annulus fibrosus lie parallel to the direction of movement, however these fibres run in opposite directions in each lamella. Therefore as the vertebrae slide relative to each other half the lateral portion fibres are placed in tension and resist the movement, while the remaining lateral fibres are relaxed and play no part in providing resistance, as shown in Figure 2.17(b). The anterior and posterior portions of the annulus fibrosus also make a contribution to resisting forward sliding however they are not as effective as the lateral portions. This is because although the amount of endpoint separation remains the same, the anterior and posterior fibres are not aligned with the direction of separation and hence are not stretched to the same degree.

Bending

Bending or rocking of the intervertebral bodies results the lowering of one edge of the vertebral body and rising of the other. This causes the annulus fibrosus to buckle in the direction of bending and stretching of the opposing edge. As this occurs the nucleus pulposus is also deformed decreasing in thickness on one side and increasing in thickness on the other, as shown in Figure 2.18.

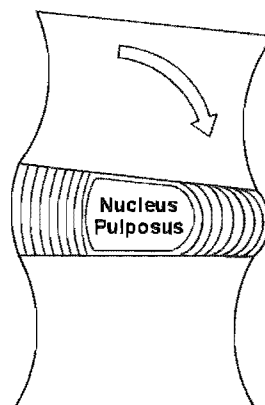


Figure 2.18 Bending of the intervertebral disc.

[Source: Bogduk et al¹]

It has been found that 5° bending of unloaded cadaveric specimens results in the nucleus pulposus pressure rising approximately 68.5 kPa⁹. This rise in pressure has been observed to be constant regardless of the applied load.

However, larger increases in intradiscal pressure are typically observed as living volunteers bend. This is attributed to the additional compressive loads applied to the intervertebral discs by the action of the back muscles which control bending¹.

Twisting

Twisting of an intervertebral disc causes the endpoints of the collagen fibres to rotate in the direction of twist, intervertebral disc height to be reduced and the nucleus pulposus to be compressed. As the collagen fibres are orientated in alternating directions in the lamellae, only the fibres orientated in the direction of twist are placed in tension, while the remaining fibres are relaxed. Therefore only half of the lamellae fibres are able to resist twisting motions, as shown in Figure 2.19.

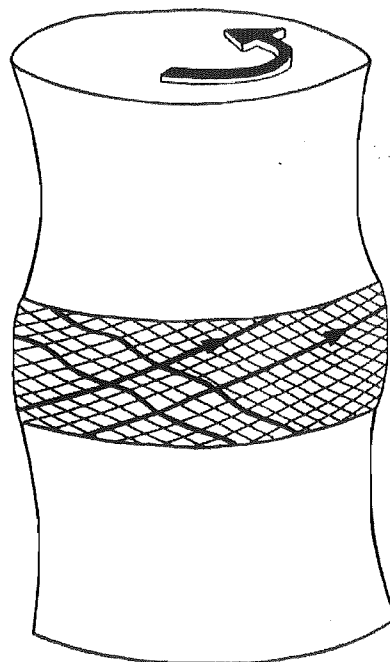


Figure 2.19 Twisting of the intervertebral disc.

[Source: Bogduk et al¹]

Summary

In summary the nucleus pulposus allows loads to be transferred between the vertebral bodies and braces the annulus fibrosus to prevent it from buckling. The nucleus pulposus makes little contribution to resisting sliding, bending or twisting of the intervertebral disc and simply deforms to comply with such movements. However, if load is applied to the intervertebral disc during such deflections the load bearing functions of the nucleus pulposus are superimposed on the intervertebral disc.

As the intervertebral disc is deflected the endpoints of the annulus fibrosus are displaced causing the collagen fibres within the annulus fibrosus to stretch and resist deflection. All the fibres of the annulus fibrosus are involved in weight bearing and resisting distraction of the intervertebral disc. However, for other movements the orientation of the fibres dictates their involvement in resisting the imposed deformations.

2.6 Zygapophysial Joints

As previously discussed in Section 2.5.2.2 with the posterior elements removed the intervertebral discs are under-constrained and can translate and rotate freely in all directions. However, for the lumbar spine to be stable and capable of bearing loads additional constraint mechanisms are required.

For example Figure 2.20 illustrates that if the posterior elements did not resist forward translation the lumbar lordosis would place the intervertebral discs in shear, destabilising the spinal column and compressing the spinal nerves. The zygapophysial joints prevent such shear from occurring and also prevent axial rotation.

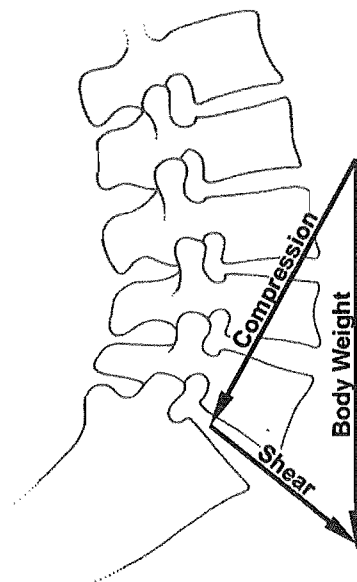


Figure 2.20 Zygapophysial joints resist shear loads.

Construction

The zygapophysial joints result from the articulation of the inferior and superior articular processes, each of which is covered with articular cartilage, as shown in Figure 2.21(a). The dorsal, superior and inferior margins of these joints are enclosed in a fibrous capsule of collagen fibres. When viewed from the rear of the spine the articular facets appear as straight faces, as shown in Figure 2.21(a), however, when viewed from above they have a curved appearance, as shown in Figure 2.21(b).

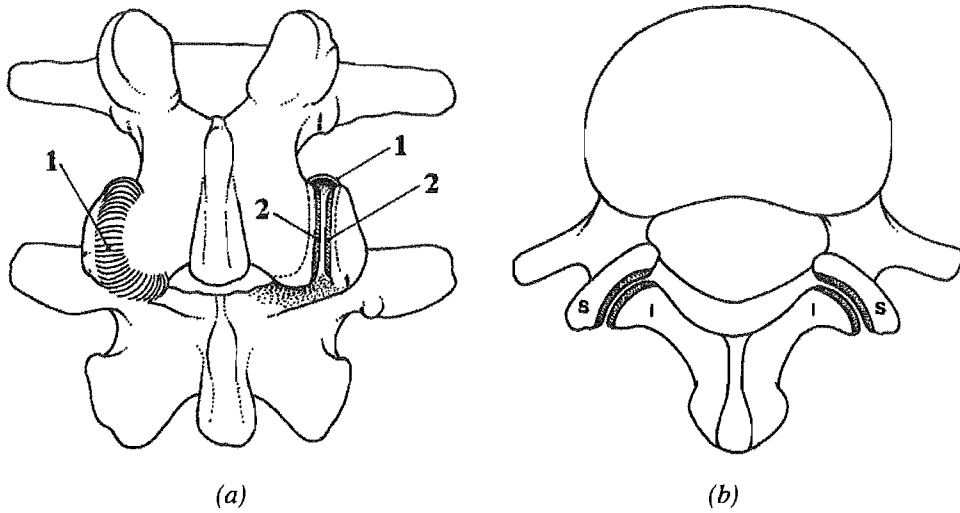


Figure 2.21 Posterior and superior views of the L3-4 zygapophysial joints.

(a) Posterior view of L3-4, the left hand side capsule (1) is shown intact; the right hand side posterior capsule is shown resected revealing the articular cartilage (2).

(b) Superior view of the L3-4 zygapophysial joints showing the curvature of the articular facets in the transverse plane. Note: I = Interior articular process of L3, S = Superior articular process of L4.

[Source: Bogduk et al¹]

Orientation

The orientation of the articular facets influences their ability to resist forward translation and axial rotation of the vertebral bodies. For example flat articular facets could be orientated to provide large contact faces to prevent either forward translation or axial rotation, however resistance to displacement in the other direction is compromised as shown in Figure 2.22.

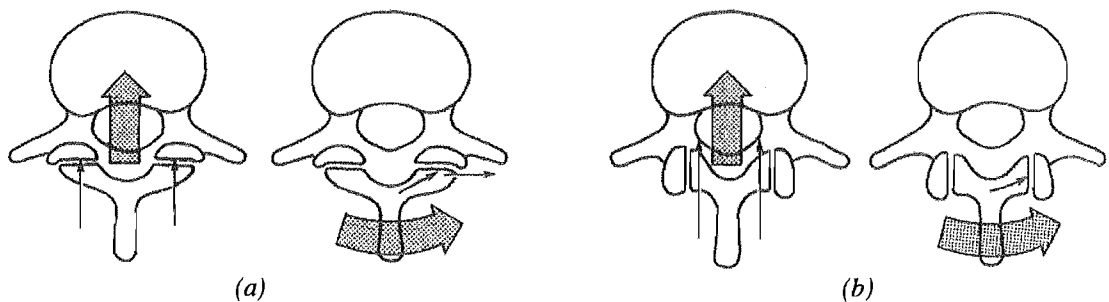


Figure 2.22 Flat zygapophysial joints.

(a) Flat articular facets parallel to the coronal plane offer strong resistance to forward translation but during axial rotation the inferior articular facet can slide relative to the superior articular facet.

(b) Flat articular facets joints parallel to the sagittal plane offer no resistance to forward translation and strong resistance to axial rotation.

[Source: Bogduk et al¹]

Curved articular surfaces such as those found in the lumbar spine provide a compromise by resisting forward translation and axial rotation. The articular surfaces of the lumbar spine are normally 'C' or 'J' shaped. Figure 2.23 shows how these curved joints have a wide backward facing anteromedial area (indicated by the bracket) which resists forward translation. Similarly there is a large contact area to resist axial rotation.

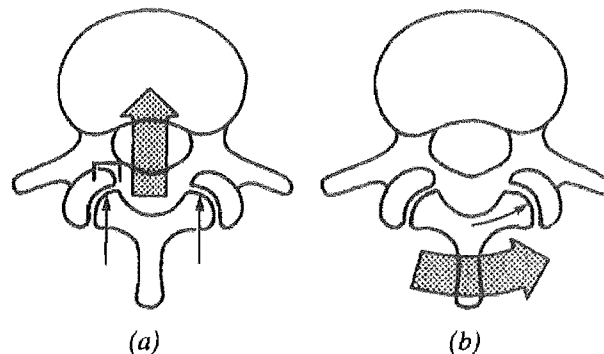


Figure 2.23 Curved zygapophysial joints.

(a) Curved zygapophysial joints have a large contact area to resist forward translation.

(b) The curved contact area also provides resistance to axial rotation.

[Source: Bogduk et al¹]

Load Carrying

In some cases, extension of the lumbar spine can cause the tips of the superior articular processes to contact the laminae of the vertebrae below. When such contact occurs a small percentage of the applied vertical load may be transmitted through the tips of the articular processes, as shown in Figure 2.24(a).

In addition to this, if a sustained axial compression is applied to a healthy intervertebral disc, the intervertebral disc height may reduce. If sufficient compression occurs the inferior articular surfaces may lower enough to contact the laminae of the vertebrae below, as shown in Figure 2.24(b). Vertical loads can then be transferred between the articular processes and laminae. This may also occur if an intervertebral joint is axially compressed while bending backwards¹.

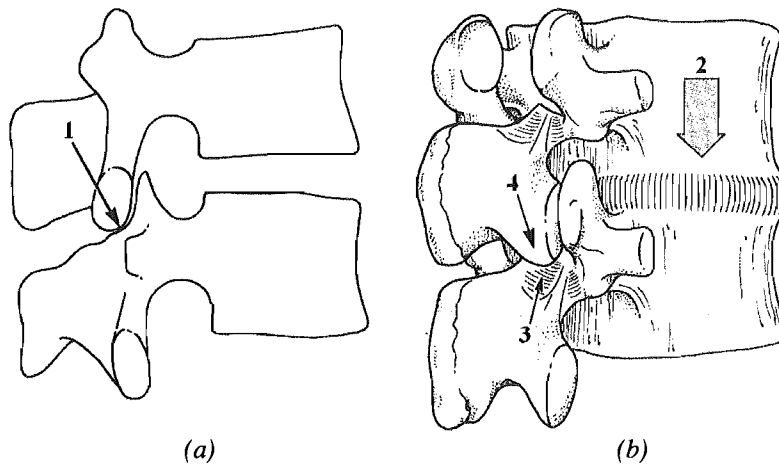


Figure 2.24 Impaction of the zygapophysial joints.

(a) When a vertebra is rocked backwards, its inferior articular processes may contact the superior articular processes of the vertebra below (1).

(b) If an intervertebral joint is compressed enough (2), the inferior articular processes of the upper vertebra may impact the laminae below (3), allowing weight to be transferred through the inferior articular process (4).

[Source: Bogduk et al¹]

2.7 Lordosis Curve

The lumbar spine has a distinct curvature known as the lordosis curve. This curvature is due to several factors. The most significant contributing factor is that the lumbosacral articular surface is tilted forwards at an angle of approximately 50° as shown in Figure 2.25.

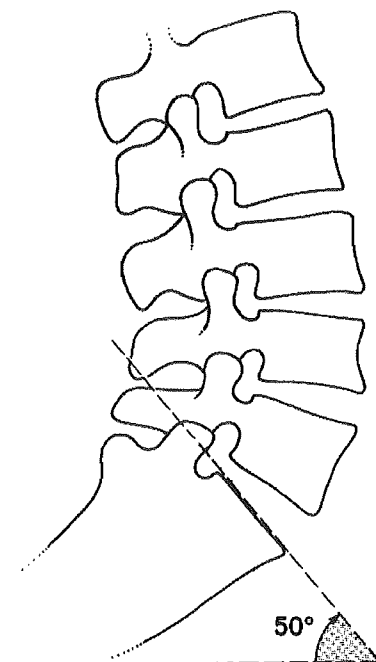


Figure 2.25 Lumbosacral angle.

[Source: Bogduk et al¹]

There are several features which help to compensate for this inclination of the lumbosacral articular surface and in doing so create the lumbar lordosis. First the lumbosacral intervertebral disc (L5-S1) is wedge shaped, with the anterior height 6-7 mm greater than the posterior height¹³. The L5 vertebral body is also wedge shaped with an anterior height approximately 3 mm greater than the posterior height³. As a result of the wedge shaped lumbosacral disc and L5 vertebral body the superior surface of L5 is much closer to horizontal than the lumbosacral articular surface.

The remainder of the lordosis curve is created by the vertebrae above L5 being placed in extension. As a result of this extension the anterior portions of the intervertebral disc are placed in tension and the posterior portions are compressed slightly.

2.8 Nerves

The spinal cord runs through the vertebral foramen from the base of the brain to the sacrum and is contained within a membrane called the dural sac. At each vertebral level, spinal nerves exit the spinal column through the intervertebral foramina as illustrated in Figure 2.26(a). It should be noted that any reduction in the intervertebral disc height can result in the spinal nerves being compressed as they pass through the intervertebral foramina.

Each of the spinal nerves is connected to the spinal cord by a dorsal and ventral root. The dorsal root transmits sensory nerve fibres from the spinal cord to the spinal nerve, while the ventral root mainly transmits motor control nerve fibres but may also transmit some sensory fibres. Where the dorsal and ventral roots separate from the spinal cord they pierce through the dural sac, however some of the dura material continues to envelope these nerve roots, this material is referred to as the dural sleeve. These structures are illustrated schematically in Figure 2.26(b).

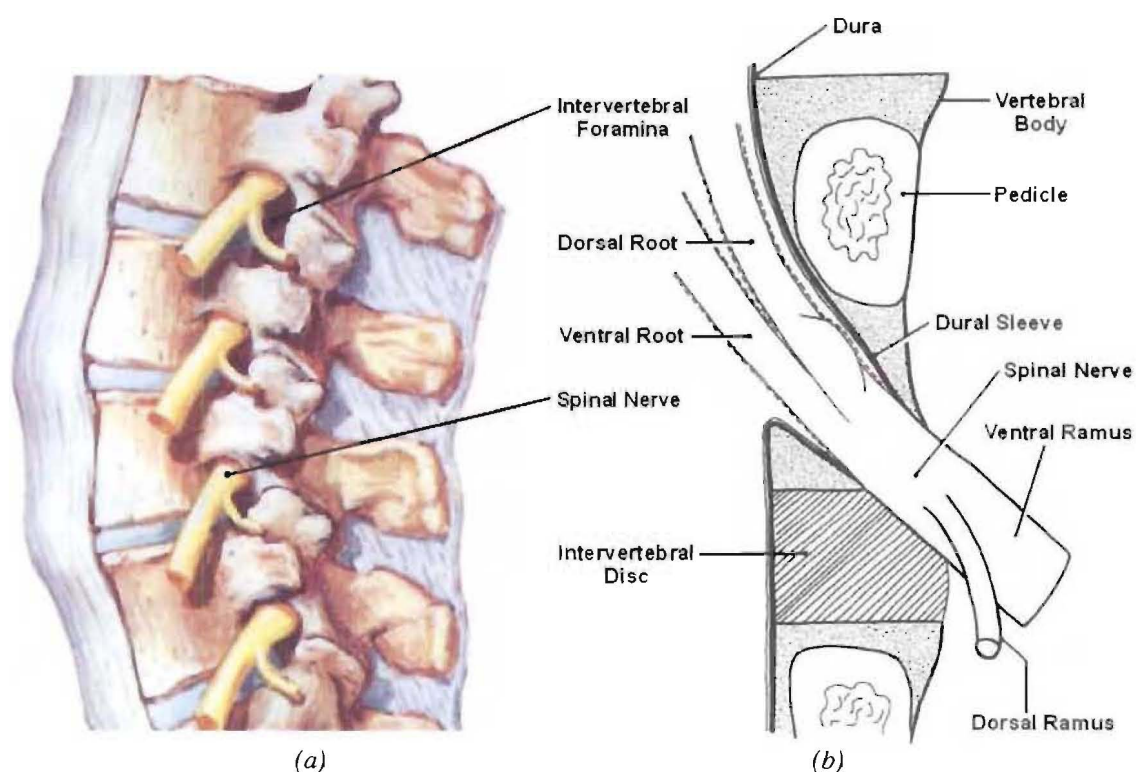


Figure 2.26 Spinal nerves.

(a) Spinal nerves and intervertebral foramina. [Source: Plate 147 Netter¹⁰]

(b) Schematic view of the dura, ventral and dorsal ramus. [Source: Bogduk et al¹]

Immediately past the intervertebral foramina the spinal nerves divide into branches called the ventral and dorsal ramus. Generally speaking the lumbar spine dorsal ramus supply nerves for the back musculature and the lumbar spine ventral ramus supply nerves for portions of the torso and lower limbs. The sinuvertebral nerves are recurrent branches of the ventral rami that re-enter the intervertebral foramina innervating the dura material, intervertebral disc and posterior longitudinal ligament. Figure 2.27 shows a schematic cross-sectional view of the nerves supplying the lumbar spine.

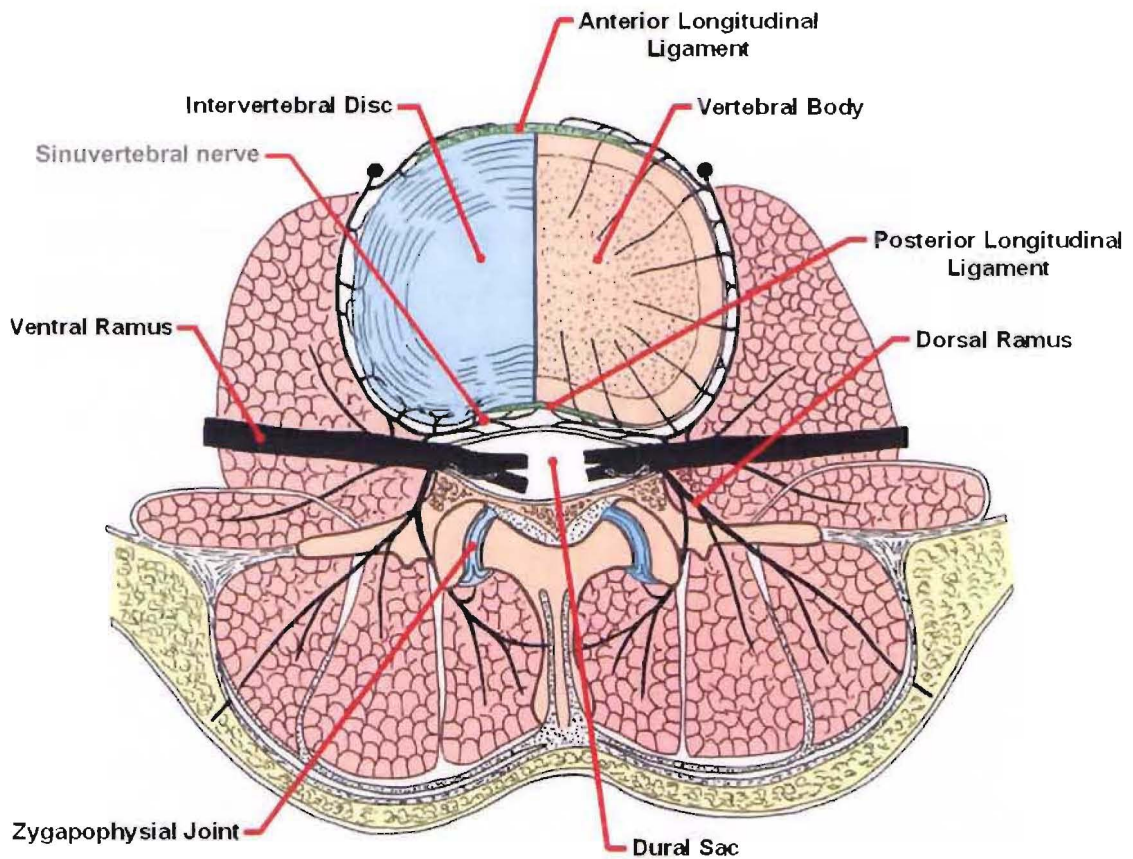


Figure 2.27 Innervation of the lumbar spine.

Cross section of the lumbar spine showing the nerves supply for the lumbar vertebral bodies, intervertebral discs and back musculature.

[Adapted from: Bogduk et al¹]

When compressive loads are applied to the lumbar spine the curvature of the lordosis curve increases, which results in the distance between the anterior edges of the vertebral bodies increasing. This in turn places the anterior fibres of the annulus fibrosus and the anterior longitudinal ligament in tension. When the tension in these fibres is equal to the force tending to separate the vertebral bodies equilibrium is reached and further deflection is prevented from occurring. Thus the anterior portion of the annulus fibrosus and anterior longitudinal ligament stabilize the lumbar lordosis. The lateral portions of the annulus also help to stabilize the lordosis curve in a similar fashion but they do not have the same influence as the anterior portion.

A key advantage of the lordosis curve is its ability to help absorb shock loads. In a straight spinal column the transfer of shock loads is only delayed by the intervertebral discs, as detailed in Section 2.5.2.1. However, in a curved spinal column shock loads also result in further compression of the posterior of the intervertebral disc and stretching of the anterior portion, effectively increasing the lumbar lordosis. As the lordosis curve increases the tension in the anterior longitudinal ligament rises, diverting some of the shock loading energy away from the vertebral bodies.

2.9 Effects of Age

The structures and functions of the lumbar spine described in the previous sections of this chapter reflect the properties of a normal, healthy, young adult spine, however, as the spine ages these properties change.

With age the number of water containing cells in the nucleus pulposus decreases and as a result the nucleus pulposus becomes drier, more granular and more fibrous^{11,17}. As these changes occur, the differences between the annulus fibrosus and nucleus pulposus also become less distinct¹⁷.

The most significant effect of the nucleus pulposus drying out it is that it is less able to exert fluid pressure and hence it is not able to transfer as much weight. As a result of this change more of the applied load is carried by the annulus fibrosus. To compensate for this increased load bearing requirement the annulus fibrosus also remodels with the collagen fibres increasing in thickness⁷. The cumulative damage sustained as the overloaded annulus fibrosus is deflected during the course of daily activities also causes the number of incomplete lamellae in the annulus fibrosus to increase^{7,17}.

With increasing age the strength of the endplates also decreases¹⁸. However the integrity of the endplates is most strongly influenced by the strength of the underlying vertebral bodies.

With age there is a general decrease in bone density and strength^{7,11}. As the bone strength reduces some of the vertical trabeculae in the vertebral body are resorbed and others are thickened. The horizontal trabeculae also resorb but are not replaced or remodelled, removing their bracing effect during weight bearing. Therefore over time the load carrying capability of the trabecular bone system decreases and more of the load is carried by the vertebral body's cortical shell. As a result of this decrease in the load carrying capability of the trabecular bone structures, the vertebral endplates can micro-fracture, deform and/or gradually become concave.

Changes due to aging also manifest themselves through a decrease in range of motion and increasing hysteresis^{14,16}. The loss of range of movement has been measured in both cadavers and living volunteers and is evident for both the entire spine and individual intervertebral joints. The increase in hysteresis is contributed to the decreased water bearing capability of the intervertebral discs.

2.10 Lumbar Spine Pain

2.10.1 Types of Pain

Lumbar spine pain can be felt and caused by a wide variety of factors and mechanisms. Typically pain is experienced in two ways.

Somatic Pain

Somatic pain arises as a result of stimulation of nerve endings in skin, bone, periosteum, ligaments joint capsules and tendons. The trademark indicator of somatic pain is that it can be localised or pin pointed to be occurring at a specific site. However the accuracy of this site location is related to the number of specific nerve endings and the representation in the sensory cortex of the brain. The spine has a very small representation compared with other structures, such as the hands.

Referred Pain

Referred pain is perceived in a region remote from the site of origin where nerve stimulation is causing the pain. An example of this is low back pain associated with pain in the buttock. The low back pain appears to be felt in the buttock, however although the lowest levels of the back and buttock are served by the same nerve supply (L4, L5, S1) the back nerves are supplied by the dorsal rami whereas the tissues of the buttocks are innervated by the ventral rami. The reason for referred pain is the convergence of the nerve tissues within the spinal cord. The nerves that serve the peripheral sites converge onto common neurones that relay to signals to higher centres. In such a case the brain is unable to distinguish which peripheral input is activating the common neuron. The trademark indicator of referred pain is that it cannot be localise, with patients often indicating an area where pain is felt, rather than the site of origin.

The neurological conditions which cause pain vary too.

Radicular Pain

Radicular pain arises as a result of irritation of spinal nerves or their roots by mechanical or chemical irritation. Intervertebral disc herniation is the most common cause of radicular pain and there is evidence that this pain is caused by the combination of inflammation as well as compression of the nerve root, rather than by compression alone⁶.

Radiculopathy

Radiculopathy it is a neurological condition in which conduction is blocked or slowed in the axons of a spinal nerve or its root. For example, compression of the axons can cause radiculopathy. This blocking of conduction in sensory axons can result in numbness or alternatively blocking motor axons can result in weakness. It should be noted however that radiculopathy does not cause pain instead it is a state of neurological loss. If radiculopathy is associated with pain, the mechanism causing that pain may not be the same as the one causing radiculopathy although it is commonly due to pressure and biochemically induced inflammation.

2.10.2 Causes of Back Pain

There are many possible causes and sites where back pain may originate from including:

- Muscles
- Ligaments
- Tendons
- Bones
- Zygapophysial Joints
- Intervertebral Discs

As illustrated in Figure 2.27 the vertebral bodies and back musculature are innervated. Accordingly any straining or tearing of the soft tissues or disorders such as tumours or fractures of the bones can understandably cause pain. Pain can also result from aspects of adjacent vertebrae colliding. For example the zygapophysial joints can be injured in various ways through collisions with the adjacent vertebrae's posterior elements.

The intervertebral disc is also well supplied with nerves and hence can be another source of back pain. Three major sources of intervertebral disc pain include discitis, torsion injuries and internal disc disruption.

Discitis

Iatrogenic discitis occurs when the intervertebral disc is infected by bacteria, normally introduced by needles used for discography and as such is a rare condition. Iatrogenic discitis is intensely painful and is evident on MRI and bone scans. However, the most significant fact highlighted by this condition is that intervertebral discs affected internally by a known and demonstrable lesion can be painful¹.

Torsion Injuries

If the spine is forcibly twisted axially, damage or torsion injuries may occur to both the zygapophysial joints and annulus fibrosus. Twisting around the normal axis of rotation, shown in Figure 2.28(a), stresses some of the collagen fibres in the annulus fibrosus as described in Section 2.5.2.2. If the vertebral body is rotated further, the centre of rotation shifts to the impacted zygapophysial joint, as shown in Figure 2.28(b). Any rotation around this secondary axis places additional lateral stress on the annulus fibrosus. This combination of axial and lateral stress can result in damage to the zygapophysial joint or circumferential tears in the annulus fibrosus, as illustrated in Figure 2.28(c) and (d). The risk of tearing fibres in the annulus fibrosus is compounded if the intervertebral discs are also flexed during rotation.

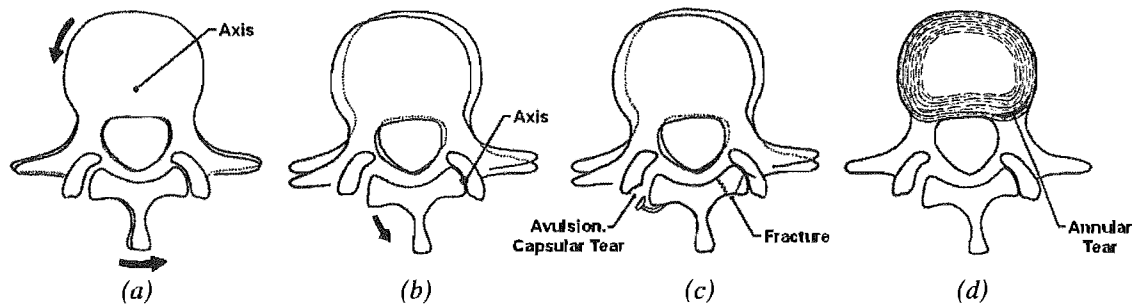


Figure 2.28 Torsion injuries.

- (a) Twisting of vertebrae around normal axis of rotation.
- (b) When the zygapophysial joint impacts, the centre of rotation shifts, placing additional stress on the annulus fibrosus and opposing zygapophysial joint.
- (c) This can result in fracture of the articular facets or tearing of the zygapophysial joint capsule.
- (d) Alternatively the annulus fibrosus may tear circumferentially.

[Source: Bogduk et al¹]

Internal Disc Disruption

Disruption of the intervertebral disc internal architecture can take several forms, but generally includes degradation of the nucleus pulposus and radial fissuring of the annulus fibrosus.

One of the common causes of intervertebral disc degradation is fracture of the endplates. In some cases endplate fractures occur and heal without any pain. However the repair of the endplate fracture can also cause degradation of the underlying nucleus pulposus, as shown in Figure 2.29(a).

If the intervertebral disc degradation remains isolated within the nucleus pulposus it can lead to localised resorption of the intervertebral disc and loss of intervertebral disc height, as shown in Figure 2.29(b). Alternatively degradation can affect the nucleus pulposus and cause radial fissuring of the annulus fibrosus, as illustrated in Figure 2.29(c). Should such fissures extend through the entire thickness of the annulus fibrosus, intervertebral disc herniation may result. This occurs when the application of sufficient load causes the nucleus pulposus to be extruded through the fissure. The extruded nucleus pulposus material may then compress the spinal nerves as illustrated in Figure 2.29(d). Intervertebral disc herniation can also result in loss of intervertebral disc height as the volume of the nucleus pulposus is no longer constant.

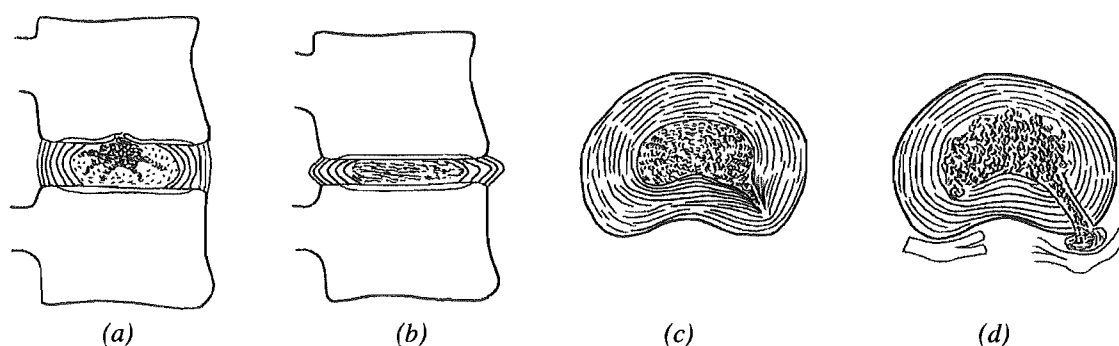


Figure 2.29 Intervertebral disc degradation.

Disruption of the nucleus pulposus (a) may lead to isolated intervertebral disc resorption (b). Alternatively the degradation may lead to radial fissures in the annulus fibrosus (c). Ultimately if the radial fissures extend far enough the degraded nucleus pulposus may herniate (d) if the intervertebral disc is subjected to sufficient load.

[Source: Bogduk et al¹]

Even if intervertebral disc degradation does not progress as far as herniation, radial fissures can cause pain. This may occur because collagen fibres which remain intact after the annulus fibrosus has ruptured are required to carry a greater percentage of the load and hence are over-strained. Alternatively the enzymes and breakdown products, resulting from the degradation of the intervertebral disc, may cause inflammation of the nerve endings exposed during the rupture of the annulus fibrosus. Figure 2.30 shows different grades of annulus fibrosus fissure.

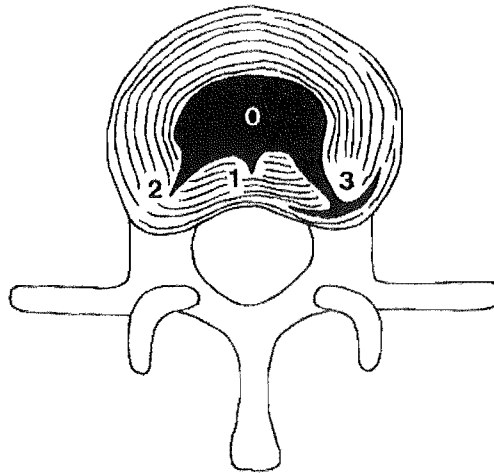


Figure 2.30 Grades of radial fissure.

Grade '0' no disruption of the annulus fibrosus. Grade '1' disruptions extend to the inner third of the annulus fibrosus. Grade '2' disruptions extend to the outer third of the annulus fibrosus. Grade '3' disruptions also extend to the outer third of the annulus fibrosus and spread between the lamellae.

[Source: Bogduk et al¹]

Aside from intervertebral disc degeneration, endplate fractures can also lead to other complications, for example contact of the nucleus pulposus and vertebral spongiosa may cause an autoimmune inflammatory response.

2.11 Summary

Ultimately there are many possible mechanisms and causes of low back pain and this area has been extensively researched. When lumbar spine pain becomes sufficiently debilitating often the only solution is surgical treatment, if a surgically correctable lesion is demonstrated.

2.12 References

1. Bogduk N, Twomey L T, *Clinical Anatomy of the Lumbar Spine*. 1987, New York: Churchill Livingstone.
2. Coventry M B, *Anatomy of the intervertebral disc*. Clin Orthop, 1969. Vol 67: pp 9-15.
3. Gilad I, Nissan M, *Sagittal evaluation of elemental geometrical dimensions of human vertebrae*. J Anat, 1985. Vol 143: pp 115-20.
4. Gray H, *Anatomy of the Human Body*. 20th Edition. 1918, Philadelphia: Lea & Febiger.
5. Inoue H, *Three dimensional architecture of lumbar intervertebral discs*. Spine, 1981. Vol 6 (2): pp 138-46.
6. MacNab I, *The Mechanism of Spondylogenic Pain*, in Hirsch C and Y Zotterman (Eds). *Cervical Pain*, 1972, Pergamon: Oxford. pp 89-95.
7. Marchand F, Ahmed A M, *Investigation of the laminate structure of lumbar disc annulus fibrosus*. Spine, 1990. Vol 15 (5): pp 402-410.
8. Markolf K L, Morris J M, *The structural components of the intervertebral disc*. J Bone Joint Surg, 1974. Vol 56A (4): pp 675-687.
9. Nachemson A L, *The influence of spinal movements on the lumbar intradiscal pressure and on the tensile stresses in the annulus fibrosus*. Acta Orthop Scandinav, 1963. Vol 33: pp 183-207.
10. Netter F H, *Atlas of Human Anatomy*. 1989, Basle, Switzerland: Ciba-Geicy Limited.
11. Panjabi M M, Goel V, Oxland T, Takata K, Duranceau J, Krag M, Price M, *Human lumbar vertebrae. Quantative three-dimensional anatomy*. Spine, 1992. Vol 417 (3): pp 299-306.
12. Roberts S, Menage J, Urban P G, *Biochemical and structural properties of the cartilage endplate and its relation to the intervertebral disc*. Spine, 1989. Vol 14: pp 166-74.
13. Schmorl G, Junghanns H, *The Human Spine in Health and Disease*, 1971, Grune & Stratton: New York. pp 18.
14. Taylor J, Twomey L, *Sagittal and horizontal plane movement of the human lumbar vertebral column in cadavers and in the living*. Rheumatol Rehab, 1980. Vol 19 (4): pp 223-232.
15. Taylor J R, *Growth of the human intervertebral discs and vertebral bodies*. J Anat, 1975. Vol 120 (1): pp 49-68.

16. Twomey L, Taylor J, *Flexion creep deformation and hysteresis in the lumbar vertebral column*. Spine, 1982. Vol 7 (2): pp 116-122.
17. Veron-Roberts B, Pirie C J, *Degenerative changes in the intervertebral discs of the lumbar spine and their sequelae*. Rheumatol Rehab, 1977. Vol 16 (1): pp 13-21.
18. White A A, Panjabi M M, *Clinical biomechanics of the spine*. 2nd Edition. 1990, Philadelphia: Lippincott Williams & Wilkins Publishers.

Table of Figures

| | |
|---|----|
| <i>Figure 3.1 Titanium mesh gage packed with autogenous cancellous bone.</i> | 46 |
| <i>Figure 3.2 Cage placed at the fusion site.</i> | 46 |
| <i>Figure 3.3 BAK/L™ implant.</i> | 47 |
| <i>Figure 3.4 LT-CAGE™.</i> | 47 |
| <i>Figure 3.5 Ovation™ Polyaxial pedicle screw fixation system.</i> | 49 |
| <i>Figure 3.6 Claris pedicle screw fixation system.</i> | 49 |
| <i>Figure 3.7 Facet screw fixation.</i> | 50 |
| <i>Figure 3.8 Anterior interbody fusion utilizing a cage and buttress plate.</i> | 52 |
| <i>Figure 3.9 Retraction of the nerve roots to facilitate posterior interbody fusion.</i> | 54 |
| <i>Figure 3.10 Postoperative anterior-posterior x-rays of a TLIF.</i> | 57 |

Traditional Surgical Treatment

Table of Contents

| | |
|--|-----------|
| CHAPTER 3 – TRADITIONAL SURGICAL SOLUTIONS | 45 |
| 3.1 SPINAL FUSION IMPLANTS | 45 |
| 3.1.1 <i>Interbody Spacers</i> | 46 |
| 3.1.2 <i>Posterior Instrumentation</i> | 48 |
| 3.1.2.1 Pedicle Screw Fixation | 48 |
| 3.1.2.2 Facet Screw Fixation | 50 |
| 3.2 SURGICAL APPROACH FOR SPINAL FUSION..... | 51 |
| 3.2.1 <i>Anterior Lumbar Interbody Fusion</i> | 52 |
| 3.2.2 <i>Posterior Lumbar Interbody Fusion</i> | 54 |
| 3.2.3 <i>Transforaminal Lumbar Interbody Fusion</i> | 56 |
| 3.2.4 <i>Circumferential Fusion (Anterior and Posterior)</i> | 58 |
| 3.3 DISADVANTAGES OF SPINAL FUSION..... | 59 |
| 3.4 REFERENCES..... | 61 |

UPDATE CHAPTER REFERENCE IN SECTION Chapter 3

UPDATE CHAPTER REFERENCE IN SECTION 3.2.1

Chapter 3 – Traditional Surgical Solutions

Spinal Arthrodesis or fusion is the traditional and currently most successful way to treat degenerative spinal problems such as trauma, disease, deformity, disc herniation or spondylolisthesis. As detailed in Chapter 2 such conditions can cause intervertebral tissue or bone to impinge on the nerve roots and may also cause adjacent vertebrae to contact, resulting in chronic pain.

Spinal fusion allows the surgeon to eliminate relative motion between two or more adjacent vertebrae, increase the space for the nerve roots, stabilize the spine and restore spinal alignment, as required to reduce the patient's pain.

Spinal fusion basically involves removing the affected intervertebral disc and packing the resulting cavity with an implant and/or bone graft to maintain the disc height. Hardware may then also be added to the vertebral bodies and posterior elements to ensure the resulting construct is stable and that no further motion occurs at the affected level.

3.1 Spinal Fusion Implants

Depending on the patient's condition, size and weight, several different types and combinations of implant are available. These implants range from simple cages used to restore the intervertebral disc spacing, to complex scaffolding systems used to restore stability and correct posture.

3.1.1 Interbody Spacers

Interbody spacers come in a variety of forms, including cylindrical mesh tube and solid spacers. However regardless of the shape or type of implant used they all serve the same purpose which is to maintain the distance between the adjacent vertebrae.

Cylindrical mesh tubes offers the advantage that the surgeon can cut the required implant(s) from stock lengths of material to match the patients intervertebral disc space in theatre. Bone graft or bone cement is then packed into the tube just prior to it being implanted, as shown in Figure 3.1. Figure 3.2 shows such a mesh tube implanted with the tube axis aligned with the anterior/posterior axis.



Figure 3.1 Titanium mesh cage packed with autogenous cancellous bone.

[Source: <http://www.spineuniverse.com/displayarticle.php/article1670.html>]

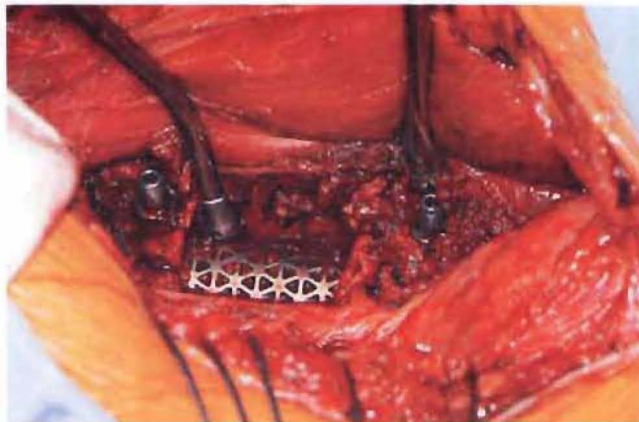


Figure 3.2 Cage placed at the fusion site.

Bolts for a lateral stabilizing plate are in situ in the vertebral bodies.

[Source: <http://www.spineuniverse.com/displayarticle.php/article1670.html>]

There are many types of solid interbody spacers available. The design of these implants varies greatly although most are available in a range of sizes to suit different patient weights and intervertebral disc spacings. Two of the more popular devices are the BAK/L™ Implant and the LT-CAGE™. These devices are illustrated in Figures 3.3 and 3.4 respectively. Solid interbody spacers are normally implanted with their long axis perpendicular to the anterior/posterior axis, as shown in Figure 3.4(b).



Figure 3.3 BAK/L™ implant.

(a) Singular BAK/L™ Implant. [Source: www.sulzerortho.eu.com]

(b) Model with two BAK/L™ implants situated in L4-5 disc space.

[Source: <http://www.spine-ctsi.com/cages.htm>]



Figure 3.4 LT-CAGE™.

(a) LT-CAGE™ shown with INFUSE™ Bone Graft Material.

(b) Schematic showing LT-Cage™ placement in L5-S1 disc space.

[Source (a): <http://www.back.com/article-infuse-surgical.html?infusebox=yep>]

[Source (b): <http://www.spineuniverse.com/displayarticle.php/article1523.html>]

Regardless of which type of interbody spacer is used they are normally packed with and surrounded by bone cement or more preferably bone grafts. Bone graft material is normally taken from either the pelvis (ileum) or from parts of the vertebrae removed as part of the fusion such as the spinous processes or laminae. In a successful fusion the bone graft grows through and/or around the interbody spacer eventually forming a solid bond with the adjacent vertebrae. Loosely, interbody spacers can be compared to building blocks and the bone graft to the mortar that binds the structure together. The intended result of an interbody fusion is a strong and stable construct.

3.1.2 Posterior Instrumentation

The purpose of posterior instrumentation is to provide the stability required for bony fusion to occur and to ensure there is no relative motion of the vertebrae at the affected spinal level(s). Ideally such posterior instrumentation provides the required strength while remaining compact in design to minimise the implants profile. There are two main types of posterior instrumentation, pedicle screw fixation and facet screw fixation.

3.1.2.1 Pedicle Screw Fixation

Pedicle screw fixation systems are one of the most commonly used types of posterior instrumentation. This is primarily because the pedicles are the ideal point to attach devices to the lumbar spine as they are strong; consist primarily of cortical bone, and are rarely affected by degenerative diseases.

Typically the pedicle screws are inserted axially down the pedicles and tie rods or plates are fastened to the screw heads to link the adjacent vertebrae together. The pedicle screws used normally have a poly-axial head which allows misalignment of the screws and scaffolding systems to be catered for.

The disadvantage of pedicle screw fixation systems is that significant muscle dissection is required to access the pedicles and to insert the implant assembly. As a result of such surgery muscle scarring and morbidity often result^{8,13}.

Figures 3.5 and 3.6 show two different pedicle screw fixation systems. Figure 3.6(a) shows a schematic cross-section of pedicle screws in relation to the vertebrae.

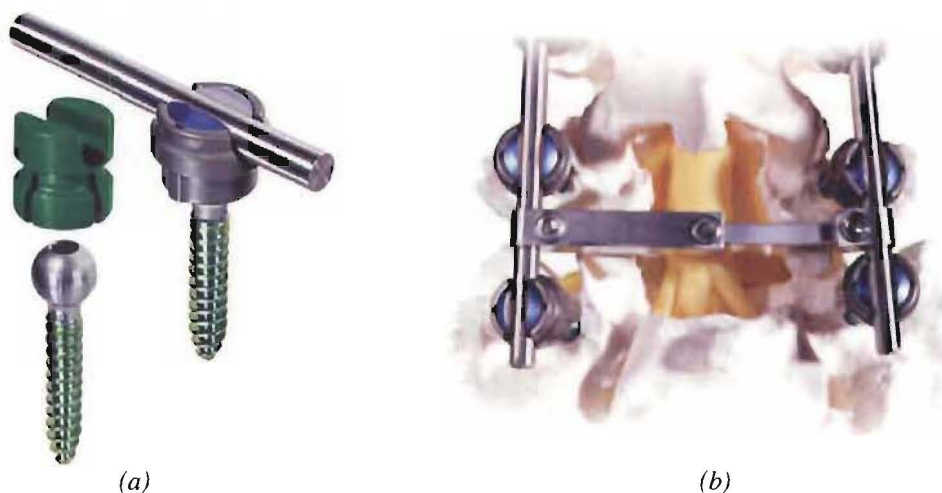


Figure 3.5 Ovation™ Polyaxial pedicle screw fixation system.

(a) Ovation™ Polyaxial System showing a poly-axial screw, trial cap and outer ring assembly.

(b) Ovation Versalink™ system in-situ on model.

[Source: <http://www.osteotech.com/prodpoly2.htm>]

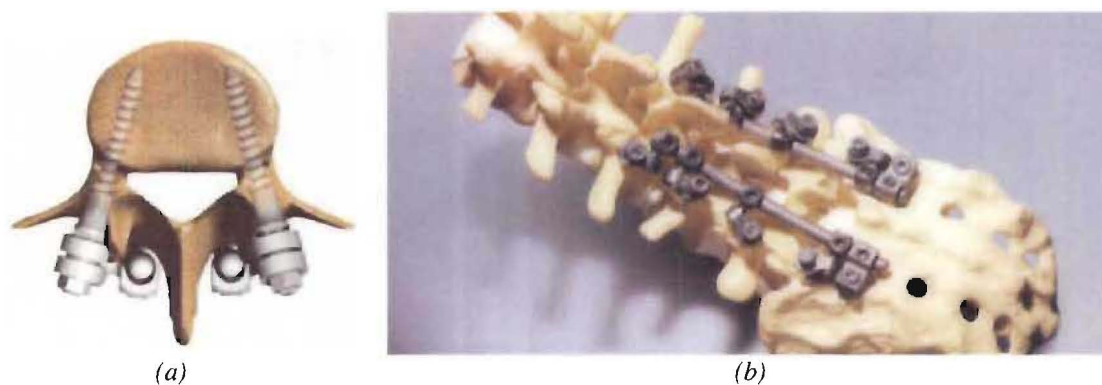


Figure 3.6 Claris pedicle screw fixation system.

(a) Schematic view of Claris pedicle screws in-situ.

(b) Claris Titanium Instrumentation on a lumbar spine model.

[Source: <http://www.eurosurgical.com/Claris.html>]

3.1.2.2 Facet Screw Fixation

Facet screw fixation involves placing a few screws through the posterior elements to prevent relative motion of the adjacent vertebrae. Typically options available to the surgeon include placing screws through the zygapophysial capsule, across the zygapophysial capsule and continuing into the pedicle, or alternatively, through the lamina and into the zygapophysial joint. This method offers the advantage of minimising the amount of hardware required. It has been also shown that for single level anterior interbody fusion facet screw fixation, with pedicle purchase, is as stable as pedicle screw fixation but it is considerably less intrusive^{1,4}. Figure 3.7 shows an example of facet screw fixation with two cortical bone screws passing through the spinous process, lamina and zygapophysial joint.

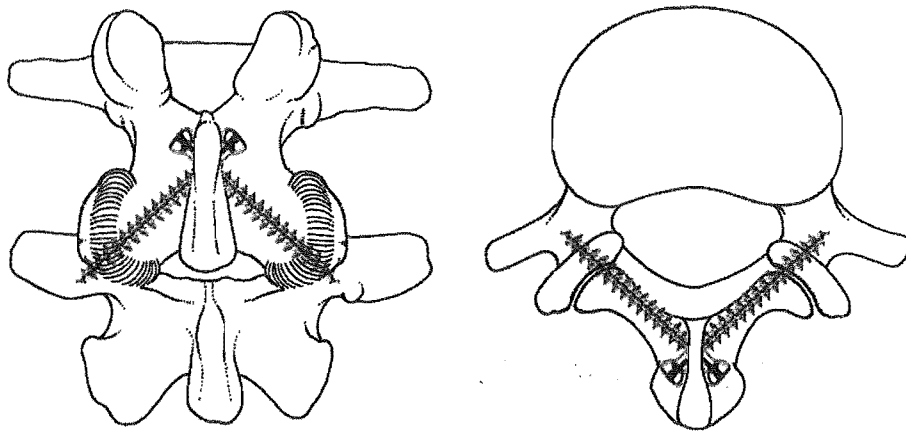


Figure 3.7 Facet screw fixation.

3.2 Surgical Approach for Spinal Fusion

When fusing the lumbar spine the intervertebral disc can be approached several ways including using anterior, posterior or lateral approaches or a combination of these. The approach used is normally determined by the patient's condition, the type of implant(s) being used and the surgeons' preference.

Some key factors in creating a successful spinal fusion include:

- Relieving any pressure applied to the nerve roots
- Removing all relative movement between vertebrae
- Maintaining correct intervertebral disc height
- Ensuring the spine remains stable
- Causing no additional damage to the nerve roots during surgery
- Minimising the formation of scar tissue.

The surgeons' ability to address these factors depends on the surgical technique used. Several common surgical techniques used to perform spinal fusion along with their relative merits and disadvantages are detailed in the Sections 3.2.1 through 3.2.4.

3.2.1 Anterior Lumbar Interbody Fusion

Anterior Lumbar Interbody Fusion (ALIF) involves making an incision in the abdomen and displacing the bowel and blood vessels in order to access the intervertebral disc. The theoretical advantages of this approach are that the vertebral bodies provide a large surface area for the cage to contact and good blood supply for fusion.

The disadvantage of ALIF is that it is often unable to restrict motion between the vertebrae adequately and it requires the surgeon to cut through abdominal compartments. An anterior approach also requires the anterior longitudinal ligament to be cut which severely diminishes the lumbar spine's ability to retard the transmission of shock loads, using the lordosis curve mechanism previously described in Section 2.7.

The graft material placed in the disc space during ALIF can also collapse under the compressive loads applied to the lumbar spine. Therefore ALIF often needs to be accompanied by posterior instrumentation to increase the stability and success rate. In the case of combined anterior and posterior surgery, instrumentation in the form of an anterior "buttress" plate may be used to keep the bone graft in place, as shown in Figure 3.8. However such additional instrumentation can damage neighbouring blood vessels.

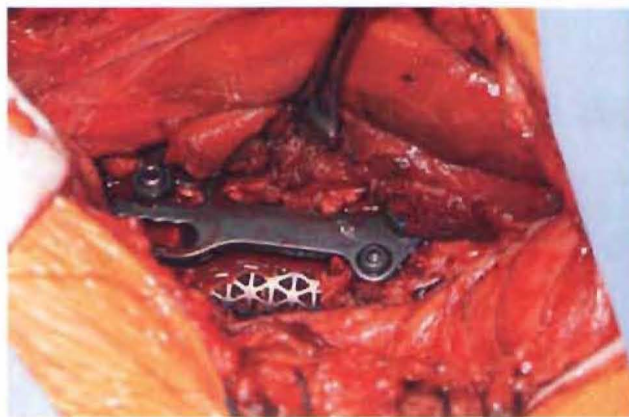


Figure 3.8 Anterior interbody fusion utilizing a cage and buttress plate.

[Source: <http://www.spineuniverse.com/displayarticle.php/article1670.html>]

In recent years there has been increased interest in anterior only fusion with anterior instrumentation in an attempt to avoid weakening and scarring of the posterior musculature. However early attempts at this type of fusion and instrumentation have not proven substantially more successful than posterior surgery. Failures have been attributed to excessive motion still present after anterior-only surgery, the collapse of the instrumentation into the vertebral bodies and malposition of the interbody spacers.

3.2.2 Posterior Lumbar Interbody Fusion

Posterior Lumbar Interbody Fusion (PLIF) involves approaching the spine through a 75 to 150 mm incision down the midline of the back. The left and right back muscles (erector spinae) are then stripped off the lamina on both sides and at multiple spinal levels.

After the initial incisions, the lamina is removed (laminectomy) which allows visualization of the nerve roots. The zygapophysial joints may also be resected to create more room for the nerve roots and to allow better visualisation of the affected area. Once the nerve roots can be moved to one side sufficiently any impinging disc material is removed. A bone graft, or interbody cage is then inserted into the disc space. Figure 3.9 shows a schematic diagram where the nerve roots have been retracted to aid in the insertion of interbody cages.

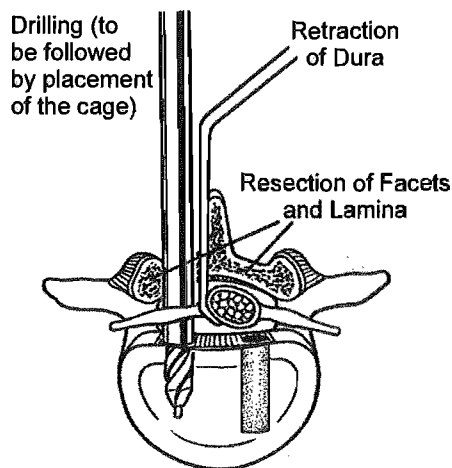


Figure 3.9 Retraction of the nerve roots to facilitate posterior interbody fusion.

[Source: http://www.lajollaspine.com/PatientCare_MinimallyInvasive.htm]

One advantage of PLIF is that the nerves of the lumbar spine can be clearly visualized and decompressed, as required. Decompression can also be achieved using an anterior approach, however it is a much more cumbersome and tedious process.

There are several disadvantages associated with posterior fusion. Substantial retraction of the nerve roots is required to gain access to the intervertebral disc space. Such traction can injure the nerve roots and may result in chronic leg pain and back pain. The pain associated with this type of nerve root injury can be severe and on-going. Currently there are no effective treatment options should such nerve damage occur.

Also in order to place the interbody cage or bone graft a substantial amount of bone, and potentially part of the zygapophysial joint(s), must be removed. Removal of this bone and joint can destabilise the spine which is counterproductive to forming a stable fusion¹². Significant trauma to the musculature also occurs due to the large incisions required. There are also numerous veins surrounding the intervertebral discs and surgery in this area may also potentially cause excessive blood loss.

Currently only 60-70% of posterior fusions for the treatment of discogenic back pain result in a satisfactory outcome⁷.

3.2.3 Transforaminal Lumbar Interbody Fusion

Transforaminal Lumbar Interbody Fusion (TLIF) is very similar to PLIF but differs in that the disc is removed using a lateral approach. This procedure is usually performed for disc problems at a single spinal level such as recurring disc herniation, instability of the spine or chronic problems related to disc rupture.

The procedure involves an incision along the midline of the back to expose the posterior elements of the spine. Once accessible the lamina at the selected spinal level is gradually resected until the nerve roots can be visualised. The nerves are then gently mobilized to expose the intervertebral disc.

The disc is removed through either side of the spinal canal, although sometimes it is possible to complete the procedure from one side only. Once the intervertebral space has been cleared it is packed with interbody spacers and bone graft material. Often posterior instrumentation is also added across the level to be fused. Additional bone grafts may also be placed across the transverse processes to ensure a solid fusion.

It is possible to leave the posterior lamina and zygapophysial joints intact during TLIF allowing the use of less invasive fixation methods. Figure 3.10 illustrates the Magerl fixation technique which is a form of facet screw fixation. This level of posterior instrumentation is sufficient as the vertebrae are already partially stabilized by the interbody spacers and the intact posterior zygapophysial joints.

TLIF still results in some scarring of the posterior musculature and also requires potentially damaging mobilisation of the nerve roots. However the key advantage of TLIF is the retention of the majority of the posterior elements, allowing a more stable fusion to be achieved.



Figure 3.10 Postoperative anterior-posterior x-rays of a TLIF.

Note that the disc has been replaced with bone graft and operative stability is achieved using the Magerl fixation technique. The two translaminar screws are clearly visible.

[Source: http://www.orthospine.com/tutorial/spinal_decompression.html#6]

Recently TLIF surgery has progressed to include the use of endoscopic instruments. Percutaneous transforaminal spinal endoscopy is performed using an endoscope that can bend up to 90 degrees and can pass around the intervertebral foramina into the spinal canal. Disc fragments can be removed and the disc reconfigured, relieving any spinal nerve compression with minimal disruption to surrounding structures, especially in cases where the disc presents itself for direct removal.²

Due to the less invasive nature of this endoscopic procedure patients are often able to return to work within weeks as opposed to waiting up to 3 months with ALIF or PLIF techniques. Other advantages of this procedure include only small incisions being required and no interference with the bone, joints or manipulation of the nerves. Additionally, as some endoscopes can be inserted through muscle, there is reduced scarring or damage to the nerves. However, endoscopic techniques are more suited to relieving pressure on the nerves as a result of bone spurs or impinging disc material, rather than conducting spinal fusions for which less favourable results are achieved, accordingly enthusiasm for endoscopic spinal arthrodesis has diminished in recent years.

3.2.4 Circumferential Fusion (Anterior and Posterior)

Circumferential fusion involves a combination of anterior and posterior lateral interbody fusions. This technique is usually performed with combination of interbody spacers, bone grafts and posterior instrumentation. The posterior instrumentation may include, but is not limited to, pedicle screws, rods, plates, wires and facet screws. The instrumentation used depends upon the degree of instability, the amount of bone structure present and the preference of the surgeon.

In general the circumferential fusion leads to a very high fusion rate. This approach is desirable in situations where postoperative stability is of concern, for example, in revision cases or for smokers. The disadvantage compared to anterior or posterior procedures alone is the invasiveness of the surgery. Due to the need for anterior and posterior incisions to access the spine, there is also an increased possibility of infection and the formation of scar tissue.

3.3 Disadvantages of Spinal Fusion

By eliminating motion at destabilised or degenerated intervertebral discs, spinal fusion allows instability to be eliminated, maintenance of normal intervertebral disc space height and preservation of sagittal balance. Spinal fusion also provides a means of halting further degeneration at the affected vertebral level(s). Depending on the approach used, fusion also provides the opportunity to remove any material impinging on nerve roots.

Good to excellent results have been reported in 52–100% of anterior lumbar interbody fusions and 50–95% of posterior lumbar interbody fusions^{6,14,17,19,20}. However spinal fusion has several key disadvantages which limit its effectiveness regardless of the surgical approach or type of intradiscal and posterior hardware used.

Spinal fusion is not a benign procedure and numerous patients develop recurrent symptoms years after surgery, as fusion disrupts the biomechanics of the adjacent spinal levels. Hypertrophic facet arthropathy, stenosis, disc degeneration, and osteophyte formation have all been reported to occur at levels adjacent to a fusion, and such pathology often results in pain for many patients^{3,5,8,10,11,15,16}. These complications often result in the need to fuse the adjacent intervertebral discs as well.

Fusion also presents a number of other disadvantages including loss of spinal mobility and graft collapse resulting in alterations of sagittal balance. Many patients also experience pain at the autograft harvest site, if bone grafts are used.

Lehman et al¹⁰ reported the long term results of lumbar fusions. A series of patients who were treated with un-instrumented fusions were followed for 21–33 years. At last follow-up approximately half the patients had lumbar pain requiring medication and 15% had required further surgery over the study period.

Biomechanical experiments on fresh cadaveric spines also indicate an increase in stresses in adjacent segments as a result of spinal fusion^{9,18}. A change in the centre of rotation of the adjacent vertebrae was also observed after fusion. Within the first five years of spinal fusion new symptoms are often observed in adjacent segments. These new symptoms are thought to be a result of accelerated degeneration of pre-existing conditions due to increased stress in the adjacent segments after fusion⁸.

All of these complications suggest that spinal fusion is not, in many cases, an adequate solution for the treatment of back pain.

Therefore an artificial intervertebral disc with natural ranges of motion, stiffness and stability could potentially provide a more successful long term solution than spinal fusion.

For an artificial disc to be successful spinal stability needs to be preserved and scarring kept to a minimum. To achieve this, a minimally invasive procedure should be used which also allows the majority if not all of the boney features, ligaments and musculature to be retained. Ideally any artificial disc should be designed so that there is no need to resect the posterior elements, particularly the zygapophysial joints which make a large contribution to spinal stability. There should also be minimal need to manipulate the nerve roots during implantation. These factors suggest that an implant designed for an anterior or lateral approach is preferable over a posteriorly inserted implant.

3.4 References

1. Chiu J C, Davis G W, Clifford T, Greenspan M. *Translaminar Facet Fixation: An Alternative Method for Lumbar Fusion: Report of 710 Cases*. The California Centre for Minimally Invasive Spine Surgery, [cited May 2003]. Available from <http://www.spinecenter.com/papers/facet/facet.htm>.
2. Ditsworth D A, *Endoscopic Transforaminal Lumbar Discectomy and Reconfiguration : A Posterolateral Approach into the Spinal Canal*. *Surgical Neurology*, 1998. Vol 49 (6): pp 588-97.
3. Frymoyer J W, Hanley E N, Howe J, Kuhlmann D, Matteri R E, *A comparison of radiographic findings in fusion and non-fusion patients 10 or more years following lumbar disc surgery*. *Spine*, 1979. Vol 4 (5): pp 435-440.
4. Heggeness M H, Esses S I, *Translaminar Facet Joint Screw Fixation for Lumbar and Lumbosacral Fusion. A clinical and biomechanical study*. *Spine*, 1991. Vol 16 (6 Suppl): pp S266-9.
5. Hutter C G, *Spinal stenosis and posterior lumbar interbody fusion*. *Clinical Orthopaedics and Related Research*, 1985. Vol 193: pp 103-114.
6. Kuslich S D, Ulstrom C L, Griffith S L, Ahern J W, Dowdle J D, *The Bagby and Kuslich method of lumbar interbody fusion. History, techniques, and 2-year follow-up results of a United States prospective, multi-center trial*. *Spine*, 1998. Vol 23 (11): pp 1267-1279.
7. La Jolla Spine Institute. *Minimally Invasive Spinal Surgery*, Updated: 17 Oct 2000 [cited Mar 2003]. Available from http://www.lajollaspine.com/PatientCare_MinimallyInvasive.html.
8. Lee C K, *Accelerated degeneration of the segment adjacent to a lumbar fusion*. *Spine*, 1988. Vol 13 (3): pp 375-377.
9. Lee C K, Langrana N A, *Lumbosacral spinal fusion: A biomechanical study*. *Spine*, 1984. Vol 9 (6): pp 574-581.
10. Lehman T R, Spratt K F, Tozzi J E, *Long-term follow-up of lower lumbar fusion patients*. *Spine*, 1987. Vol 12 (2): pp 97-104.
11. Leong J C Y, Chun S Y, Grange W J, Fang D, *Long-term results of lumbar intervertebral disc prolapse*. *Spine*, 1983. Vol 8 (7): pp 793-799.
12. Low Back-Pain.Com. *Posterior lumbar interbody fusion (PLIF)*, Updated: 08 Mar 2003 [cited Mar 2003]. Available from <http://www.lowback-pain.com/surgery.PLIF.htm>.
13. Madan S S, Boeree N R, *Comparison of Instrumented Anterior Interbody Fusion with Instrumented Circumferential Lumbar Fusion*. *Eur Spine J*, 2003. Vol 12: pp 567-575.

14. Ray C D, *Threaded titanium cages for lumbar interbody fusions*. *Spine*, 1997. Vol 22 (6): pp 667-680.
15. Traynelis V, Haid R W J. *Spinal Disc Replacement: The Development of Artificial Discs*. Spine Universe, Updated: 30 Apr 2002 [cited Mar 2003]. Available from <http://www.spineuniverse.com/displayarticle.php/article501.html>.
16. Vaughan P A, Malcolm B W, Maistrelli G L, *Results of L4-L5 disc excision alone versus disc excision and fusion*. *Spine*, 1988. Vol 13 (6): pp 690-695.
17. Watkins R G, *Results of anterior interbody fusion*, in White A H, Rothman R H, and Ray C D (Eds). *Lumbar Spine Surgery: Techniques and Complications*, 1987, C V Mosby: St. Louis. pp 408-432.
18. Yang S W, Langrana N A, Lee C K, *Biomechanics of lumbosacral spinal fusion in combined compression-torsion loads*. *Spine*, 1986. Vol 11 (9): pp 937-941.
19. Yuan H A, Garfin S R, Dickman C A, Mardjetko S M, *A historical cohort study of pedicle screw fixation in thoracic, lumbar, and sacral spine fusions*. *Spine*, 1994. Vol 19 (20S): pp 2279S-2296S.
20. Zucherman J F, Selby D, DeLong W B, *Failed posterior lumbar interbody fusion*, in White A H, Rothman R H, and Ray C D (Eds). *Lumbar Spine Surgery: Techniques and Complications*, 1987, C V Mosby: St. Louis. pp 296-305.

Chapter 4 – Specification & Analysis of Existing Artificial Discs

4.1 Expansion of Problem Statement in Engineering Terms

This chapter details the final design specification for this intervertebral disc implant project and the justification of these parameters. This specification was also used to evaluate some of the other artificial disc implants currently available.

In 1997, Kostuik³¹ developed criteria for the design of an intervertebral disc prosthesis. These criteria were used during the design of the Kostuik disc. To date only a few researchers have published intervertebral disc design criteria and of those published Kostuik's are the most comprehensive. Therefore during the development of the design specification for this project some of Kostuik's criteria were used, however parameters were expanded on and modified as required.

4.1.1 Load Carrying Requirements

The intervertebral disc implant is required to carry a percentage of the patient's static body weight and the additional loads applied as the patient carries out various activities.

When the patient is standing upright and stationary the head, torso and arms apply vertical loads on the lumbar spine segments. These masses represent between 50 and 58 percent of the patient's total body weight^{16,29,41,63}. Therefore for a patient weighing 100 kg the intervertebral disc implant will be required to support a 50 to 60 kg nominal load.

During daily activities, the lumbar spine is subjected to significant biomechanical forces. Studies indicate that a intervertebral disc may experience axial compressive loads ranging from 400 N during quiet standing to more than 7000 N during heavy lifting^{40,60}. Large loads resulting from activities like heavy lifting only occur infrequently as opposed to low load situations, like walking and lifting small weights, which occur with a much higher frequency.

In order to withstand a maximum load of 7000 N a very bulky, resilient disc would be required, therefore the maximum design load was limited to 1200 N for the purposes of this project. This load limit was considered acceptable on the basis that the patient's spine would already be compromised and the patient could be instructed to avoid strenuous activities such as heavy lifting.

As previously detailed in Section 2.6 the zygapophysial joints can carry a small percentage of the applied vertical loads in certain conditions. There have been several studies investigating this load carrying capability in the lumbar spine with results varying from the zygapophysial joints bearing 28%³⁶ to 40%²⁷ percent of the vertical load, to the zygapophysial joints carrying none of the load provided the lumbar spine is placed in slight flexion². The reasons for these differences in findings are due to the techniques used and researchers differing appreciations of the zygapophysial joint anatomy and behaviour.

The morphology of the patient will also influence the loads applied to the implant. For example patients with good abdominal muscle tone are able to use their torso as a hydraulic tube thus allowing some weight bearing to occur through the pressurised abdomen. Conversely patients with poor abdominal muscles, for example those with a large gut, are unable to support weight in this fashion and as a result tend to lean backwards so they can balanced all their weight on the lumbar spine.

However, for the purposes of this project the intervertebral discs were considered to carry all of the applied loads and the zygapophysial joints and abdomen to carry none. Hence the intervertebral disc implant will be required to carry a nominal load of 600 N and a maximum load of 1200 N.

4.1.2 Kinematics

The motion properties of the lumbar spine have been investigated using theoretical studies⁵³, cadaveric specimens^{7,40,51,62} and healthy volunteers^{19,43,44,45,46}. Studies which utilised physical specimens were completed using a variety of measurement techniques. The principal method for measuring the motion in healthy volunteers was bi-planar radiography. In cadaveric studies direct measurements were normally taken.

| Source | Flexion | Extension | Lateral Flexion | | Axial Rotation | Study Type |
|----------------------------------|---------|-----------|-----------------|-------|----------------|------------|
| | | | Left | Right | | |
| Shirazi-Adl ⁵³ | 7° | 6.5° | 6.2° | 6° | - | Theory |
| Schultz et al ^{7,40,51} | 5.5° | 3° | 5° | 5.6° | 1.5° | Cadaver |
| Yamamoto ⁶² | 8.9° | 5.8° | 5.5° | 5.9° | 2.2° | Cadaver |
| Pearcy et al ^{45,46} | 13° | 2° | 3° | 5° | 1.5° | Volunteer |
| Pearcy ⁴³ | 13° | 3° | 3° | 3° | 1° | Volunteer |
| Dvorak ¹⁹ | 18.2° | | 9.5° | | - | Volunteer |

Table 4.1 Mean values of range of motion of L4-5.

The variations in the range of motion (ROM) values given in Table 4.1 may be due to several factors, including the method used to measure the range of motion, the age of the subjects and any pre-existing degeneration of the intervertebral discs.

There are also variations between the results obtained from living volunteers and cadaver specimens. One reason for this discrepancy is that often in cadaveric studies the applied loads are typically restricted to 10.6 Nm to reduce the chance of damaging or excessively deforming the spinal segment. However, in studies with living volunteers the subject often bends to the most extreme position they can endure. Studies of cadaveric specimens have additional disadvantages resulting from post-mortem changes. Also these studies are often completed with the back musculature removed, thus the measurements obtained may not accurately reflect the mobility of a living subject.

After consultation with an orthopaedic surgeon¹³ the design ranges of motion for the intervertebral disc implant were set as shown in Table 4.2.

| Motion | Design ROM |
|-----------------------|------------|
| Flexion | 8° |
| Extension | 2° |
| Left Lateral Flexion | 5° |
| Right Lateral Flexion | 5° |
| Axial Rotation | 0° |

Table 4.2 Design range of motion.

These design range of motions values are lower than the values shown in Table 4.1 for healthy volunteers, however these ranges of motion were considered to be adequate and appropriate for a spinal column which has previously been damaged or diseased. While larger design ranges of motion would match those values in the healthy lumbar spine, such motions may result in further damage to the already compromised annulus fibrosus and/or zygapophysial joints.

It is however noted that for patients suffering from ligamentous laxity, a condition where the longitudinal ligaments are loose or stretched, these ranges of motion may be insufficient. Patients should therefore be carefully screened prior to implantation of the intervertebral disc implant.

The intervertebral disc implant could be designed so that the ranges of motion in lateral bending are different to those for flexion and extension. However, if this is the case then the implant should include alignment features to ensure correct orientation with the patient's spine. Also, as the specification does not allow for any axial rotation, facility should be provided to ensure accurate alignment of the implants' endplates relative to each other during the implantation procedure to prevent any additional loading of the zygapophysial joints.

4.1.3 Centre of Rotation

Full flexion of the lumbar spinal segments involves a combination of 8° of anterior sagittal rotation and 1-3 mm of forward translation. This combination of rotation and translation results in each vertebra exhibiting a curved or arc motion relative to the vertebrae below. In a healthy spine the centre of this arc lies below the moving vertebra and is known as the instantaneous axis of rotation (IAR), as shown in Figure 4.1(a).

As the lumbar spine moves from full extension to full flexion the amount of sagittal rotation versus sagittal translation changes. Consequently the location of the IAR for each phase of motion differs slightly. Essentially, the axis of movement is not constant. If the instantaneous axes of rotation are determined for each phase of motion and plotted in sequence, they depict a locus known as the centroid of motion, as illustrated in Figure 4.1(b).

In healthy volunteers, the instantaneous axes of rotation fall in tight clusters, centred near the superior endplate of the lower adjacent vertebra as shown in Figure 4.1(c)⁴⁴. As Kostuik³¹ stated *“Replicating the position of these axes in an intervertebral disc prosthesis is critical in restoring the sagittal plane motions and in constraining the motion of the nervous structures with physiological limits”*.

For the purposes of this project it was considered sufficient to create an intervertebral disc implant with a fixed centroid of motion as shown in Figure 4.1(a). Such a centroid of motion should be located in the posterior third of the disc space. However, where possible a centroid of motion similar to that illustrated in Figure 4.1(b) should be used to ensure normal loading of the zygapophysial joints.

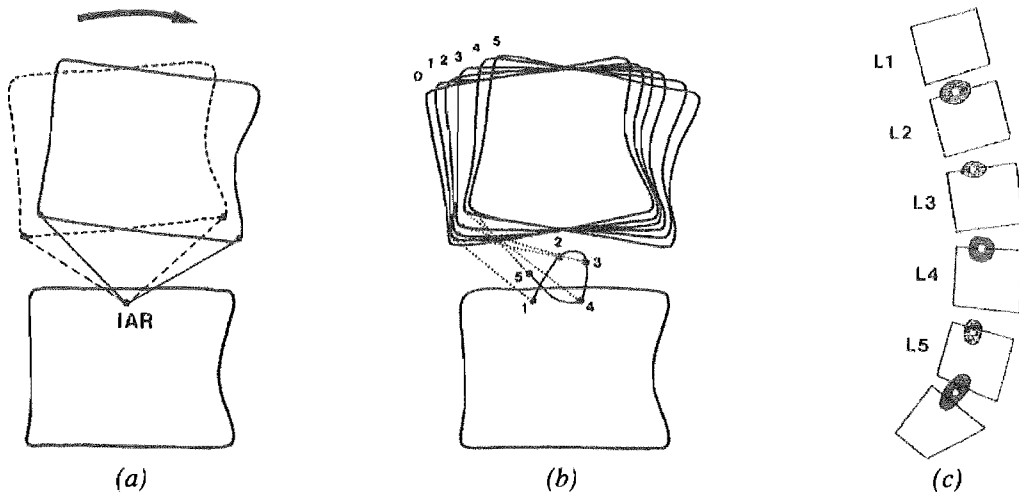


Figure 4.1 Instantaneous axis of rotation.

(a) Instantaneous Axis of Rotation (IAR).

(b) When the IAR are connected in sequence they depict a locus or path known as the centroid of motion.

(c) The mean location and distribution of IAR for a healthy lumbar spine. The central dot depicts the mean location; the outer ellipse depicts the two standard deviation range.

[Source: Pearcy M J, et al¹⁴]

4.1.4 Fatigue Requirements

The mean age of spinal fusion patients in the United States of America is 46 years¹. To reduce the trauma to the patient, it is desirable that the number of surgical operations required be kept to a minimum. As Kostuik³¹ stated “*the disc prosthesis should last for the life of the recipient. Therefore the life span of the implant should exceed 40 years*”.

“The number and amplitude of load cycles experienced by a lumbar intervertebral joint during the period of a year is a matter of speculation. However by assuming that the average person experiences 2 million strides per year (1 million gait cycles), 125,000 significant bends (flexion and extension), and disregarding the 6 million breaths that this person would take in a year, a conservative estimate of the number of spinal loading cycles during the 40-year period would be 85 million cycles. Consequently, it was determined that the device and the materials should be tested to at least 100 million cycles”.

It was not clear what Kostuik’s load cycle assumptions were based on, or whether these assumptions were reasonable. Therefore to determine the fatigue specification for this project the frequencies of typical activities were tallied. These values were then cross-referenced to deflection types and ranges of motion for the same activities. This allowed the number and severity of daily excursions in each direction to be determined.

The lumbar spine movements were first categorised, as either causing large or small angular deflections. Large angular deflections are those that occur when a patient sits down, stands up, bends to pick up an object or plays sport. Small angular deflections are those that occur while performing tasks such as walking or breathing.

Large angular deflections were found to vary in magnitude between patients and also depending on the technique used to carry out the activity, for example patients have different methods of putting on a sock. Hsieh et al³⁰ studied the level of flexion that occurred in the whole lumbar spine when performing four daily tasks. The results of this study suggest that activities such as picking an object up off the floor require full flexion of the lumbar spine. However, activities such as sitting down or standing up while resulting large angular deflections do not require full flexion of the lumbar spine, as shown in Table 4.3. Large deflection activities were therefore further sub-divided into full flexion deflection activities (8°) and moderate deflection activities (5°).

| Activity | Peak Flexion Angle (deg) | Percentage of Maximum Flexion |
|------------------------------|---------------------------------|--------------------------------------|
| Full Flexion when Standing | 61.3 (± 10.5) | 100 |
| Full Extension when Standing | 23.0 (± 8.7) | - |
| Stand to Sit | 34.6 (± 13.7) | 55.8 (± 22.1) |
| Sit to Stand | 41.8 (± 14.2) | 65.9 (± 21.4) |
| Pick up object off floor | 60.4 (± 18.4) | 95.3 (± 22.2) |
| Put on Right Sock | 56.4 (± 15.1) | 89.0 (± 14.3) |
| Put on Left Sock | 56.8 (± 15.9) | 90.3 (± 15.2) |

Table 4.3 Mean (\pm SD) lumbar motion and percentage of normalised flexion for four daily activities.

[Source: Hsieh et al³⁰]

Small angular deflections resulting from activities such as walking cannot be neglected when considering the fatigue life of the intervertebral disc implant. Although the stresses resulting from these deflections may be small they occur with greater frequency than the high stress significant bends. As a result these small angular deflections can cause cumulative damage which influences the fatigue life of the implant.

Kostuik's fatigue requirements were based on an average person completing 2 million strides per year, however, some researchers now consider up to 4 million cycles per year to be normal¹⁴. Given patients requiring an intervertebral disc implant may be less active than an average person, Kostuik's value of 2 million cycles per annum was considered to be acceptable.

The lumbar spine angular deflections for patients walking on flat, level ground have been reported by several researchers. In each of these studies the results were reported as a total deflection for the whole lumbar spine, as shown in Table 4.4. The variation in the values reported by different researchers is most probably due to the different measurement techniques used.

To determine the deflection per spinal level these reported values were evenly divided across the five lumbar spine intervertebral discs. As a result the deflection per lumbar spine level while walking was estimated to be 1° in each of the three angular deflection planes, as shown in Table 4.4.

| Motion | Angular Deflection | | Source |
|----------|--------------------|-------------------|-------------------------|
| | Whole Spine | Per Level | |
| Flex/Ext | 3° | $<1^\circ$ | Taylor ⁵⁶ |
| | $3-4^\circ$ | $\approx 1^\circ$ | Callaghan ¹⁵ |
| Lateral | $2-4^\circ$ | $\approx 1^\circ$ | Whittle ⁶¹ |
| | $8-12^\circ$ | $>2^\circ$ | Taylor ⁵⁶ |
| | $1-2.5^\circ$ | $<1^\circ$ | Callaghan ¹⁵ |
| Axial | $2-4^\circ$ | $\approx 1^\circ$ | Whittle ⁶¹ |
| | 6.5° | $>1^\circ$ | Taylor ⁵⁶ |
| | $2-3^\circ$ | $<1^\circ$ | Callaghan ¹⁵ |

Table 4.4 Lumbar spine angular deflections when walking.

Motion coupling also exacerbates the number of deflections the intervertebral discs are subjected to. Motion coupling means that as the spine deflects in one plane, deflections also occurs in the other two planes. For example when a patient bends forward to pick up an object off the floor the primary motion is flexion, however coupled rotations (axial and lateral) and translations also occur. This is illustrated in Table 4.5 for flexion and extension movements.

| | Spinal Level | Mean (SD) Rotation (degrees) | | | Mean (SD) Translation (mm) | | |
|------------------|--------------|------------------------------|---------|-------|----------------------------|---------|-------|
| | | Sagittal | Coronal | Axial | Sagittal | Coronal | Axial |
| Flexion | L1 | 8 (5) | 1 (1) | 1 (1) | 3 (1) | 0 (1) | 1 (1) |
| | L2 | 10 (2) | 1 (1) | 1 (1) | 2 (1) | 1 (1) | 1 (1) |
| | L3 | 12 (1) | 1 (1) | 1 (1) | 2 (1) | 1 (1) | 0 (1) |
| | L4 | 13 (4) | 2 (1) | 1 (1) | 2 (1) | 0 (1) | 0 (1) |
| | L5 | 9 (6) | 1 (1) | 1 (1) | 1 (1) | 0 (1) | 1 (1) |
| Extension | L1 | 5 (1) | 0 (1) | 1 (1) | 1 (1) | 1 (1) | 0 (1) |
| | L2 | 3 (1) | 0 (1) | 1 (1) | 1 (1) | 0 (1) | 0 (1) |
| | L3 | 1 (1) | 1 (1) | 0 (1) | 1 (1) | 1 (1) | 0 (1) |
| | L4 | 2 (1) | 1 (1) | 1 (1) | 1 (1) | 0 (1) | 1 (1) |
| | L5 | 5 (1) | 1 (1) | 1 (1) | 1 (1) | 1 (1) | 0 (1) |

Table 4.5 Mean movements coupled with flexion and extension of the lumbar spine.

[Source: Bogduk N, et al¹¹]

Given these activity ranges of motion the final fatigue specification would ideally be determined by cross-referencing these values with the frequencies at which these activities occur. However, there is little data available on the frequencies of typical spinal activities. The test data that is available normally focuses on one activity and gives a deflection range but no frequency value.

Therefore in order to determine the number of daily deflections in each direction, two approximations were made. First the number of cycles occurring over a given time period was estimated for several activities, as shown in Table 4.6. Next the time spent carrying out these activities was estimated, allowing a tally of daily deflections to be generated. The resulting deflections per day in each direction are listed in Table 4.7.

| Activity | Cycles |
|-------------------|----------------|
| Walking | 80 per Minute |
| Running | 120 per Minute |
| Sits | 20 per Hour |
| Significant Bends | 100 per Hour |

Table 4.6 Estimated cycles per time period for typical daily activities.

| Activity | Time (Hrs) | Time (Min) | Multiplier (Table 4.6) | Cycles (per Day) | Number of Angular Deflections per Day | | | | | | | | | |
|-------------|------------|------------|------------------------|------------------|---------------------------------------|------|-----|---------------|-----------|-----|---------|----|-------|---------------|
| | | | | | Flexion | | | | Extension | | Lateral | | Axial | |
| | | | | | 1° | 2° | 5° | 8° | 1° | 2° | 1° | 5° | 1° | |
| Sleeping | 8 | 480 | 0 | 0 | 0 | 0 | 0 | 0 | 0 | 0 | 0 | 0 | 0 | |
| Walking | 1 | 60 | 80 | 4800 | 4800 | 0 | 0 | 0 | 4800 | 0 | 4800 | 0 | 4800 | |
| Sitting | 12 | 720 | 20 | 240 | 0 | 0 | 240 | 0 | 0 | 240 | 0 | 0 | 0 | |
| Standing | 2 | 120 | 0 | 0 | 0 | 0 | 0 | 0 | 0 | 0 | 0 | 0 | 0 | |
| Running | 0.25 | 15 | 120 | 1800 | 0 | 1800 | 0 | 0 | 1800 | 0 | 1800 | 0 | 1800 | |
| Sig Bending | 0.75 | 45 | 100 | 75 | 0 | 0 | 0 | 75 | 0 | 75 | 0 | 75 | 75 | Total per Day |
| Totals | 24 | 1440 | - | 6915 | 4800 | 1800 | 240 | 75 | 6600 | 315 | 6600 | 75 | 6675 | 27180 |
| | | | | | | | | Flexion Total | 6915 | | | | | |

Table 4.7 Estimates of daily activities, angular deflections and frequencies.

From the data in Table 4.7 it can be seen that the majority of the daily deflections occur in the sagittal plane (flexion and extension). The positive component (flexion) will have the greatest influence on the fatigue life of the implant, as it has the greatest number of daily excursions and the largest deflection range. By extrapolating the flexion data from Table 4.7 for 40 years of continuous service, as shown in Table 4.8, the fatigue requirements of the implant were determined.

| Required Deflection (Flexion) | Percentage | Number of Deflections over 40 years |
|--|-------------------|--|
| 1 degrees | 69.5% | 70 M |
| 2 degrees | 26.0% | 26 M |
| 5 degrees | 3.5% | 3.5 M |
| 8 degrees | 1% | 1 M |
| Total | | 100.5 M |

Table 4.8 Fatigue requirements of implant in flexion over 40-year life span.

This fatigue analysis relies on the assumption that the fatigue properties of the implant are not adversely affected by deflections in other directions. That is lateral deflections do not affect the flexion fatigue properties, and visa versa. It should be noted that this fatigue analysis yielded a similar total value to the 85 M specified by Kostuik³¹.

4.1.5 Materials

The primary consideration when selecting materials for a biomedical application is biocompatibility. That is, when implanted, the material selected should have no adverse effects on the bone or soft tissues, such as inflammation, degeneration, toxicity, immune response, carcinogenicity, or mutation, to list a few⁴.

For the purposes of this project the materials considered were limited to those that have already been well tested and proven commercially in other medical implant applications. This restricted the number of candidate materials available and eliminated many of the new implant grade alloys currently being developed. However, the use of unconventional or untested materials would increase the development costs and time span required, as more *in-vitro* testing would be required to ensure *in-vivo* compatibility.

The implant should also be designed to minimise, or preferably remove all together, articulating, contacting and gliding surfaces. As the surfaces of any contact couple move against each other small particles shear off the parent material. These small particles are referred to as wear debris.

The body's natural mechanisms can transport a small amount of polymer or metallic wear debris away from the implant site using the lymphatic system. However when thousands of sub-micron polymer particles are generated, for example with every step taken by a hip implant, the lymphatic system becomes overwhelmed. The particles that are not transported away from the joint capsule stimulate a macrophage induced inflammatory response that can lead to bone loss and subsequent implant loosening.

The severity of the reaction depends on the volume, size and reactivity of the particles and any biological incompatibilities with the debris. Cement particles were once exclusively blamed for such osteolysis. However research has shown that any particle debris can result in bone resorption^{48,54}. Therefore materials selected for any remaining contact couples should be chosen to maximise wear resistance.

Fatigue strength of the chosen material(s) is also of importance in order for the implant to meet the fatigue life of 100 million cycles previously specified in Section 4.1.4. For most materials this will require a design which results in stresses which are below the endurance strength of the material selected. However, cyclic testing of the chosen material(s) and complete implant will also be required to verify that the cumulative damage effects do not adversely affect the fatigue life of the implant.

Kostuik³¹ also identified that "*Galvanic corrosion is a concern if dissimilar metals are used*".

4.1.6 Geometry

Kostuik³¹ stated “The implant should be contained primarily within the normal disc space” to achieve this several factors must be considered including:

- Preservation of the intervertebral disc wedge angle
- Preservation of the annulus fibrosus
- Endplate size
- Disc height
- Allowance for projections
- In-growth of tissue

Preservation of the Intervertebral Disc Wedge Angle

As previously detailed in Section 2.7 the L5-S1 intervertebral disc and lumbar vertebral bodies are wedge shaped. The lumbar intervertebral discs are also placed in extension slightly at rest. Any intervertebral disc implant developed should therefore have endplates which match the intervertebral disc wedge angle or be capable of conforming to the required shape *in-vivo*.

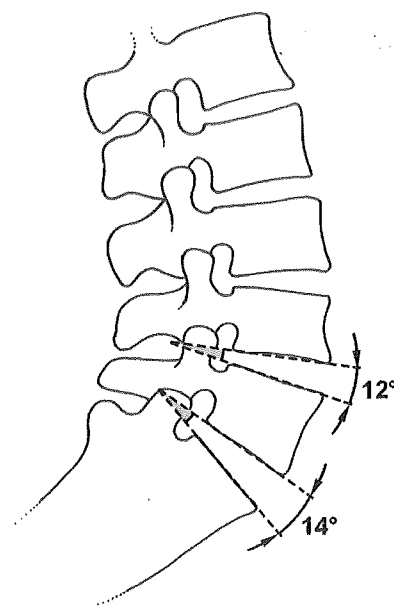


Figure 4.2 Intervertebral disc wedge angles.

[Source: Bogduk et al¹¹]

Several researchers have reported intervertebral disc wedge angles which were found by utilising measurements of the anterior and posterior disc height in combination with the sagittal diameter^{3,5,24,57}. These intervertebral disc wedge angles were typically reported for the spine in a neutral or un-deflected position. The L5-S1 level has the most pronounced wedge angle, with a mean size of 14.3°. The remainder of the lumbar intervertebral discs have a smaller wedge angle that increases from L1-2 to L4-5 as shown in Table 4.9. Figure 4.2 illustrates the wedge angles for the L4-5 and L5-S1 intervertebral discs.

| Level | Wedge Angle (Degrees) | |
|-------|-----------------------|------------|
| | Range (Deg) | Mean (Deg) |
| L1-2 | 6.7 – 11.3 | 9 |
| L2-3 | 5.1 – 11.0 | 9.2 |
| L3-4 | 5.5 – 13.6 | 10.4 |
| L4-5 | 10.4 – 14.4 | 12.0 |
| L5-S1 | 12.2 – 15.4 | 14 |

Table 4.9 Intervertebral disc wedge angles.

If devices are added to the intervertebral disc implant to restrict the range of motion in the sagittal plane (flexion and extension) they should not be affected by any pre-deformation of the implant, such as the implants' endplates being deflected to conform to the intervertebral disc wedge angle. Alternatively a range of implants with different wedge angles should be developed.

Preservation of Annulus Fibrosus

Ideally the majority of the annulus fibrosus should be preserved, as it performs several important functions as detailed below.

- With the nucleus pulposus removed the annulus fibrosus alone is capable of supporting virtually the same compressive loads as an intact intervertebral disc.
- The fibres of the annulus fibrosus limit distraction, sliding and bending movements of the intervertebral joint, thus preservation of the annulus fibrosus will help to ensure normal loading of the zygapophysial joints.
- The anterior fibres of the annulus fibrosus and to some extent the lateral portions, help to stabilize the lumbar lordosis.
- When an artificial disc is added to the spinal column and load is applied, the tapered endplates may cause the implant to displace anteriorly, effectively ejecting it from the disc space, as shown in Figure 4.3. If the anterior portion of the annulus fibrosus is retained it will prevent this from occurring by blocking the implant's path.

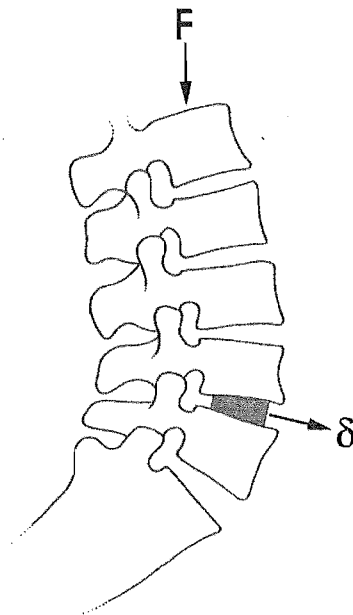


Figure 4.3 Ejection of the implant from the disc space.

The angular relationship between the vertebral bodies may result in an implant being ejected from the disc space when load is applied. Retaining the anterior portion of the annulus fibrosus will prevent this from occurring.

Therefore to preserve these natural load carrying, stabilising and motion-limiting mechanisms, any resection of the annulus fibrosus during the insertion of the implant should be minimised. However some resection of the annulus fibrosus is unavoidable during the insertion of artificial disc implants. The ideal site for resection is dependant on several factors.

The anterior portion of the annulus is normally healthy, free of deformities and makes a significant contribution to weight bearing, spinal stability and retaining the implant. An anterior approach also requires the anterior longitudinal ligament to be cut and the surgeon must operate through the abdominal chambers as detailed in Section 3.2.1. Therefore resection of the anterior portion of the annulus fibrosus should be avoided wherever possible.

The posterior portion of the annulus only makes a small contribution to spinal stability. However if a posteriorly inserted implant is used it must be small and compact to minimise the need to manipulate the nerve roots. Also such an implant should not require the posterior elements to be resected. These requirements make a posteriorly implanted intervertebral disc implant less viable and considerably more complex to design.

The lateral portions of the annulus fibrosus support some of the applied compressive loads and also help to stabilise the lumbar lordosis. However these contributions are small provided the zygapophysial joints and the anterior portion of annulus fibrosus are intact.

Therefore the most viable option is to resect and reflect one lateral wall of the annulus fibrosus to facilitate insertion of the intervertebral disc implant.

Endplate Size

The size of the lumbar vertebral endplates has been studied using radiographs^{24,28,42}, cadaveric specimens⁸, CT and MRI scans³. Figure 4.4 shows the vertebral body parameters that are normally measured. The results of these studies exhibit some variation depending on the disc level, age and sex of the patient. However, in general, the endplates tend to increase in size from T12 to S1, with the transverse diameter increasing approximately 15% and the sagittal diameter increasing approximately 10%. The transverse diameter has been found to range between 25-63 mm with an average dimension of 50 mm. The sagittal diameters reported range between 27-45 mm with an average of 35 mm.

As already detailed, the intervertebral disc implant should be contained within the normal disc space and the majority of annulus fibrosus should be preserved where possible. The anterior portion of annulus is approximately 7-10 mm thick, and the posterior portion is significantly thinner at 3-5 mm thick. Therefore the sagittal diameter of the implant should not exceed 25 mm.

The wall thickness of the annulus fibrosus decreases from the anterior portion to the lateral portions. Therefore given the lateral wall of the annulus is approximately 7.5 mm thick, the transverse diameter should be less than 35 mm.

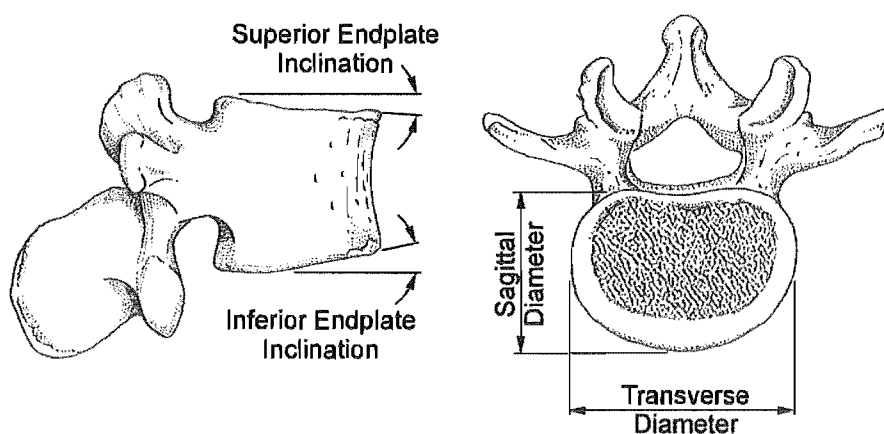


Figure 4.4 Vertebral body dimension parameters.

Figure 4.4 also shows the typical superior and inferior vertebral body inclinations. Panjabi et al⁴² reported a constant inclination of approximately 1.3° for both the superior and inferior endplates at all levels of the lumbar spine.

As detailed in Section 2.4.1.1 the vertebral bodies have high strength cortical bone on their periphery and less dense, soft spongiosa material at the centre. The mean failure load of the lumbar endplates has been found to range between 140-225 N at the periphery and 50 N in the central regions²⁵. The underlying vertebral cortical bone has also been found to have regional variations, with the strongest points closest to the pedicles^{6,25}.

The addition of an artificial disc will result in the load being carried by three structures - the vertebral body endplate, the trabecular bone and the implant endplate. If the implant does not transmit the normal physiological stresses to the adjacent tissues a detrimental response may occur. For example, if the surrounding bone is subjected to a stress lower than naturally experienced then bone resorption may occur. Conversely if the stress transmitted is greater than naturally experienced, bone deposition or stress fractures may result.

In the case of the intervertebral disc implant, if the implant-bone interface is too stiff the vertebral body will only be loaded at the outer edge of implant endplate while the central area of trabecular bone will be under-loaded. This redistribution, or change, in the stress profile is sometimes referred to as 'stress shielding'.

The implant should therefore exert the majority of the forces on the periphery of the vertebral body, with the remaining portion of the load distributed across the remainder of the endplate to ensure resorption of the underlying trabecular bone does not occur. To achieve this, the stiffness of the implant endplate should be minimised, allowing the implants endplates to conform to the vertebral body superior and inferior surfaces.

Disc Height

As previously described in Section 2.8 the spinal nerves exit the spinal canal through the intervertebral foramina, and it is at this point that the nerve roots are particularly vulnerable to compression³². Therefore maintenance of the disc height, especially the posterior aspect, is important. Long term restoration of the intervertebral disc height will also ensure correct loading of the zygapophysial joints^{11,31}.

The height of lumbar intervertebral discs has been studied by several researchers, using lateral radiographs, MRI and CT scans^{3,5,24,57}. The intervertebral disc height measurements were normally taken where the lateral dimension was largest, typically at the anterior edge of the disc. From these studies the intervertebral disc height was found to range between 6-14 mm with an average height of 10 mm.

Projections

Kostuik³¹ stated that, “Parts of the implant may project outside the normal disc space to provide short term fixation points. There should be provision for discs to be implanted at contiguous levels with no overlap of projections”. While interlocking projections could be utilised, the implant should ideally be fully contained within the disc space to avoid interference with the surrounding soft tissues. Also if interlocking projections are included in the final design these should not compromise the adjacent vertebral bodies. For example Figure 4.5 shows two designs for fixation protrusions, (a) shows a poor design which will result in splitting of the vertebral body if the implant is used at contiguous levels, (b) illustrates a better design which alleviates this issue.

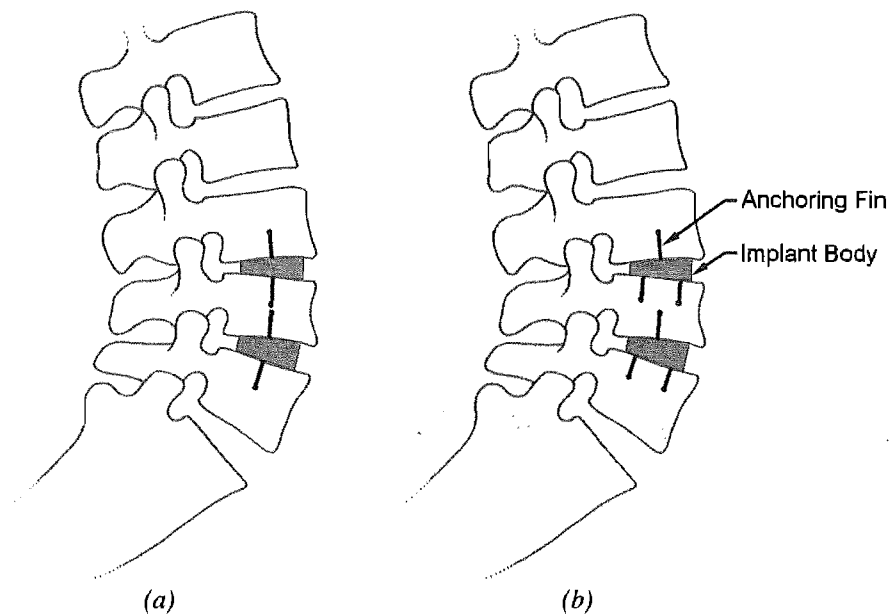


Figure 4.5 Allowance for using of the implant at contiguous levels.

- (a) Poor protrusion design, the vertebral body may split due to alignment of the anchoring fins.
 (b) Better alignment of the anchoring fins, by staggering the fins there is less chance of splitting the vertebral bodies.

In-growth of Tissue

Should biological material grow into the implant’s cavities, the implant should be able to continue operating with little or no loss of function. Alternatively the implant should prevent such in-growth from occurring. Periprosthetic ossification, or the growth of bone around the implant, may also occur and similarly this should be prevented or be of negligible importance.

Summary

The intervertebral disc implant must meet several geometry requirements. Where possible the majority of the annulus fibrosus should be preserved to take advantage of the natural load bearing and stabilising mechanisms; this is particularly relevant for the anterior portion of the annulus.

Ideally the implant should be inserted using a lateral approach to avoid compromising the annulus fibrosus and posterior elements of the vertebral bodies. Using such an approach the implant profile during the insertion procedure can potentially be as large as 25 x 10 mm (sagittal diameter x disc height). However the implant insertion dimensions should be minimised where possible so a small surgical window can be used.

Allowance must also be made for fixation to the adjacent vertebral bodies and the intervertebral disc wedge angle.

Figure 4.6 shows a summary of the key implant geometry requirements.

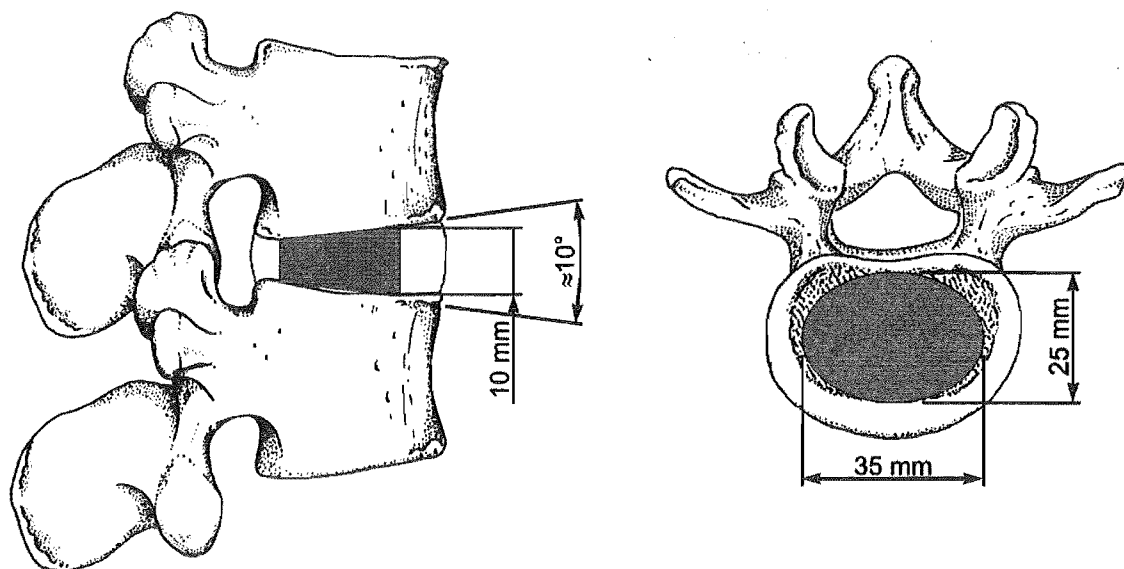


Figure 4.6 Summary of implant geometry requirements.

4.1.7 Stiffness

Kostuik³¹ identified that in order to replicate load transmission between vertebral levels the disc implant should “...duplicate fully the intact disc's stiffness in all three planes of rotation plus axial compression. Because of the predominance of sagittal plane motions in the lumbar spine; duplication of physiological stiffness in flexion and extension was deemed a critical aspect of design and a significant first step toward duplication of joint stiffness”.

Reported values for the stiffness and maximum load properties of healthy intervertebral discs are shown in Table 4.10.

| Testing Condition | Stiffness Coefficient | Maximum Load | Spine Region Measured | Reference |
|-------------------|-----------------------|--------------|-----------------------|----------------------------|
| Compression | 2.5 MN/m | 4500 N | Lumbar | Virgin ⁵⁹ |
| | 2.3 MN/m | 5300 N | Lumbar | Brown et al ¹² |
| | 1.8 MN/m | 1800 N | Thoracic & Lumbar | Markolf ³⁷ |
| Tension | 1.0 MN/m | 1800 N | Thoracic & Lumbar | Markolf ³⁷ |
| Shear | 0.26 MN/m | 150 N | Thoracic & Lumbar | Markolf ³⁷ |
| Flexion | 2.0 Nm/deg | 7 Nm | T7-8/L3-4 | Markolf ³⁸ |
| Extension | 2.6 Nm/deg | 7 Nm | T7-8/L3-4 | Markolf ³⁸ |
| Lateral Bending | 1.7 Nm/deg | - | Lumbar | Yamamoto ⁶² |
| Axial Rotation | 4.0 Nm/deg | 8 Nm | Lumbar | Farfan et al ²² |

Table 4.10 Average stiffness coefficients from representative functional spines.

If the stiffness of the intervertebral disc implant is significantly lower than the naturally occurring values the stability of the spinal column may be compromised. Conversely if the implant is too stiff additional exertion will be required for the patient to bend or the implant will act as a rigid body and all deflection will occur at the remaining spinal levels. Therefore the intervertebral disc implant should have stiffness coefficients similar to those found in a healthy lumbar spine.

If the implant is designed with directional stiffness, location and alignment features should be provided to ensure correct alignment of the implant *in-vivo*.

4.1.8 Fixation to Bone

Immediate and long-term fixation of the implant to the adjacent vertebral bodies is essential. There are several types of fixation device which could potentially provide the level of fixation required. These include screws, spikes, fins and in-growth of bone into porous coated or macro-textured surfaces.

Kostuik³¹ categorised these fixation methods as follows. *“Screws can be expected to provide adequate fixation for no more than 6 weeks. Press fit type fixation components (spikes, pegs, posts) are inadequate under tensile loading and also may be effective only for a relative short time. Porous coated and macro-textured surfaces require approximately 6 weeks of no or small amplitude motion to establish fibrous bone in-growth”*.

Consultation with an orthopaedic surgeon¹³ suggested that screws were capable of providing fixation over periods greater than six weeks, but that the level of fixation does degrade under high loads. If screws are used to provide fixation the implant should also incorporate locking mechanisms which result in the screws becoming an integral part of the implant, thus reducing the potential for wear debris generation.

Otherwise Kostuik's summary of the fixation techniques was considered to be accurate. The fixation system selected should therefore utilise a combination of some or all of these methods to ensure long-term fixation.

Adequate access to the fixation system during surgery should also be provided. For example, if screws are used to retain the implant there should be sufficient space for an insertion tool and visualisation of the screw head. Tooling may need to be developed to aid insertion and fixation of the implant. The fixation system should also allow for the use of the implant at contiguous levels, as detailed in Section 4.1.6.

4.1.9 Failsafe

Kostuik³¹ specified that, “*The device should be designed such that failure of different components of the implant will not cause catastrophic failure of the lumbar intervertebral joint or damage the surrounding nervous or vascular tissues. The integrity of the implants should be maintained in the event of an accident or an unexpected mechanical shock to the spine*”.

In order to ensure that these requirements are met any intervertebral disc implant developed should be extensively tested *in-vitro* prior to any clinical trials. These tests can, at least in part, be completed using test rigs that replicate all the loads and motions normally applied to a healthy spinal segment. The intervertebral disc implant should also be tested to destruction so that all the failure modes can be identified and analysed. In conjunction with a failure mode and effects analysis, the aim of these *in-vitro* studies should be verification that the implant is safe and reliable.

The surgical technique used to implant the device should be simple and repeatable such that consistent results can be achieved following adequate surgical training. Accurate positioning of the implant will also be critical to the success of the device. Accordingly any instrumentation developed to aid in the insertion of the device should provide adequate orientation and positional guides.

The final implant design should also allow for extraction should partial or catastrophic failure occur. If extraction is required the surrounding anatomy should not be compromised to a point where a standard spinal fusion cannot be carried out. Simple extraction procedures and tooling should also be developed as required to aid in the removal of the implant.

It should be noted that the design of surgical procedures and instrumentation would require extensive clinical consultation, and as such these tasks would be subsequent to verifying that the concept developed during this project is feasible.

4.1.10 Specification

Table 4.1 shows the final specification for the intervertebral disc implant. Each specification item is ranked as either being of high or low importance. This ranking allows critical implant features to be differentiated from features that are simply desires.

| Item | Importance |
|--|-----------------------|
| <i>Load Carrying Requirements</i> | |
| Support 60 kg nominal load | High - ⑤4 3 2 1 - Low |
| Support 120 kg maximum load | High - 5④3 2 1 - Low |
| <i>Motions Requirements</i> | |
| Flexion: 8° | High - ⑤4 3 2 1 - Low |
| Extension: 2° | High - ⑤4 3 2 1 - Low |
| Lateral bending: ±5° | High - ⑤4 3 2 1 - Low |
| Axial rotation: <1° | High - 5④3 2 1 - Low |
| Match physiological stiffness | High - 5④3 2 1 - Low |
| Features to prevent ROM and stiffness misalignment | High - 5 4③2 1 - Low |
| Prevent excessive deflection | High - 5 4 3②1 - Low |
| <i>Material Properties</i> | |
| Biocompatible material | High - ⑤4 3 2 1 - Low |
| Minimise wear debris generation | High - ⑤4 3 2 1 - Low |
| <i>Geometry Requirements</i> | |
| Maintain disc height | High - ⑤4 3 2 1 - Low |
| Cross section dimensions 25x35 mm (max) | High - 5④3 2 1 - Low |
| Height dimension 10 mm (max) | High - 5④3 2 1 - Low |
| Wedge Angle 9-14° | High - 5 4③2 1 - Low |
| Implant using lateral approach | High - 5 4③2 1 - Low |
| Allow for use at contiguous levels | High - 5 4③2 1 - Low |
| Minimise stiffness of implant endplates | High - 5 4 3②1 - Low |
| <i>Design Requirements</i> | |
| 40 year (100 million cycle) lifespan | High - ⑤4 3 2 1 - Low |
| Not fail catastrophically | High - ⑤4 3 2 1 - Low |
| Long-term anchoring to adjacent vertebral bodies | High - 5④3 2 1 - Low |
| Apply loads on periphery of adjacent vertebrae | High - 5④3 2 1 - Low |
| Simple surgical technique | High - 5④3 2 1 - Low |
| Preserve the anterior of the annulus | High - 5 4③2 1 - Low |
| No pinch points | High - 5 4③2 1 - Low |
| In-growth of tissue not affect implant performance | High - 5 4③2 1 - Low |
| Centre of rotation close to inferior endplate | High - 5 4 3②1 - Low |
| Allow for standard treatment if required | High - 5 4 3②1 - Low |

Table 4.11 Specification.

4.2 Artificial Discs

The idea of developing an intervertebral disc implant is not a new one. Several different styles of artificial disc have previously been developed and tested by other researchers. The designs developed can be grouped into the following categories, articulating, hydraulic and elastic. An explanation of each style of artificial disc follows, along with assessments of the implants that have been developed to date.

4.2.1 Articulating Discs

Articulating discs are defined as those having two or more components that slide relative to each other to provide the required motions. Articulating discs can be further categorised as those having polymer-metallic wear couples and those with metallic-metallic wear couples. Discs with a polymer-metallic wear couple are often referred to as composite discs.

The most commonly developed and clinical trialed discs are the polymer-metallic or composite wear couple variety. Typically these artificial discs have concave metallic endplates and a convex polymer insert. The most significant limitations of this type of disc are the generation of wear debris and cold flow or creep of the polymer insert.

The softer of the two articulating materials will be the predominant source of wear debris, which in the case of composite disc implants will be the polymer material. As previously discussed if there is sufficient volume wear debris a macrophage response may occur. This will in turn result in resorption of the surrounding bone stock and implant loosening. Currently only one articulating disc implant includes a sheath to contain any wear debris generated.

The compressive loads applied to composite discs may result in cold flow of the polymer insert with resulting loss of disc height leading to narrowing of the intervertebral foramina. In turn this may lead to compression of the nerve root and incorrect loading of the facet joints. Ultimately, if the polymer insert deforms enough, the implant endplates may not be able to slide freely over the insert surface causing the implant to have a reduced or complete loss of function.

Several metallic-metallic articulation or ball type artificial discs have also been developed for the lumbar spine. One of the first attempts to produce an artificial disc involved implanting stainless steel spheres in the intervertebral disc space. In 1966 Fernstrom²³ reported on 191 such implants in 125 patients. Subsidence occurred in 88% of patients during the 4 to 7 year follow up period.

Metallic-metallic articulating discs also suffer from the same wear debris issues that effect composite articulating discs, however with metallic discs the volume of wear debris generated does not tend to be as great.

Neither type of articulating discs have any capability for axial compression and as a result they are not able to retard shock loads as a healthy intervertebral disc would. Any shock loads applied are therefore transmitted directly to the adjacent intervertebral discs.

4.2.1.1 Link SB Charité Disc

The most widely implanted artificial disc to date is an articulating disc called the Link SB Charité disc, which is shown in Figure 4.7. This device is a composite disc consisting of a ultra high molecular weight polyethylene (UHMWPE) spacer and two metallic endplates and it is available in a variety of different sizes. It also features a ring around the periphery of the spacer to improve its visibility on x-rays.



Figure 4.7 Link SB Charité Disc.

[Source: <http://www.medscape.com/viewarticle/442451>]

One advantage of the Link SB Charité disc is that it has a ‘mobile sliding core’ as shown in Figure 4.8, which allows the rotation and translation movements of a healthy intervertebral disc to be approximated.

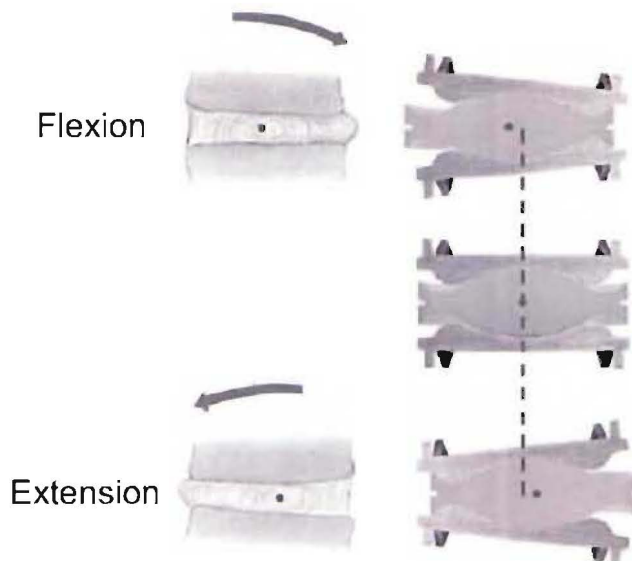


Figure 4.8 Link SB Charité Disc mobile sliding core.

[Source: Link³⁵]

The Charité disc has been implanted in over a thousand European patients with relatively good results. Additional clinical trials using the Charité III disc are ongoing in Europe, the United States, Argentina, China, Korea and Australia. A number of follow up studies have been reported by various authors.

David¹⁸ reported on 85 patients who received Charité disc implant(s). Five years post-implantation 68% of the patients had good or better results, while 16% of patients had poor results. Fourteen of the patients with poor results underwent secondary arthrodesis at the prosthesis level.

Griffith et al²⁶ reported the results of 93 patients 1 year post surgery, with the majority experiencing pain reduction and increased mobility, however 5.6% of patients experienced implant failure, dislocation or migration of the implant, three instance of UHMWPE ring deformation were also reported.

Lemaire et al³³ reported on 105 patients with a mean of 51 months of follow-up, 82% of patients experienced low back and radicular pain relief. The study also reported that 11 patients experienced complications including vascular problems, temporary neurological deficits, periprosthetic ossification, and implant settling.

The Charité disc is unable to prevent anterior translation of the vertebral bodies and as a result the zygapophysial joints may be abnormally loaded. Wear debris generation is another factor which needs to be considered when evaluating the Charité disc and opinion ranges from there being no wear debris issues³⁴ to these effects needing to be investigated further³⁹.

The loss of disc height due to deformation or cold flow of the UHMWPE spacer could also limit the long-term success of the Charité disc. Cold flow or plastic deformation of the UHMWPE spacer may occur as a result of the small contact patches between the endplates and spacer, the high compressive loads applied and the low compressive strength of the spacer when compared to the endplates. If such cold flow occurs it will affect the stiffness of the device and the rate at which wear debris is produced.

4.2.1.2 ProDisc

The ProDisc was developed in the late 1980's and is based on a composite spherical articulation. The implant consists of three pieces, two cobalt chromium molybdenum alloy endplates and a convex UHMWPE load-bearing surface. Figure 4.9 shows the implant in its assembled form. The convex UHMWPE bearing surface snap-fits into the inferior endplate.

The implant is attached to the vertebral bodies by a large central keel and two spikes on each endplate. Physiologically the ProDisc can match the ranges of motion of a normal spine in flexion, extension, axial rotation, and lateral bending, however the implant makes no allowance for axial compression.



Figure 4.9 ProDisc implant.

[Source: <http://www.medscape.com/viewarticle/442451>]

As the implant is modular the surgeon can customize the device to each patient's spine. There are two endplate sizes (medium and large), three heights of the polyethylene component (10, 12, and 14 mm), and two lordosis angles (6 and 11 degrees) available. This range of implant sizes allows the ProDisc to be used at L3-4, L4-5 or L5-S1 levels.

Between 1990 and 1993, 64 patients were implanted with the ProDisc implant. In 1999 the surviving 61 patients were extensively studied. At the time of these 7-11 year follow-ups all the implants were intact and functioning. There had been no implant removals, revisions or failures. No evidence of subsidence was seen on follow-up radiographs and 90.8% of patients were reported as having excellent results, 7.4% had good results and 1.8% had a fair result.⁹

Two-thirds of the patients had implants at a single spinal level while the remainder of the patients had multiple implants at adjacent levels. There was no difference in the outcome between the single and multi level implantations⁹. However if the implant is used at contiguous levels the alignment of the fixation keels could potentially cause the vertebral bodies to split, as previously discussed in 4.1.6.

A multi-centre trial of the ProDisc implant is currently in progress to compare the ProDisc to 360° (front and back) fusion using allograft in the intervertebral space and pedicle screws with autograft posteriorly. The ProDisc has been implanted in over 500 patients in Europe since December 1999 and a multi-centre FDA study was started in the United States in October 2001.⁶⁴

However as for the Link SB Charité disc the ProDisc implant has the potential for complications resulting from the production of wear debris and/or cold flow of the polymer bearing surface. ProDisc also makes no allowance for preventing anterior translation of the vertebral bodies, thus the zygapophysial joints may be subjected to additional loads.

4.2.1.3 Bryan Cervical Disc

The Bryan Cervical Disc System, shown in Figure 4.10, is another composite articulating disc. This design consists of a low friction, wear resistant, elastic nucleus with two circular titanium endplates. A flexible membrane forms a seal around the implant to contain a lubricant and to prevent the migration of wear debris. The implant allows normal ranges of cervical spine motion and comes in five sizes ranging from 14 to 18 mm in diameter.



(a)



(b)

Figure 4.10 Bryan Cervical Disc.

(a) Photograph of the Bryan Cervical Disc.

(b) Partially sectioned CAD model of Bryan Cervical Disc.

[Source (a): <http://www.medscape.com/viewarticle/442451>]

[Source (b): <http://www.spineuniverse.com/displayarticle.php/article1883.html>]

Initial clinical experience with the Bryan Total Cervical Disc Prosthesis has been reported as promising, with 51 patients being implanted. Twenty-six of the patients implanted were followed for 6 months, after this time 92% of these patients had good to excellent results with no significant subsidence or migration.^{55,58}

The nucleus of the Bryan disc will be subject to wear, which could limit the service life of the implant. However the Bryan disc has been tested under laboratory conditions to a total of 45 human equivalent years of neck movement with only a little wear noted⁵². The Bryan Cervical Disc also reduces the risks of aseptic loosening by containing any wear debris generated within the lubricant and flexible membrane. The membrane also serves to stop biological in-growth.

One of the key factors working in favour of the Bryan Cervical Disc is that it is designed for use in the cervical spine where the applied loads are significantly lower than those found in the lumbar spine. These lower loads will in turn help reduce the volume of wear debris that is generated and amount of cold flow that occurs.

4.2.1.4 Kostuik Disc

The Kostuik disc has metal on metal articulation surfaces and a hinge pin mechanism which allows it to provide full ranges of motion in the required directions. The implant consists of two hot isostatically pressed Cobalt Chrome endplates and two Ti-6Al-4V springs, as shown in Figure 4.11.

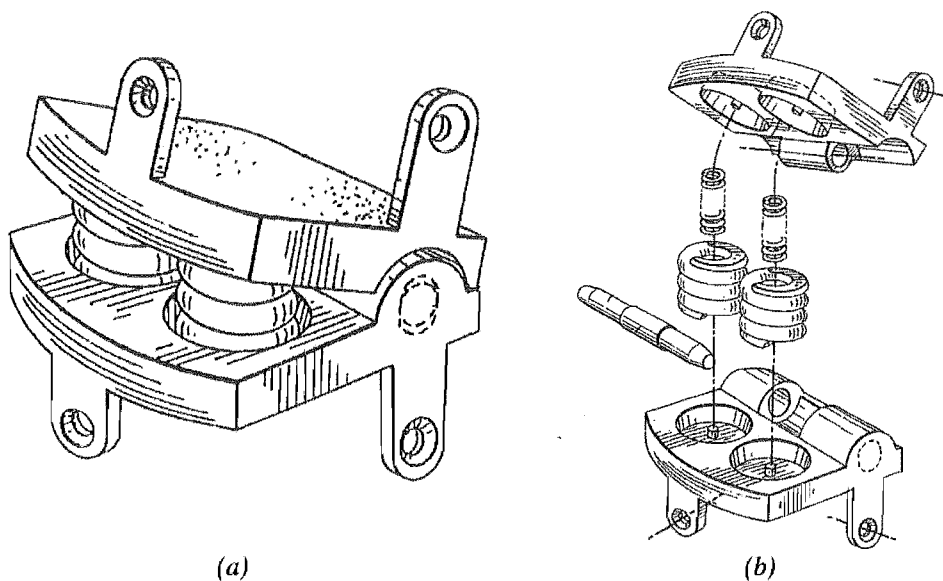


Figure 4.11 Kostuik Disc.

(a) Assembled view.

(b) Exploded view showing the hinge pin and springs.

[Source: US Patent 4,759,769]

The disc is able to rotate around the hinge pin to provide the flexion and extension movements. The ends of the hinge pin also decrease in diameter and the pin holes are elongated which allows 3-6° of lateral flexion to occur. The Kostuik disc also features two springs which are intended to duplicate the intervertebral discs stiffness in flexion and extension.

The implant is rigidly anchored to the intervertebral bodies using cortical bone screws. Spikes on the endplate also act to prevent implant migration and the endplates are porous coated to provide long term rigid fixation.

There are however, a number of potential sources of wear debris with this implant design. Schmiedberg et al⁴⁹ tested the implant and found the spring pocket interfaces accounted for 90% of the wear debris generated. On average, the hot isostatically pressed CoCr spring-pocket interfaces were found to produce 2.889 mm³ of wear debris per million cycles. Forged CoCr spring-pocket interfaces were found to produce 1.216 mm³ per million cycles⁴⁹. These values are higher than those typically seen for Metasul hip implants⁴⁸.

There are also a number of sites where biological in-growth into the implant mechanisms may occur.

Six *in-vivo* trials have been conducted in sheep. After periods of three and six months the soft tissue samples from these trials showed no signs of giant cell reaction and no foreign bodies or foreign body reaction were detected³¹. No human clinical trials of this implant have been reported to date.

4.2.1.5 Bristol Cervical Disc

The Bristol disc, originally developed in Bristol, England, has a ball and socket articulation and is made entirely of stainless steel. It is secured to the vertebrae with screws and allows unconstrained motion in all axes of rotation.

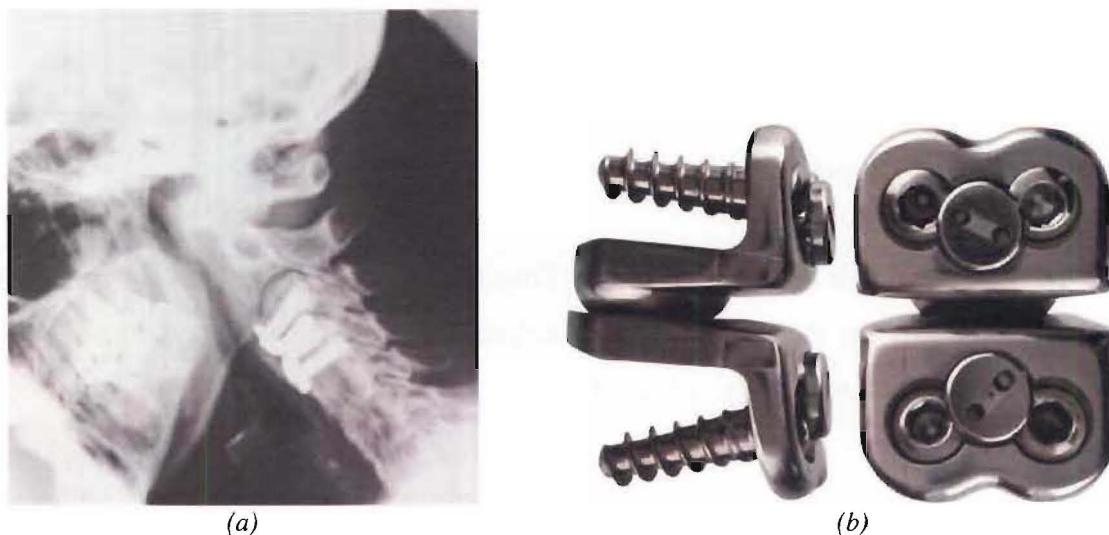


Figure 4.12 Bristol Cervical Disc.

(a) Lateral cervical radiographs demonstrating the Bristol disc in flexion.

(b) Photographs of the Bristol disc. Left: Lateral view. Right: Anterior view.

[Source: <http://www.medscape.com/viewarticle/442451>]

The clinical results for 20 patients with a mean follow-up period of 2.4 years were reported by Cummins et al¹⁷. Patients with radiculopathy improved, and those with myelopathy either improved or their symptoms stabilized. Two screws broke and there were two cases of minor screw back-out; further surgery was not required in these patients.

One joint was removed because it was loose, a failure that was thought to be due to a manufacturing error. At the time of removal, the joint was firmly attached to the bone and was covered anteriorly by a smooth scar. A detailed examination revealed that the surrounding tissues did not contain any significant wear related debris.

Joint motion was preserved in all but two patients. Both of these patients had undergone implantation of the device at the C6-7 level and in these cases the implant was so large that the facets were completely separated. This size mismatch was thought to be the reason motion was not maintained. No subsidence of the disc was reported. As per the Bryan Cervical Disc the Bristol Disc is only intended for use in the cervical spine where the applied loads are lower than those found in the lumbar spine. If exposed to higher loads, such as in the lumbar spine, such an implant design may exhibit wear and fatigue related problems.

It should be noted that the Bristol Cervical Disc incorporates locking screws which are intended to constrain the fixation screws helping to prevent the generation of wear debris at the fixation screw/implant interface.

The device is currently being manufactured in an assortment of sizes and additional clinical studies are being conducted in Europe and Australia.

4.2.2 Hydraulic Discs

Hydraulic disc designs attempt to recreate the natural intervertebral disc mechanisms detailed in Section 2.5.2.1. These discs consist of a fixed volume of fluid surrounded by a flexible, high strength outer skin.

When a compressive weight is applied to a hydraulic disc the fluid pressure rises exerting a radial load on the outer skin. The radial pressure in the fluid braces the outer skin and the pressure on the endplates transmits the load from one vertebral body to the next. During angular deflections of a hydraulic disc the outer skin in the direction of movement is compressed and buckles while the skin on the opposite side is stretched.

Hydraulic discs have several advantages - they can be fully contained within the disc space and they can absorb shock loads provided either the fluid is compressible or the outer skin has some resilience.

4.2.2.1 Prosthetic Disc Nucleus

The most widely studied nucleus replacement is the Prosthetic Disc Nucleus (PDN) with over 550 patients having been treated with this implant. The PDN replicates the physiological functions of the nucleus and can restore disc space height. It is also the only artificial disc implant currently available which allows the majority of the annulus fibrosus to be preserved.

The PDN consists of a hydrogel core constrained within a woven polyethylene jacket and is available in 5, 7 and 9 mm sizes. It is available in a wedge-shaped anterior configuration and a rectangular posterior configuration, as shown in Figure 4.13.

Before being implanted, the PDN is compressed and dehydrated to minimize its size. Once implanted, the woven outer cover allows fluid to pass through to the core, which immediately begins to absorb fluid and swell. Most of the expansion takes place in the first 24 hours after surgery, although it takes 4-5 days for the hydrogel core to reach its maximum expansion. Placement of two PDN implants within the disc space provides sufficient lift to restore and maintain disc space height in most patients.

Another advantage of the PDN is that it is the only artificial disc that can distract the intervertebral disc space. This distraction capability allows the Prosthetic Disc Nucleus to be implanted into disc spaces as small as 5 mm.

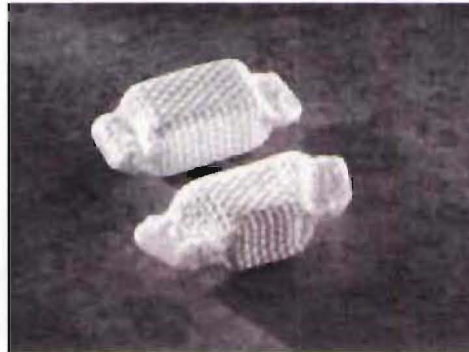


Figure 4.13 Prosthetic Disc Nucleus (PDN).

[Source: <http://www.medscape.com/viewarticle/442451>]

In-vitro fatigue testing of the device has been performed at loads ranging between 200 N and 800 N for 50 million cycles, with the device continuing to function as intended⁴⁷. However it should be noted that a test load of this magnitude only accounts for the loads applied during quiet standing. Therefore the results obtained may differ when the implant is subjected to higher loads for example those that occur during bending or lifting.

Schönmayr et al⁵⁰ reported on 10 patients treated with the PDN with a minimum of 2 years of follow-up data, segmental motion was preserved all in cases. Migration of the implant occurred in three patients, but only one required corrective surgery.

In a further study of 243 patients, Bertagnoli et al¹⁰ noted marked improvement in most patients, however they also noted that implant migration was the primary source of complications. Moderate endplate remodelling was also observed in the majority of patients with the endplates adapting to the contours of the implants. In a few cases extreme remodelling resulted in a loss of disc height. This remodelling is probably due to changes in the load distribution on the endplates.

Further clinical evaluations of this implant are being conducted in Europe, South Africa and the United States.

4.2.3 Elastic Discs

Elastic discs rely on the deformation of an elastic material to provide the required angular motions and vertical compression.

The elastic compound used must have sufficient stiffness to support the applied compressive loads but remain soft enough to allow the angular movements. If the compound is too stiff additional exertion will be required for the patient to bend. Conversely if the elastic compound is too soft spinal stability may be compromised or cold flow of the elastomer may occur.

A number of elastic disc concepts have been patented, however only one has been developed and clinically trialed.

4.2.3.1 Acroflex Disc

The Acroflex Disc uses a hexane based polyolefin rubber core vulcanised to two titanium endplates²⁰ and is only able to function correctly if there is good osteo-integration of the endplates.

The results of initial clinical trials with this device were mixed. Six patients received the Acroflex disc and were evaluated after a minimum of 3 years. At the time of evaluation the outcomes were reported as: 1 excellent, 2 good, 1 fair, and 2 poor. One of the patients with a poor result developed a tear in the rubber at the junction of the vulcanisation²⁰.

The second generation Acroflex-100 has since been developed. This later model implant consists of an HP-100 silicone elastomer core bonded to two titanium endplates and is shown in Figure 4.14. Although additional patients have undergone implantation of the Acroflex-100, the outcomes of these clinical trials have not been published²¹.



Figure 4.14 Acroflex Disc.

[Source: <http://www.medscape.com/viewarticle/442451>]

4.3 Summary

A number of artificial discs have previously been developed for the lumbar spine. While some of these discs have been successfully trialed none meet all the criteria laid out in the specification component of this chapter.

The focus of this project was therefore to develop a new intervertebral disc implant which meets all of the specification requirements. Particular focus was paid to developing an implant that minimised or preferably eliminated all wear debris generation. This decision effectively ruled out the use of articulating discs. However a number of new elastic and hydraulic disc concepts were developed, as detailed in Chapter 5.

4.4 References

1. *Statistics for 1995 HCUP-3 Nationwide Inpatient Sample, by expanded CCHPR diagnosis (principle diagnosis only)*. 1995, Agency for Healthcare Research and Quality Rockville, USA www.ahrq.gov.
2. Adams M A, Hutton W C, *The mechanical function of the lumbar apophysial joints*. Spine, 1983. Vol 8: pp 327-330.
3. Aharinejad S, Bertagnoli R, Wicke K, Firbas W, Schneider B, *Morphometric analysis of vertebrae and intervertebral discs as a basis of disc replacement*. Am J Anat, 1990. Vol 189 (1): pp 69-76.
4. American Society for Testing and Materials, *F981 - Standard Practice for: Assessment of Compatibility of Biomaterials for Surgical Implants with Respect to Effect of Materials on Muscle and Bone*. ASTM Standards, 2002, ASTM: Philadelphia. pp 344-348.
5. Amonoo K H, *Morphometric changes in the heights and anteroposterior diameters of the lumbar intervertebral discs*. J Anat, 1991. Vol 175: pp 159-68.
6. Amstutz H C, Sissons H A, *The Structure of the Vertebral Spongiosa*. J Bone Joint Surg Br, 1969. Vol 51: pp 540-550.
7. Berkson M H, Nachemson A, Shultz A B, *Mechanical Properties of Human Lumbar Spine Motion Segments - Part II: Responses in Compression and Shear, Influence of Gross Morphology*. Journal of Biomechanical Engineering, 1979. Vol 101: pp 53-57.
8. Berry J L, Morgan J M, Berg W S, Steffee A D, *A morphometric study of human lumbar and selected thoracic vertebrae*. Spine, 1987. Vol 12 (4): pp 362-7.
9. Bertagnoli R, Kumar S, *Indications for full prosthetic disc arthroplasty: A correlation of clinical outcome against a variety of indications*. Eur Spine J, 2002. Vol 11 (Suppl 2): pp S131-S136.
10. Bertagnoli R, Schönmayr R, *Surgical and clinical results with the PDN prosthetic disc-nucleus device*. Eur Spine J, 2002. Vol 11 (Suppl 2): pp S143-S148.
11. Bogduk N, Twomey L T, *Clinical Anatomy of the Lumbar Spine*. 1987, New York: Churchill Livingstone.
12. Brown T, Hanson R, Yorra A, *Some mechanical tests on the lumbo-sacral spine with particular reference to the intervertebral discs*. J Bone Joint Surg, 1957. Vol 39A: pp 1135.
13. *Personal Communication*, Burn J. *Implant Requirements*, Christchurch, 1 May 2002.

14. *Personal Communication, Discussion: Burn J. Review of Implant Requirements*, Christchurch, 21 May 2003.
15. Callaghan J P, Patla A E, McGill S M, *Low back three-dimensional joint forces, kinematics, and kinetics during walking*. *Clinical Biomechanics*, 1999. Vol 14 (3): pp 203-216.
16. Clauser C E, McConville J T, Young J W, *Weight, Volume and Centre of Mass of Segments of the Human Body. AMRL Technical Report (TR-69-70)*. 1969, Wright-Patterson Air Force Base, OH
17. Cummins B H, Robertson J T, Gill S S, *Surgical experience with an implant cervical joint*. *J Neurosurg*, 1998. Vol 88: pp 943-948.
18. David T H, *Lumbar disc prosthesis: a study of 85 patients reviewed after a minimum follow-up period of five years*. *Rachis Revue de Pathologie Vertebrale*, 1999. Vol 11 (4-5).
19. Dvorak J, Panjabi M M, Chang D G, Theiler R, Grob D, *Functional Radiographic Diagnosis of the Lumbar Spine*. *Spine*, 1991. Vol 16 (5): pp 562-571.
20. Enker P, Steffee A, Mcmillin C, *Artificial disc replacement. Preliminary report with a 3-year minimum follow-up*. *Spine*, 1993. Vol 18: pp 1061-1070.
21. Enker P, Steffee A D, *Total disc replacement*, in Bridwell K H and DeWald R L (Eds). *The Textbook of Spinal Surgery*, 1997, Lippincott-Raven: Philadelphia. pp 2275-2288.
22. Farfan H F, Cossette J W, Roberston G H, Wells R V, Kraus H, *The Effect of Torsion on the Lumbar Intervertebral Joint: The Role of Torsion in the Production of Disc Degeneration*. *J Bone Joint Surg*, 1970. Vol 52A: pp 468-497.
23. Fernstrom U, *Arthroplasty with intercorporal endoprosthesis in herniated disc and in painful disc*. *Acta Chir Scand*, 1966. Vol Suppl 357: pp 154-159.
24. Gilad I, Nissan M, *A study of vertebra and disc geometric relations of the human cervical and lumbar spine*. *Spine*, 1986. Vol 11 (2): pp 154-7.
25. Grant J P, Oxland T R, Dvorak M F, *Mapping the Structural Properties of the Lumbrosacral Vertebral Endplates*. *Spine*, 2001. Vol 26 (8): pp 889-896.
26. Griffith S L, Shelokov A P, Buttner-Janzen K, LeMaire J P, Zeegers W S, *A multicenter retrospective study of the clinical results of the LINK SB Charité intervertebral prosthesis. The initial European experience*. *Spine*, 1994. Vol 19: pp 1842-1849.
27. Hakim N S, King A I. 1976. *Static and dynamic facet loads*. *Proceedings of the Twentieth Stapp Car Crash Conference*. pp 607-39.

28. Hall L T, Esses S I, Noble P C, Kamaric E, *Morphology of the lumbar vertebral endplates*. Spine, 1998. Vol 23 (14): pp 1517-23.
29. Hatze H, *A Mathematical Model for the Computational Determination of Parameter Values of Anthropometric Segments*. J Biomechanics, 1980. Vol 13: pp 833-43.
30. Hsieh C-Y J, Pringle R K, *Range of Motion of the Lumbar Spine Required for Four Activities of Daily Living*. Journal of Manipulative and Physiological Therapeutics, 1994. Vol 17 (6): pp 353-358.
31. Kostuik J P, *Intervertebral Disc Replacement*. Clinical Orthopaedics and Related Research, 1997. (337): pp 27-41.
32. LeClercq T, Kruse J J, Awasthi D. *Lumbar Interbody Fusion with Titanium Cages: Five Year Follow-Up*. Department of Neurosurgery; Louisiana State University Medical Center; New Orleans, Louisiana, [cited Apr 2003]. Available from <http://www.medschool.lsumc.edu/Nsurgery/PLIFcages.html>.
33. Lemaire J P, Skalli W, Lavaste F, Templier A, Mendes F, Diop A, Sauty V, Laloux E, *Intervertebral disc prosthesis. Results and prospects for the year 2000*. Clinical Orthopaedics and Related Research, 2000. Vol 337 (April): pp 64-76.
34. Link H D, *LINK SB Charité III Intervertebral dynamic disc spacer*. Rachis Revue de Pathologie Vertébrale, 1999. Vol 11.
35. Link H D, *History, design and biomechanics of the Link SB Charité artificial disc*. Eur Spine J, 2002. Vol 11 (Suppl 2): pp S98-S105.
36. Lorenz M, Patwardhan A, Vanderby R, *Load-bearing characteristics of lumbar facets in normal and surgically altered spinal segments*. Spine, 1983. Vol 8: pp 122-30.
37. Markolf K L. 1970. *Stiffness and damping characteristics of the thoracic-lumbar spine*. Proceedings of Workshop on Bioengineering Approaches to Problems of the Spine, NIH. pp.
38. Markolf K L, *Deformation of the Thoracolumbar Intervertebral Joint in Response to External Loads: A Biomechanical Study using Autopsy Material*. J Bone Joint Surg, 1972. Vol 54A: pp 511-533.
39. Martz E O, Goel V K, Pope M H, Park J B, *Materials and design of Spinal Implants - A Review*. Journal of Biomedical Materials Research, 1997. Vol 38 (3): pp 267-288.
40. Nachemson A L, Schultz A B, Berkson M H, *Mechanical Properties of Human Lumbar Spine Motion Segments: Influence of Age, Sex, Disc Level and Degeneration*. Spine, 1979. Vol 4: pp 1-8.

41. Nigg B M, *Inertial Properties of the Human or Animal Body*, in Nigg Benno M and Herzog Walter (Eds). *Biomechanics of the Musculo-Skeletal System*, 1994, John Wiley & Sons: Chichester. pp 337-64.
42. Panjabi M M, Goel V, Oxland T, Takata K, Duranceau J, Krag M, Price M, *Human lumbar vertebrae. Quantative three-dimensional anatomy*. Spine, 1992. Vol 17 (3): pp 299-306.
43. Pearcy M J, *Stereo Radiography of the Lumbar Spine Motion*. Acta Orthop Scandinav, 1985. Vol Supp 212: pp 1-41.
44. Pearcy M J, Bogduk N, *Instantaneous Axes of Rotation of the Lumbar Intervertebral Joints*. Spine, 1988. Vol 13: pp 1033-1041.
45. Pearcy M J, Portek I, Sheppard J, *Three-Dimensional Analysis of Normal Movement in the Lumbar Spine*. Spine, 1984. Vol 9: pp 294-297.
46. Pearcy M J, Tibrewal S B, *Axial Rotation and Lateral Bending in the Normal Lumbar Spine Measured by Three-Dimensional Radiography*. Spine, 1984. Vol 9 (6): pp 582-587.
47. Ray C D, *The PDN prosthetic disc-nucleus device*. Eur Spine J, 2002. Vol 11 (Suppl 2): pp S137-S142.
48. Rieker C, Windler M, Wyss U, eds. *Metasul: A Metal-on-Metal Bearing*. 1999, Hans Huber.
49. Schmiedberg S K, Chang D H, Frondoza C G, Valdevit A D, Kostuik J P, *Isolation and characterization of metallic wear debris from a dynamic intervertebral disc prosthesis*. Journal of Biomedical Materials Research, 1994. Vol 28 (11): pp 1277-1288.
50. Schonmayr R, Busch C, Lotz C, Lotz-Metz G, *Prosthetic disc nucleus implants: The Wiesbaden feasibility study - 2 years follow-up in ten patients*. Rivista Di Neuroradiologia, 1999. Vol 12 Suppl. 1: pp 163-170.
51. Schultz A B, Warwick D N, Berkson M H, Nachemson A L, *Mechanical Properties of Human Lumbar Spine Motion Segments - Part I: Response in Flexion, Extension, Lateral Bending, and Torsion*. Journal of Biomechanical Engineering, 1979. Vol 101: pp 46-52.
52. Sekhon L. *Artificial Disc Surgery in the cervical spine*. SpineUniverse.com, Updated: 18 Feb 2003 [cited May 2003]. Available from <http://www.spineuniverse.com/displayarticle.php/article2035.html>.
53. Shirazi-Adl A, *Biomechanics of the Lumbar Spine in Sagittal/Lateral Moments*. Spine, 1994. Vol 19 (21): pp 2407-2414.

54. Sinha R, Peris M. *The Effects of Osteolysis and Aseptic Loosening*. MedScape, Updated: 17 Jan 2001 [cited Mar 2003]. Available from <http://www.medscape.com/viewarticle/418875>.
55. Spenciner D. *Byran Cervical Disc Prosthesis*. Brown University, [cited Mar 2003]. Available from <http://bms.brown.edu/curriculum/b108/discs/Bryan.htm>.
56. Taylor N F, Evans O M, Goldie P A, *Angular movements of the lumbar spine and pelvis can be reliably measured after 4 minutes of treadmill walking*. *Clinical Biomechanics*, 1996. Vol 11 (8): pp 484-486.
57. Tibrewal S B, Pearcy M J, *Lumbar intervertebral disc heights in normal subjects and patients with disc herniation*. *Spine*, 1985. Vol 10 (5): pp 452-4.
58. Traynelis V, Haid R W J. *Spinal Disc Replacement: The Development of Artificial Discs*. *Spine Universe*, Updated: 30 Apr 2002 [cited Mar 2003]. Available from <http://www.spineuniverse.com/displayarticle.php/article501.html>.
59. Virgin W, *Experimental investigations into the physical properties of intervertebral disc*. *J Bone Joint Surg*, 1951. Vol 33B: pp 607.
60. White A A, Panjabi M M, *Clinical biomechanics of the spine*. 2nd Edition. 1990, Philadelphia: Lippincott Williams & Wilkins Publishers.
61. Whittle M W, Levine D, Pharo E C, *Sagittal plane motion of the pelvis and lumbar spine during level, uphill and downhill walking and running*. *Gait and Posture*, 2000. Vol 11: pp 162-163.
62. Yamamoto I, Panjabi M M, Crisco T, Oxland T, *Three-Dimensional Movements of the Whole Lumbar Spine and Lumbosacral Joint*. *Spine*, 1989. Vol 14 (11): pp 1256-1260.
63. Zatziorsky V, Seluyanov V, *The Mass and Inertia Characteristics of the Main Segments of the Human Body*, in Matsui H and Kabayashi K (Eds). *Biomechanics VIII-B*, 1983: Champaign, IL. pp 1152-9.
64. Zigler J. *Lumbar Artificial Disc Surgery for Chronic Back Pain*. *Spine-health.com*, Updated: 1 July 2002 [cited May 2003]. Available from <http://www.spine-health.com/research/discupdate/artificial/artificial01.html>.

Chapter 5 – Conceptual Design

This chapter details the generation and evaluation of conceptual designs for the intervertebral disc implant.

5.1 Conceptual Design Process

To develop a design specification of any product, the task must be accurately expressed in terms which are easily understood. This often requires the problem statement to be broken down and associated with previous knowledge. Naturally during this process some conceptual designs are generated.

Once the specification has been developed there can be a tendency to take a favourite idea and start to refine and develop it as the final design. However, this is a weak methodology and can lead to resources being expended on concepts which are not optimal. A better practice is to generate as many conceptual designs as possible and then evaluate each concept in relation to the design specification before making a final selection for further development.

5.1.1 Concept Generation

Several concept generation methods were used during this project, a brief description of each follows.

- *Brainstorming* is a group orientated exercise, during which group members contribute unique ideas and build on ideas suggested by others. All of the ideas generated are recorded. One of the key elements of brainstorming is that ideas are not evaluated or criticised, in fact wild and outlandish ideas are often encouraged as they can lead to new trains of thought and thus the development of new and original concepts.
- *Incubation* occurs in the subconscious mind. When presented with a problem that cannot be readily solved, the subconscious mind continues to seek a solution after the initial period of thought has ended. Given the problem and an array of facts and past experiences the mind is able to form a variety of shifting, continually changing solutions. When a workable solution is found a picture is flashed into the conscious mind¹.
- *Patents*. Searching patents can yield good ideas, however there are several potential problems with this method. It can be hard to find or interpret the appropriate material and interesting concepts which do not directly relate to the problem can be distracting².
- *Discussions with outside parties* can also lead to the development of new concepts. People outside the development group are often able to see the overall picture from a new perspective and can come up with new ideas accordingly. Discussions with experts in the field can also help generate new ideas based on previous knowledge they have acquired. However, this method can have drawbacks as experts may sometimes dismiss a potential solution because it has not been done before or is considered to be unconventional.
- *Evolution* or the merging of previously generated ideas can also lead to new concepts being developed.

5.1.2 Refinement and Initial Design

Once the generation of conceptual designs has been completed the concepts can be refined as required. The aim of this task is to identify designs which have merit and discard those which are impractical or are technically unsound.

If brainstorming has been used as a method of generating concepts then there may be some concepts which can be quickly discarded as being impractical. However, some concepts may require rudimentary analysis to determine if they are viable.

The refinement of ideas and initial design work can also lead to new concepts being developed as the potential of each concept is fully realised.

5.1.3 Evaluation

During the evaluation of the concept designs the goal is to select the concept(s) which has the greatest probability of succeeding while minimising the effort expended.

There are many methods for evaluating engineering conceptual designs. One of the most common systems is to break the design specification into sub-tasks and weight the importance of each item. Once this has been done, each concept can be evaluated by scoring its effectiveness in fulfilling each sub-task. By multiplying the task weighting and the concept's score a total can be found for each design, as shown in Table 5.1. The concept which achieves the highest score should have the highest likelihood of meeting all of the design requirements.

| | Load 5 | Size 1 | Wear 3 | Total |
|-----------|-----------|-----------|-----------|-------|
| Concept A | 10 50 | 7 7 | 1 3 | 60 |
| Concept B | 4 20 | 6 6 | 8 24 | 50 |
| Concept C | 2 10 | 3 3 | 5 15 | 28 |

Table 5.1 Sample evaluation table.

Note: each sub-task is score against a common total. In this case each score is out of 10.

This method of selecting a final design can also highlight any areas of the selected design which need additional work. For example in Table 5.1, Concept A achieves the highest overall total but the low score for the wear component indicates that this area needs further development.

It should be noted however, that this evaluation method does rely on the specification correctly identifying all the requirements and on the assignment of appropriate weights and scores. However, other evaluation systems also suffer from similar issues. For the purposes of this project, in the author's opinion, an objective view was taken during the evaluation process and an effort was made to avoid favouring any of the concepts.

5.2 Conceptual Design of the Intervertebral Disc Implant

As detailed in Section 4.1.5 wear particles can trigger a macrophage cellular response which can lead to inflammation and the resorption of bone. For this reason a key decision was made at the time of generating the intervertebral disc implant specification and conceptual designs to develop an implant which produced no wear debris. The implant was therefore required to have no sliding or articulating components. This decision was made in spite of a number of articulating implants having already been developed by other researchers. However, as discussed in Section 4.2.1 these implants can be prone to wear debris generation issues. This decision did restrict the number and type of concept designs that were generated though.

The conceptual designs that were generated are shown in Appendix 1. These designs can be subdivided into three groups: metallic springs, hydraulic devices and elastomer devices.

During the refinement of the metallic spring concepts it became clear that the material properties would play an important role. Accordingly the properties of Titanium, Stainless Steel and Nitinol alloys were investigated as detailed in Appendices 2 to 4. Table 5.2 shows some of the key mechanical properties for the materials investigated.

| | Density (g/cm ³) | Young's Modulus (GPa) | Yield Strength (MPa) | Fatigue Strength (MPa) |
|---------------------------|---------------------------------|--------------------------|---------------------------|---------------------------|
| Ti-6Al-4V | 4.428 | 105-116 | 870 | 575 (a) |
| CP Titanium Grades 1-4 | 4.51 | 103-107 | 200-480 (b) | 300-350 |
| 316L Stainless Steel | 7.95 | 195 | 800-950 | 260 |
| Nitinol | 6.45 | 40 (c) 75 (d) | 195-790 (c) 70-140 (d) | 250 (e) |

Table 5.2 Key mechanical properties of the materials investigated.

Where: (a) Fine duplex microstructure.

(b) Increasing from 200 MPa for Grade 1 to 480 MPa for Grade 4 Commercially Pure Titanium.

(c) Austenitic phase.

(d) Martensitic phase.

(e) Stress controlled fatigue with an endurance limit of 10^6 cycles.

The stiffness and peak stresses for each metallic spring concept were then determined. A sample analysis of the z-spring concept is shown in Appendix 5. These investigations revealed that the main issue with the metallic spring concepts was that if they fulfilled the angular stiffness requirements then they had insufficient strength to support the applied loads. Conversely, if the spring concepts were strong enough to support the applied loads then their stiffness was too high and they would not allow any significant deflections to occur. Therefore all of the metallic spring concepts were determined to be unworkable.

The final design was therefore selected from the remaining pool of hydraulic and elastomer conceptual designs using the evaluation method detailed in Section 5.1.3. Evaluation sub tasks were determined from the specification developed in Chapter 4 and are detailed in Appendix 6. Of the concepts evaluated the fluid filled bellows was found to be the most viable solution, as shown in Table 5.3.

The decision was therefore made to proceed with developing an intervertebral disc implant based on the fluid filled bellows concept.






| | | Support Loads | Motions | Match Stiffness | Wear Debris | Endplate | Cross Section | Disc Height | Axis of Rotation | 40 Year Life | Total |
|-----------------------------|--|---------------|----------|-----------------|-------------|----------|---------------|-------------|------------------|--------------|-------|
| | | 5 | 4 | 4 | 5 | 3 | 3.5 | 4.5 | 2 | 4 | |
| <i>Fluid Filled Bellows</i> |  | 8 40 | 10 40 | 2 8 | 10 50 | 8 24 | 5 17.5 | 9 40.5 | 5 10 | 8 32 | 262 |
| <i>Urethane Spiral</i> |  | 5 25 | 8 32 | 8 32 | 4 20 | 4 12 | 10 35 | 3 13.5 | 5 10 | 6 24 | 203.5 |
| <i>Urethane Block</i> |  | 5 25 | 6 24 | 6 24 | 10 50 | 6 18 | 9 31.5 | 3 13.5 | 4 8 | 6 24 | 218 |
| <i>Urethane Annulus</i> |  | 5 25 | 8 32 | 8 32 | 2 10 | 8 24 | 5 17.5 | 3 13.5 | 5 10 | 6 24 | 188 |
| <i>Urethane Balls</i> |  | 5 25 | 4 16 | 4 16 | 2 10 | 6 18 | 10 35 | 3 13.5 | 2 4 | 6 24 | 161.5 |

Table 5.3 Intervertebral disc evaluation table.

Note: An explanation of each sub task can be found in Appendix 6.

5.3 References

1. Wallas G, *The Art of Thought*. 1926, New York: Harcourt, Brace and Company.
2. Ullman D G, *The Mechanical Design Process*. 1992: McGraw-Hill.

Chapter 6 – Embodiment Design

This chapter details the principles behind the bellows intervertebral disc implant and the design of key implant components.

6.1 Principles of the Bellows Intervertebral Disc Implant

In many ways the fluid filled bellows concept selected for further development is similar to an intervertebral disc. Like an intervertebral disc the implant consists of a fluid centre surrounded by a flexible pressure vessel. Figure 6.1 shows a stylised version of the bellows intervertebral disc implant.

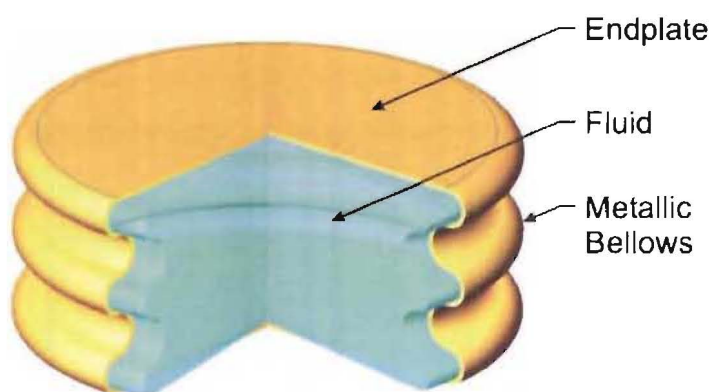


Figure 6.1 Stylised bellows intervertebral disc implant components.

Note: Components are shown partially sectioned, not to scale and are not representative of final design.

Metallic bellows, like the annulus fibrosus, are able to support internal pressure, compress axially and deflected angularly. Bellows can also resist relative lateral deflections of the endplates and twisting over short lengths. However, on their own metallic bellows are unable to transfer compressive loads like the stiff fibres of the annulus fibrosus. Bellows are also unable to stretch elastically to provide radial expansions.

The fluid fill medium in the bellows intervertebral disc implant acts in a similar way to the nucleus pulposus, it can be deformed by applied loads but it cannot be compressed. When vertical loads are applied to the bellows intervertebral disc implant the fluid fill medium tries to reduce in height and expand outward radially. This outward expansion is resisted by the metallic bellows.

The fluid fill medium also exerts pressure on the implant's endplates, however these too resist deformation. Therefore the fluid fill medium is unable to deform either radially or axially despite the application of loads and as a result the internal pressure increases. This creates an effectively rigid structure that allows compression loads to be transmitted from one endplate to the other and thus from vertebral body to vertebral body, while still allowing angular deflections to occur.

Healthy intervertebral discs have the ability to slow the transfer shock loads by the temporarily diverting some energy into stretching the elastic collagen fibres of the annulus fibrosus. However, as metallic bellows effectively do not allow radial expansions to occur, any shock loads will be directly transferred from one vertebra to the next. It is not anticipated that this will be a significant issue provided the adjacent intervertebral discs are healthy and are able to retard some of the shock loading.

6.2 Components

The primary components of the bellows intervertebral disc implant are the metallic bellows and fluid fill medium, however several other components must also be considered including:

- Endplates and fixation mechanisms
- Any additional load carrying features
- Overload protection features
- Motion limiting devices
- Protective coatings

The design of the metallic bellows and other components is detailed in the remainder of this chapter.

6.2.1 Metallic Bellows

Various forms of bellows have been used in many applications for several centuries. Bellows were first manufactured from wood and leather and used to supply air to forges and furnaces. Metallic bellows were developed early in the 20th century and since this time have been used extensively as flexible joints in pressurised piping systems. In the last 20 years bellows construction has become more sophisticated with complex construction and material combinations being used to produce bellows which can be used for engine thermostats, air conditioning expansion joints, fluid couplings, aerospace components and expansion devices, to name a few applications.

6.2.1.1 Types of Metallic Bellows

There are two types of metallic bellows, formed bellows and welded bellows, both of which have similar features. In general all metallic bellows consist of one or more corrugations or 'convolutions' and each of these convolution has flat annular areas called 'diaphragms'. The diaphragms are able to be distorted, in turn allowing the ends of the bellows to be deflected. Figure 6.2 shows typical bellows terminology. It should be noted that individual diaphragms are a feature of welded bellows but not formed bellows.

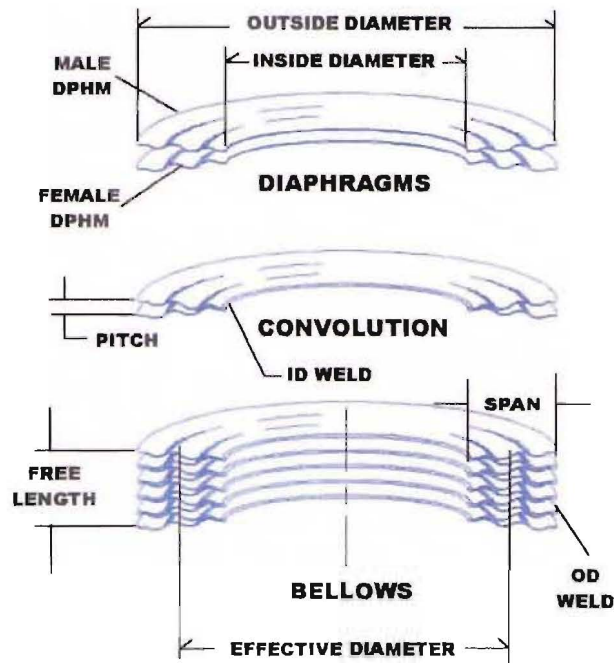


Figure 6.2 Sectioned view of welded bellows showing common terminology.

[Source: Flexial Corporation⁶]

Figure 6.3 shows photographs of typical formed bellows (a) and welded bellows (b). Other components can also be added to metallic bellows, for example Figure 6.3(b) shows a welded bellows which has a machined end cuff added.

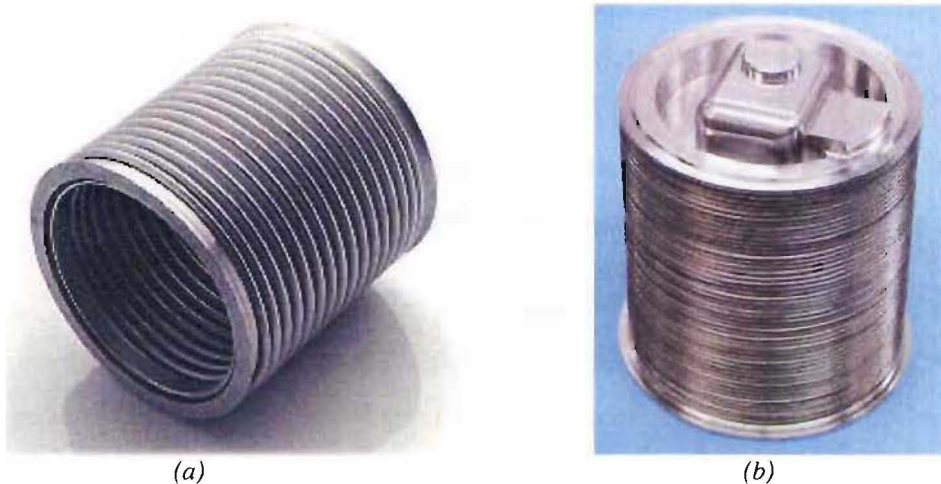


Figure 6.3 Types of bellows.

(a) Formed bellows. [Source: <http://www.weldlogic.co.uk/level%202/Appilpage.htm>]

(b) Welded bellows. [Source: Flexial Corporation⁶]

The processes used to manufacture formed and welded metallic bellows along with a summary of each type of bellows strengths and weaknesses are detailed below.

Formed Bellows

Formed bellows are manufactured from tubular stock using a complex die set and the application of internal pressure, as illustrated in Figure 6.4. In the first stage of the manufacturing process, stock material is loaded into the die set (a) and the inside of the tube is then pressurised. As the stock material begins to bulge (b) the spacers between the die plates are retracted while the internal pressure is maintained (c). Finally the die plates are moved together to form the convolutions (d). The last part of the formed bellows manufacturing process is to trim the bellows cuff to the desired length (e).

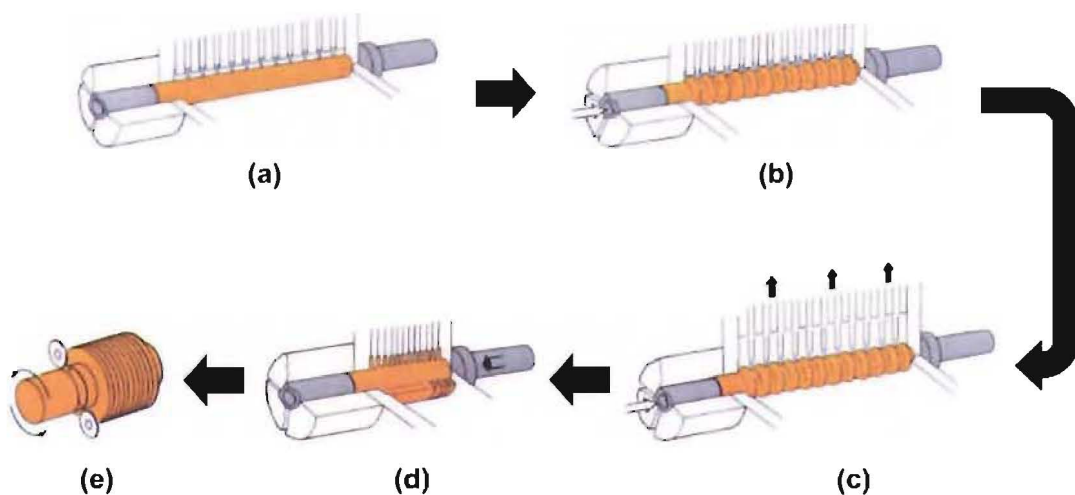


Figure 6.4 Formed bellows manufacturing process.

[Source: <http://www.caradonhydroflex.com/munufacturing.html>]

The main advantage offered by formed bellows is their ability to withstand high internal and external pressures.

However, as the stock material must be drawn into the die set and stretched to form the bellows only relatively shallow convolutions (spans) can be produced without excessively thinning or rupturing the bellows wall. This small span size limits the amount of deflection formed bellows can undergo before being damaged.

The need for die plates during the manufacturing process also means that large radiuses are formed at the root and crest of each convolution. These radii do not contribute anything to the bellows ability to deflect. The convolution radii also limit the number of convolutions which can be formed per unit length. This in turn results in fewer diaphragms per unit length and thus the deflection range of formed bellows is reduced further.

The need to draw material into the die set and the physical size of the die sets means there are limits to how long continuous lengths of formed bellows can be.

Welded Bellows

Welded bellows are also sometime referred to as welded edge bellows. Figure 6.5 shows the manufacturing process for welded bellows. First individual diaphragms are formed by punching them from a sheet of stock material (a). The inside edges of two diaphragms are then welded together to form a convolution (b). Finally multiple convolutions are welded together to create a welded bellows (c).

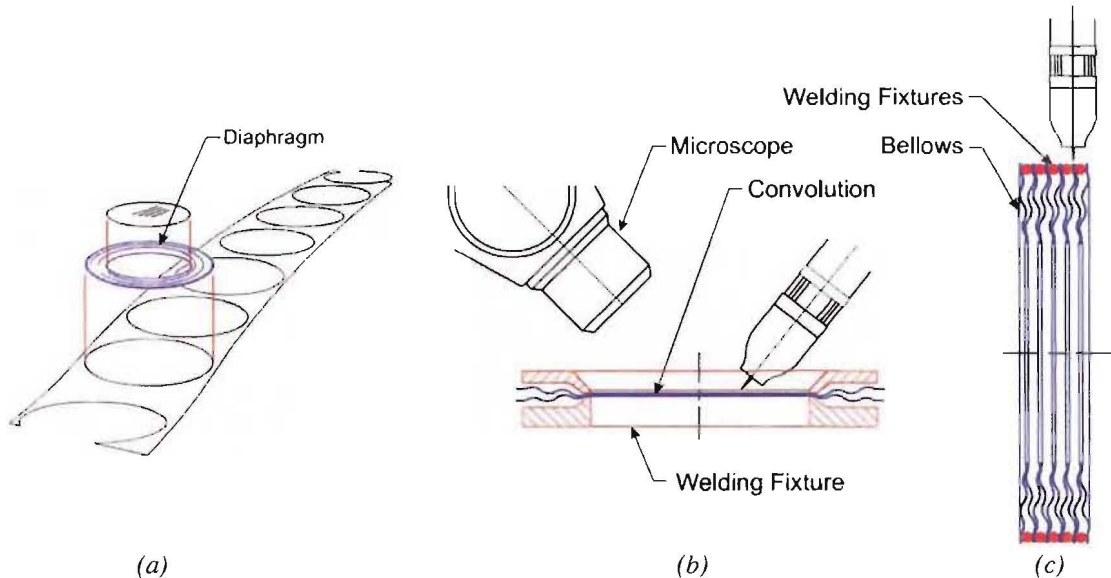


Figure 6.5 Welded bellows manufacturing process.

[Source: Flexial Corporation⁶]

Welded bellows are not able to withstand the same pressures as formed bellows, however they do offer several advantages.

No radiuses are formed at the inner and outer edges of the convolutions during the manufacturing process which allows the diaphragms of welded bellows to be much closer together. Thus compact welded bellows can be produced with significantly more diaphragms and a greater deflection range per unit length than formed bellows.

Welded bellows with large spans can also be produced as there are no forming limits which restrict the ratio of the diaphragms inside and outside diameters. This means welded bellows can be produced which have large amounts of flexibility.

Formed bellows can only be manufactured from materials which exhibit good formability and elongation characteristics; however welded bellows can be produced from any material which can be welded. Welded bellows also offer the advantage of being able to collapse to a solid height where diaphragm welds contact each other, as shown in Figure 6.6. In a collapsed state welded bellows can transfer very high loads and pressures and then be released with no permanent damage. If formed bellows are collapsed to a 'solid height' the inner and outer radiuses will be crushed.

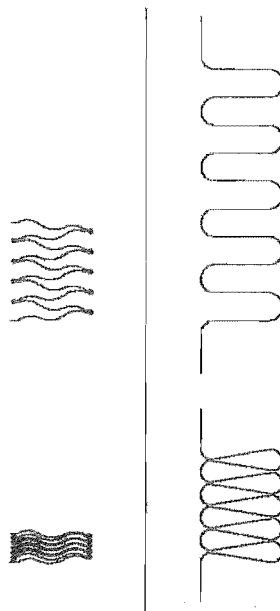


Figure 6.6 Bellows solid height.

[Source: Flexial Corporation⁶]

The inner and outer radiuses of formed bellows are also sensitive to scratches and nicks as these areas are highly stressed. However, the weld beads of welded bellows are approximately 3 times thicker than the diaphragm material and can tolerate wear and scratches without resulting in any degradation of the welded bellows performance. This feature allows welded bellows to be used for applications such as valve stem seals where valve stems may repeatedly contact and rub against the inner diaphragm welds.

Contours or ripples can be added to the diaphragms of welded bellows during the manufacturing process. These features allow stress resulting from the application of pressure and deflections to be redistributed across the diaphragms. Diaphragm contours can also be used to increase or decrease the spring rate of welded bellows. Figure 6.7 shows some typical diaphragm contours.

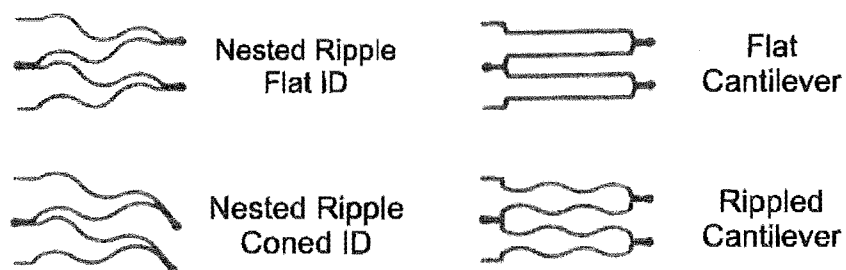


Figure 6.7 Welded bellows diaphragm contours.

The major disadvantage of welded bellows is that they are not suited to dirty working environments. Any solid material which gets between the diaphragms can act as a fulcrum when the welded bellows are deflected, creating high localised stress in the welds, which can in turn lead to premature failure of the welded bellows.

Multi-Ply Bellows

Formed and welded bellows can be constructed to have single or multi ply walls. Multi-ply bellows consist of several layers of material as opposed to one layer.

Given an identical overall wall thickness, single and multi-ply bellows can support the same internal or external pressures. However, given the same overall wall thickness multi-ply bellows experience less strain than single-ply bellows when they are deflected. This characteristic means that multi-ply bellows can be designed to support the same pressures and deflections as a single-ply bellows but they can be shorter or have a higher fatigue life.

When forming multi-ply welded bellows, all the diaphragms are joined with common welds at the inner and outer edges. Figure 6.8 shows a partial section of a two-ply welded bellows convolution.

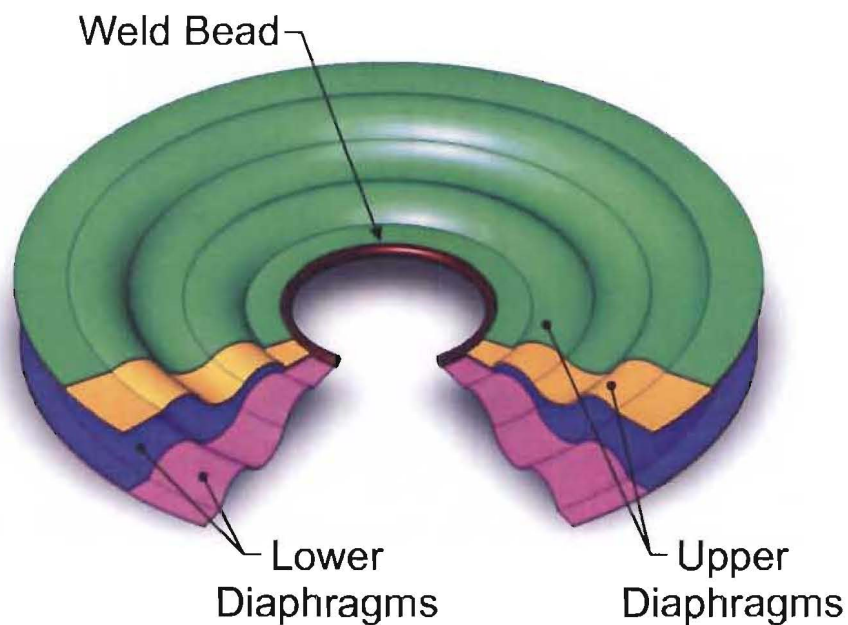


Figure 6.8 Welded bellows multi-ply convolution.

It should be noted that for most multi-ply applications a maximum of two plies are normally specified so both layers of material can be visually inspected as required.

6.2.1.2 Selection of Bellows Type and Manufacturer

Several metallic bellows manufacturers were contacted to determine whether formed or welded bellows could meet the requirements laid out in the specification for the intervertebral disc implant. Initial contact with manufacturers was by phone, followed by a written specification.

The information provided during the phone calls and in the specification was intentionally kept brief and broadly worded to reduce the possibility of compromising any intellectual property associated with the project. The specification sent to manufacturers can be found in Appendix 7.

Of the five bellows manufacturers contacted, three responded. Two of these responses were from formed bellows manufacturers and the remaining response was from a welded bellows manufacturer.

Both formed bellows manufacturers stated that the specified length of the bellows was insufficient to produce the required deflection range and life^{5,28}.

The welded bellows manufacturer that responded was Flexial Corporation who are based in the United States of America. Flexial stated that given the potential for debris around the implant site they did not consider welded bellows were a viable option⁹. However, if the welded bellows could be shielded from debris then Flexial were confident they could design a bellows capable of performing the specified motions for the required number of cycles¹⁰.

Given these responses the decision was made to continue development of the bellows intervertebral disc implant using welded bellows supplied by Flexial Corporation.

6.2.1.3 Detail Design of the Welded Bellows

After some discussion with the Engineering Manager at Flexial it was determined that the analytical design of welded bellows is a difficult task. This is because analytical studies of welded bellows often do not reflect the performance of the bellows once manufactured. Instead it is common practice in the welded bellows industry to modify analytical results based on past empirical experience. This also applies to finite element studies of welded bellows.

Therefore given these complications and as Flexial is an industry leader in the design of welded bellows, the decision was made to subcontract the bellows specific design work to Flexial. During the design of the welded bellows, a process which took approximately 9 months, Flexial took the lead role, with the author providing instructions and detailed specification information and conducting verification calculations were appropriate.

The first detail dealt with was the selection of a material. The initial bellows specification called for either Commercially Pure Titanium or Ti-6Al-4V to be used. Although Ti-6Al-4V has the highest fatigue strength of these materials it has poor formability and can work harden, affecting the forming of the diaphragm contours. Therefore after consultation with Flexial, Commercial Pure Grade 4 Titanium was selected. This material was chosen as it can be easily formed and it has the highest fatigue and yield strengths of the Commercial Pure alloys.

During the design process several areas of the bellows specification were refined to more accurately reflect the implant's needs and to include any additional information needed. These changes included altering the number of deflection cycles the bellows were required to undergo and reducing the internal pressure the welded bellows were required to support. The reasons for these changes are detailed below.

Number of Angular Deflection Cycles

The initial bellows specification called for the bellows to be able to deflect angularly 8° for 100 million cycles. However as detailed in Section 4.1.4 the implant does not undergo 100 million 8° angular deflections. The majority of the deflections are significantly smaller. Table 6.1 below shows the final angular deflection specification for the welded bellows.

| Required Deflection (Flexion) | Number of Deflections over 40 years |
|--|--|
| 1 degrees | 70 M |
| 2 degrees | 26 M |
| 5 degrees | 3.5 M |
| 8 degrees | 1 M |
| | 100.5 M |

Table 6.1 Bellows fatigue requirements.

Another factor considered was that the fatigue performance of welded bellows is not adversely affected by the angular deflections occurring in a variety of planes and directions. That is, lateral deflections do not affect the flexion fatigue properties, and visa versa. This was discussed with Flexial who stated that in their experience when welded bellows are deflected around several axes, the fatigue properties around each axis of deflection are unrelated. However in order to validate that this is the case for the intervertebral disc implant, multi-axis fatigue testing of the bellows should be undertaken.

Internal Pressure

The most significant difficulty encountered while designing the welded bellows was that the internal pressure was too high.

Initial design work indicated that to provide the specified ranges of motion a 2-ply bellows with 15 convolutions was required. The inner and outer diaphragm diameters of these bellows were 10.6 and 23.6 mm respectively and each ply was 0.0762 mm (0.003 inches) thick. Using these dimensions the effective area of the bellows was determined using Equation 1 [Source: Flexial Corporation⁶].

$$\begin{aligned} \text{Effective Area} &= \frac{\pi}{4} \cdot \frac{(OD + ID)^2}{4} \\ &= 230 \text{ mm}^2 \end{aligned} \quad (\text{Eq. 1})$$

The load carrying requirements for the implant were specified to be 600 N for static loads and up to 1200 N during dynamic loading. Based on the above effective area the static load applied to the fluid filled bellows implant would result in an internal pressure of 2.6 MPa. However, the bellows specified by Flexial were only able to support a peak pressure of 690 kPa¹⁴. Therefore, for the fluid filled bellows concept to be successful, it was determined that either the pressure capacity of the bellows would have to be increased or the load applied to the bellows reduced.

Theoretically, increasing the thickness of the diaphragms would raise the bellows pressure capacity while reducing the deflection range, assuming the peak stress in the bellows wall remains constant. However, after consultation with Flexial it was determined that while increasing the wall thickness of the bellows would analytically improve the bellows pressure capabilities any significant increase in thickness would make the bellows un-manufacturable. Specifically, with thicker diaphragms more heat input is required to achieve a satisfactory weld. However, as the specified bellows have a small diameter and pitch only small welding fixtures can be used. Any increase in the heat input during the welding operations would result in the fixtures being unable to chill the diaphragms sufficiently. This would in turn result in burning of the parent material and/or the weld fixtures being melted and drawn into the convolution welds^{11,12}.

It was therefore decided that increasing the bellows pressure capability was not a viable solution and the loads applied to the bellows would have to be reduced. Three potential methods of achieving this were identified:

- The internal pressure could be decreased by using bellows of a larger diameter. However, as the bellows were already close to the maximum envelope specified this was not considered to be a viable option.
- An internal support could be added to the implant to carry some or all of the applied loads. Any wear debris generated by this mechanism would be contained within the welded bellows helping to prevent any osteolysis problems associated with wear debris from occurring. However, the use of a support mechanism would increase the complexity of the implant and may adversely affect the life of the metallic bellows.
- The final load sharing mechanism considered was utilisation of the annulus fibrosus. As previously described in Section 2.5.2.1 the annulus fibrosus is able to support virtually the same compressive loads as an intact intervertebral disc. Therefore by using a lateral approach to preserve the majority of the annulus fibrosus the load the metallic bellows are required to support could be reduced.

The favoured method of reducing the loads applied to the metallic bellows was the utilisation of the annulus fibrosus. To determine if this was viable several factors were considered.

Markolf et al²¹ observed that during the first loading of post-discectomy intervertebral discs they displayed increased deformation and reduced stiffness. This change in performance compared to an intact disc was attributed to fibres of the annulus fibrosus "*mechanically altering*" to form a new stable configuration. Some of the intervertebral discs also exhibited bulging after application of load. However, the key and unexpected finding of this study was that when loaded repeatedly the response of the reconfigured annulus fibrosus was very similar to that of an intact intervertebral disc. These trends are illustrated in Figure 6.9(a). Markolf suggested this could be the reason patients who have had some or all of a nucleus pulposus removed do so well postoperatively.

Markolf also conducted creep tests during which the post-discectomy specimens were loaded for a period of 15 minutes, before being unloaded. This loading and unloading procedure was repeated several times for each specimen. During the first loading cycle accelerated creep was observed, which was attributed to buckling of lamellae. However during subsequent loadings the post-discectomy discs were observed to behave in a similar fashion to intact intervertebral discs as shown in Figure 6.9(b).

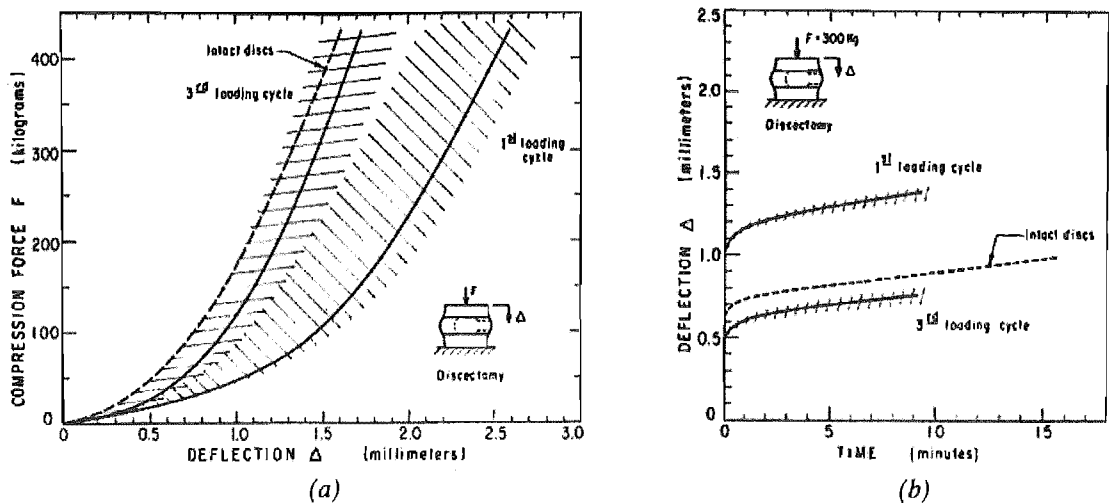


Figure 6.9 Load carrying capabilities of annulus fibrosus following discectomy.

(a) Load-deflection of annulus fibrosus post-discectomy.

(b) Creep of annulus fibrosus post discectomy.

[Source: Markolf et al²¹]

If the annulus fibrosus is to successfully carry a high percentage of the applied loads the bellows intervertebral disc implant must conform to the same load-deflection curve as the annulus fibrosus. For example Figure 6.9(a) shows that during the application of a 60 kg load the annulus fibrosus compresses approximately 0.5 mm. If the bellows intervertebral disc implant does not compress as far as the annulus fibrosus, then once compression of the annulus fibrosus ceases any additional loads will have to be entirely supported by the fluid filled bellows implant. To allow such compression to occur the implant's fluid would have to contain a compressible component. The simplest method of achieving this would be to only partially fill the metallic bellows with fluid.

In summary, if the bellows intervertebral disc implant can be designed to match the annulus fibrosus load-deflection curve, there is no reason why the annulus fibrosus can not be used to support a high percentage of the applied static and dynamic loads.

Utilising the annulus fibrosus as a load carrying member also offers the advantage of improving the stiffness of the bellows intervertebral disc implant. Typically welded metallic bellows have a low stiffness. If a bellows intervertebral disc implant were used on its own it could potentially result in the spinal column becoming unstable. By utilising both the annulus fibrosus and the metallic bellows their combined stiffness will be close to the stiffness of a healthy intervertebral disc.

After additional consultation with Flexial it was determined that using such a strategy suitable metallic bellows could be designed. However, the maximum compression the welded bellows could sustain was 0.5 mm. As an additional safe guard the bellows intervertebral disc implant should include an internal support which prevents deflections in excess of 0.5 mm from occurring. If the implant is compressed 0.5 mm and the internal support components contact, the annulus fibrosus will cease to carry any additional loads. Therefore the internal support must also be capable of carrying compressive loads. The design of the internal support is detailed in Section 6.2.2.

While utilising the annulus fibrosus as a load carrying component is a viable option for the bellows intervertebral disc implant, it would not work for the metallic spring concepts previously detailed in Chapter 5. By utilising the annulus fibrosus the load carrying requirements for the metallic springs would be reduced and the spring cross sections and spring stiffness could also be reduced. However, the combined stiffness of the spring and annulus fibrosus would still be too high and would result in insufficient deflection occurring at the affected spinal level.

6.2.1.4 Welded Bellows Specification

Given the modified fatigue and internal pressure requirements a final bellows specification was developed and supplied by Flexial Corporation as detailed below^{12,13}.

| | |
|---|---|
| Outside Diameter | 23.6 mm |
| Inside Diameter | 10.61 mm |
| Estimated Free Length | 9.5 mm |
| Material | Commercial Pure Titanium Grade 4 |
| Thickness | 0.0762 mm (0.003 in) |
| Number of Plies | 2 ply |
| Number of Convolutions | 15 |
| Maximum Axial Stroke | 0.5 mm (Compression only) |
| Maximum Angular Deflection | ± 8 deg |
| Maximum Pressure | 100 psi (690 kPa) |
| Maximum Leakage Rate | 1x10 ⁻⁶ cc/sec of He @ 1 atmosphere differential |
| Predicted Life | |
| 0.5mm Compression and 8° angular deflection | 1x10 ⁶ Cycles |
| 0.5mm Compression and 5° angular deflection | 150x10 ⁶ Cycles |

At the completion of the design work a quote for bellows with these specifications was requested from Flexial.

The resulting quote was split into two components, a unit cost of US\$884 per welded bellows based on an order of 8 units and a non-recurring engineering and tooling charge of US\$7800.²³ The non-recurring engineering and tooling charge included preparation of engineering drawings and the manufacture of tooling such as male and female diaphragm stamping dies, weld tooling and gauging. This non-recurring charge would only apply to the initial bellows order.

Details of the diaphragm contours and the weld specification were not released by Flexial at the time of quotation as they considered this material to be commercial sensitive. However, Flexial were prepared to release this data on receipt of a confirmed order.¹²

6.2.2 Internal Support

As previously described an internal support is required to prevent the bellows from being compressed more than 0.5 mm. The internal support must be capable of performing the same angular deflections as the bellows, while also separating to allow the implant to move from an uncompressed to a compressed state and visa versa. The internal support should also be able to carry applied loads once 0.5 mm of compression has occurred.

Figure 6.10(a) shows the implant in an unloaded state with a gap between the internal support components. When load is applied to the implant it decreases in height, compressing the gas and raising the internal pressure. Once sufficient load has been applied the support components contact and prevent further deflection as shown in Figure 6.10(b)

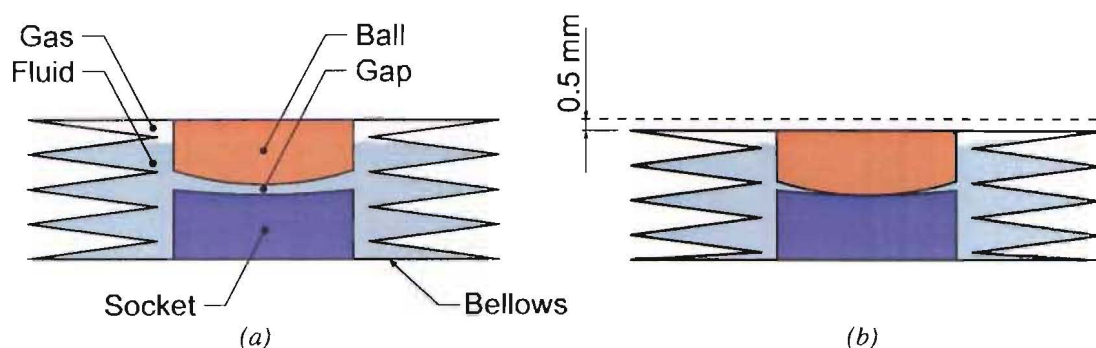


Figure 6.10 Support separation and contact.

(a) Unloaded implant assembly with a gap between support components.

(b) Loaded implant assembly, when sufficient load is applied the support components contact.

The simplest mechanism which can support compression loads and deflect angularly while still being able to separate, is a pair of spherical contact surfaces. Spherical contact surfaces have also been used in several other medical implants. Hip implants utilise a ball and socket arrangement to provide the required motions. Similarly, knee implants have two spherical surfaces which slide and roll relative to each other to provide angular deflections. Hip and knee implants have also been found to exhibit small separations when deflected *in-vivo*^{16,17,18,20,22}.

The decision was made to develop an internal support mechanism which incorporated spherical contact surfaces. Several factors were considered during the design of the internal support including optimising the design and size of the support components, material selection and surface roughness. Another factor considered when optimising the internal support was minimising the volume of wear debris produced by the internal support. This was deemed important as any solid material which gets between the convolutions can adversely affect the life of the welded bellows, as detailed in Section 6.2.1.1.

6.2.2.1 Conceptual Designs

When metallic bellows are deflected angularly they tend to rotate around their centre of geometry, as indicated in Figure 6.11. Any support system added to the implant assembly must not alter this centre of rotation. Failure to achieve this may result in the bellows being subjected to additional or abnormal loads and deflections, which may in turn result in a reduction in the bellows life.

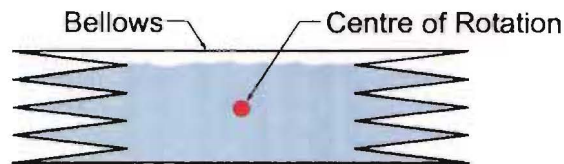


Figure 6.11 Bellows natural centre of rotation.

Two different groups of spherical support concepts which allow the bellows to rotate around their centre of rotation were developed.

The first group consisted of a ball and socket arrangement similar to a hip implant. When angular deflections occur one surface “slides” relative to the other, as indicated in Figure 6.12. While this support arrangement meets all the requirements the sliding motion may produce wear debris. As previously detailed in Section 6.2.1.1 any material, including wear debris, which gets between the bellows diaphragms can act as a fulcrum producing high localised stress in the bellows welds and potentially lead to premature failure of the bellows. Therefore if a sliding support is used it should be designed to produce minimal wear debris.

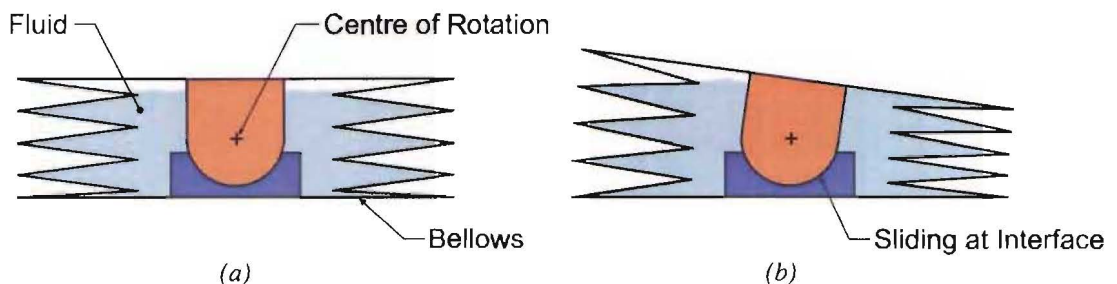


Figure 6.12 Internal support causing sliding at interface.

(a) Load applied compressing bellows and closed support gap, no angular deflection.

(b) Load applied compressing bellows and closed support gap, with angular deflection.

The second support arrangement considered is similar to a knee implant with the required motions being provided by the two support surfaces “rolling” relative to each other. Figure 6.13(a) shows the implant assembly in a loaded but undeflected state. As the implant deflects angularly the convex support component rolls over the surface of the concave component, as indicated in Figure 6.13(b). This system offers the advantage of producing less wear debris than the sliding support. However, when a rolling support is deflected the central points separate and the overall height of the implant increases. It may be possible to accommodate this change in height or ‘lift’ though, as it effectively results in the bellows being decompressed.

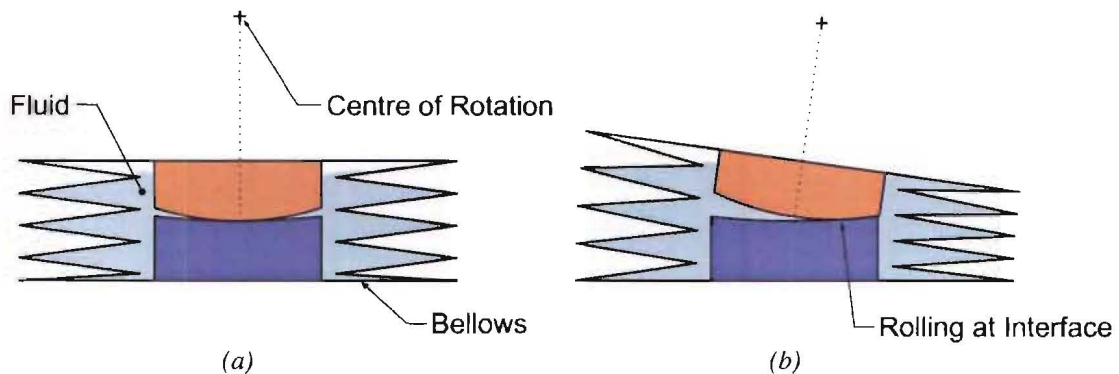


Figure 6.13 Internal support causing rolling at interface.

- (a) Load applied compressing bellows and closed support gap, no angular deflection.
 (b) Load applied compressing bellows and closed support gap, with angular deflection.

6.2.2.2 Size Optimisation

The most significant factor influencing the design of rolling and sliding supports is the contact stress at the interface of the two components when they are loaded. The magnitude of the contact stress is dependent on the size of the spheres and the elastic properties of the two components. Hertz^{8,27} developed theory to determine the contact stress for a sphere in a spherical socket as shown below in Figure 6.14 and Equation 2.

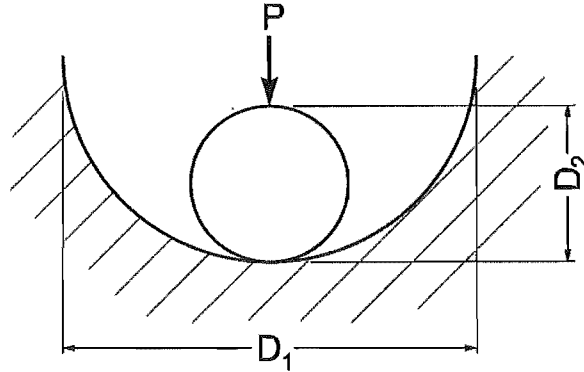


Figure 6.14 Sphere in a spherical socket.

$$\text{Max } \sigma_c = 0.918 \sqrt[3]{\frac{P}{K_D^2 C_E}} \quad (\text{Eq. 2})$$

Where

$$K_D = \frac{D_1 D_2}{D_1 - D_2}$$

$$C_E = \frac{1 - \nu_1^2}{E_1} + \frac{1 - \nu_2^2}{E_2}$$

Where: Max σ_c = Maximum Contact Stress (MPa)

P = Load (N)

D = Diameter (m)

E = Elastic Modulus (GPa)

ν = Poisson Ratio (-)

Determining the size of the sliding internal support components was relatively simple as the component dimensions are only influenced by the contact stress, internal diameter of the bellows and the thickness of the support socket. These limiting dimensions are shown in Figure 6.15.

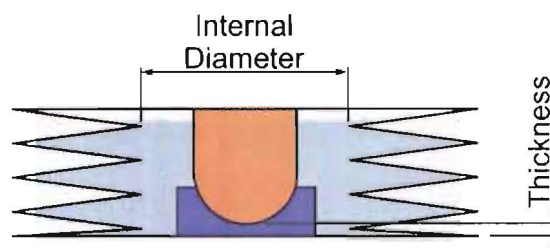


Figure 6.15 Thickness of sliding support socket.

There are several factors which influence the size of the rolling internal support components including:

- The contact stress.
- The internal geometry of the metallic bellows.
- The position of the contact point when the implant is deflected.
- The amount of lift that occurs as the implant is deflected.

The internal diameter of the bellows limits the size of the rolling support components. However, unlike the sliding support the radii of the spherical faces can be larger than the inside diameter of the metallic bellows. Specifically, there is no need for the roller's spherical face (R_2) to be tangential to the cylindrical face of the roller as shown in Figure 6.16.

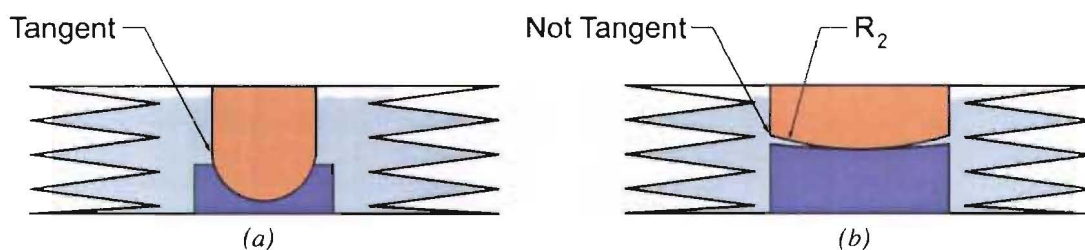


Figure 6.16 Cylindrical-to-spherical tangency comparison for the internal support.

- (a) The sliding support requires the spherical contact surface to be tangential to the cylindrical face of the concave component.
- (b) The spherical contact surface for the rolling support can have a large radius (R_2) as there is no need for the contact surface to be tangential to the outer face of the concave component.

It is important that during 8° deflections the rolling support's contact point is not too close to the edge of the components. Failure to do so may result in the edge of the support components being damaged or the implant becoming unstable. The position of the contact point (R_{Contact}) is dependent on the radii of the components and the amount the implant deflected (θ) as indicated in Figure 6.17.

Given the importance of the contact point radius (R_{Contact}) it was set to be a controlling variable along with the socket radius (R_1). The peak deflection (θ) of the implant was previously specified to be 8° . Given these variables the roller radius (R_2) could be determined, as shown in Equation 4.

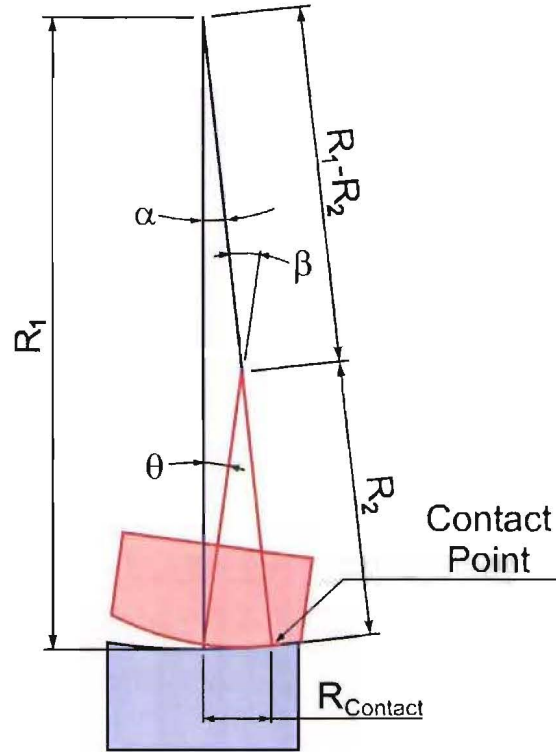


Figure 6.17 Rolling support contact point radius during deflection.

$$\beta = \text{Sin}^{-1} \left(\frac{R_1 (\text{Sin} \theta)}{R_1 - R_2} \right)$$

$$\alpha = \beta - \theta$$

Where: R_1 = Socket Radius

R_2 = Roller Radius

θ = Deflection Range (8°)

$$R_{\text{Contact}} = R_1 \text{Sin} \alpha \quad (\text{Eq. 3})$$

Therefore

$$R_2 = R_1 - \frac{R_1 \text{Sin} \theta}{\text{Sin} \left(\text{Sin}^{-1} \left(\frac{R_{\text{Contact}}}{R_1} \right) + \theta \right)} \quad (\text{Eq. 4})$$

The final factor influencing the design of the rolling internal support is the amount the roller lifts as the implant is deflected as indicated in Figure 6.18. This lift will, as previously noted, result in the implant being decompressed. The amount of lift is dependent on the radii of the roller components (R_1 & R_2), the contact radius ($R_{Contact}$) and the amount the implant is deflected (θ) as shown in Equation 5

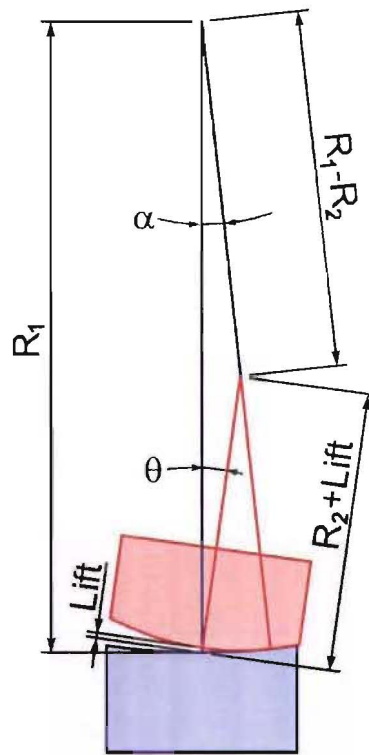


Figure 6.18 Lift as a result of rolling support deflection.

$$\frac{R_1 - R_2}{\sin \theta} = \frac{R_2 + \text{Lift}}{\sin \alpha}$$

$$\text{Lift} = \left(\sin \alpha \left(\frac{R_1 - R_2}{\sin \theta} \right) \right) - R_2$$

Substituting for $\sin \alpha$ from Equation 3

$$\text{Lift} = \left(\left(\frac{R_{Contact}}{R_1} \right) \cdot \left(\frac{R_1 - R_2}{\sin \theta} \right) \right) - R_2 \quad (\text{Eq. 5})$$

Using the relationships developed in Equations 2, 4 and 5 the effects of varying the rolling support's socket diameter (R_1) and contact radius (R_{Contact}) were investigated. In each case a peak deflection of 8° was used.

As shown in Figure 6.19 increasing the radius of either the socket (R_1) or the contact point (R_{Contact}) results in an increase in the roller radius (R_2).

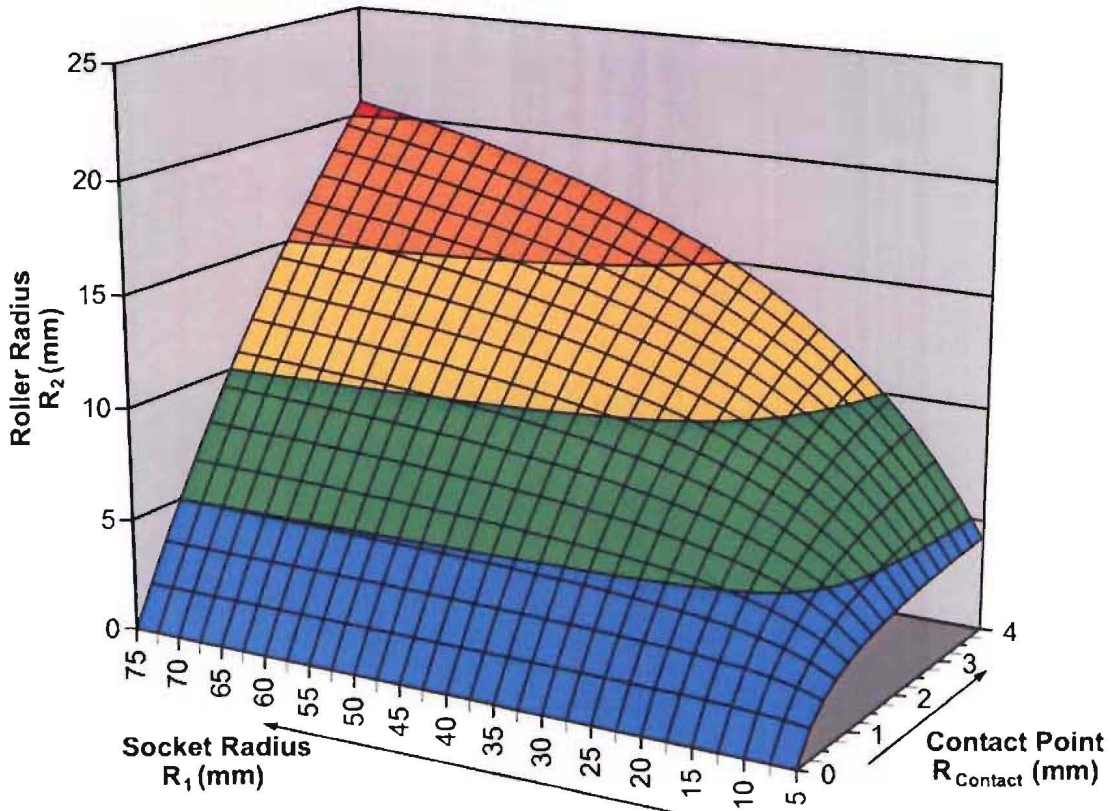


Figure 6.19 Required roller radius (R_2) for varying socket and contact point radii.

The main factor influencing the amount of lift that occurs as the implant is deflected is the contact point radius (R_{Contact}) as shown in Figure 6.20. Changing the socket radius (R_1) has little effect, except for small values of R_1 and larger values of R_{Contact} when a discontinuity occurs and the amount of lift increases.

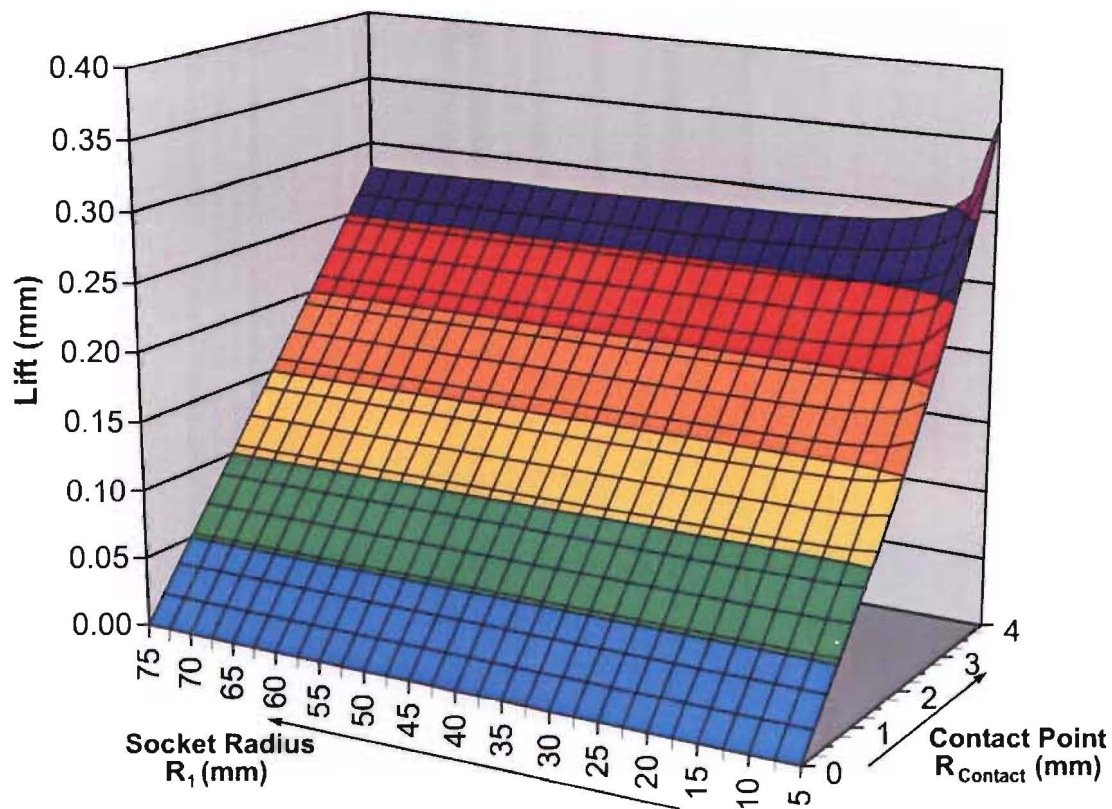


Figure 6.20 Lift resulting from 8° angular deflection for varying socket and contact point radii.

Altering the socket radius (R_1) has very little effect on the resulting contact stress as shown in Figure 6.21. However the contact point radius (R_{Contact}) has a strong influence, with small values resulting in high contact stresses. It should be noted that the contact stress values shown in Figure 6.21 are indicative only and were determined using a unit load applied to a cobalt chrome roller and socket.

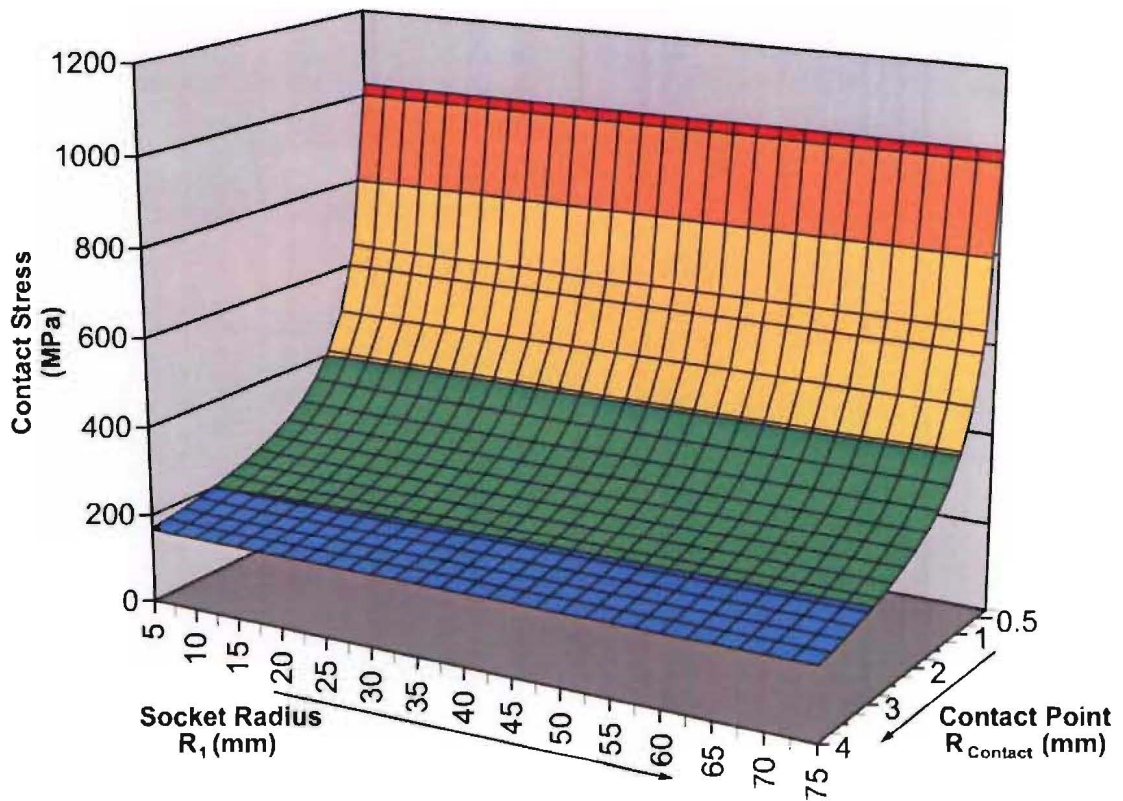


Figure 6.21 Contact stress for varying socket and contact point radii.

The contact stress was determined using a unit load applied to a roller support system constructed from chrome cobalt and thus is indicative only.

Note: For clarity the socket radius (R_1) and contact point radius (R_{Contact}) axes are reversed when compared to Figures 6.19 and 6.20.

A summary of the effects the socket radius (R_1) and the contact point radius (R_{Contact}) have on the rolling internal support are shown in Table 6.2. As can be seen, it is not possible to achieve a low contact stress while also minimising the amount of lift that occurs. Therefore mid-range socket radius and contact point radius values are required to achieve a workable balance between the lift and contact stress.

| Socket Radius | Contact Radius | Roller Radius | Lift | Contact Stress |
|---------------|----------------|---------------|-------|----------------|
| Small | Small | Small | Small | High |
| Large | Small | Small | Small | High |
| Small | Large | Small | Large | Low |
| Large | Large | Large | Large | Low |

Table 6.2 Summary of socket and contact point radii effects.

6.2.2.3 Material Selection

There are several factors which influence material selection for sliding and rolling internal supports, these include the following.

The magnitude of the contact stresses generated between spherical surfaces is influenced by the material's properties as can be seen in the C_E component of Equation 2. By maximising C_E the contact stresses can be minimised. This can most easily be achieved by selecting materials with low moduli of elasticity.

Material combinations with differing hardness are sometimes utilised so one component wears predominantly. This can be used to advantage, for example, in the sliding support with the socket component being made of a softer material. As the soft socket wears the size of the contact patch will increase and the surface stresses will decrease. Differing hardness can be a disadvantage however if the surface of the harder component is damaged and a cutting edge is effectively created. In such a case additional wear debris will be produced. By utilising materials which have similar or identical hardness it is possible to produce a system in which both components wear more uniformly.

The use of two hard materials can result in a system which produces small volumes of wear debris. For example the use of two chrome cobalt surfaces will result in a system which produces low volumes of wear debris and the wear particles produced will typically be small in size. However a support system with two chrome cobalt surfaces will have high contact stresses.

Table 6.3 shows a summary of the materials considered for the internal support components. Several combinations of these materials were trialed for both types of internal support as shown in Tables 6.4 and 6.5.

| Material | Modulus of Elasticity (E) (GPa) | Poisson's Ratio (ν) (-) | Compressive Yield Strength (σ_{cy}) (MPa) |
|-----------------------------|---|---|--|
| Chrome Cobalt ⁷ | 241 | 0.3 | 930 [†] |
| CP Ti Grade 4 ³¹ | 105 | 0.35 | 550 |
| Ti-6Al-4V ³¹ | 110 [†] | 0.26 | 917 |
| Radel R4400 ³² | 2.0 | 0.45 | 98 |
| Radel R5500 ³² | 1.7 | 0.45 | 99 |
| UHMWPE | 0.69 ³⁰ | 0.45 ²⁴ | 14 ⁴ |

Table 6.3 Summary of internal support material properties.

Note: Radel is a trade name for Polyphenylsulfone.

Note: † = value estimated from tensile value.

6.2.2.4 Stress Analysis

The contact stresses at the interface of the sliding and rolling internal supports were determined analytically using Equation 2. Finite element studies of the internal support components were also conducted in a FEA package called Ansys.

Sliding Support

The dimensions of the sliding support components were set to be as large as possible, thus maximising the K_D component of Equation 2 and minimising the maximum contact stress. As previously noted the internal geometry of the bellows limits the size of the sliding support components. Therefore, with an internal bellows diameter of 10.61 mm it was determined that a sliding support diameter of 7.5 mm was appropriate. Support components of this size will fit in the bore of the metallic bellows while not interfering with the diaphragm welds when the implant is deflected. This value also ensures the socket is not too thin, as previously indicated in Figure 6.15. The diameter of the convex support component was set to be 0.1 mm smaller than the socket diameter to allow for manufacturing and assembly tolerances. This diametrical clearance is typical of those found in hip implants¹⁹. This resulted in the final sliding support system having a socket diameter of 7.5 mm and a ball diameter of 7.4 mm.

Contact stresses were then determined analytically using Equation 2 and an applied load of 600 N. Table 6.4 below shows the resulting contact stresses for several material combinations. From these results it can be seen that any of the material combinations trialed are capable of supporting the applied loads.

| | Material Combinations | | | | | |
|----------------------|-----------------------|---------------|------------|-----------|-------------|-------------|
| Socket Material | Chrome Cobalt | UHMWPE | UHMWPE | UHMWPE | Radel R4400 | Radel R5500 |
| Support Material | Chrome Cobalt | Chrome Cobalt | Ti Grade 4 | Ti-6Al-4V | Radel R4400 | Radel R5500 |
| C_E | 0.008 | 1.160 | 1.164 | 1.164 | 0.798 | 0.938 |
| Max σ_C (MPa) | 297.8 | 10.4 | 10.4 | 10.4 | 13.3 | 12.0 |
| Factor of Safety | 3.1 | 1.3 | 1.4 | 1.4 | 7.4 | 8.3 |

Table 6.4 Sliding support contact stresses.

A finite element analysis of the sliding support with a chrome cobalt-chrome cobalt material combination was completed in Ansys. Figure 6.22 shows the resulting contact stress contour plot for this study. The peak contact stress found was 320 MPa which is 7 percent higher than the value found analytically using Equation 2. Despite this small difference in the peak contact stress values, the chrome cobalt sliding support components can still be deemed capable of supporting the applied loads with a high degree of confidence.

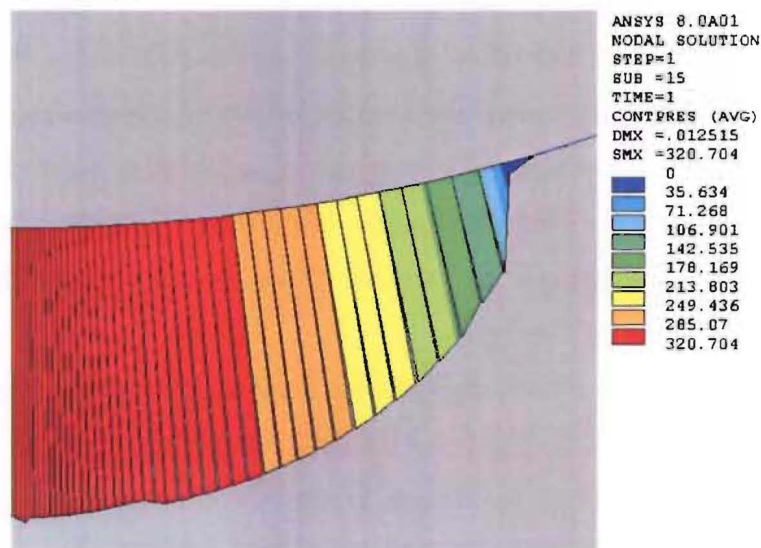


Figure 6.22 FEA contact stress plot for chrome cobalt-chrome cobalt sliding support.

Rolling Support

The dimensions of the rolling support components were determined by choosing values which minimised the contact stress and lift. However, as previously noted these terms are inversely related, that is, dimensions which result in low contact stresses cause significant lift as the implant is deflected, and vice versa. In Section 6.2.2.2 the contact point radius (R_{Contact}) was found to have the greatest influence on both the peak stress and lift. A mid-range R_{Contact} value of 3.75 mm was therefore selected, which will result in a low contact stress and moderate amount of lift. The socket radius has little effect on the contact stress and lift as shown in Figures 6.20 and 6.21, except at low values when a discontinuity causes the amount of lift to increase significantly. The socket radius was therefore set to be 35 mm and using Equation 4 the roller radius was determined to be 15.1 mm. This combination of dimensions results in a system which produces 0.26 mm of lift during 8° deflections, which was considered to be acceptable.

The contact stresses for the rolling support were determined analytically using Equation 2 and an applied load of 600 N. Table 6.5 below shows the resulting contact stresses for several material combinations. From these results it can be seen that only the Radel-Radel material combinations are capable of supporting a 600 N load.

| | Material Combinations | | | | | |
|----------------------|-----------------------|---------------|------------|-----------|-------------|-------------|
| Socket Material | Chrome Cobalt | UHMWPE | UHMWPE | UHMWPE | Radel R4400 | Radel R5500 |
| Support Material | Chrome Cobalt | Chrome Cobalt | Ti Grade 4 | Ti-6Al-4V | Radel R4400 | Radel R5500 |
| C_E | 0.008 | 1.160 | 1.164 | 1.164 | 0.798 | 0.938 |
| Max σ_C (MPa) | 1425.8 | 49.7 | 49.6 | 49.6 | 63.8 | 57.3 |
| Factor of Safety | 0.7 | 0.3 | 0.3 | 0.3 | 1.5 | 1.7 |

Table 6.5 Rolling support contact stresses.

Finite element analyses were conducted for two of the rolling support material combinations.

For comparison purposes a chrome cobalt-chrome cobalt material combination was analysed first. As shown in Figure 6.23 the peak contact stress found in this study was 1440 MPa which is approximately 1 percent higher than the value determined analytically using Equation 2, showing a good correlation between the studies. This also highlights the difference in peak contact stress between the sliding (320 MPa) and rolling (1440 MPa) support systems. The large contact stresses found for the rolling supports suggests an increased potential for wear debris production. Therefore although the rolling support reduces the volume of wear debris produced by eliminating sliding this will be offset by the high contact stresses at the interface of the two components.

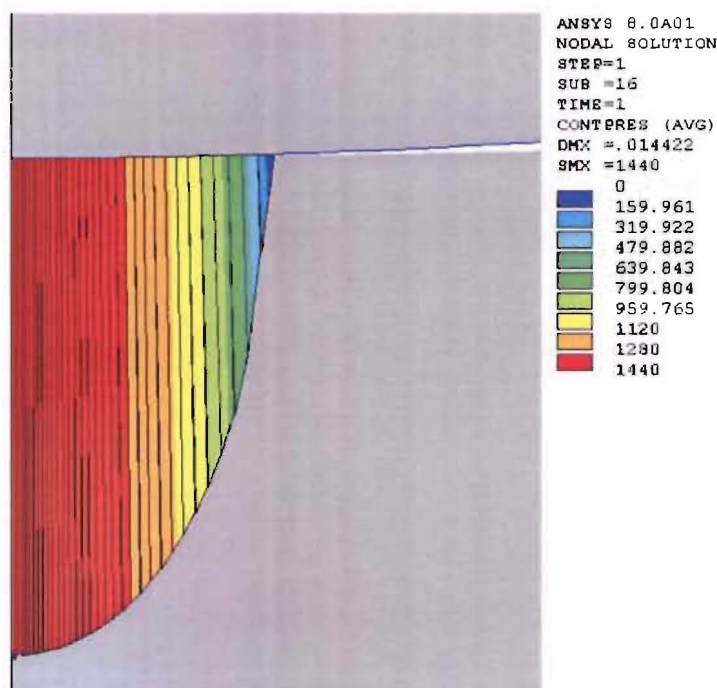


Figure 6.23 FEA contact stress plot for chrome cobalt-chrome cobalt rolling support.

A finite element analysis of the Radel R5500-Radel R5500 material combination was also conducted in Ansys. From Figure 6.24 it can be seen the peak contact pressure found in was 72 MPa which is 26 percent higher than the value found analytically. This different was attributed to some localised plastic deformation occurring in the finite element analysis. This may also account for the fluctuations in the stress profile shown in Figure 6.24. It is not envisaged that such plastic deformation would affect the performance of the Radel R5500-Radel R5500 rolling support as it would manifest itself as bedding-in of the contact faces. Such bedding-in is a common occurrence in hip implants^{15,29,33}. Therefore the Radel R5500–Radel R5500 material combination remains a viable option for the rolling internal support components.

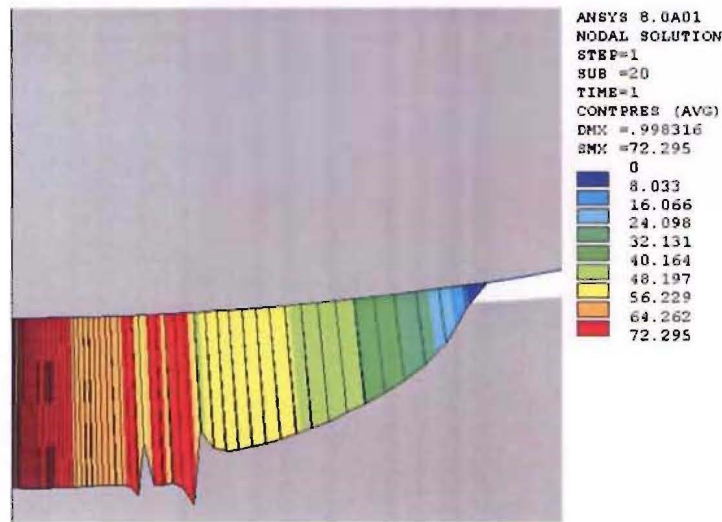


Figure 6.24 FEA contact stress plot for Radel R5500-Radel R5500 rolling support.

6.2.2.5 Surface Roughness

The surface roughness of the internal support components also needs to be considered.

Surface roughness affects the friction coefficient between two parts. More importantly, in the case of the internal support components, the roughness also determines how the surfaces will wear and how well they will support the applied loads.

Surface roughness is normally quantified by a roughness average (R_A). The roughness average is determined by summing of the absolute values of all the areas above and below the nominal surface divided by the length sampled, as shown in Figure 6.25 and Equation 6.

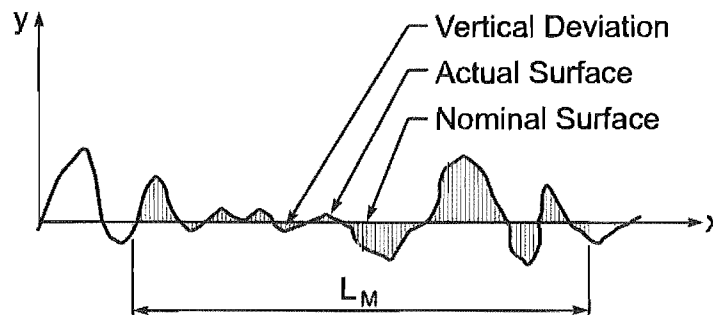


Figure 6.25 Average surface roughness.

$$R_A = \int_0^{L_M} \frac{|y|}{L_M} dx \quad (\text{Eq. 6})$$

Where: R_A = Roughness average.

y = Vertical deviation of the actual surface from the nominal surface.

L_M = Length over which the surface deviations are measured.

If the internal support surfaces have large R_A values, i.e. rough surfaces, there is greater potential for wear debris to be generated. This occurs because the components only contact each other at a few isolated points. As the internal support components move relative to each other the protrusions in contact are subjected to high shear loads. Some of these protrusions may then break away from the parent material producing wear particles, as shown in Figure 6.26.

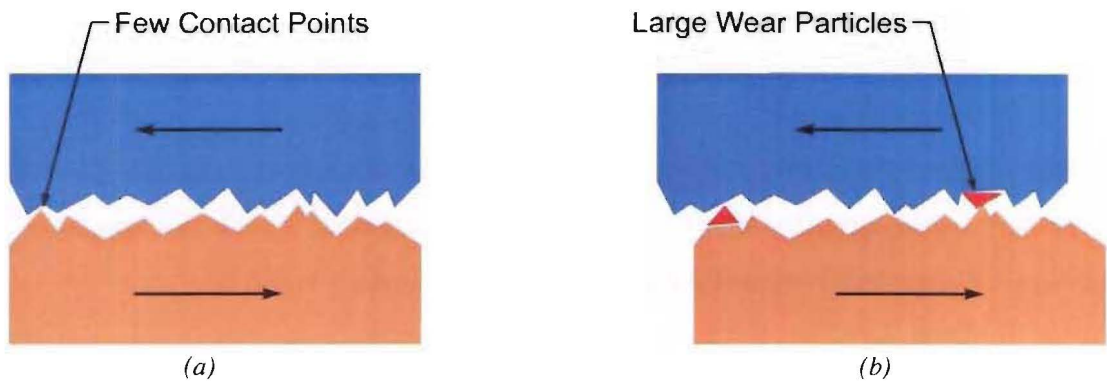


Figure 6.26 Wear resulting from rough surface.

(a) Rough surfaces only contact and transfer loads through a few points.

(b) As the surfaces move relative to each other some of the highly loaded protrusions may break away forming wear debris.

Note: The surface roughness and wear particle size are exaggerated for illustration purposes.

Conversely for components with a high surface finish, low R_A , the two components contact at a greater number of points. Thus the shear loads in these protrusions are lower and there is less chance of them breaking away. Smooth surfaces therefore tend to produce less wear debris and the wear particles generated are smaller in size, as indicated in Figure 6.27.

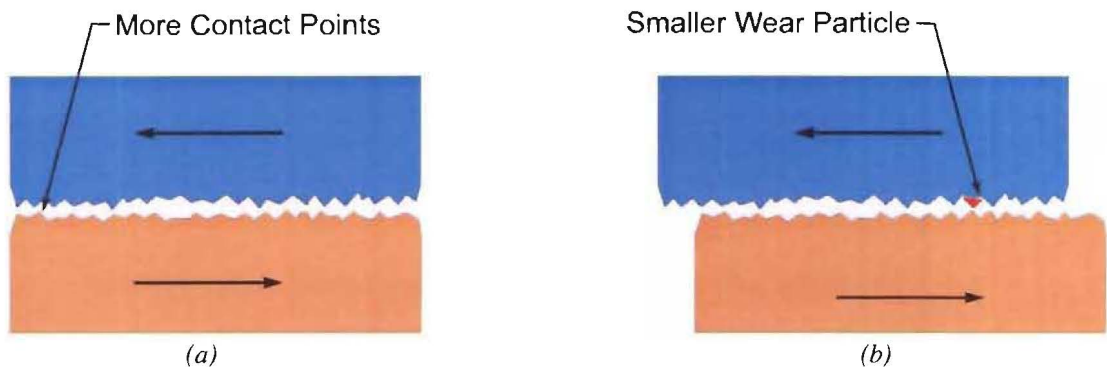


Figure 6.27 Wear resulting from smooth surface.

(a) Smooth surfaces contact and transfer loads through a greater number of points.

(b) As a result of the reduced load there is less potential for protrusions to break free of the parent surface. Any wear debris that is formed also tends to be smaller in size.

Note: The surface roughness and wear particle size are exaggerated for illustration purposes.

The hardness of the components also affects amount of wear debris generated by contact pairs. For example, if hard and soft materials are utilised together the protrusions on the surface of the harder component will tend to penetrate the softer material when compressive loads are applied. This may in turn result in the softer material being cut by the hard protrusions or the formation of features which are prone to fracturing, as illustrated in Figure 6.28.

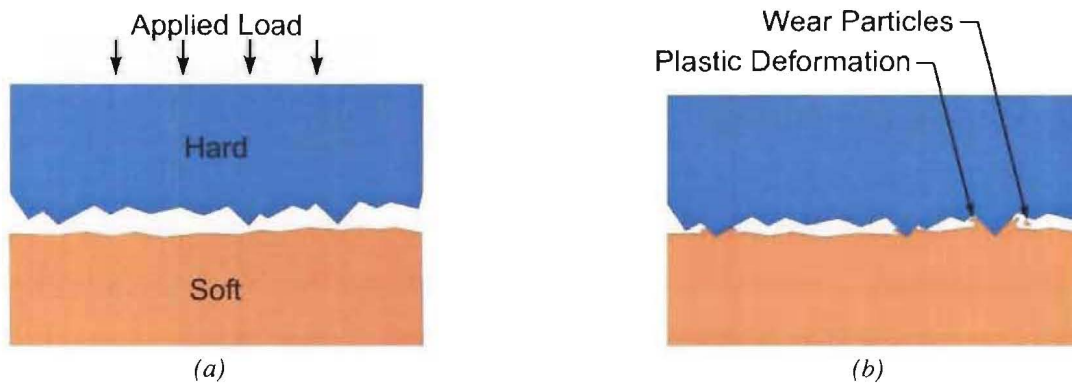


Figure 6.28 Contact couple of differing hardness.

(a) System comprising of a hard and soft contact couple prior to loading.

(b) Once loaded the hard component may plastically deform the soft component, creating wear debris or features which are prone to separating from the parent material.

Note: The surface roughness and wear particle size are exaggerated for illustration purposes.

Therefore the spherical surfaces of the internal support components should have a high surface finish (low R_A) to help ensure minimal wear debris is produced. Hip implants typically have a surface roughness (R_A) of $0.01 \mu\text{m}^{19}$. A similar surface roughness value should be suitable for the bellows intervertebral disc implant support components.

6.2.2.6 Selection of an Internal Support

Both the sliding and rolling internal support could be viable for use in the bellows intervertebral disc implant.

The sliding support offers the advantage of having significantly lower contact stresses at the interface of the two support components. The main disadvantage of this system is that the relative motion between the two components may result in the production of wear debris. The volume of wear debris produced may be minimised though with appropriate material selection.

The rolling support offers the advantage of potentially producing less wear debris than the sliding support. However the contact stresses are higher than the sliding support and it also decompresses the implant as it is deflected. Both of these factors may reduce the viability of the rolling internal support.

To aid in the final selection and design of the internal support mechanism several studies need to be conducted, these should include the following:

- Testing to determine the ideal material combination, including factors such as ensuring compressive failure of the material does not occur and quantification of the volume of wear debris produced.
- Testing to quantify the volume of wear debris produced by the different support systems
- Testing to determine the effects of wear products on the life of the bellows, including whether the wear products do act as fulcrum points and increase the stress at the bellows diaphragm welds.
- Analysis of implants with rolling supports to ensure that the decompression of the implant as it deflects does not adversely affect the life or performance of the metallic bellows.
- Analysis of both support systems to determine their performance when separated repeatedly to simulate complete loading and unloading of the implant.
- Testing of both support systems to confirm they can support the applied loads while the implant is in a deflected state. Also checking to ensure the implant remains stable and there is no tendency for the support components to slip or disarticulate.
- Investigation to determine whether the 0.5 mm gap between the support components when the implant in an unloaded condition, is appropriate.

To aid such testing three test rigs were developed. The details of these test rigs can be found in Chapter 7.

In summary, it is not possible at this time to finalise the design of the internal support for the bellows intervertebral disc implant until testing has been completed. However investigation of the internal support components to date suggests either of the proposed support systems could be viable.

Note: For the remainder of this document the bellows intervertebral disc implant is shown with a roller support, however that this is for illustration purposes only.

6.2.3 Fill Medium Selection

The bellows intervertebral disc implant requires a two part fill medium which includes compressible and incompressible components. The selection of these components is detailed below.

6.2.3.1 Incompressible Component

The majority of the fill medium is required to be incompressible.

The first incompressible fill mediums considered were fluids such as distilled water and silicone. A potential advantage of using a fluid fill medium is that it could be 'injected' into the implant after it has been inserted. This would allow the bellows to be inserted in a compressed form and 'inflated' once correctly positioned. However, the success and long term operation of the bellows intervertebral disc implant would then rely on systems being developed which would allow the surgeon to correctly fill and seal the bellows. The disadvantage of fluid fill mediums is that if the metallic bellows are damaged and leak, the fluid will be ejected into the intervertebral disc space.

Semi-rigid fill mediums such as aerated silicone and closed cell foams were also considered. These materials offer the advantage of not leaking and allowing limited operation of the implant should the metallic bellows fail. These materials could also include voids or be aerated to include the compressible component of the fill medium. The disadvantage of semi-rigid fill mediums is that they can not occupy space between the diaphragms as this would prevent deflection of the implant. Therefore semi-rigid fill mediums would only be able to fill the space between the internal support and inner bellows welds. As a result only a thin walled tube of semi-rigid material could be used, which may have insufficient rigidity to support the applied loads.

Ultimately the decision was made to use a fluid fill medium due to the simplicity of these materials and their ability to conform to the bellows convolutions. Distilled water was dismissed from the selection process as it may cause corrosion of the metallic bellows or become rancid over the life of the implant. The final incompressible fill medium selected was a product called Silbione.

Silbione is produced by Rhodia and is also referred to as Rhodia MDM Fluid. This material was designed as a substitute for Dow Corning Medical Grade 360 Fluid. Silbione is pure, clear, colourless polydimethylsiloxane and is available in standard viscosities of 20, 100, 350, 1000 and 12500 cps. All of Rhodia's medical implant products, including Silbione, are designed and tested to meet many of the ISO 10993 biocompatibility test requirements for long term implantable materials.

Silbione has also been used for application such as lubricating the barrels of plastic syringes to insure smooth operation of the plunger. It can be used to lubricate rubber or plastic tubes and metal instruments that are inserted into the body. Silbione is also used as a lubricant for artificial limbs and eye sockets. This wide spread and successful usage of Silbione in medical applications provides some confidence in its selection as the fill medium for the bellows intervertebral disc implant. Some of Silbione's other properties include:

- High purity
- Chemically inert
- High water repellent
- Low volatility
- Low surface tension
- Resistance to decomposition by heat and oxidation
- Effective defoamer for many fluids

For the purposes of this implant a 20 cps Silbione was selected. The low viscosity of this fluid will allow it to be easily displaced from between the diaphragms during angular deflections, helping to prevent hydraulic damage of the bellows welds from occurring. A technical data sheet for this material can be found in Appendix 8.

6.2.3.2 Compressible Component

As previously described the fill medium must include a compressible component so the implant can match the load deflection curve of the annulus fibrosus. The simplest and most effective mechanism of achieving this is to add a fixed volume of gas (Nitrogen or air) to the implant.

As the gas volume can not be totally compressed a small height of gas must remain once the implant has been compressed 0.5 mm. This remaining gas height (L_2) can be determined as shown in Equation 7.

$$P_1 A_1 L_1 = P_2 A_2 L_2 \quad (\text{Eq. 7})$$

$$101(0.5 + x) = 690x$$

$$x = 0.0857 \text{ mm}$$

Where:

$$P_1 = 101 \text{ kPa} \quad (\text{Atmospheric pressure})$$

$$P_2 = 690 \text{ kPa} \quad (\text{Maximum pressure welded bellows can withstand})$$

$$A_1 = A_2 \quad (\text{Effective area of welded bellows})$$

$$L_1 = 0.5 + x \quad (\text{Length of uncompressed bellows and gas height})$$

$$L_2 = x \quad (\text{Gas height})$$

In an uncompressed state, the bellows intervertebral disc implant will therefore require a compressible gas height of 0.585 mm giving a total gas volume of 134.7 mm³.

The gas component could be enclosed in a flexible bladder separating it from the Silbione fluid or alternatively the bellows could only be partially filled with Silbione. However as the internal support also needs to be accommodated it was decided that only partially filling the bellows was the easiest and most effective option.

6.2.4 Endplates

The endplates are the interface between the metallic bellows and the vertebral bodies and must perform several functions including:

- Provide a leak free, resilient attachment to the bellows diaphragms.
- Induce no additional stresses in the bellows.
- Provide short and long term fixation to the vertebral bodies.
- Allow the disc wedge angle to be replicated.
- Allow installation of internal components as required.
- Locate and transfer loads to and from the internal support components.
- Provide features to aid insertion and retraction.

The design of the endplates is detailed below.

6.2.4.1 Attachment of Endplates to Bellows

A well designed endplate should mimic the configuration of the stamped diaphragms. The endplates must be designed so that they do not interfere with the free movement or contours of the diaphragms⁶. The endplates should also contact the diaphragm flats in such a way that if the bellows are compressed to their solid height the diaphragms are not damaged.

Two potential methods of attaching the endplates to the metallic bellows were identified these were the use of an adhesive or welding.

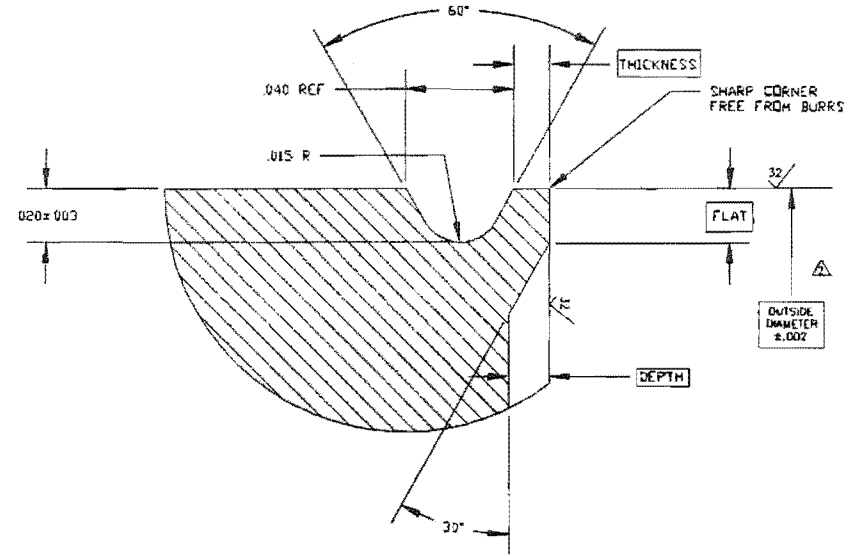
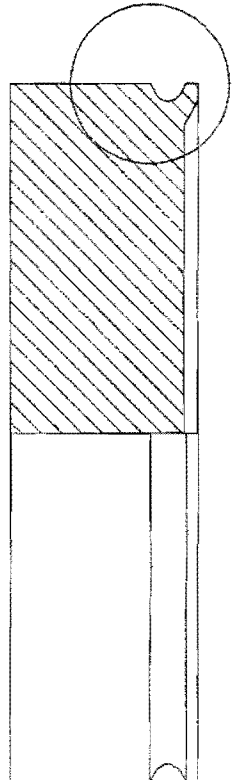
Adhesives offer the advantage of allowing the endplates to be attached to the bellows after the bellows have been manufactured and all the internal components have been installed. Also the use of adhesives does not require the use of specialist equipment and allows final assembly to occur in a sterile environment if necessary. The key disadvantage of adhesives is that they introduce another material and process into the implant assembly which must be proven to be biocompatible and capable of lasting the full life of the implant.

To achieve a good bellows-endplate bond using an adhesive there should ideally be a large contact patch between the two components. During correspondence with Flexial it was established that it is possible to remove the internal diameter diaphragm punch during the manufacture of some diaphragms¹². This allows capping diaphragms to be produced and welded to the ends of the bellows thus providing a large contact area for the endplates to be glued to.

The other option considered was to weld the endplates directly to the bellows diaphragms using the same equipment and techniques used to manufacture the bellows. Welding the endplates in place offers the advantage of not introducing a new processes or materials to the manufacture of the implant. The resulting joint will also have similar performance to the rest of the bellows. Welding the endplates in place does require internal components, such as the internal supports, to be fitted prior to the last endplate being welded in position, however this should not be an issue. To achieve a high quality weld between the endplates and bellows diaphragms, care must be taken to correctly prepare the endplates. Figure 6.29 shows a weld preparation suggested by Flexial Corporation.

NOTES
 1. **EXCEL** DIMENSIONS AND TOLERANCE GIVEN ON INDIVIDUAL DRAWING.
 2. OUTSIDE DIAMETER TOLERANCE APPLIES TO WELD PREP.
 SEE INDIVIDUAL DRAWING FOR TOLERANCE ON REMAINDER OF DIAMETER.

| REVISIONS | | | TOPNO | |
|-----------|------------|---------------------|----------|-----|
| REV | CHANGE NO. | DESCRIPTION | DATE | BY |
| A | 128 | NEW DRAWING | 11/20/95 | RRL |
| B | 1785 | DEPTH WAS .015/.010 | 01/08/01 | JDB |



TYPICAL APPLICATION

| | | | |
|--|---|--|--------------|
| DRAWN BY <u>RRL</u> DATE <u>11/20/95</u> DES. APPD _____ DWG CHKD _____ DWG APPD _____ | UNLESS OTHERWISE SPECIFIED DIMENSIONS ARE IN INCHES TOLERANCE UNLESS SPECIFIED DECIMALS ± .005 DECIMALS >.01 CAST SURFACES ± .033 ANGLES ± 0.5° REMOVE BURRS -- BREAK CORNERS .015 MAX | FLEXIAL CORPORATION COOKEVILLE, TENNESSEE BELLOWS WELD PREP STANDARD FORM C CYLINDRICAL CONFIGURATION | |
| MATERIAL: _____ | SPECIFICATIONS _____ | DWG NO <u>FES-006C</u> | REV <u>B</u> |
| APPROV DWG SCALE <u>NO SCALE</u> (REF 1) | | CADFILE NO <u>FES001C.DWG</u> | |

NOTICE: THIS DRAWING IS ONLY CONDITIONALLY ISSUED AND, EXCEPT FOR RIGHTS EXPRESSLY GRANTED TO THE UNITED STATES GOVERNMENT, NEITHER RECEIPT NOR POSSESSION THEREOF CONFERES OR TRANSFERS ANY RIGHT IN, OR LICENSE TO USE THE SUBJECT MATTER OF THE DRAWING OR ANY DESIGN OR TECHNICAL INFORMATION SHOWN THEREON, NOR ANY RIGHT TO REPRODUCE THIS DRAWING OR ANY PART THEREOF, EXCEPT FOR MANUFACTURE BY VENDORS FOR FLEXIAL CORPORATION, AND FOR MANUFACTURE UNDER FLEXIAL CORPORATION'S WRITTEN PERMISSION.

Figure 6.29 Example of a typical endplate weld preparation
 [Source: Flexial Corporation⁶]

Welding the endplates to the bellows was selected as the preferred method of attachment. The main reasons for this decision were that the welding process was already included in the manufacture of the implant and welding will produce a strong bond which is directly comparable to the rest of the diaphragm joints.

The welding process used to produce bellows is autogenous, that is the edges of the diaphragms melt together and fuse without the addition of filler material. Utilising the same material for the bellows diaphragms and endplates will help to simplify the welding processes and reduce the risk of different material compositions playing a part in the weld's performance. The decision was therefore made to manufacture the endplates from Grade 4 Commercially Pure Titanium.

To facilitate adding the internal support components after the endplates have been welded in position the use of a large removable endplate plug was considered. This endplate plug could also be used to adjust the size of the gap between the internal support components as required. However, this idea was dismissed due to a lack of space for the required features.

6.2.4.2 Fixation to Vertebral Bodies

When considering fixation of the implant to the adjacent vertebral bodies several factors must be considered including:

- The profile of the endplates
- Distribution of loads
- Short and long term fixation
- Use at contiguous levels

The vertebral endplates are not flat and have a profile which varies from patient to patient. To ensure suitable contact between the vertebral and implant endplates the profile of implant's endplates could be tailored to suit each individual patient. However a more practical approach is to reshape the vertebral endplates during the implantation procedure to suit a standard implant endplate profile. The decision was made to use flat implant endplates. A matching flat vertebral endplate contact surface can then be created using standard orthopaedic techniques and instrumentation.

As detailed in Section 4.1.6 the intervertebral disc implant should exert the majority of the forces on the periphery of the vertebral bodies. The central portions of the vertebral endplates must also be loaded to some extent to prevent resorption of the underlying trabecular bone. Reshaping of the vertebral endplates to match the implant's endplates also allows such a load distribution to be achieved.

As the vertebral endplates and underlying trabecular are relatively soft, any high spots on the vertebral endplates will be compressed when load is applied to the implant-vertebral body interfaces. As the implant endplates are relatively stiff this will result in the majority of the loads being applied at the periphery of the implant's endplates and thus the periphery of the vertebral bodies.

A small percentage of the load will also continue to be transferred through the high spots on the surface of the vertebral endplate, which were compressed during the initial loading of the implant-vertebral body interface. As a result the underlying trabecular bone will continue to be loaded, helping to prevent resorption from occurring. The trabecular bone could be loaded further by adding small protrusions, such as small blunt spikes or bumps to the implant endplates, however the effectiveness of, and need for such features needs to be investigated further.

As described in Section 4.1.8 short and long term fixation of the implant to the vertebral bodies requires different mechanisms.

Screws provide good short term fixation, however they are not suitable for use over long periods, or in situations where they are highly loaded. Press fit fixation methods, such as spikes, pegs and fins, provide good initial fixation and a positive means of locating the implant, but they do not perform well under tensile loads.

The best method of providing long term fixation is to utilise bone in-growth into porous surfaces. This fixation method provides a high strength bond which continues to remodel itself over the life of the implant. For bone in-growth to establish there must be little to no relative movement between the implant and surrounding bone for at least 6 weeks. Bone in-growth does not therefore provide good short term fixation. Bone will adhere to machined titanium surfaces, however porous surfaces are normally utilised as they provide a network of holes and under-cut surfaces for bone to grow through and key into, allowing a high strength bond to be created.

For the bellows intervertebral disc implant the chosen fixation system was a combination of fins and porous in-growth surfaces. Fins also offer the advantage of providing an increased surface area for bone in-growth to occur over, thus increasing the strength of the implant-bone interface. The fin design used is similar to that used in the ProDisc implant previously detailed in Section 4.2.1.2. However, the disadvantage of the ProDisc fins is that they are aligned thus there is potential for the vertebral body to split if ProDisc implants are used at contiguous levels. The solution as suggested in Section 4.1.6 was to use offset fins.

Figure 6.30 shows rendered images of the bellows intervertebral disc top and bottom endplate fins and porous in-growth surfaces. It should be noted that in this figure and any proceeding figures which show the endplates, the fixation fins are shown orientated for an anterior insertion, however the fixation fins could be orientated for a lateral approach.



Figure 6.30 Rendered of implant endplates showing fixation features.

(a) Top endplate with two fins and a central filling port.

(b) Bottom endplate with only one fin.

The fins and end surfaces are shown with a porous coating for bone in-growth to key into. Other endplate features are shown in an as-machined condition.

To prevent damage to bone growing into the porous surfaces during the months following implantation, the patient could be advised to only perform light duties and deflections.

6.2.4.3 Replication of the Intervertebral Disc Wedge Angle

As detailed in Section 4.1.6 the intervertebral implant should be capable of conforming to, or have endplates which match, the intervertebral disc wedge angle.

Using flat endplates and having the implant conform to the intervertebral disc wedge angle is not viable for the bellows intervertebral disc implant. Such an approach would require the metallic bellows to be able to deflect in excess of 8° . A more viable option is to produce an implant with non-parallel endplate surfaces as shown in Figure 6.30. Using this approach a range of implants could be manufactured with different intervertebral disc wedge angles to suit different spinal levels and patients.

6.2.4.4 Provision for Filling Bellows

Consideration must be given for adding the fluid fill medium to the implant assembly.

It is not practical to add the fill medium to the implant assembly prior to welding the last endplate in place as this may cause deterioration of the fluid fill medium and any cooling effects the fluid provides may adversely affect the weld(s). Therefore the fluid fill medium must be added through a port in the implant assembly once all the welding processes have been completed.

As the metallic bellows are very thin and highly stressed it is not possible to add a port to one of the bellows diaphragms. Instead the fill medium must be introduced through a port in one of the endplates. Two potential endplate port designs were identified.

The most feasible and chosen solution is to add a recessed port to the flat face of one endplate. A pre-measured volume of fluid can then be added via this port and the implant sealed by the addition of a threaded plug and o-ring. An exploded view of this system is shown in Figure 6.31.

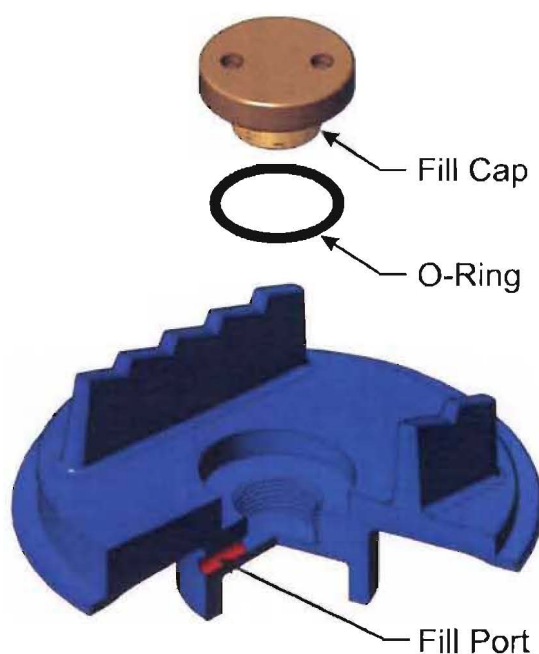


Figure 6.31 Exploded view showing the preferred endplate fill port arrangement.

The endplate is shown partially sectioned to show the fill port (red).

Adding fluid fill medium through a port in the outer cylindrical face of the endplate was also considered. This could be achieved by drilling a hole parallel to the top face of the endplate and then cross drilling, as shown in Figure 6.32. Ultimately this method was rejected though, as there is insufficient space for the required features.

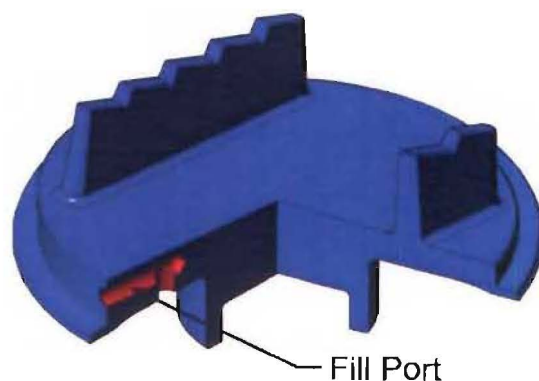


Figure 6.32 Alternative endplate fill port.

The endplate is shown partially sectioned to show the fill port (red) which consists of two cross drilled holes.

6.2.4.5 Internal Support Location and Support

The internal support components must be located centrally in the intervertebral disc implant and remain fixed in position for the duration of the implant's life. Any polymer support components should also be supported around their periphery to help prevent them deforming as a result of cold flow.

The simplest and most efficient way of providing these features is to add a socket to each of the implant's endplates. A light transition fit between the support components and endplate sockets will help ensure the support components remained fixed in place for the life of the implant.

Figure 6.33 shows an endplate socket with and without a polymer support component in place.

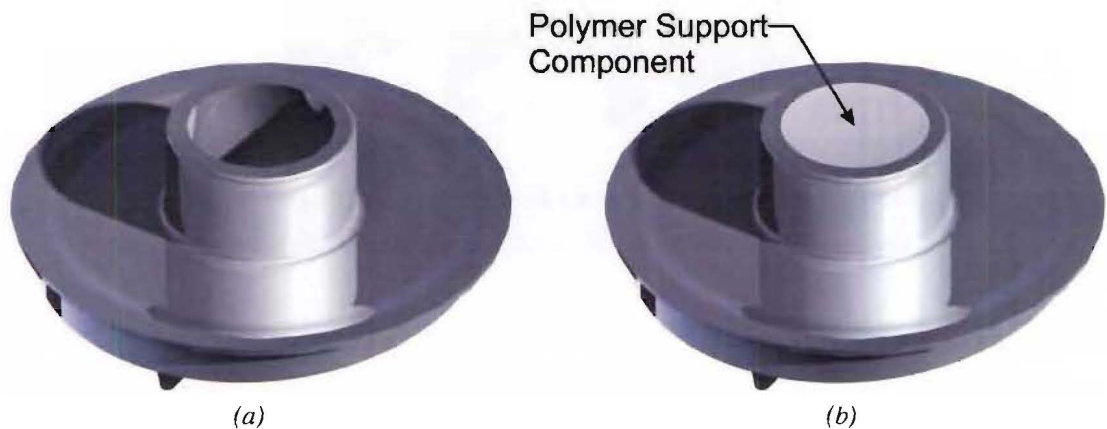


Figure 6.33 Endplate socket.

(a) Bottom endplate and socket for a support component.

(b) Bottom endplate with a polymer support component in place.

6.2.5 Motion Restriction

In order to ensure the metallic bellows are not damaged by being over deflected, motion restricting devices must be provided. Three potential methods of achieving this were identified; the use of the annulus fibrosus, bump stops and tethers.

In a healthy intervertebral disc the zygapophysial joints and the annulus fibrosus restrict the lumbar spine's deflection range. If the majority of the annulus fibrosus is retained as previously described then these natural deflection limiting mechanisms will also be retained and can be utilised. However, in some cases these natural motion restricting mechanisms allow deflections greater than 8° to occur, as detailed in Section 4.1.2. Therefore additional motion restricting devices must be provided to prevent the implant being damaged.

The simplest method of restricting the implant's range of motion is to add bump stops to the implant's endplates. However, this may not be effective. Figure 6.34(a) shows an un-deflected implant with bump stops. Initially the implant deflects angularly around the centre of the bellows until the bump stops contact as shown in Figure 6.34(b). If the implant is forced then to undergo further angular deflection the centre of rotation shifts to the point where the bump stops have contacted, and deflection can then continue to occur, as indicated in Figure 6.34(c). Therefore bump stops alone are not able to limit the deflection range of the intervertebral disc implant.

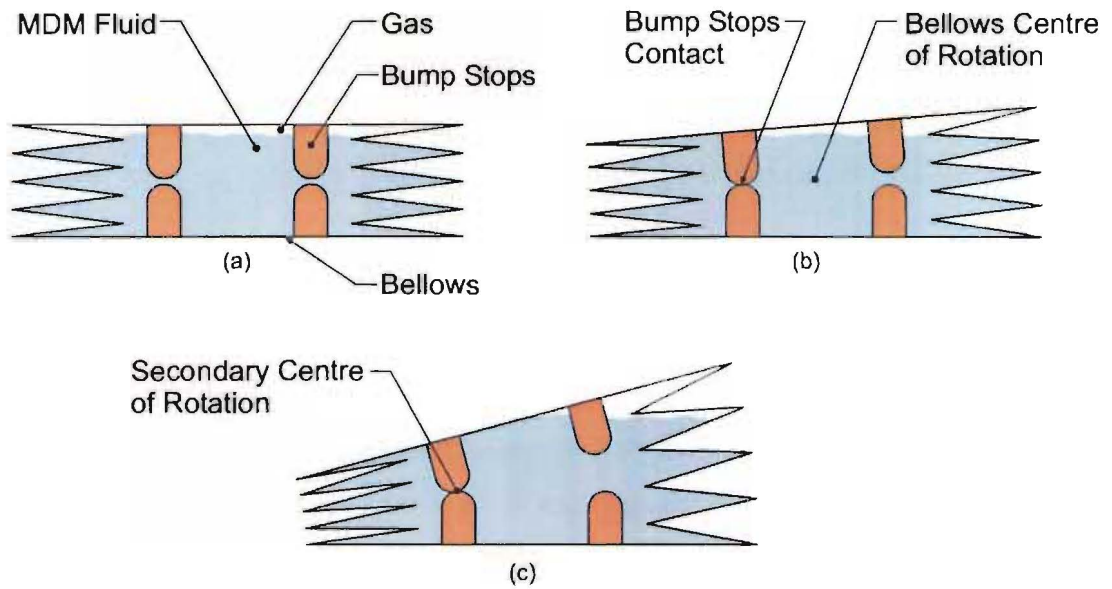


Figure 6.34 Schematic diagrams of bump stops.

(a) Un-deflected implant.

(b) Implant deflected 8° until bump stop contacts.

(c) Implant over deflected, rotation occurs around bump stop stretching opposing side of bellows.

Note: For clarity simplified bellows and bump stops are shown and the internal support is hidden.

Another method of restricting the deflection range of the implant is to use tethers. Tethers are flexible fixed length linkages which prevent further deflection of the implant when taut. Effectively tethers act as a secondary annulus fibrosus, the length of which can be set when the implant is manufactured.

Figure 6.35(a) shows an un-deflected implant with tethers and the internal support. As the implant is deflected the tethers on one side are placed in tension while the opposing tethers are placed in compression. When the tether in tension becomes taut it prevents further extension of the bellows. Further compression of the bellows on the opposing side is prevented by the internal support components contacting, as illustrated in Figure 6.35(b).

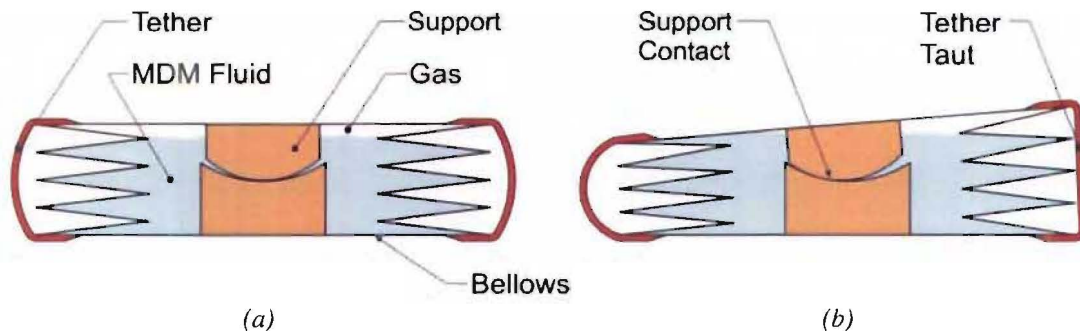


Figure 6.35 Schematic diagrams of externally tethered implant.

(a) Un-deflected implant.

(b) Deflection of the implant places tether in tension preventing further deflection of the implant.

Note: For clarity simplified bellows and internal support are shown.

The tethers could be positioned on the exterior of the implant as illustrated in Figure 6.35(a) or alternatively they could be positioned on the interior of the implant between the internal support and internal wall of the bellows as illustrated in Figure 6.36. However, as there is only a small space between the internal support and inner wall of the bellows, exterior tethers were considered to be more practical.

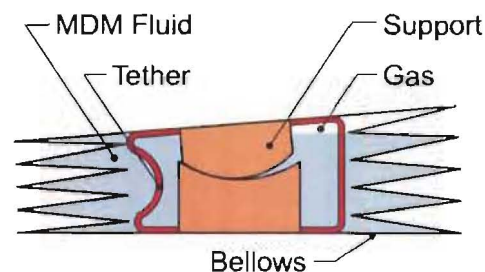


Figure 6.36 Schematic diagram of internally tethered implant.

Note: The implant is shown in a deflected state with simplified bellows and internal support components for clarity.

The disadvantage of restricting the implant's deflection range with tethers is that there is potential for the implant to separate from the vertebral bodies. This will occur when the patient reaches the implant's extreme range of motion and then continues to exert a bending force on the implant. Unable to deflect any further the implant endplates will try to separate from the vertebral body endplates. This may result in the implant's endplates or vertebral bodies being damaged. This would be particularly significant in the first six months following implantation when osteo-integration of the bone into the implant endplates is occurring.

One way of overcoming this problem would be to attach tethers to the vertebral bodies. However to attach sufficient tethers the entire periphery of both vertebral bodies would need to be accessed, a procedure which would be very invasive. This would also rely on the surgeon correctly fitting the tethers. Attaching tethers directly to the vertebral bodies was therefore not considered to be a viable solution.

The final solution selected was utilisation of both the annulus fibrosus and exterior tethers. Provided the majority of the annulus fibrosus is preserved, the combination of these two mechanisms should be sufficient to control the range of motion at the affected spinal level(s).

The external tethers added to implant could consist of a continuous ring of material or be discrete bands which are arranged to coincide with the major axes of deflection. Either of these options would be workable, however a continuous ring of material would allow the tether material to also be used as a protective outer sheath, as detailed in Section 6.2.6.

6.2.6 Protective Outer Sheath

Welded bellows can be damaged by the ingress of debris into the gaps between the convolutions as detailed in Section 6.2.1.2. To prevent such damage from occurring, a flexible protective sheath needs be fitted to the exterior of the implant. The Bryan Cervical Disc described in Section 4.2.1.3 also utilises a sheath to prevent the ingress of biological material and to stop the egress of wear debris and lubricant.

As suggested in the previous section, the sheath material could also be utilised as a tether to prevent over deflection of the implant. This has the advantage of reducing the number of implant components required. To allow the sheath to also act as a tether, it would have to be constructed from a material which does not stretch, is flexible and prevents the in-growth of biological material.

Several textiles have been used extensively for *in-vivo* applications including woven polytetrafluoroethylene (Teflon), polypropylene and polyester. These materials have been used for artificial tendons, ligaments and vascular grafts. To prevent biological in-growth these textiles are normally covered with a silicone membrane, with the exception of materials used for vascular grafts where in-growth is encouraged²⁶. These materials are also produced in woven forms which allow little or no stretch.

The combination tether-sheath could therefore be constructed from any of these materials provided they have sufficient strength and the outer surface is covered by a silicone membrane to prevent in-growth occurring.

The tether-sheath must be firmly anchored to the implant's endplates. Any slipping of the tether will result in it lengthening and no longer correctly limiting the implant's range of motion. Anchoring of the tether-sheath could most easily be achieved by using a clamping ring as illustrated in Figure 6.37. This clamping ring could take several forms such as a preformed circlip style spring or alternatively a crimped ring could be used.

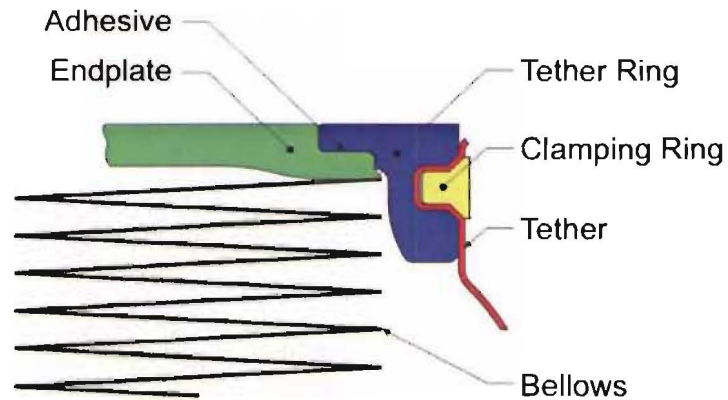


Figure 6.37 Tether retaining components.

Note: Simplified bellows are shown for clarity.

The clamping arrangement shown in Figure 6.37 features a 'tether ring' which the tether-sheath is fastened to. Ideally this tether ring should be incorporated into the implant's endplate, although there must also be sufficient room to access the bellows-endplate weld(s) during the manufacturing process. The diameter of the tether ring should also be reduced where possible. These refinements of the tether ring were not completed as part of this project. Instead the tether ring is located on the implant endplate by a spigot and held in place by a medical grade adhesive.

Two medical grade adhesives for retaining the tether ring were identified. Both of these products are produced by NuSil and are called Med-1511 and Med1-4213. Both adhesives cure at room temperature and their adhesion to titanium is enhanced with the use of a primer²⁵. The two systems differ in the way they cure. Med-1511 cures in the presence of atmospheric moisture hence the relative humidity of the assembly environment will influence the rate of cure. Med1-4213 is a two-part product which cures within 24 hours of mixing. Data sheets for both adhesives and primers can be found in Appendix 8.

6.2.7 Surface Treatment

Care must be taken to ensure that the surface condition of the finished implant is suitable for implantation. To achieve this ASTM F86-01³ recommends the following conditions be met:

- The surface must be free of imbedded or deposited finishing materials or other foreign contaminants.
- Surfaces should be free of imperfections, such as tooling marks, nicks, scratches, cracks, cavities, burrs and other defects that impair the serviceability of the device.
- All traces of oils, greases, paints or other loose surface contaminants should be removed.
- Any passive oxide films should be restored to provide maximum corrosion resistance.

For implants made of titanium ASTM B600-91¹ suggests several treatment options to ensure the implant is clean, free of scale and that the passive oxide film is optimised. The treatment options in this standard include the use of propriety solutions or molten salt baths. As the intervertebral disc implant has many small features, particularly the metallic bellows which may distort when heated, treatment in molten salt baths is not desirable.

The intervertebral implant should therefore be treated in the following manner following completion of all the manufacturing processes.

- Remove lubricants oils grease using alkaline or emulsion soak-type cleaners and electrolytic alkaline cleaning systems.
- Remove any coarse scale using sand, shot or vapour blasting, if possible or required.
- Treat using propriety caustic-based solutions to remove any scale, lubricant residues, embedded iron, interstitial carbon, oxygen and nitrogen.
- Immerse in sulphuric acid solution to remove any converted scale product, as required by the previously used propriety caustic-based solution.
- Final brightening of the implant can be achieved by brief cycle in nitric-hydrofluoric solution.
- Rinse well.
- Visually inspect for any surface contamination.

6.2.8 Surface Marking

Permanent marking of the implant is a small but important issue. ASTM F983-86² recommends that all implants should be able to be positively identified through the use of permanent markings. Where there is sufficient space, markings should include the following information:

- Manufacturer
- Material
- Catalogue or model number
- Serial or lot number

If space is available additional information can be included such as implant size or the orientation in which the implant is intended to be used.

Permanent marking of medical implants can be achieved in several ways including, but not limited to, the use of mechanical imprinting, chemical etching, traditional mechanical engraving or lasers. ASTM F86-01³ states that whatever marking process is used it should not impair the mechanical or corrosion properties of the implant, nor should the markings cause an adverse tissue response. The location of any markings should also be recorded on the manufacturing drawings for the implant.

In the case of the bellows intervertebral disc implant the ideal location for markings is on the machined outer face of either endplate, as shown in Figure 6.38.



*Figure 6.38 Example of laser engraving on the outer face of the top endplate.
The engraving is shown positioned either side of the insertion/retraction tooling hole.*

The serial or lot number should be cross referenced to the raw material certificates and the job and inspection sheets for each manufacturing task. Such records allow the implant's performance to be related back to the raw components and processes as required.

6.2.9 Insertion/Extraction Tooling

Instrumentation needs to be developed to aid in the insertion and retraction of the implant. However, the primary focus of this project was the development of the intervertebral disc implant and as such the design of insertion and retraction instrumentation was not considered in depth during this project. However one potential insertion procedure is described below.

Removal of the nucleus pulposus can be achieved using standard instrumentation already developed and used for spinal fusion procedures. However, more effective tools may need to be developed. Markolf et al²¹ noted during their studies of the intervertebral discs that, despite having easier access to the nucleus pulposus than can normally be accomplished surgically, a surprisingly large percentage of the nucleus pulposus (approximately 50%) remained even after their most thorough discectomy procedure.

Flat vertebral endplate surfaces must be created so the intervertebral disc implant distributes loads appropriately, as detailed in Section 6.2.4.2. This can be achieved using standard orthopaedic tools such as chisels and scraping devices.

The most complex tooling required will be that used to pre-cut slots for the fixation fins the correct distances apart and in the correct orientation between the vertebral bodies. This could be achieved using a reciprocating saw and guide block. However, provision should be made for locking the guide block in position for the duration of all the saw cuts.

Finally an insertion tool is required to impact the implant into position. While the bellows intervertebral disc implant is being inserted the implant's endplates should be fixed relative to each other to prevent any deflection of the implant. Fixing the endplates relative to each other will also prevent the bellows being damaged. For example if one endplate were to advance into the intervertebral disc space ahead of the other, the bellows would be placed in shear. The insertion tool should also be anchored to the implant to reduce the risk of the surgeon slipping and impacting the bellows rather than the endplates.

Accordingly threaded instrumentation holes could be added to the implant endplates as can be seen in Figure 6.38. By screwing the insertion tool into these holes, the endplates are constrained and the position of the instrumentation relative to the bellows can also be controlled.

Figure 6.39 shows an example of an insertion tool suitable for impacting the implant into position. It should be noted that the threaded instrumentation holes and insertion tool are shown orientated for an anterior insertion. This is because for the endplate design shown the instrumentation holes are best accommodated by the anterior aspect of the endplate. However, the insertion features and thus the insertion tool could be orientated for a lateral approach.

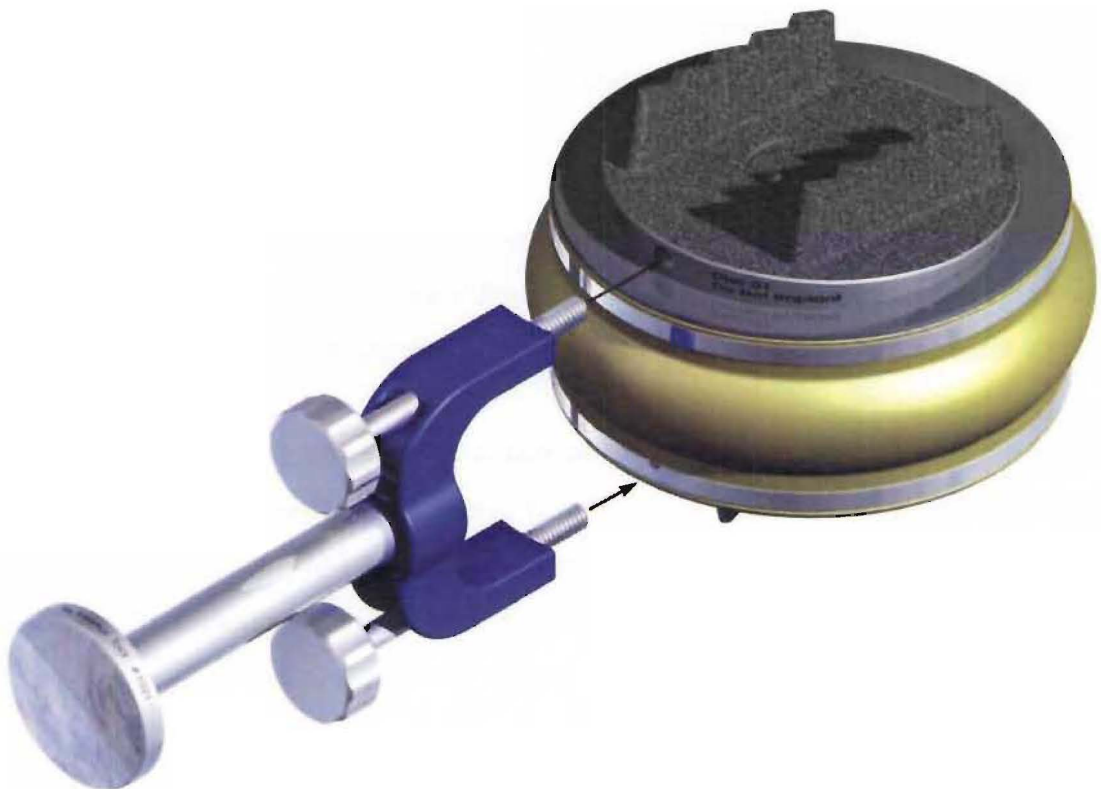


Figure 6.39 Suggested intervertebral disc implant insertion tooling.

Instrumentation is also required to remove the intervertebral disc implant should the implant need to be revised or a traditional fusion carried out. However, as previously stated the development of such instrumentation was not considered during the course of this project.

6.3 Assembled Implant Renders and Drawings

Figure 6.40 below shows a rendered, partially sectioned isometric view of the bellows intervertebral disc implant in an uncompressed state. For clarity the fluid fill medium is not shown.

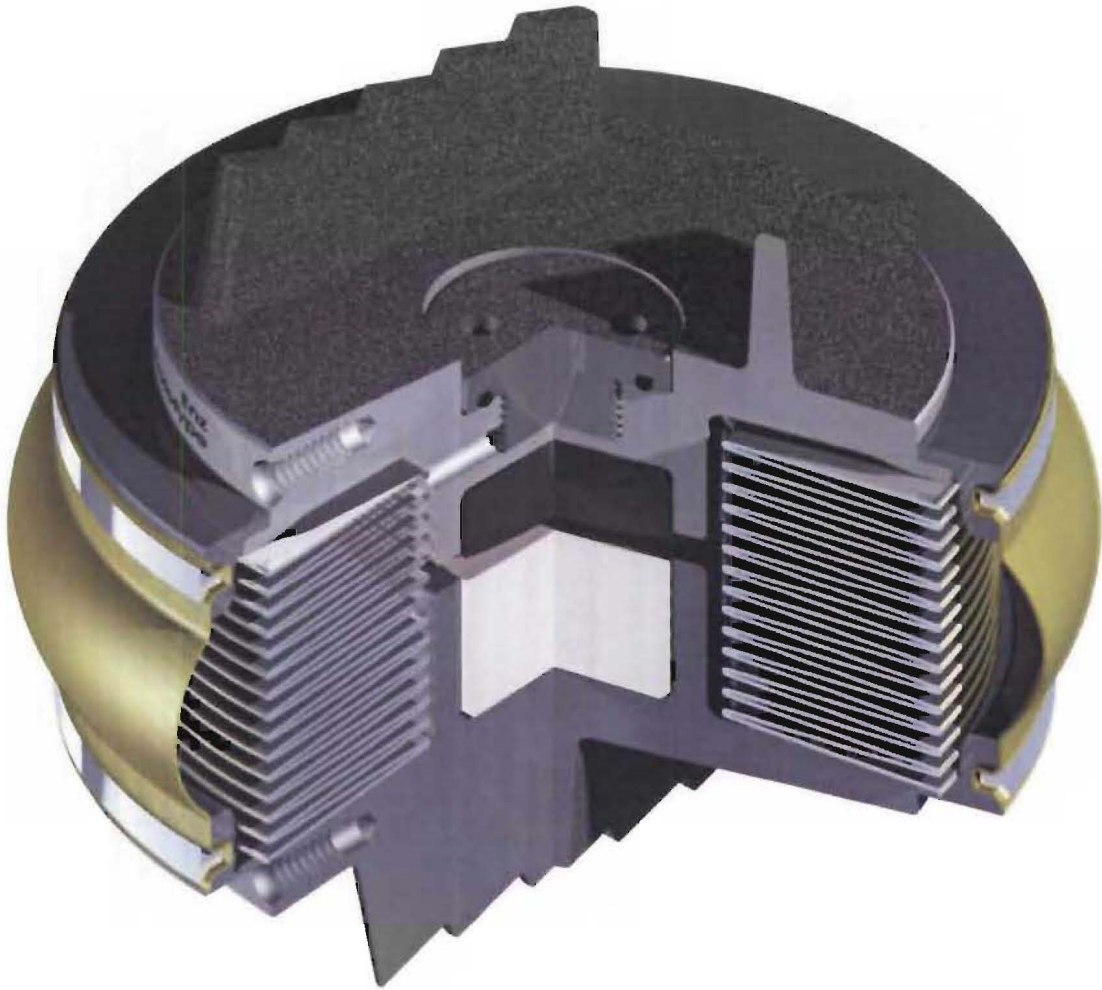


Figure 6.40 Rendered partial isometric of bellows intervertebral disc.

Note: the fluid fill medium is not shown for clarity.

Figure 6.41 shows a general assembly drawing of the bellows intervertebral disc implant.

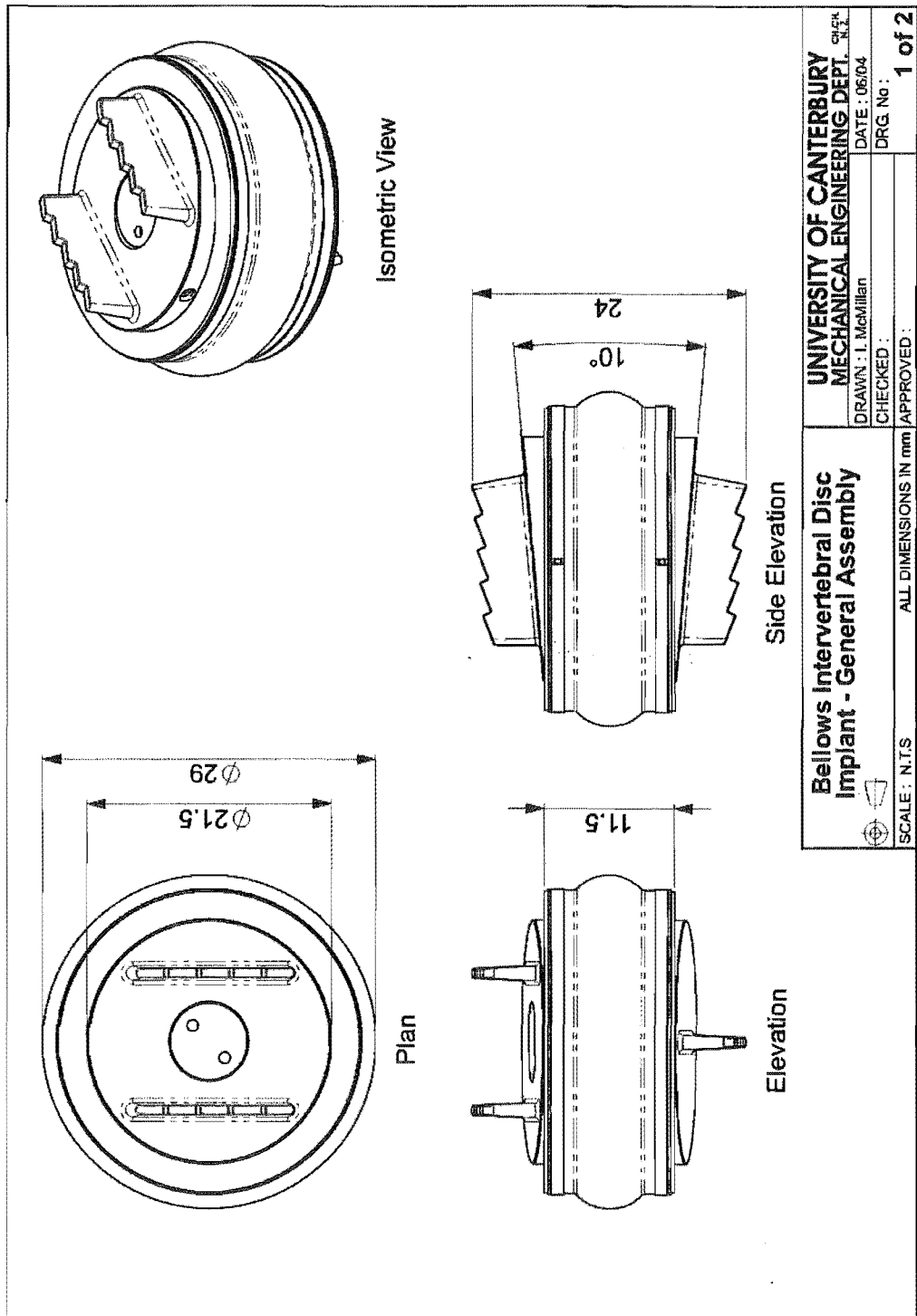


Figure 6.41 General assembly of bellows intervertebral disc implant.

Figure 6.42 shows a sectioned view and bill of materials for the bellows intervertebral disc implant. As previously discussed in Section 6.2.6 and as can be seen in Figures 6.41 and 6.42 the tether and clamping rings require further refinement to reduce the overall diameter of the implant. However, such refinement was not completed as part of this project.

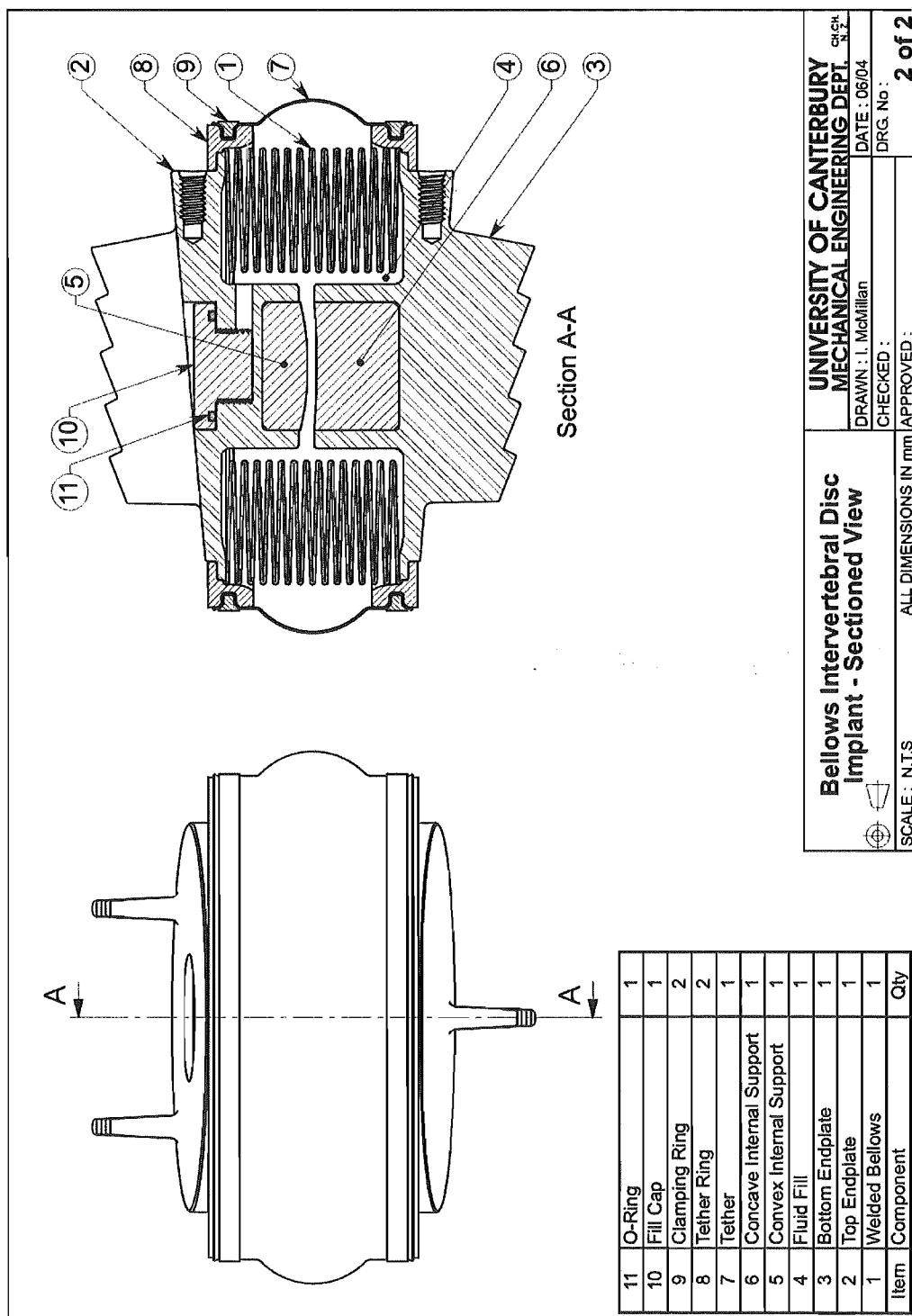


Figure 6.42 Sectioned view of bellows intervertebral disc implant.

6.4 Advantages and Disadvantages of Bellows Intervertebral Disc Implant

The bellows intervertebral disc implant has several advantageous features when compared to existing devices, as detailed below.

The bellows intervertebral disc implant closely replicates the arrangement of a healthy intervertebral disc, consisting of a flexible pressure vessel which contains an incompressible fluid. The bellows intervertebral disc implant also incorporates additional load carrying and overload protection features. The implant assembly is able to withstand compressive loads and angular deflections while having a low angular stiffness.

The bellows intervertebral disc implant is designed to be inserted using a lateral approach thus minimising the trauma to musculature and nerves surrounding the patient's spine. This approach also allows the majority of the annulus fibrosus to be preserved. Preservation of the anterior portion of the annulus fibrosus is particularly relevant as this portion of the annulus fibrosus is able to support a high percentage of the applied compression loads. The annulus fibrosus also helps to prevent anterior displacement of the vertebral bodies, helping to ensure normal loading of the zygapophysial joints.

The bellows intervertebral disc implant has a low angular stiffness. The combination of this low stiffness and preserving the majority of the annulus fibrosus will allow the affected spinal level to have an angular stiffness which is similar to that of a healthy intervertebral disc. This will help to ensure the stability of the spine is preserved and that additional exertion is not required for the patient to bend.

The bellows intervertebral disc implant does not produce any wear debris, helping to prevent the onset of osteolysis. Any wear particles produced by the internal support components will remain encapsulated by the bellows. The bellows intervertebral disc implant is also able to perform 100 million deflections giving the implant a serviceable life of approximately 40 years *in-vivo*.

In a healthy spine the intervertebral discs retard the transmission of shock loads by utilising the elastic properties of the annulus fibrosus. The welded bellows are not able to stretch elastically and thus cannot retard shock loads to the same degree as a healthy intervertebral disc. However some shock retardation may occur through compression of the gaseous component of the fill medium, although this can only occur if the internal support components are not already in contact. However, with the exception of the Prosthetic Disc Nucleus, none of the other artificial intervertebral discs detailed in Section 4.2 are able to absorb shock loads either.

The main disadvantage of the bellows intervertebral disc implant is that it is complex with multiple load carrying mechanisms, including the annulus fibrosus, the fluid filled bellows and the internal support. However the use of multiple load carrying mechanisms means there is less chance of the bellows intervertebral disc implant failing catastrophically.

The main factor contributing to the complexity of the design is that the welded bellows on their own do not have sufficient pressure capacity to support all the applied loads. This requires the use of the annulus fibrosus and internal support to carry a percentage of the loads. If welded bellows with a higher pressure capability can be developed this may remove the reliance on the annulus fibrosus.

Another factor which strongly influenced the design of the intervertebral disc implant was the specification requirement that the implant was to produce no wear debris. If this restriction were removed a less complex system may have been developed. The Link SB Charité disc and ProDisc implant are examples of intervertebral disc implant which produce wear debris and have relatively simple components. However, the role of wear debris in the spine is a contentious issue. This issue will be resolved only after a large number of wear debris producing artificial discs have been in service for an extended period of time. If debris problems do arise there will be a need for an artificial disc which does not produce wear debris, such as the bellows intervertebral disc implant.

The bellows intervertebral disc implant requires a protective sheath to prevent the ingress of debris into the bellows convolutions to ensure the bellows internal diameter welds are not damaged. A sheath could also be incorporated into existing implants that produce wear debris, such as the Charité or ProDisc implants. By using a sheath, any wear debris that was produced could be contained, nullifying the issue of wear debris generation and osteolysis. However, this would complicate insertion of the polyethylene cores into the Charité and ProDisc implants and thus would require a significant redesign of these implants.

Therefore, in spite of its limitations the bellows intervertebral disc implant still has significant merits that warrant further development and testing.

6.5 Patent

In September 2001 a provisional specification for the bellows intervertebral disc implant was submitted for patenting in New Zealand. This provisional patent has since been amended several times. The current New Zealand Patent Application Number is 525179/526019.

In May 2004 a Patent Cooperation Treaty (PCT) application was also lodged. The content of this application is the same as that for the New Zealand patent. The current PCT International Application Number is PCT/NZ2004/000069.

Full text for the current NZ Patent Application can be found in Appendix 9.

6.6 References

1. *Standard Guide for Descaling and Cleaning Titanium and Titanium Alloys Surfaces. Annual Book of ASTM Standards, 2002*, ASTM International: West Conshikocken, PA, USA. Vol 02.04. pp 574-576.
2. *Standard Practice for Permanent Marking of Orthopaedic Implant Components. Annual Book of ASTM Standards, 2002*, ASTM International: West Conshikocken, PA, USA. Vol 13.01. pp 353-354.
3. *Standard Practice for Surface Preparation and Marking of Metallic Surgical Implants. Annual Book of ASTM Standards, 2002*, ASTM International: West Conshikocken, PA, USA. Vol 13.01. pp 10-11.
4. Boedeker Plastic Inc. *Polyethylene Specifications*. Boedeker Plastics Inc, [cited Nov 2002]. Available from http://www.boedeker.com/polye_p.htm.
5. *Personal Communication*, Elliott J. *Bellows Enquiry*. Senior Aerospace Bird Bellows - Engineering Department, Congleton, UK, 2 May 2002.
6. Flexial Corporation, *Welded Bellows Engineering Handbook*. 2002, Cookeville USA.
7. *Personal Communication*, Foo C. *Quotation of BioDur CCM Plus Alloy - Uni of Canterbury*. Carpenter Technology Asia Pacific, 30 August 2002.
8. Hertz H, *Gesammelte Werke*. Leipzig, 1895. Vol 1.
9. *Personal Communication*, Higbie S. *Bellows Inquiry 1*. Flexial Corporation, Cookeville USA, 1 May 2002.
10. *Personal Communication, Email*: Higbie S. *Bellows Inquiry 2*. Flexial Corporation, Cookeville USA, 14 May 2002.
11. *Personal Communication, Email*: Higbie S. *Bellows Inquiry 3*. Flexial Corporation, Cookeville USA, 8 August 2002.
12. *Personal Communication*, Higbie S. *Bellows Inquiry 4*. Flexial Corporation, Cookeville USA, 8 August 2002.
13. *Personal Communication*, Higbie S. *Bellows Inquiry 5*. Flexial Corporation, Cookeville USA, 28 August 2002.
14. *Personal Communication*, Higbie S. *Bellows Inquiry 6*. Flexial Corporation, Cookeville USA, 5 November 2002.
15. Hu X Q, Isaac G H, Fisher J, *Changes in the contact area during the bedding-in wear of different sizes of metal on metal hip prostheses*. *Biomed Mater Eng*, 2004. Vol 14 (2): pp 145-9.

16. Komistek R D, Dennis D A, Mabe J A, *In-vivo determination of patellofemoral separation and linear impulse forces*. Orthopade, 1998. Vol 27 (9): pp 612-8.
17. Komistek R D, Dennis D A, Mabe J A, Walker S A, *An in-vivo determination of patellofemoral contact positions*. Clinical Biomechanics, 2000. Vol 15: pp 29-36.
18. Komistek R D, Dennis D A, Ochoa J A, Haas B D, Hammill C, *In-Vivo Comparison of Hip Separation after Metal-on-Metal or Metal-on-Polyethylene Total Hip Arthroplasty*. Journal of Bone and Joint Surgery, 2002. Vol 84-A (10): pp 1836-1840.
19. Liao Y-S, Hanes M, Fryman C, Turner L. 2004. *Effects of Head Size, Clearance and Start-Stop Protocol on Wear of Metal-on-Metal Hip Bearings*. 7th World Biomaterials Congress, Sydney. pp 82.
20. Lombardi A V, Mallory T H, Dennis D A, Komistek R D, Fada R A, Northcut E J, *An in-vivo determination of total hip arthroplasty pistoning during activity*. Journal of Arthroplasty, 2000. Vol 15 (6): pp 702-708.
21. Markolf K L, Morris J M, *The structural components of the intervertebral disc*. J Bone Joint Surg, 1974. Vol 56A (4): pp 675-687.
22. Northcut E J, Komistek R D, Dennis D A, Ochoa J A, Hoff W A, *In vivo determination of hip separation and forces generated due to implant loading conditions*, Presented at the Twenty-First Annual Meeting of the American Society of Biomechanics. 1997, Clemson University, South Carolina <http://asb-biomech.org/onlineabs/abstracts97/106/>.
23. *Personal Communication*, Prowse D. *Bellows Quotation*. Flexial Corporation, Cookeville USA, 17 December 2002.
24. Reeves E A, Barton D C, FitzPatrick D P, Fisher J, *A two-dimensional model of cyclic strain accumulation in ultra-high molecular weight polyethylene knee replacements*. Proc Instn Mech Engrs, 1998. Vol 212 (H): pp 189-198.
25. *Personal Communication*, Reilly B T. *Titanium Biocompatible Adhesives*. Nusil, 15 May 2002.
26. Rigby A J, Anand S C, *Medical Textiles*, in Horrocks A R and Anand S C (Eds). *Handbook of Technical Textiles*, 2000, Woodhead Publishing Limited in association with The Textile Institute: Cambridge. pp 407-24.
27. Roark R J, Young W C, *Roark's formulas for stress and strain*. 6th Edition. 1989, New York: McGraw-Hill.
28. *Personal Communication*, Schreiber S. *Bellows Inquiry*. Witzmann, Germany, 8 May 2002.

29. Smith S L, Dowson D, Goldsmith A A, *The effect of femoral head diameter upon lubrication and wear of metal-on-metal total hip replacements*. Proc Inst Mech Eng, 2001. Vol 215 (2): pp 161-70.
30. Stein H L, Ticona LLC, *Ultra High Molecular Weight Polyethylene (UHMWPE)*, 1998, ASM International: Ohio, USA. pp 167-171.
31. Welsch G, Boyer R, Collings E W, eds. *Materials Properties Handbook: Titanium Alloys*. 1994, ASM International: Materials Park, OH.
32. Westlake Plastics Company, *Products for Medical Applications*. 2002, Lenni, PA, USA.
33. Wroblewski B M, Siney P D, Dowson D, Collins S N, *Prospective Clinical and Joint Simulator Studies of a New Total Hip Arthroplasty Using Alumina Ceramic Heads and Cross-Linked Polyethylene Cups*. The Journal of Bone and Joint Surgery, 1996. Vol 78B (2): pp 280-5.

<Blank Page>

Chapter 7 – Test Rig Design

7.1 Introduction

As suggested in the previous chapter, to aid in the development of the bellows intervertebral disc implant testing of individual components and the implant assembly needs to be conducted. This chapter details the development of three test rigs which could be used to conduct such *in-vitro* testing. It should be noted that these test rigs are not designed specifically for the bellows intervertebral disc implant and could be used to test any artificial disc implant.

7.2 Background

There is currently no validated animal model for testing and evaluating intradiscal implants or artificial disc implants¹. The use of baboons has been suggested, however this model presents several disadvantages including biological and biomechanical dissimilarities as well as availability and ethical issues. Therefore mechanical test rigs need to be developed.

Wilke et al⁴ recommended the development of agreed *in-vitro* testing conditions to allow test results from various research groups to be compared. The proposed standard was primarily aimed at *in-vitro* tests which utilised functional cadaver spinal segments. The standard included recommended loading methods, specimen conditions and analysis parameters. It was also recommended that spinal test rigs incorporate the following features:

- Specimens should be able to move freely in all six degrees of freedom.
- Test rigs should be capable of simulating the six loading components separately. These include flexion/extension, lateral bending and torsion along with axial compression, tension and shear in the sagittal and horizontal planes.
- All possible loading combinations should be provided.
- Loading should be applied either continuously or in a stepwise fashion.
- Specimens should be able to be loaded in the positive and negative directions continuously (flexion/extension or left-right) so load displacement curves that reflect the full cycle of motion in a given direction can be obtained.

Wilke et al³ reported the design and construction of a multi-axis test rig for *in-vitro* experiments. This test rig was designed to test functional cadaver spinal segments and included the six load components detailed above as well as the option of including muscle forces. To create the required motions this test apparatus utilised a gimbal system which was connected to an overhead gantry. The three gimbal axes were driven using stepper motors and gearbox-clutch assemblies to provide flexion/extension, lateral bending and axial twisting motions. The gantry consisted of a support carriage which translated on rails to provide the required shear, compression and tension movements. Figure 7.1 shows schematic diagrams of this apparatus.

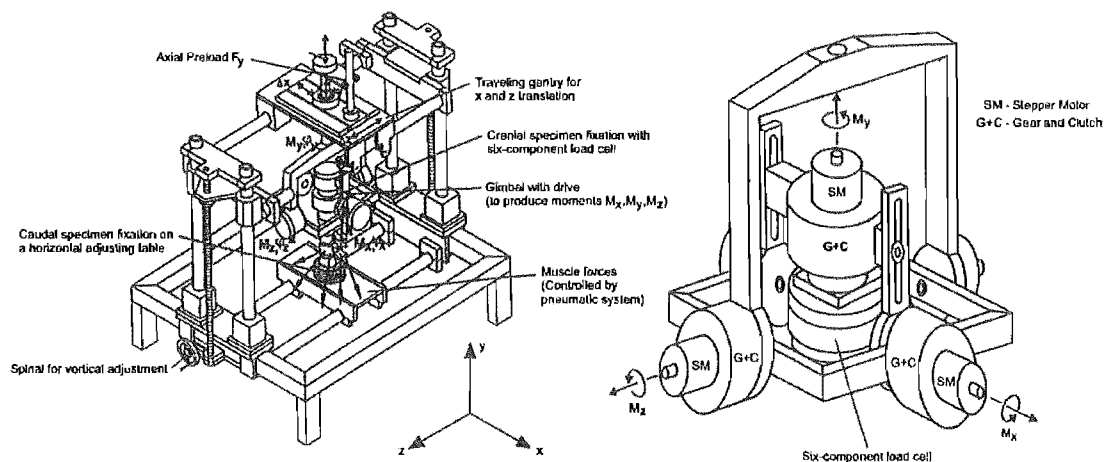


Figure 7.1 Schematic diagram of the multi-axis test rig designed by Wilke et al.

[Source: Wilke et al³]

Add-on modules are also available for universal testing machines which allow multi-axis testing of spinal implants and cadaver specimens. Figure 7.2 shows a flexion/extension and axial twisting module for a MTS tensile testing machine.



Figure 7.2 Flexion/extension and axial twisting module for a MTS machine.

[Source: MTS Systems Corporation²]

The main disadvantage of the Wilke³ test rig and add-on modules is the frequency at which they are able to perform tests. Both the Wilke and MTS test systems are only able to perform around 5000 deflection cycles per day. At this rate, testing the bellows intervertebral disc implant to destruction could take in excess of 20000 days, assuming an implant life of 40 years (100 million cycles).

Therefore, to aid in the development of the bellows intervertebral disc implant and its constituent components faster test rigs and simple testing procedures needed to be developed. To achieve this, the functions of the intervertebral disc implant were broken down into groups of loads and movements that are more or less independent. This allowed simpler test rigs and testing procedures to be developed. Another benefit of this approach is that it allows parallel development and testing of different implant functions thus reducing the overall testing time frame. This approach does rely on there being no interactions between the different groups of functions. Accordingly it would be advisable to perform complete testing procedures prior to using the implant *in-vivo*.

Ultimately, three test rigs to test different implant functions were designed. These test rigs were designed to complete the following tasks:

- Test how specimens perform during angular deflections around one axis.
- Test the compression response of specimens.
- Test specimens in flexion/extension, lateral bending and compression.

7.3 Common Features

The test rigs designed have several common requirements and features as detailed below.

7.3.1 Environmental Considerations

The test temperature is important as the physical properties of materials, especially polymers, are temperature dependant. All testing should therefore be carried out at a constant temperature of 37°C to simulate *in-vivo* conditions.

Corrosion and chemical interactions between components and fluids must also be considered. For example when testing the internal support components they should be surrounded by the fluid fill medium used in the bellows intervertebral disc implant. Similarly, if the metallic bellows are being tested the exterior should be exposed to conditions as close to those *in-vivo* as possible, while the interior faces should be exposed to the fill fluid medium. To simulate *in-vivo* conditions stabilised bovine serum, otherwise known as Hank's solution, is normally used.

The vessels used to contain the test fluids must meet several requirements including:

- The vessels should be non-reactive so they do not affect the test results.
- Removable top covers should be provided.
- Provision should be made for adding and draining the test fluids.
- The vessels should ideally be transparent to allow visual monitoring of the test specimens.

All the test rigs developed utilised Perspex vessels to contain the testing fluid. The top of these vessels can be easily sealed using plastic cling film. To prevent localised overheating and burning of the test fluids, 316L stainless steel tube can be coiled in the bottom of the fluid containment vessels and water preheated to 37°C pumped through the tubing. This reticulating hot water system allows the temperature of the testing fluids to be accurately controlled while not exposing them to temperatures greater than 37°C. Conversely, if heat needs to be removed from the system cold water could be circulated through the stainless steel tubing.

Wear debris generated by test rig components should under no circumstances come into contact with the test specimens or fluids as this may influence the test results. Therefore no sliding or articulating test rig components should be located in the fluid containment vessels.

7.3.2 Monitoring

The performance of the test specimens and test rigs needs to be monitored for the duration of all the tests and all the results recorded. Parameters of interest may include the applied loads or a tally of the excursions test specimens have been subjected to. Specific parameters which should be recorded are detailed in each test rig's specification.

Monitoring accessories may also be added to some test specimens to record parameters such as pressure, temperature or strain gauge readings. Therefore there should be space in the fluid containment vessels for these devices and their connections.

If a computer is used to monitor and record the test rig and test specimen parameters then the results should be permanently stored, rather than just cached, so that the results are not lost if the power supply to the computer system is disrupted.

7.3.3 Safety

The test rigs should have physical guards to prevent the operator or any bystanders being injured.

7.3.4 Control Systems

If a control system is used to manage the test rigs it should also have provisions for:

- Stepping through the test sequence.
- Pausing and recommencing the test sequence.
- Automatic operation.

If power is lost to the test rigs or monitoring systems, the test rigs should automatically cease all operations and return to an unloaded position until further intervention by an operator.

7.4 Single-Axis Testing

The ability of the metallic bellows and internal support components to withstand angular deflections needs to be tested. To simplify the analysis of test specimens and to increase the testing speed a test rig should be developed which deflects test specimens angularly around one axis only. The complexity of the test rig and testing procedure can be decreased further by using deflections of a constant magnitude for the duration of each test. For example a set of test specimens could be repeatedly deflected 8° around one axis.

Data from such tests would be used to determine the number of deflections the implant can withstand in one direction. This data could also be used to provide a coarse estimate the implant's overall fatigue behaviour. Alternatively the wear properties of the internal support components could be determined allowing the sliding and rolling internal support systems to be accessed and the material selection finalised.

While the test specimens are being deflected angularly, compressive loads should be applied to replicate the contact stresses and internal pressures the components will be exposed to *in-vivo*.

The test specimens should be constrained so they can only deflect around one axis. The angular deflection moments and compressive loads should then be applied through these constraint mechanisms. The axes of the constraint mechanisms should be aligned concentrically so that the test specimens are not subjected to additional shear loads. Provision should also be made for positioning the test specimens so their axes of rotation coincide with the test rigs axis of rotation.

The single-axis test rig should be able to repeatedly test the specimens using the procedure given below:

- Starting with the test specimen(s) in an unloaded and undeflected state.
- Increase the compressive load applied to the test specimen(s) until a constant predetermined load is reached.
- Deflect the test specimen(s) angularly around one axis through a fixed angle, as many times as is required.
- Return the specimen(s) to an undeflected position.
- Remove all loads from the test specimen(s).
- Repeat as required.

The implant's performance should be monitored through out the duration of the single-axis deflection testing procedure with the following parameters being recorded:

- Angular deflection range.
- Number of angular deflections completed.
- Magnitude of the loads applied.
- Room temperature and fluid bath temperature.

7.4.1 Test Rig Design

Two methods of deflecting the implant angularly were considered, these were using a stepper motor and a four bar linkage system. The main advantage of stepper motors is that the angle they operate through can be easily adjusted, by altering a parameter in the control system. However, stepper motors and their control systems are expensive.

It was determined that the simplest and cheapest way to constantly deflect the test rig and test specimens through a fixed angle was to use a four bar linkage mechanism. By fixing the length of the linkages the angle the test specimens are deflected through can be easily and accurately set. To allow fine adjustment of the deflection range variable length linkages were included in test rig where possible. A flywheel was added to the test rig drivetrain to ensure minimal fluctuations in the testing speed.

The internal pivot components or implant assembly do not require great force to deflect them angularly therefore the decision was made to develop a multi-station test rig. This allows a greater number of samples to be tested simultaneously, reducing the overall testing time frame.

The decision to develop a multi-station test rig design made it impractical to use weights to provide the compressive loads on the test specimens. Instead pneumatic cylinders were utilised to provide the compressive loads. Regulators can be used to limit the air pressure supplied to the cylinders, thus allowing the force applied to the test specimens to be controlled. By utilising solenoid operated control valves the pneumatic cylinders can also be configured to unload the test specimens should the power supply to the test rig be interrupted.

To allow accurate alignment of the constraint mechanisms tight tolerances were added to the relevant features on the manufacturing drawings and a fine adjustment mechanism was built into one end of the test rig. This adjustment mechanism allows the upper constraints to be moved relative to bottom constraints, thus allowing them to be accurately aligned.

The test specimens must also be able to be adjusted vertical to ensure their axes of rotation are coincident with the test rig's axis of rotation. Accordingly, fine pitched adjustment screws were added to the non-reciprocating constraints. By winding these adjustment screws up or down the height of the test specimens can be adjusted.

Figure 7.3 shows an isometric view of the final 4-station single-axis test rig.

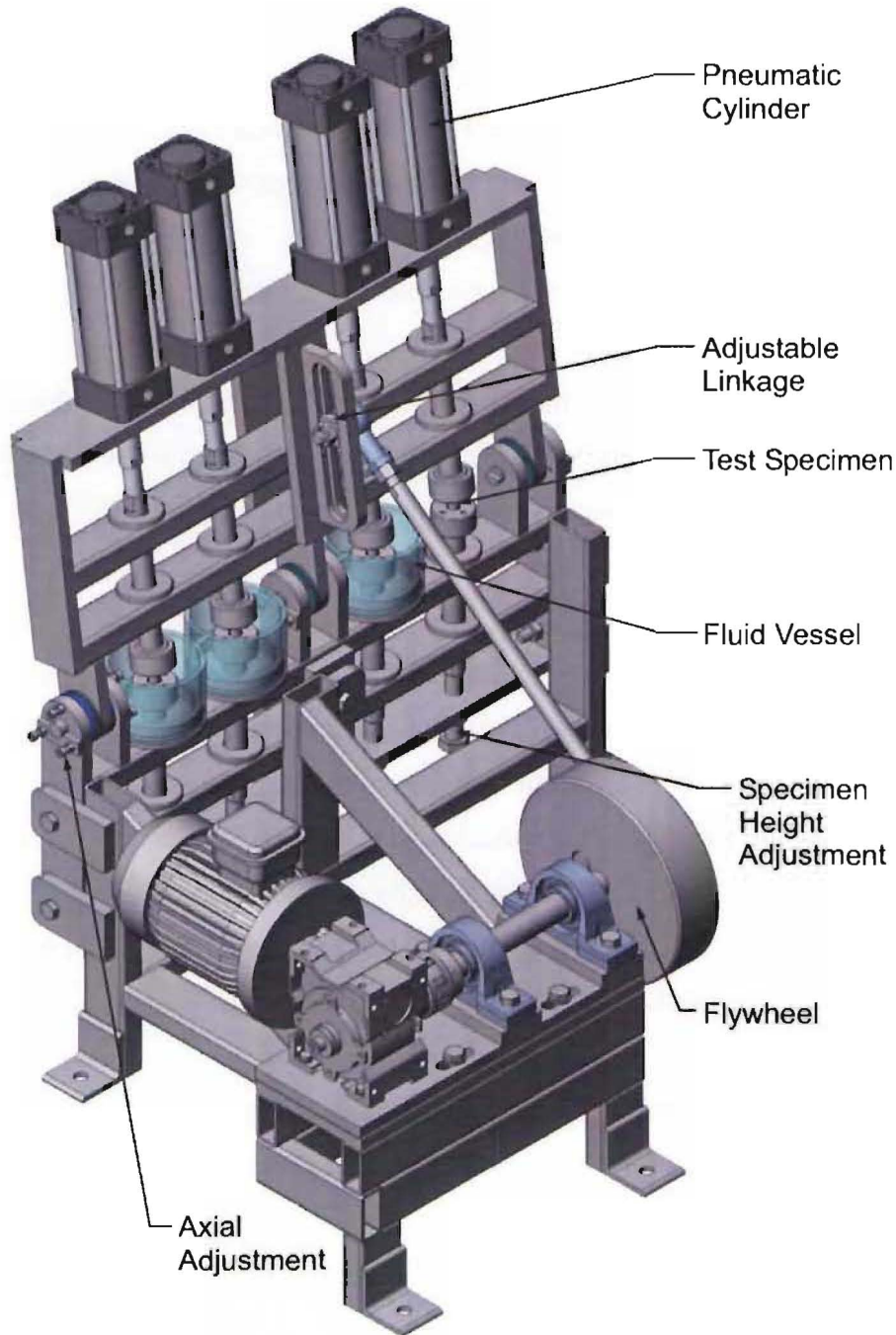


Figure 7.3 CAD model of the single-axis test rig.

Note: The temperature control system and right hand fluid vessel are not shown for clarity.

Figure 7.4 shows the single-axis test rig in two different positions.

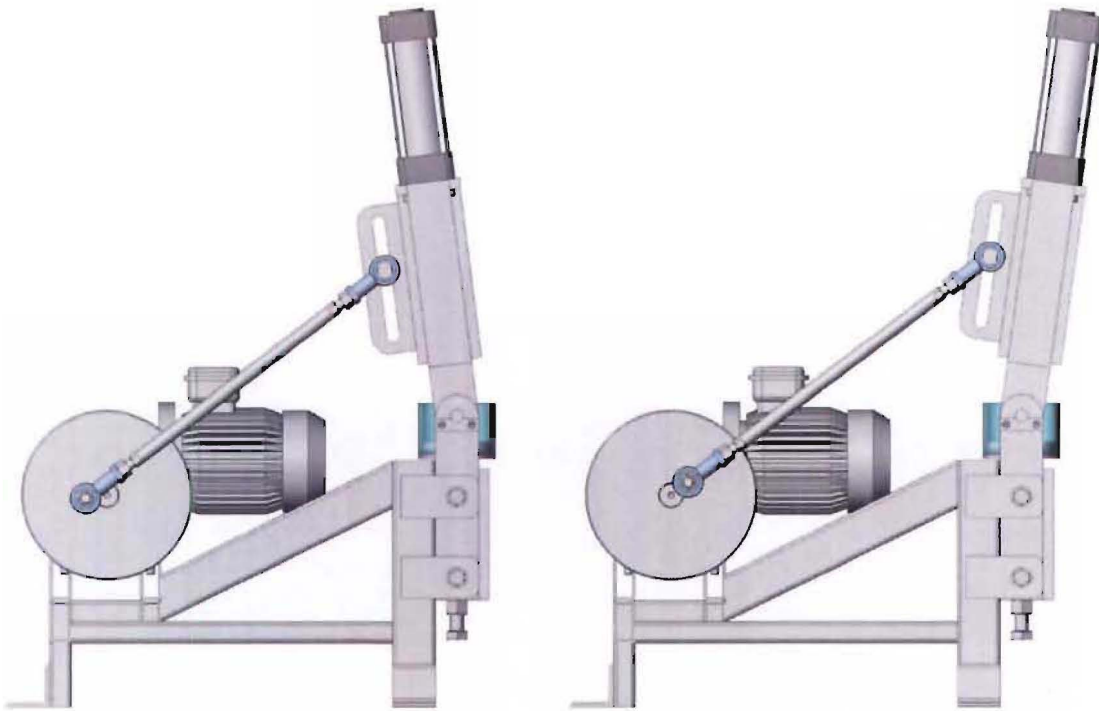


Figure 7.4 Single-axis test rig range of motion.

The single-axis test rig was manufactured during the course of this project so testing of the internal support components could be conducted. However, complications with the supply of test specimens prevented this testing being conducted.

Front and side views the test rig manufactured are shown in Figure 7.5.

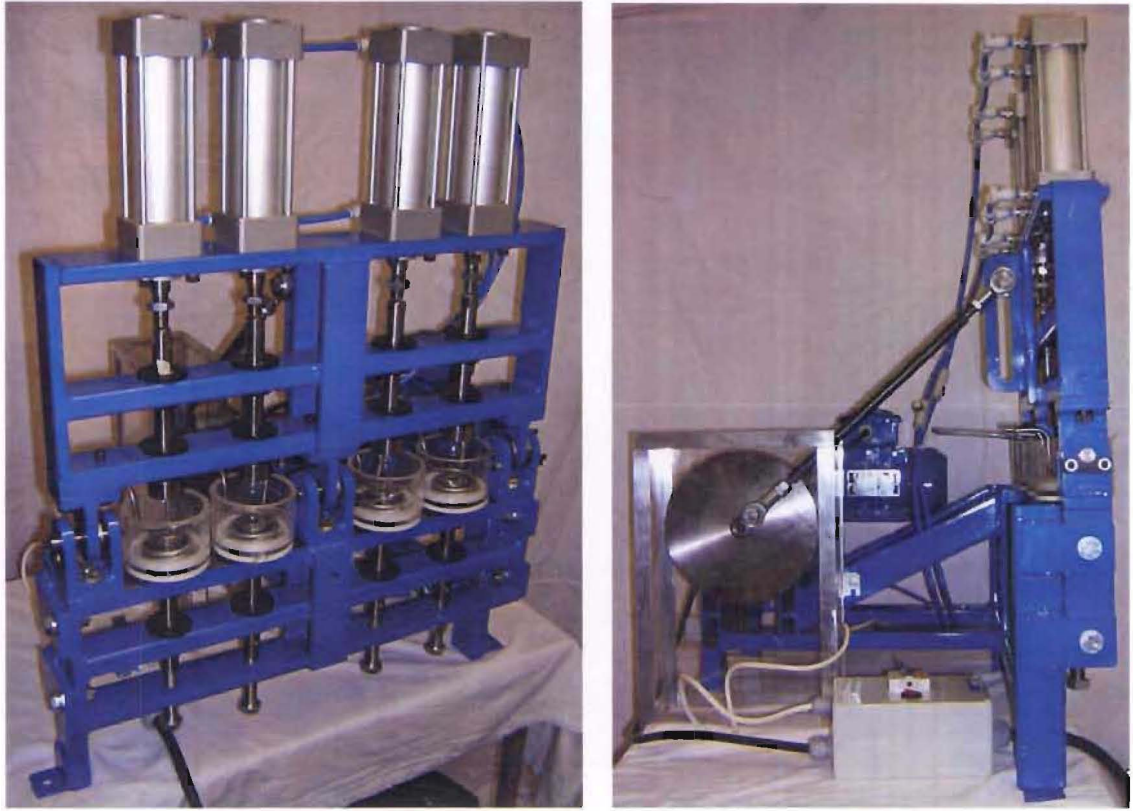


Figure 7.5 As built single-axis test rig.

(a) Front View.

(b) Side View.

Figure 7.6 shows two of the test specimen constraint mechanisms, fluid containment vessels and 316L stainless steel heating coils.



Figure 7.6 Single-axis test rig constraint mechanisms, fluid vessels and heating coils.

Note: the fluid containment vessels are shown with a protective layer of plastic film.

7.5 Vertical Load Testing

A test rig needs to be developed which allows the ability of the internal support and assembled implant to withstand static and dynamic loads to be assessed. The test results would be used to confirm that the internal support components do not suffer fatigue failure, surface degradation or cold flow. Alternatively, the effects of separating and contacting the internal support surfaces could be evaluated. The number of axial compressions and decompressions the metallic bellows can withstand could also be quantified using this test rig.

Vertical load testing should be carried out by constraining the top and bottom faces of the test specimens so no angular deflections can occur. The vertical load test rig should then repeatedly load the test specimen(s) using the procedure given below:

- Starting with the test specimen in an unloaded state.
- Apply loads to the test specimens through the constraint mechanisms until a constant predetermined load is reached. During this loading procedure no angular deflection should occur. For the bellows intervertebral disc implant the static load was specified to be 600 N.
- As required, apply shock loads to the test specimen(s) via the constraint mechanisms to simulate dynamic loading effects such as those present when walking or running.
- Remove all loads from the test specimen(s).
- Repeat.

The test specimen's performance should be monitored through out the duration of the vertical load testing procedure with the following parameters being recorded:

- Number of static loading cycles.
- Number of dynamic loading cycles.
- Magnitude of the loads applied.
- Room temperature and fluid bath temperature.

7.5.1 Test Rig Design

Two methods of applying compressive loads to the implant were considered, these were the use of weights or a pneumatic/hydraulic system. Weights were rejected as they can not easily be removed in the advent of a power failure, also the loads specified would require large masses of material. Pneumatics were the preferred option compared to hydraulics, as pneumatic components are easier to service and cheaper to purchase than hydraulic components.

Based on this decision a test rig utilising a pneumatic cylinder was developed. By using a regulator to limit the air pressure supplied to the pneumatic cylinder the load applied to the test specimens can be accurately controlled.

Furthermore, by utilising two pressure regulating valves, one pneumatic cylinder can be used to provide both the static and dynamic loads. This can be achieved by pressurising the top of the cylinder (out stroke) to the sum of the static and dynamic loads, while the lower half of the cylinder (in stroke) can be pressurised to provide the dynamic load. With such a system, when both sides of the cylinder are energised the forces balance, resulting in only the static load component being applied to the test specimen. If the lower half of the cylinder is then depressurised both the static and dynamic loads are applied. This system also offers the advantage of allowing the dynamic loads to be rapidly applied to the test specimens.

Solenoid operated valves were added to the pneumatic circuit. These valves can be configured to depressurise both sides of the pneumatic cylinder, thus unloading the test specimens, should the power supply to the test rig be interrupted.

Figure 7.7 shows an isometric view of the proposed test rig assembly. This arrangement could be used to create a multi-station test rig, however given the cheap construction of the apparatus, building individual test rigs was considered to be more practical.

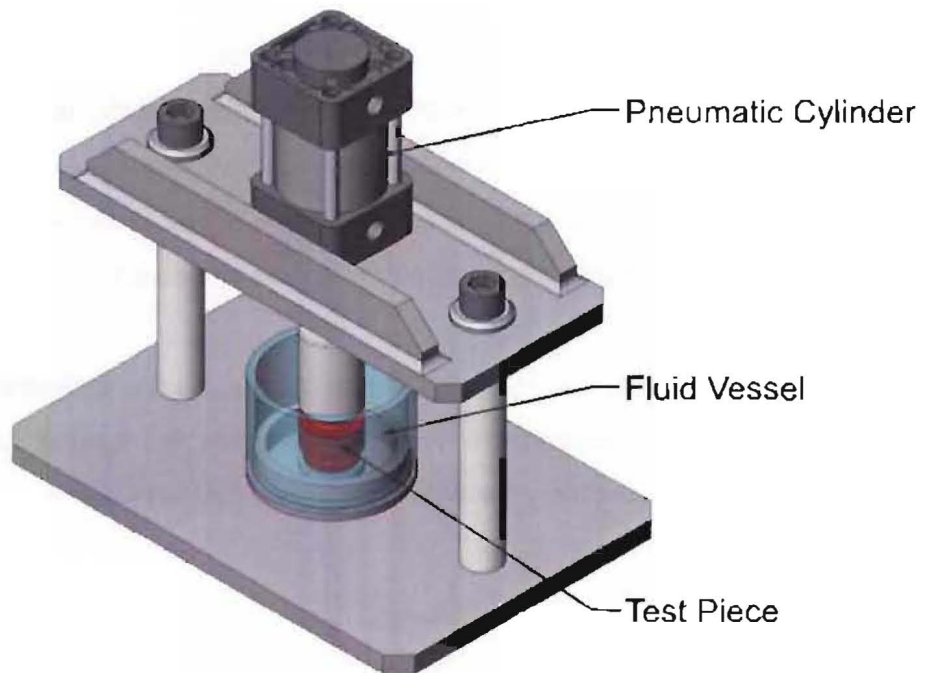


Figure 7.7 CAD model of the vertical load test rig.

Note: the temperature control system is not shown for clarity.

7.6 Multi-Axis Testing

A multi-axis test rig needs to be developed which applies flexion/extension and lateral bending moments to the bellows intervertebral disc implant. Static and dynamic loads should also be applied to the test specimens to accurately represent *in-vivo* conditions. The results of such multi-axis testing will allow the fatigue and wear performance of the bellows intervertebral disc implant and its components to be quantified.

Testing should be carried out by constraining the implant's endplates. Angular deflection moments and compressive loads should then be applied through these constraint mechanisms replicating the way the bellows intervertebral disc implant will be deflected and loaded *in-vivo*.

The constraint mechanisms used to locate and deflect the test specimens should be aligned so they place no additional loads on the test specimens. Provision should also be made for correctly positioning the test specimen so its axes of rotation coincide with the test rig's axes of rotation.

Depending on the type of internal support used, sliding or rolling, there may be some decompression of the test specimens during angular deflections. The test rig should not prevent such decompression from occurring.

During a typical testing sequence the following ranges and numbers of deflections should be applied to the test specimens.

Axis 1 – Positive Direction (Flexion)

1 deg – 4800 cycles

2 deg – 1800 cycles

5 deg – 240 cycles

8 deg – 75 cycles

Axis 1 – Negative Direction (Extension)

1 deg – 6600 cycles

2 deg – 315 cycles

Axis 2 – Both Directions (Lateral Bending)

1 deg – 6600 cycles

2 deg – 75 cycles

These deflections should be programmed to occur in a mixed order rather than all the deflections in one direction being applied consecutively. As previously determined in Section 4.1.4 such a sequence of deflections represents one days worth of typical lumbar spine deflections. Therefore, to simulate a 40 year implant life span the programmed sequence of deflections should to be repeated approximately 14,500 times.

The multi-axis test rig should be able to repeatedly deflect test specimens using the following procedure:

- Starting with the test specimen(s) in an unloaded state.
- Increase the compressive load applied to the test specimen(s) until a constant predetermined load is reached. For the bellows intervertebral disc implant the static load was specified to be 600 N.
- Deflect the test specimen(s) angularly through the programmed series of angular deflections around both axes.
- During these angular deflections, pre-programmed shock loads should also be applied to the test specimen(s) to simulate dynamic loading effects such as those present when walking or running.
- Return the test specimen(s) to an undeflected position.
- Remove all loads from the test specimen(s).
- Repeat the testing sequence as required.

The implant's performance should be monitored through out the duration of the multi-axis testing procedure with the following parameters being recorded:

- Magnitude and number of static loading cycles.
- Magnitude and number of dynamic loading cycles.
- Magnitude and number of angular deflections completed in both axes.
- Number of pre-programmed deflection sequences completed.
- Room temperature and fluid bath temperature.

7.6.1 Test Rig Design

Given the need for the test piece to rotate varying amounts around two axes, a stepper motor powered gimbal arrangement, similar to that proposed by Wilke et al³, was considered to be the most practical solution. While stepper motors and their associated control systems are expensive they allow the test rig to have the required flexibility. Stepper motors also allow a reasonable compact test rig design to be developed.

The final design was developed by an undergraduate student closely supervised by the author. The general design and layout of the components was discussed and rationalised by both parties based on Wilke et al³ findings, while the detail design work, such as sizing of components, was completed by the undergraduate student.

A pneumatic cylinder was utilised to provide the required compressive loads. As previously described for the vertical load test rig, by utilising two pressure regulating valves one pneumatic cylinder can be configured to provide both the static and dynamic loads.

Counterweights should be added to the gimbal rings as required, to balance out the weights of the stepper motors and pneumatic cylinder. This will prevent the test specimens being subjected to additional loads or deflections.

To allow the constraint mechanisms to be accurately aligned tight tolerances should be added to the relevant features on the manufacturing drawings and an adjustment mechanism was built into each of the gimbal axes. These mechanisms allow each of the gimbal rings to be adjusted relative to each other and relative to the base plate of the test rig, thus allowing the two constraint mechanisms to be aligned concentrically.

The test rig designed also includes a vertical adjustment mechanism so the test specimen's axes of rotation can be aligned with the gimbal axes. As for the single-axis test rig, this was achieved by adding a fine pitched adjustment screw to the bottom constraint mechanism. By winding this adjustment screw up or down the height of the test specimen can be adjusted.

Figure 7.8 shows an isometric view of the proposed multi-axis test rig.

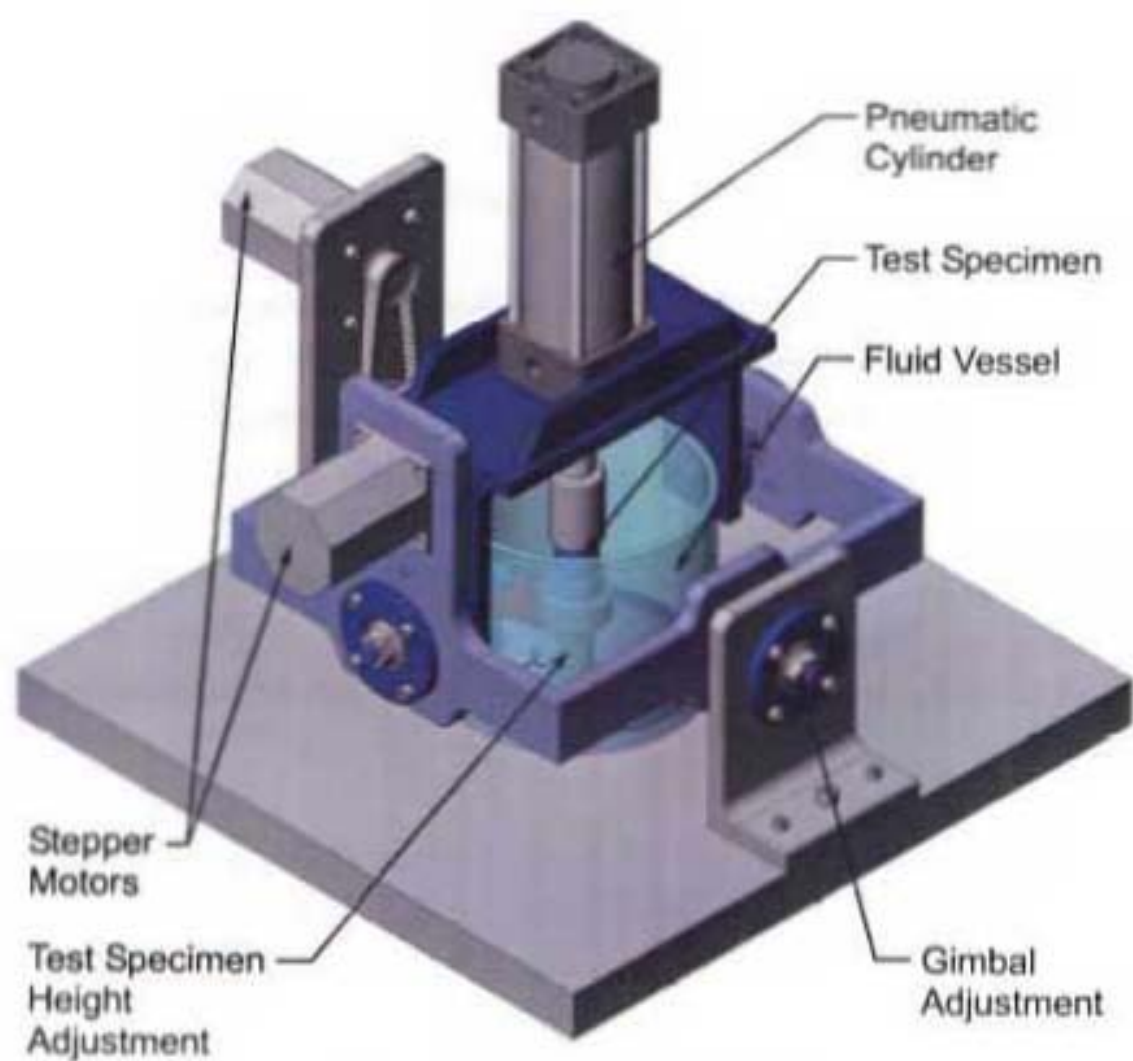


Figure 7.8 CAD model of the multi-axis test rig.

Note: the temperature control system is not shown for clarity.

The multi-axis test rig is shown in two deflected states in Figure 7.9.

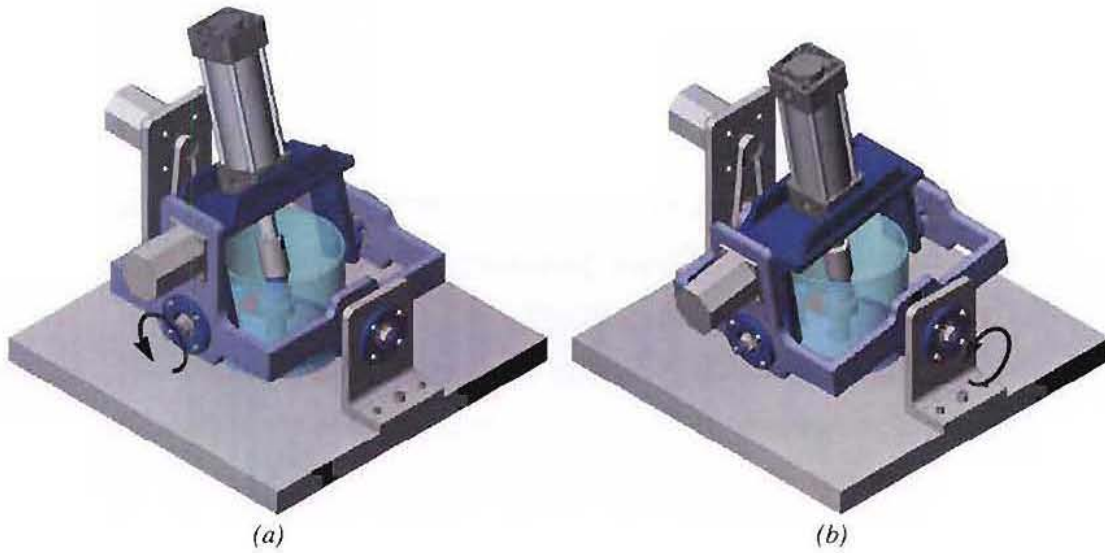


Figure 7.9 Multi-axis test rig axes.

(a) Angular deflection around Axis 1.

(b) Angular deflection around Axis 2.

A multi-station test rig could be created by manufacturing several gimbals and connecting them with linkages so that one set of stepper motors could be used to test several test specimens. However this would require more powerful stepper motors and the manufacturing tolerances in the linkages and connections may result in the additional test rigs not deflecting accurately. Therefore, if multiple test stations are required it would be more prudent to build several independent test rigs each with their own stepper motors and control system.

7.7 Conclusion

In order to aid development and testing of the bellows intervertebral disc implant, specifications and designs for three test rigs were developed. These test rigs are intended to complete the following tasks:

- **Single-Axis Test Rig** - Deflects angularly around one axis a constant amount, allowing the wear and fatigue properties of individual components and the metallic bellows to be rapidly assessed.
- **Vertical Load Test Rig** - Applies static and dynamic compression loads to individual components or the complete implant assembly allowing any fatigue failure or surface degradation issues to be identified.
- **Multi-Axis Test Rig** - Deflects the assembled implant angularly around two axes while applying static and dynamic compression loads. This test rig allows the performance of the implant to be assessed when it is subjected to loading conditions similar to those found *in-vivo*.

As discussed in Section 7.2 by breaking the implant functions into groups of loads and movements that are independent, the testing procedures could be simplified and parallel testing of implant functions could be carried out. This approach allowed simpler test rigs to be developed and the overall testing time frame could be reduced. Another benefit was that higher testing frequencies could be achieved. For example, the single axis-test rig was design to test components at 1.17 Hertz (70 cycles per minute) which is significant improvement over the 3.5 cycles per minute offered by the Wilke et al³ or MTS test rigs².

At the conclusion of this project no testing had been carried out using these test rig designs. As previously stated in Section 7.4.1 testing of internal support components was intended to be done but due to issues with the supply of test specimens this work could not be started. Testing of the welded bellows was considered but once the cost and timeframe were disclosed it was unrealistic to include such testing as part of the project. Additionally the detail design of such testing procedures is a task which turned out to be well beyond the scope of this project.

7.8 References

1. Allen M J. 2004. *Animal Models in Spine Surgery*. 7th World Biomaterials Conference, Sydney. pp 214.
2. MTS Systems Corporation, *Solutions for Biomaterials and Biomechanics Testing*. 2004, Eden Prairie, MN, USA: MTS Systems Corporation.
3. Wilke H J, Claes L, Schmitt H, Wolf S, *A universal spine tester for in-vitro experiments with muscle force simulation*. Eur Spine J, 1994. Vol 3: pp 91-97.
4. Wilke H J, Wenger K, Claes L, *Testing criteria for spinal implants: recommendations for the standardization of in-vitro stability testing of spinal implants*. Eur Spine J, 1998. Vol 7: pp 148-154.

<Blank Page>

Chapter 8 – Conclusion

Disorders of the lumbar intervertebral discs may occur for a variety of reasons including trauma, disease or deformity. Currently, the most common surgical treatment for such disorders is spinal arthrodesis which involves fusing the vertebrae adjacent to the affected intervertebral disc. In 1997 it was estimated that over 150,000 lumbar fusions were performed in the United States. However, spinal arthrodesis has many disadvantages which limit both its short and long term success rates.

The aim of this project was to develop an implant which allowed damaged intervertebral discs to be replaced and which also allowed the patient to retain full motion at the affected level. Several other researchers have developed intervertebral disc implants, however as detailed in Chapter 4 these implants have their own inherent problems. The most significant problem the majority of these existing artificial disc implants present is that they generate wear debris, which may in turn lead to the onset of osteolysis. Therefore the specification for this project stated that the intervertebral disc developed should produce no wear debris.

The implant developed consists of a welded metallic bellows which acts as a flexible pressure vessel containing a semi-compressible fluid/gas core. This arrangement is similar to that of a healthy intervertebral disc in which the fluid nucleus pulposus is encapsulated by the elastic collagen fibres of the annulus fibrosus.

This implant is able to withstand compressive loads and angular deflections while having a low angular stiffness. The implant utilises multiple load carrying mechanisms and also incorporates overload protection features. The presence of multiple load carrying mechanisms also helps to further reduce the chance of the bellows intervertebral disc implant failing catastrophically.

To minimise the trauma to musculature and nerves surrounding the patient's spine the bellows intervertebral disc implant was designed to last in excess of 40 years and to be inserted using a lateral approach. This approach also allows the majority of the annulus fibrosus, particularly the anterior aspect, to be preserved. This was deemed to be important as the anterior portion of the annulus fibrosus plays a significant role in supporting the applied loads and helping to preserve the stability of the lumbar spine.

Metallic bellows and thus the bellows intervertebral disc implant have a low angular stiffness. However, when implanted the combination of the implant and retained annulus fibrosus will result in an angular stiffness which is similar to that of a healthy intervertebral disc. This will help to ensure that the stability of the spine is preserved and that the patient does not have to exert additional energy to bend at the affected level.

The bellows intervertebral disc implant is more complex than the other artificial discs. A less complex intervertebral disc implant could have been developed during the course of this project by allowing the production of wear debris, as other artificial disc implants do. However, the role of wear debris in the spine is a contentious issue. Accordingly as further research into new and existing intervertebral discs is conducted it may become apparent that there is a need for an artificial disc which does not produce any wear debris. The bellows intervertebral disc implant meets this requirement.

To allow testing of the bellows intervertebral disc implant three rig designs were developed which could be used to conduct accelerated *in-vitro* testing. Each of the test rigs is intended to test one component of the implant's performance. For example, the implant's performance when bearing compressive loads, or deflecting around one or two axes could be appraised. Such testing of individual aspects of the implant will allow the testing procedures to be simplified and accelerated while still allowing representative data about the implant's long term performance to be obtained.

Areas of the bellows intervertebral disc implant which should be tested and refined to ensure safe and optimum *in-vivo* performance include the following:

- Testing of the metallic bellows specified to confirm they can meet the fatigue and pressure requirements
- Testing to finalise the internal support geometry and material combination.
- Testing to determine the effects of internal and external debris on the life of the metallic bellows.
- Testing of the tether/sheath assembly to ensure it correctly limits the implants range of motion and prevents the ingress of debris into the welded bellows convolutions.
- Refinement of the tether/sheath fixation mechanisms.

In summary, a new lumbar intervertebral disc implant has been designed which has the unique feature of not producing any wear debris. This implant has sufficient potential to warrant further refinement and *in-vitro* testing to determine whether it is viable for *in-vivo* use. Ultimately, the use of such an implant should bring new levels of comfort and confidence to those many patients requiring treatment for lower back disorders.

<Blank Page>

Part B

**BioModelling
and the
Development of a Femoral Endoprosthesis**

<Blank Page>

Chapter 9 - BioModelling

9.1 Problem Statement

The proposal for the BioModelling component of this project was prepared before any research into intervertebral disc implants was completed, it stated the following:

Develop the capability to produce computer models, and consequently plastic and metal replicas from CT scans of patients' vertebrae.

It is essential for custom implants to duplicate the patients' bones. It is unacceptable for an orthopaedic surgeon to find in the middle of an operation that replacement parts do not fit. A spinal implant, unlike a hip replacement, has to fit the surrounding bones, it has to clear the spinal cord and other structures and it is by comparison a complex shape.

Therefore, for this project it is essential to have tools which allow boney structures to be faithfully model and reproduced. It may be possible some time in the future to develop a range of standard sized implant components, but at this stage this is not realistic. Vertebrae are just too complex.

The technical steps to developing this models-from-CT-scans capability are:

- *Acquire software and learn methods to convert CT scan data to CAD models.*
- *Acquire suitable CT scan data to work on.*
- *Develop a process for producing NC machined metal bone models.*
- *Develop a process for producing FDM plastic bone models.*

As the research into the development of an intervertebral disc implant progressed, it became apparent that a BioModelling capability was not necessary. Provided the implant meets the simple endplate form requirements there is no need to replicate the boney structures. However, by the time this was realised research into BioModelling was almost complete.

Aside from 'aiding' in the development of intervertebral disc implants, BioModels can also be used for visualisation and preoperative planning purposes. This is particularly relevant for maxillofacial and plastic surgery applications, where the preservation of bony features *is* critical if an accurate aesthetic result is to be achieved. Therefore, given these other visualisation and planning applications, the decision was made to complete research into BioModelling techniques. The resulting processes have since been offered to local surgeons as a service.

The following areas were focused on during the BioModelling section of the project.

- Developing working relationships with hospital staff involved in CT scanning.
- Determining methods for accessing and copying CT scan data.
- Acquiring software and methods to convert CT scan data to 3d models.
- Output of 3d data in formats suitable for rapid prototyping.
- Production of plastic models, or BioModels.
- Production of CAD models for modelling and NC machining purposes.

Note: The images shown in this chapter were generated by the author during the course of this work, unless otherwise noted.

9.2 Medical Imaging

There are several different types of medical imaging system available, including Computed Tomography (CT), Magnetic Resonance Imaging (MRI) and Positron Emission Tomography (PET) scanning. Bone is most commonly imaged using CT scanning as it offers the best resolution of hard tissues. A brief explanation of CT scanning follows.

9.2.1 Computed Tomography Imaging

Computed Tomography (CT) imaging, is also known as "CAT scanning" (Computed Axial Tomography). The word Tomography comes from the Greek words "tomos" meaning "slice" or "section" and graphia meaning "describing".

Computed Tomography is based on standard x-ray principals. As x-rays pass through the body they are attenuated or weakened at differing rates depending on the density of the material being scanned. The key difference is that in a CT scanner an arc shaped detector measures the x-ray profile, as opposed to a film when taking a conventional x-ray image. The x-ray tube is mounted on one side of a rotating frame inside the CT scanner and an arc shaped detector mounted on the opposite side, as shown in Figure 9.1.

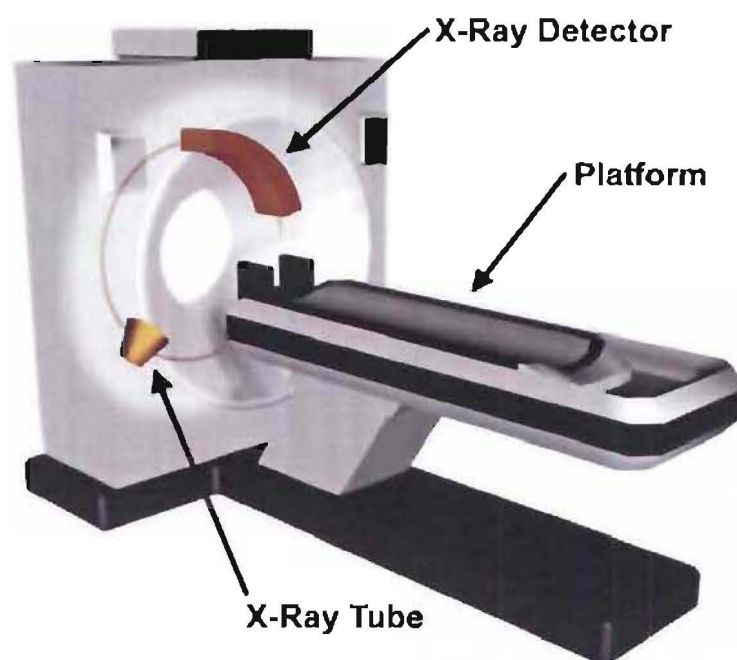


Figure 9.1 Schematic of modern CT scanner.

[Adapted from: <http://science.howstuffworks.com/cat-scan2.htm>]

As the rotating frame spins the x-ray tube and detector around the patient, a fan shaped beam of x-rays is created as shown in Figure 9.2.

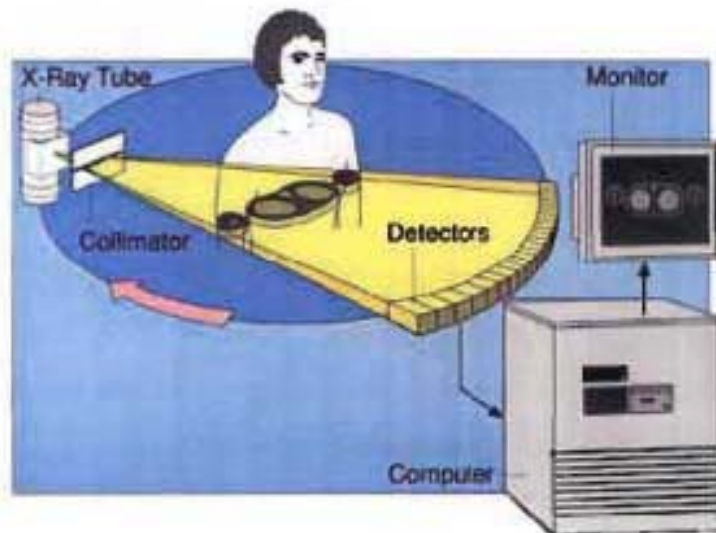


Figure 9.2 Relationship of the x-ray tube, patient, detector, and image reconstruction computer.

[Source: http://imagingis.com/ct-scan/how_ct.asp]

The detector takes numerous snapshots or “profiles” of the attenuated x-ray beam. Typically during one 360 degree rotation, approximately 1000 profiles are collected. A dedicated computer then reconstructs each slice from these profiles. The thickness of the CT slices can be varied by adjusted lead shutters which are positioned in front of the x-ray tube and detector. Typically slice thicknesses of 1-10 mm are used.

The latest multi-slice CT systems can collect 4 slices of data in 350 ms and reconstruct a 512 x 512 matrix image in less than a second. This allows an entire adult chest to be scanned in five to ten seconds, during which time 40 - 8 mm slices are typically collected.

9.2.2 Spiral CT

Early model CT scanners transferred power to the x-ray tube using high voltage cables wrapped around an elaborate set of rotating drums and pulleys. The rotating frame would spin 360° in one direction capturing one slice of data; the frame would then spin back 360° in the other direction to capture a second slice. In between each slice, the rotating frame would come to a complete stop and reverse directions while the patient table was moved forward incrementally thus generating the slice thickness.

In the mid 1980's power slip rings were added to CT scanners allowing the cable and drum systems to be abandoned. Using slip rings power can be transferred between a stationary power source and a continuously rotating gantry. In modern CT scanners the x-ray tube and deflector rotate continuously while the patient is moved constantly through the scanning aperture. This results in one CT image, as opposed to multiple discrete slices. This process is referred to as spiral or helical scanning, a visual representation of which is shown in Figure 9.3.



Figure 9.3 Simulation of the x-ray beam path during spiral CT scanning.

{Source: <http://imagingis.com/ct-scan/spiral.asp>}

As spiral CT data represents the patient anatomy in one slice it minimises the potential of the scan data being misaligned as a result of the patient moving or breathing. This continuous data set can be converted into discrete slice data or reconstructed to provide three-dimensional images.

During the evaluation of the reconstruction software it was found that some software packages were not able to import spiral CT data. Although this problem could be overcome by instructing the radiologist to scan using discrete slices, it is desirable to be able to use spiral CT data where possible.

9.2.3 Clinical Benefits of CT Imaging

MR, ultrasound and digital x-ray fluoroscopy have all made significant improvements in their ability to image the chest, lungs and abdomen. However, spiral CT remains the primary digital imaging technique for the chest, lungs, abdomen and bones due to the combination of fast data acquisition and high resolution. CT scanning is also unique in that it can provide detailed information of nearly every organ in the upper abdomen and pelvis in one examination.

CT imaging provides both good soft tissue resolution (contrast) as well as high spatial resolution. This allows CT imaging to be used for visualisation of joints such as the shoulder, hip or spine. For example Figure 9.4 shows a CT image of a prolapsed intervertebral disc.



Figure 9.4 Axial CT image of the lumbar spine.

Note: This CT image shows a slight prolapse of the intervertebral disc with the ejected nucleus pulposus material impinging on the spinal cord.

{Source: http://imagnis.com/graphics/ct-scan/ct_lumbar_disk.gif}

9.3 Medical Reconstruction

Traditionally, medical images have been viewed as a series of planar images, each of which shows a sectional cut through the patient's anatomy. Basic software algorithms have been available for several years which allow approximate 3d reconstructions to be made directly from the raw slice data. However, these reconstructions typically have poor resolution and accuracy. The BioModelling software packages investigated during the course of this research offer the advantage of allowing high quality accurate 3d reconstructions to be created. This high resolution data can then be used to produce graphical or physical models.

Figure 9.5 shows a CT scan output as traditional planar images and a three-dimensional image produced using BioModelling software.

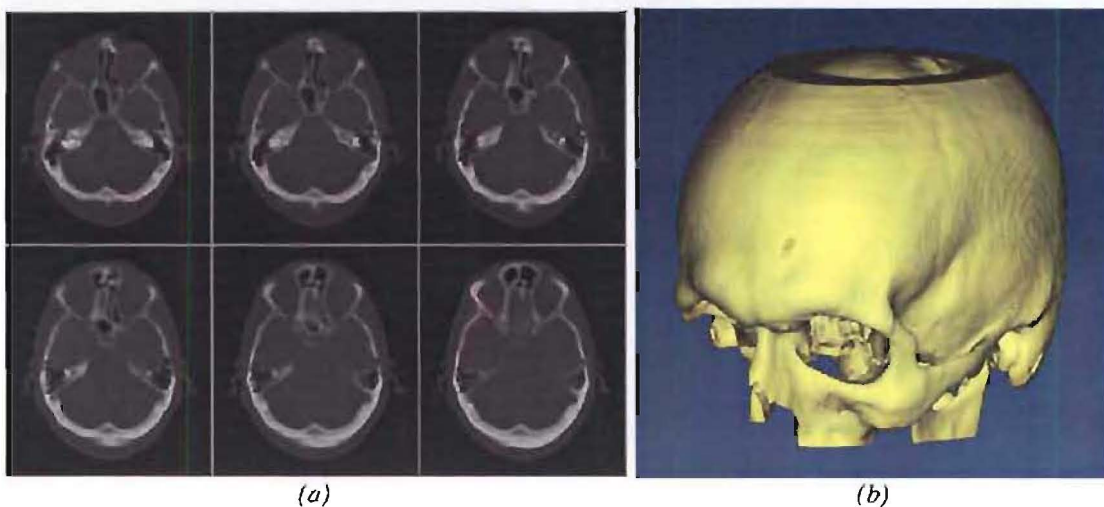


Figure 9.5 CT planar images and three-dimensional reconstruction image.

- (a) Slice data from a CT scan of a skull, skill and experience are required to diagnose such images.*
- (b) Reconstructed 3d model of the same CT data, this model can be rotated and magnified allowing the surgeon to focus on diagnosis rather than interpretation of the slice data.*

A recent high profile case where BioModelling was used was the separation of conjoined twins. CT scans of the twin's skulls were taken and then three stereolithography models were grown; one of each twin's skull and one of the area where the twins were joined as shown in Figure 9.6. These models allowed the surgical team to fully understand what anatomy the twins shared and to plan the surgical procedure to separate them.



Figure 9.6 BioModels of craniopagus twins.

[Source: <http://www.blamodel.com/twinsinfo.htm>]

9.3.1 Reconstruction Process

Several software packages designed to reconstruct medical imaging data are commercially available. The general sequence of operations for these packages is:

1. Import the slice data.
2. Organise the slice data, as required.
3. Adjust contrast and brightness.
4. Set threshold levels to isolate material of required density.
5. Create masks using the threshold data.
6. Adjust the masks as required (draw/erase).
7. Calculate the 3d volume of selected mask data.
8. View the 3d volume.
9. Export the 3d volume as required.

Importing slice data is a simple process that involves selecting a set of images to be reconstructed. As there is no standardised data format for CT scanners different import filters are required for each brand of scanner. The software packages tested were capable of importing most common formats, however in some cases the import filters were sold as individual modules.

Patients are sometimes scanned with gantry tilt as shown in Figure 9.7. This is normally done so the anatomy of interest can be visualised more clearly when the slice data is viewed as planar images. Gantry tilt must be removed when creating 3d reconstructions. Some of the software packages investigated were capable of importing and realigning CT data with gantry tilt. However, it was found that the interpolation required to realign the slice data, often resulted in inferior quality 3d volumes being created. It is therefore advisable not to use gantry tilt for scans which are going to be reconstructed.

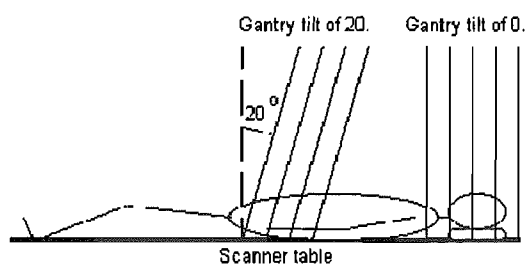


Figure 9.7 Gantry tilt schematic.

Once the slice data has been imported the images can be removed, added or reordered as required. A typical dialogue box for organising slice data is shown in Figure 9.8.

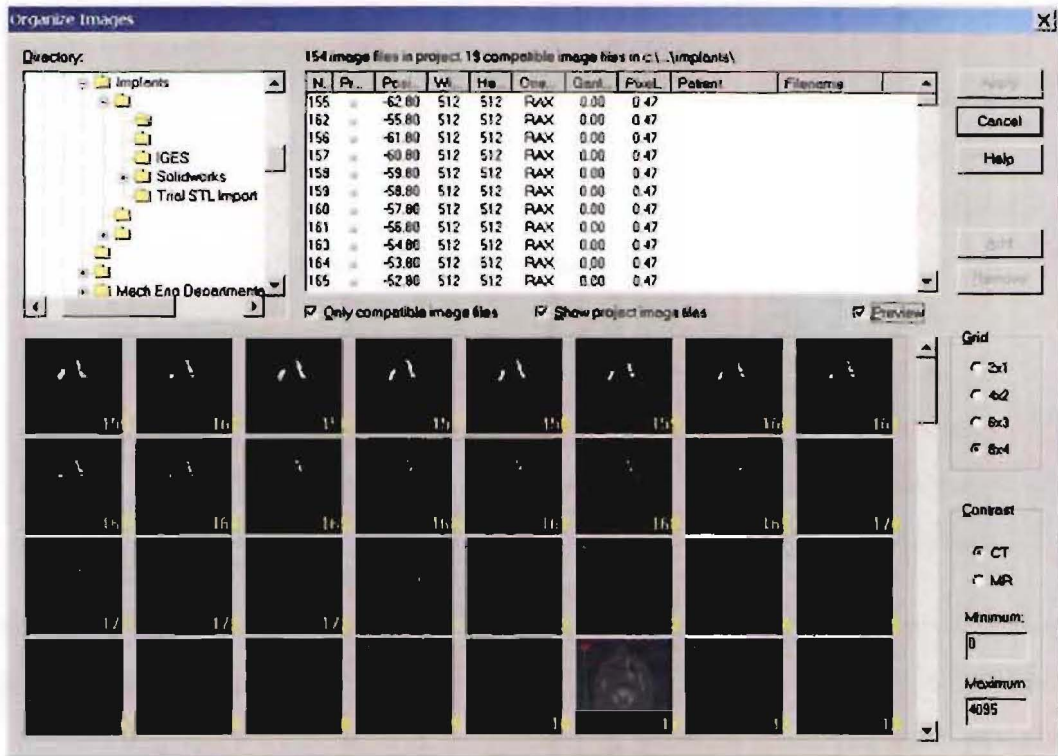


Figure 9.8 Organise images dialogue box.

The "Organise Images" dialogue box can be used to remove, add or reorder slice data as required.

Shown is the "Organise Images" dialogue box for the Mimics software package.

The basic unit of CT or MR slice data is the voxel or volume element. Voxels represent a pixel in the display of CT or MR images. By manipulating and filtering the voxels, specific groups of tissue can be isolated for reconstruction. For this project, the primary area of interest was the reconstruction of bones, however it is possible to reconstruct individual blood vessels, nerve tissue or muscle groups. Standard voxel manipulation and isolation tools include contrast adjustment and thresholding, which are detailed in Sections 9.3.2.1 and 9.3.2.2 respectively.

Once the target voxels (tissues) have been isolated they can be modified using draw and erase tools. This allows unwanted cavities to be filled and unwanted data removed. These tools are detailed in Section 9.3.2.3.

The next step in the reconstruction process is to calculate the three dimensional volume. By triangulating between the edges of voxels in adjacent slices, a three dimensional solid can be created. Typically during this phase of the reconstruction process low, medium or high quality reconstruction options can be selected. The number of voxels grouped together in one triangular facet determines the quality level. If fewer voxels are grouped together more triangles are required to describe the surface, and in turn the quality of the reconstruction increases.

The reconstructed volume can then be viewed. A typical reconstruction 3d view is shown in Figure 9.5(b). All of the software packages investigated allowed the reconstructed model to be rotated, panned and zoomed as required.

Once the required geometry has been isolated and reconstructed the next step is to export the 3d volume. All of the software packages investigated were capable of exporting reconstructed data in an STL format and some packages were also capable of exporting VRML files. Both of these file formats use triangular facets to describe 3d surfaces. As detailed in Section 9.6.1.1, BioModelling software packages often produce large STL and VRML files which contain thousands of triangular facets.

STL files were the export format of choice, especially for rapid prototyping purposes where STL files are the industry standard. VRML files are primarily intended for visualisation purposes and are not editable.

The time required to complete a reconstruction varied from package to package and from case to case. Typically the time from receipt of the data to output of an STL file was under an hour.

9.3.2 Standard Voxel Manipulation Tools

Most reconstruction software packages have three main voxel manipulation tools, contrast, threshold and draw/erase. The operation of these tools varies from package to package however, the effect on the slice data is the same.

9.3.2.1 Contrast

Contrast tools change the number of grey values available for display. Basically adjusting the contrast makes whites whiter and blacks blacker. The objective when adjusting the greyscale values is to allow different densities of material to be identified without the image becoming washed out. The contrast also affects the thresholding of images.

Figure 9.9 shows three different contrast levels for the same CT slice. The first image, Figure 9.9(a), has a wide range of grey values, but the edges of the bone and soft tissues are hard to distinguish. Figure 9.9(b) has a reduced range of grey values which allows the boney features and their edges to be more readily identified. If the available grey scale range is too small as shown in Figure 9.9(c) the image becomes washed out and finer details are lost.

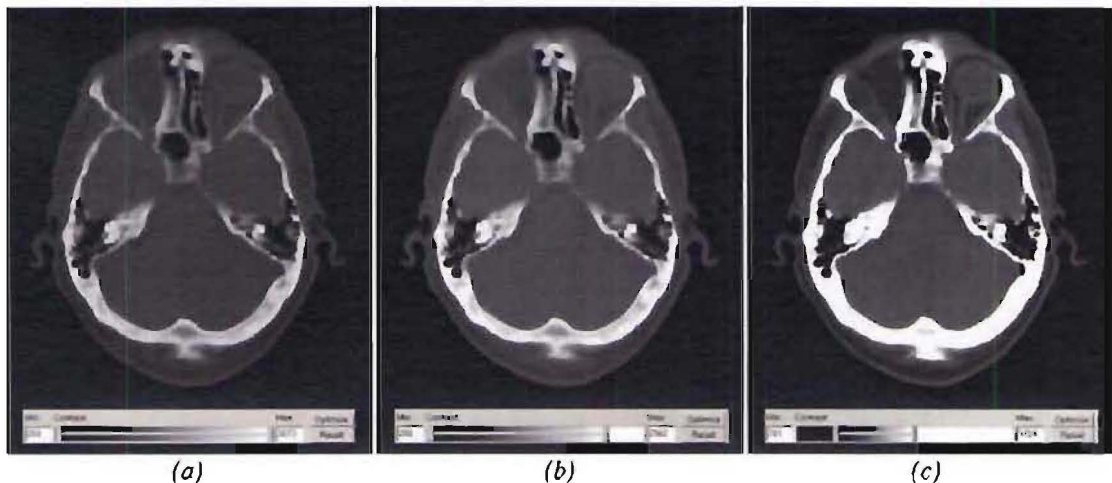


Figure 9.9 CT slices with increasing contrast.

9.3.2.2 Threshold

Thresholding is used to select and isolate the voxels required for the reconstruction. Typically the data selected is added to a mask for reconstruction purposes. The threshold limit(s) defines which voxels are included in the mask based on the greyscale value of each voxel. The material which is to be isolated can be selected using either one or two thresholding limits. In the case of using one threshold, all the voxels in the image with a greyscale value higher than or equal to the threshold value are added to the mask. In the case of using two thresholding limits voxels with greyscale values equal to and between both values are selected.

Figure 9.10 shows a CT image with three different thresholding values. In each case the goal is to isolate the bony features using a lower thresholding limit. In Figure 9.10(a) the thresholding value used is too low and some soft tissue is also selected, this would result in the reconstruction of soft tissues as well as bony features. Figure 9.10(b) shows a more ideal thresholding value, all of the high density bone is selected but the lower density soft tissues are not. If the thresholding value is too high, as shown in Figure 9.10(c) some of the bony features will be lost.

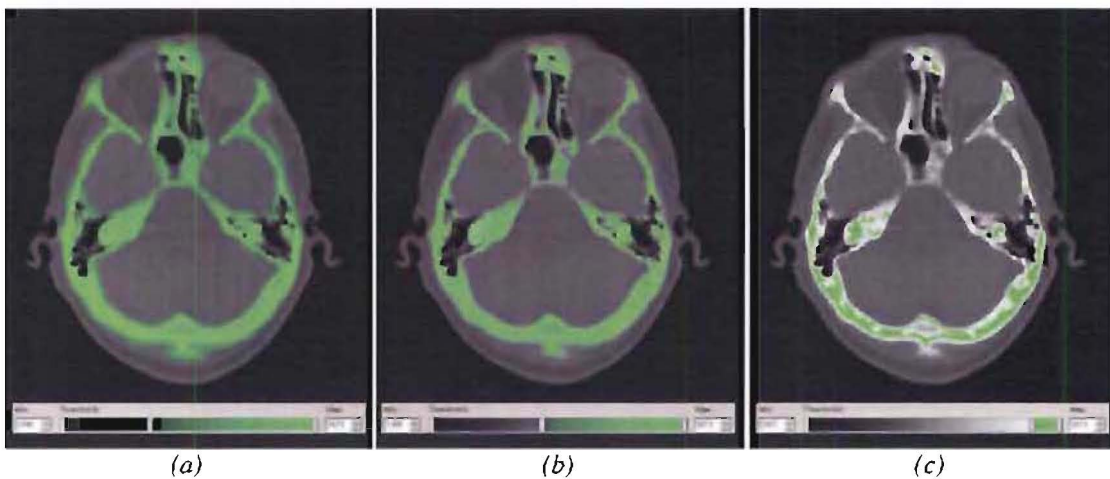


Figure 9.10 CT slices with varying thresholding limits.

Correctly setting the threshold value(s) is essential to creating an accurate reconstruction. This can be difficult to achieve especially if raw slice data or image contrast are poor.

9.3.2.3 Draw/Erase

Draw and erase tools allow the mask data to be manually edited. These tools may be required to remove artefacts from the mask, such as flares from other implants, dental fillings or portions of the scanner platform that were included in the slice data. The draw tool is also useful to simplify areas which contain unwanted detail such as the sinus or eardrum cavities, as shown in Figure 9.11(b).

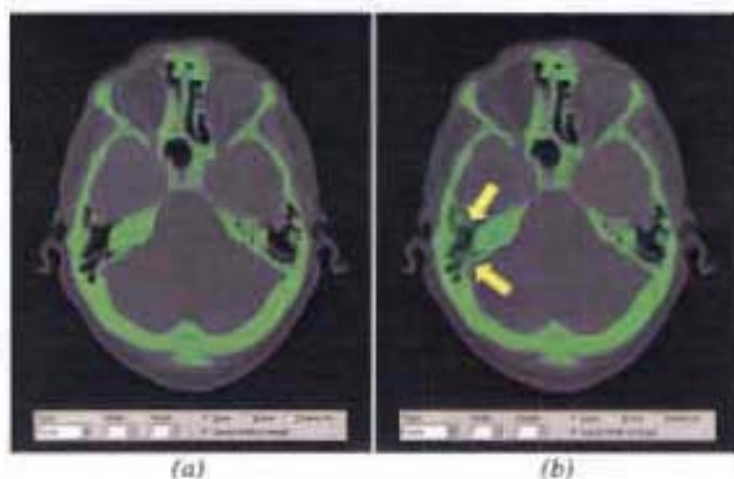


Figure 9.11 Draw and Erase tools.

(a) Raw mask data.

(b) The draw and erase tools can be used to modify the mask data, in this case the ear drum and associated passages have been filled in to simplify the model.

9.3.3 Software Solutions Tried

Three commercially available reconstruction packages that are capable of importing CT slice data and exporting reconstructed 3d volumes were investigated during the course of this project. A summary of each software package and the findings are detailed below.

9.3.3.1 3D Doctor

3D Doctor is a software package for researchers requiring medical, engineering or scientific 3d image viewing and reconstruction tools. It is able to create 3d models from medical images for diagnosis, surgical planning, and rapid prototyping applications. It is also able to reorient the slice plane for CT and MRI images allowing the patient anatomy to be viewed from any angle or direction¹.

The basic reconstruction process using 3D Doctor is as follows:

1. Import the CT slice images into 3D Doctor.
2. Create object boundaries using the auto or manual segmentation functions.
3. Use 3D Doctor's surface rendering to create a 3d model.
4. Export the resulting model as an STL file.

The cost of 3D Doctor at the time of investigation was NZ\$9600.

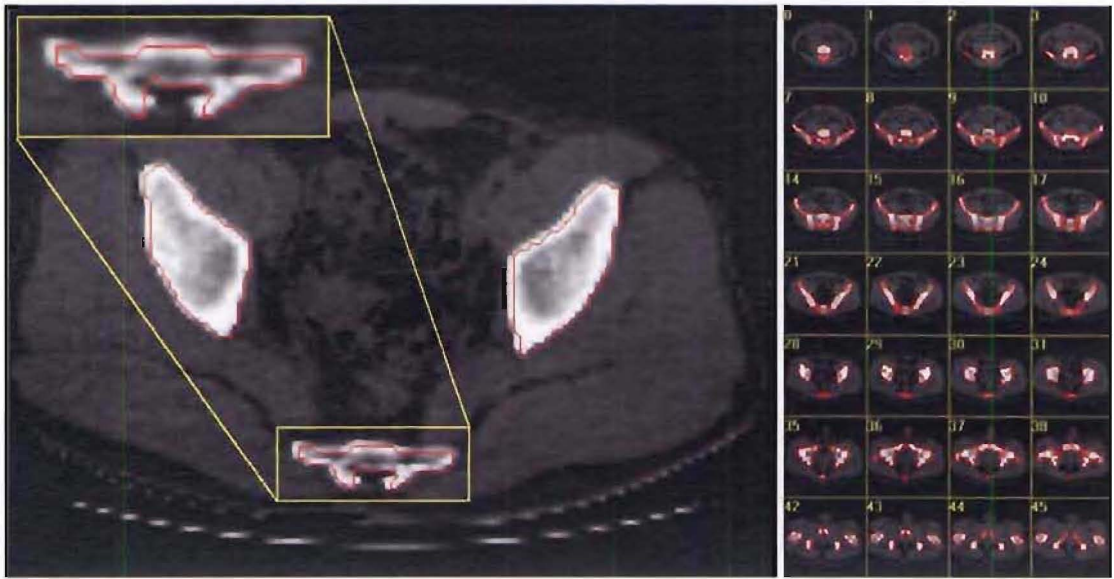


Figure 9.12 3D Doctor workspace and image mosaic.

A magnification of the sacrum and its associated object boundary are shown.

[Source: <http://www.ablesw.com/3d-doctor/tutor.html>]

During the trial of 3D Doctor it was found that the thresholding or segmentation tools produced very coarse masks, as shown in Figure 9.12. This limited the accuracy of the reconstruction that could be created using 3D Doctor and for this reason it was not considered to be a viable option.

9.3.3.2 Mimics

One of the most extensively tested packages was Mimics. This package is commonly used in industry to create medical reconstructions. The reconstructions produced using Mimics were found to be of a high quality, yet simple and quick to produce. The general reconstruction procedure using Mimics is as follows:

1. Select and import the slice data into Mimics.
2. Remove any unnecessary slice data.
3. Adjust the contrast of the images and threshold to isolate the required material.
4. Using a region-growing tool, select one voxel within the region of interest. Mimics adds all the inter-connecting voxels within the thresholding limit(s) to a new mask.
5. The “Calculate 3d” tool is then used to create a 3d reconstruction. Different reconstruction quality levels can be selected at this stage.
6. A rendering of the 3d model is displayed which can be rotated, scaled and measure as required.
7. Export the resulting model as an STL file.

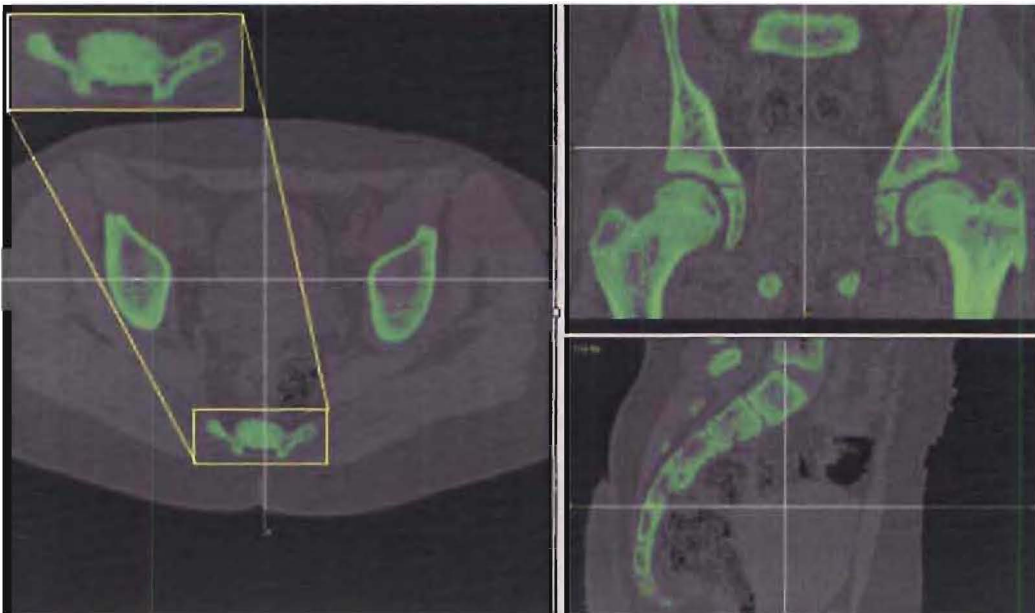


Figure 9.13 Mimics workspace.

A magnification of the sacrum and its associated mask are shown.

The masks and reconstructions created using Mimics were found to have a high resolution as shown in Figure 9.13.

However, the image manipulation tools in Mimics were quite basic. Some of the software packages tested included filtering algorithms that allowed noisy data to be improved and soft tissues to be more readily isolated, but Mimics did not offer such functionality.

Mimics was also the most expensive package tested, with the base module costing NZ\$19,800, at the time of investigation. In addition to this, Mimics also required individual raw data filters to be purchased so data could be imported from different brands of CT scanner.

The main advantage of Mimics was that it was easy to use, with simple tools and menu structures.

9.3.3.3 Velocity² Pro

The other software package that was tested extensively was Velocity² Pro, which is produced by Image3. The Velocity reconstruction software was originally developed for UNIX based computer systems, however at the time of investigation Image3 were in the process of re-writing the software to run on Microsoft Windows. The reconstruction process using Velocity² Pro is as follows:

1. Select and import the slice data into Velocity² Pro.
2. Remove any unnecessary slices.
3. Adjust the greyscale and apply filters to each slice as required.
4. Using a flood-select tool threshold each image to isolate the required data and create masks.
5. Modify the mask data as required to remove cavities and artefacts using logic, filtering and manual selection tools.
6. Create a three dimensional model using the Surfer function.
7. View the model.
8. The model file size and complexity can be reduced if required by merging surfaces that lie within a specified angular tolerance.
9. Export the resulting model as a STL file.

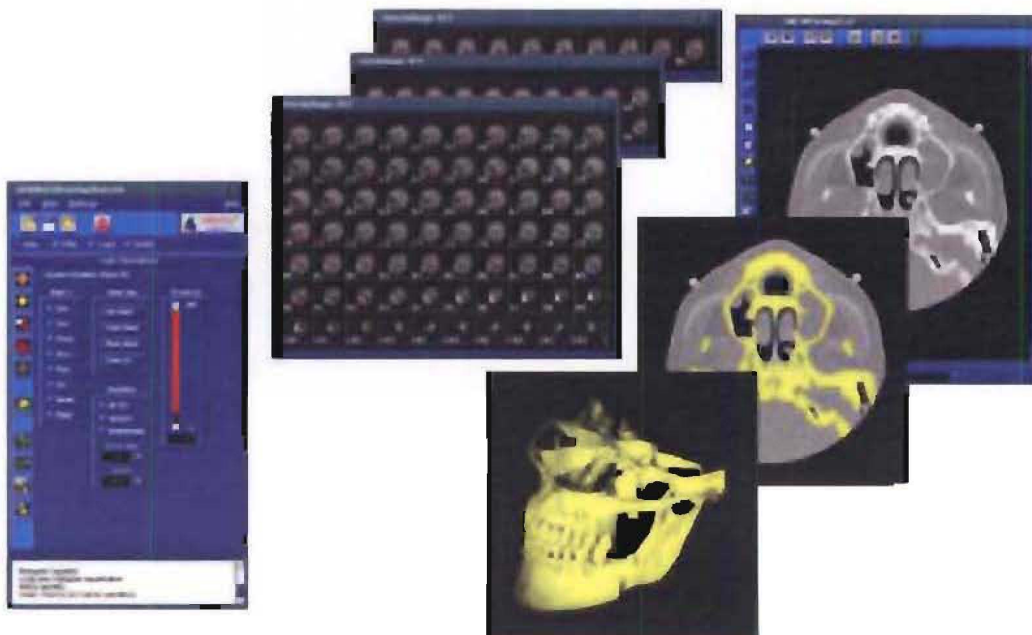


Figure 9.14 Velocity² Pro workspace (Unix Version).

[Source: Velocity² Pro Tutorial Exercise completed as part software evaluation]

The models produced using Velocity² Pro were found to be of a high quality and noisy or poor data could be manipulated using the wide range of tools and filters available in the package. These tools also allowed varying densities of tissue to be readily isolated and reconstructed. All of the data manipulation tools only affect one data slice at a time however scripts could be created to automate the manipulation process. The additional tools and functionality offered by Velocity² Pro increased the complexity of the package and resulted in a more complex reconstruction process. The cost of Velocity² Pro at the time of investigation was NZ\$16,000.

9.3.4 Final Software Package Chosen

After evaluating these three reconstruction software packages the decision was made to purchase Velocity² Pro. This decision was influenced by the lower cost of this software package and by the potential offered by the more advanced data manipulation and filtering functions.

However, with use it was found that the Velocity² Pro software was quite cumbersome to use. Also, as the majority of the work completed using the software has only involved the reconstruction of high-density boney features, the majority of the filtering and manipulation tools have not been required.

9.3.5 Problem Highlighted With Use

Several other problems were identified as the reconstruction software was used as discussed below.

9.3.5.1 Data Retrieval

In New Zealand, CT images are primarily used for planar visualisation purposes hence the scan data is normally copied to x-ray film and the raw data is deleted. In order for BioModelling to be completed the raw data must be retained. Therefore systems had to be set up which allowed the raw data to be copied.

CT scan data is normally stored on magnetic optical discs. Once the scan data has been transferred to film these discs are recycled and the raw data is discarded. At Christchurch Public Hospital magnetic optical discs are reused every 2-3 days.

The magnetic optical discs could be transported off the hospital sites for downloading of the scan data. However, magnetic optical discs and their associated drives are expensive and as there is no standard disc format each brand of disc requires a different proprietary drive. This is not an issue for the hospitals concerned as they normally only use one brand of disc. However, the need for multiple magnetic disc drives and time restrictions makes it impractical to transport the discs to another location for downloading.

The CT scan data therefore had to be copied to another storage medium, such as CD, on the hospital premises. It was found that due to sensitivity and high demands on the CT scanner systems, hospitals were not prepared to allow peripheral devices such as CD writers to be attached to the CT scanners. The final solution was to have the medical physics departments in each hospital copy the data over their networks and then burn the data to CD. The data could then be released for reconstruction.

To facilitate this process, forms were generated to ensure the patient data was copied with the appropriate consent and at the correct time. An example of such a form can be seen in Figure 9.20.

9.3.5.2 Data Accuracy

During the trials of reconstruction software, test data was obtained from the Medical Physics Department at Christchurch Public Hospital, New Zealand. Initially this data was modified by the Medical Physics Department allowing it to be imported directly into the software packages without the need for additional import filters. However, it was found that the reconstructions created from this data were very coarse. This was attributed to the low sampling rate used during the modification of the data. This problem was resolved by using the raw scan data and import filters supplied by the reconstruction software vendors.

9.4 Rapid Prototyping

The next task research task was the creation of plastic BioModels using rapid prototyping technology.

Rapid prototyping systems create parts by adding thin layers of material in the x-y plane. Once one layer is built the model is lowered by a small amount in the z direction, and the construction of the next layer begins. By continuing to add more layers of material three dimensional parts can be constructed as shown in Figure 9.15. This process differs from conventional machining techniques which remove material from a piece of stock material to form the final shape.

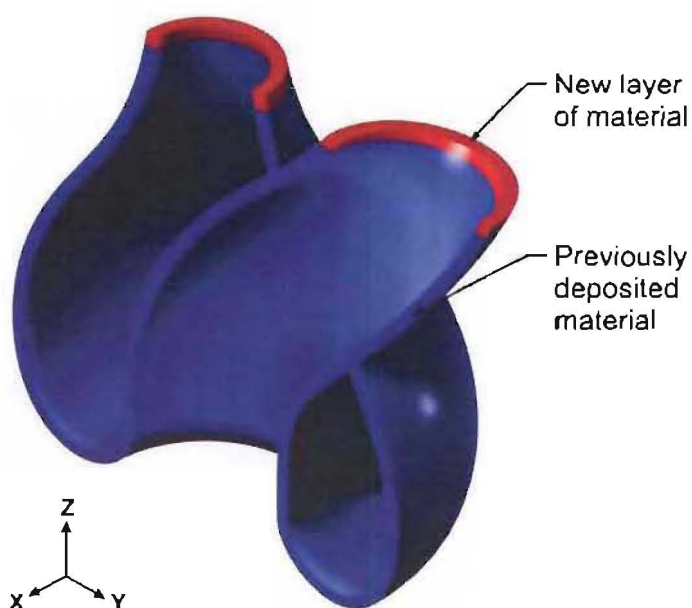


Figure 9.15 Rapid prototyping part creation.

Rapid prototyping systems create parts by adding material in thin layers in the x-y plane to form the final shape. Once one layer is completed the model is lowered and creation of the next layer begins.

As rapid prototyping systems build models in layers, each new layer must have a solid layer of material below it to support the new material as it is added. For models with unsupported features, supports are created, as shown in Figure 9.16. These supports are then removed from the model after the building process has been completed.

Examples of where the addition of support material may be necessary include:

- Holes with horizontal axes.
- Overhanging protrusions.
- Hollow shells.
- Items with bases that are not flat.

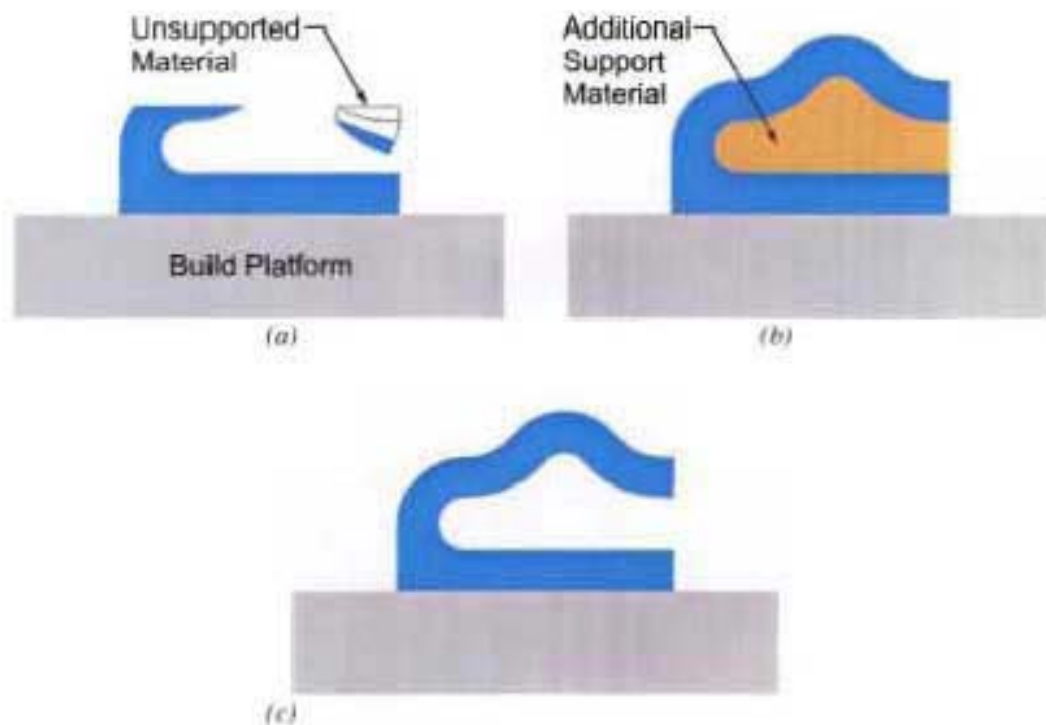


Figure 9.16 Addition of support material.

(a) Material being added to a rapid prototyped model must be supported.

(b) The addition of supports to the model allows such unsupported geometry to be created.

(c) Once the part is completed the support material is to be removed leaving only the required geometry.

The three most common types of rapid prototyping system are Stereo-Lithography, Fusion Deposition Modelling and Three Dimensional Printing. A summary of each of these modelling methods and their relative advantages follows.

9.4.1 Stereo-Lithography

Stereo-lithography is often referred to as SLA and is the most widely known and used rapid prototyping system for medical prototyping purposes.

This layered manufacturing method utilizes a photo-curable liquid resin in combination with an ultraviolet laser. The resin sits underneath the laser in a vat and the laser traces over the top of liquid in the x-y plane. When the ultraviolet laser beam hits the resin it hardens a small layer of resin at that point. By controlling the areas the ultraviolet beam traverses over, specific areas of the resin surface can be solidified. Once each layer of material has been solidified the part is lowered a small amount and a new layer of resin is spread over the top surface. The process is then repeated until the entire part has been formed.

Once completed, the part is removed from the resin vat and cleaned to remove any remaining uncured resin. Any support material is removed and the part is then post-cured in an ultraviolet light chamber for several hours. Figure 9.17 shows a stereo-lithography model of a maxilla and mandible.



Figure 9.17 Stereo-lithography model of a maxilla and mandible.

[Source: <http://www.protomed.net/content/products/SLA.html>]

Stereo-lithography offers a high level of accuracy and resolution. The finished parts also have a smooth surface that requires very little finishing. However, these models have several disadvantages including being brittle, expensive and slow to produce. Some of the resins used are also hygroscopic which means that the parts are susceptible to absorbing moisture from the atmosphere. Moisture absorption can result in distortion and dimensional instability of the models. In addition to this, if the models are handled for extended periods of time, moisture from the hands can cause stereo-lithography models to feel greasy.

9.4.2 Fusion Deposition Modelling

Fusion deposition modelling, otherwise known as FDM, produces parts using extruded ABS plastic. The process involves an ABS plastic filament being fed into an extrusion head where the plastic is heated to a semi-liquid state. The softened plastic is then forced through a small diameter nozzle onto a build platform. By traversing the nozzle in the x-y plane the contour of a part can be created and filled in. Once one layer has been completed the build platform is lowered and the process is repeated. Support material is added using an identical process. Modern FDM machines usually have a separate extrusion head for the support material which may consist of a plastic, wax or water-soluble material. Figure 9.18 shows a maxilla and mandible grown using fusion deposition modelling.



Figure 9.18 Fusion deposition model of a maxilla and mandible.

Because it uses high strength ABS plastic, FDM is the favoured technology for prototyping plastic parts that require some strength. This is particularly relevant for parts which are intended for pre-operative planning purposes. The strength of FDM models allows the surgeon to cut and drill them, whereas stereo-lithography parts often chip, crack or break when handled this way.

The main disadvantage of FDM parts is that they have a slightly corrugated surface, which is a function of the layer thickness. These corrugations can result in surgeons incorrectly viewing FDM models as being less accurate. However this is textural issue can be resolved with education or finishing processes such as sanding and painting.

9.4.3 Three Dimensional Printing

Three dimensional printers utilise inkjet technology to bind powder and produce parts.

Three dimensional printers first spread a thin layer of powder over the work platform. An inkjet print head then deposits liquid binder over the cross-section being created. Once one layer has been fully solidified the build platform is lowered and the process is repeated. Once the part is finished, it is removed from the surrounding loose powder.

Currently two materials are used with this system, a plaster based powder and a starch based powder. The plaster powder offers high strength and detail while the starch based powders allow high modelling speeds and very low cost models to be produced. Starch based powders are also suitable for investment casting.

Typically these parts have a low strength and are approximately 50% porous however, they can be post treated for additional strength and durability. This post treatment involves spraying or dipping the part in wax, urethane or resin depending on the required material properties. Figure 9.19 shows an untreated model of a human skull.



Figure 9.19 Human skull model created using three dimensional printing.

[Source: <http://www.3corp.com/industries/spotlight.asp?ID=12>]

The key advantages of the three dimensional printing system are the high build speed and low capital and consumable costs. Another advantage of this system is that the non-solidified powder remains around the model supporting any overhanging features, hence there is no need to add addition support material.

Table 9.1 shows a comparison of the three rapid prototyping systems considered.

9.4.4 Summary of Rapid Prototyping Formats

| Process | Maximum Resolution X-Y (mm) | Layer Thickness (mm) | Material | Relative Comparisons (Best (5) – Worst (1)) | | | | | | |
|-----------------------------|-----------------------------|----------------------|---------------------|---|----------------------|---------------------|--------------------------|-----------------------|------|------------|
| | | | | Clean up Required | Post Build Finishing | Mechanical Strength | Untreated Surface Finish | Dimensional Stability | Cost | Build Time |
| Stereo-Lithography | ±0.125 | 0.05 | Photo Curable Resin | 5 | 5 | 3 | 5 | 1 | 1 | 1 |
| Fusion Deposition Modelling | ±0.25 | 0.125 | ABS Plastic | 3 | 1 | 5 | 2 | 5 | 3 | 3 |
| Three Dimensional Printing | ±0.2 | 0.10 / 0.17 | Plaster / Starch | 1 | 2 | 2 | 2 | 2 | 5 | 5 |

Table 9.1 Comparison of three rapid prototyping formats.

9.4.5 Selection of a Rapid Prototyping Format

Partly as a result of this research, rapid prototyped CT scan reconstructions, or BioModels, are being offered to Australasian surgeons and medical consultants, by a local company Enztec Limited.

These BioModels are generally used for orthopaedic pre-operative planning purposes and allow surgeons to clearly visualise the affected area, plan the patient's treatment and check the placement of implants and fixation devices. The models must therefore be robust enough to be able to accommodate regular handling and standard medical practices, such as cutting, drilling and the addition of screws.

BioModels are also being used for the development of custom implants. This requires the models to be robust enough to withstand cutting and drilling in a workshop environment. The BioModels are also used on occasion as forming dollies, press tools and welding fixtures too.

Therefore, for the purposes of the Australasian BioModelling market, fusion deposition modelling was considered to be the most appropriate rapid prototyping format.

9.5 BioModelling Ordering Process

For the BioModelling service to be effective and efficient, procedures were developed which allow surgeons and Enztec Limited to accurately communicate with each other.

The current procedure for ordering a BioModel is as follows:

1. The surgeon is provided with a pad of CT Data Archive Request forms and CT Scanning Protocols.
2. Surgeon decides a BioModel is required.
3. Surgeon completes standard radiology CT scanning forms and a CT Data Archive Request.
4. Both of these forms are sent to the surgeon's preferred Radiology Department.
5. If necessary, the radiology department consults with Enztec Limited to clarify the CT scanning requirements.
6. The patient is scanned and the CT data archived.
7. The archived data is sent to Enztec Limited.
8. The data is reconstructed and Area of Interest Diagrams are generated.
9. The Area of Interest Diagrams are then sent to the surgeon.
10. Using horizontal and vertical lines the surgeon isolates the area(s) they wish to have BioModelled on the diagrams. The surgeon also indicates whether a quotation is required.
11. The completed Area of Interest Diagrams are returned to Enztec Limited.
12. A quote is supplied if required and if accepted the surgeon provides billing details.
13. The data required is then isolated, as per the indication diagrams, and the BioModel grown.
14. The BioModel is then inspected and dispatched to the surgeon.

Typically BioModels are delivered to surgeons within 5 working days of Enztec Limited receiving confirmation of the order and the billing details. The maxilla and mandible shown in Figure 9.18 were grown using the process detailed above. At the time of this report the maxilla BioModel cost NZ\$550 and the mandible cost NZ\$600. The cost of BioModels does vary though depending on the physical size of the patient, as the cost of the model is directly related to the build time and volume of ABS plastic used.

A sample CT Data Archive Request form is shown in Figure 9.20. Figure 9.21 shows a partial set of Area of Interest Diagrams for a mandible BioModel.


| | | | |
|--|---|---------------------------|---|
| DATE: | CT DATA ARCHIVE REQUEST | |  |
| PATIENT NAME: | | | |
| PATIENT DOB: | CONSULTANT: | | 4045 Scores Rd Christchurch Ph: 64-3-348-0203 Mobile: 021-293-3033 Fax: 64-3-348-0182 E-mail: info@enztec.co.nz |
| AFFIX PATIENT STICKER HERE: | | | |
| SCAN DESCRIPTION/SPECIAL INSTRUCTIONS: For Biomodel of (R) post maxillary alveolus & zygoma | | | |
| PLEASE TICK ONE: | PUBLIC PATIENT <input type="checkbox"/> PRIVATE PATIENT <input type="checkbox"/> | CONSULTANT AUTHORIZATION: | |
| FOR OFFICE USE ONLY DATA ORDER NUMBER: | | | |

Figure 9.20 CT Data Archive Request form

Shown with a typical description of the BioModel geometry required, as given by the surgeon.

enztec BIOMODEL Enztec Limited
Unit 4/45 Sonnet Road, Sockburn, Christchurch
Ph: 03 348 0202, Fax: 03 345 6182
Email: nichie@enztec.co.nz

CT Scan Reconstruction

Area of Interest Indication Diagrams

Patient Name _____

Patient ID / Scan ID _____

Date of Birth _____

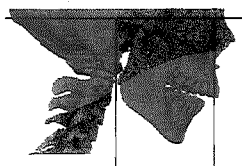
Enztec Ref _____

Project Initiator _____

The checked views are present on the accompanying pages.

| | |
|--|---|
| View of Patients Left <input type="checkbox"/> | View of Patients Right <input type="checkbox"/> |
| View of Patients Anterior <input type="checkbox"/> | View of Patients Posterior <input type="checkbox"/> |
| Pictorial View of Patients Left Anterior <input type="checkbox"/> | Pictorial View of Patients Right Anterior <input type="checkbox"/> |
| Pictorial View of Patients Left Posterior <input type="checkbox"/> | Pictorial View of Patients Right Posterior <input type="checkbox"/> |
| Scan Description: _____ | Other <input type="checkbox"/> |

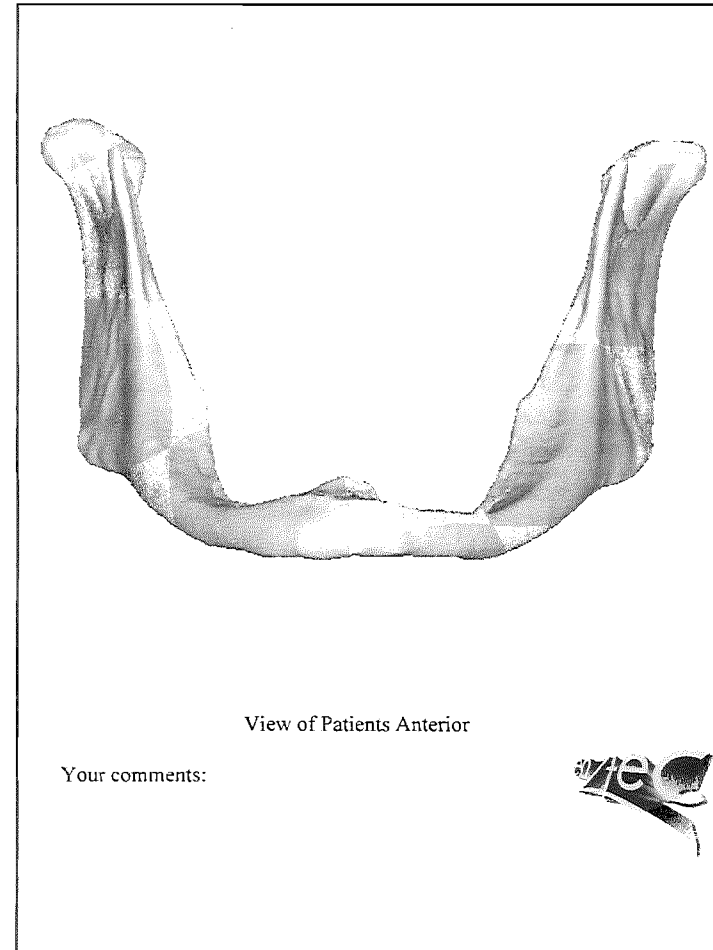
Please indicate using horizontal and vertical lines only, the area(s) of interest for use as a Biomodel.
Where necessary use a written explanation in the comments space provided.
Example Only:



(example only)
Mandible and TMJ only please
Maxilla not required.

View of Patients Right

(a)



(b)

Figure 9.21 Area of Interest Diagrams supplied to the surgeon.

(a) Cover sheet with patient identification summary, description of views attached and mark up instructions.

(b) Typical image of reconstructed data, the surgeon marks the area required using horizontal and vertical lines, multiple images are normally provided for clarity.

9.6 Machined BioModels

9.6.1 Problem statement

In some cases it is necessary to produce metallic BioModels for *in-vivo* use. To achieve this NC machine code and/or CAD compatible files must be produced from the reconstructed slice data. All the CT data reconstruction software packages investigated were capable of exporting STL files and in the case of Mimics, contour files could also be exported in an IGES format.

Each of these output formats presents its own problems when creating data for CAD or NC machining purposes. Several different software solutions were investigated to overcome these issues.

9.6.1.1 STL Files

The STL file format was developed for the rapid prototyping industry and describes the surfaces of three-dimensional models using triangular facets. Figure 9.22 shows a simple model which has been exported as an STL file. Each surface is broken down into a number of triangular facets. The size of the facets decreases wherever small features or large changes in surface curvature occur.

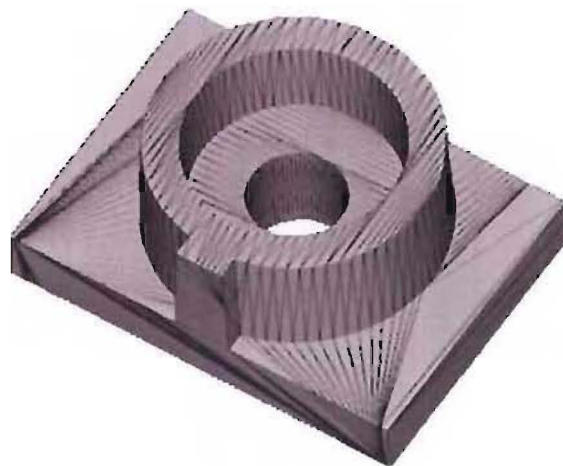


*Figure 9.22 Simple CAD generated model exported in STL format.
[Source: http://rpdrc.ic.polyu.edu.hk/old_files/stl_introduction.htm]*

Some software for generating NC code allows STL files to be directly imported. However, as each facet has to be individually toolpathed, directly NC machining parts from STL files would be a time consuming and difficult task.

Furthermore, as BioModels typically contain very complex, fine features, the resulting STL files typically contain millions of facets and have a large file size. This large volume of data makes these files very difficult to visualise, manipulate or toolpath. Hence additional processing of these files is required if they are to be used for NC machining purposes.

9.6.1.2 IGES Contour Files

Mimics is able to export IGES contours of the reconstructed anatomy. The spacing of these contours can be adjusted as required. Figure 9.23 shows an example of the IGES contours produced for a reconstructed femoral head. IGES contours can be imported into most CAD packages and, theoretically, could be used to create lofted surfaces which could then be toolpathed.

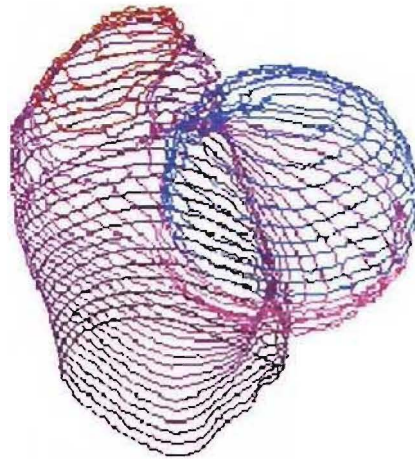


Figure 9.23 IGES contour file of a reconstructed femoral head.

However, it was found that the IGES contours exported consisted of many small segments and the end points of the contours did not line up. This resulted in the contours either failing to loft, or alternatively the lofted sections produced were twisted and distorted.

One solution was to rebuild the contours in a CAD package so they had the same number of points and the endpoints were aligned. This process was found to produce marginal results, an example of which is shown in Figure 9.24.



Figure 9.24 Lofted model of a partial femoral head developed from IGES curves.

It was found that recreating the profiles still resulted in some distortion of the geometry and there were curvature discontinuities at each contour. It was also difficult to construct transition areas using this process. For example it was not possible to accurately loft the transition area between the femoral head and the peak of the greater trochanter, as shown in Figure 9.25. The process of rebuilding the contours was also very time consuming. The geometry shown in Figure 9.24 took approximately 15 man hours to construct.

It was therefore decided that lofting exported IGES contours was not an acceptable way to produce accurate CAD models of reconstructed CT data.

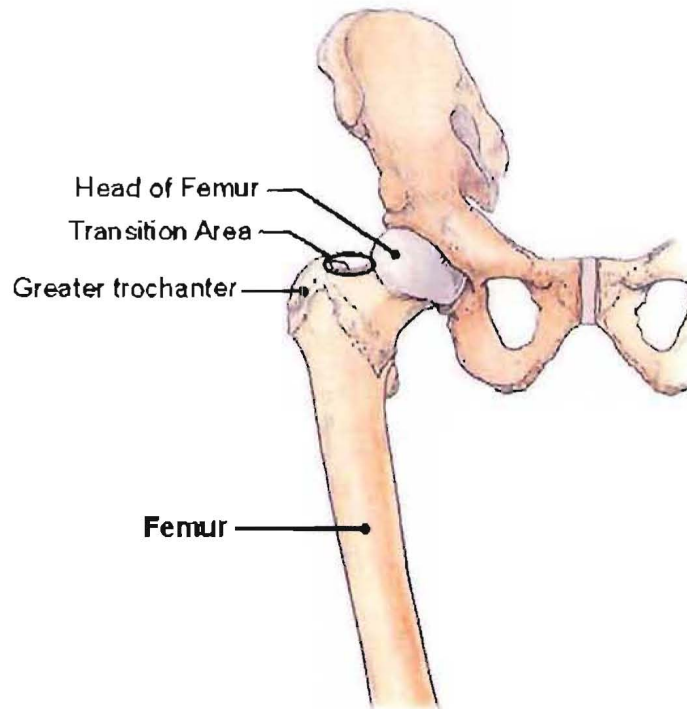


Figure 9.25 Anterior view of the right femur and pelvis.

[Source: Moore K L³]

9.6.1.3 Rhinoceros®

Rhinoceros®, otherwise known as Rhino, is a NURBS based modelling package primarily used for modelling freeform shapes. NURBS stands for Non-Uniform Rational B-Spline and is a mathematical way of defining curves, surfaces, and solids.

Although Rhino primarily works with NURBS objects it does have some tools for manipulating triangular meshes. Specifically, STL files can be converted into NURBS based models. These resulting NURBS models can then be imported into most CAD packages.

This process was found to be computationally intensive, with only small models being able to be converted to NURBS geometry. The reconstructed hip shown in Figure 9.26 took in excess of 3 hours to open, convert to a NURBS based file and import into a CAD package.



Figure 9.26 Hip geometry produced in Rhinoceros® from an imported STL file.

The NURBS files imported into CAD packages were also faceted as per the original STL files. Therefore generating and exporting NURBS models offers few advantages over directly importing STL files into NC toolpathing software.

Using the imported NURBS geometry as a template, additional modelling could be completed in a CAD package to recreate critical features. However, as detailed in Section 9.6.1.2 this reconstruction process was found to be a time consuming and difficult task.

Recently several CAD packages have introduced the ability to directly import STL files. The resulting CAD models are still faceted as found using the Rhinoceros[®] methodology, however this direct importation ability does eliminate the need for Rhinoceros[®].

9.6.1.4 Reverse Engineering Software

Several reverse engineering software packages are currently commercial available. These software packages use sophisticated algorithms to manipulate surface data and output it in a variety of different formats.

These software packages can typically import point cloud data, volume meshes and polygonal meshes, such as STL files. The raw data can then processed using a number of tools to create watertight smooth polygonal models.

Of the software packages available, Raindrop Geomagic® Studio was selected for extensive testing. A typical Geomagic Studio workflow is detailed below. Note: Figures 9.27 – 9.29 were created using a tutorial data set which was included with the Raindrop Geomagic® Studio software.

The first step is to import the raw data. In Figure 9.27(a) a point cloud is shown, but an STL file can be used instead. Noisy data can be improved and sampling algorithms used to reduce the data set. Reducing the data set allows polygon surfaces to be generated faster and a higher quality polygonal surface may also result. The data chosen for removal is selected based on curvature with more data retained in areas of high curvature while point data is removed from flat, less detailed areas. For example multiple data points in the middle of large flat surfaces make no contribution to the accuracy or definition of the model and hence can be removed. However, if required the data filtering and reduction steps can be skipped and the full data set used to construct the model. Figure 9.27(b) shows the model after filtering and data reduction, the faceted appearance of the model does not reflect the final shape of the model.

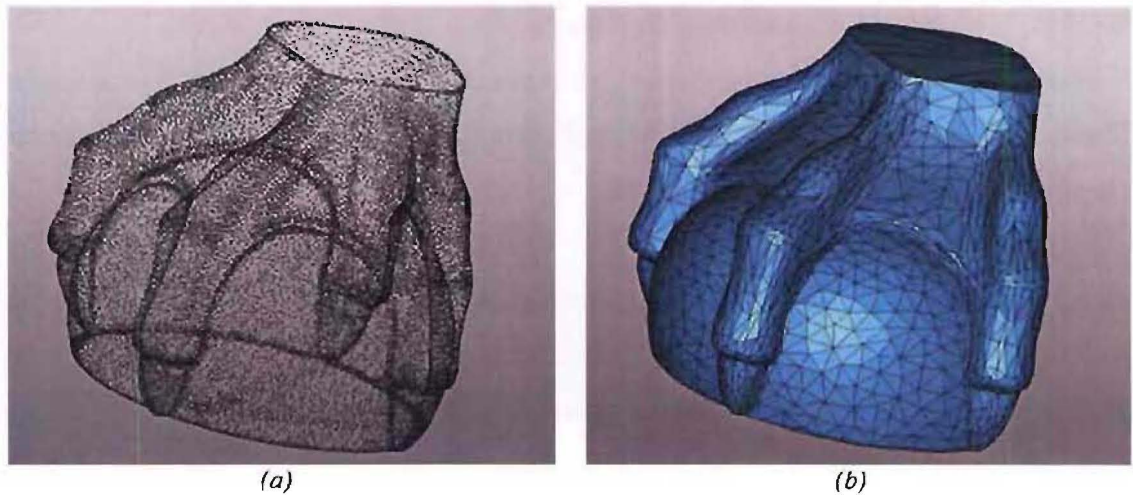
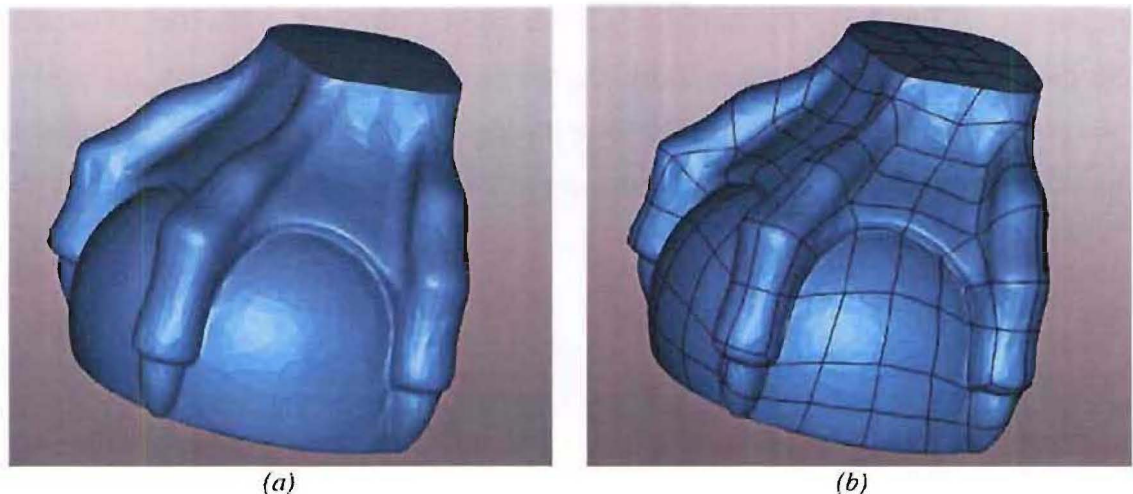


Figure 9.27 Data input and pre-processing.

(a) Raw data input.

(b) Filtering and data point reduction.

After pre-processing of the raw data, construction of the polygonal model can begin. The Geomagic software uses a series of geometric rules to create polygonal surfaces over the surface of the raw data. This process is automated, however, sometimes topology errors occur. For example, some regions of the model may be filled that should not be, or holes may be created which require filling. These repairs can be completed using smoothing algorithms, triangle deletion and hole filling tools. Automatic feature detection and sharpening can also be carried out at this stage to ensure hard edges and corners are retained. Figure 9.28(a) shows the model after the polygonal surfaces have been created and any topology errors have been repaired.



(a)

(b)

Figure 9.28 Surface generation and patch manipulation.

(a) Wrapped NURBS surface, with topology errors repaired.

(b) Final layout of the NURBS patches after manipulation of the patch boundaries and positions.

Once polygonal surfaces have been created they can be broken down into smaller patches; and a NURBS surface is fitted to each patch. The key to producing a sound NURBS model is good patch structure. The ideal structure is:

- *Regular*: Each patch should be approximately rectangular with four vertices meeting at the same point.
- *Shape Appropriate*: There should be no severe or multiple curvature changes in the centre of the patch.
- *Economy*: The model should ideally contain a minimum of patches.

The Geomagic software has automatic construction tools which aim to achieve these NURBS patch goals. After the initial creation of the patches, manual editing tools can be used to improve the structure and position of patch boundaries, as required. The final patch boundaries for the previous example are shown in Figure 9.28(b).

Once suitable patches have been created the NURBS model can be exported in a variety of formats and then import directly and cleanly into most CAD packages. Figure 9.29 shows a completed CAD compatible model.



Figure 9.29 Final NURBS model.

This process was found to be effective for converting 3d models of reconstructed CT scan data into CAD and toolpathing compatible models.

The key disadvantage of this approach is the cost. Geomagic Studio has all the functionality required but cost NZ\$15,000 at the time of investigation. However, other methods investigated for converting reconstructed CT data into CAD and toolpathing compatible files were found to be inaccurate and inefficient. It is therefore recommended that a software package such as Raindrop Geomagic® Studio should be used to convert STL files into CAD and toolpathing compatible forms.

9.7 Case Study

After research into rapid prototyped and CAD compatible BioModels had been completed, a request was received to develop an implant for a patient who required their right hand cheek and orbital socket boney structures to be replaced.

9.7.1 Case History

The patient had previously had a radical maxillectomy and orbital exenteration for a right maxillary squamous cell carcinoma. Or simply put, had an operation to remove a large tumour which included some of the bones which form the cheek bone and eye socket. As a result of this surgery the patient required an implant to replace their right zygoma and maxilla. Figure 9.30 shows the position and general form of these boney structures.

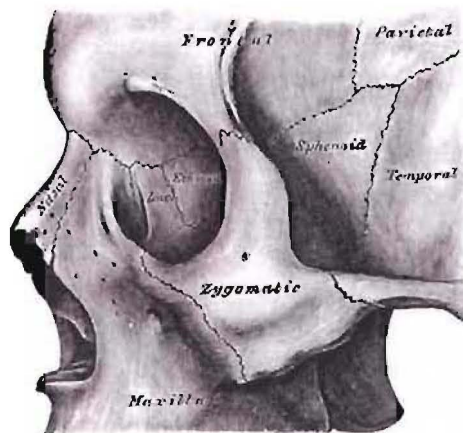


Figure 9.30 Left zygomatic bone and maxilla in-situ.

[Source: Gray H, Anatomy of the Human Body. Figure 164²]

CT scans of the patient's skull were taken with a slice spacing of 1mm and the resulting data was reconstructed. A rendering of the reconstructed data is shown in Figure 9.31.



Figure 9.31 Rendering of the reconstructed CT data.

The missing zygomatic and maxilla boney structures on the right hand side can be clearly seen.

The reconstructed data was then used to create a FDM BioModel. After consulting with the surgeon involved with the case and reviewing the BioModel, the decision was made to create the bulk of the implants form by mirroring the patient's left hand side zygomatic and maxilla structures.

9.7.2 Generation of the Implant Geometry

The reconstructed data was imported into Raindrop Geomagic® Studio. Using this software the surface data for the left hand boney features was isolated and exported. This data was referred to as the implant parent data.

The entire skull geometry was then simplified to remove all internal structures and non-critical features. This was done so the skull geometry could be imported into the CAD package for implant planning and design purposes. During this simplification of the skull data, care was taken to preserve the accuracy of the implant parent data and the areas of the skull where the implant was to be located. The simplified skull was then exported in a CAD compatible format. Figure 9.32 shows the simplified skull data and the implant parent data (red).

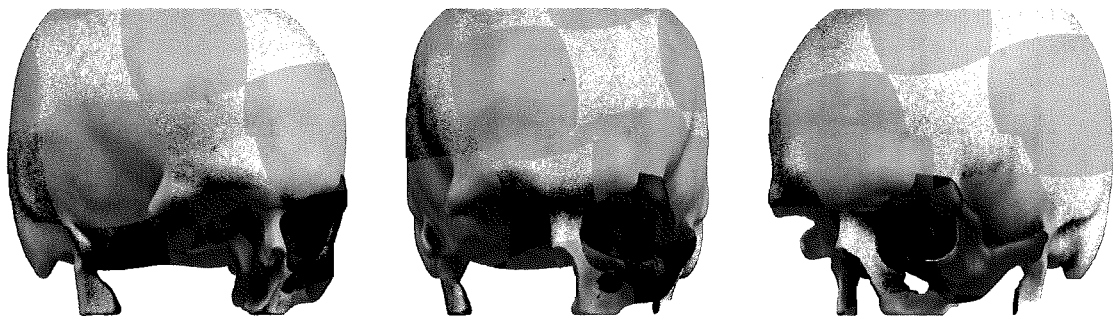


Figure 9.32 Rendering of the implant parent data.

The implant parent data, shown in red, was copied from the underlying reconstructed CT data.

A temporary coordinate system was created in the centre of the skull. The implant parent data was mirrored about the sagittal plane of this coordinate system to create the implant template data. Figure 9.33 shows the implant template data positioned on the reconstructed and simplified skull. It was decided not to include the frontal process of the maxilla, which forms part of the nasal structure in the implant parent data. The specification called for this structure to be manually formed once the bulk of the implant had been created.



Figure 9.33 Rendering of the implant template data.

The implant parent data extracted from patient's left zygomatic and maxilla boney structures were mirrored and positioned to create a template for the implant.

9.7.3 Implant Manufacturing Processes

A prototype implant was NC machined from a billet of aluminium for evaluation purposes. The prototype implant, shown in Figure 9.34(a), was found to have a good overall form but the areas where it contacted the skull needed to be adjusted to increase the size of the contact patches. This poor fit was due to the fact the human body is not symmetrical. Two potential methods of improving the fit at the contact points were considered, these included:

- Manually adjusting the thickness of the implant at the contact areas to reduce the gap between the skull and implant surfaces.
- Removing some the protruding bone at the contact points, allowing more of the implant to be contact with the remaining reshaped bone.

It was decided that adjusting the implant to suit the patient was the best choice, however if necessary the fit could be further improved in theatre by removing a small amount of bone.

The final implant was manufactured from Commercial Pure Grade 2 Titanium. Due to the cost of this material it was decided to form the bulk of the implant using press tools rather than NC machining from billet. A die set was produced using the implant template data and the implant was formed from 2mm sheet. An untrimmed implant blank is shown in Figure 9.34(b).



Figure 9.34 Skull implant prototypes.

(a) NC machined implant prototype.

(b) Pressed implant prototype prior to trimming operations.

The implant blank was then trimmed to the required shape and some minor manual curvature adjustments were made. The areas of the implant which contacted the patient skull were then manually reduced in thickness to approximately 1mm. This had two benefits:

- It allowed the contact between the skull and implant to be improved, as previously detailed.
- It allowed the implant thickness to be reduced at the attachment points meaning that the implant did not sit as proud of the skull surface as it would have otherwise.

The finished implant was polished and anodised. Anodising the implant offered several benefits. It improves the visual appeal of the implant and it hardens the implant surface. The hardened implant surface does not wear as readily as raw titanium. This reduction in implant wear and the associated reduction in wear debris volume helps prevent staining of the surrounding tissue and decolourisation of the skin. In this case, staining of the skin was an important issue due to the close proximity of the implant to the skin and the visibility of the implant site.

The implant was successfully implanted in mid 2002, using maxillofacial bone screws. The implant site remained inflamed and required aspiration for a period of two months. The patient also experienced some thinning of the skin in the region of the maxilla frontal process where the nasal structure had been manually created. This thinning was probably due to the amount of subcutaneous fat that was removed during the implantation procedure. These complications have since been overcome and the patient continues to make a full recovery.

9.7.4 Improvements and Future Work

During a post-implantation review of this implant and its manufacture, several key areas for potential improvement were identified.

9.7.4.1 Adjustment of the Implant Attachment Points

As previously discussed in Section 9.7.3 the implant and/or skull had to be manually adjusted to improve the contact between the implant and skull. A more desirable solution is to modify the implant template data prior to manufacturing the implant. One method of achieving this is detailed below.

The implant template data should be positioned on the reconstructed skull geometry as accurately as possible. Figure 9.35 shows the implant template data (blue) in position.



Figure 9.35 Rendering of the raw implant template data.

As the human body is not symmetrical the implant template mirrored from the contralateral side does not fit the implant site exactly.

The implant template data should be trimmed back a sufficient distance so there is space to create a transition surface between the remaining implant template data and the desired contact area. Surfaces from the underlying skull geometry can then be copied into the implant data file to form contact patch component of the implant. These skull contact surfaces (red) should be trimmed to the desired shape as shown in Figure 9.36. The gap between the implant template data (blue) and the reconstructed skull can also be clearly seen in Figure 9.36.

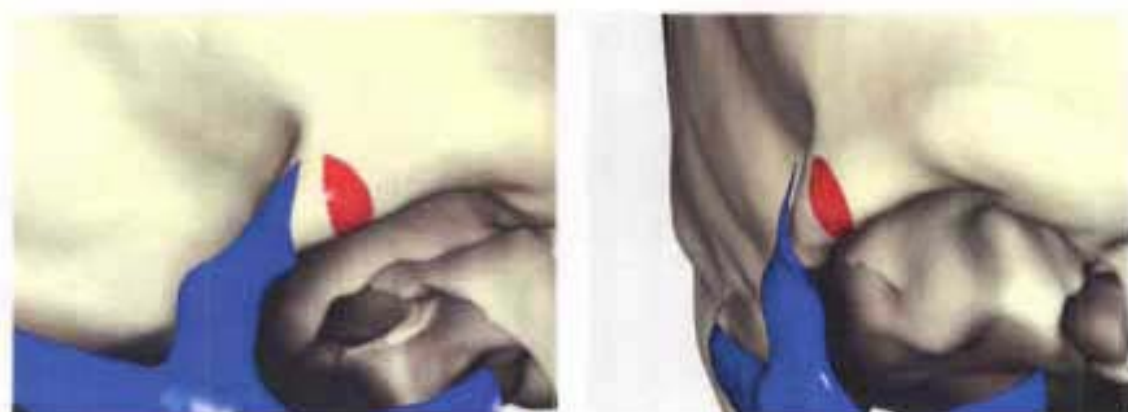


Figure 9.36 Rendering of the modified implant template and contact patch.

The implant template was reduced and the data extracted from the implant contact site. The mismatch between the template data and reconstructed skull can also be clearly seen.

Boundary curves should then be generated between the trimmed implant and contact patch surfaces. A bridging surface can then be generated between these two surfaces. Where possible curvature controls should also be used to help create a smooth transition between the implant surfaces. The bridging surface (yellow) is shown in Figure 9.37.



Figure 9.37 Rendering of the bridge between the implant template and contact patch.

A surface is created between the edges of modified implant template and contact patch. This allows the general implant form to be retained while ensuring a well fitting implant is created.

Figure 9.38 shows the final implant form after knitting of the implant, bridge and contact patch surfaces. Using this technique the implant will accurately fit the patient's skull and no additional manipulation of the implant or skull should be required.



Figure 9.38 Rendering of the final implant and contact patch.

9.7.4.2 Modification of the Manufacturing Process

In order to take advantage of the modified contact surface(s) the manufacturing process must be accurate enough to replicate the CAD model features. This is easily achieved if the implant is NC machined from billet, as most NC machining centres are more than capable the required tolerances. However as previously discussed, it is preferable to press the implant from thin sheet rather than NC machining from billet due to cost constraints. Well designed press tooling is capable of producing the required tolerances, however the design of such tools is a difficult and time consuming task and prohibitive for one off items such as custom implants.

The proposed solution is a two step manufacturing process. First the implant CAD model should be used to produce a series of press tools which form the bulk of the implant geometry. Pressing cannot be used to form small and critical features, such as the contact areas, as spring-back reduces the accuracy of final part. Instead critical areas of the implant geometry should be NC machined into the pressed implant blank once all the pressing procedures have been completed. This second step allows surfaces that need to be accurately formed, such as the contact surfaces, to be produced efficiently and economically.

This technique is only suitable for applications where implants with non-uniform thickness are acceptable. However, for cosmetic, non-structural implants, such as the zygomatic and maxilla implant, non-uniformity is a desirable feature as it allows the implant to sit flush with the surrounding bone.

9.8 Summary and Conclusion

Several software packages for manipulating and reconstructing medical scan data were investigated during this component of the project. These packages allow 3d graphical models to be developed from planar medical scan data for visualisation purposes. The software packages investigated offered varying levels of functionality and complexity.

The reconstructed 3d models can be exported in a rapid prototyping compatible format allowing plastic models of the required geometry to be produced. Procedures were also developed and implemented to facilitate the timely release of raw scan data with appropriate patient consent, for modelling purposes.

The final component of this research was to develop methods of producing metallic models of reconstructed data for *in-vivo* applications. Several potential solutions were investigated, however ultimately a commercial software package was determined as being the best solution. Methods of manipulating the scan data were also developed which allow accurate mating of metallic models and the patient anatomy.

The reconstruction processes and BioModelling techniques detailed in this chapter have been offered to Australasian medical professionals as a service. Currently this facility is being well utilised and has been well accepted by the orthopaedic, maxillofacial and plastic surgery communities. The bulk of requests are for FDM BioModels, however the number requests for custom implants for *in-vivo* use continues to increase.

9.9 References

1. Able Software Corp. *3D-Doctor*, [cited March 2003]. Available from <http://www.ablesw.com/3d-doctor/>.
2. Gray H, *Anatomy of the Human Body*. 20th Edition. 1918, Philadelphia: Lea & Febiger.
3. Moore K L, *Clinically Oriented Anatomy*. 3rd Edition. 1985, Baltimore: Williams & Wilkins.

<Blank Page>

Chapter 10 – Femoral Endoprosthesis

10.1 Problem Statement

A request was received to design a femoral endoprosthesis for a patient who had the brittle bone disease, Osteogenesis Imperfecta.

10.2 Case History

The 46-year-old male patient had suffered multiple long bone fractures throughout his life and presented with significant orthopaedic problems. His right femur had a Bent Kuntscher nail (Figure 10.1a). He had long multi-holed plates on both tibia and stress fractures at the lower end of each tibia. However, the most pressing problem was the patient's left femur.

The left femur had previously been fitted with a tri-fin nail plate (Figure 10.1b) at the proximal end and a condylar screw plate (Figure 10.1c) intended for adolescents at the inferior end. There was a non-union in the middle, and multiple broken screws throughout the shaft of the femur. An x-ray of the patient's femur is shown in Figure 10.2.

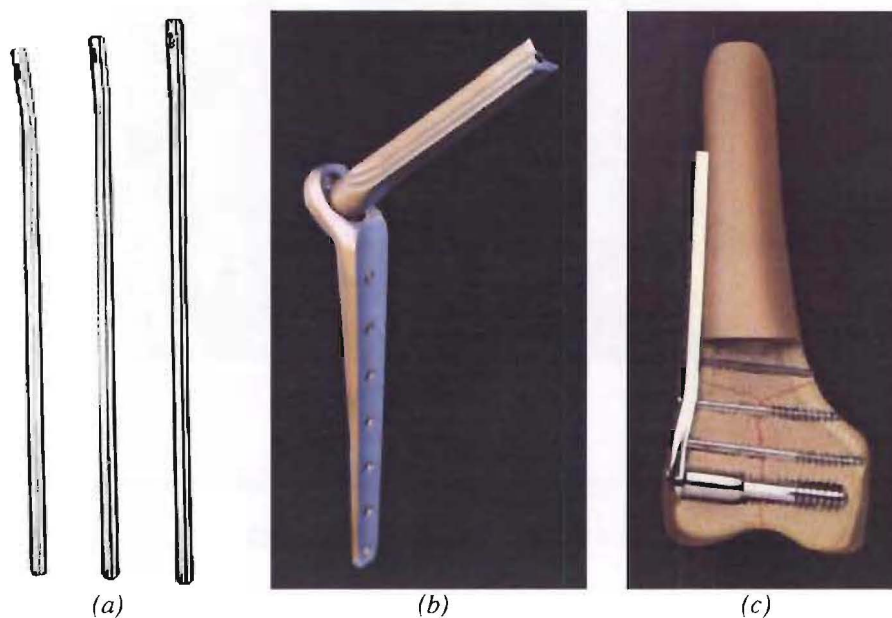


Figure 10.1 Examples of existing fixation devices.

(a) Bent Kuntscher nail. [Source: <http://narang.com/nails.html>].

(b) Tri-fin nail plate.

(c) Condylar screw plate. [Source: <http://tristan.membrane.com/aona/tech/ortho/dhs/dhs0005.html>]



Figure 10.2 X-ray of the patient's left femur.

The patient had undergone six previous operations to rectify various fractures of the left femur. The remaining bone was small in diameter and sclerotic. The patient's left limb was also shorter and there was a significant varus mal-alignment due to the previous fractures. However, the patient's hip and knee joints were in good condition and it was specified that these joints should not be compromised during the treatment of the patient.

One reason the existing implants had failed was because they were designed for load sharing applications. That is, these devices were not designed to support the patient's full weight. Instead the existing implants would be intended to provide some reinforcement while the adjacent bone carried the majority of the loads. However, in this case the femoral bone stock did not have sufficient strength to carry the requisite percentage of the applied loads. There were also non-union areas where the implants were required to carry all of the applied loads.

Two treatment options for the patient's left femur were considered:

- Patch up the femur with bone graft material and add more fixation plates and wires to the non-union site.
- Remove all the existing implants and insert an endoprosthesis which incorporated the patient's healthy hip and knee joints. Such an endoprosthesis would be required to carry all applied loads and not require the bone to heal.

Ultimately the surgeon involved in the case elected to use a femoral endoprosthesis.

10.3 Literature Review

A literature search was conducted to determine if any suitable femoral endoprotheses had already been developed. Four different endoprosthesis systems were identified.

10.3.1 Nerubay and Katznelson Total Femoral Replacement

Between 1973 and 1983, 19 patients were fitted with a total femoral prosthesis after treatment of sarcoma of the femur⁵. This prosthesis consisted of a Thompson femoral head with a long stem which was inserted into the tibia. This procedure required the knee joint to be removed and left the patient with a straight leg. To compensate for this loss of knee motion the affected leg was shortened 1cm in some cases to accommodate free swinging of the limb while walking. Five of the patients treated had excellent results and nine had good functional results. Complications included infection of the implant site and fracture of the implant. The implant fractures occurred in the stem where the implant meet the tibia. It is noted that this implant was an improvement on amputation, the only other surgical option at the time.

10.3.2 Marcove et al Total Femur and Knee Replacement

In 1976 Marcove et al³ reported a total femur and knee replacement. This implant was reported as being made entirely of metal. It consisted of a femoral head and hinged knee implant which were connected by a rigid shaft, as shown in Figure 10.3. The device was implanted in 19 patients with an average age of 20.3 years. The patients were followed for 3 to 29 months. Thirteen of the patients had functional results, with nine patients able to climb stairs one at a time while using aids such as crutches. The affected limbs were reported as being weak, but functional. Patients were able to walk without support, but their gait was found to be better with a cane and/or an ischial weight bearing brace. Complications included infection and local reoccurrence of sarcomas requiring disarticulation of the hip.



Figure 10.3 Marcove et al total femur and knee replacement.

[Source: Marcove et al³]

10.3.3 Steinbrink et al Total Femoral Prosthesis

Several different variants of the Steinbrink et al⁶ Total Femoral Prosthesis were produced, all of which utilised hinged knee and total hip prostheses. In the first version of the prosthesis the hip and knee devices were cemented into a polyethylene shaft, as shown in Figure 10.4(a). This design was versatile and economic to produce, but suffered from a lack of rigidity and fatigue fractures. Also in order to withstand the stresses the polyethylene component had to be bulky, which made closure of the wound difficult in some cases.

A titanium version of the implant was developed, which allowed the prosthesis to withstand higher loads while reducing the bulk of the implant, this version of the implant is shown in Figure 10.4(b). However, a ceramic femoral head was necessary due to the poor wear characteristics of the selected titanium alloy.

The final version of this implant was manufactured from a Chrome-Cobalt-Molybdenum alloy and was called the Durchsteck prosthesis it is shown in Figure 10.4(c). This implant incorporated a removable distal end which allowed the implant to be pushed through the reamed out lower end of the femur. This arrangement allowed the femoral muscle and ligament attachments to be preserved.

Between 1973 and 1980, 32 total femoral replacements were undertaken using the Durchsteck prosthesis. Eleven patients experienced post-surgery infection, but after treatment there was no reoccurrence of infection. Twelve patients could walk for half an hour or more. Most patients had satisfactory hip movement, but the knee range of motion was restricted when compared to a standard knee implant. Three patients required revision due to implant fracture or infection, but none required disarticulation.

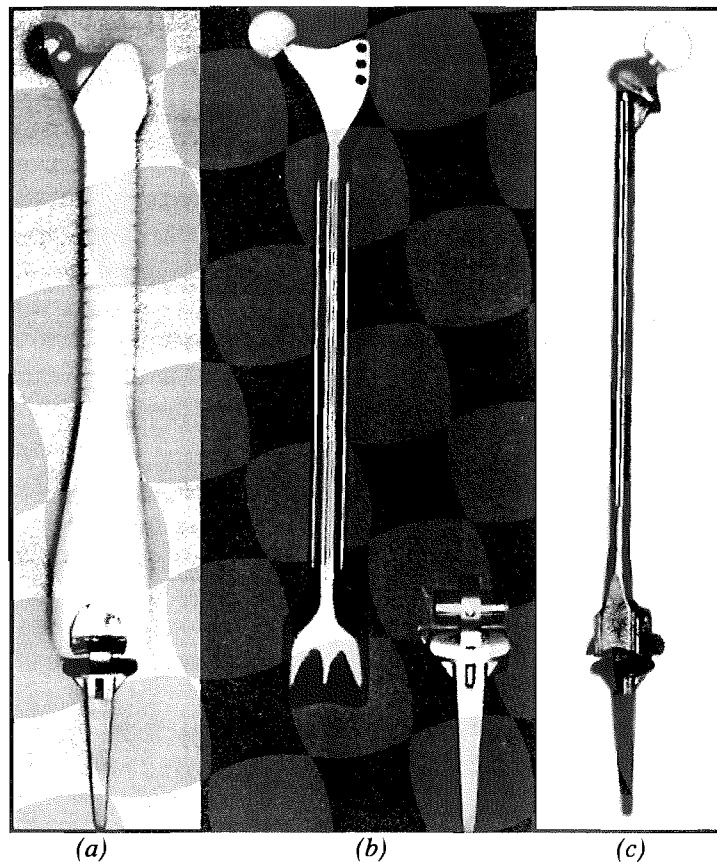


Figure 10.4 Steinbrink et al total femoral prostheses.

(a) Polyethylene prosthesis.

(b) Titanium prosthesis with ceramic head.

(c) Durchsteck prosthesis with ceramic head.

[Source: Steinbrink et al⁶]

10.3.4 Kotz Modular Femur and Tibia Reconstruction System

The Kotz Modular Femur and Tibia Reconstruction System (KMFTR), is a commercially available 26 piece modular system for reconstructing the lower extremity bones from the femoral head to the distal third of the tibia^{1,2}. The implant is made of cast Chrome-Cobalt-Molybdenum alloy, known as Vitallium. Figure 10.5 shows exploded and assembled views of the Kotz Distal Femoral Modular Endoprosthesis.

Between 1982 and 1989, 100 lower limb reconstructions were completed using the KMFTR system after resection of malignant tumours. The overall survival rate of the prostheses was 85% after 3 years, 79% after 5 years, and 71% after 10 years. The most common reason for implant failure was aseptic loosening. The other reasons for revision surgery were implant fracture and infection. Early repair of minor prostheses related complications, such as worn polyethylene bushings, resulted in a significant reduction in implant failures.⁴

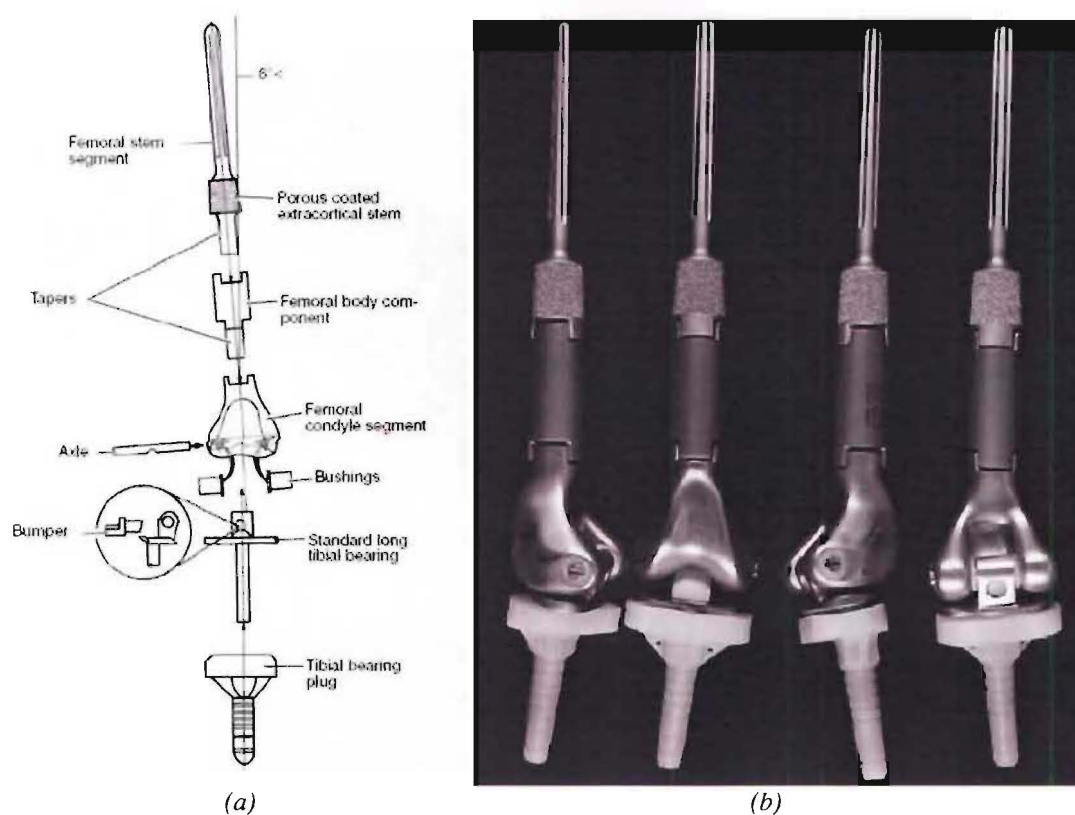


Figure 10.5 Kotz distal femoral modular endoprosthesis.

(a) Exploded view of the endoprosthesis components.

(b) Composite photograph of assembled endoprosthesis.

[Source: Malawer²]

10.4 Proposed Solution

None of the implant systems identified in the literature search were considered appropriate, as they all required the hip and/or knee joints to be resected, contrary to the requirements for this patient. Therefore, the decision was made to design a new femoral endoprosthesis.

Discussions were held with the surgeon involved with the case, to refine the form and design of various endoprosthesis components. The surgeon requested an endoprosthesis that had a screw or nail device for the hip connection and a condylar screw for the knee connection. A tee cross-section was specified to bridge between the knee and the hip joints. It was also specified that the web of the tee cross section should be able to be inserted into a slot cut in the remaining femoral bone stock, as shown in Figure 10.6.

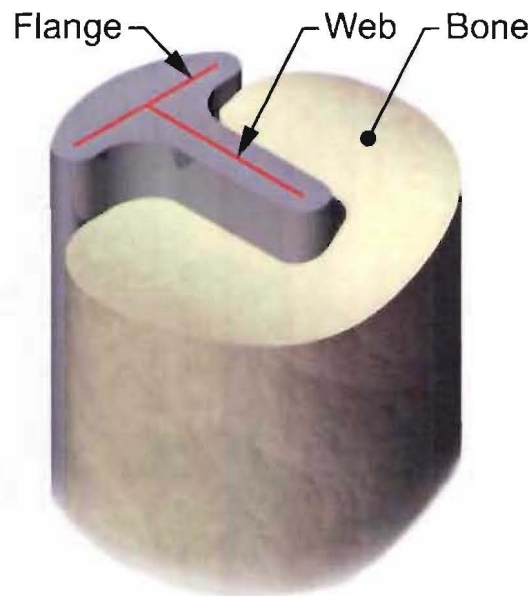


Figure 10.6 Tee section positioned in femur.

The endoprosthesis was required to withstand all physiological loads. It was noted that the endoprosthesis was unlikely to experience large dynamic loads due to the patient's other ailments limiting strenuous activities. The patient weighted 85 kg, therefore when standing still and supporting the patient's full weight the endoprosthesis would be required to support an applied load of approximately 1000 N. Ultimately a design load of 2000 N was selected to allow for small dynamic loading effects.

Initial design concepts for the hip connection used a tri-fin nail similar to the one already implanted. Ideally, by using a tri-fin nail the trauma to the femoral head could be reduced by re-using the cavity created by the existing implant. However, analysis of tri-fin nails indicated that the fins may buckle under the applied load. Although tri-fin nail implants are designed to be used for such hip connections, they are, as previously discussed, intended for load sharing applications. Therefore the decision was made to develop a custom screw for the hip connection.

The endoprosthesis assembly order was required to be flexible so the surgeon could implant components in any order as circumstances dictated in theatre. The main development focus was therefore on the design of connections between the screw devices and implant body.

Appendix 10 shows some of the concept sketches generated during the development of the final endoprosthesis design.

10.5 Endoprosthesis Geometry

The majority of the endoprosthesis form was determined by the patient's morphology. The procedure used to determine the key implant dimensions is detailed below.

Ideally, the endoprosthesis dimensions could be determined using the BioModelling techniques detailed in Chapter 9. However, this was not possible as the large number of pre-existing implants in the patient's femur would result in any CT scans having a large number of artefacts, such as flares. Endoprosthesis dimensions were therefore determined by directly measuring from the parallax corrected x-ray shown in Figure 10.7(a).

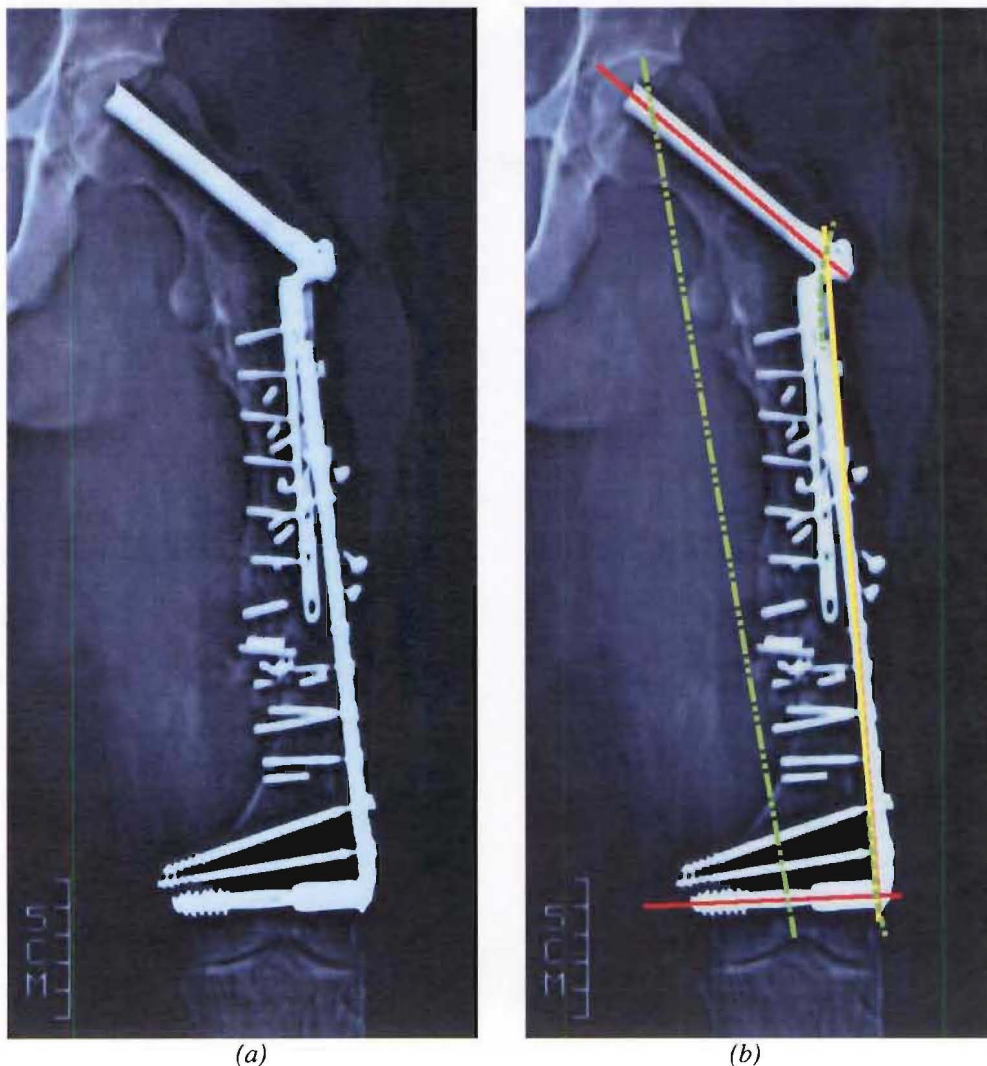


Figure 10.7 Geometry extracted from x-ray.

(a) Original x-ray image.

(b) X-ray image and key axes.

Several key axes were identified from the x-ray as shown in Figure 10.7(b). First the current screw and nail axes, shown in red, were identified. These axes were connected together by a line, shown in yellow, which met the axes at the outer cortex of the bone. Finally the length of the femur was determined by constructing a line between the highest point of the femoral head and the valley between the two condyles of the knee, as shown in green.

Figure 10.8(b) shows the data extracted, from which several key observations were made. The patient's left femur was found to be 10mm shorter than the right hand side. The angles measured between the screw axes and reference lines were also found to be abnormal. The decision was made to correct these deformities, as shown in Figure 10.8(c). The femur length reference line was made vertical and the length increased by 10mm. The hip angle was also increased from 135 degrees to a more standard 150 degrees and the knee angle was also adjusted slightly. The modification of the hip and knee angles also helped to improve the varus mal-alignment problem. The hip axis was also rotated anteriorly 15 degrees as shown in Figure 10.8(a) to replicate healthy hip geometry. The green curve shown in Figure 10.8(c) represents the desired bone/endoprosthesis interface.

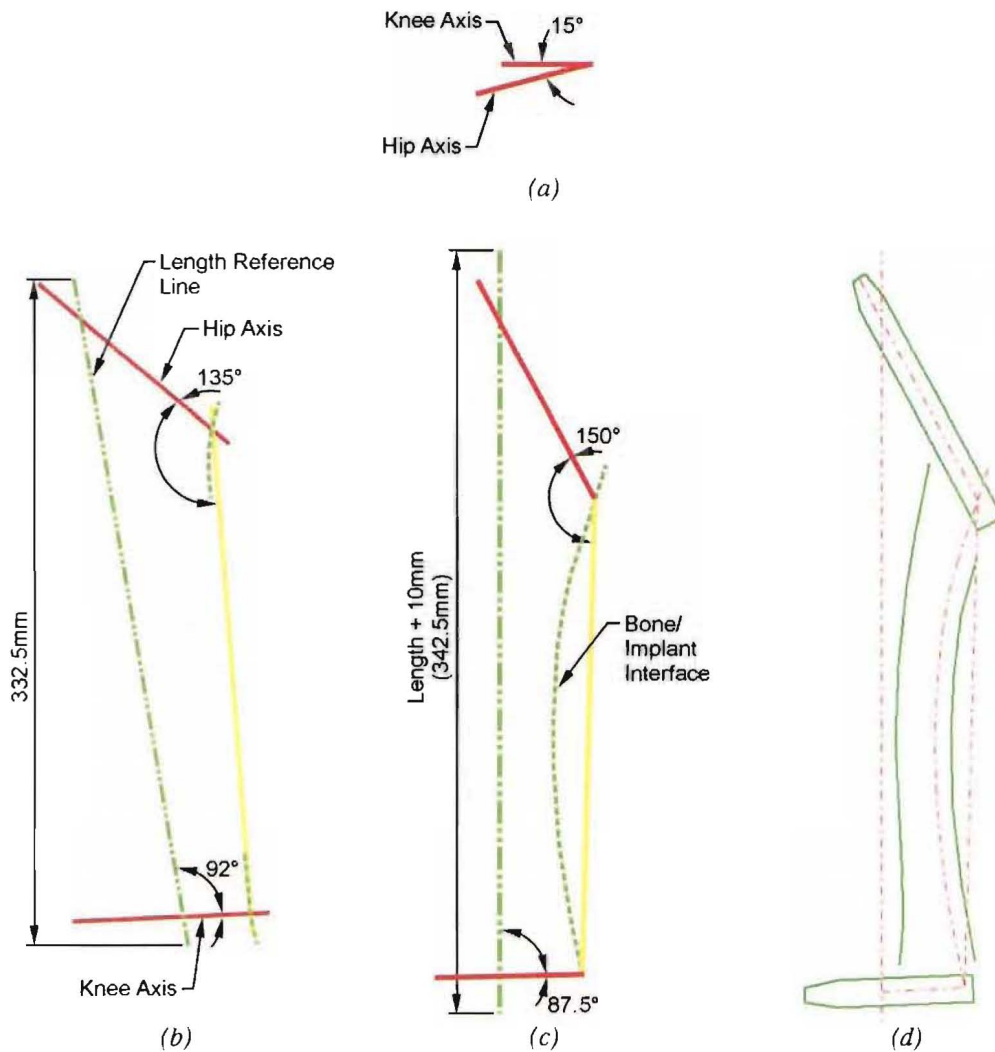


Figure 10.8 Endoprosthesis geometry.

(a) Key axes as measured from X-rays.

(b) Corrected geometry.

(c) Anterior rotation of the hip axis.

(d) Endoprosthesis geometry and boundaries.

Once the key geometry had been defined, guide curves were created to define the screw and tee cross-section boundaries, as shown in Figure 10.8(d).

10.6 Final Solution

The final endoprosthesis design consisted of 6 unique parts as illustrated in Figure 10.9.

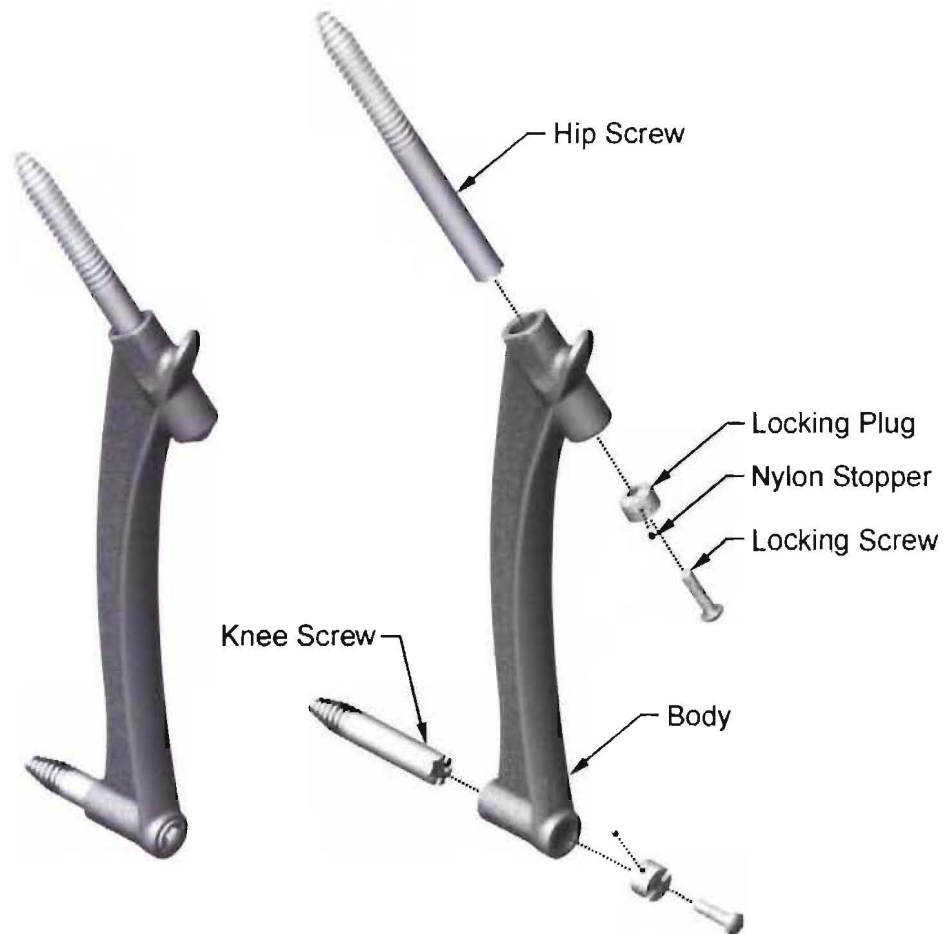


Figure 10.9 Assembled & exploded views of the femoral endoprosthesis.

Details of each component and the assembly order of the endoprosthesis follow.

10.6.1 Endoprosthesis Body

The body component forms the bulk of the endoprosthesis and is used to locate the hip and knee screws. It has a tee cross-section and is manufactured from Ti-6Al-4V. The overall dimensions of the body are 254.5 x 57.25 x 31.5 mm ($h \times w \times d$).

The hip and knee bosses have an outside diameter of 17.5 mm. To reduce the volume of bone that must be removed from the femoral head, two flats were machined into the anterior and posterior faces of the hip boss. These cuts are 14 mm long and reduce the width of the hip boss to 16 mm.

Surfaces which may be in contact with any remaining femoral bone stock were carborundum blasted to aid bone ingrowth and adhesion. The outer surfaces of the endoprosthesis which are placed in tension when the implant is loaded were polished. Figure 10.10 shows a rendering of the endoprosthesis body.



Figure 10.10 Endoprosthesis body.

10.6.2 Hip and Knee Screws

The hip and knee screws shown in Figure 10.11 are 12.5 mm in diameter and are 130 mm and 70 mm long respectively. Both screws have a 3 mm pitch buttress thread for screwing into the femoral bone stock.

The ends of both screws have 6 castellations and a $\frac{1}{4}$ " UNF x 12.5 mm long thread. The primary purpose of the castellations is to engage with the locking plugs and prevent the screws from rotating *in-vivo*. The castellations also provide driving surfaces which can be used during the implantation procedure. The $\frac{1}{4}$ " UNF thread, in conjunction with the locking screws, tie the assembled endoprosthesis together and also keep the hip and knee screws engaged with the implantation tooling.

The hip and knee screws were produced from Ti-6Al-4V bar stock on an NC lathe and machining centre. The thread forms were then hand polished to remove any machining marks.



Figure 10.11 Hip and knee screws.

10.6.3 Locking Plugs and Nylon Stoppers

The locking plugs are screwed into the endoprosthesis body once the hip and knee screws have been fitted. Both locking plugs were identical and had a M14.5 x 1 threaded exterior and are 9.7 mm long. They were manufactured from Ti-6Al-4V. There is also a $\text{Ø}2.5 \times 3$ mm deep hole in the side of the locking plugs for a nylon stopper. This nylon stopper deforms as the locking plug is screwed into the endoprosthesis body. Once sufficient deformation of the nylon stopper occurs, the locking plug thread binds preventing them from unscrewing *in-vivo*.

One end of the locking plugs has male castellations which engage with the hip and knee screws. As previously described these castellations help prevent the hip and knee screws from rotating relatively to the locking plugs and endoprosthesis body *in-vivo*.

The other end of the locking plug has a slot which is used to drive the locking plug into position.

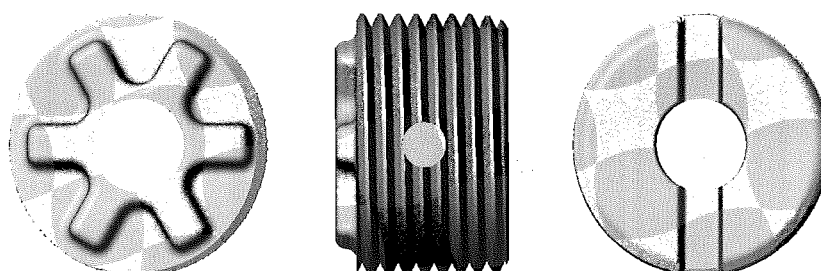


Figure 10.12 Locking plug.

10.6.4 Locking Screws

The locking screws were $\frac{1}{4}$ " UNF x 20 mm long. They were manufactured from commercially available Ti-6Al-4V bolts. The bolt head was reduced in thickness and all corners were rounded to create a smooth profile.

Detailed engineering drawings of each part can be found in Appendix 11.

10.6.5 Assembly Sequence

The assembly order of the femoral endoprosthesis was flexible allowing the surgeon to assemble the components in different sequences. The hip and knee screws can be inserted through the endoprosthesis body. This allowed the surgeon to position the endoprosthesis body and then use the screw holes in the endoprosthesis body as guides when drilling and inserting the hip and knee screws. Alternatively the surgeon could fit one of the screws, followed by the endoprosthesis body and the other screw.

Once the endoprosthesis body and screws are in place, locking plugs can be screwed into the body. These locking plugs were fitted with nylon stoppers to prevent them unscrewing *in-vivo*. Once the locking plugs are in place and their castellations are engaged with the hip or knee screw castellations, locking screws can be used to tie the whole assembly together.

10.7 Analysis

The endoprosthesis design was analysed using first principles and CosmosWorks. CosmosWorks is a Finite Element Analysis (FEA) package which runs embedded within the SolidWorks modelling environment. One of the key advantages of CosmosWorks is that any changes made to the CAD model are automatically made to the FEA model as well. This allowed different endoprosthesis designs and cross sections to be quickly evaluated.

To simplify the FEA analysis and reduce the computation time the hip and knee screws were simplified. The castellations, $\frac{1}{4}$ " UNF holes and thread at the ends of the screws were all removed, as shown in Figure 10.13. The locking plugs, nylon stoppers and locking bolts were also removed from the FEA study and were replicated with boundary conditions.



Figure 10.13 Knee screw simplified for FEA purposes.

Contact elements were used between the endoprosthesis body and the modified screws. Loads of 2000 N and 2500 N were then applied to the assembly. 2000 N was the specified design load, however an overload case of 2500 N was also considered.

Figure 10.14 shows deflection and stress plots for the endoprosthesis during the application of a 2500 N load. The resultant deflection of the endoprosthesis assembly was 2.3 mm and the Von-Mises stress was found to be approximately 510 MPa. The yield strength of Ti-6Al-4V is 870 MPa. These results were considered to be acceptable. The hip and knee screw were the most highly stressed components. The diameter of the screws could be increased to reduce the magnitude of the deflections, however this was considered to be unnecessary and undesirable, as it would also require additional bone to be removed from the hip and knee joints.

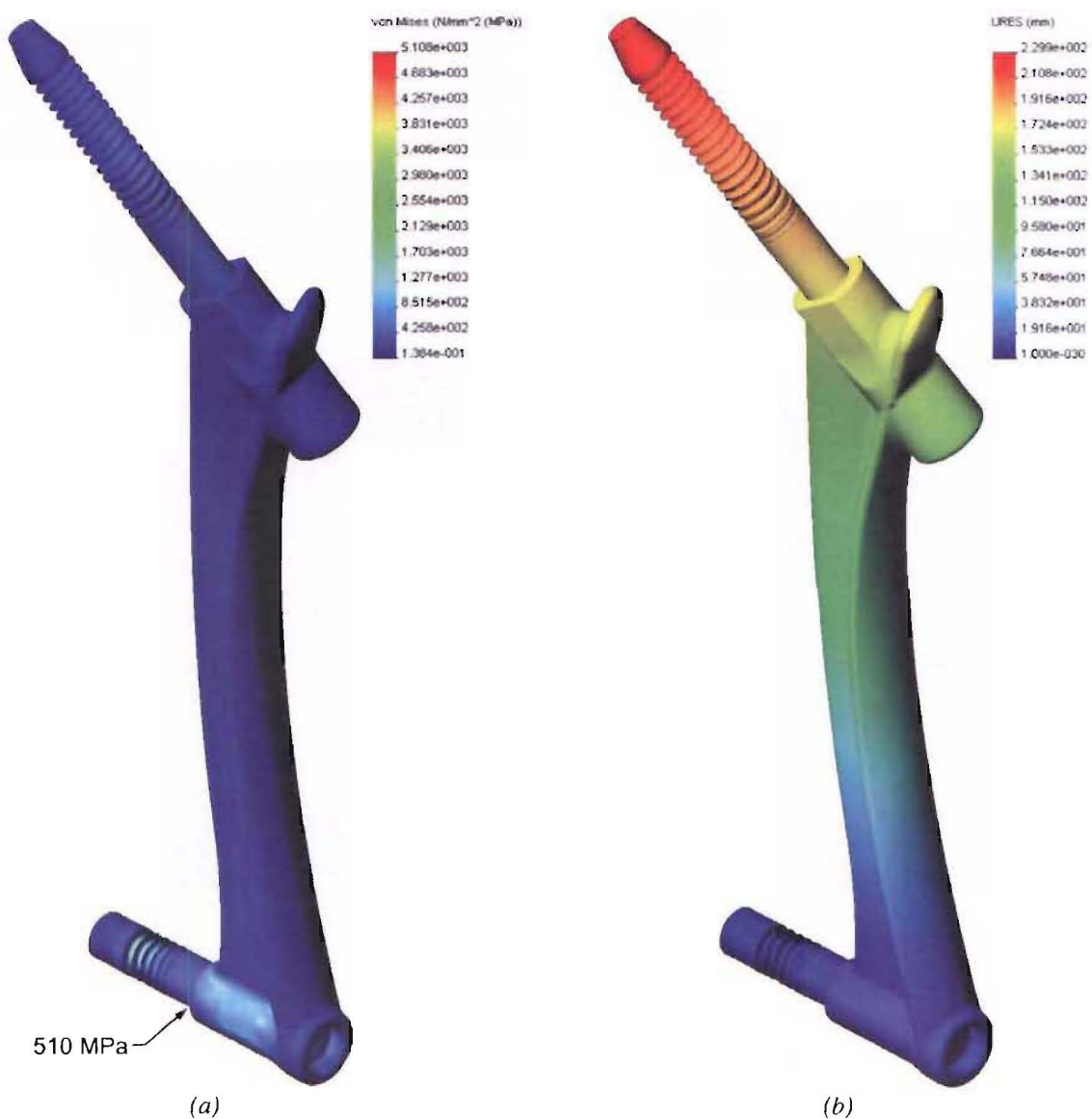


Figure 10.14 FEA deflection and stress plots.

(a) Stress plot showing a maximum Von-Mises stress of 510 MPa with an applied load of 2500 N.

(b) Deflection plot showing a peak deflection of 2.3 mm during the application of a 2500 N load.

Due to the tight timeframe of this project, once design of the endoprosthesis was finalised and all the components were manufactured there was insufficient time for mechanical testing. As part of the design and verification process a second endoprosthesis was to have been manufactured for testing purposes. However due to budgetary and resource limitations this was not completed until 12 months after the implantation of the first device, after which time the second device was used primarily for marketing purposes.

10.8 Instrumentation

Instrumentation was manufactured to aid in the implantation of the endoprosthesis. Figure 10.15 shows an introducer which was used during the insertion of the hip and knee screws. This instrument had a castellated end which engaged with the hip and knee screw castellations. The instrument also featured a $\frac{1}{4}$ " UNF threaded rod which was used to ensure that the hip and knee screws remained firmly engaged with the introducer castellations during the implantation procedure.

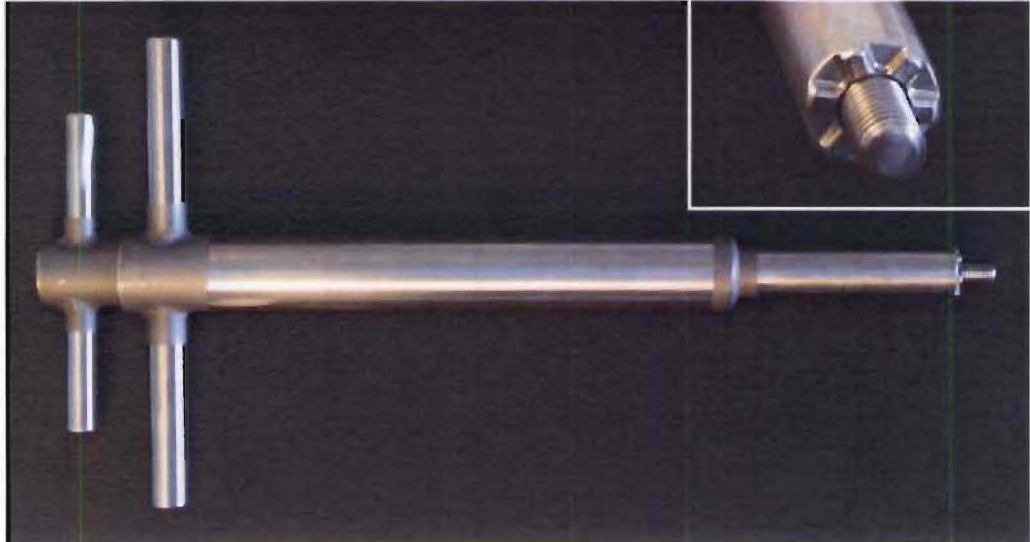
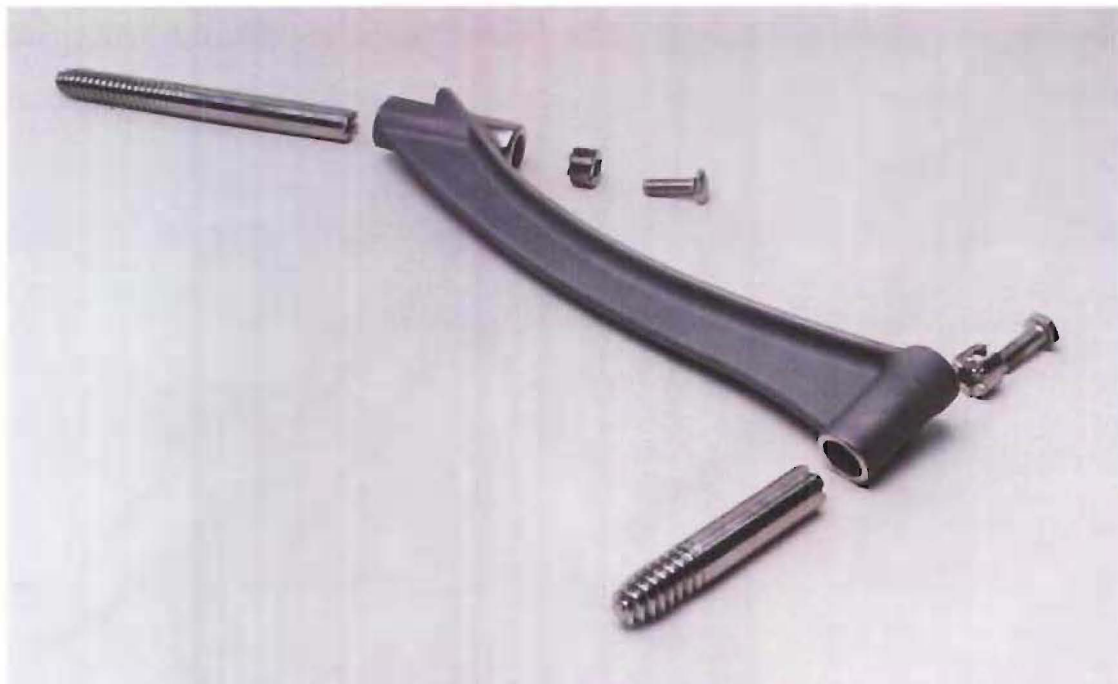


Figure 10.15 Hip and knee screw introducer.

Figure 10.16 shows the finished endoprosthesis in an assembled and disassembled state.



(a)



(b)

Figure 10.16 Femur endoprosthesis photos.

(a) Assembled femoral endoprosthesis.

(b) Femoral endoprosthesis components (the nylon stoppers are not shown).

10.9 Surgical Outcome

In November 1999 the patient underwent surgery to implant the femoral endoprosthesis. The most difficult part of the procedure was the removal of the existing implants as the bone stock was firmly adhered to the broken screws and tri-fin nail.

A slot was cut in the remaining femoral bone stock to accommodate the web of the endoprosthesis body. This was a laborious process as the outer cortical bone was hard and the burrs used proved to be inefficient. However, insertion of the endoprosthesis body was a simple matter once the slot had been produced.

During the insertion of the hip screw there was concern that if the screw was advanced to the full depth the femoral head may fracture, as shown in Figure 10.17(a). As a result the decision was made to leave the hip screw only partial inserted and not fit the locking plug for the hip screw. This was an acceptable solution, as if the hip screw slides axially as shown by the red arrow in Figure 10.17(b) the load is carried by the remaining bone stock and the body of the endoprosthesis, as illustrated by the green arrows.

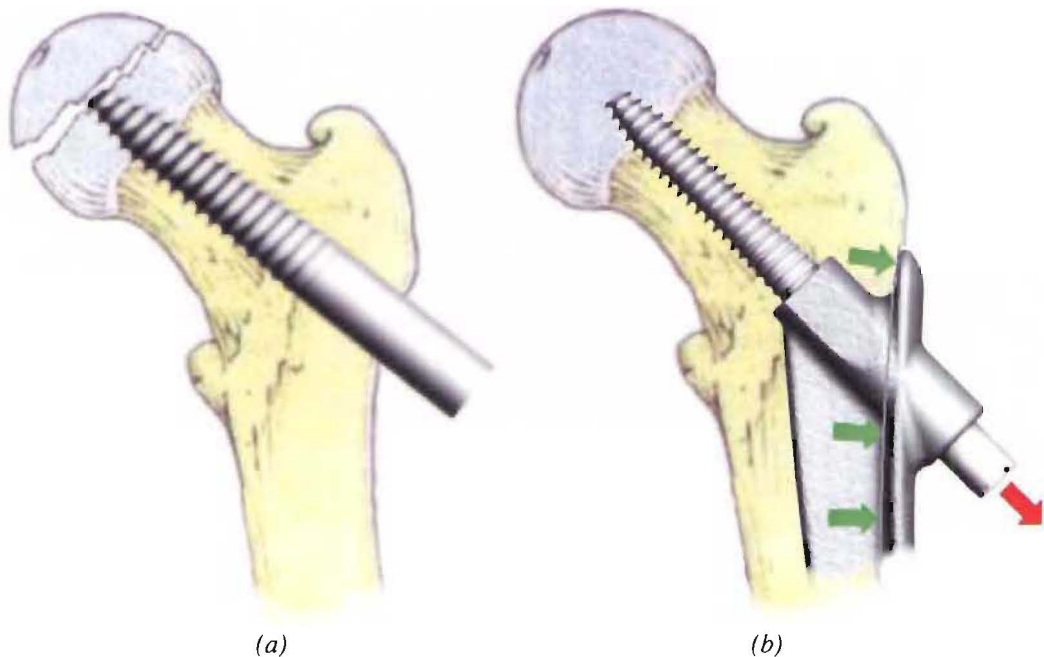


Figure 10.17 Hip screw length issue and in-theatre solution.

(a) Inserting the hip screw to full depth may have resulted in the femoral head fracturing.

(b) As a result the locking plug was left out and the endoprosthesis body carries the load (green arrows).

Note: The length of exposed screw is exaggerated for illustration purposes.

The knee screw was inserted without any complications and the wound was closed in a standard fashion. The patient reported the next day that his leg felt as if was “solid” again. Within two weeks of the surgery the patient was fully weight bearing through the implant. The patient has had no evidence of infection and continues to improve.

10.10 Potential Improvements

Several areas that could be improved were identified during the post implantation review of the femoral endoprosthesis.

10.10.1 Hip and Knee Screw Length

During the design of the hip and knee screws the overall length was determined from the x-ray shown in Figure 10.7(b). Care was taken to ensure the length of the screws was correct. However, due to complications during the implantation procedure the hip screw was found to be too long, as discussed in Section 10.9. This complication could be overcome in future by supplying the surgeon with several screws of varying lengths.

10.10.2 Hip and Knee Screw Castellations

The hip and knee screws and the locking plugs had castellations on their mating surfaces to prevent them from rotating *in-vivo*. The original design, shown in Figure 10.18(a), only allowed the screw castellations to engage in six orientations. This resulted in the surgeon having to either loosen or over-tighten the screws and/or locking plugs in order to engage the castellations. A more desirable solution would be to use a larger number of small castellations, as shown in Figure 10.18(b).

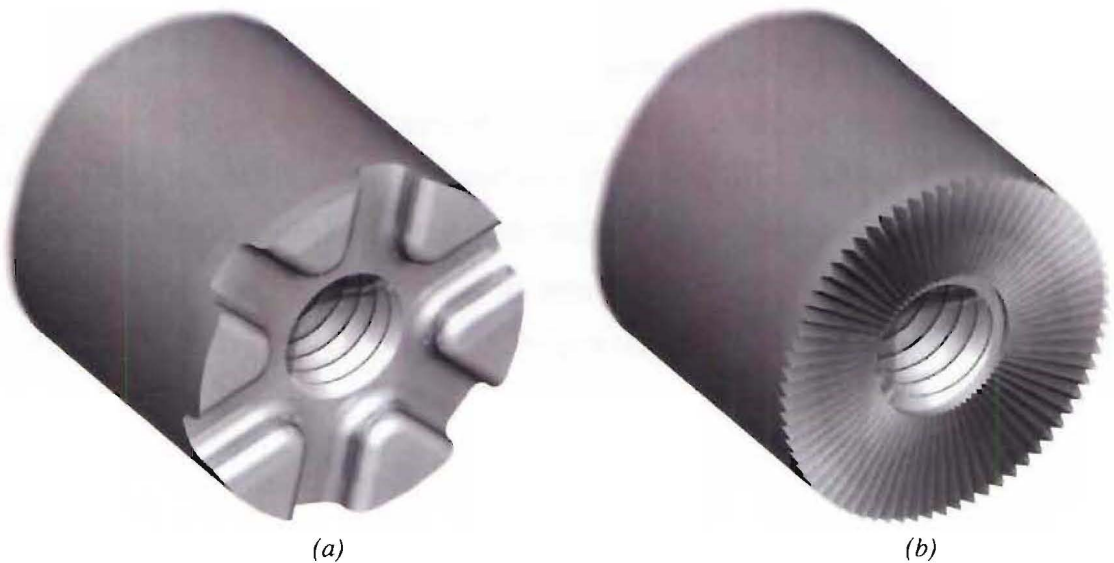


Figure 10.18 Hip and knee screw castellation design.

(a) Original six castellation design.

(b) Improved fine castellation design.

10.10.3 Locking Screw Profile

Locking screws were used to retain the hip and knee screws. The original endoprosthesis design called for button head cap screws to be used, as shown in Figure 10.19(a). However, contrary to information originally provided by the supplier involved, it was not possible to source these screws in the required alloy, so machined down standard bolts were used instead. These bolts had a head profile as shown in Figure 10.19(b). In hindsight neither of these screw head designs are desirable due to their raised profiles. A potential improvement would be to recess the screw heads into the locking plugs as shown in Figure 10.19(c).

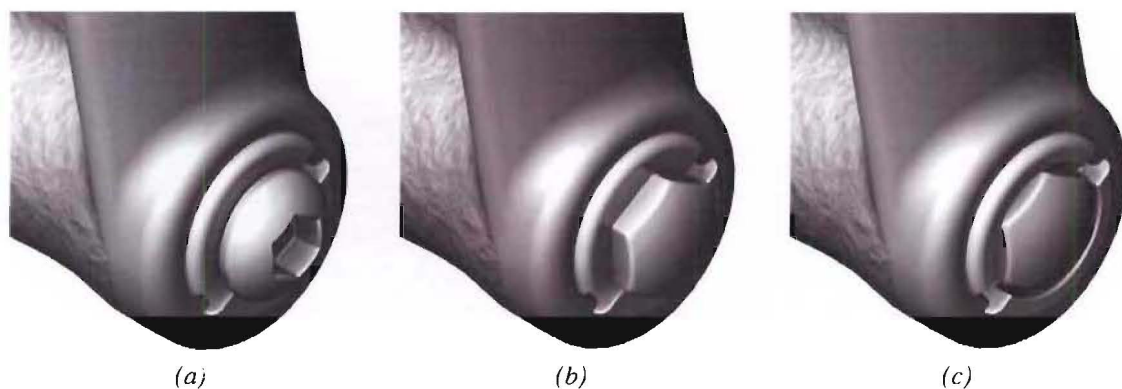


Figure 10.19 Locking screw profiles.

(a) Design locking screw.

(b) Supplied locking screw.

(c) Revised locking screw profile.

10.10.4 Miscellaneous Improvements

Two other potential improvements were highlighted during the review of the femoral endoprosthesis, these include:

- The hip and knee screw should be reduced in diameter if possible.
- When the stock material was ordered the grain direction was not specified. As a result the material was supplied and machined with the endoprosthesis body running across the grain instead of with the grain. Ideally the grain direction should be along the endoprosthesis long axis as shown in Figure 10.20 to optimise the strength and deflection properties of the endoprosthesis.



Figure 10.20 Endoprosthesis body, supplied and preferable grain directions.

10.11 Summary and Conclusion

A femoral endoprosthesis was required for a patient who suffers from Osteogenesis Imperfecta. The implants previously fitted to the patient's femur had failed catastrophically. These failures were almost certainly due to the implants not being designed to support all the loads applied to the femur.

An endoprosthesis was therefore required which was able to support all the applied loads whilst still allowing the patient's healthy hip and knee joints to be retained. Accordingly, an endoprosthesis with a tee cross section was designed. Connections to the patient's hip and knee joints were made with custom bone screws. Locking mechanisms were included in the endoprosthesis to minimising the potential of wear debris being generated at the screw/body interfaces. The endoprosthesis was also designed to allow the surgeon to assemble the components in any order.

During the surgical procedure to implant the endoprosthesis it was found that the hip screw was too long. This was due to the surgeon being unable to insert this screw to its full depth without potentially damaging the femoral head. As a result this screw was only partially inserted. A post-implantation review of the endoprosthesis found that this would not reduce its performance; however a solution was developed to overcome this issue in any future cases.

The patient continues to make a good recovery and is able to walk short distances without any walking aids. However, for the majority of daily activities the patient continues to use crutches. The primary reason is to prevent further deterioration of the patient's other ailments such as the tibia stress fractures. After recovering from the femoral endoprosthesis surgery, the patient has requested additional surgery to rectify his other lower limb problems.

In summary, the novel femoral endoprosthesis designed during this project has been successful and allowed the patient to remain mobile. The experience of designing and manufacturing this device also helped the author to develop strong working relationships with the surgeon and other biomedical engineers involved with this case.

10.12 References

1. Kotz R, Ritschl P, Trachtenbrodt J, *A Modular Femur-Tibia Reconstruction System*. Orthopedics, 1986. Vol 9 (12): pp 1639-52.
2. Malawer M M, *Distal Femoral Resection with Endoprosthetic Reconstruction*, in Malawer Martin M and Sugarbaker Paul H (Eds). *Musculoskeletal Cancer Surgery: Treatment of Sarcomas and Allied Diseases*, 2001, Kluwer Academic Publishers. pp 459-84.
3. Marcove R C, Lewis M M, Rosen G, Huvos A G, *Total Femur and Total Knee Replacement*. Clinical Orthopaedics and Related Research, 1976. (126): pp 147-52.
4. Mittermayer F, Krepler P, Dominkus M, Schwameis E, Sluga M, Heinzl H, Kotz R, *Long-term Follow-up of Uncemented Tumor Endoprostheses for the Lower Extremity*. Clinical orthopaedics and related research, 2001. (388): pp 167-77.
5. Nerubay J, Katznelson A, Tichler T, Rubinstein Z, Morag B, Bubis J J, *Total Femoral Replacement*. Clinical Orthopaedics and Related Research, 1988. Vol 229: pp 143-8.
6. Steinbrink K, Engelbrecht E, Fenelon G, *The Total Femoral Prosthesis*. J Bone Joint Surg, 1982. Vol 64B (3): pp 305-312.

Part C

Appendices

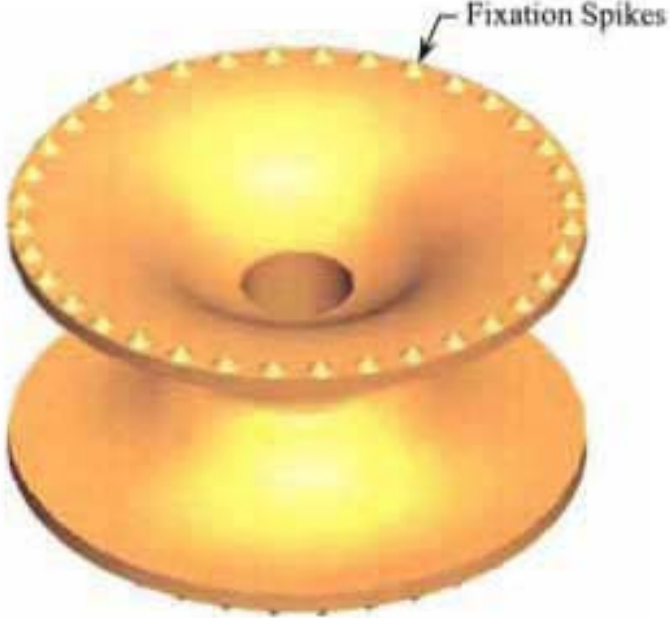
<Blank Page>

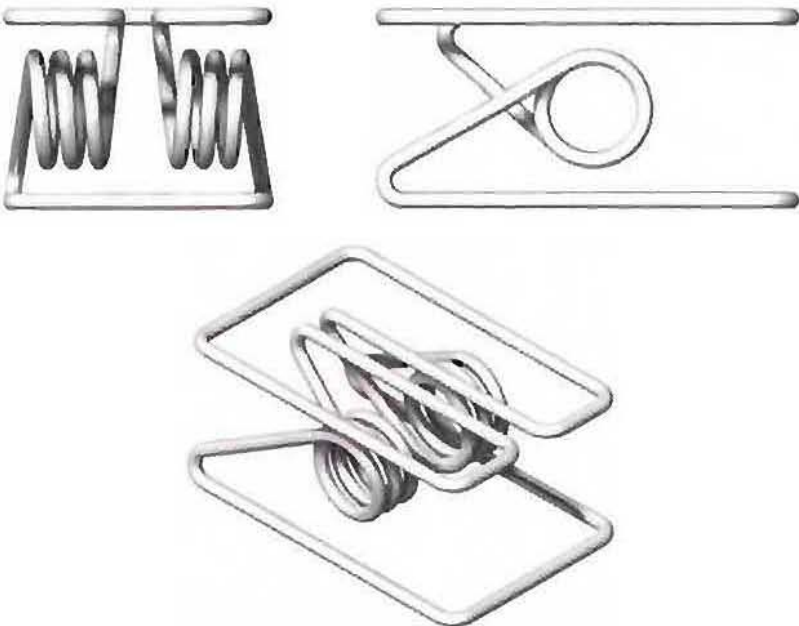
Appendix 1 – Conceptual Designs


A number of conceptual designs for the intervertebral disc implant were generated, including the following:

- Belleville Washer
- Torsion Spring
- Side Mounted Torsion Spring
- Z-Spring
- Z-Spring Variant
- C-Spring
- Side C-Spring
- Toroidal C-Spring
- Fluid Filled Bellows
- Urethane Spiral
- Urethane Block
- Urethane Annulus
- Urethane Balls

A brief description and analysis of each concept is provided in this appendix.

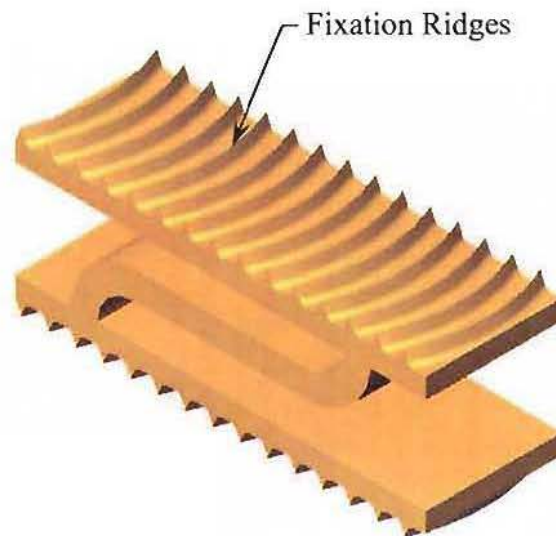
| | | |
|--|--------------------------|-----------------|
| Project: Spine | Belleville Washer | 01 of 13 |
| Date: 25/12/03 | | |
|  | | |
| <p>Summary:</p> | | |
| <p>This metallic spring design is based on two Belleville Washers which are commonly used to provide apply preloads in bolted connections or machine tools.</p> | | |
| <p>Pros:</p> | | |
| <ul style="list-style-type: none"> - Simple design. - Capable of supporting large vertical loads. - No wear debris generated during deflections. - Will exert the majority of the forces on the periphery of the vertebral bodies. | | |
| <p>Cons:</p> | | |
| <ul style="list-style-type: none"> - The cross section required to support the compressive loads will result in a very stiff implant which is hard to deflect angularly. - Difficult to cater for the intervertebral disc wedge angle. - The large cross section of this implant would require a large section of the annulus fibrosus to be reflected. | | |

| | | |
|--|-----------------------|-----------------|
| Project: Spine | Torsion Spring | 02 of 13 |
| Date: 25/12/03 | | |
|  | | |
| <p>Summary:</p> | | |
| <p>This concept was based on a spring commonly found in clothes pegs and could be constructed from a single length of spring wire. A single spring of this design could be used or alternatively two narrower springs could be used side by side.</p> | | |
| <p>Pros:</p> | | |
| <ul style="list-style-type: none"> - Simple design. - Minimal wear debris will be generated during angular deflections. Some debris will be generated though if the torsion coils rub. - The angular stiffness can be varied by changing the wire diameter and spring geometry. - Able to absorb vertical shock loads. | | |
| <p>Cons:</p> | | |
| <ul style="list-style-type: none"> - Difficult to create a structure strong enough to support compressive loads. - May be affected by in-growth of tissue. | | |

| | | |
|--|------------------------------------|-----------------|
| Project: Spine | Side Mounted Torsion Spring | 03 of 13 |
| Date: 25/12/03 | | |
|  | | |
| Summary: | | |
| <p>This concept relies on the deflection of a torsion spring to provide the required motions. Multiple instances of such an implant would be required around the periphery of the intervertebral disc space.</p> | | |
| Pros: | | |
| <ul style="list-style-type: none">- Simple design.- No wear debris generated during angular deflections, unless the torsion coils rub during deflections. | | |
| Cons: | | |
| <ul style="list-style-type: none">- May project outside the intervertebral disc space.- Accurate positioning of the implants is required to ensure correct function of the implant assembly.- In order to support the compressive loads multiple springs may be required, however this will result in the angular stiffness of the implant assembly being too high.- Placing multiple instances of such an implant around the periphery intervertebral disc space would be a very invasive procedure. | | |

Project: Spine

Date: 25/12/03

Z-Spring**04 of 13****Summary:**

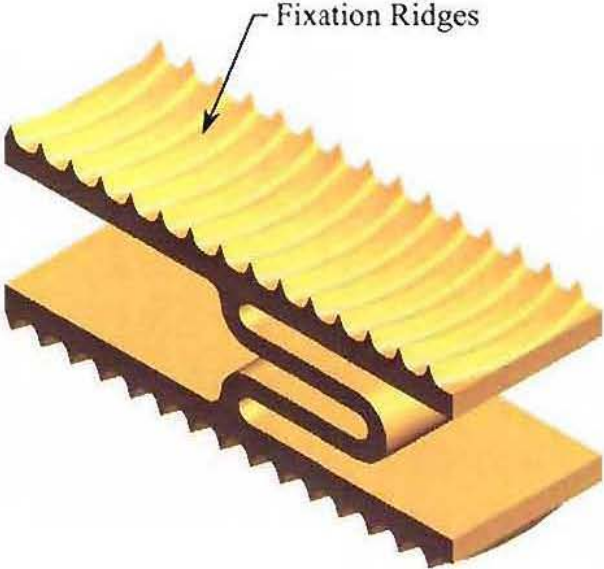
This concept relies on a thin beam (spring) bending to provide the required motions.

Pros:

- Simple design.
- No wear debris generated during deflections.
- Able to support compressive loads.
- Able to absorb shock loads.
- Small cross section which will allow minimal invasive surgical procedures to be used.

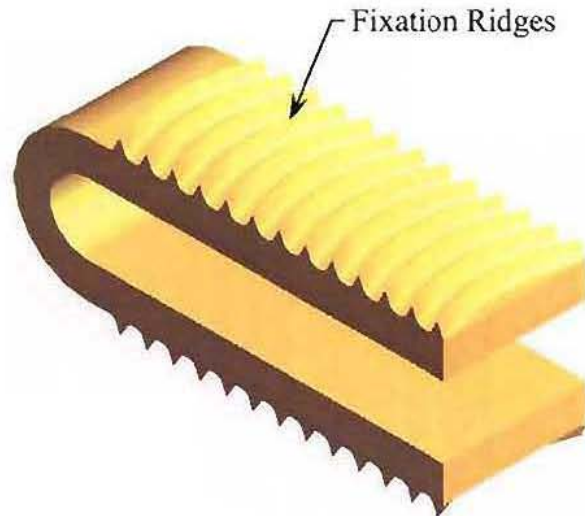
Cons:

- In order to be able to withstand the compressive loads the stiffness of the spring must be substantial, which in turn makes the angular stiffness too high.
- Lateral deflections would require twisting of the spring and hence it would be very stiff when deflected in this direction. Alternatively, two of these devices could be used. In such a case lateral deflections would require the z-spring to be compressed, however in order to support the compressive loads the spring would have to be very stiff. Therefore supporting compressive loads and allowing lateral deflections are mutually exclusive.

| | | |
|---|-------------------------|-----------------|
| Project: Spine | Z-Spring Variant | 05 of 13 |
| Date: 25/12/03 | | |
|  <p>A 3D perspective rendering of a Z-spring variant. The spring is shown in a compressed state, with its zig-zag profile clearly visible. It is mounted on a rectangular base. The top surface of the spring features a series of small, raised ridges, which are labeled with an arrow and the text 'Fixation Ridges'. The spring is colored in a gradient from yellow to orange.</p> | | |
| <p>Summary:</p> | | |
| <p>This concept is a variation of the Z-Spring concept which features twice as many spring elements.</p> | | |
| <p>Pros:</p> | | |
| <ul style="list-style-type: none"> - Simple design. - No wear debris generated during deflections. - Able to support compressive loads and shock loads. - Small cross section which will allow minimal invasive surgical procedures to be used. | | |
| <p>Cons:</p> | | |
| <ul style="list-style-type: none"> - In order to be able to withstand compressive loads the stiffness of the spring must be substantial, which in turn makes the angular stiffness too great. - This concept does not improve on the lateral stiffness performance offered by the previous z-spring concept. | | |

Project: Spine

Date: 25/12/03

C-Spring**06 of 13****Summary:**

This concept is similar in design to a tuning fork. When compressive loads are applied to the tips of the spring they close, allowing angular deflection of the vertebral bodies to occur.

Pros:

- Simple design.
- No wear debris generated during deflections.
- Angular stiffness can be changed by altering the spring geometry.
- Able to support compressive loads.
- Small cross section which will allow minimal invasive surgical procedures to be used.

Cons:

- Only able to be deflected angularly in one direction. Therefore if the spine is flexed in the opposite direction the vertebral bodies will separate from the implant endplates.
- Not able to absorb vertical shock loads.
- In order to be able to withstand compressive loads the stiffness of the spring must be substantial, which in turn makes angular stiffness too high.

| | | |
|-----------------------|----------------------|-----------------|
| Project: Spine | Side C-Spring | 07 of 13 |
| Date: 25/12/03 | | |

Summary:

This concept is similar to the C-Spring design however in this case angular deflections of the vertebral bodies causes both bending and twisting in the C-Spring to occur. Two of these devices could be used on either side of the intervertebral disc space to create a stable assembly.

Pros:

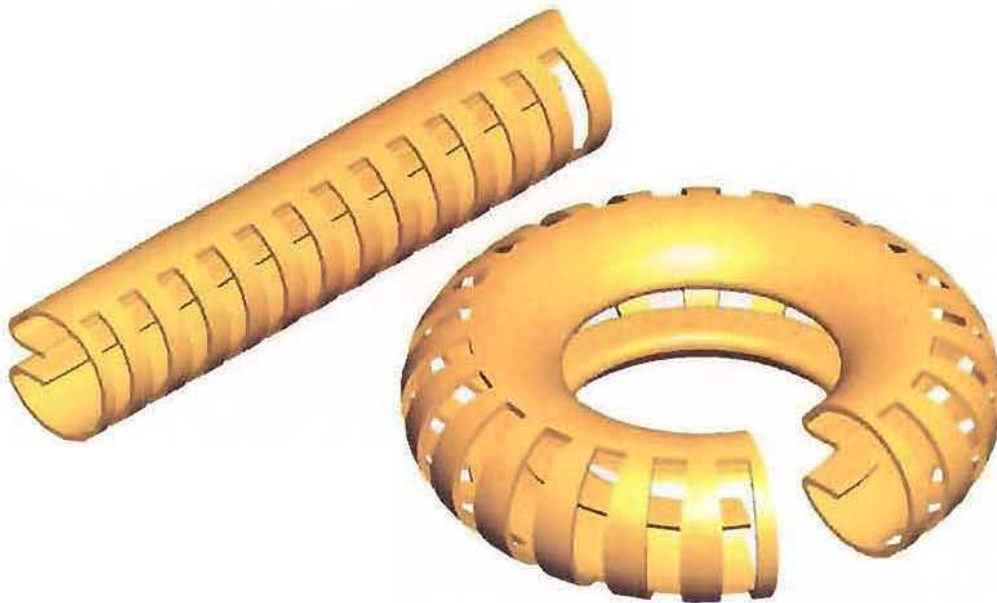
- Simple design.
- No wear debris generated during deflections.
- Able to support compressive loads.

Cons:

- In order to be able to withstand compressive loads the stiffness of the c-spring must be substantial, which in turn results in the angular stiffness being too high.
- Lateral deflections would require the spring component to be compressed, however in order to support the compressive loads the spring would have to be very stiff. Therefore supporting the compressive loads and allowing lateral deflections are mutually exclusive.
- May project outside the intervertebral disc space.

Project: Spine

Date: 25/12/03

Toroidal C-Spring**08 of 13****Summary:**

This concept is also similar to the C-Spring, however in this case a number of small C-Springs are placed around the periphery of the disc space. This design could be manufactured in a linear form and then deformed into a toroidal form as it was inserted, thus only requiring a small incision in the annulus fibrosus.

Pros:

- No wear debris generated during deflections.
- Large contact area which would allow forces to be applied to the periphery of the vertebral bodies.
- The angular stiffness can be alter by changed the spring geometry.
- Able to support compressive loads.
- Can be inserted through a small surgical window.

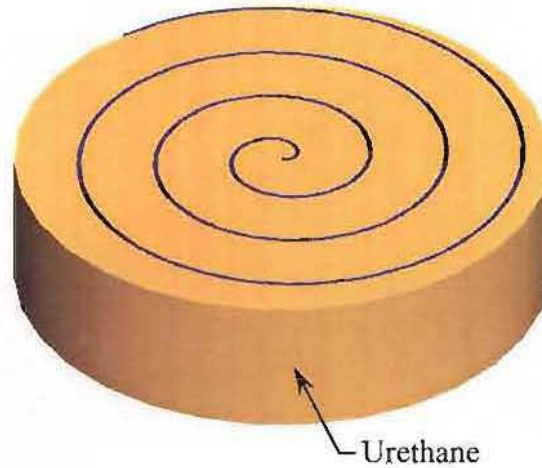
Cons:

- A stiff design is required to support compressive loads which would require significant effort to deflect angularly.
- Difficult to cater for intervertebral wedge angle.

| | | |
|--|-----------------------------|-----------------|
| Project: Spine | Fluid Filled Bellows | 09 of 13 |
| Date: 25/12/03 | | |
| <div data-bbox="491 380 1114 766" data-label="Image"></div> <p data-bbox="249 775 397 812">Summary:</p> <p data-bbox="249 829 1362 1087">This concept consists of a thin walled, fluid filled vessel with convoluted walls. As the fluid fill supports the compressive loads, the wall thickness of the vessel can be reduced and thus the angular stiffness of the implant could also be reduced. This design is quite similar to a natural intervertebral disc which consists of a flexible pressure vessel and fluid core.</p> <p data-bbox="249 1161 323 1199">Pros:</p> <ul data-bbox="268 1216 1362 1474" style="list-style-type: none">- No wear debris generated during deflections.- Large contact area which would allow forces to be applied to the periphery of the vertebral bodies.- Angular stiffness can be varied.- Able to support compressive loads. <p data-bbox="249 1548 332 1585">Cons:</p> <ul data-bbox="268 1603 1362 1742" style="list-style-type: none">- Complex construction.- The large cross section of this implant would require a large section of the annulus fibrosus to be reflected. | | |

Project: Spine

Date: 25/12/03

Urethane Spiral**10 of 13****Summary:**

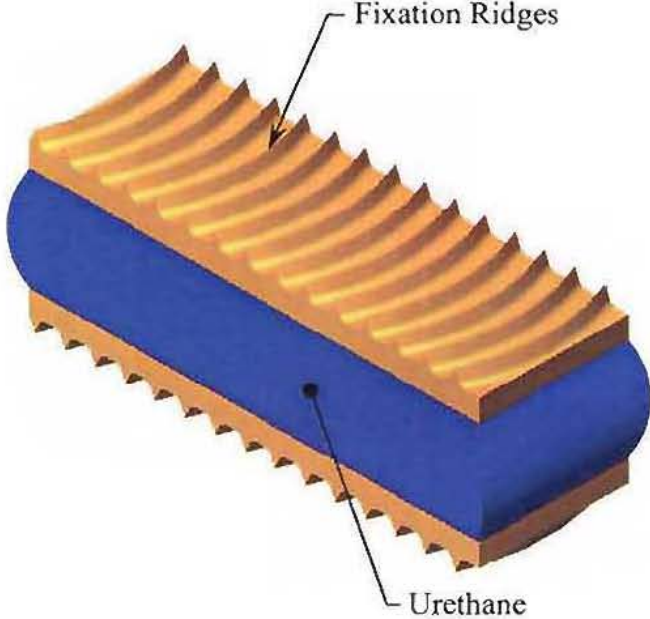
This concept utilises a soft urethane rubber (or similar material) which can compress and deform to supply the required motions. This is similar to the function of the Acroflex Disc. This design could be inserted in a similar way to the toroidal c-spring. By straightening the spiral it could be feed into the intervertebral disc space through a small incision in the annulus fibrosus, once in the intervertebral disc cavity it would recoil into a spiral.

Pros:

- Large contact area which would allow forces to be applied to the periphery of the vertebral bodies.
- Able to absorb vertical shock loads.
- Easy to manufacture.
- Can be inserted though a small incision in the annulus fibrosus.
- The directional stiffness could be varied with the addition of holes or voids.

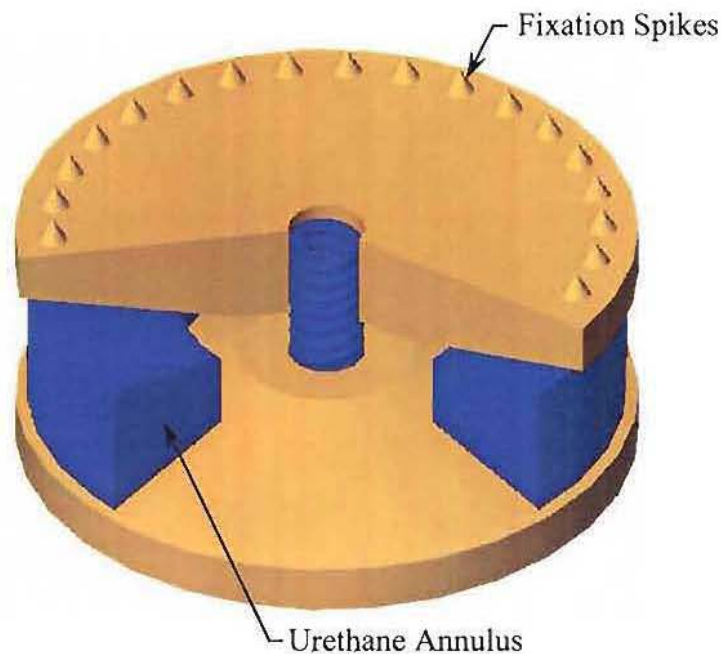
Cons:

- Wear debris may generated if parts of the spiral rub against each other.
- May cold flow when subjected to sustained vertical loads.
- Reliant on the material properties to provide required deflections.
- Previously patented in 1975 (US Patent 3867728).

| | | |
|--|-----------------------|-----------------|
| Project: Spine | Urethane Block | 11 of 13 |
| Date: 25/12/03 | | |
|  | | |
| <p>Summary:</p> | | |
| <p>This urethane block is similar to the Acroflex Disc. It utilises a soft deformable urethane rubber (or similar material) which can compress and stretch to provide the required motions. Two of these devices could be inserted though a small incision in the annulus fibrosus to provide the required level of support.</p> | | |
| <p>Pros:</p> | | |
| <ul style="list-style-type: none"> - Large contact areas. - Able to absorb vertical shock loads. - Can be inserted though a small incision in the annulus fibrosus. - Directional stiffness could be varied by adding voids to the flexible material. | | |
| <p>Cons:</p> | | |
| <ul style="list-style-type: none"> - May cold flow when subjected to sustained vertical loads. - Reliant on the material properties to provide required deflections. - Similar to Acroflex Disc and hence may suffer from the same cold flow and endplate delamination problems. | | |

Project: Spine

Date: 25/12/03

Urethane Annulus**12 of 13****Summary:**

This urethane annulus is a variation of the urethane spiral concept. It utilizes a soft deformable urethane rubber (or similar material) which compresses and stretches radially to provide the required motions. A flexible spring in the centre of the device would be required to help keep the endplate components located centrally to each other. Note: this device shown above is partially sectioned for clarity.

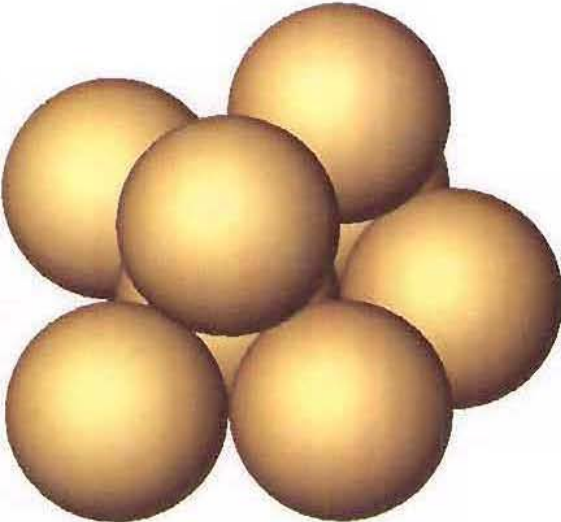
Pros:

- Able to absorb vertical shock loads.
- Directional stiffness could be varied by changing thickness of the urethane annulus in certain areas or by adding voids.

Cons:

- May cold flow when subjected to sustained vertical loads.
- Reliant on the material properties to provide required deflections.
- Wear debris will be generated as the urethane moves relative to the endplates.
- The large cross section of this implant would require a large section of the annulus fibrosus to be reflected.

| | | |
|-----------------------|-----------------------|-----------------|
| Project: Spine | Urethane Balls | 13 of 13 |
| Date: 25/12/03 | | |



Summary:

This concept involves a number of soft urethane balls being placed through a hole in the annulus fibrosus to fill the space normally occupied by the nucleus pulposus. The annulus fibrosus could then be repaired to prevent the balls from being ejected. The required motions would be provided by the urethane balls being compressed and displaced within the intervertebral disc space.

Pros:

- Can be inserted though a very small incision in the annulus fibrosus.
- Able to absorb vertical shock loads.
- Easy to manufacture.

Cons:

- Difficult to control the stiffness of the device *in-vivo*.
- Reliant on correct number of balls being inserted into the intervertebral disc space.
- May cold flow when subjected to sustained vertical loads.
- Reliant on the material properties to provide required deflections.
- The annulus fibrosus must be repaired and remain healthy to retain the balls.
- Wear debris will be generated as balls move relative to each other.

Appendix 2 – Titanium

As detailed in Chapter 5, during the refinement of the metallic spring concepts it was established that the material properties would play an important role. One of the material groups investigated was Titanium and its alloys. This appendix details the physical properties of Ti-6Al-4V and Commercially Pure Titanium Alloys, both of which are commonly used for *in-vivo* applications.

A2.1 Background

Titanium alloys range from high ductility commercially pure alloys which can be used where formability is essential, to heat treatable high strength alloys with high strength to weight ratios. Titanium alloys can be worked using conventional machining processes, fabrication, forging and casting allowing complex forms to be manufactured in large and small volumes.

When selecting materials for *in-vivo* use bio-compatibility is a critical consideration however strength, elastic modulus, density and the capacity for osteo-integration with bone and other tissues must also be considered. There are several titanium alloys which meet these requirements. Pure titanium is inert and immune to corrosion by body fluids and is therefore considered wholly biocompatible. Titanium alloys also have a high strength and a low modulus compared to steel which helps to prevent bone resorption from occurring. With appropriate surface treatment bone and tissues will also firmly adhere to titanium implants.

Titanium and its alloys have been used in a wide range of medical applications, as detailed below.

The most common medical applications of titanium have been the production of bone screws, partial and total hip joints, knee joints and instrumentation. Titanium alloys are also used for dental implants where titanium 'root' implants are implanted into the mandible and maxilla.

Soft commercial pure titanium alloys are used extensively for maxillofacial fixation plates. These plates are used to restore facial features which have been affected by trauma, disease or deformity. The high malleability of these alloys allows surgeons to easily deform the plates in theatre to suit the patient's facial structure.

A wide range of surgical instruments are also made from titanium. These instruments are often anodised to create non-reflective surfaces which minimise glare from surgical lights. Titanium instruments also can withstand repeated sterilisation without compromising edge and surface qualities, corrosion resistance or strength.

A2.2 Available Alloys

There are many commercially available titanium alloys which are suitable for medical implant purposes. The most commonly used alloys are Ti-6Al-4V and the Commercial Pure (CP) Grades.

A number of other Titanium alloys have also been developed for medical implant purposes including Ti-6Al-7Nb, Ti-5Al-2.5Fe, Ti-13Nb-13Zr and Ti-12Mo-6Zr-2Fe however these alloys are not as common. Data regarding the properties of these alloys is also less common and due to difficulties finding vendors for these materials they were not included in the material selection process for the intervertebral disc implant. This decision fulfils the specification requirement that conventional biocompatible materials be used to limit testing and development costs.

A2.3 Ti-6Al-4V

Ti-6Al-4V is the most widely used titanium alloy and it accounts for more than 50% of all the titanium used worldwide. Approximately 80% of the Ti-6Al-4V produced is used in the aerospace industry, with the medical industry accounting for approximately 3% of the total produced. The remainder of the Ti-6Al-4V produced is used in the automotive, marine and chemical industries⁶.

A number of different methods and formulations are used to produce Ti-6Al-4V. Depending on the production method and formulation the oxygen content may vary from 0.08 to 0.2% (by weight), the aluminium content may be as high as 6.75% and vanadium content may vary up to 4.5%. In general the higher the percentage of alloying elements added, particularly oxygen, the greater the strength of the material. Conversely lower oxygen, nitrogen and aluminium content improves ductility, fracture toughness and stress corrosion resistance⁶.

Ti-6Al-4V is also available as a Ti-6Al-4V ELI grade. This is a grade with 'extra low interstitial' oxygen and iron which exhibits improved damage tolerance properties.

A2.3.1 Mechanical Properties

The mechanical properties of Ti-6Al-4V at room temperature are detailed below in Table A2.1.

| Property | Value |
|---------------------------------|-----------|
| Density (g/cm ³) | 4.428 |
| Elastic Modulus Tensile (GPa) | 105-116 |
| Shear Modulus (GPa) | 41-45 |
| Poisson's Ratio | 0.26-0.36 |
| Ultimate Tensile Strength (MPa) | 925 |
| Tensile Yield Strength (MPa) | 870 |

Table A2.1 Ti-6Al-4V – Mechanical properties at room temperature.

[Source: Welsch et al⁶]

A2.3.2 Fatigue life

There are several factors which affect the fatigue performance of Ti-6Al-4V including surface effects and microstructure.

High cycle fatigue typically occurs as a result of micro-cracks forming and growing to become macro-cracks. These micro-cracks propagate until the fracture toughness of the material is exceeded and final fracture occurs. However, *as a rule of thumb, the fatigue life for small, highly stressed components (small critical flaw size) is mainly controlled by micro-crack initiation and growth, while for large components operating at low stress levels (large critical flaw size), macro-crack growth behaviour is more important*⁵. For the intervertebral disc implant the former is the case, as the implant will have a small cross section and is highly stressed, therefore its high cycle fatigue performance will be micro-crack controlled.

A2.3.2.1 Surface Effects on Fatigue Life

Mechanical surface treatments such as shot peening, polishing, or surface rolling can be used to improve the fatigue life of most metals. In most cases three surface properties are altered: surface roughness, degree of cold work (dislocation density) and residual stress. The influence of these surface effects on high cycle fatigue are shown in Table A2.2.

| Surface Effect | Crack Nucleation | Crack Propagation |
|-----------------------------|--------------------|-------------------|
| Surface roughness | Accelerates | No effect |
| Cold work | Retards | Accelerates |
| Residual compressive stress | Minor or no effect | Retards |

Table A2.2 Surface effects on high cycle fatigue.

[Source: Welsch et al⁶]

Surface roughness determines whether fatigue strength is primary crack nucleation controlled (smooth) or crack propagation controlled (rough). Fatigue cracks normally initiate at or near singularities on or near the surface of the specimen. These singularities may include but are not limited to scratches, pits or inclusions. Therefore, a good surface finish is a fundamental requirement for high endurance strength.

Residual compressive stress is also an important factor in fatigue performance and is most prominent in the infinite life stress range (10^7 cycles or more) as it can significantly retard micro-crack growth once cracks are present⁵. For high cycle fatigue residual stress is more important than surface finish, although the two are often closely related. For example surface roughness and residual stress are often associated with machining and finishing operations process, for example shot peening.

Figure A2.1 shows the effects of electropolishing, shot peening and stress relieving on Ti-6Al-4V. From this graph it can be seen that the high cycle fatigue properties of an electropolished sample with fine lamellar structure is improved by shot peening. However, stress relieving shot-peened samples results in a significant decrease in fatigue strength. Adding an electropolishing process to a shot peened and stress relieved sample results in most of the benefits of shot peening being restored.

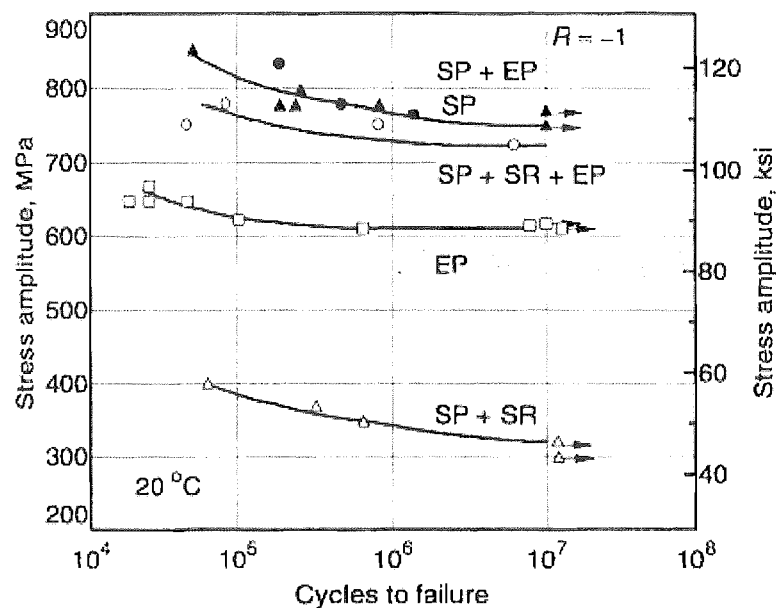


Figure A2.1 Ti-6Al-4V - Effect of shot peening and electropolishing on fatigue life.

Rotating beam test on fine lamellar microstructure in air, at 20°C.

EP = Electropolished, SP = Shot peened, SR = Stress relieved.

[Source: Welsch et al⁶]

Two potential surface treatment processes were considered to increase the fatigue life of the intervertebral disc implant, as detailed below.

Shot Peening

As previously stated shot peening places the outer surface of the material in compression but increases the surface roughness. The residual compressive stresses inhibit slip and delay the nucleation of cracks. However, the majority of the intervertebral disc concept designs developed were small and had undercut features which would be hard to access with shot peening equipment. Therefore, shot peening was not considered to be a viable option for increasing the high cycle fatigue strength of the intervertebral disc implant.

Electropolishing

Electropolishing creates highly polished surfaces on metallic workpieces by removing material through an electrochemical process similar to, but the reverse of, electroplating.

Typically the object to be electropolished is immersed in a container containing electrolyte along with another metallic conductor. A direct electric current is then passed through the workpiece and metallic conductor via the electrolyte. The workpiece is maintained anodic, with the cathodic connection being made to the metal conductor.

During the electropolishing process, a film of varying thickness covers the surface of the workpiece. This film is thickest over micro-depressions and thinnest over micro-projections. Electrical resistance is at a minimum wherever the film is thinnest which in turn results in the high rates of metallic dissolution at any micro-projections.

The material removed becomes a metallic salt. The metal removal rate is controllable to a degree and tolerances between 0.00254 and 0.0635 mm can normally be achieved.

Titanium is difficult to electropolish as it has a strong oxide layer which is hard to break down. As a result a highly reactive electrolyte is required, for example in the case of electropolishing Ti-6Al-4V an electrolyte of the following composition is typically used.

- 600ml methanol
- 360ml butanol-2 (C₄-H₁₀-O)
- 60ml perchloric acid (H-Cl-O₄)

Note: As perchloric acid is highly reactive and dangerous at room temperature this electrolyte should be stored at -20°C when not in use.

No commercial vendors carrying out electropolishing of titanium alloys were located during this investigation. Most vendors stated that due to the reactivity of the required electrolytes and the difficulties associated with polishing titanium alloys they were not interested in such work. However, titanium is polished in laboratory environments for experimental work. It was reported by the Technische Universitaet Hamburg that they regularly polish titanium alloys for experimental work using the previously detailed electrolyte ⁴.

It was noted by the Technische Universitaet Hamburg that during the polishing process the electrolyte should be maintained at -30°C and stirred constantly using a magnetic stirrer to achieve optimum results. For best results the workpiece should also be cooled down to -30°C in the electrolyte bath prior to the application of the electric current.

As material removal occurs with the conduction of current from the workpiece to the cathode, the surfaces and edges nearest the cathode have the greatest amount of material removed. Technische Universitaet Hamburg achieved uniform electropolished of fatigue testing specimens by rotating the workpiece in a cylindrical metallic vessel which acts as both the electrolyte bath and cathode. However, most of the intervertebral disc concept designs have undercut surfaces which would not be readily exposed to fresh electrolyte or be included in the current conduction path. As a result electropolishing of undercut areas could be difficult to achieve.

Given this inability to reliably electropolish critical implant features and the high reactivity of the electrolyte, it was determined that electropolishing the intervertebral disc implants was not a viable option.

These surface modification findings are not unique to titanium and its alloys. Therefore regardless of the material selected for the intervertebral disc implant the fatigue properties for unmodified surfaces should be used.

A2.3.2.2 Microstructure Effects on Fatigue Life

As previously stated fatigue cracks normally initiate at or near singularities on the surface of the workpiece. However even if metallic samples have a highly polished surface and no stress concentrations are present, alternating stress can cause slip bands to form and in turn fatigue failure to occur.

The application of a fluctuating stress causes dislocation motion in alternating directions. This localised irreversible dislocation movement occurs in narrow bands along slip planes in individual grains and as a result slip bands are formed. Since these bands terminate at a free, unconstrained surface, roughness in the form of ridges and grooves is created on the surface of the workpiece. These features are called *slipband extrusions* and *slipband intrusions*. The formation such features is illustrated in Figure A2.2.

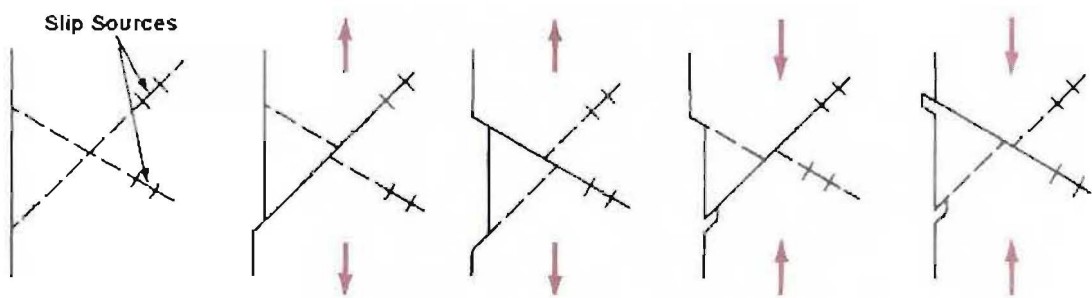


Figure A2.2 Slip band formation mechanism.

Operation of two intersecting slip bands, with the application of a reversing load.

{Source: Fine et al³}

The high concentrations of plastic strain developed within these localised bands ultimately serve as sites for the initiation of micro-cracks. As dislocation movement and thus slip band formation can occur below the materials' yield strength, fatigue failure can be initiated below the yield or proof stress.

The most significant factor in slowing down the propagation of micro-cracks is their interaction with grain boundaries. As micro-cracks reach grain boundaries they slow down or stop growing altogether. This is due to the fact that slip systems are discontinuous across grain boundaries. The length of the slip planes, known as the effective slip length, determines the amount of subsequent accumulated damage that occurs.

In the case of Ti-6Al-4V the effective slip length is limited by ‘critical’ micro-structural dimensions which can include but are not limited to the grain size, the length of the interfaces between the alpha (α) and beta (β) phases and the Widmanstätten packet size. In duplex materials an additional effective length parameters include grain size and the volume fraction of primary alpha (α_p). The fatigue properties of Ti-6Al-4V can therefore be improved by refining the grain structure.

For example when Ti-6Al-4V alloy is slowly cooled from the β region, the final microstructure consists of α phase plates which are separated by β phase, this arrangement is known as a Widmanstätten structure. A typical Widmanstätten microstructure is shown in Figure A2.3. This structure has large effective slip lengths and thus a low resistance to fatigue crack nucleation.

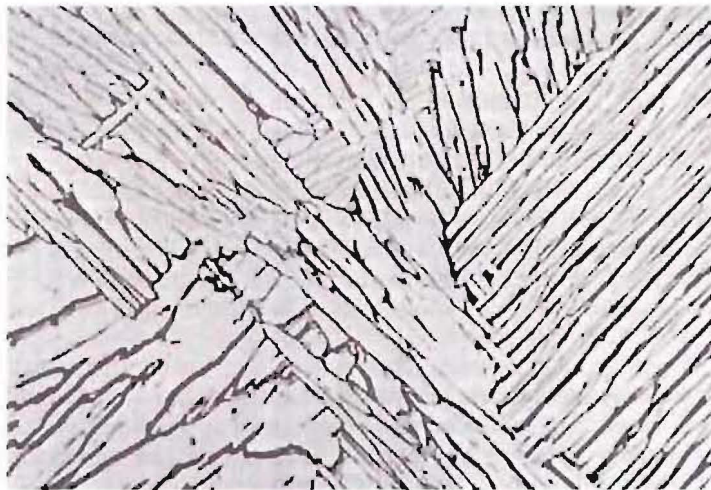


Figure A2.3 Typical Ti-6Al-4V Widmanstätten microstructure.

Widmanstätten microstructure of Ti-6Al-4V after slow cooling from above the β transus. The white plates are α phase and the dark regions between them are β phase. Optical micrograph 500x.

[Source: Donachie²]

The fatigue performance and typical crack nucleation sites for three other Ti-6Al-4V microstructures are detailed below.

Lamellar Microstructure

When carrying out solution heat treatments above the β transus the resulting microstructure depends on the degree of homogenization during solution treatment and on the cooling rate.

Quenching from above the β transus suppresses the diffusion controlled β to α transformation and leads to the formation of needle-like α' martensite. The resulting martensitic material has high yield strength but low fracture toughness hence once fatigue cracks nucleate, brittle failure quickly occurs.

For slower cooling rates as the temperature falls below the β transus, nucleation of α begins and diffusion controlled partitioning between the α and β phases occurs. The resulting microstructure is lamellar, in which broad α and fine β lamellae alternate to form packets. The size of the lamellar packets depends on the prior β grain size and the cooling rate with results ranging from fine acicular structures to coarse lamellar structures as indicated in Figure A2.4.⁶

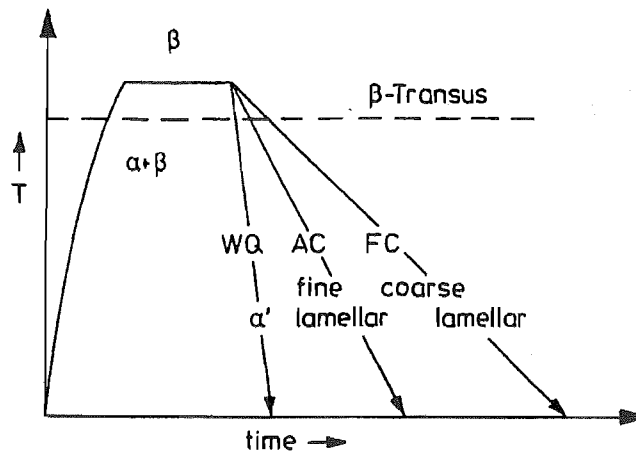


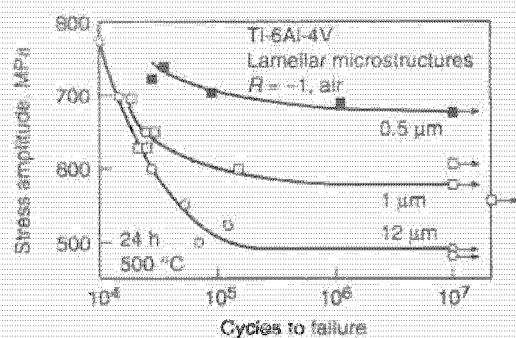
Figure A2.4 Formation of lamellae microstructure.

The cooling rate through the transus determines the fineness of the lamellar microstructure.

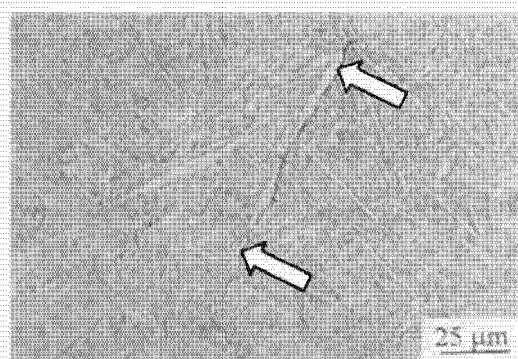
Note: WQ = Water quenched. AC = Air Cooled. FC = Furnace Cooled.

[Source: Welsch et al⁶]

Figure A2.5(a) shows the fatigue performance of a fully lamellar Ti-6Al-4V microstructure with the width of the alpha lamellae decreasing from 10 to 0.5 μm . With decreasing lamellae size an improvement in fatigue strength from 480 to 600 MPa is observed. Crack nucleation sites in lamellae microstructures are normally located in slip bands within the alpha lamellae. Because resistance to both dislocation motion and fatigue crack nucleation depend on the width of the alpha lamellae there is a strong correlation between the yield strength and fatigue strength for this microstructure.⁵



(a)



(b)

Figure A2.5 Ti-6Al-4V - Lamellar microstructure.

(a) Effect of a lamellae width on fatigue life.

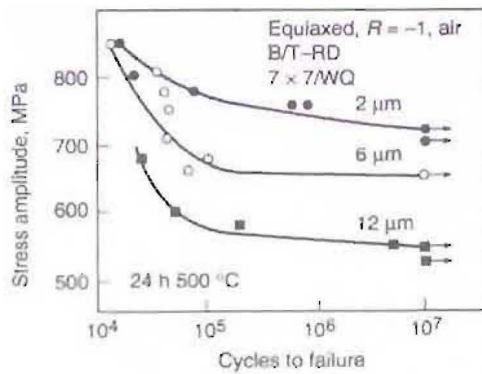
(b) Fatigue crack nucleation site.

[Source: Wagner⁵]

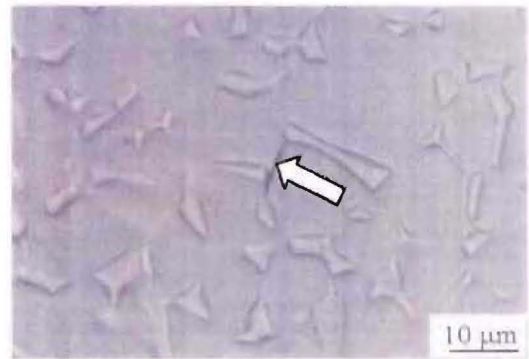
Equiaxed Microstructure

Equiaxed grain structures result from hot working the material in the α and β phase field and then recrystallising below the transus temperature. The presence of both phases during hot-working prevents the coarsening of the microstructure which occurs if only β grains are present. If this material is then recrystallization-annealed below the martensite start temperature, a fine equiaxed microstructure consisting of α and β grains forms.

Figure A2.6(a) shows that for a fully equiaxed Ti-6Al-4V grain structure, a decrease in the alpha grain size from 12 to 2 μm results in an increase of the fatigue strength from 550 to 720 MPa. Fatigue cracks in this material nucleate at slip bands within the alpha phase as indicated in Figure A2.6(b).



(a)



(b)

Figure A2.6 Ti-6Al-4V - Equiaxed microstructure.

(a) Effect of a grain size on fatigue life.

(b) Fatigue crack nucleation site.

[Source: Wagner⁵]

Duplex Microstructure

Duplex microstructures are formed in a similar way to equiaxed structures, except the material is recrystallization-annealed above the martensite start temperature. At this temperature, diffusion controlled partitioning between the α and β phases occurs resulting in a microstructure which consists of α grains and fine lamellar regions. The duplex annealing temperature determines the relative amounts of α and fine lamellar (transformed β) as shown graphically in Figure A2.7.

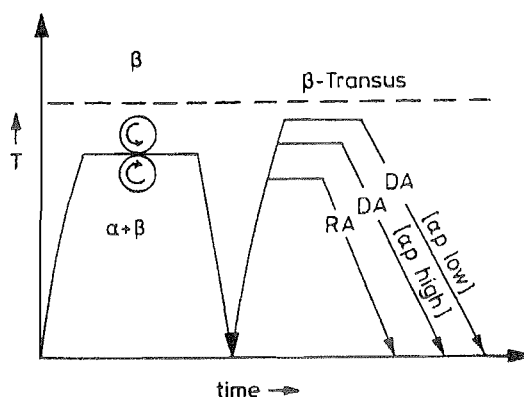


Figure A2.7 Processing path for recrystallization and duplex annealed microstructures. Although not indicated on this diagram recrystallization annealing has a slower cooling rate.

RA = Recrystallization Anneal. DA = Duplex Anneal. op = Primary Alpha.

[Source: Welsch et al⁶]

Figure A2.8 shows the microstructures which results from two different annealing temperatures. The microstructure in Figure A2.8(a) results from a low annealing temperature and consists of 40% primary alpha, while a higher annealing temperature results in 20% primary alpha phase as shown in Figure A2.8(b).

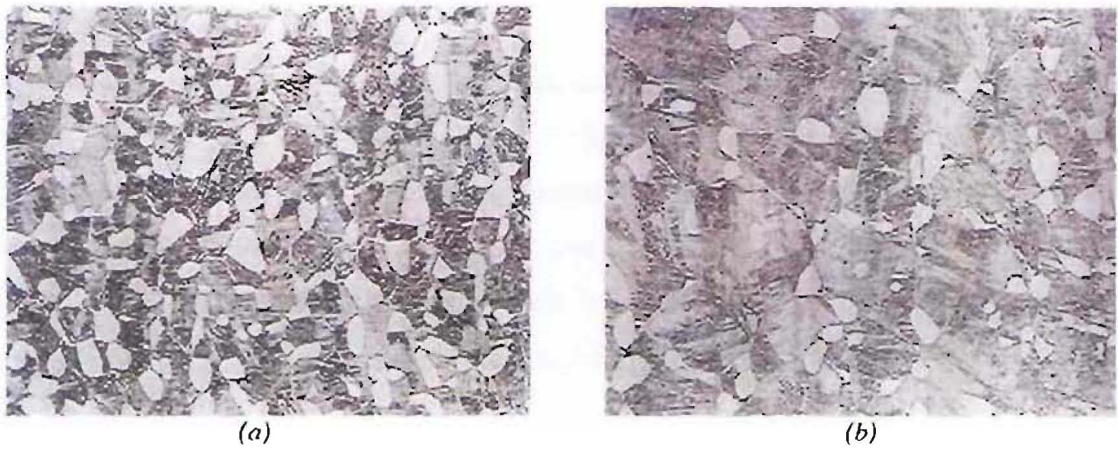


Figure A2.8 Ti-6Al-4V – Duplex microstructure.

(a) 40% primary alpha (α_p) 200x.

(b) 20% primary alpha 200x.

[Source: Welsch et al⁶]

For duplex Ti-6Al-4V decreasing the width of the alpha lamellae from 1 to 0.5 μm increases the fatigue strength from 480 to 575 MPa, as shown in Figure A2.9(a). Fatigue cracks in duplex microstructures can occur in the lamellae matrix, within the α_p phase or at the interface between the lamellae matrix and α_p phase⁵. Figure A2.9(b) shows a fatigue crack nucleating in a lamellae region.

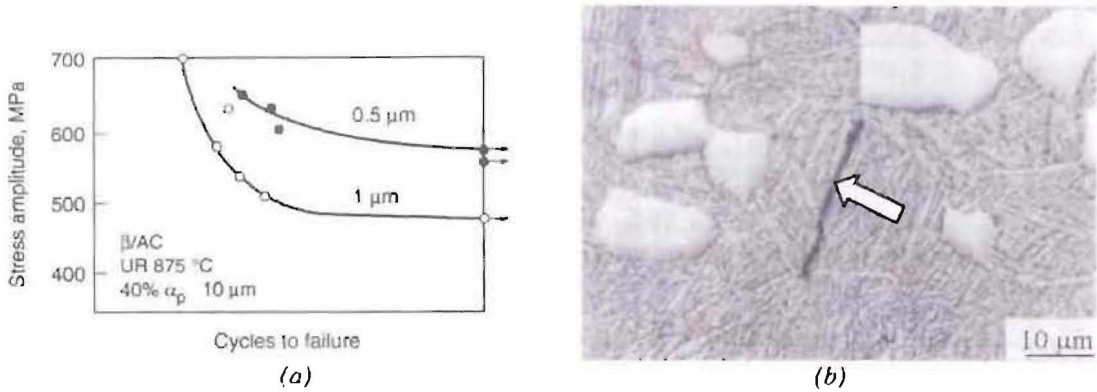


Figure A2.9 Ti-6Al-4V – Duplex microstructure and fatigue.

(a) Effect of a lamellae width on fatigue life.

(b) Fatigue crack nucleation site.

[Source: Wagner⁵]

Heat Treatment Environment

One of the disadvantages of titanium alloys is the high solubility of interstitial oxygen and nitrogen. Heating titanium to high temperatures in air not only causes oxidation but the inward diffusion of oxygen, nitrogen and hydrogen. This in turn results in the formation of a hard surface or 'alpha-case' which reduces the fatigue strength and ductility of the material. Therefore, if the titanium alloy is to be heated either as part of a forming process or to refine the microstructure, care must be taken to ensure the alpha case is removed. Alternatively careful control of the environment during heating must be ensured to prevent exposure to oxygen, nitrogen and hydrogen.

A2.3.2.3 Endurance Strength Summary

When Ti-6Al-4V is air cooled from above transus the temperature a lamellar microstructure with an endurance strength of up 600 MPa results. Provided the implant can be heated and cooled without distorting, this microstructure may be a viable option for the intervertebral disc implant.

Of the heat treatment processes investigated, the highest endurance strength results from a fine equiaxed microstructure. To achieve this grain structure a hot forming process is required during the manufacture of the implant. However, hot forming of the intervertebral disc implant may not be desirable or the forming process used may be too inhomogeneous or of insufficient magnitude to refine the grain sufficiently. Therefore, this heat treatment process was dismissed from the intervertebral disc implant material selection process.

Duplex microstructures also require a hot forming process however most titanium vendors are able to supply semi-finished Ti-6Al-4V products (bar, wire, tubes, etc) in a duplex condition. An advantage of manufacturing the intervertebral disc implant from semi-finished duplex material is that there is no need to heat treat the material. This means there is also no need to remove alpha-case material or have access to environment controlled heat treatment facilities either of which will increase the cost and complexity of the manufacturing process. It should be noted however that if such semi-finished duplex material is used, care must be taken to ensure that any heat treatment and forming operations are limited to sub-transus temperatures. The maximum endurance strength reported for duplex microstructures was 575 MPa.

A2.4 Commercially Pure Titanium

There are four ASTM grades of Commercially Pure (CP) titanium. These grades differ in the amount of impurities they contain, with the primary differences being in the oxygen and iron content. Table A2.3 shows the composition of the different commercially pure grades and associated ASTM standards.

| Grade | ASTM Spec | C | Fe | H | N | O | OT | Other |
|------------|-------------------|-----|-----|--------|------|-------|---------|--------|
| CP Grade 1 | B348 ¹ | 0.1 | 0.2 | 0.0125 | 0.03 | 0.018 | 0.4 | Bal Ti |
| CP Grade 2 | B348 ¹ | 0.1 | 0.3 | 0.0125 | 0.03 | 0.25 | 0.4 max | Bal Ti |
| CP Grade 3 | B348 ¹ | 0.1 | 0.3 | 0.0125 | 0.05 | 0.35 | 0.4 | Bal Ti |
| CP Grade 4 | B348 ¹ | 0.1 | 0.5 | 0.0125 | 0.05 | 0.4 | 0.4 | Bal Ti |

Table A2.3 Commercial Pure Titanium grades and composition (% Weight).

Note: OT = Other Total (for impurity content).

[Source: Welsch et al⁶]

Higher purity CP alloys (Grade 1) have a lower strength and hardness than the less pure alloys (Grade 4). The high purity grades also exhibit higher ductility. In general commercial pure grades of titanium are normally selected for their excellent corrosion resistance and biocompatibility for applications where high strength is not required. The most commonly used grade of commercial pure titanium alloy is Grade 2.

A2.4.1 Mechanical Properties

The mechanical properties of commercial pure titanium alloys at room temperature are detailed in Table A2.4.

| | ASTM Specification | | | |
|---------------------------------|--------------------|-----------|-----------|-----------|
| | Grade 1 | Grade 2 | Grade 3 | Grade 4 |
| Density (g/cm ³) | 4.51 | 4.51 | 4.51 | 4.51 |
| Elastic Modulus Tensile (GPa) | 103-107 | 103-107 | 103-107 | 103-107 |
| Shear Modulus (GPa) | 45 | 45 | 45 | 45 |
| Poisson's Ratio | 0.34-0.40 | 0.34-0.40 | 0.34-0.40 | 0.34-0.40 |
| Ultimate Tensile Strength (MPa) | 275 | 345 | 445 | 550 |
| Tensile Yield Strength (MPa) | 205 | 275 | 380 | 480 |

Table A2.4 Commercially Pure Titanium - Mechanical properties at room temperature.

[Source: Welsch et al⁶]

Figure A2.10 shows the fatigue properties for ASTM Grade 4 commercial pure titanium alloy. From this graph it can be seen that this alloy exhibits an endurance limit which is strongly dependent on temperature. The other grades of commercial pure titanium have similar fatigue strength and also exhibit a decrease in endurance strength with increasing temperature.

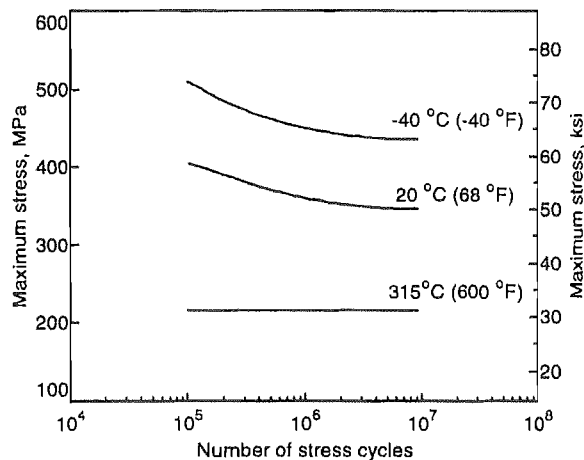


Figure A2.10 Commercially Pure Grade 4 Titanium Alloy - Rotating beam fatigue strength.

For un-notched, polished specimens machined from annealed bar stock.

[Source: Welsch et al⁶]

A2.5 Summary

Both Ti-6Al-4V and the commercial pure grades of titanium are suitable for use in the intervertebral disc implant. The final choice of material will depend on the required endurance strength, ductility and availability of the material in the required cross section.

A2.6 References

1. *Specification for Titanium and Titanium Alloy Bars and Billets. Annual Book of ASTM Standards*, 2002, ASTM International: West Conshikocken, PA, USA. Vol 02.04. pp 204-213.
2. Donachie M J, *Titanium : A Technical Guide*. 1988, Metals Park, OH: ASM International.
3. Fine M E, Ritchie R O, *Fatigue-crack initiation and near-threshold crack growth. Fatigue and Microstructure*, 1979, American Society for Metals: St Louis. pp 245-278.
4. *Personal Communication*, Sauer C. *Electropolishing Ti*, Hamburg, 2 November 2000.
5. Wagner L, *Fatigue life behaviour*, in Lampman S R (Eds). *ASM Handbook: Volume 19 - Fatigue and Fracture*, 1996, ASM International. pp 837-845.
6. Welsch G, Boyer R, Collings E W, eds. *Materials Properties Handbook: Titanium Alloys*. 1994, ASM International: Materials Park, OH.

<Blank Page>

Appendix 3 – Stainless Steel

As detailed in Chapter 5, during the refinement of the metallic spring concepts it became clear that the material properties would play an important role. One of the materials investigated was Stainless Steel. This appendix details the physical properties of Stainless Steels commonly used for *in-vivo* applications.

A3.1 Background

Stainless steel is used extensively for medical applications such as instrumentation, implants and auxiliary equipment. Some of the advantages of stainless steel include its corrosion resistance, ease of cleaning and aesthetic appearance.

The first orthopaedic application for stainless steel was the use of molybdenum-free 18-8 stainless steel to replace vanadium plates and screws. However this alloy was susceptible to corrosion *in-vivo*. In 1946 the American College of Surgeons endorsed 316 and 317 as the preferred grades of stainless steel in place of 18-8 alloys (302 and 304). Currently the most commonly used stainless steel alloy for implant purposes is 316L.

A3.2 316L Stainless Steel

316L stainless steel is a low carbon, high molybdenum grade of the standard 316 alloy. The composition of 316 and 316L alloys are detailed below in Table A3.1.

| Grade | ASTM Spec | C | Mn | Si | Cr | Ni | P | S | Other |
|-------|-------------------|------|-----|-----|---------|---------|-------|------|----------|
| 316 | A276 ¹ | 0.08 | 2.0 | 1.0 | 16-18.0 | 10-14.0 | 0.045 | 0.03 | - |
| 316L | A276 ¹ | 0.03 | 2.0 | 1.0 | 16-18.0 | 10-14.0 | 0.045 | 0.03 | 2-3.0 Mo |

Table A3.1 316 Stainless steel grades and composition (% Atomic).

Note: Balance of material is Iron

{Source: Davis²}

316L stainless steel can be supplied in several different processing states and with slight variations in composition, the most common states for medical implant purposes are 316LVM and 316LS. These versions of the base 316L alloy are vacuum arc remelted and offer the advantages of having higher purity and fewer non-metallic inclusions.

A3.2.1 Mechanical Properties

The mechanical properties of 316LS at room temperature are detailed in Table A3.2.

| Property | Value |
|-------------------------------|-------|
| Density (g/cm ³) | 7.95 |
| Elastic Modulus Tensile (GPa) | 195 |
| Shear Modulus (GPa) | 75 |
| Poisson's Ratio | ~0.25 |

Table A3.2 Mechanical properties of 316LS annealed bar at room temperature.

[Source: CarTech²]

Most stainless steel suppliers can supply 316 stainless steels in either an annealed or cold worked state. As can be seen in Table A3.3 increasing the percentage cold work of 316LS causes an increase in hardness and strength, while also resulting in a corresponding decrease in ductility.

| Mechanical Property | Annealed | Cold Work Percentage | | | |
|---------------------------------|----------|----------------------|------|------|------|
| | | 35 | 52 | 70 | 90 |
| Hardness (Rockwell C) | 88 | 26 | 36 | 38 | 40 |
| Ultimate Tensile Strength (MPa) | 586 | 862 | 1034 | 1172 | 1541 |
| Tensile Yield Strength (MPa) | 434 | 793 | 848 | 896 | 946 |
| Elongation at Break (%) | 57 | 18 | 16 | 17 | 13 |
| Reduction in Area (%) | 88 | 72 | 62 | 60 | 57 |

Table A3.3 316LS - Mechanical properties as a function of cold work.

[Source: CarTech²]

A3.2.2 Fatigue life

The endurance strength of 316L stainless steel in air is approximately 260 MPa, as shown in Figure A3.1^{3,4,5}.

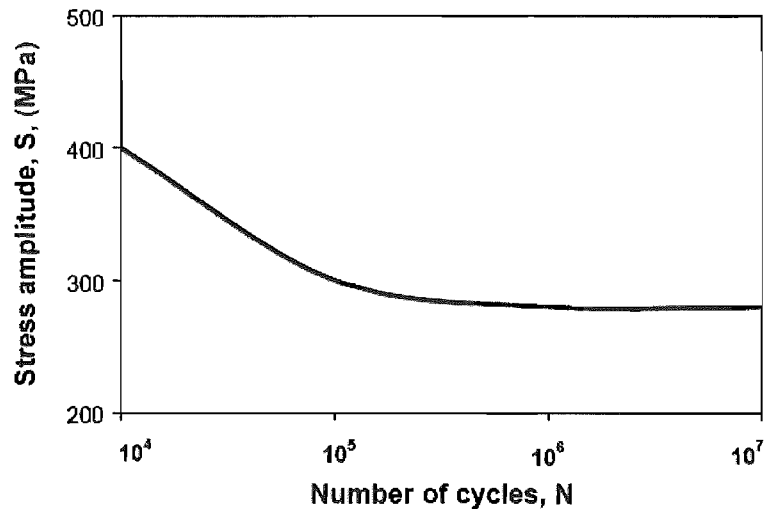


Figure A3.1 S-N curve for 316L stainless steel in air.

[Source: Leffler⁴]

The fatigue limits of stainless steels are influenced by the service environment. The more aggressive the corrosion conditions and the lower the loading frequency, the greater the effect the environment has on the fatigue life. For example during high frequency loading there is little time for corrosion to occur and the fatigue properties of the 316L alloy are primarily determined by the service life. However, at lower loading frequencies corrosion effects are more pronounced and any corrosion deposits which form can act as stress concentration sites which in turn reduce the fatigue life^{4,5}. Figure A3.2 shows the effect of pH on fatigue strength of three stainless steels alloys. The pH of saliva and urine are typically 6.4.

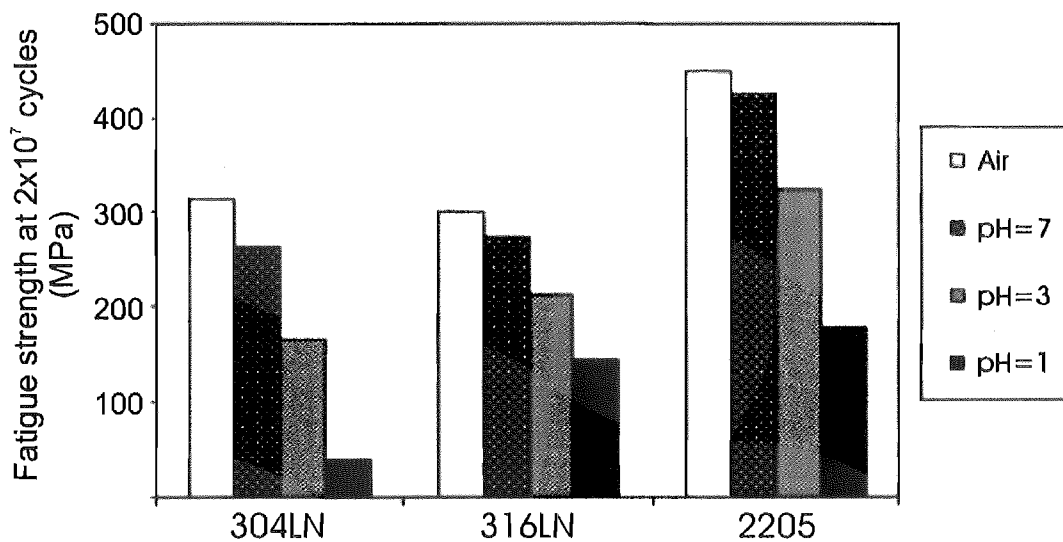


Figure A3.2 Effect of pH on fatigue strength of stainless steel.

Values were determined from rotating bending fatigue tests conducted at 100 Hz and 40°C. Results are presented for sample tested in air and 3% NaCl solution of various pH strengths.

Note: 316LN is a modified 316L alloy with additional Nitrogen to improve its strength and damage tolerance properties.

[Source: Leffler⁴]

A3.3 Summary

Stainless steel alloys, particularly 316L and its variants could be used to produce intervertebral disc implant components. However, the relatively low endurance strength of these materials means they can only be used in low stress situations.

A3.4 References

1. *Standard Specification for Stainless Steel Bars and Shapes. Annual Book of ASTM Standards*, 2002, ASTM International: West Conshikocken, PA, USA. Vol 01.03. pp 86-92.
2. Carpenter Specialty Alloys, *BioDur 316LS Stainless*, in Carpenter Specialty Alloys (Eds). *BioDur and Other Specialty Alloys for Medical Applications*, 2003.
3. Davis J R, ASM International. Handbook Committee., *Stainless steels*. ASM specialty handbook. 1994, Materials Park, Ohio: ASM International.
4. Leffler B. *Stainless - Stainless Steels and their properties*. Outokumpu Group, [cited Feb 2004]. Available from www.outokumpu.com.
5. Peckner D, Bernstein I M, *Handbook of stainless steels*. 1977, New York: McGraw-Hill.

Appendix 4 – Nitinol

As detailed in Chapter 5, during the refinement of the metallic spring concepts it became clear that the material properties would play an important role. One of the materials investigated was Nitinol. This appendix details the characteristics, shape memory properties and physical properties of Nitinol.

A4.1 History

In 1932 a new class of alloys was discovered, these materials exhibited the ability to restore themselves to an undeformed state when heated. Some of these alloys also exhibited super-elastic properties depending on past processing and environmental conditions. This new class of alloys was named Shape Memory Alloys or SMA for short. However due to the expensive nature of the alloys involved (most SMA at this time contained significant amounts of Gold and Cadmium) and the poor performance of these alloys, Shape Memory Alloys were not utilised in industry.

However in 1962 Nickel-Titanium Alloy was discovered by Buehler and co-workers at the Naval Ordnance Laboratory, this alloy consisted of half Nickel and half Titanium atoms. Nickel-Titanium alloy was found to exhibit superior properties when compared to all other shape memory alloys and the constituents were not prohibitively expensive.

With the discovery of NiTiNOL, so named to recognize its Naval Ordnance Laboratory origins, the level of product development utilizing shape memory alloys began to accelerate. Several companies smelted ingots of Nitinol often with poor results and numerous inventors filed patents on potential products through the late sixties and early seventies. However, most of these products were not practical and were never marketed.

In 1969, Raychem Corporation developed a product which is still the most financially successful product utilizing Nitinol, the Cryofit[®] hydraulic pipe coupling. This coupling is used in high performance hydraulic systems such as those for military aircraft and navy ships. Over one million have been put into service without a single in-service failure being reported and million dollars of this product are still sold each year⁹.

A4.2 Characteristic Properties of Nitinol

Nitinol has several unique characteristics which can be taken advantage of when designing medical implants and instrumentation. These characteristics are detailed in this section along with a brief description of an application for each. A more detailed explanation of the mechanisms behind these characteristics is provided in Section A4.5.

A4.2.1 Elastic Deployment

Nitinol offers elasticity approximately 20 times greater than that of stainless steel¹. This elasticity can be used to advantage where complex instruments need to be passed through narrow trochars and then deployed. Such instruments may include suture passers, retractors and retrieval bags. Another example is the Homer Mammalok illustrated in Figure A4.1, when deployed the wire in this device forms a tight 9 mm radius hook. If this device were made from stainless steel the hook radius would have to be increased to 50 mm, or the wire diameter reduced to 0.05 mm, either of which would cause the instrument to become unusable.

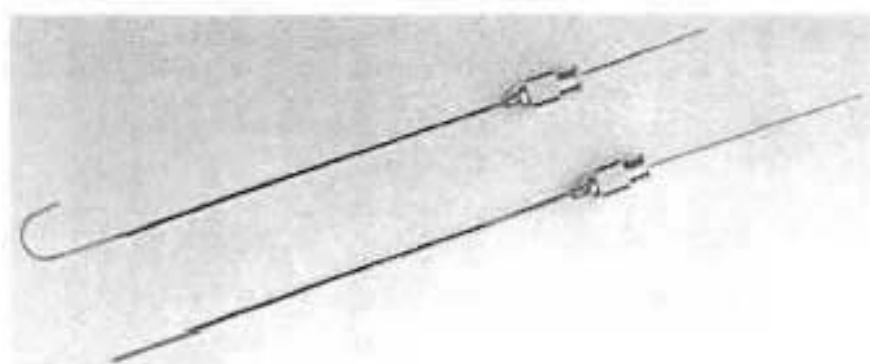


Figure A4.1 Homer Mammalok®, shown in retracted and deployed configurations.

[Source: T.W Duerig et al¹]

A4.2.2 Biocompatibility

Nitinol contains approximately 50% nickel, which is considered toxic in pure form. However, the presence of nickel does not necessarily indicate toxicity, for example stainless steel (Grade 316L) contains 10-14% nickel but the nickel is prevented from interacting with the environment by a protective oxide layer. In the case of Nitinol, the nickel is held 'captive' in a very stable TiO_2 oxide layer. Extensive *in-vivo* testing has shown Nitinol to be highly biocompatible^{1,8} more so than stainless steel, although it is less stable than pure titanium¹⁵.

Nitinol implants have been used extensively in dentistry, orthopaedics and many other branches of medicine, with large numbers of permanent implant being reported in Japan, Germany, China and Russia dating back to the early 1980s⁶. Also several Class III Nitinol implants have been approved for use in the USA. One such product is the Simon vena cava filter shown in Figure A4.2.

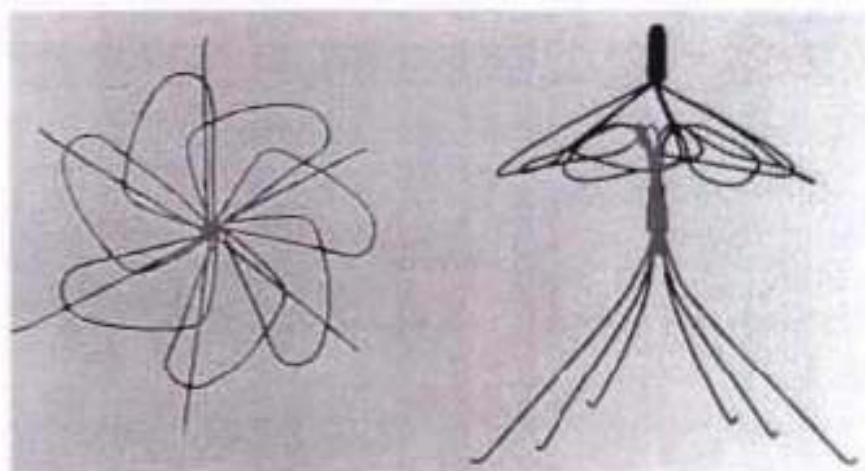


Figure A4.2 Longitudinal and transverse views of a Simon vena cava filter in its deployed state.

This device was the first Class III Nitinol Implant approved by the FDA.

[Source: T.W Duerig et al¹]

A4.2.3 Kink Resistance

Within reasonable limits Nitinol cannot be kinked. This characteristic is related to the high elasticity previously mentioned and the shape of stress-strain curve. When strains are increased locally beyond the plateau strain, stresses increase rapidly. As this occurs the strain is redistributed into areas of lower strain instead of increasing the peak strain. Thus kinking or strain localisation is prevented by the creation of a more uniform strain profile than would occur in a conventional elastic-plastic material⁴.

The first application to utilise this property was guide wires, which must pass through tortuous paths without kinking. Even very small permanent bends in these guide wires can cause “whipping” which destroys the ability to steer the wire. Another application for this kink resistance is small diameter instruments that can still operate smoothly while bent, an example of which is shown in Figure A4.3.

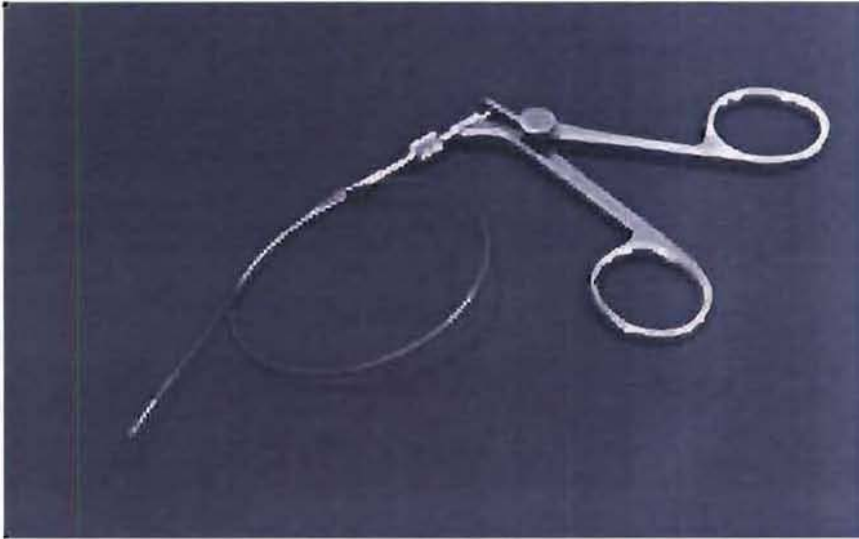


Figure A4.3 Kink resistance 1 mm diameter grasper designed for use in urology.

The instrument shaft is composed of very thin walled Nitinol tube and wire, able to be bent around radii of less than 30 mm without kinking.

[Source: T.W Duerig et al⁴]

A4.2.4 Constancy of Stress

When a deformed Nitinol component is unloaded the resulting stress-strain curve exhibits constant stress over large strains, as shown in Figure A4.4. In conventional metals the stress during unloading is dependent on the percentage strain. However, for super-elastic materials operating temperature is the controlling factor. As a result with constant temperature, as found in the human body, super-elastic devices can be designed to exert a constant load over a wide range of shapes⁴.

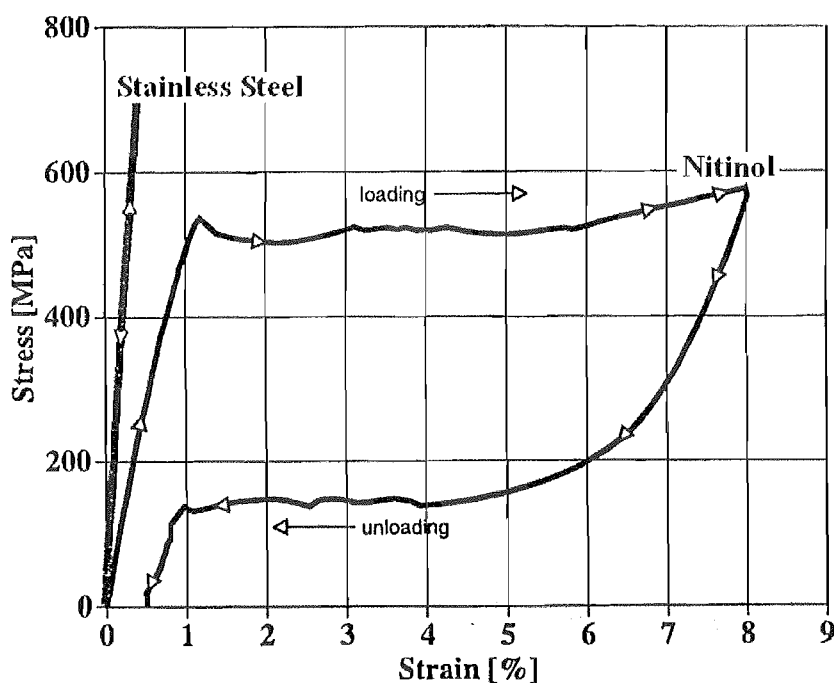


Figure A4.4 Stress-Strain curve for Nitinol compared to Stainless Steel.

Nitinol is non-linear, exhibits a hysteresis and follows different paths on loading and unloading. The elasticity of Nitinol is approximately twenty times that of Stainless Steel. Nitinol also exhibits a very flat unloading curve, i.e. a constant stress is exerted over large strains.

[Source: T.W Duerig et al³]

Orthodontic arch-wires were the first product to take advantage of this property. Orthodontists often tighten conventional arch-wires to the point of causing pain. As the treatment continues the teeth move and the forces on the arch-wire rapidly relax retarding tooth movement and slowing the treatment process. In contrast Nitinol arch-wires, shown in Figure A4.5, are able to exert constant force and move the teeth for an extended period of time, meaning fewer visits to the orthodontist and less pain⁷.

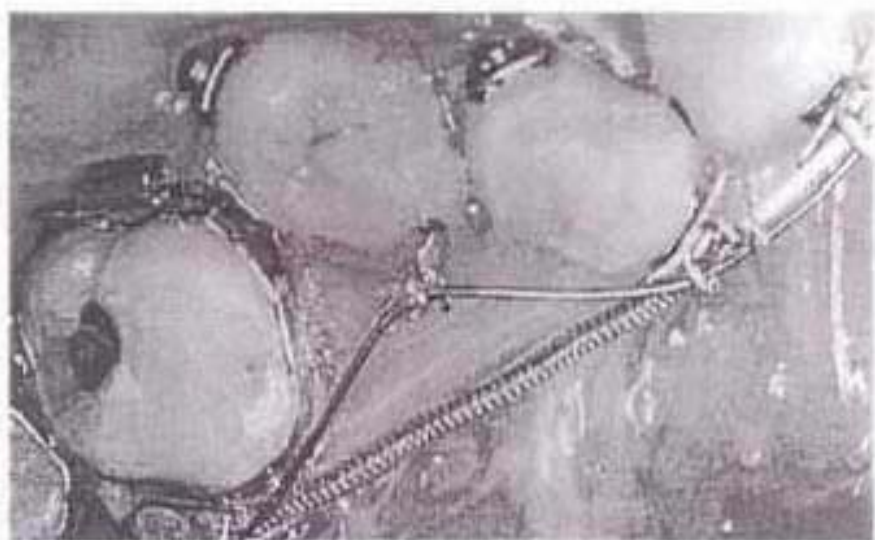


Figure A4.5 Nitinol orthodontic arch-wires apply constant stress to the teeth.

[Source: T.W Duerig et al.]

A4.2.5 Physiological Compatibility

Stainless steel, titanium and other biocompatible metals are very stiff and yield little, if at all, as a result of pressure from the surrounding tissues. The high compliance of Nitinol makes it one of the metals most mechanically similar to bone. This improved physiological similarity promotes bone growth⁸ and healing by sharing loads with the surrounding tissue. This characteristic has led to applications such as hip implants, bone staples and bone spacers⁷ an example of which is shown in Figure A4.6.



Figure A4.6 An intervertebral disc spacer in martensitic and deployed super-elastic states. The properties of Nitinol promote rapid recovery due to the similarities between the implant and the surrounding tissue.

[Source: T.W Duerig et al³]

However, this physiological compatibility comes at a price, computational complexity. Conventional metals are linearly elastic and readily lend themselves to both analytical and Finite Element Analysis (FEA) methods. Nitinol, like biological materials is much more difficult to model, not only is it's behaviour non-linear but it also exhibits strain dependent hysteresis, a strong temperature dependency and a permanent set (which is also strain dependent). However, it has been reported that there is a vendor in the United States of America who is able to conduct FEA analysis of Nitinol²².

A4.2.6 Thermal Deployment

One of the most popular attributes of Nitinol devices is that they can be deployed using the shape memory effect. One of the most common thermally deployed medical devices is self-expanding stents, an example of which is shown in Figure A4.7. These self-expanding stents are often used as a follow up to balloon angioplasty to internally brace the walls of tubular passages, such as blood vessels.

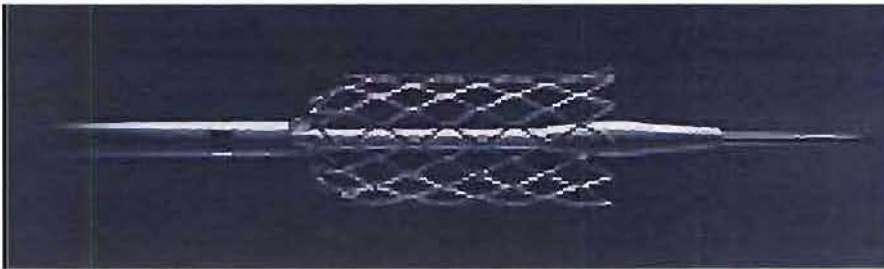


Figure A4.7 SMA stent in the process of being deployed from a catheter.

The equilibrium shape of the stent increases six-fold as it is warmed to body temperature. The catheter provides mechanical constraint that prevents premature recovery of the deployed shape.

[Source: T.W Duerig et al⁴]

Flushing chilled saline solution through the catheter keeps the Nitinol stent in the deformed (collapsed) state until the surgeon is ready to deploy the device. When released from the catheter, the stent is warmed by its new surroundings, recovers its pre-programmed shape and becomes a super-elastic device.

A4.2.7 Dynamic Interference

Stents also take advantage of another useful Nitinol property, dynamic interference or a constant force pushing radially outwards onto the vessel wall. Traditional inflated stents require a balloon to expand and plastically deform them to the desired shape. However, following traditional deployment as the balloon is collapsed the stent elastically recovers causing it to become loose in the vessel. The only way to overcome this loosening problem is to over expand the balloon and stent, but this can cause damage to the vessel. In contrast Nitinol stents expand outward to a pre-programmed form with no spring-back. Therefore, after deployment correctly sized Nitinol stents continue to push outward with a gentle force. Nitinol stents will also expand outwards to fill irregular or oblong cross sections as opposed to balloon inflated stents which always adopt the round shape of the balloon.

A4.2.8 Fatigue Resistance

Nitinol has a fatigue behaviour that is quite atypical for metallic materials¹⁷. Fatigue environments can be divided into two groups; strain-controlled and stress-controlled. As the names imply the former describes a device alternately deformed between two set shapes, while the latter describes the influences of a fluctuating load.

To illustrate the differences consider the fatigue behaviours of a rubber band and a loop of steel wire. In a stress-controlled environment (e.g. load cycling between 10 and 100kg) the steel loop will survive far longer than the rubber band. In a strain-controlled environment (e.g. alternately stretching from 100 to 200mm), the rubber band will outperform the steel loop.

Nitinol is much the same; in a strain-controlled environment it will dramatically outperform conventional metals^{2,10}. However, in stress-controlled environments it may fail in fatigue rapidly. An example of where this strain controlled fatigue could be used to advantage is pacemaker leads which require a conductive metal that can survive a high number of flexing motions without failing⁴.

A4.2.9 Biased Stiffness

Conventional materials load and unload along an identical path. For example the force applied by a spring is dependent on how far it is stretched not on whether the spring is being stretched or released. However super-elastic components are path dependent, with the position of the spring being less important than whether the spring is being stretched or released.

This biased stiffness or hysteresis is illustrated in Figure A4.8 for a stent which is manufactured in the open configuration and then deformed to the closed position (A). When the stent is deployed by releasing it from the catheter it follows the unloading arrows, until the vessel is filled and expansion stops (B). The gentle pressure against the vessel wall is controlled by the unloading arrows, but efforts to re-collapse the stent and vessel are resisted by the stiffness indicated by the loading arrows. Also if further expansion of the stent occurs the same biased stiffness is maintained.

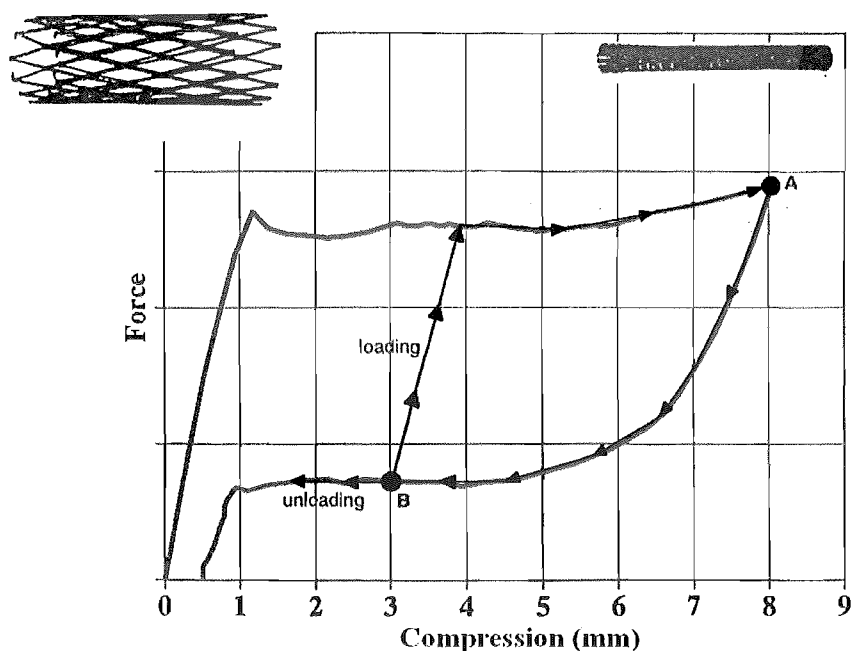


Figure A4.8 Biased stiffness illustrated in a stent.

[Source: T.W Duerig et al³]

A4.2.10 MRI Compatibility

Nitinol provides crisp, clear MRI images which is potentially useful in open MRI procedures. Applications for needles and instruments have also been proposed, though to date few of these products are commercially available³.

A4.3 Properties of Nitinol

Several studies to determine the properties of Nitinol have been carried out; a compilation of some of the results is shown below^{2,5,9}.

Physical Properties

| | | |
|-------------------------|------------|---|
| Melting Point | | 1300 °C |
| Density | | 6.45 g/cm ³ |
| Electrical Resistivity | Austenite | ~76–100 μΩ/cm |
| | Martensite | ~70–82 μΩ/cm |
| Magnetic Susceptibility | Austenite | 3.7 x 10 ⁻⁶ emu/g |
| | Martensite | 2.4 x 10 ⁻⁶ emu/g |
| Thermal Conductivity | Austenite | 0.18 watt/cm - °C |
| | Martensite | 0.085 watt/cm - °C |
| Thermal Expansion | Austenite | 11 x 10 ⁻⁶ m/°C |
| | Martensite | 6.6 x 10 ⁻⁶ m/°C |
| Corrosion Resistance | | Similar to 300 series Stainless Steel or Titanium Alloys |

Mechanical Properties

| | | |
|-----------------------|------------|--|
| Young's Modulus | Austenite | ~ 40 GPa (5.6 x 10 ⁶ psi) |
| | Martensite | ~ 75 GPa (10.8 x 10 ⁶ psi) |
| Yield Strength | Austenite | 195–790 MPa (28–100 x 10 ³ psi) |
| | Martensite | 70–140 MPa (10–20 x 10 ³ psi) |
| Ultimate Strength | | 900 MPa (130 x 10 ³ psi) |
| Elongation at Failure | | 20–40% |

Transformation Properties

| | |
|----------------------------|---------------|
| Transformation Temperature | -200 to 110°C |
| Shape Memory Strain | 8.5% maximum |

Typical Loading and Unloading Characteristics

| | |
|---|-------------------------|
| Loading Plateau (σ_l) | 450–700 MPa |
| Unloading Plateau (σ_u) | Up to 250 MPa |
| Maximum Spring-back | 11% |
| Maximum Deformation with % Permanent Set (ϵ_p) | 6% |
| Maximum Stored Energy | 40–50 J/cm ³ |

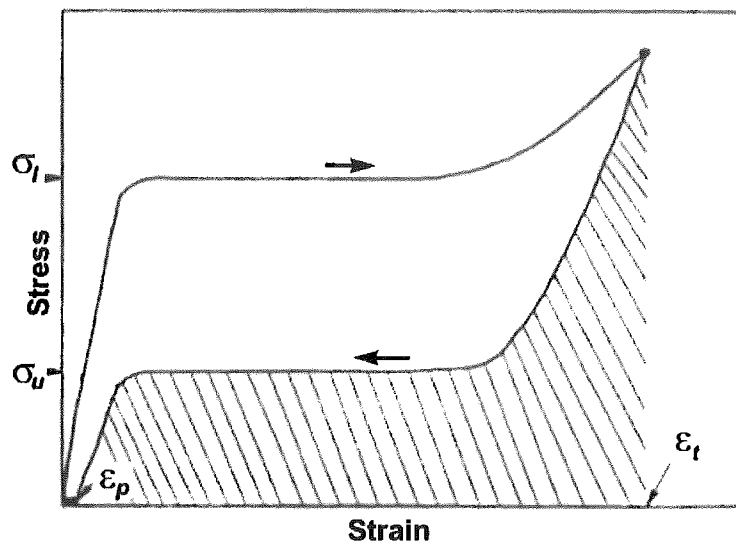


Figure A4.9 Schematic showing super-elasticity descriptors.

Stored Energy indicated by shaded area.

[Source: Duerig *et al*²]

Note: These values are only approximate indications of the properties of Nitinol. Exact figures vary depending on the alloy composition, past processing history and the number of shape memory effect cycles with material has been subjected to.

A4.4 Theory of the Austenite to Martensite Transformation

The basis of the shape memory effect lies in the alloy's ability to undergo a thermo-elastic martensitic transformation. The martensitic transformation can be defined as lattice transformation involving shearing deformation which in turn results from cooperative atomic movement. The martensitic transformation is athermal, as the amount of new phase produced is dependent on temperature rather than the period of time spent at a given temperature.

The transformation from austenite to martensite is often interpreted as a two-fold sequence, involving Bain strain and lattice-invariant shear.

Bain strain, or lattice deformation, accounts for the atomic movements needed to produce the new martensitic structure from the old austenitic material. Figure A4.10(a) shows the lattice movements of conventional metals such as stainless steel which exhibit Hookian elasticity. In contrast, Figure A4.10(b) shows the progressive transformation of austenite to martensite observed in shape memory alloys. As the magnitude of the stress increases (from left to right) the amount of martensite increases as more layers of the lattice are deformed.

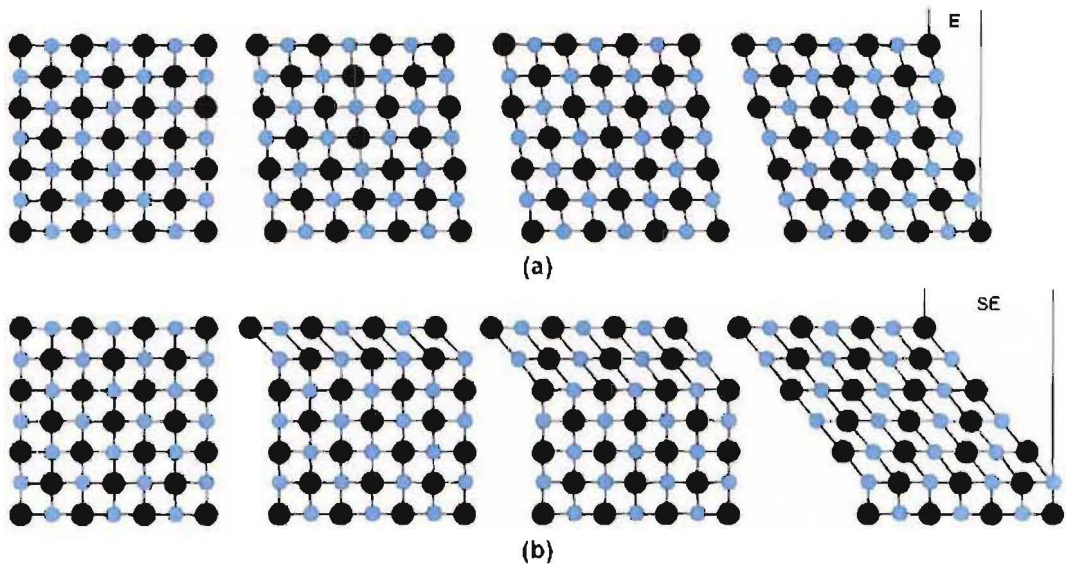


Figure A4.10 2d schematic of the austenite to martensite transformation.

(a) Lattice movements associated with Hookian elasticity.

(b) Progressive lattice deformation observed in shape memory alloys.

Where 'E' is traditional elasticity and 'SE' is super-elasticity.

[Source: Stockel et al¹⁶]

The second part of the martensite transformation, the invariant-lattice shear, is an accommodation process. The martensite produced during lattice deformation has a different shape and volume to the surrounding austenite. To accommodate these changes either one of two deformation mechanisms, slip or twinning, may occur. Slip shown in Figure A4.11(a) is a permanent and irreversible accommodation process and is common in many martensites. Twinning is able to accommodate shape changes in a reversible way and is illustrated in Figure A4.11(b). For the shape memory effect to occur to any significant extent twinning must be the predominant accommodation process. However regardless of which accommodation mechanism occurs each of the resulting crystals has a martensitic structure but the shape of the original austenite structure.

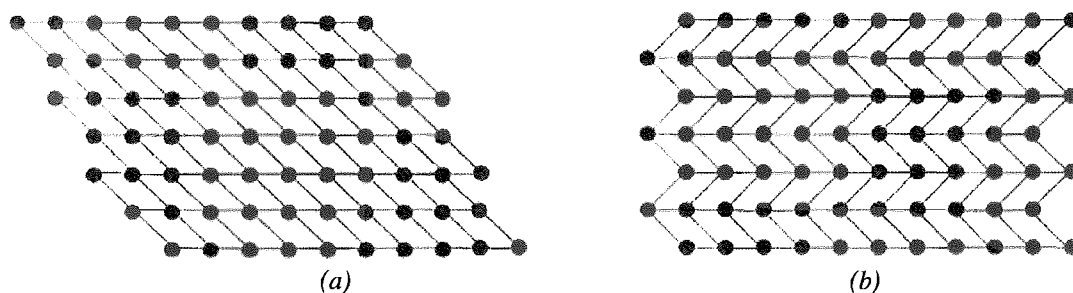


Figure A4.11 Stress-induced martensitic shape and volume accommodation mechanisms.

(a) Slip causes irreversible damage.

(b) Twinning is reversible and the predominant accommodation process for shape memory alloys.

[Source Gil et al⁷]

In the absence of an external applied stress and when the volume change is negligible, the thermally induced martensitic transformation is characterized by random martensite plate variants, as shown in Figure A4.12. Such a transformation results in a minimum or even nil macroscopic shape change⁷.



Figure A4.12 Microstructure of martensite.

[Source Gil et al⁷]

If a constant externally applied uniaxial stress assists the thermally induced martensitic transformation, only a limited number of thermo-elastic martensite variants grow. Or alternatively in the case of martensite formations around pre-existing dislocation stress fields, certain martensite plate variants will be dominant as can be observed in Figure A4.13. These processes will lead to a macroscopic shape change⁷.



Figure A4.13 Microstructure of stress-induced martensitic.

[Source Gil et al⁷]

In order to induce the austenite to martensite transformation, the chemical free energy of the martensite must be lower than that of the austenite. Since the transformation requires an excess of non-chemical free energy (such as transformation strain and interface energy), the transformation will only take place if the difference between the chemical free energies of both phases are greater than the necessary non-chemical free energy⁷.

Or in other words, a driving force is necessary. The austenite to martensite transformation will only proceed if the material is under-cooled to a suitably low temperature, M_s . This temperature is below the equilibrium temperature T_0 where the chemical free energy of the martensite and austenite are equal. A driving force is also necessary for the reverse transformation therefore the specimen must be overheated to a suitably high temperature, A_s , as illustrated in Figure A4.14.

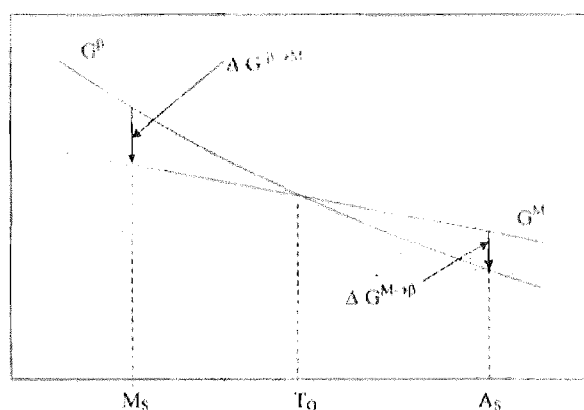


Figure A4.14 Relationship between free energy of martensite (M) and austenite (β).

[Source Gil et al⁷]

The required under-cooling and overheating as well as the activation energies are much smaller for martensitically transforming shape memory alloys than those required for steels. $\Delta G_{\text{Chemical}}$ on cooling for shape memory alloys, is about 10-15 J/Mol and ΔT about 5-50°C. While for steels, $\Delta G_{\text{Chemical}}$ ranges from 1000 to 1500 J/Mol and ΔT ranges from 200 to 400°C.

M_F and A_F are defined as the temperatures needed to complete the transformation and retransformation respectively. This need to under-cool and overheat the material results in a temperature hysteresis as shown in Figure A4.15.

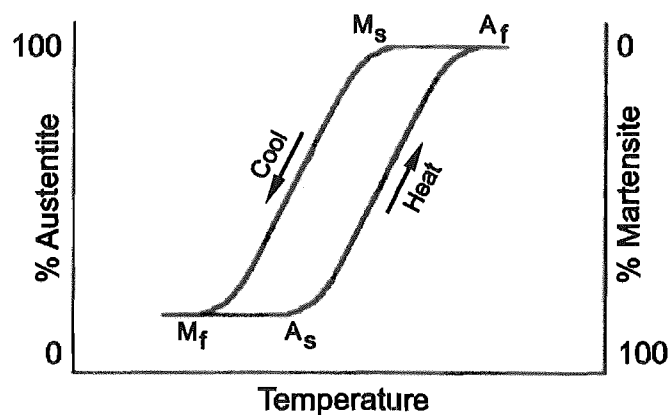


Figure A4.15 Temperatures hysteresis.

[Source: Waram²⁰]

All of the physical properties of Shape memory alloys which are dependent on the crystal structure, such as electrical resistivity, optical reflectivity, damping characteristics and specific heat, are different in the austenitic and martensitic phases and therefore show similar hysteresis loops. By following one of these properties during the forward and reverse transformations the four characteristic temperatures M_S , M_F , A_S and A_F as well as the shape of the hysteresis loop can be determined.

A4.5 Shape Memory Alloy Mechanisms

A4.5.1 Thermal - Mechanical Cycling

As previously described shape memory alloys have the unique property known as shape memory effect. This refers to the alloys ability to be deformed at low temperatures and retain this deformation until it is heated, at which point the material returns to its original undeformed state. The transformation back to the undeformed shape occurs as a result of the materials crystal structure changing.

At high temperatures the crystal structure of shape memory alloys is Austenitic, while at low temperatures martensitic structures are formed. The austenite structure is often referred to as the parent phase. As previously described when shape memory alloy is cooled the martensite lattice does not all tilt in the same direction; instead a twinned structure is observed, as shown in Figure A4.16.

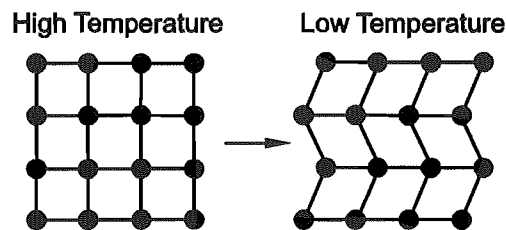


Figure A4.16 Nickel Titanium alloy atomic arrangement upon cooling.

[Source: Waram²⁰]

When a load is applied to this martensitic material it deforms (i.e. accumulates strain), causing the twins to reorient so they lie in the same direction. This process is called de-twinning, in shape memory alloys the stress required to reorient the twins is relatively low. A de-twinned structure is illustrated in Figure A4.17.

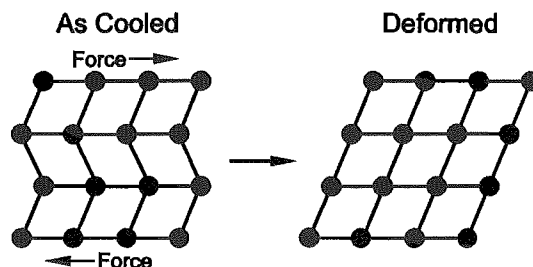


Figure A4.17 Deformation of lattice or de-twinning.

[Source: Waram²⁰]

When the applied load is released at a temperature below A_S any shape change persists since rearrangement of the twins and martensite variants does not occur. However, upon heating through the A_S to A_F temperature range the material recovers its original shape as a result of the reverse transformation from martensite to austenite. As the structure of the martensite has low symmetry, the reverse transformation is highly restricted in the crystallographic sense and usually only one variant of the parent phase (austenite) is nucleated. Full recovery of the original shape will not occur, however, if any slip occurred during the accommodation process or if the material was over strained during the deformation stage.

Once the shape is recovered at the A_F temperature, there is no change in shape when the unloaded material is cooled down below M_F and the shape memory effect can only be reactivated by deforming the martensitic specimen again.

This shape memory effect is a one-way process, proceeding from cold shape to hot shape and it cannot be reverse. The process is shown schematically in Figure A4.18 is sometimes referred to as *one-way shape memory effect*.

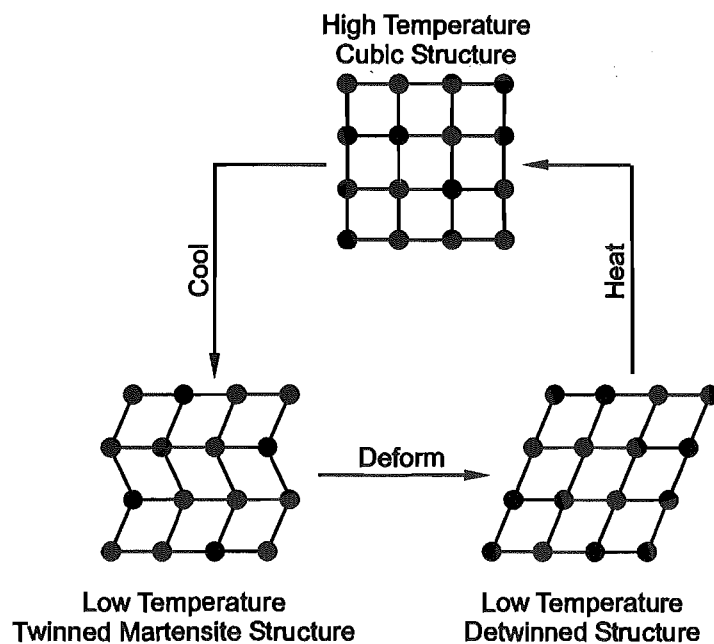


Figure A4.18 Transformation between high and low temperature structures.

[Source: Waram²⁰]

A4.5.2 Two-Way Shape Memory Effect

It is possible to create shape memory devices which can cycle between fixed shapes in both the parent and martensite phases. In effect, the material remembers the high temperature shape and the low temperature shape, as well as the shapes at all temperatures between these two extremes. It is then possible to cycle fairly repeatedly between these different shapes by simply changing the temperature. This effect is called the *two-way shape memory* or reversible shape memory effect and is shown schematically in Figure A4.19.

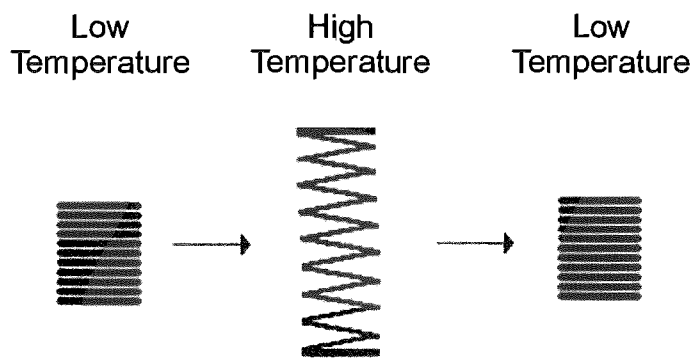


Figure A4.19 Schematic diagram of the two-way memory effect.

[Source: Waram²⁰]

Two-way shape memory behaviour is achieved as a result of training. Training limits the number of martensite variants which can be formed when the alloy is heated and cooled through the transition temperature range. During training cycles the material is deformed in the low temperature state. This deformation introduces dislocations which stabilize the pre-existing configuration of martensites. On heating to temperatures above A_F , the martensite-austenite transformation occurs but the dislocations remain. On cooling below M_S , martensite forms in such a way as to accommodate the stress fields associated with the previously formed dislocations. Therefore, if there are sufficient dislocations only a few stable martensite configurations, including the original configuration, can exist.

It should be noted that only during heating can work (force and motion) be generated for both the one-way and two-way shape memory effects. During cooling with the two-way effect, the material simply recovers its low temperature shape and it cannot provide force to external components.

A4.5.3 All-Round Shape Memory Effect

The all-round shape memory effect differs from the two-way effect in the following ways:

- A greater amount of shape memory change is possible with the all-round effect.
- The high and low temperature shapes are exact inverses of each other. i.e. a complete reversal of curvature is possible as shown in Figure A4.20.

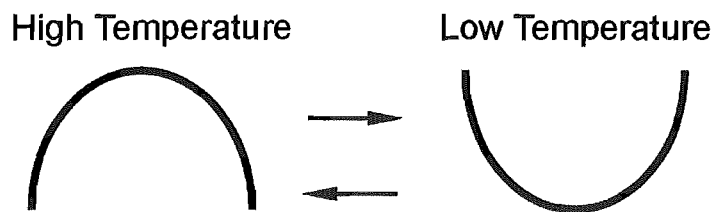


Figure A4.20 All-round shape memory effect.

[Source: Waram²⁰]

Because of the extra processing involved and the lack of reliability associated with the two-way and all-round shape memory effects, they are usually not used to provide motion in the reverse direction. Instead an outside biasing force is normally used to determine the cold shape and any two-way effect that is present helps to reduce the amount of biasing force needed. Figure A4.21 shows an example of an actuator where the outside biasing force is provided by a steel spring.

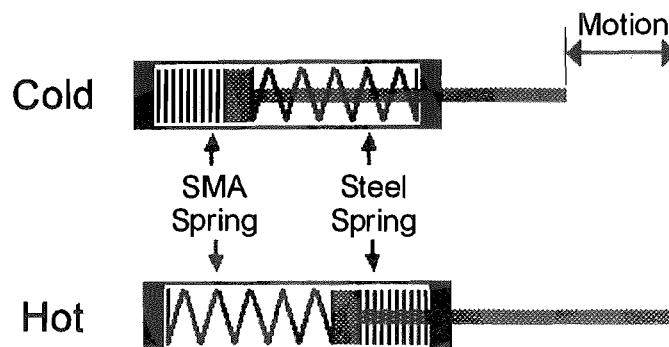


Figure A4.21 Two-way motion using a biasing (steel) spring.

[Source: Waram²⁰]

A4.5.4 Super-Elasticity

Super-Elasticity or Pseudo-Elasticity can be defined as the ability of certain alloys to return to their original shape upon unloading after substantial deformation.

Shape memory alloys are able to exhibit such super-elasticity due to their ability to form stress-induced martensite. Just as water can be condensed from steam by pressurization or cooling, shape-adaptive martensite can be formed by stressing as well as cooling.

When shape memory alloy components are stressed at temperatures greater than A_F , and below M_D , stress-induced martensite is formed. If the material is then unloaded the stress-induced martensite becomes unstable and the material returns to its original austenitic form. Super-elastic devices for medical applications therefore require an A_F temperature below 37°C .

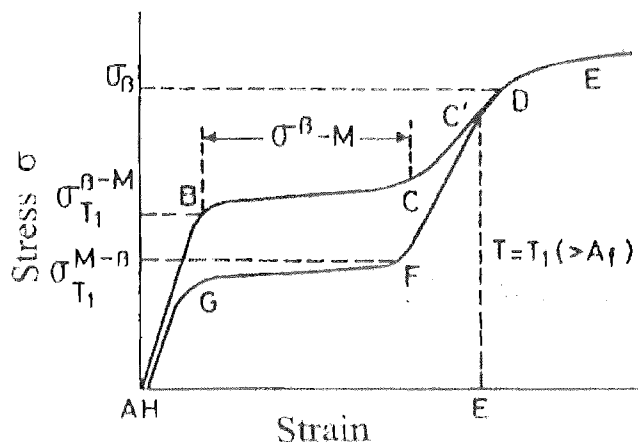


Figure A4.22 Stress-Strain for a super-elastic material.

[Source Gil et al⁷]

Figure A4.22 shows a typical pseudo-elastic stress-strain curve. The linear portion AB represents the elastic deformation of the parent martensite phase. Point B corresponds to a stress level $\sigma_{T_1}^{\beta \rightarrow M}$ where the first stress-induced martensite plates start to be formed. The martensite transformation is completed at point C. The slope of the region BC reflects the energy dissipated by the material due to internal friction and the formation of defects.

When material fully transformed into stress-induced martensite is stressed further, it will deform elastically as represented by region CD. At point D the plastic yield stress σ_{β} , of the material is reached and the material continues to deform plastically up to fracture (E). If the stress is released before reaching point D, for example at point C', the induced strain is recovered again through several stages. The region C'F of the curve corresponds to the elastic unloading of the stress-induced martensite. Upon reaching the stress $\sigma_{T_1}^{M \rightarrow \beta}$ at point F, the reverse martensitic transformation starts and the fraction of stress-induced martensite decreases until the parent phase is completely restored at point G. Region GH represents the elastic recovery of the parent phase. Super-elastic materials may exhibit some set, or failure to recover the total strain, if irreversible deformation occurs during the loading or unloading processes.

The stress required to induce the formation of stress-induced martensite $\sigma_{T_1}^{\beta \rightarrow M}$ and the corresponding to the reverse transformation $\sigma_{T_1}^{M \rightarrow \beta}$ are both linear functions of temperature, as can be seen in Figure A4.23.

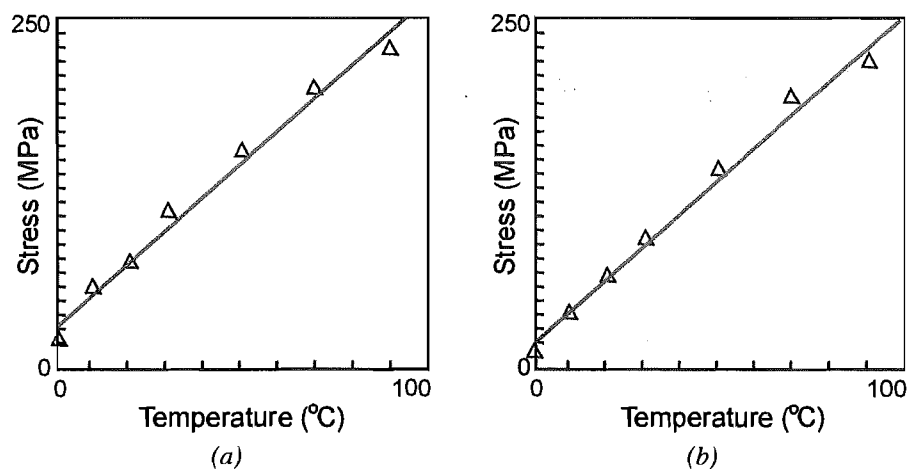


Figure A4.23 Effect of temperature on transformation stress.

(a) Temperature versus transformation stress (Austenite \rightarrow Martensite).

(b) Temperature versus reverse transformation stress (Martensite \rightarrow Austenite).

[Source Gil et al⁷]

In general super-elastic shape memory alloys can be strained up ten times more than ordinary spring materials and can store considerably more energy, as shown in Table A4.1.

| Material | Elastic Strain | Stored Energy (Joules/cm³) |
|-----------------|-----------------------|--|
| Steel | 0.8% | 8 |
| Cu-Zn-Al | 5.0% | 14 |
| Ni-Ti | 10.0% | 40-50 |

Table A4.1 Stored energy of different materials.

[Source: Waram²⁰]

A4.5.5 Hysteresis

Mechanisms at an atomic scale cause hysteresis to occur. The austenite to martensite transformation (cooling phase of the transformation) occurs over a lower temperature range than the martensite to austenite transformation. An idealised temperature hysteresis is shown in Figure A4.24.

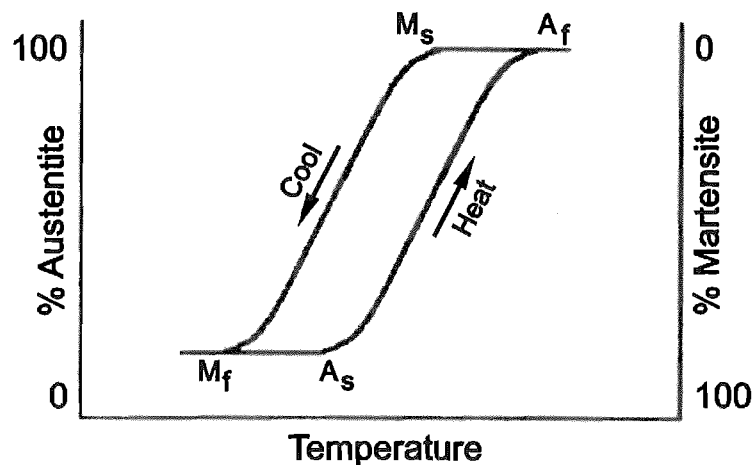


Figure A4.24 Idealised temperature hysteresis.

[Source: Waram²⁰]

The absolute values of the transformation temperatures, the hysteresis width and shape (skew) depend on the alloy composition and processing history. Most shape memory alloys have a hysteresis loop width of 10-50°C. The main causes of hysteresis are the internal friction caused by the movement of the austenite-martensite interface and the creation of defects within the crystal structure.

Hysteresis also denotes an energy dissipation mechanism and associated high damping capacity. The damping capacity is highest in the martensite phase, particularly in the region of M_s . This damping could be used to advantage in energy-absorbing devices.

A4.5.6 Stress-Induced Martensite Limit

As the temperature increases it becomes more difficult to stress-induce martensite. Above a temperature, M_D , the critical stress required to induce martensite is greater than that needed to move dislocations. Therefore, M_D is the highest temperature at which it is possible to form martensite. Thus the temperature range for stress-inducing martensite varies from M_S to M_D .

Permanent deformation of shape memory alloys also starts to occur 25°C above A_F and a significant deterioration in super-elasticity occurs 50°C above A_F . Fortunately A_F temperatures between $10\text{-}30^\circ\text{C}$ are easily achieved using Nitinol allowing excellent super-elasticity to be achieved at body temperature³.

A4.5.7 Summary of Shape Memory Alloy Deformation Processes

The thermo-mechanical behaviour of shape memory alloys is summarized graphically in Figure A4.25. The right hand portion of this graph shows the stress-strain curve corresponding to the deformation of martensite below M_F . The induced strain recovers between A_S and A_F after the applied stress has been removed and the specimen heated, thus allowing Nitinol to exhibit the shape memory effect. At temperatures above M_S , but below M_D , stress-induced martensite is formed, leading to a super-elastic loop with an upper and lower plateau. At temperatures above M_D no stress-induced martensite is formed and the austenite undergoes plastic deformation.

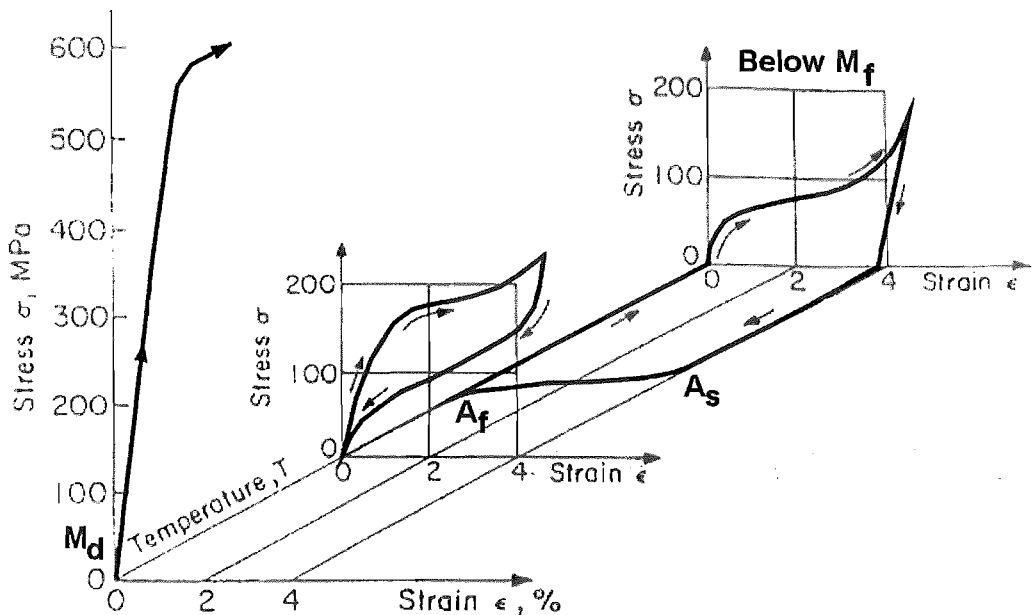


Figure A4.25 Three dimensional stress-strain-temperature diagram for a Nitinol.

Deformation and shape memory behaviour of a Nitinol alloy when deformed below M_F , above A_F and above M_D .

[Source: Wayman et al²¹]

A4.6 Fatigue Characteristics

A4.6.1 SMA Cyclic Behaviour

Shape memory actuators can exhibit two different failure modes when subjected to repeated thermal-mechanical cycling, these are:

- Classic fatigue failure.
- Loss of motion (i.e. recovery strain) with continued thermal cycling.

Classic fatigue failure occurs when a localised defect initiates the formation of a micro-crack which continues to progressively grow as the device is cycled. Ultimately once the crack has grown sufficiently large enough the device fails catastrophically.

Loss of motion failure occurs when a shape memory actuator fails to recover its original form after heating above A_F . The extent of motion loss that occurs with thermal cycling is dependent on the applied stress. Waram²⁰ found that Nitinol spring actuators thermally cycled with a shear stress of 172 MPa experienced a loss in motion of approximately 15% after 100,000 cycles. This loss of motion was linear with the logarithm of the number of cycles, with a large percentage of the total loss of motion occurring in the first few thousand cycles.

A4.6.2 Super-Elastic Cyclic Behaviour

It has been found that during super-elastic cycling of Nitinol alloys, parameters such as the maximum loading plateau stress and the available stored energy can decrease. These changes in the materials properties have been reported to occur relatively rapidly during the initial cycles, but after approximately 100 cycles these changes become less noticeable³.

Shape memory alloys also fail as a result of fatigue damage during super-elastic cycling. As described in Section A4.2.8, shape memory alloys perform better in strain controlled rather than stress controlled environments. Figure A4.26 shows the fatigue life for a 50% Ni-Ti alloy (atomic) in a strain controlled environment at various temperatures. From this graph a trend of decreasing fatigue life with increasing temperature can also be observed.

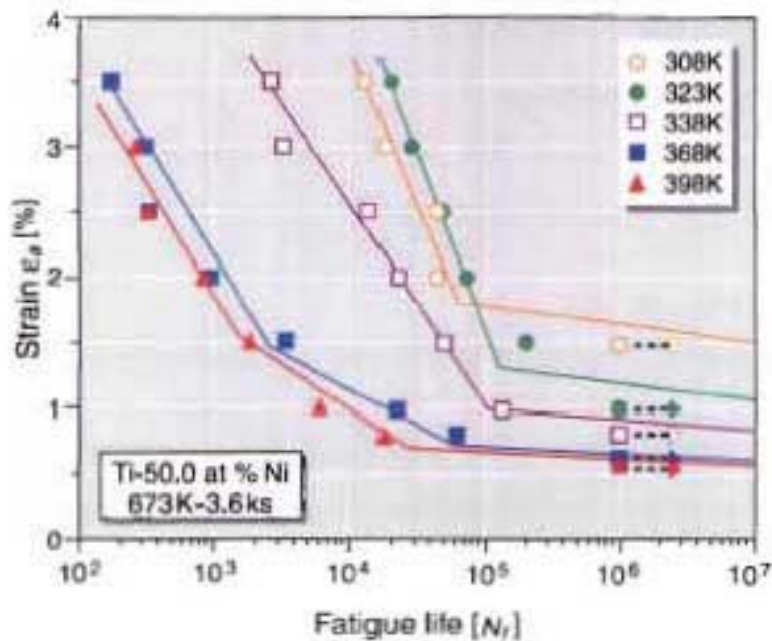


Figure A4.26 Strain controlled fatigue.

The effect of strain on the rotary bending fatigue life of Ti-50at%Ni alloy at various test temperatures.

The endurance limit increases with decreasing test temperature.

[Source: Pelton et al¹⁰]

Figure A4.27 shows the fatigue performance of a 50.9% Ni/Ti alloy (atomic) in a stress controlled environment at three different temperatures. From this plot it can be seen that to ensure a fatigue life in excess of 10^6 cycles at 293K (20°C) the applied stress must be below 200MPa.

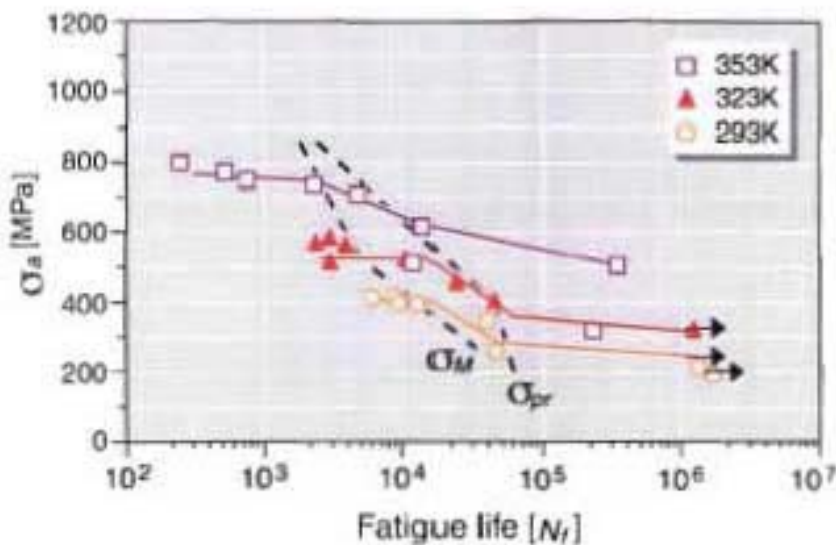


Figure A4.27 Stress controlled fatigue.

The influence of stress on the fatigue life for rotary bending of Ti-50.9at%Ni alloy.

[Source: Pelton et al¹⁰]

A4.7 Biocompatibility

A number of *in-vivo* and *in-vitro* studies have been carried out to investigate the biocompatibility of Nitinol alloys. The results of these studies are often varied, inconclusive and recommend further studies be carried out. However, some broad generalizations can be made from the literature reviewed during the course of this project, these include:

- Equi-atomic nickel-titanium alloys exhibit a better corrosion resistance than austenitic stainless steels and similar corrosion resistance to titanium-based alloys^{1,8,11,12,19}.
- Histological analyses of tissues recovered after *in-vivo* studies tend not to exhibit any adverse reactions^{1,13}.
- Surface preparation and roughness of components can affect biocompatibility with surface nickel levels varying depending on the finishing process used^{12,18,19}.
- Nickel-Titanium alloys exhibit good biocompatibility with human osteoblasts and fibroblasts^{11,14}.
- Nitinol induces no toxic effects, decrease in cell proliferation and do not inhibit the growth of cells in contact with the metal surface^{1,13,14}.
- Although toxic, the nickel in nickel-titanium alloys does not adversely affect biocompatibility due to the very stable TiO₂ layer formed^{13,19}.

Also despite the suggestions that further studies be carried out, most authors state that nickel-titanium alloys appear to be suitable for *in-vivo* use.

A4.8 Conclusions

Nitinol is a useful material for the design and manufacture of medical implants as many of the properties it exhibits are unique including:

- Shape Memory Effect
- Thermal Deployment
- Biased Stiffness
- Kink Resistance

Other important properties exhibited by Nitinol are its biocompatibility and low stiffness. This low stiffness (elastic modulus) allows stress-shielding effects on surrounding bone to be reduced in well designed implants.

Some design tables are available for designing Nitinol tension and compression coil springs. However even with the use of such design tables, the calculation of loads and deflections for Nitinol springs is considered computationally difficult and in most cases only approximations can be made. Processing effects play a large part in determining the performance of Nitinol devices. As a result of these factors the design and manufacture of Nitinol implants is often noted as being an empirical process.

The key disadvantage when considering Nitinol for use in the intervertebral disc implant is the low fatigue limit exhibited in stress controlled environments. To produce a Nitinol intervertebral disc implant with a fatigue life in excess of 100,000,000 cycles the applied stress would have to be approximately 200 MPa.

As a result of this poor fatigue performance and the difficulties associated with designing Nitinol devices, the decision was made to eliminate Nitinol as being a viable material selection for the intervertebral disc implant.

A4.9 References

1. Castleman L S, Motzkin S M, Alicandri F P, Bonawit V L, *Biocompatibility of Nitinol Alloy as an implant material*. J Biomed Mater Res, 1976. Vol 10: pp 695-731.
2. Duerig T W, Pelton A R, Corporation N D, *Ti-Ni shape memory alloys*, in Boyer R, Welsch G, and Collings E W (Eds). *Material Properties Handbook - Titanium Alloys*, 1994, ASM International: Materials Park, OH 44073-0002, USA. pp 1035-1048.
3. Duerig T W, Pelton A R, Stöckel D, *The utility of super-elasticity in medicine*. Biomedical Materials and Engineering, 1996. Vol 6: pp 255-266.
4. Duerig T W, Pelton A R, Stöckel D. *Superelastic Nitinol for medical devices*. Devicelink.com, Updated: 1997 [cited Mar 2003]. Available from <http://www.devicelink.com/mpb/archive/97/03/003.html>.
5. Duerig T W, Zadno G R, in Duerig T W, Melton K N, et al. (Eds). *Engineering Aspects of Shape Memory Alloys*, 1990, Butterworth-Heinemann Ltd: Boston. pp 369.
6. Fukuyo S, *Shape Memory Implants*, in Duerig T W, Melton K N, et al. (Eds). *Engineering Aspects of Shape Memory Alloys*, 1990, Butterworth-Heinemann Ltd: Boston. pp 470.
7. Gil F J, Panell J A, *Shape memory alloys for medical applications*. Proc Instn Mech Engrs, 1998. Vol 212 (Part H): pp 473-488.
8. Gyunter V E, Itin V I, Monasevich L A, Yu I, *Shape memory effects and their application in medicine*, 1992, Nauka: Novosibirsk, Russia. pp 600-602.
9. Hodgson D E, *Using shape memory alloys*. 1988, Sunnyvale, CA, USA: Shape Memory Applications, Inc.
10. Pelton A R, DiCello J, Miyazaki S, *Optimisation of processing and properties of medical grade Nitinol wire*. Min Invas Ther & Allied Technol, 2000. Vol 9 (1): pp 107-118.
11. Putters J L M, Kaulesar D M, Zeeuw G R D, Bijma A, *Comparative cell culture effects of shape memory metal (Nitinol), nickel and titanium: a biocompatibility estimation*. European Surgical Research, 1992. Vol 24 (6): pp 378-382.
12. Rondelli G, Vicentini B, Cigada A, *The corrosion behaviour of Nickel Titanium shape memory alloys*. Corrosion Science, 1990. Vol 30 (8/9): pp 805-812.
13. Ryhanen J, Kallionen M, Tuukkanen J, Junila J, Niemela E, Sandvik P, Serlo W, *In vivo biocompatibility evaluation of nickel-titanium shape memory metal alloy - muscle and perineural tissue responses and capsule membrane thickness*. Journal of Biomedical Materials Research, 1998. Vol 41 (3): pp 481-488.

14. Ryhanen J, Niemi E, Serlo W, Niemela E, Sandvik P, Pernu H, Salo T, *Biocompatibility of Nickel-Titanium shape memory metal and its corrosion behaviour in human cell cultures*. Journal of Biomedical Materials Research, 1997. Vol 35 (4): pp 451-457.
15. Speck K, Fraker A, *Anodic polarization behaviour of Ni-Ti and Ti-6Al-4V in simulated physiological solutions*. J Dent Res, 1980. Vol 59 (19): pp 1590.
16. Stockel D, Yu W, *Superelastic Ni-Ti wire*. Wire J Int, 1991. pp 45-50.
17. Tolomeo D, Davidson S, Santinoranont M. 2000. *Cyclic properties of superelastic Nitinol: design implications*. SMST-2000: Proceedings of the International Conference on Shape Memory and Superelastic Technologies, Pacific Grove, California. pp 471-476.
18. Trigwell S, Hayden R D, Nelson K F, Selvaduray G, *Effects of surface treatment on the surface chemistry of NiTi alloy for biomedical applications*. Surface & Interface Analysis, 1998. Vol 36 (7): pp 483-489.
19. Venugopalan R, Trepanier C, *Assessing the corrosion behaviours of Nitinol for minimally-invasive device design*. Min Invas Ther & Applied Technol, 2000. Vol 9 (2): pp 67-74.
20. Waram T C, *Actuator design using shape memory alloys*. 2nd (Metric) Edition. 1993, 1063 King St. W., Suite 204, Hamilton, Ontario L8S 1L8, Canada: T.C. Waram.
21. Wayman C M, Duerig T W, *An introduction to martensite in shape memory*, in Duerig T W, Melton K N, et al. (Eds). *Engineering Aspects of Shape Memory Alloys*, 1990, Butterworth-Heinemann Ltd: Boston. pp 5-10.
22. *Personal Communication*, Yun M. *Technical advice - Nitinol.com*, Fremont, CA, 9 August 2000.

Appendix 5 – Sample Z-Spring Calculation

This appendix details the analytical analysis of the metallic Z-Spring intervertebral disc concept to determine angular stiffness and peak stress relationships. The effects of varying the spring geometry are also discussed. However, it was determined that there are no combinations of length and radius which allow both the stiffness and peak stress requirements to be met.

A5.1 Analysis of the Z-Spring Concept

When the patient is standing upright a uniformly distributed load (UDL) will be applied to intervertebral disc implant, this load was specified to be 600 N in Section 4.1.1. A moment (M_{Ang}) will also be applied to the implant during angular deflections. Figure A5.1 shows these two loads applied to the Z-Spring concept.

The magnitude of the moment can be determined from the stiffness coefficients specified in Section 4.1.7. For example, during flexion the ideal stiffness of the implant was specified to be 2 Nm per degree. That is, the application of a 2 Nm moment should cause a 1 degree deflection of the spring.



Figure A5.1 Schematic showing the loads applied to the Z-Spring concept.

The Z-Spring supports a uniformly distributed load (UDL) due to the patient's weight and a moment (M_{Ang}) during angular deflections.

The application of loads will result in the Z-spring deflecting and the generation of stresses.

Figure A5.2 shows a simplified version of the Z-Spring geometry with the endplates removed. This system was broken down into three sections for analysis purposes. These sections were a cantilevered arc (A-B), a straight cantilever (B-C) and another cantilevered arc (C-D).

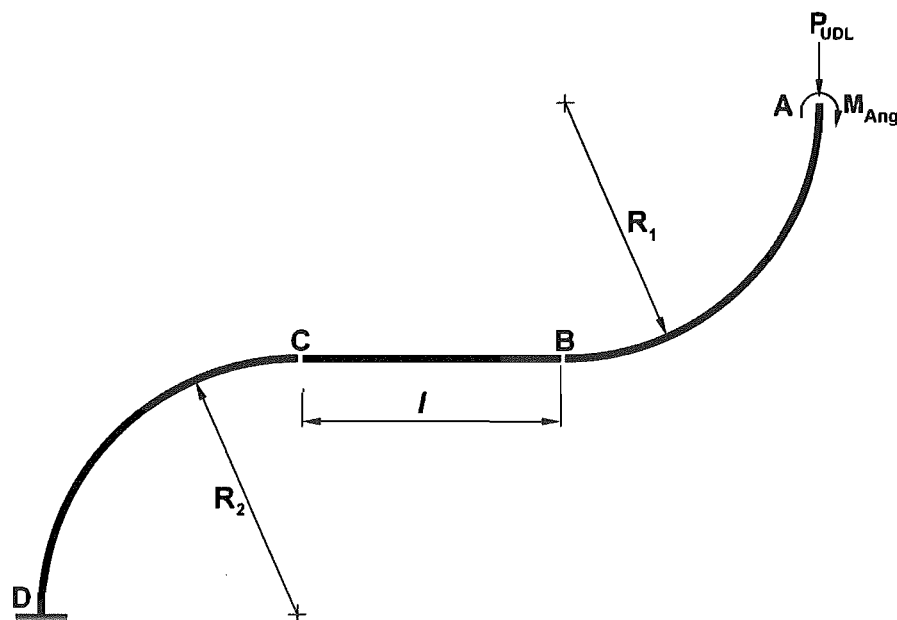


Figure A5.2 Simplified Z-Spring geometry.

With the compressive load (P_{UDL}) and moment (M_{Ang}) applied, the deflections for each component of the Z-Spring were found analytically using Castigliano's Second Theorem which states.

$$\Delta = \int_0^l \left(\frac{M}{EI} \right) \frac{\partial M}{\partial P} dx$$

Or in radial terms

$$\Delta = \int_0^\theta \left(\frac{M}{EI} \right) \frac{\partial M}{\partial P} R d\theta$$

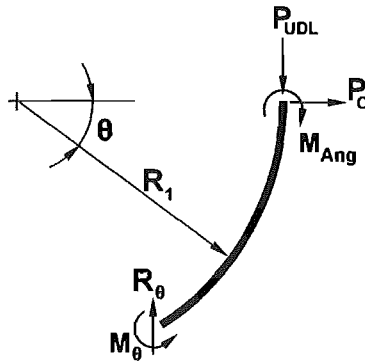
These deflection relationships were then used to determine the stiffness of the whole z-spring. The peak stress which results from the application of the loads was also determined.

A5.2 Arc Deflections (A-B)

The horizontal and vertical tip deflections of the arc section A-B when subject to a compressive load and moment were found as detailed below.

Horizontal Displacement

To determine the horizontal displacement (Δx_{A-B}) an imaginary point load P_0 was applied at the free end of the arc section.



Using Castigliano's Second Theorem

$$\Delta x_{A-B} = \frac{\partial U}{\partial P_0} = \int_0^{\frac{\pi}{2}} \left(\frac{M_\theta}{EI} \right) \frac{\partial M_\theta}{\partial P_0} R_1 d\theta$$

$$\text{where } M_\theta = M_{Ang} + P_{UDL} R_1 (1 - \cos \theta) + P_0 R_1 \sin \theta$$

$$\text{and } \frac{\partial M_\theta}{\partial P_0} = R_1 \sin \theta$$

Now $P_0 = 0$, so

$$M_\theta = M_{Ang} + P_{UDL} R_1 (1 - \cos \theta)$$

Therefore

$$\Delta x_{A-B} = \int_0^{\frac{\pi}{2}} \left(\frac{M_{Ang} + P_{UDL} R_1 (1 - \cos \theta)}{EI} \right) (R_1 \sin \theta) R_1 d\theta$$

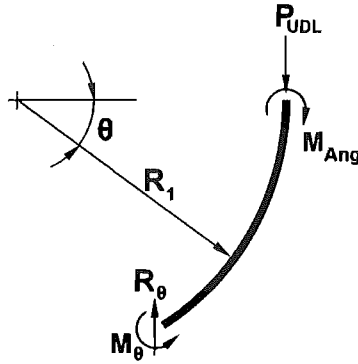
$$\Delta x_{A-B} = \frac{R_1^2}{EI} \int_0^{\frac{\pi}{2}} (M_{Ang} \sin \theta + P_{UDL} R_1 \sin \theta - P_{UDL} R_1 \cos \theta \sin \theta) d\theta$$

$$\Delta x_{A-B} = \frac{M_{Ang} R_1^2}{EI} + \frac{P_{UDL} R_1^3}{2EI}$$

(Eq 5.1)

Vertical Displacement

Similarly, to determine the vertical displacement (Δy_{A-B}) at Point A, Castigliano's Second Theorem was solved with respect to P_{UDL} .



$$\Delta y_{A-B} = \frac{\partial U}{\partial P_{UDL}} = \int_0^{\frac{\pi}{2}} \left(\frac{M_{\theta}}{EI} \right) \frac{\partial M_{\theta}}{\partial P_{UDL}} R_1 d\theta$$

where $M_{\theta} = M_{Ang} + P_{UDL} R_1 (1 - \cos \theta)$

and $\frac{\partial M_{\theta}}{\partial P_{UDL}} = R_1 (1 - \cos \theta)$

Therefore

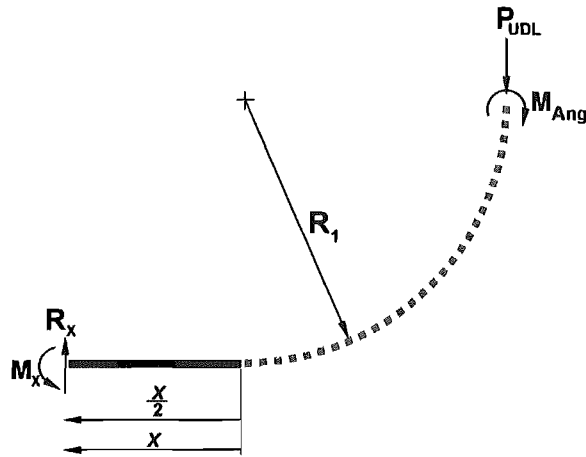
$$\Delta y_{A-B} = \int_0^{\frac{\pi}{2}} \left(\frac{M_{Ang} + P_{UDL} R_1 (1 - \cos \theta)}{EI} \right) (1 - \cos \theta) R_1^2 d\theta$$

$$\Delta y_{A-B} = \frac{R_1^2}{EI} \int_0^{\frac{\pi}{2}} (M_{Ang} - M_{Ang} \cos \theta + P_{UDL} R_1 - 2P_{UDL} R_1 \cos \theta + P_{UDL} R_1 \cos^2 \theta) d\theta$$

| | |
|--|----------|
| $\Delta y_{A-B} = \frac{M_{Ang} R_1^2}{4EI} (2\pi - 4) + \frac{P_{UDL} R_1^3}{4EI} (3\pi - 8)$ | (Eq 5.2) |
|--|----------|

A5.3 Cantilever Deflections (B-C)

The vertical displacement (Δy_{B-C}) at point A which results from the straight cantilever section B-C deflecting was determined as detailed below.



Using Castigliano's Second Theorem

$$\Delta y_{B-C} = \frac{\partial U}{\partial P_{UDL}} = \int_0^l \left(\frac{M_x}{EI} \right) \frac{\partial M_x}{\partial P_{UDL}} dx$$

$$\text{where } M_x = M_{Ang} + P_{UDL}(R_1 + x)$$

$$\text{and } \frac{\partial M_x}{\partial P_{UDL}} = R_1 + x$$

Therefore

$$\Delta y_{B-C} = \int_0^l \left(\frac{M_{Ang} + P_{UDL}(R_1 + x)}{EI} \right) (R_1 + x) dx$$

$$\Delta y_{B-C} = \frac{1}{EI} \int_0^l (M_{Ang} + P_{UDL}R_1 + P_{UDL}x)(R_1 + x) dx$$

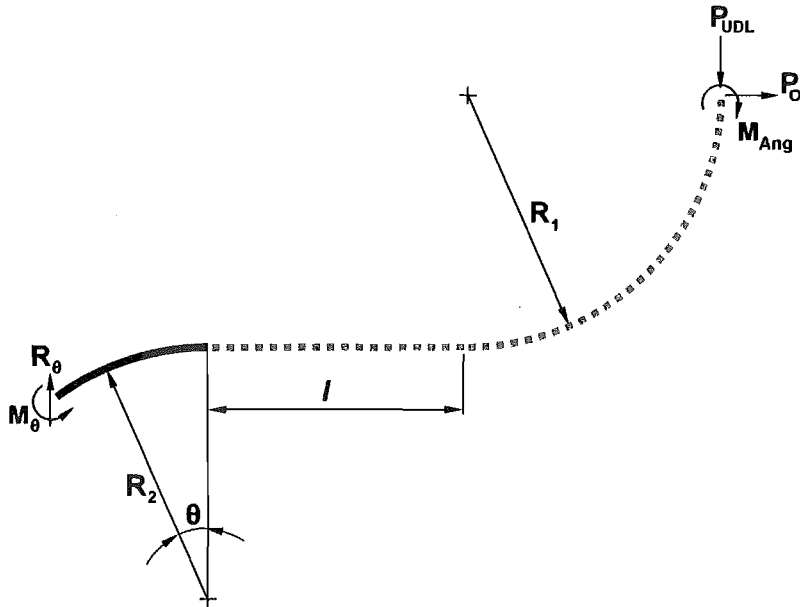
$$\boxed{\Delta y_{B-C} = \frac{M_{Ang}l}{2EI} (2R_1 + l) + \frac{P_{UDL}l}{3EI} (3R_1^2 + 3R_1l + l^2)} \quad (\text{Eq 5.3})$$

A5.4 Arc Deflections (C-D)

The horizontal and vertical displacements at Point A which result from the arc section C-D deflecting were determined as detailed below.

Horizontal Displacement

To determine the horizontal displacement (Δx_{C-D}) an imaginary point load P_0 was applied at Point A.



Using Castigliano's Second Theorem

$$\Delta x_{C-D} = \frac{\partial U}{\partial P_0} = \int_0^{\frac{\pi}{2}} \left(\frac{M_\theta}{EI} \right) \frac{\partial M_\theta}{\partial P_0} R_2 d\theta$$

$$\text{where } M_\theta = M_{Ang} + P_{UDL}(R_1 + l + R_2 \sin \theta) + P_0(R_1 + R_2 - R_2 \cos \theta)$$

$$\text{and } \frac{\partial M_\theta}{\partial P_0} = R_1 + R_2 - R_2 \cos \theta$$

Now $P_0 = 0$, so

$$M = M_{Ang} + P_{UDL}(R_1 + l + R_2 \sin \theta)$$

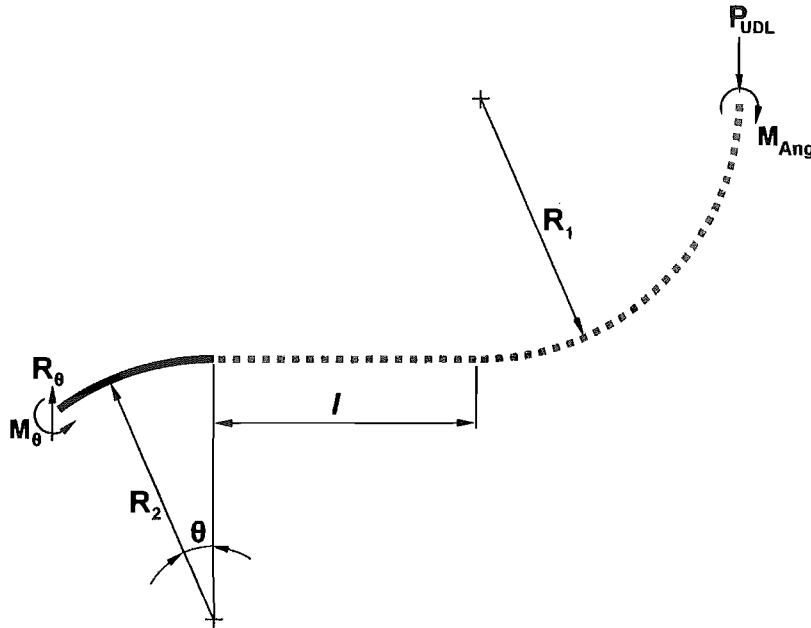
$$\Delta x_{C-D} = \int_0^{\frac{\pi}{2}} \left(\frac{M_{Ang} + P_{UDL}(R_1 + l + R_2 \sin \theta)}{EI} \right) (R_1 + R_2 - R_2 \cos \theta) R_2 d\theta$$

$$\Delta x_{C-D} = \frac{M_{Ang} R_2}{2EI} (\pi R_1 + \pi R_2 - 2R_2) + \frac{P_{UDL} R_2}{2EI} (\pi R_1^2 + \pi R_1 R_2 + \pi R_1 l + \pi R_2 l - 2R_2 l + R_2^2)$$

(Eq 5.4)

Vertical Displacement

Similarly, to determine the vertical displacement (Δy_{C-D}) at Point A, Castigliano's Second Theorem was solved with respect to P_{UDL} .



$$\Delta y_{C-D} = \frac{\partial U}{\partial P_{UDL}} = \int_0^{\frac{\pi}{2}} \left(\frac{M_\theta}{EI} \right) \frac{\partial M_\theta}{\partial P_{UDL}} R_2 d\theta$$

where $M_\theta = M_{Ang} + P_{UDL}(R_1 + l + R_2 \sin \theta)$

and $\frac{\partial M_\theta}{\partial P_{UDL}} = R_1 + l + R_2 \sin \theta$

Therefore

$$\Delta y_{C-D} = \int_0^{\frac{\pi}{2}} \left(\frac{M_{Ang} + P_{UDL}(R_1 + l + R_2 \sin \theta)}{EI} \right) (R_1 + l + R_2 \sin \theta) R_2 d\theta$$

$$\Delta y_{C-D} = \frac{M_{Ang} R_2}{2EI} (\pi R_1 + \pi l + 2R_2) + \frac{P_{UDL} R_2}{4EI} (2\pi R_1^2 + 4\pi R_1 l + 2\pi l^2 + \pi R_2^2 + 8R_1 R_2 + 8R_2 l)$$

(Eq 5.5)

A5.5 Total Deflections

Using Equations 5.1 to 5.5 the total deflection of the Z-Spring system at point A were found to be:

$$\Delta x_{@A} = \frac{M_{Ang}}{2EI} (2R_1^2 + \pi R_2^2 - 2R_2^2 + \pi R_1 R_2) + \frac{P_{UDL}}{2EI} (R_1^3 + \pi R_2^2 l - 2R_2^2 l + \pi R_1^2 R_2 + \pi R_1 R_2^2 + \dots \\ \dots + \pi R_1 R_2 l + R_2^3)$$

$$\Delta y_{@A} = \frac{M_{Ang}}{2EI} (\pi R_1^2 + l^2 + 2R_1 l + \pi R_1 R_2 + \pi R_2 l) + \frac{P_{UDL}}{12EI} (9\pi R_1^3 - 24R_1^3 + 4l^3 + 12R_1 l^2 + \dots \\ \dots + 12R_1^2 l + 6\pi R_1^2 R_2 + 12\pi R_1 R_2 l + 3\pi R_2^3 + 6\pi R_2 l^2 + 24R_1 R_2^2 + 24R_2^2 l)$$

And in the unique cases where $R_1 = R_2 = R$

$$\Delta x_{@A} = \frac{M_{Ang} \pi R^2}{EI} + \frac{P_{UDL} R^2}{EI} (R + \pi l - l + \pi R) \quad (\text{Eq 5.6})$$

$$\Delta y_{@A} = \frac{M_{Ang}}{2EI} (2\pi R^2 + l^2 + 2Rl + \pi Rl) + \frac{P_{UDL}}{6EI} (9\pi R^3 + 2l^3 + 6Rl^2 + 18R^2 l + 6\pi R^2 l + 3\pi Rl^2) \quad (\text{Eq 5.7})$$

When determining the stiffness of the Z-Spring only the deflections which results from the application of the moment, M_{Ang} , are of interest. Therefore from (Eq 5.7) the vertical (Δy_{Ang}) and angular ($\Delta \theta_{Ang}$) deflections which result from the application of M_{Ang} were found to be:

$$\Delta y_{Ang} = \frac{M_{Ang}}{2EI} (2\pi R^2 + l^2 + 2Rl + \pi Rl) \quad (\text{Eq 5.8})$$

$$\Delta \theta_{Ang} = \text{Tan}^{-1} \left(\frac{\Delta y_{Ang}}{2R + l} \right)$$

$$\Delta \theta_{Ang} = \text{Tan}^{-1} \left(\frac{M_{Ang} (l + \pi R)}{2EI} \right) \quad (\text{Eq 5.9})$$

Therefore the overall stiffness of the Z-Spring system is:

$$\text{Stiffness} = \frac{M_{Ang}}{\text{Tan}^{-1} \left(\frac{M_{Ang} (l + \pi R)}{2EI} \right)} \quad (\text{Eq 5.10})$$

A5.6 Peak Stress

The peak stress was found to occur at point D, the fixed end of the second arc component, as indicated in Figure A5.3.

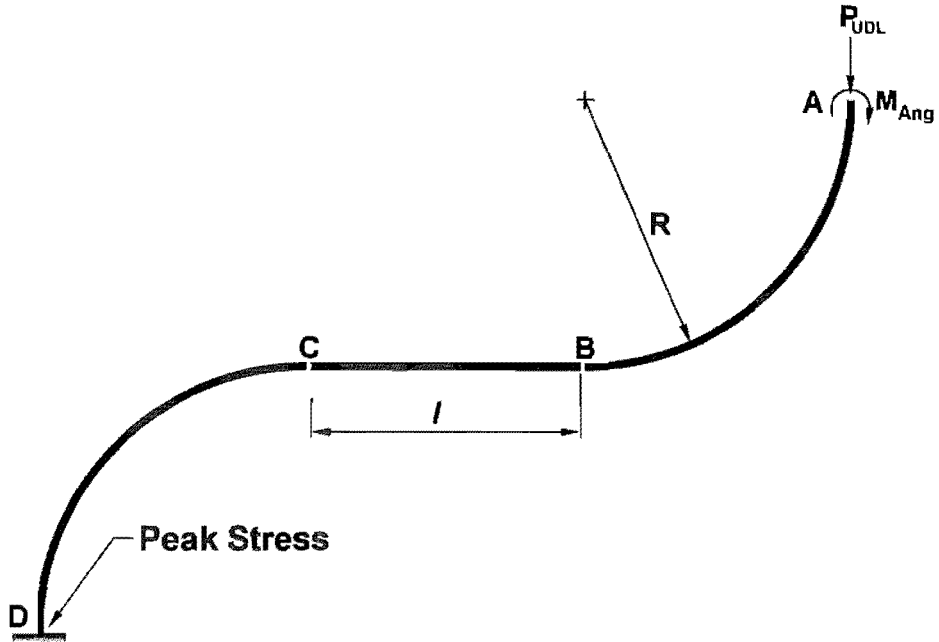


Figure A5.3 Z-Spring peak stress location.

As previously determined in Section A5.4 the moment for this component of the spring (C-D) was determined as being:

$$M_{\theta} = M_{Ang} + P_{UDL}(R_1 + l + R_2 \sin \theta)$$

Hence if $R_1 = R_2 = R$ the peak moment and stress can be found to be:

$$M_{Max} = M_{Ang} + P_{UDL}(2R + l)$$

and

$$\sigma_{Max} = \frac{(M_{Ang} + P_{UDL}(2R + l))y}{I} \quad (\text{Eq 5.11})$$

A5.7 Effect of Varying Length and Radius

The effects of varying the Z-Spring geometry were determined using the stiffness and peak stress relationships (Equations 5.10 & 5.11). The two most critical variables are the length (l) and radius (R).

The maximum implant envelope was previously defined in Section 4.1.6 to be 25 x 35 x 10 mm (Sagittal Diameter x Transverse Diameter x Height). Given these size restrictions the Z-Spring length parameter (l) was set to be less than 10 mm and the radius (R) less than 5 mm.

The stiffness and stress values for a range of length and radius values were then determined and plotted as shown in Figures A5.4 and A5.5. For the purposes of this analysis the Modulus of Elasticity (E) was set to be 115 GPa and a rectangular spring cross section (Width 15 mm x Thickness 2 mm) was used.

Figure A5.4 shows the effect varying the length and radius has on the stiffness of the Z-Spring. As detailed in Section A5.1 the intervertebral disc implant should have a stiffness of 2 Nm/deg during flexion. In Figure A5.4, values which are less than or equal to this limit are highlighted in green. From this plot it can be seen a small number of configurations meet this stiffness requirement.

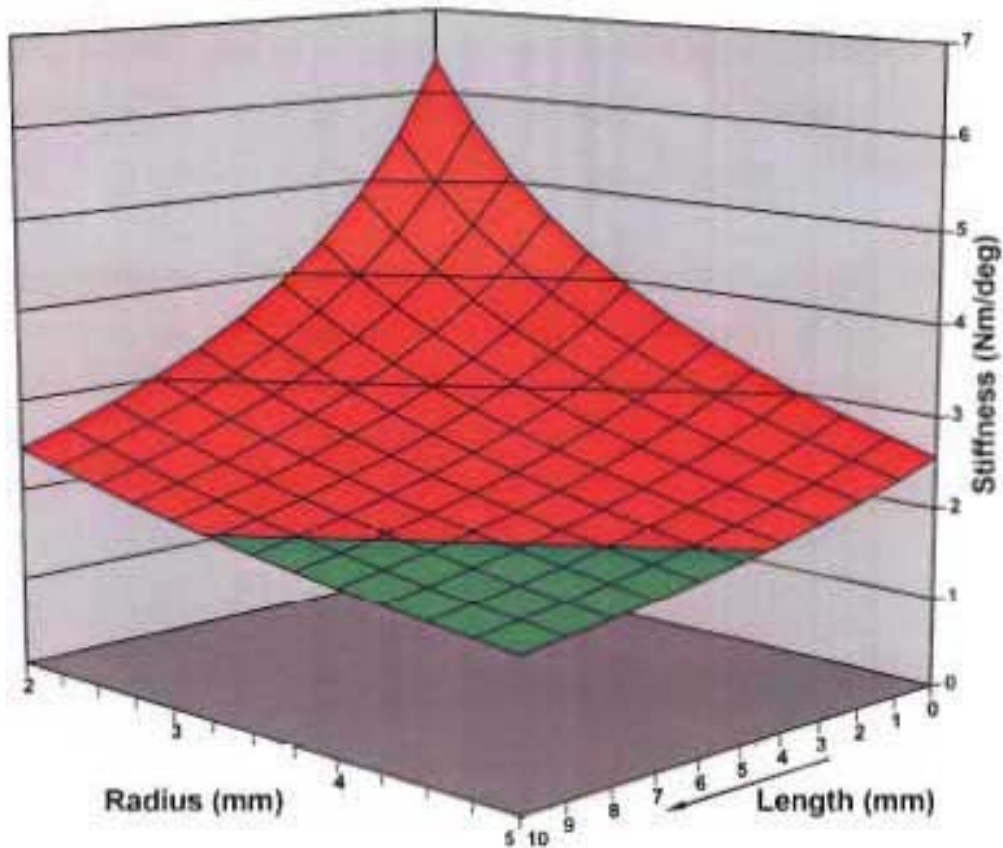


Figure A5.4 Z-Spring stiffness as a function of length and radius.

For flexion the specified stiffness was 2Nm/deg, configurations which result in a stiffness less than this value are highlighted in green.

In Section 5.2 it was noted that Ti-6Al-4V had the highest fatigue limit of the materials investigated. In order to achieve a life in excess of 100 million cycles using this material, the peak stress in the Z-Spring should be less than 600 MPa for a lamellar microstructure. Figure A5.5 shows the peak stress in the Z-Spring for different length and radius values. The values shown apply for $M_{\text{Ave}} = 2 \text{ Nm}$ and $P_{\text{UDL}} = 600 \text{ N}$. Configurations which result in a stress less than 600 MPa are highlighted in green.

It should be noted that for clarity the length axis is reversed when compared to the stiffness plot (Figure A5.4).

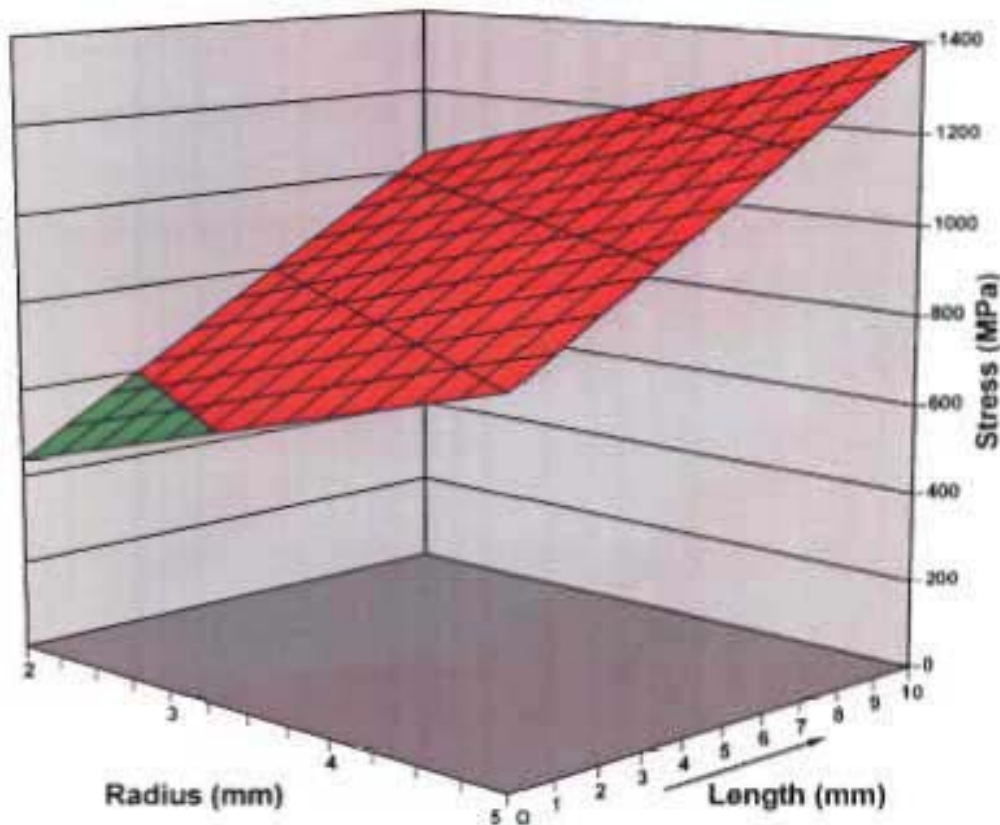


Figure A5.5 Z-Spring peak stress as a function of length and radius.

For Ti-6Al-4V alloy the maximum acceptable stress is 600MPa, configurations which have a stress less than this are highlighted in green.

Note: for clarity the length axis is reversed (compared the stiffness plot).

When Figures A5.4 and A5.5 are compared it can be seen there are no suitable combinations of length and radius which allows both the stiffness and peak stress requirements to be met. The configurations that do meet the stress requirements result in very stiff Z-Springs which would require excessive exertion by the patient in order to bend.

The cross section of the Z-Spring also affects the stiffness and stress values. Reducing the Z-Spring width or depth results in a decrease in stiffness but also causes a significant increase in the peak stress. Conversely increasing the spring cross section causes the stiffness to increase and the peak stress to decrease.

A5.8 Summary

From this analysis it can be seen that the Z-Spring concept presented is not a workable solution for the intervertebral disc implant.

Similar studies were carried out for the other metallic spring concepts shown in Appendix 1. However, as for the Z-Spring concept, the other spring configurations investigated also yielded no workable stiffness and peak stress relationships. Therefore the other metallic spring concepts were also declared to be unsuitable for use as intervertebral disc implants.

Appendix 6 – Evaluation Subtasks

The appendix contains definitions of the evaluation sub-task used in Section 5.2.

Definitions

Support Loads

The implant must be able to support all the applied static and dynamic loads.

Motions

The implant should ideally provide a natural range of motion as detailed in Section 4.1.2

Match Stiffness

The implant should aim to replicate the stiffness of a healthy intervertebral disc. If the stiffness of the disc implant is significantly lower than that of a natural intervertebral disc the stability of the spinal column may be compromised. Conversely, if the implant is too stiff additional exertion will be required for the patient to bend, or alternatively the implant may act as a rigid body and all the deflection will occur at the remaining spinal levels.

Wear Debris

Wear debris products can result in osteolysis, which in turn can lead to the implant loosening or inflammation. Therefore the implant should produce no wear debris.

Endplate

The implant should exert the majority of the forces on the periphery of the intervertebral body, however, a portion of the load should also be distributed across the central portion of the vertebral body endplate to prevent resorption of the underlying trabeculae.

The endplates must also have provisions for short and long term anchoring of the implant to the adjacent vertebral bodies.

Cross Section

The intervertebral disc implant must meet several cross sectional requirements. It should be fully contained within the nucleus pulposus space and the majority of the annulus fibrosus should be preserved. Preservation of the anterior portion of the annulus fibrosus is particularly important as it makes a significant contribution to the stability of the spinal column and load carrying.

Disc Height

The implant should restore the intervertebral disc height immediately after implantation and maintain it for the duration of the implant's life. Failure to do so may result in compression of the nerve roots or incorrect loading of the zygapophysial joints.

Axis of Rotation

The natural axis of rotation for a healthy intervertebral disc is located close to the inferior endplate, as described in Section 4.1.3. The intervertebral disc implant should replicate this where possible.

40 Year Life

To reduce trauma to the patient the intervertebral implant should ideally last 40 years and must be capable supporting all the required motions and loads during this period.

<Blank Page>

Appendix 7 - Initial Bellows Specification

As detailed in Chapter 6, several metallic bellows manufacturers were contacted to determine whether formed or welded bellows could meet the requirements laid out in the specification for the intervertebral disc implant. Initial contact with manufacturers was by phone, followed by a written specification.

The information provided during the phone calls and in the written specification was intentionally kept brief and broadly worded to reduce the possibility of compromising any intellectual property associated with the project. The specification sent to manufacturers is detailed in this appendix.

408

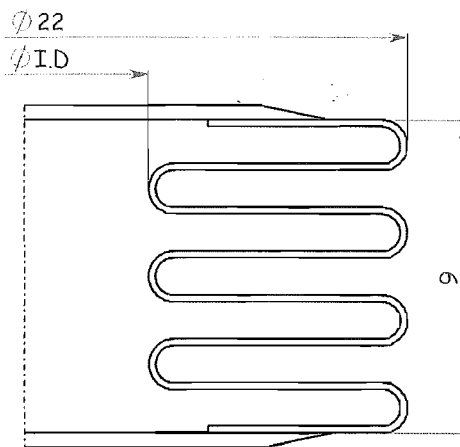
Iain McMillan
PhD Student
Mechanical Engineering
University of Canterbury
Private Bag 4800
Christchurch
New Zealand
Phone: +64 3 364 2987 ext 7257 (day)
Fax: +64 3 343 6182
Email: i.mcmillan@mech.canterbury.ac.nz

Date: XX XXX XXXX

Attn: X XXXXXXX

Further to our conversation yesterday regarding formed/welded bellows I am writing to detail my bellows requirements, in confidence.

The bellows will be required to act as a flexible pressure vessel with both ends capped in close proximity to the convolutions, as shown below.



I am happy for the bellows to be supplied with tangent ends, flanges etc, (i.e. as standard bellows are), as I am able to cut the bellows down to suit my application.

The bellows depicted on the previous page are for illustrative purposes only and the bellows length (9mm) and the outside diameter (22mm) are the only critical dimensions. Other variables can be changed as required, including those listed below.

- Wall thickness.
- Convolution span.
- Convolution pitch.
- Number of convolutions.
- Inside diameter.

The required pressure capabilities, ranges of motion and critical dimensions are detailed on Page 410. I recognise that these details may be insufficient to design an appropriate bellows therefore please do not hesitate to contact me should you have any queries.

I look forward to your reply on this matter.

Regards

Iain McMillan

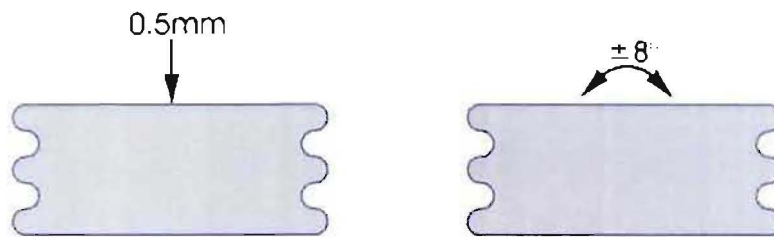
Bellows Specification

Pressure

| | | |
|---------------------|------------|------------------|
| Operating Pressure: | Inside: | 1MPa (approx) |
| | Outside: | Atmospheric |
| Maximum Pressure: | Inside: | 1.75MPa (approx) |
| | Outside: | Atmospheric |
| Shock Pressure: | Infrequent | |

Displacement

| | |
|----------------------------|--|
| Axial Displacement: | 0.5mm |
| Parallel Offset (Lateral): | nil |
| Peak Angular Rotation: | 8° |
| Service Life: | 100 million cycles (angular deflections) |
| Frequency: | <1Hz |



Deformation Modes

Dimensions

| | |
|------------------------|---|
| OD: | 22mm |
| Installed Length: | 10mm |
| Material: | Commercially Pure Titanium (CP-Ti) or Ti-6Al-4V |
| Operating Temperature: | ≈30°C |
| Fluid: | Water (5% aerated) |

The bellows will not normally be angularly deflected. They will have to undergo a maximum angular deflection of 8°, however for the majority of the cycles the deflection will be less than this (≈1-5°).

If necessary the outside diameter of the bellows could be increased to 25mm but ideally the outside diameter should be 22mm as previously specified.

Appendix 8 –Technical Data Sheets

This appendix contains technical data sheets for the following products:

- Silbione 40047
- NuSil Med-1511
- NuSil Med1-4213
- NuSil SP-120
- NuSil SP-124

<Blank Page>

A8.1 Silbione 40047

S I L I C O N E S

**SILBIONE® 40047, 40073, 40074,
40098, 40104**

August 1999

TECHNICAL DATA SHEET

PRODUCT DESCRIPTION

Rhodia's MDM Fluid was designed as a substitute for Dow Corning Medical Grade 360 Fluid. Rhodia's MDM Fluids are pure, clear colorless polydimethylsiloxane. They are available in standard viscosities of 20, 100, 350, 1000, and 12,500 cps. Custom viscosities to 2,000,000 cps are also available. These fluids are ideal for lubrication of critical medical devices. MDM is soluble in a variety of aliphatic, aromatic, chlorinated and oxygenated solvents and is compatible with many pharmaceutical, cosmetic and medical device preparations.

Special features include:

- High purity
- Chemical inertness
- High water repellency
- Low volatility
- Low surface tension
- Low order of toxicity and skin sensitization
- Resistance to decomposition by heat and oxidation
- Good lubrication characteristics for plastics and rubber

BIOCOMPATIBILITY

Our medical implant products are designed and tested to meet many of the ISO 10993 biocompatibility test requirements for long term implantable materials which can create substantial savings in product development testing and time-to-market. All materials used in each manufactured lot are screened beforehand by an MEM tissue culture test. It is the responsibility of the user to perform appropriate confirmatory testing on the final product to determine its safety. Additional testing is available by request.

Our medical grade products are manufactured under a fully traceable quality system that is ISO 9001 Certified. An FDA Master File reference including formulation, manufacturing methods, testing and toxicology is available.

The user must carefully review literature for uses where adverse effects are reported for certain applications of silicone in medical devices. The user of this material must independently determine that any product incorporating this material is safe and effective.

APPLICATIONS

MDM Fluid is intended for use in a variety of medical applications including: lubricant for plastic or rubber devices and instruments, inert protective coating and water repellent film on the skin, and a hydrophobic surface on glass and ceramic substrates.

MDM Fluid can be applied to the barrels of plastic syringes to insure smooth operation of the plunger. It may also be used to lubricate rubber or plastic tubes and metal instruments that are inserted into the body. MDM Fluid is recommended for application to hypodermic needles to allow easy insertion and is ideal for lubricating instruments to permit easier movement of the instrument and to minimize injury to body tissue. MDM Fluid may be used in conjunction with Rhodia's Silbione® 40097 RTV Silicone Lubricant for adherent thin, lubricant release coatings used in applications such as hypodermic needles and scalpel blades.

MDM Fluid can be used as an effective lubricant for the sockets of artificial limbs and eyes. It serves as a surface coating on latex urethral catheters to reduce irritation to the urethra. This product is not a suitable lubricant for repetitive rubbing contact on metals.

MDM Fluid can be used as a condom lubricant. Films of MDM Fluid transmit water vapor readily, yet are highly repellent to water and water-based fluids. They can be formulated into effective barrier creams and sprays to protect the skin from water, waterborne irritants and from many solvents.

MDM Fluid is ideal for treating the surfaces of glass, ceramics, enamels, plastics, rubbers, and metals. The fluid film provides a temporary water repellent, biologically inert barrier over the treated material. This barrier lessens damage to blood and delays its clotting.

MDM Fluid is an effective defoamer for many foaming fluids, both aqueous and nonaqueous. Rhodia also supplies specially formulated defoamers for medical applications requiring high defoaming efficiency.

BLENDING

MDM Fluid permits any desired blending of different viscosity grades. Although the fluid is available in a number of standard viscosity grades, occasionally an application will call for a fluid of a viscosity between the standard grades.

LOT TESTING

Each production lot is certified as having passed cytotoxicity and physical properties. Additional testing is available upon request.

TYPICAL PROPERTIES

These values are not intended for use in preparing specifications.

| <u>Test</u> | <u>Results</u> |
|--------------------------------|----------------------|
| APPEARANCE | CRYSTAL CLEAR LIQUID |
| COLOR, BARRETT | < 2.5 |
| SPECIFIC GRAVITY @ 77°F (25°C) | |
| 20 cps | 0.95 |
| 100 cps | 0.98 |
| 350, 1000, 12,500 cps | 0.98 |
| REFRACTIVE INDEX | 1.400 - 1.405 |
| VISCOSITY @ 77°F (25°C) | |
| 20 AND 12,500 cps | ±10% OF NOMINAL |
| 100, 350 AND 1000 cps | ±5% OF NOMINAL |
| PART NUMBERS: | |
| 20 cps = 40074 | |
| 100 cps = 40104 | |
| 350 cps = 40073 | |
| 1000 cps = 40047 | |
| 12,500 cps = 40098 | |
| VOLATILE CONTENT | 20 cps < 15% |
| | 100 - 1.25k < 15% |
| CYTOTOXICITY | NON TOXIC |

PACKAGING AND STORAGE

Packaging is available in 8, 40, and 420 lbs. epoxy lined metal containers. Suggested retest at twelve months from the date of shipment.

NOTE: All information is offered in good faith, without guarantee or obligation for the accuracy or sufficiency thereof, or the results obtained, and is accepted at user's risk. Nothing herein shall be construed as a recommendation for uses which infringe patents or as extending a license under valid patents.



SILBIONE® is a Trademark of Rhodia

Rhodia is Registered to ISO 9001

320 W. Stanley Avenue
Ventura, CA 93001
TEL: 805-653-5638 -- FAX: 805-653-2315

A8.2 NuSil Med-1511



10000 Parkway • Fremont, CA 94538

NuSil Technology
 2010 Quail Lane • Cupertino, CA 95014
 408/254-0700 • 408/254-0669 fax
 www.nusil.com

© 2004 NuSil Technology Company

Product Profile

MED-1511 and MED-2000 Silicone Adhesive

Description:

NuSil Technology's MED-1511 and MED-2000 are one component, self-leveling silicone RTV materials for bonding silicone elastomers to each other and to some synthetics and metals.

MED-1511 and MED-2000 contain no solvents and cure at room temperature upon exposure to atmospheric moisture. During the curing process, the silicone adhesives release acetic acid vapor as a by-product. After final cure, the resulting silicone elastomers possess the appearance, texture and general composition of many conventional silicone elastomers.

Advantages of these products include:

- Cures at room temperature at moderate relative humidity
- Self-leveling flow
- Provided in various sizes of ready-to-use tubes for easy application

Applications:

NuSil Technology MED-1511 and MED-2000 are used for bonding silicone elastomers to each other and to some synthetics or metals. MED-1511 and MED-2000 are produced without any additives and do not contain solvents or plasticizers.

The purchaser should thoroughly test products made in part or otherwise incorporating NuSil Technology MED-1511 and MED-2000 to determine the

acceptability of the products' performance in a specific application.

Instructions For Use:

Surface Preparation

Surfaces to be bonded or built-up with silicone adhesive should be cleaned thoroughly to remove possible surface contaminants. Use a non-oily cleaner or mild soap. Do not use synthetic detergents or oil-based soaps, as these soaps may be absorbed and may subsequently leach out. Rinse copiously with hot water and follow by rinsing thoroughly with distilled water. Compatible degreasers, such as 1,1,1-trichloroethane, may be used to clean metal surfaces.

The catalytic system of the adhesive is inhibited by traces of alcohol. For this reason alcohols should not be stored near the work site.

Bonding Applications:

Spread a layer of silicone adhesive on one of the surfaces. Squeeze together both surfaces to be bonded. Apply sufficient pressure to ensure full contact, without forcing the silicone adhesive out from between the pieces.

Curing Time:

Curing or vulcanization time depends upon the thickness of the silicone adhesive layer, the relative humidity, and the accessibility of atmospheric moisture to the curing adhesive.

For sections of typical thickness, a relative humidity level between 20 to 60 percent is recommended to cure the adhesive at room temperature, since controlled atmospheric moisture is an important factor for vulcanization.

Usually the adhesive forms a tack-free outer skin for thick section films within a few minutes after application. The vulcanization rate will be slowed where very thin films are exposed to excessive humidity ($\geq 80\%$ relative air humidity). For films below 80 microns, the relative air humidity should be within 30% - 50%.

Because MED-1511 and MED-2000 cure upon exposure to moisture vapor, the tubes must be kept tightly closed when not in use. A plug of cured material may form in the tip of the tube. Remove or dispense the plug from the tube before using.

Packaging:

The acidic nature of MED-1511 and MED-2000 provides a natural bactericidal effect. While MED-1511 and MED-2000 containers may be relatively free of microorganisms, it cannot be considered sterile unless subjected to a validated sterilization process. When the adhesive is fully cured it can withstand sterilization with ethylene oxide, dry heat, or steam autoclaving.

The size and shape of fabricated articles must be considered when establishing conditions of sterilization. Larger quantities and larger parts may require longer periods of heating and may retain ethylene oxide longer than small parts. It is the responsibility of the user to determine the outgassing time required for a particular application if ethylene oxide sterilization methods are used.

MED-1511 AND MED-2000 are available in non-sterile tubes.

Slab

1/10 Gallon Tube
Two Ounce Tube
Two Ounce Case (24 x 2 oz)
Five Ounce Tube
Five Ounce Case (24 x 5 oz)
Six Ounce Tube
Six Ounce Case (24 x 6 oz)
Twelve Ounce Tube
Eight Gram Tube

Eight Gram Case (36 x 8mm)
Five Gallon Container

Caution:

MED-1511 and MED-2000 should not be used in the uncured state to repair or encapsulate living tissue in the body since acetic acid is evolved in vapor form during the cure process. On contact, uncured adhesive irritates eyes. Avoid contact with eyes and skin. Contact lens wearers should take appropriate precautions. In case of contact, flush eyes with water. Call a physician. Remove from skin with dry cloth or paper towel. Adhesive releases acetic acid (vinegar-like odor) during cure. Keep out of reach of children.

Shipping Limitations:

None

Typical Properties as Supplied:

| | <u>MED-1511</u> | <u>MED-2000</u> |
|--|-----------------|-----------------|
| Tack Free (minutes) | 20 | 14 |
| Flow (in./1 min.) | 1 | 3 |
| Specific Gravity | 1.10 | 1.08 |
| Durometer, Shore A | 25 | 30 |
| Tensile Strength (lb/in ²) / MPa | 1100 / 7.6 | 900 / 6.2 |
| Elongation, % | 750 | 600 |
| Tear Strength (lb/in) / kN/m | 60 / 10.5 | 50 / 8.8 |

Test Methods:

| | <u>MED-1511</u> | <u>MED-2000</u> |
|-----------------------|-----------------|-----------------|
| Appearance | NTM - 002 | NTM - 002 |
| Specific Gravity | NTM - 003 | NTM - 003 |
| Tack Free Time | NTM - 005 | NTM - 005 |
| Durometer, Shore A | NTM - 006 | NTM - 006 |
| Tensile Strength | NTM - 007 | NTM - 007 |
| Elongation | NTM - 007 | NTM - 007 |
| Tear Strength | NTM - 009 | NTM - 009 |
| Tissue Culture | NTM - 061 | NTM - 061 |
| Emission Spectroscopy | NTM - 071 | NTM - 071 |

FDA Master File:

A Master File for MED-1511 AND MED-2000 has been filed with the U.S. Food and Drug Administration. The Master Files will contain the results of applicable chemical and mechanical equivalency tested as well as confirmatory biological

testing. Customers interested in authorization to reference these files must contact NuSil Technology.

Warnings About Product Safety:

NuSil Technology believes that the information and data contained herein is accurate and reliable; however, it is the user's responsibility to determine suitability and safety of use for these materials. NuSil Technology can not know the specific requirements of each application and hereby makes the user aware that it has not tested or determined that these materials are suitable or safe for any application. It is the user's responsibility to adequately test and determine the safety and suitability for their application and NuSil Technology makes no warranty concerning fitness for any use or purpose. There has been no testing done by NuSil Technology to establish safety of use in any medical application.

NuSil Technology has tested this material only to determine if the product meets the applicable specifications. (Please contact NuSil Technology for assistance and recommendations when establishing specifications.) When considering the use of NuSil Technology products in a particular application, you should review the latest Material Safety Data Sheets and contact NuSil Technology for any questions about product safety information you may have.

No chemical should be used in a food, drug, cosmetic, or medical application or process until you have determined the safety and legality of the use. It is the responsibility of the user to meet the requirements of the U.S. Food and Drug Administration (FDA) and any other regulatory agencies. Before handling any other materials mentioned in the text, you should obtain available product safety information and take the necessary steps to ensure safety of use.

Specifications:

The typical properties shown in this technical profile should not be used as a basis for preparing specifications. Please contact NuSil Technology for assistance and recommendations in establishing particular specifications.

Patent Warning:

NuSil Technology disclaims any expressed or implied warranty against the infringement of any patent. NuSil Technology does not warrant that the use or sale of the products described herein will not infringe the claims of any United States patents or other country's patents covering the product itself or the use in combination with other products or in the operation of any process.

Warranty Information:

NuSil Technology's warranty period is 6 months from date of shipment when stored below 40°C in original unopened containers. Unless NuSil Technology provides you with a specific written warranty of fitness for a particular use, NuSil Technology's sole warranty is that the product will meet NuSil Technology's then current specification. NuSil Technology specifically disclaims any other express or implied warranty, including warranties of merchantability and of fitness for use. Your exclusive remedy and NuSil Technology's sole liability for breach of warranty is limited to refund of purchase price or replacement of any product shown to be other than as warranted, and NuSil Technology expressly disclaims any liability for incidental or consequential damages.

<Blank Page>

A8.3 NuSil Med1-4213



www.nusil.com • 800-541-1111

NuSil Technology
 100000100 • 100000101 • 100000102

100000103 • 100000104 • 100000105

100000106

© 2011 NuSil Corporation

Product Profile

MED1-4213 & MED2-4213 Fast Cure Silicone Adhesives

Description:

NuSil Technology MED1-4213 and MED2-4213 silicone adhesives are two-part, 1:1 mix, translucent, silicone system for bonding silicone elastomers to each other and to some metals and plastics. MED1-4213 will cure at room temperature but cure time can be rapidly reduced at elevated temperatures. MED2-4213 will only partially cure at room temperature but can be rapidly cured at elevated temperatures. See the typical cure schedule section. Both adhesives are pourable, self-leveling, high tear strength silicone materials. In many cases the use of a silicone primer may not be needed to obtain suitable adhesion.

Applications:

MED1-4213 and MED2-4213 are designed for applications requiring the use of silicone adhesives to bond silicones to each other and to other substrates such as metals and plastics. After mixing the A and B sides together, cure begins. Advantages of these products are:

- Unlike one-part RTV silicone adhesives, MED1-4213 and MED2-4213 do not require atmospheric moisture for curing.
- There is no curing byproduct such as acetic acid or methyl alcohol.

MED1-4213 cures at room temperature; MED2-4213 cures rapidly at elevated temperatures

- Unlike one-part RTV adhesives, cure rate of both products may be rapidly accelerated by

application of heat in an oven, or by heat gun or heat lamp.

- Good adhesion to silicones, and in many unprimed metal and plastic substrates can be obtained.
- Relatively low viscosity allows the packaging of the products into easy-to-use, airless, side-by-side kits that eliminate the difficulty of mixing and dosing.

Mixing:

In side-by-side kits, MED1-4213 and MED2-4213 are mixed in a 1:1 ratio through the use of a static mix and dispense cartridge. A disposable static mix tip is attached to the cartridge and the Part A and Part B are extruded through the static mix tip, dispensing directly onto the substrate. Note: it is sometimes prudent to discard the first few grams of extruded material, as good static mixing often does not occur until after this point. MED1-4213 and MED2-4213 can also be purchased in standard two-part 2-part, 2-gallon, 10-gallon, and 2-drum kits. When using these standard kits, care should be used to minimize air entrapment during mixing. The mixed product should be placed in a vacuum chamber to remove entrapped air, which reduces bubble formation during curing.

Typical Properties as Supplied:

| | <u>MED1-4213</u> |
|-------------------------|------------------|
| Chemical Classification | VMQ |
| Color | Translucent |
| Viscosity, cP Part A | 80,000 |

| | |
|----------------------|-------------|
| Viscosity, cP Part B | Thixotropic |
| Mix Ratio | 1:1 |
| Work Time, Minutes | 5 |

Typical Properties as Supplied:

| | |
|-------------------------|------------------|
| | <u>MED2-4213</u> |
| Chemical Classification | VMQ |
| Color | Translucent |
| Viscosity, cP Part A | 80,000 |
| Viscosity, cP Part B | Thixotropic |
| Mix Ratio | 1:1 |
| Work Time, Hours | 2 |

Test Properties:

Cured 24 hours @ 25°C (77°F)

| | |
|--------------------------------|------------------|
| | <u>MED1-4213</u> |
| Specific Gravity @ 25°C (77°F) | 1.10 |
| Durometer, Shore A | 15 |
| Tensile Strength, psi | 600 |
| Elongation, % | 650 |
| Tear Strength, pli, Die B | 75 |

| | |
|--------------------------------|------------------|
| | <u>MED2-4213</u> |
| Specific Gravity @ 25°C (77°F) | 1.10 |
| Durometer, Shore A | 15 |
| Tensile Strength, psi | 600 |
| Elongation, % | 650 |
| Tear Strength, pli, Die B | 75 |

Typical Cure Schedule:

| <u>Temperature</u> | <u>MED1-4213</u> | <u>MED2-4213</u> |
|--------------------|------------------|------------------|
| 25°C | 4-6 Hours | N/A |
| 70°C | 10 Minutes | N/A |
| 100°C | 5 Minutes | 30 Minutes |
| 150°C | 1 Minute | 15 Minutes |

Substrate Consideration:

MED1-4213 & MED2-4213 will cure in contact with most materials common to biomedical assemblies. Exceptions include sulfur cured organic rubbers, latex, chlorinated rubbers, some RTV silicones and unreacted residues of some curing agents. Units to be encapsulated or potted should be clean and free of surface contaminants. Containers and dispensers to be used with MED1-4213 & MED2-4213 should also be clean and dry. Cure inhibition can usually be prevented by washing all containers with clean solvent or volatilizing the contaminants by heating.

Packaging:

Fifty ML Side by Side Kit
 Two Hundred ML Side by Side Kit
 Four Hundred ML Side by Side Kit
 Two Pint Kit
 Two Gallon Kit
 Ten Gallon Kit

FDA Master File:

A Master File for MED1-4213 has been filed with the U.S. Food and Drug Administration. These Master Files contain the results of applicable chemical and mechanical equivalency tested as well as confirmatory biological testing. A Master File for MED2-4213 is in process with the U.S. Food and Drug Administration. These Master Files will contain the results of applicable chemical and mechanical equivalency tested as well as confirmatory biological testing. Customers interested in authorization to reference these files must contact NuSil Technology.

Warnings About Product Safety:

NuSil Technology believes that the information and data contained herein is accurate and reliable; however, it is the user's responsibility to determine suitability and safety of use for these materials. NuSil Technology can not know the specific requirements of each application and hereby makes the user aware that it has not tested or determined that these materials are suitable or safe for any application. It is the user's responsibility to adequately test and determine the safety and suitability for their application and NuSil Technology makes no warranty concerning fitness for any use or purpose. There has been no testing done by NuSil Technology to establish safety of use in any medical application.

NuSil Technology has tested this material only to determine if the product meets the applicable specifications. (Please contact NuSil Technology for assistance and recommendations when establishing specifications.) When considering the use of NuSil Technology products in a particular application, you should review the latest Material Safety Data Sheets and contact NuSil Technology for any questions about product safety information you may have.

No chemical should be used in a food, drug, cosmetic, or medical application or process until you have determined the safety and legality of the use. It is the responsibility of the user to meet the requirements of the U.S. Food and Drug Administration (FDA) and any other regulatory agencies. Before handling any other materials mentioned in the text, you should obtain available product safety information and take the necessary steps to ensure safety of use.

Specifications:

The typical properties shown in this technical profile should not be used as a basis for preparing specifications. Please contact NuSil Technology for assistance and recommendations in establishing particular specifications.

Patent Warning:

NuSil Technology disclaims any expressed or implied warranty against the infringement of any patent. NuSil Technology does not warrant that the use or sale of the products described herein will not infringe the claims of any United States patents or other country's patents covering the product itself or the use in combination with other products or in the operation of any process.

Warranty Information:

NuSil Technology's warranty period is 6 months from date of shipment when stored below 40°C in original unopened containers. Unless NuSil Technology provides you with a specific written warranty of fitness for a particular use, NuSil Technology's sole warranty is that the product will meet NuSil Technology's then current specification. NuSil Technology specifically disclaims any other express or implied warranty, including warranties of merchantability and of fitness for use. Your exclusive remedy and NuSil Technology's sole liability for breach of warranty is limited to refund of purchase price or replacement of any product shown to be other than as warranted, and NuSil Technology expressly disclaims any liability for incidental or consequential damages.

<Blank Page>

A8.4 NuSil SP-120

SP-120

SP-121

Silicone Primers



10000 Parkside Drive • San Jose, CA 95135

Phone: (408) 261-1000 • Fax: (408) 261-1001

Website: www.nusil.com

© 2004 NuSil

SP-120 and SP-121 are registered trademarks of NuSil Technology.

Product Profile

Description

- Specially formulated primers designed for use with one- and two-part RTV silicone rubber compounds
- SP-120 is clear and SP-121 is red
- One-component primers require no mixing
- Air-drying
- Convenient container sizes produce less waste

Applications

- Improve the adhesion of NuSil Technology's one- and two-part RTV silicone rubbers to various substrates including metals (e.g. stainless steel, steel, copper and aluminum), ceramics, glass, some coppers, rigid plastics and wood.
- SP-120 is clear to preserve visibility with clear product
- SP-121 is red to provide easy visual determination of surface coverage

| Typical Properties | Result | | Metric Conv. | ASTM | NT-TM |
|--------------------------------|----------------|--------|--------------|----------------|-------|
| | SP-120 | SP-121 | | | |
| Color | Clear | Red | - | - | - |
| Viscosity | 1.0 cP | - | - | D-1084, D-2198 | 001 |
| Non-Volatile Content | 5% | 3.5% | - | D-2288 | 004 |
| Specific Gravity @ 25°C (77°F) | 0.78 | - | - | D-792 | 003 |
| Flash Point, (TCC) | 63°F | - | 17°C | D-92 | 002 |
| Solvent Type | VMMA/P-Naphtha | | - | - | - |
| D.O.T. Classification | Flammable | | - | - | - |

Instructions for Use

Applying

Apply by brushing, wiping or dipping a uniform thin film onto the substrates. The following procedures are recommended for best bonding results:

1. Clean and degrease the surface being primed with an appropriate solvent and a coarse lint-free cloth.
2. Rinse the surface off with clean solvent.
3. When completely dry, apply a uniform thin coat by dipping, spraying or brushing. A camel hair brush may be used, or on smooth surfaces, a lint-free tissue. Dried primer coatings vary from being clear to having a slight haze. If dried to a whitish haze or chalky appearance, the coating is too thick. Clean and reapply.
4. Allow to dry for 30 minutes at room temperature and 50% relative humidity. This primer is actuated by atmospheric moisture, so lower levels of humidity require longer drying times.
5. Apply the appropriate NuSil Technology adhesive/sealant.

Storage

Containers should remain sealed when not in use. This material hydrolyzes in the presence of atmospheric moisture and it is recommended that an inert gas, such as argon or nitrogen, be used to blanket the product before closing the container. Hydrolyzation is indicated by a milky appearance, and once occurred, the material cannot be reclaimed and will contaminate any unreacted primers.

Note: NuSil Technology's primers are supplied in flammable hydrocarbon solvents. Keep away from heat and open flames. Use only with adequate ventilation.

Packaging

2 Ounce Bottle
4 Ounce Bottle
8 Ounce Bottle
16 Ounce Bottle
1 Gallon Container
5 Gallon Container

Warranty

6 Months

Warnings About Product Safety

NuSil Technology believes that the information and data contained herein is accurate and reliable. However, the user is responsible to determine the material's suitability and safety of use. NuSil Technology cannot know each application's specific requirements and hereby notifies the user that it has not tested or determined this material's suitability or safety for use in any application. The user is responsible to adequately test and determine the safety and suitability for their application and NuSil Technology makes no warranty concerning fitness for any use or purpose. NuSil Technology has completed no testing to establish safety of use in any medical application.

NuSil Technology has tested this material only to determine if the product meets the applicable specifications. (Please contact NuSil Technology for assistance and recommendations when establishing specifications.) When considering the use of NuSil Technology products in a particular application, review the latest Material Safety Data Sheets and contact NuSil Technology with any questions about product safety information.

Do not use any chemical in a food, drug, cosmetic, or medical application or process until having determined the safety and legality of the use. The user is responsible to meet the requirements of the U.S. Food and Drug Administration (FDA) and any other regulatory agencies. Before handling any other materials mentioned in the text, obtain available product safety information and take the necessary steps to ensure safety of use.

Specifications

Do not use the typical properties shown in this technical profile as a basis for preparing specifications. Please contact NuSil Technology for assistance and recommendations in establishing particular specifications.

Patent Warning

NuSil Technology disclaims any expressed or implied warranty against the infringement of any patent. NuSil Technology does not warrant the use or sale of the products described herein will not infringe the claims of any United States' or other country's patents covering the product itself, its use in combination with other products or its use in the operation of any process.

Warranty Information

NuSil Technology's warranty period is 6 months from the date of shipment when stored below 40°C in original unopened containers. Unless NuSil Technology provides a specific written warranty of fitness for a particular use, NuSil Technology's sole warranty is that the product will meet NuSil Technology's then current specification. NuSil Technology specifically disclaims any other expressed or implied warranty, including warranties of merchantability and fitness for use. The exclusive remedy and NuSil Technology's sole liability for breach of warranty is limited to refund of purchase price or replacement of any product shown to be other than as warranted. NuSil Technology expressly disclaims any liability for incidental or consequential damages.

A8.5 NuSil SP-124



Customer Product and Technical Support

Phone: 800-828-6889

2000 Lakeside Drive • Covington, LA 70011

800-828-6889 • 504-835-1111

www.nusil.com

© 2000 NuSil Technology, Inc.

Product Profile

SP-124 Silicone Primer

Description:

NuSil Technology SP-124 Silicone Primer are specially formulated, one-component primers. SP-124 is designed to be used for improved bonding to NuSil Technology's one-part and two-part RTV silicone rubber compounds. SP-124 is a air-drying primer supplied ready to use as pourable solvent solutions in convenient small containers.

NuSil Technology's SP-124 is a clear, colorless primer designed for applications where discoloration of the substrate is undesirable.

Applications:

When properly applied, SP-124 silicone primer is designed to improve the adhesion of NuSil Technology's one and two-component RTV silicone rubbers to various substrates. Included are metals (such as stainless steel, steel, copper, and aluminum) ceramics, glass, some composites, rigid plastics and wood.

Advantages:

- Single-component, no mixing required
- Convenient container size, less waste
- Transparent to preserve visibility with clear product

CAUTION: NUSIL TECHNOLOGY'S PRIMERS ARE SUPPLIED IN FLAMMABLE HYDROCARBON SOLVENTS. KEEP AWAY

FROM HEAT AND OPEN FLAMES. USE ONLY WITH ADEQUATE VENTILATION.

Typical Properties as Supplied:

| | SP-124 |
|-------------------------------------|-------------|
| Color | Transparent |
| Yellow | |
| Viscosity, cP | 1.0 |
| Non-Volatils Content, % | 5 |
| Specific Gravity @ 25°C (77°F) | 0.77 |
| Flash Point, (TCC) | 48°F |
| Solvent, Type | VM&P Naptha |
| Drying Time @ 25°C (77°F), 50% R.H. | 30 minutes |
| D.O.T. Classification | Flammable |

Applying:

NuSil Technology's SP-124 primer may be applied by brushing, wiping or dipping. A uniform thin film is required. For best bonding results the following procedures are recommended.

1. Thoroughly clean and degrease the surface to be primed with an appropriate solvent and a coarse lint-free cloth.
2. Rinse off surface with clean solvent.
3. When the parts are completely dry, apply a uniform thin coat of SP-124 primer by dipping, spraying or brushing. A camel hair brush may be used, or on smooth surfaces, a lint-free tissue. The dried primer coating will vary from clear to a slight haze. If the surface dries to a heavy whitish haze or

a chalk appearance, the coating is too thick. Clean and reapply.

4. At room temperature and 50% relative humidity, the primer coat should be allowed to dry for ½ hour, with atmospheric moisture. Lower humidity will require a longer drying time.

5. Apply appropriate NuSil Technology adhesive / sealant.

Storage:

This material cures in the presence of atmospheric moisture. It is recommended that an inert gas, such as Argon or Nitrogen, be used to blanket the product before securely re-closing the container.

Packaging:

Four Ounce Bottle

Eight Ounce Bottle

Sixteen Ounce Bottle

One Gallon Container

Five Gallon Container

Containers should remain sealed when not in use. These primers will hydrolyze upon contact with atmospheric moisture and reduce or destroy their effectiveness. Hydrolyzation is indicated by a milky appearance in the primers. Once occurred, the material cannot be reclaimed and will contaminate any unreacted primers.

Warnings About Product Safety:

NuSil Technology believes that the information and data contained herein is accurate and reliable; however, it is the user's responsibility to determine suitability and safety of use for these materials. NuSil Technology can not know the specific requirements of each application and hereby makes the user aware that it has not tested or determined that these materials are suitable or safe for any application. It is the user's responsibility to adequately test and determine the safety and suitability for their application and NuSil Technology makes no warranty concerning fitness for any use or purpose. There has been no testing done by NuSil Technology to establish safety of use in any medical application.

NuSil Technology has tested this material only to determine if the product meets the applicable

specifications. (Please contact NuSil Technology for assistance and recommendations when establishing specifications.) When considering the use of NuSil Technology products in a particular application, you should review the latest Material Safety Data Sheets and contact NuSil Technology for any questions about product safety information you may have.

No chemical should be used in a food, drug, cosmetic, or medical application or process until you have determined the safety and legality of the use. It is the responsibility of the user to meet the requirements of the U.S. Food and Drug Administration (FDA) and any other regulatory agencies. Before handling any other materials mentioned in the text, you should obtain available product safety information and take the necessary steps to ensure safety of use.

Specifications:

The typical properties shown in this technical profile should not be used as a basis for preparing specifications. Please contact NuSil Technology for assistance and recommendations in establishing particular specifications.

Patent Warning:

NuSil Technology disclaims any expressed or implied warranty against the infringement of any patent. NuSil Technology does not warrant that the use or sale of the products described herein will not infringe the claims of any United States patents or other country's patents covering the product itself or the use in combination with other products or in the operation of any process.

Warranty Information:

NuSil Technology's warranty period is 6 months from date of shipment when stored below 40°C in original unopened containers. Unless NuSil Technology provides you with a specific written warranty of fitness for a particular use, NuSil Technology's sole warranty is that the product will meet NuSil Technology's then current specification. NuSil Technology specifically disclaims any other express or implied warranty, including warranties of merchantability and of fitness for use. Your exclusive remedy and NuSil Technology's sole liability for breach of warranty is limited to refund of

purchase price or replacement of any product shown to be other than as warranted, and NuSil Technology expressly disclaims any liability for incidental or consequential damages.

<Blank Page>

Appendix 9 - New Zealand Patent Application

As detailed in Chapter 6, a provisional specification for the bellows intervertebral disc implant was submitted for patenting in New Zealand in September 2001. This provisional patent has since been amended several times. The current New Zealand Patent Application Number is 525179/526019.

This appendix contains the full text for the current NZ Patent Application.

NEW ZEALAND
PATENTS ACT 1953

PROVISIONAL SPECIFICATION

“LOAD BEARING STRUCTURES”

We, **ENZTEC LIMITED**, a company duly incorporated under the laws of New Zealand of 4/45 Sonter Road, Christchurch, New Zealand, do hereby declare this invention to be described in the following statement:

TECHNICAL FIELD

The present invention relates to load bearing structures.

There have been a number of devices proposed for use as disk replacements. There are none that meet all of the preferences below.

The present invention in one aspect relates to intervertebral disk replacement (including replacement for similar low displacement joints). Since, therefore, there is contemplation of body joints (including vertebral facet joints or vertebral joints to the pelvis, etc.) the terms thereafter "intervertebral", "proximal vertebral body", etc. should take as an option corresponding meanings.

A collapsed disk can cause pain, partial paralysis and limited mobility. If the situation is serious enough the current medical solution is for the patient to have a "spinal fusion" operation in which the collapsed disk is removed and, by one of several similar methods, the adjoining vertebrae are induced to grow together and in time become fused. This operation is successful in reducing the paralysis and pain but limits the flexibility of the spine and puts more load on to adjacent disks. As a result there is increased potential for the neighbouring disks to degenerate as well.

BACKGROUND

THE SOUGHT-AFTER CHARACTERISTICS IN A DISK REPLACEMENT:

The ideal replacement would be a component:

1. That will bond to the vertebrae.
2. That will have the flexibility in all respects similar to that of a healthy disk. This involves vertical and angular flexibility.
3. It should have stability similar to a healthy disk (for example it should not allow the adjacent vertebra to slide fore and aft or laterally in relation to one another).
4. It should spread the load into the vertebrae much in the manner of healthy disk.

Other preferences are that:

5. It should be no more difficult to insert than the hardware at present used in the operation.
6. It should if possible use the same procedures as presently used.
7. Once in place it should have good survivability.
8. If anything should go wrong, it should not fail catastrophically.
9. It should be able to be replaced by hardware used in current methods.
10. It should not have sliding surfaces that produce wear debris.
11. It should be eminently biocompatible

Whilst there have been a number of devices mooted to be used as disk replacements, none has all of the preferences above.

An object of this invention in some of its embodiments is to meet at least several (if not all) of these criteria and thereby provide for the surgeon and patient a realistic alternative to spinal fusion as the method of choice for dealing with a collapsed intervertebral disk or to at least provide an alternative. Similarly with other joint application.

Another object of this invention in some of its embodiments is to meet all these criteria and thereby provide for the surgeon and patient a realistic alternative to spinal fusion as the method of choice for dealing with degenerate intervertebral disk.

The invention in one aspect in several forms is shown (cut in half) in Figures 13 through 20.

The invention in this form comprises a tough sealed outer casing in the form of a cushion or bellows arrangement filled with a bio compatible fluid medium (eg; liquid and/or otherwise) possibly incorporating a gas (eg; air) cavity or gas cavities. It may have other applications as discussed hereafter.

BRIEF DESCRIPTION OF THE INVENTION

In one aspect the present invention consists in **a load transferal device**, said device being defined at least in part by

a space confinement housing which provides spaced exterior surface adapted to bear against surfaces of spaced members which are to have a capability over at least some distance and some angular disposition of moving relatively towards each other and/or angling relative to each other, and

at least one force transferring media within said housing.

Preferably said device is an implant useful for cushioning directly or indirectly bone members.

In another aspect the present invention consists in **an implant useful as a prosthetic replacement of an intervertebral disk**, said implant being defined at least in part by

a space confinement housing which provides, as an at least in part simulation of such a disk, top and bottom surfaces adapted (directly or indirectly) to bear at least in part respectively on the upper and lower vertebral bodies between which it might be interposed as an implant, and

at least one force transferring media within said housing,

wherein said housing under the influence of the confined media has a capability of allowing said top and bottom surfaces to be angularly disposed relative to each other in a number of different conditions (simulating those of an intervertebral disk) as a result of an ability of the housing under diverse loadings (such as those of real or simulated angular dispositions of proximate vertebral bodies between which the implant might be inserted) to compact in part and substantially correspondingly expand in part.

Preferably said implant has as a motion limiting feature (one or more) to restrict the maximum separation of said top and bottom surfaces.

Preferably said housing is in the form of a bellows or some equivalent (whether or unitary or fabricated form). Additional implant forms could include circular, spiral, horseshoe or banana profiles.

Preferably said housing is substantially of or is an adaption of a form substantially as depicted in any one or more of the accompanying drawings.

Preferably said media is at least in part liquid and/or at least in part gaseous and/or a resilient (at least in part) solid(s) material(s).

In another aspect the invention consists in **the use of an implant as previously defined** as a replacement for an intervertebral disk.

In yet another aspect the invention consists in **a method of replacing an intervertebral disk** which comprises or includes at least

(if necessary) opening the annulus,

(if necessary) removing the damaged or defective intervertebral disk, or residue thereof, and

interposing an implant as previously defined between the related proximal vertebral bodies,

(and if possible and/or necessary and/or desirable) restoring to its functional positioning the annulus),

(and, if the implant is not of a kind motion limited internally and/or externally of the housing to itself, at any appropriate stage, motion limiting the implant to one or other, or both, of said related proximal vertebral bodies).

In a further aspect the present invention consists in, **interposed between, or for imposition between, vertebral bodies in a spinal structure, an implant as a prosthetic replacement of an intervertebral disk,**

wherein said implant confines a force transferring media inside a housing capable of being compressed and/or angularly distorted by the effect of proximate vertebral bodies, whereby any such angular distortion, in part, compresses (and displaces some of the media) and, in part, expands (under the action at least in part of displaced media),

and wherein the media assisted expansion is limited by at least one of:

- (i) motion limiters external of yet attached to the housing,
- (ii) motion limiters internally of yet attached to the housing, and/or
- (iii) motion limiters between each adjacent vertebral body and distal parts of the housing or motion limiters not attached to the housing.

BRIEF DESCRIPTION OF THE DRAWINGS

Preferred forms of the present invention will now be described with reference to the accompanying drawings in which

Figure 1 (two views, Figures 1A and 1B) shows simplified front and isometric pictorial views of normal spine anatomy and physiology,

Figure 2 shows a simplified isometric view of position of a bellows type implant in accordance with the present invention relative to spine anatomy and physiology,

Figure 3 (shows artists renderings of the lumbar spine anatomy and physiology (Source: *Frank H. Netter, M.D.; Atlas of Human Anatomy; Plate 144*), **Figure 3A** showing the second lumbar vertebra: superior view, **Figure 3B** shows the intervertebral disk, **Figure 3C** shows the third and fourth lumbar vertebrae: posterior view and **Figure 3D** shows the lumbar vertebrae, assembled: left lateral view),

Figure 4A shows in cross section a bellows type housing in accordance with the present invention in a relaxed mode with two motion limiting devices on opposed sides each being in a relaxed state, and **Figure 4B** shows the same view as in Figure 4A but with an angular distortion as a result of applied force in the arrowed direction which has the effect of further relaxing the motion limiting device on the side to which the greater force is applied until such time as the other diametrically opposed motion limiting device pulls taut and those the forces F_t apply to limit further expansion, such limitation of further expansion ensuring there is sufficient force transferring media interposed on the more compressed side to prevent further and excessive contraction,

Figure 5A (Figures 5A and 5B) show front and isometric pictorial views of a spine at rest with surrounding anatomy and physiology and a bellows implant (the bellows being partly obscured in Figure 5B and an annulus comprised during insertion of the implant being shown with no thickness for clarity in the drawing),

Figure 6 (Figures 6A and 6B) shows front and isometric pictorial views of a deflected spine with surrounding anatomy and physiology and bellows implant, these figures being similar to those of Figure 5 but showing the nature of the performance,

Figure 7 (Figures 7A and 7B) shows front and isometric pictorial views of a spine at rest with an externally tethered bellows implant (note the annulus has been omitted for clarity),

Figure 8 (Figures 8A and 8B) shows front and isometric pictorial views of a deflected spine with externally tethered bellows implant (again the annulus being omitted for clarity),

Figure 9 shows an isometric pictorial view of an internally tethered bellows type implant,

Figure 10 shows an isometric pictorial view of an externally tethered bellows type implant,

Figure 11 (Figures 11A and 11B) shows front and isometric pictorial views of a spine at rest with the vertebral bodies tethered (note the annulus has been omitted for clarity),

Figure 12 (Figures 12A and 12B) shows front and isometric pictorial views of a deflected spine with the vertebral bodies tethered (note the annulus has been omitted for clarity),

Figure 13 is a simple housing form shown in section that could be used as a compressible/expandable housing,

Figure 14 shows an alternative form to that of Figure 13 for such a housing again shown in section, this time as a bellows type housing having a number of concertina type convolutions,

Figure 15 shows a more preferred form to that of Figure 14 showing welded seams or (if integrally formed) sharper transitions in the concertina regions,

Figure 16 is a variation of the housing of Figure 13 showing vertebral body engagement projections,

Figure 17 shows a variation of the embodiment of Figure 13 having a plug capable of being fitted after filling with the force transferring media,

Figure 18 is a further variation of the arrangement of Figure 13 showing how the force transferring media can be more than a mere bio-compatible liquid in that it can include compressible spheres or other shapes therein, such as a gas filled bubble form,

Figure 19 shows a further variation of Figure 13 where a compressible foam or like at least in part solid(s) material(s) media is provided as the force transferring media,

Figure 20 shows how, if desired, some more resistant to compression forms can be provided internally as motion limiting device(s), such provisions being instead of and/or in addition to any other motion limiting in accordance with the present invention,

Figure 21 is a plan view of bean shaped forms, and

Figure 22 shows a device of the present invention being interposed as cushioning below a tibial tray.

DETAILED DESCRIPTION OF THE INVENTION

This invention in one form is shown (cut in half and without tethers) in Figure 13 and described in detail below.

The housing in this form comprises a tough sealed outer casing in the form of a cushion or bellows arrangement filled with a biocompatible fluid medium possibly incorporating a gas cavity or cavities.

The housing of casing can be made of a suitable biocompatible material such as titanium or stainless steel. The outer edge of this structure could be thin and flexible, and may involve one or more convolutions (as for example in Figure 14) depending on the requirements of space and flexibility. This design is not unlike flexible metal bellows found in steam piping. The bellows may be formed bellows as shown in Figure 14 or edge-welded bellows, as shown in Figure 15.

All the figures show the implant being circular, because this was the easiest configuration to draw however ideally it would be "bean" shaped. The plan view "bean" shape (as in Figure 21) allows insertion from a posterior or more lateral approach - one being inserted from each side, or two from the same.

The vertebral bodies have increasing compressive strength closer to the periphery. Hence the geometry of the implant needs to mimic this profile to place the loads as close as possible this higher strength material thus ensuring the vertebral body endplates are not damaged, by the applied loads.

The ends of the structure could be thicker and might be coated (on the surfaces next to the bond) with a suitable bioactive agent or an appropriately roughened surface, the purpose of which is to encourage osteo-integration. They could contain barbed spikes (Figure 16), deflectable spikes or the like, to help locate and fix them into the vertebral bodies during insertion.

The bellows wall may be coated

- i) Internal coating to stop interacting of housing material and fill medium.
- ii) Internal coating to help retain fill medium (fluid in this case) if a crack develops in the housing.
- iii) Anodised outer surface to improve wear properties of implant should surrounding anatomy rub against implant (example similar treatment is applied to pacemakers).

The connection between the flexible sides and the thicker ends is suitably designed to avoid stress concentrations.

The ends may contain an opening filled for example with a flush screwed-in cap (Figure 17) allowing insertion after manufacture of the internal medium

The housing confined force transferring media may take a number of forms. In its simplest form it could be gas (eg; air, nitrogen, CO₂, or the like), but this will not allow the structure to carry much load without collapse, and, should there be a crack in the outer casing, it would leak gas into the patient's body.

Alternatively it could be a simple liquid such as sterile saline. This would avoid the problem of gas leakage on rupture. However it would allow collapse of the casing structure if leakage occurred.

Having the casing completely filled with a fluid like saline would perhaps not provide sufficient compressibility, especially if the casing was metal. This however can be improved by providing a sealed plastic gas bubble or bubbles of known volume, floating within the fluid (Figure 18). These would act as springs to any shock pressure loadings applied to the structure, and would provide some axial flexibility to the structure and prevent end plate overload and fracture.

Another alternative to the internal medium could be a flexible plastic material such as a suitable polyurethane or silicone polymer or the like. This would have the advantages that should cracking of the outer casing occur, the internal medium would not leak out but would retain its function for a considerable period before plastic creep and fretting cause problems. Compressibility of such a plastic filling could be ensured by embedding a gas cavity within it. This gas cavity could be purposefully chosen to be the right size and shape to give the chosen axial compressibility and rocking stiffness to the overall structure.

Another alternative as the internal medium could be a closed-cell foam of a chosen density (Figure 19). Again this could have the advantages that it could be chosen to have the right resilience. Should cracking of the outer casing occur, this would not leak out but would retain its function, like the more solid plastic media.

The various internal media could have varying stiffness properties and/or the housing geometry could have varying sectional properties at different locations within the disk to suit the needs of rocking and vertical stiffness, and the compression of the bellows.

The structure could also include rigid internal buffer stops to prevent any overloading of the structure (Figure 20).

A particular advantage of the structures of Figures 13 to 20 is that they emulate the behaviour of a live disk in the respect that:

- a) it can carry large vertical loads by virtue of the fact that it has an internal fluid under pressure (albeit a somewhat plasticised fluid),
- b) it has a small amount of axial compressibility,
- c) it is relatively flexible to rocking motions,
- d) it is very stiff to torsional motions, and
- e) it is very stiff to shear between the top and bottom surfaces.

As a result of the semi fluid interior and the internal gas cavity(s), the cushion can be “tuned” to the required axial and rocking flexibilities by varying the stiffness of the internal material, and varying the size, shape and location of the gas cavity(s). As disk spaces are not always parallelograms in shape, the flexibility allows congruency.

A particular advantage of the structure is that it is completely enclosed within a casing such as titanium or a suitable alloy of titanium, which has long been used as an implant material.

Another particular advantage is that there are no external sliding surfaces producing friction and wear debris, known particularly with plastics, to cause toxic responses within the body.

Another advantage is that there are not titanium (or other metal) surfaces bearing on one another. As such it avoids the potential for wear, galling and wear debris with the titanium.

Another advantage over prior art is that this structure is relatively rigid against shear movements between the top and bottom ends. Unlike some earlier products, this design is able to maintain spinal stability with this feature.

Another particular advantage is that this cushion can be inserted in the same space and with the same procedures and operations as used currently for spinal fusion operations. In fact this design allows simpler insertion as it does not require to be filled with the bone particles required for spinal fusion.

A further advantages are that, should the unit need to be removed, a spinal fusion procedure can be implemented in its place - this design has not excluded a subsequent spinal fusion operation.

Another feature is that the large loads are carried by pressure in the internal fluid and this allows that walls of the cushion to be thin. This means that significant deflections can take place without raising the wall stress beyond critical values. This means the device can be designed to have a very long life in terms of metal fatigue.

Another is that since where internal material is biocompatible and solidified it means that if the outer titanium shell should crack, for example by fatigue or trauma, no material comes out, and there is no toxic reaction as a result. Further, since the gas cavity is well embedded within the plastic, no gas can escape into the body either. The wall thickness can be varied so critical area adjacent to the disk have greater protection in the event of a wall failure directing any extruded material away from this zone.

A related feature is that should failure occur, the consequences are not catastrophic. In fact that unit should still function with cracks through the thin wall. What is likely to happen is that the cracks would eventually develop wear debris that may be rejected by the body. The overall result is that should failure occur there is a long time available before the implant has to be replaced, if at all.

While the designs described and drawn are intended primarily for the replacement of intervertebral disks they could also be used (with a suitable size alteration) in other body joints such as the vertebral facet joints. Importantly joints with complex movements (such as the wrist and subtarsal joints) could use this implant device with slight shape variations. It may also be incorporated under knee replacement implants or incorporated into the tibial tray design.

Figure 22 shows a device in accordance with the present invention on a tibia below a tibial tray (eg; of CoCr metal) which itself is preferably below, for example, a polyethylene bearing.

Persons skilled in the art will appreciate other joint applications.

In a non medical application, i.e. industry it could be used for suspension systems, variable if the "bubble" volume were able to be adjusted during use.

The motion restricting systems described in this document are important to the success of the intervertebral implant for several reasons where there is no inherent mechanism within the bellows or other housing of the implant to prevent excessive deflection occurring. Over deflection could result in several issues, including:

- a) Bellows implant being damaged causing immediate loss, or partial loss of function.
- b) If the level of over deflection is minor, (i.e. there is no loss of function) but repeatedly occurs the implant life could be significantly reduced.
- c) Bone/implant interface union could be damaged.
- d) Surrounding anatomy and physiology could be damaged.

For these reasons motion-restricting systems have been developed to complement the bellows implant and prevent over deflection.

In the healthy lumbar spine there are several mechanisms that restrict the degree of deflection an intervertebral disc can travel through. These mechanisms include:

- a) The surrounding ligaments and muscles groups
- b) The facet joints
- c) And the annulus

Shown in Figure 1 is a simplified pictorial view of the lumbar spine. The intervertebral disc 4 consists of two “components” the annulus 1 and the nucleus pulposus 2 as shown in Figure 3B.

The bellows implant (as one example of a housing type) will normally be used in situations where the annulus is damaged and often the facet joints 3 may be damaged as well. During surgery approximately 30% of the annulus will be reflected to allow insertion of the bellows implant. The remaining nucleus will then be removed and the bellows implant 6 will sit in the nucleus cavity 8 surrounded by the remaining annulus 5, as shown in Figure 2.

Therefore with two of the natural deflection restriction mechanisms potentially compromised, deflection of the bellows implant 6 must be able to controlled by adding other mechanisms to the implant.

To date, three different motion restriction mechanisms have been considered. These have included:

- a) Bump Stops
- b) Bellows Geometry
- c) Tethers

Bump stops limit the maximum distance a mechanism can travel through. The bump stops may be configured as shown in Figure 20, they may in either or both internally or externally of the bellows cavity.

The bump stops may be singular, plural, or continuous.

This method consists simply of two surfaces that come into contact when the maximum travel is reached. This method has the advantage of being very simple.

If the implant introduces a shearing motion when deflected, the bump stop surfaces will produce wear debris as they make contact. As the bellows implant will not introduce any shear motion, such wear debris would not be produced.

If the bump stops were situated within the housing cavity wear debris generation issues would be further minimised ; as any such debris would be contained within the housing and would not be able to make contact with the surrounding anatomy and physiology.

Such bump stops could also be designed to incorporate cushioning, reducing any impact loads as the bump stops come into contact.

Bump stops have been used in several intervertebral disc implants including Kostuik et al (US Patent: 4,759,769).

The maximum deflection of the implant could also be controlled by the bellows geometry. Factors such as the bellows thickness, convolution pitch and convolution height all affect the level of deflection which results from an applied force. Therefore the bellows could be engineered to meet a specified maximum deflection.

Welded edge bellows as shown in Figure 15 also offer the advantage of being able to deflect without incurring damage until the convolutions contact, or become “bound”, once bound no further deflection can occur.

This method would require a specific bellows for each patient based on his or her age, weight, muscle strength etc. Also the geometry of the bellows affects the peak stress the bellows experience and this stress in turn affects the life span of the bellows implant.

Tether systems are our favoured method for restricting the deflection of the implant.

Preferably there is a plurality of tethers.

Preferably said tethers are external of said housing.

Alternatively said tethers are internal of said housing.

In other forms the tethering can be distinct from the implant ie can be from one proximal vertebral bodies to the other.

In yet a different embodiment, (less preferred) there is a plurality of tethers with one or more attached to the housing towards one said surface for subsequent attachment to a vertebral body distal to said one said surface, and with one or more attached to the housing towards the other said surface for subsequent attachment to a vertebral body proximal to said one said surface.

Preferably said tethers are flexible ties that span between its existing or intended attachments so as not to provide any substantial fetter on compaction.

Preferably said tethers are flexible so as to not provide any substantial fetter on compaction.

Tether systems have been used in some conceptual intervertebral disc implant designs including Xavier et al (US Patent 6,063,121). It should also be noted that Kostuik et al (US Patent 4,759,769) also used tethers to prevent excessive extension of their implant.

Tether systems work by taking advantage of the incompressible fluid within the bellows or other implant. See Figure 4A. As the implant deforms one side of the disc implant is compressed as in Figure 4B and at the least in part media inside the implant (eg; perhaps an incompressible confined liquid) is forced to the other side of the housing. This movement of the fluid 11 places the other side of the implant in tension. Around the periphery of the implant housing 9, or close to it, are fixed length tethers 10. As the disc deforms the tether 10A on the compressed side of the disc becomes relaxed and the tether 10B on the other side of the disk are placed in tension. When the tether 10B in tension becomes taut it stops any further skewing motion of the housing. Hence by controlling the length of all tethers 10 the maximum deflection on the opposing side can be fixed.

Tethers could be a continuous ring around the entire circumference (periphery) of the implant housing (i.e. not just discrete tethers) and hence the terms “at least one tether”, “one or more tethers”, etc encompasses such variations.

Several tether systems have been developed as an example which use this principle.

USE OF SURROUNDING ANATOMY TETHER

This method of restricting motion requires no additions to the bellows implant and relies on the surrounding anatomy and physiology to limit deflections. In a healthy lumbar spine the annulus, facet joints, surrounding ligaments and muscles naturally act to restrict motion; hence this method is a continuation of this philosophy.

During insertion of the implant approximately 30% the annulus would have to be reflected however where possible the remainder of the annulus would be preserved.

The remaining annulus, facet joints etc would then be relied on to continue protecting the implant and anatomy and physiology from over deflection using the tether system as detailed in respect of Figures 4A and 4B.

This tethering system has the advantages of not adding complexity to the bellows implant design and using the patient's anatomy and physiology to the implants advantage. The potential problems with this method are that it may place unnecessary stress on the annulus, which will have already been weakened during implant insertion.

EXTERNALLY TETHERED BELLOWS

The bellows implant could be altered to include bands or a continuous ring of material around the outside of the bellows. These bands or ring would consist of a flexible, non-stretching material anchored to the implant. The length of the bands could be set at the time of manufacture to provide the required levels of deflection.

As for the previous method of tethering the bellows, "the surrounding anatomy and physiology tether", the majority of the annulus would be left intact. In the views shown below the remaining annulus has been omitted for clarity.

Advantages of this system include, no reliance on the annulus to restrict movement, easy access to tether and the possibility of using the ring of material as a secondary fluid containment system, should the bellows fail. Disadvantages of this system include the need for the tether material to be biocompatible.

As the tether is not anchored to the bone if the patient continues to bend after the tether has become taut the vertebral bodies may separate from the implant damaging the implant/bone union. This separation of the implant and vertebral bodies is unlikely to occur though as the remaining annulus and ligaments will continue to limit deflection to safe levels as detailed previously.

INTERNALLY TETHERED BELLOWS

The bellows implant design could also be altered to include bands or a continuous ring of material on the inside of the bellows. These bands or ring would consist of a flexible, non-stretching material anchored to the inside of the implant.

The internally and externally tethered bellows are inserted in an identical fashion. Hence the at-rest and deflected views of the internally tether bellows are very similar to the external tethered bellows shown in Figure 7 & 8.

Partial cross-sections of the internally and externally tethered bellows are shown below, as can be seen from these figures the implants are identical apart from the placement of tether.

Advantages of internal tethers include, the tether material need not be biocompatible and the possibility of using the ring of material as a system to contain the majority of the fluid should the bellows fail.

The major disadvantage of this tether system is increased difficulty accessing the tether material making construction potentially more difficult.

Once again as the tether is not anchored to the bone if the patient continues to bend after the tether has become taut the vertebral bodies may separate from the implant damaging the implant/bone union. This separation of the implant and vertebral bodies is unlike to occur though as the remaining annulus and ligaments will continue to limit motion to safe levels.

INDEPENDENT TETHER

This method of tethering the implant in effect recreates the annulus by fixing the tether rigidly to the vertebral bodies or other parts of the patients anatomy and physiology. This tether system would therefore prevent the patient from over deflecting hence removing the risk of the vertebral bodies separating from the implant and hence damaging the implant/bone union.

This method of tethering the implant would however dramatically increase the complexity of inserting the implant. The surgeon would be required to staple the tethers onto the vertebral bodies in the correct places and with the correct length of tether in each position. Due to lack of access to the lumbar spine anatomy during insertion of the implant, independent tethers could only be used to reinforce the reflected annulus. Independent tethers could also be used in conjunction with internally or externally tethered bellows, with the same restriction above.

It should be noted that the positions of the tethers on the periphery of the vertebral bodies in Figure 11 & Figure 12 are purely schematic and the tethers could be placed in other positions.

Suitable biocompatible tethering or other materials include any of those disclosed in the aforementioned patents. Attachment thereof to a housing can be by adhesion (eg; with a biocompatible adhesive) or otherwise. Attachment thereof to bone can be by adhesion, or screws, etc. See again aforementioned patents.

CLAIMS

1. **A load transferal device**, said device being defined at least in part by a space confinement housing which provides spaced exterior surface adapted to bear against surfaces of spaced members which are to have a capability over at least some distance and some angular disposition of moving relatively towards each other and/or angling relative to each other, and

at least one force transferring media within said housing.

2. A device of claim 1 which is an implant useful for cushioning directly or indirectly bone members.

3. **An implant useful as a prosthetic replacement of an intervertebral disk**, said implant being defined at least in part by

a space confinement housing which provides, as an at least in part simulation of such a disk, top and bottom surfaces adapted (directly or indirectly) to bear at least in part respectively on the upper and lower vertebral bodies between which it might be interposed as an implant, and

at least one force transferring media within said housing,

wherein said housing under the influence of the confined media has a capability of allowing said top and bottom surfaces to be angularly disposed relative to each other in a number of different conditions (simulating those of an intervertebral disk) as a result of an ability of the housing under diverse loadings (such as those of real or simulated angular dispositions of proximate vertebral bodies between which the implant might be inserted) to compact in part and substantially correspondingly expand in part.

4. An implant of claim 3 which has one or more motion limiting feature to restrict the maximum separation of said top and bottom surfaces.

5. An implant of claim 4 wherein said implant confines a force transferring media inside a housing capable of being compressed and/or angularly distorted by the effect of proximate vertebral bodies, whereby any such angular distortion, in part, compresses (and displaces some of the media) and, in part, expands under the action at least in part of displaced media),

and wherein the media assisted expansion is limited by at least one of:

- (i) motion limiters external of yet attached to the housing, and/or
- (ii) motion limiters internally of yet attached to the housing.

6. A device of claim 3, 4 or 5 wherein said housing is in the form of a bellows or some equivalent (whether or unitary or fabricated form).

7. A device of claim 6 wherein said housing is substantially of or is an adaption of a form substantially as depicted in any one or more of the accompanying drawings.

8. A device of any one of claims 4 to 7 said media is at least in part liquid and/or at least in part gaseous and/or a resilient (at least in part) solid(s) material(s).

9. **The use of an implant defined** in any one of claims 4 to 8 as a replacement for an intervertebral disk.

10. **A method of replacing an intervertebral disk** which comprises or includes at least

(if necessary) opening the annulus,

(if necessary) removing the damaged or defective intervertebral disk, or residue thereof, and

interposing an implant as defined in any one of claims 4 to 8 between the related proximal vertebral bodies,

(and if possible and/or necessary and/or desirable) restoring to its functional positioning the annulus),

(and, if the implant is not of a kind motion limited internally and/or externally of the housing to itself, at any appropriate stage, motion limiting the implant to one or other, or both, of said related proximal vertebral bodies).

11. **Interposed between, or for imposition between, vertebral bodies in a spinal structure, an implant as a prosthetic replacement of an intervertebral disk,**

wherein said implant confines a force transferring media inside a housing capable of being compressed and/or angularly distorted by the effect of proximate vertebral bodies, whereby any such angular distortion, in part, compresses (and displaces some of the media) and, in part, expands (under the action at least in part of displaced media),

and wherein the media assisted expansion is limited by at least one of:

(i) motion limiters external of yet attached to the housing,

(ii) motion limiters internally of yet attached to the housing, and/or

(iii) motion limiters between each adjacent vertebral body and distal parts of the housing or motion limiters not attached to the housing.

ABSTRACT

An implant useful as a prosthetic replacement of an intervertebral disk which consists of a housing providing at least a part simulation of a disk yet containing a force transferring media. The housing is in the form of a bellows or equivalent structure preferably restricted as to maximum separation between those surfaces of the housing to be in contact with the proximate vertebral bodies thereby to limit angular distortion under the effect of the proximate vertebral bodies.

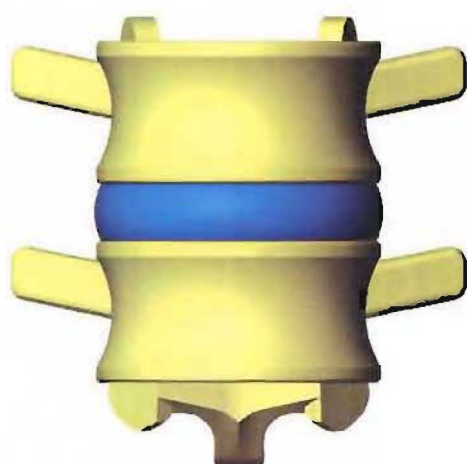


FIGURE 1A

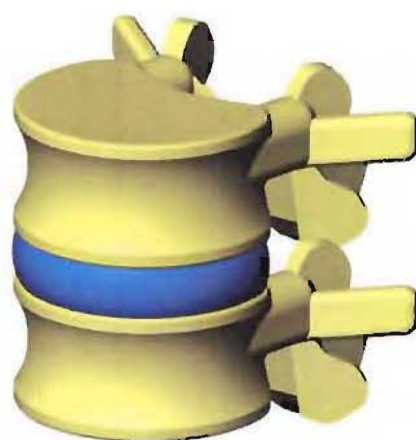


FIGURE 1B

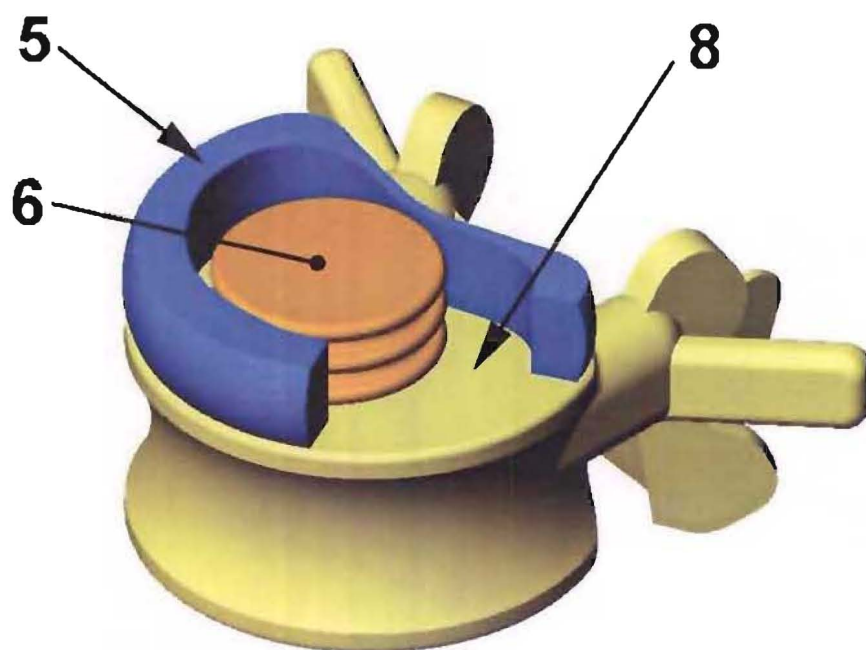


FIGURE 2

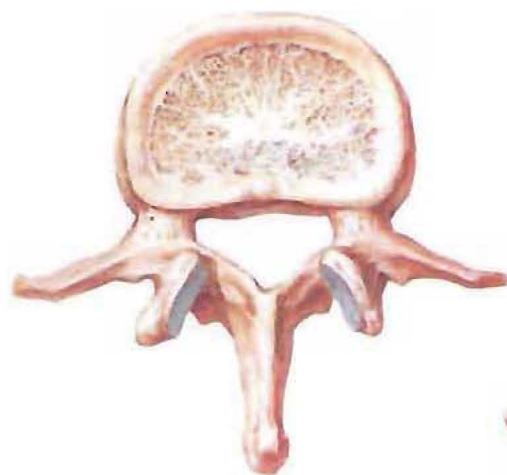


FIGURE 3A

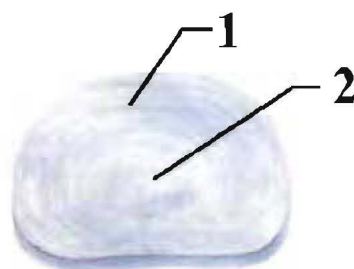


FIGURE 3B

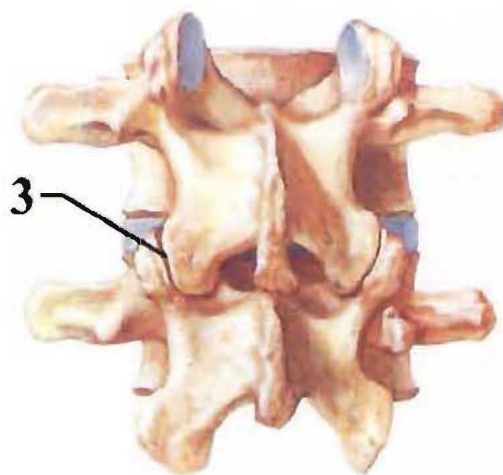


FIGURE 3C

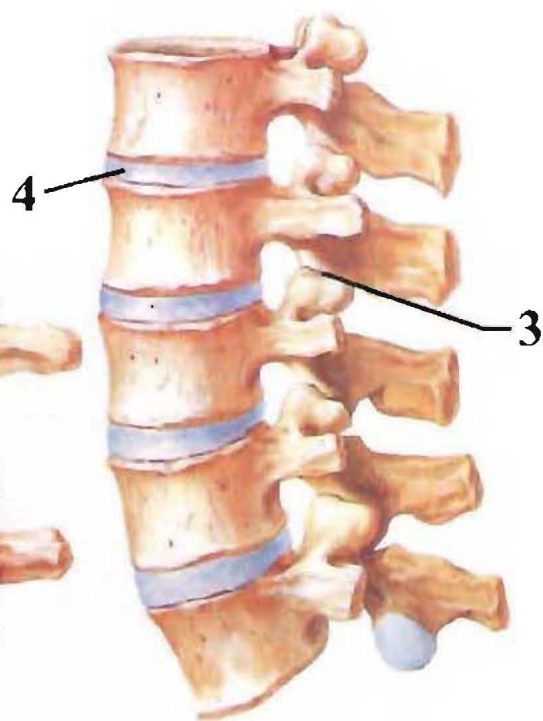


FIGURE 3D

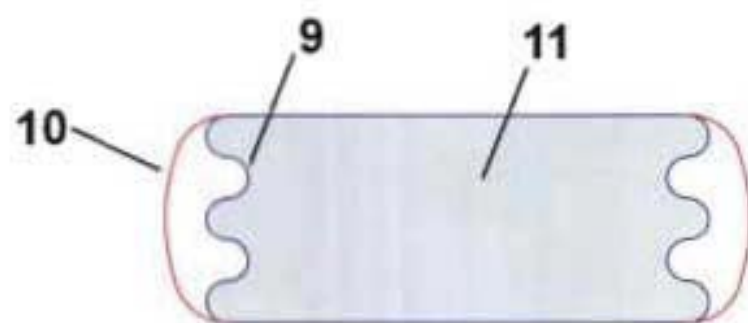


FIGURE 4A

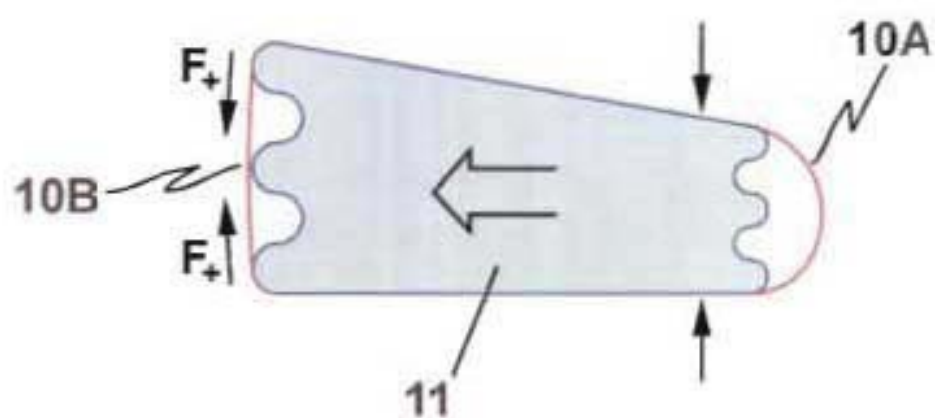


FIGURE 4B

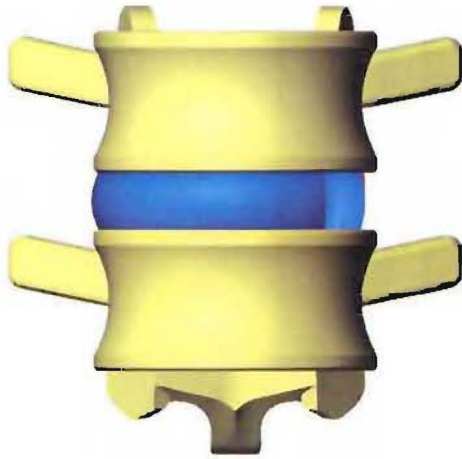


FIGURE 5A

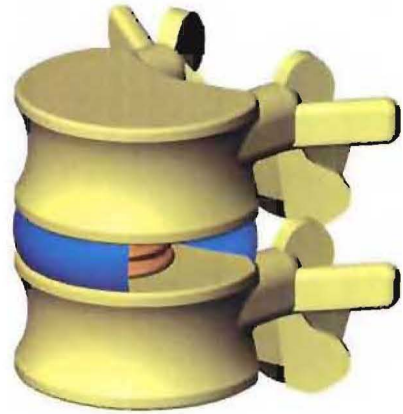


FIGURE 5B

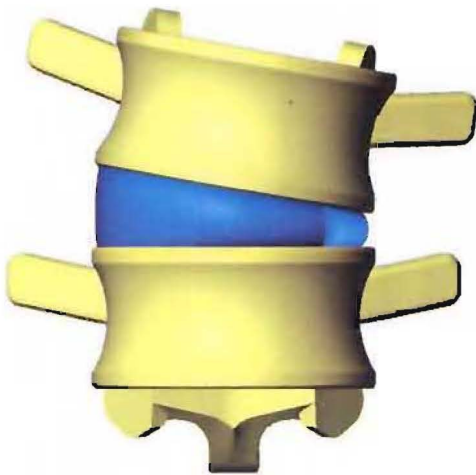


FIGURE 6A

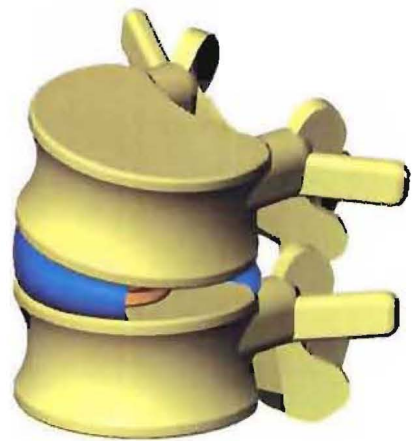


FIGURE 6B

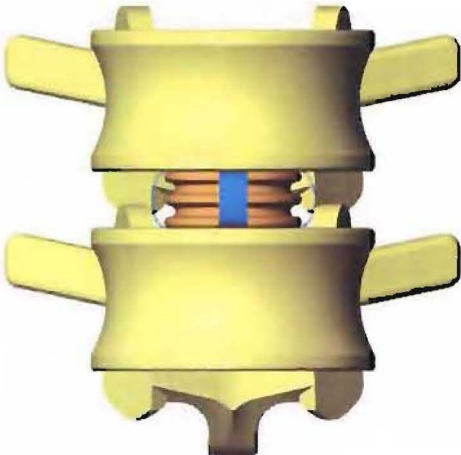


FIGURE 7A

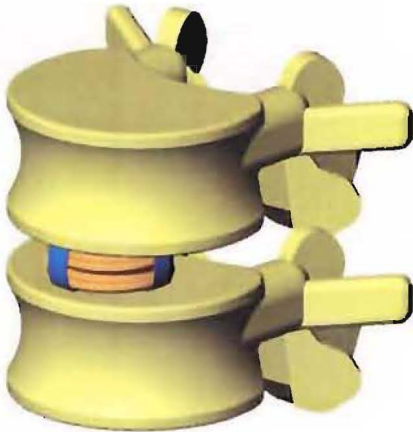


FIGURE 7B

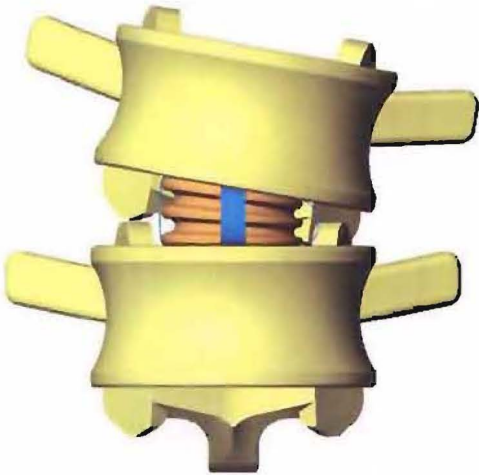


FIGURE 8A

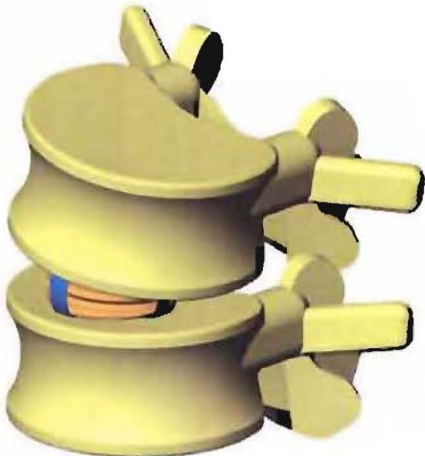


FIGURE 8B

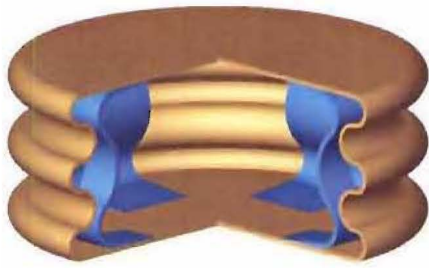


FIGURE 9



FIGURE 10

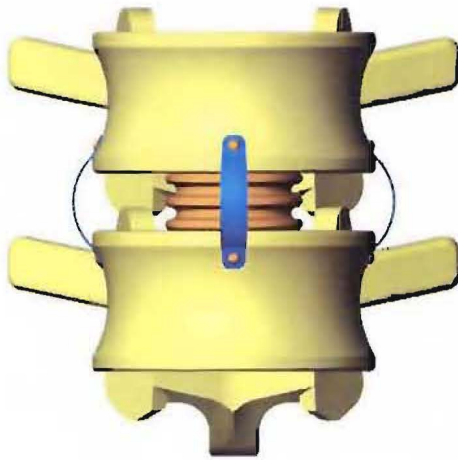


FIGURE 11A

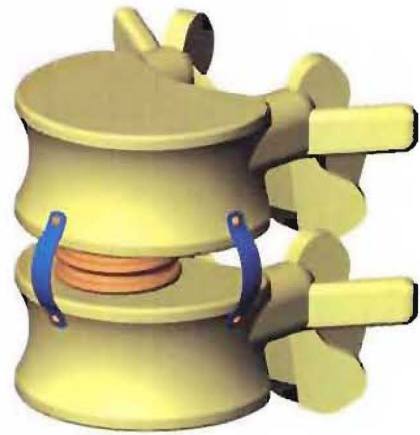


FIGURE 11B

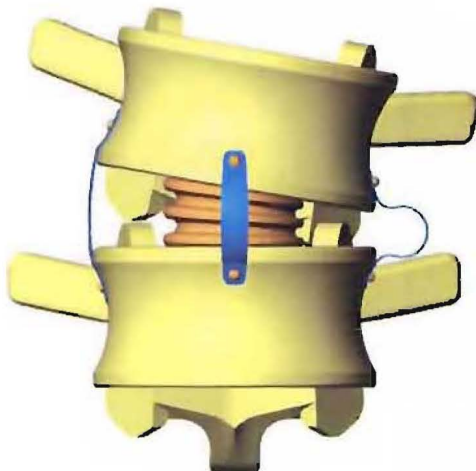


FIGURE 12A

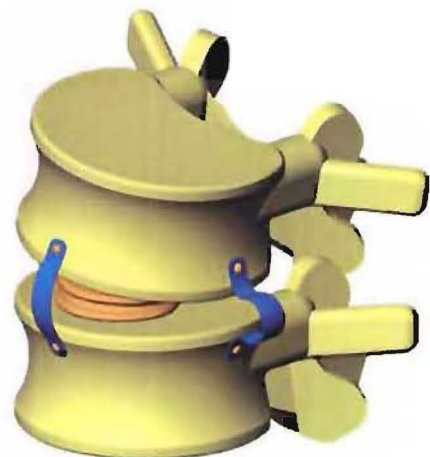


FIGURE 12B

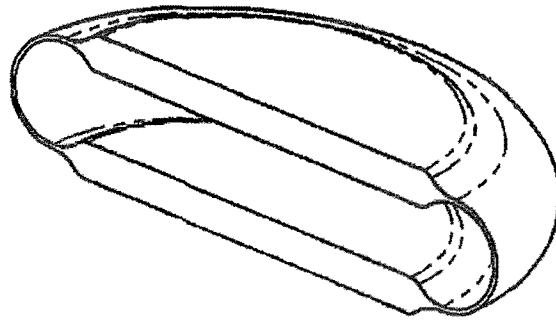


FIGURE 13

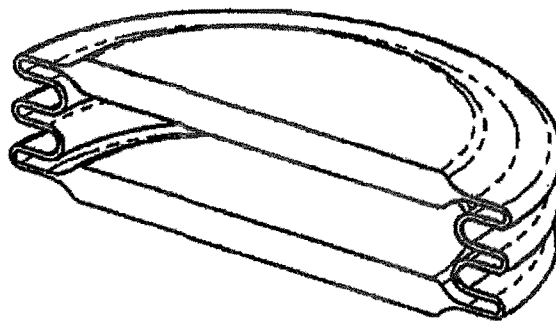


FIGURE 14

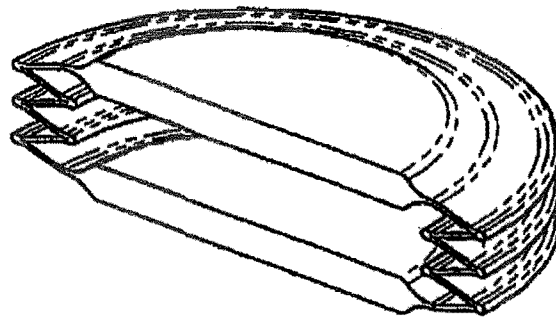


FIGURE 15

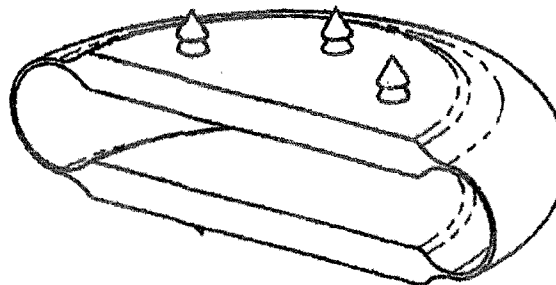


FIGURE 16

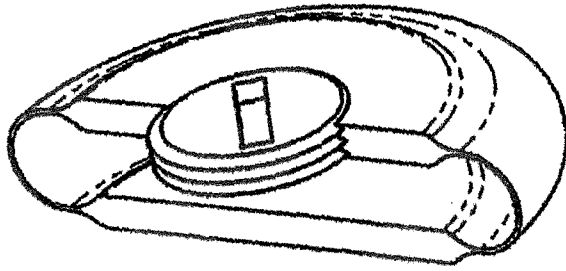


FIGURE 17

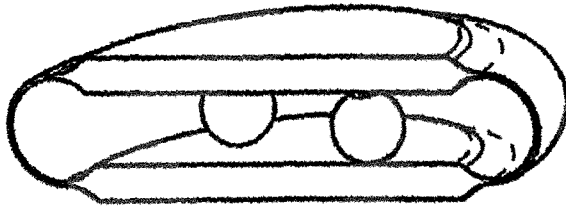


FIGURE 18

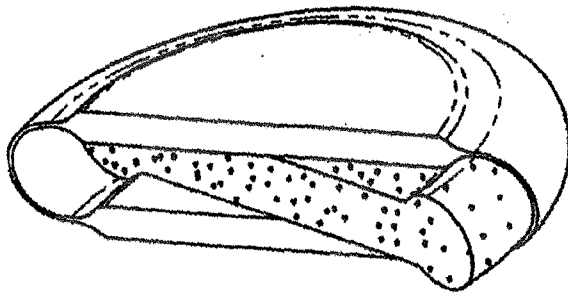


FIGURE 19

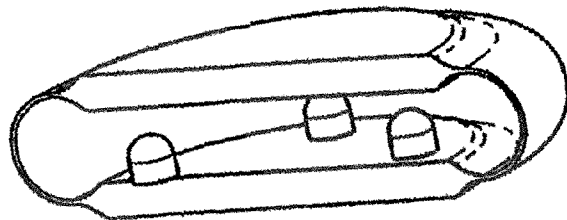


FIGURE 20

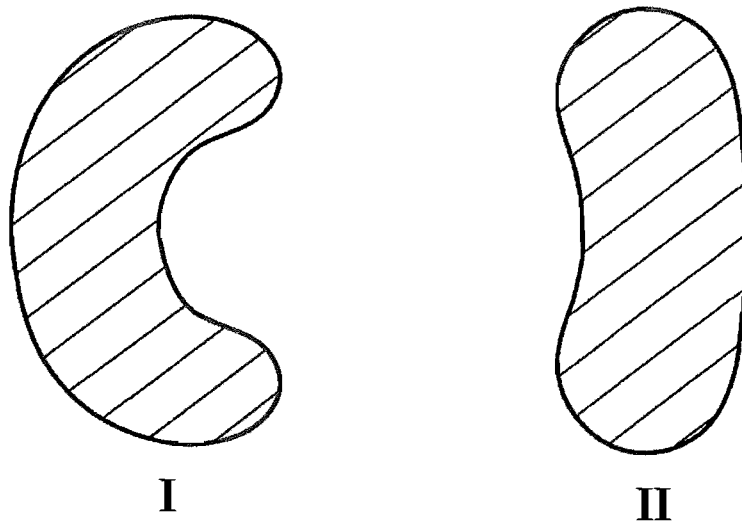


FIGURE 21

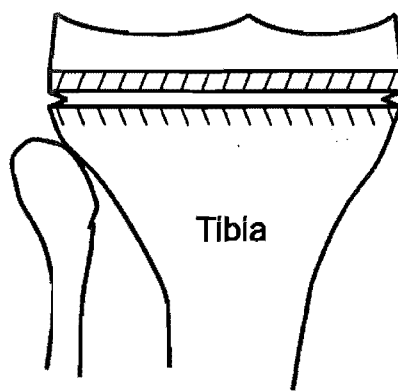


FIGURE 22

<Blank Page>

Appendix 10 – Femoral Endoprosthesis Conceptual Designs

Numerous sketches were generated during the development and detail design of the femoral endoprosthesis as discussed in Chapter 10. A few of the more significant concept sketches are shown in this appendix.

The concept sketches shown in Figure A10.1 show the development of tee cross section for the endoprosthesis body. The first concept sketch Figure A10.1(a) required a broad slot to be cut in the femur to accommodate the tee web. As the cross-section was refined the tee web was reduced in width as shown in Figure A10.1(b). A concave flange design, shown in Figure A10.1(c), was developed which would wrap around the remaining bone stock, however this was rejected due to problems associated with modelling and manufacturing such a structure. The cross section shown in Figure A10.1(d) is most similar to the final design. It features a right angle relationship between the web and flange faces and a small transition curve between the web and the flange.

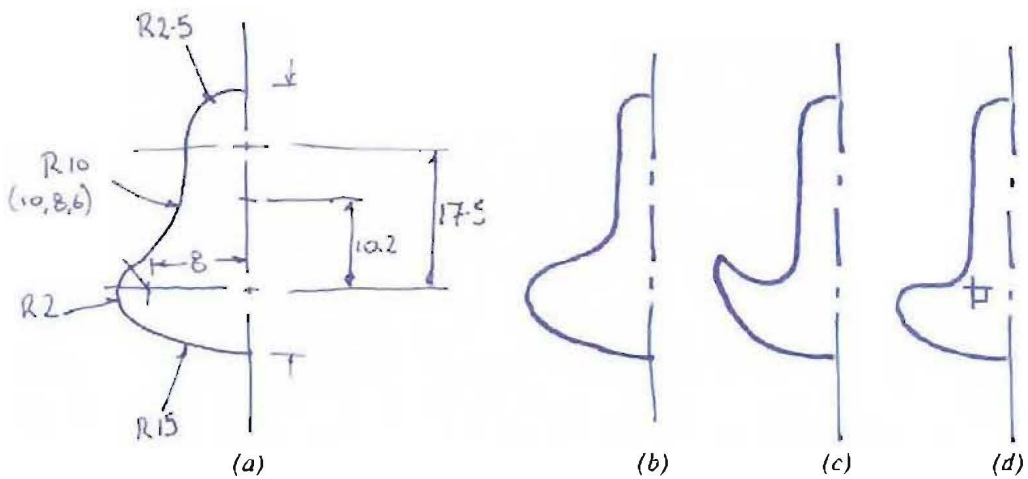


Figure A10.1 Cross section sketches.

(a) Initial tee cross section.

(b) Tee cross section with reduced web thickness.

(c) Tee cross section with a concave flange to wrap around the remaining bone stock.

(d) Final tee cross section.

Figure A10.2 shows the one of the first concept sketches of the endoprosthesis body. Several versions of the femoral endoprosthesis profile were developed, however the final design selected was similar to this sketch. Note this sketch shows screws for the hip and knee connections.

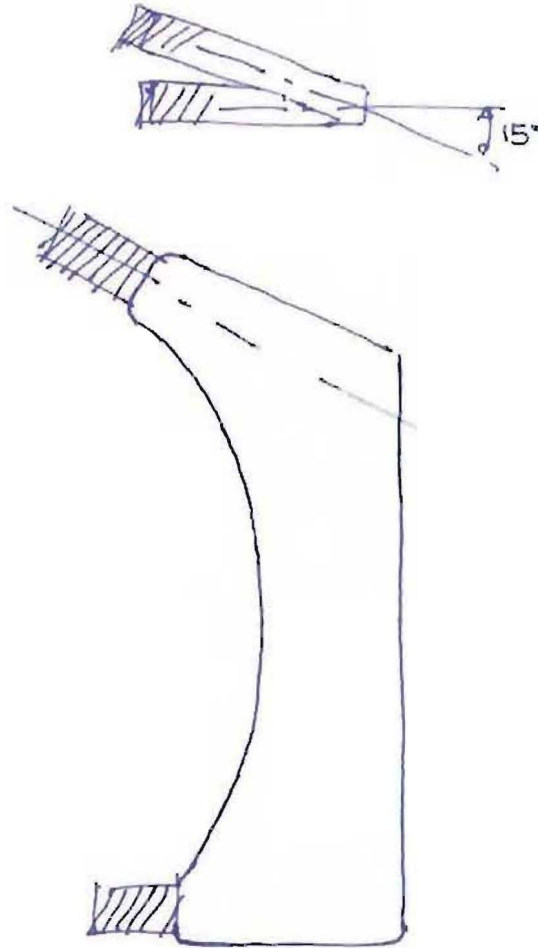


Figure A10.2 First endoprosthesis concept sketch.

Several endoprosthesis designs were developed which allowed a tri-fin nail, identical to the one already implanted in the patient's hip, to be used. Sketches of these designs are shown in Figure A10.3. These designs were ultimately rejected though as tri-fin nails were found to have insufficient strength to bear the patients full weight over an extended period of time. There were also wear debris, fretting and manufacturability concerns with these designs.

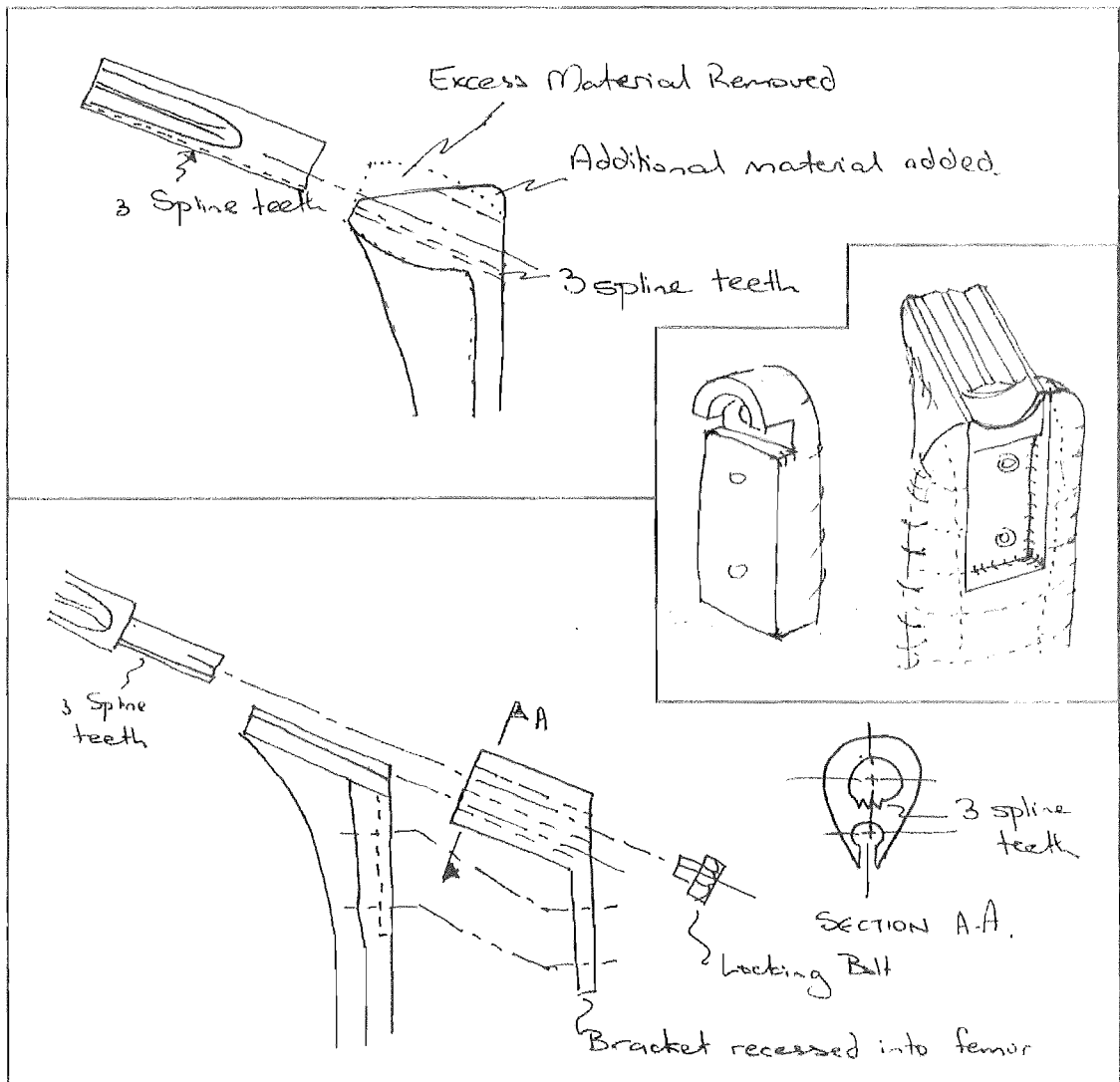


Figure A10.3 Endoprosthesis designs for retaining a tri-fin nail.

Figure A10.4 shows some of the hip screw retention systems considered. The final solution adopted was Idea 2. Although this concept required a boss on the outer face of the endoprosthesis body it was felt that this was the simplest, most secure design which also minimised any potential wear debris issues.

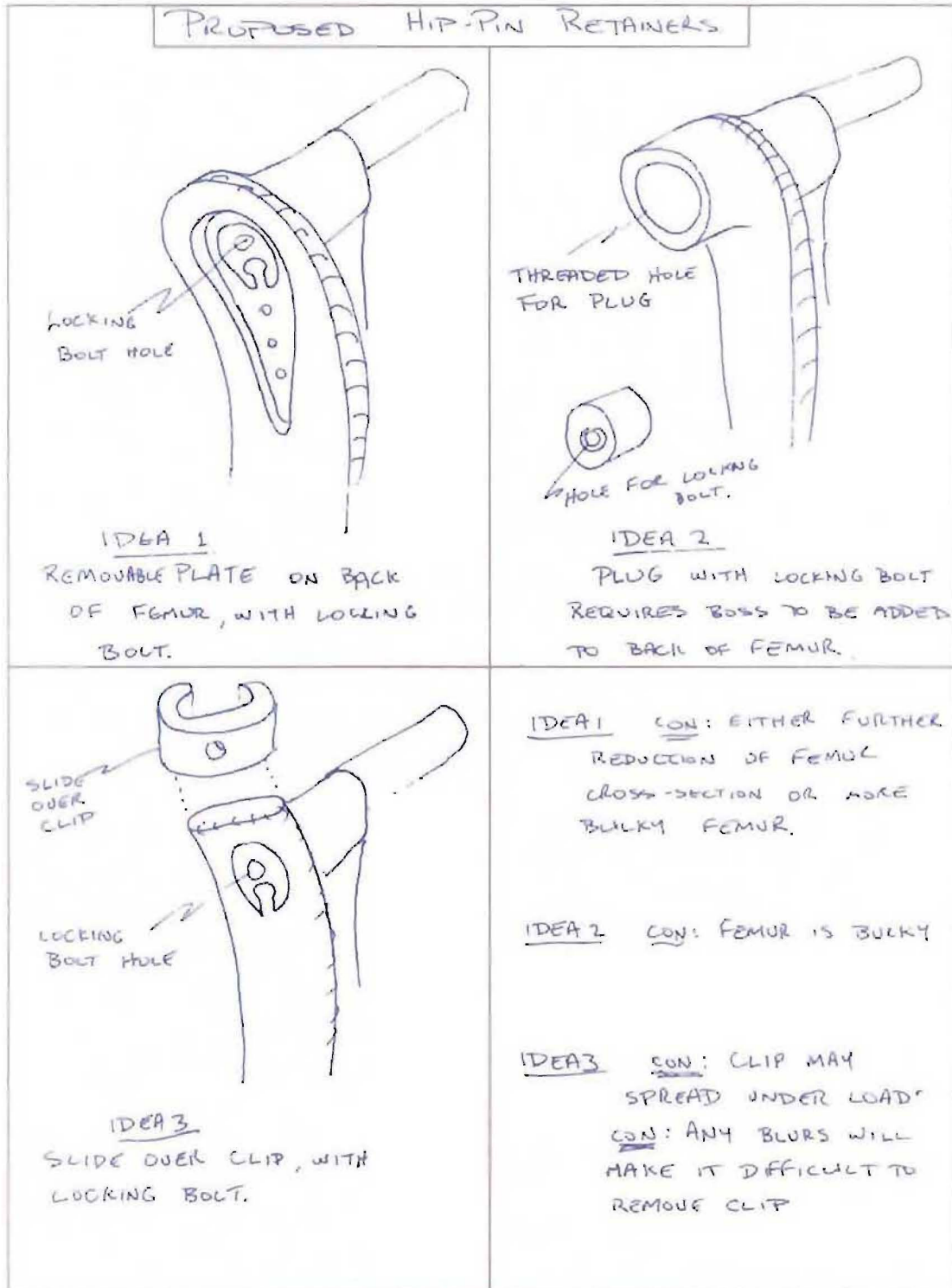


Figure A10.4 Endoprosthesis designs for retain the hip screw.

<Blank Page>

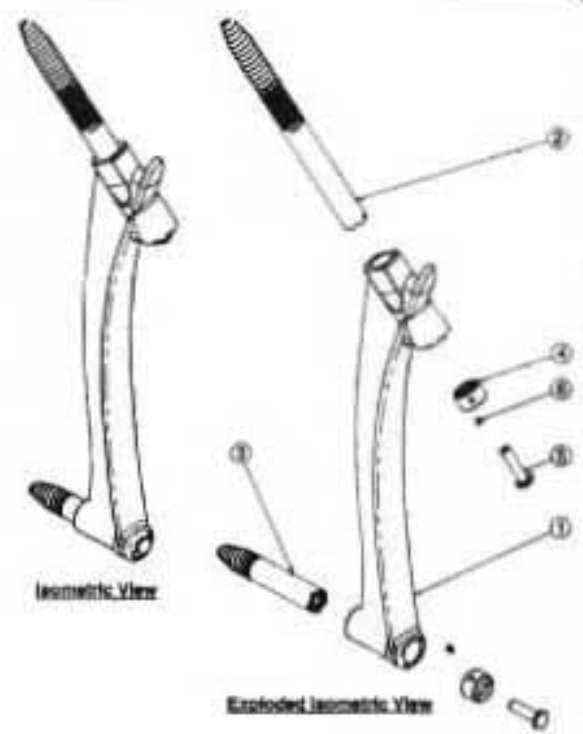
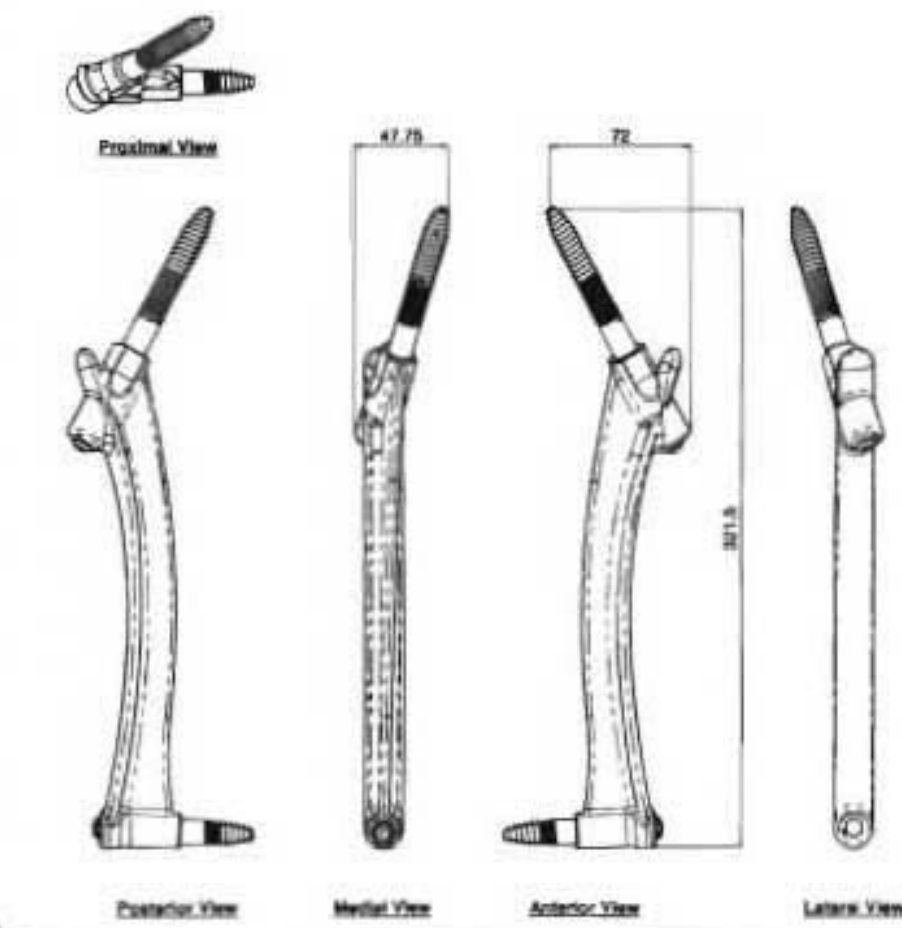
Appendix 11 – Femoral Endoprosthesis Drawings

This appendix contains engineering drawings of the femoral endoprosthesis detailed in Chapter 10. These drawing detail the following components.

- General Assembly
- Endoprosthesis Body
- Hip Screw
- Knee Screw
- Locking Plug

Figure A11.1 Femoral Endoprosthesis General Assembly

All Dimensions ±0.1 Unless Otherwise Stated.
 All Dimensions in Millimetres.
 Stock Material: Ti-6Al-4V.
 Quantity: 2 Required.
 Carborundum Blast All Compression Surfaces,
 with Fine Grit, 40 P₆₁, 90 Blast Angle.



| 5 | Nylon Stopper | 2 | - |
|------|--------------------|----------|-------------|
| 5 | 1/4" UNF x 20 Bolt | 2 | - |
| 4 | Locking Plug | 2 | SW_1299_02 |
| 3 | Knee Screw | 1 | AC_1198_02 |
| 2 | Hip Screw | 1 | AC_1198_01 |
| 1 | Femur Main Body | 1 | SW_1299_01 |
| Item | Description | Quantity | Drawing No. |

Custom L.H. Femur

General Arrangement

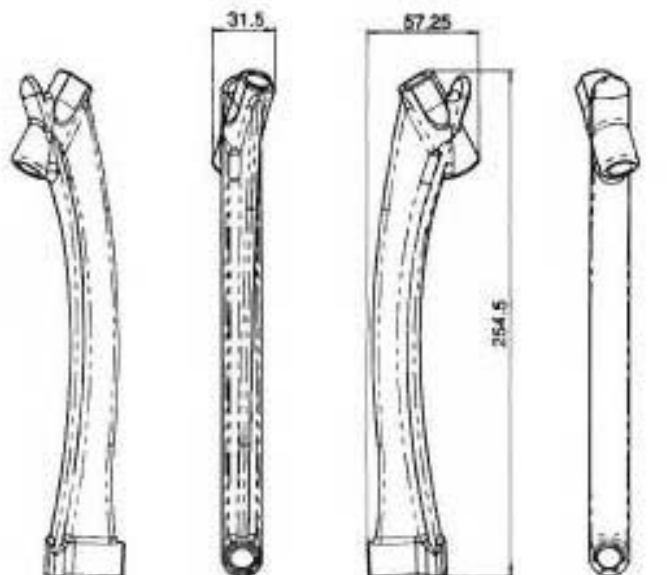
| | | | |
|-------------|------------------------------|------|-------|
| DESIGNED BY | J.E., I.M., P.M., R.V., M.N. | DATE | 1.1 |
| DRAWN BY | I. McMillan | DATE | 12/95 |
| CHECKED BY | | DATE | A |
| SW_1299_GA | | | |



All Dimensions ± 0.1 Unless Otherwise Stated.
 All Dimensions in Millimetres.
 Stock Material: Ti-6Al-4V.
 Quantity: 2 Required.
 Carborundum Blast All Compression Surfaces,
 with Fine Grit, 40 Psi, 90° Blast Angle



Proximal View



Posterior View

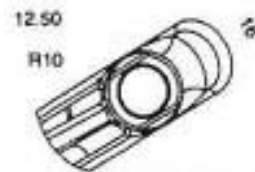
Medial View

Anterior View

Lateral View



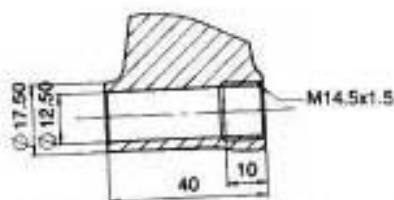
Typical Cross Section



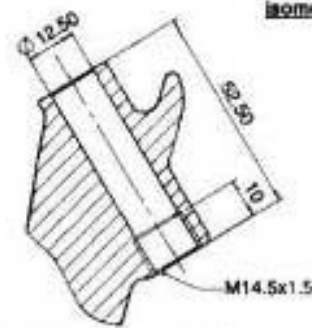
Auxiliary View of Hip Boss



Isometric View



Detail Sectional View of Knee Boss

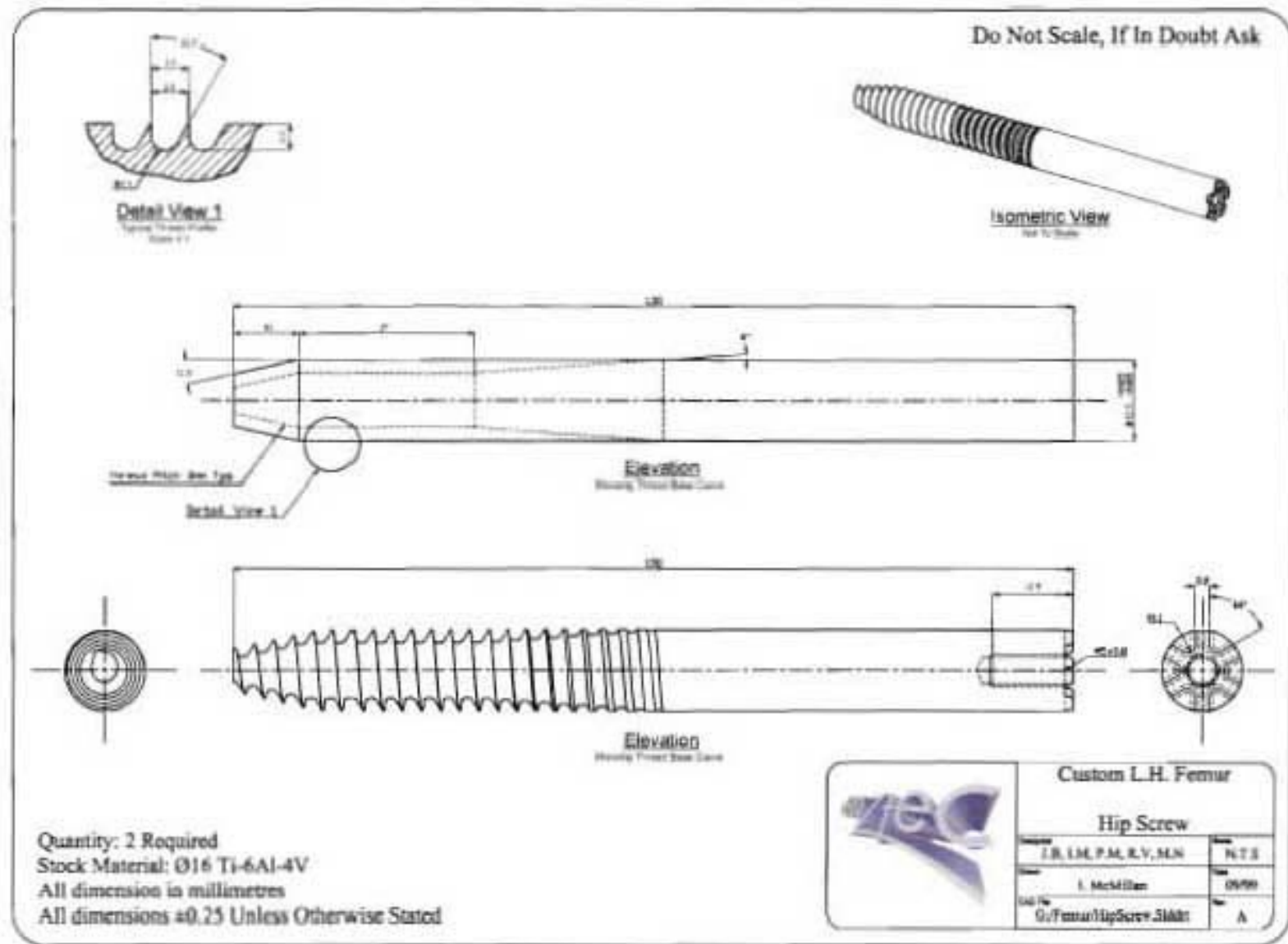


Detail Sectional View of Hip Boss

| | | |
|-----------------------|-------------------------------------|---------------|
| | Custom L.H. Femur | |
| | Femur Main Body | |
| | Designed J.B, I.M, P.M, R.V, M.N | Scale 2:1 |
| | Drawn I. McMillan | Date 09/99 |
| QC'd By SW_1299_01 | Rev A | |

Figure All 2 Endoprosthesis Body.

Figure A1.3 Hip Screw



Do Not Scale, If In Doubt Ask

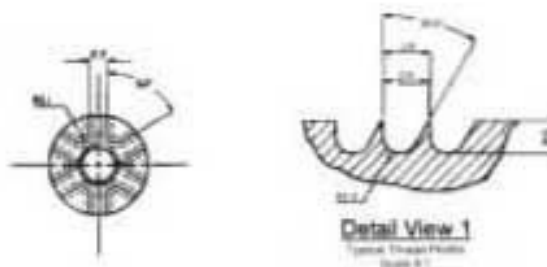
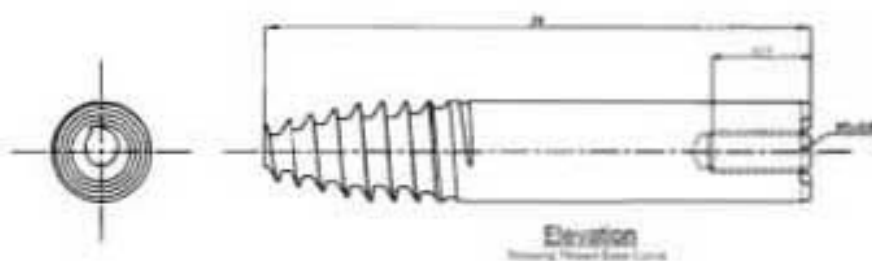
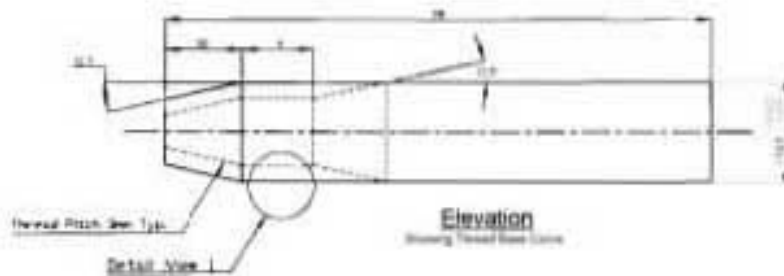
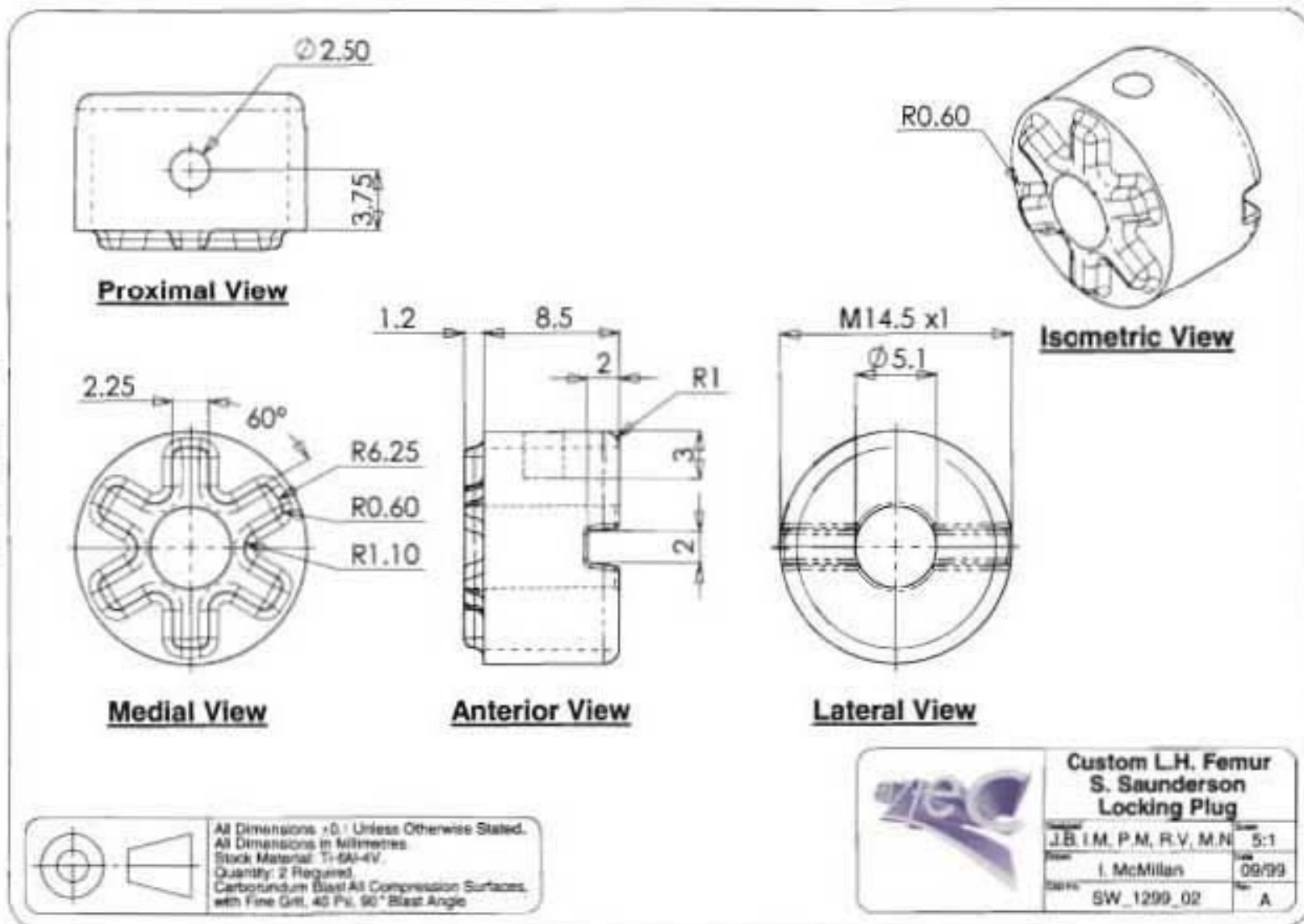


Figure A11.4 Knee Screw

Quantity: 2 Required
 Stock Material: Ø16 Ti-6Al4V
 All dimension in millimetres
 All dimensions ±0.25 Unless Otherwise Stated

| | | |
|------|---------------------------|-------|
| | Custom L.H. Femur | |
| | Knee Screw | |
| | J.B. LM, P.M., R.V., M.H. | N.T.S |
| | I. McMillan | 09/99 |
| DATE | G:\Femur\KneeScrew.Slabbt | A |

Figure A11.5 Locking Plug



The End